

Keiichi Sasaki · Osamu Suzuki  
Nobuhiro Takahashi *Editors*

# Interface Oral Health Science 2014

Innovative Research on  
Biosis–Abiosis Intelligent Interface



Springer Open

# Interface Oral Health Science 2014



Keiichi Sasaki • Osamu Suzuki  
Nobuhiro Takahashi  
Editors

# Interface Oral Health Science 2014

Innovative Research on Biosis–Abiosis  
Intelligent Interface



Springer Open

*Editors*

Keiichi Sasaki  
Division of Advanced Prosthetic  
Dentistry  
Tohoku University Graduate  
School of Dentistry  
Sendai, Miyagi, Japan

Osamu Suzuki  
Division of Craniofacial Function  
Engineering  
Tohoku University Graduate  
School of Dentistry  
Sendai, Miyagi, Japan

Nobuhiro Takahashi  
Division of Oral Ecology  
and Biochemistry  
Tohoku University Graduate  
School of Dentistry  
Sendai, Miyagi, Japan

ISBN 978-4-431-55125-6

ISBN 978-4-431-55192-8 (eBook)

DOI 10.1007/978-4-431-55192-8

Springer Tokyo Heidelberg New York Dordrecht London

Library of Congress Control Number: 2014951841

© The Editor(s) (if applicable) and the Author(s) 2015. The book is published with open access at SpringerLink.com

**Open Access.** This book is distributed under the terms of the Creative Commons Attribution Noncommercial License, which permits any noncommercial use, distribution, and reproduction in any medium, provided the original author(s) and source are credited.

All commercial rights are reserved by the Publisher, whether the whole or part of the material is concerned, specifically the rights of translation, reprinting, re-use of illustrations, recitation, broadcasting, reproduction on microfilms or in any other way, and storage in data banks. Duplication of this publication or parts thereof is permitted only under the provisions of the Copyright Law of the Publisher's location, in its current version, and permission for commercial use must always be obtained from Springer. Permissions for commercial use may be obtained through RightsLink at the Copyright Clearance Center. Violations are liable to prosecution under the respective Copyright Law.

The use of general descriptive names, registered names, trademarks, service marks, etc. in this publication does not imply, even in the absence of a specific statement, that such names are exempt from the relevant protective laws and regulations and therefore free for general use.

While the advice and information in this book are believed to be true and accurate at the date of publication, neither the authors nor the editors nor the publisher can accept any legal responsibility for any errors or omissions that may be made. The publisher makes no warranty, express or implied, with respect to the material contained herein.

Printed on acid-free paper

Springer is part of Springer Science+Business Media ([www.springer.com](http://www.springer.com))

# Preface

This book, containing review articles from the 5th International Symposium for Interface Oral Health Science held January 20–21, 2014, at Sakura Hall in Tohoku University, Sendai, Japan, is being published in 2014 under the title of *Interface Oral Health Science 2014*. I am very pleased and honored to deliver the book for publication.

Interface oral health science is a new concept in dentistry, established by the Tohoku University Graduate School of Dentistry in 2002, and is based on the following principles: Normal oral function is maintained through harmony between three biological and biomechanical systems: structure of the mouth, including teeth, the mucous membrane, bones, and muscles; microorganisms in the mouth (parasites); and biomaterials. Tooth decay, periodontal disease, and other oral disorders can be recognized as interface disorders, which are caused by the collapse of the interface between the systems. This concept is shared not only by dentistry and dental medicine but also by a variety of disciplines, including medicine, material science, engineering, and others.

Since 2002, the Tohoku University Graduate School of Dentistry has regarded interface oral health science as the main theme of dental research in the twenty-first century. We are committed to advancing dental studies by implementing interface oral health science, while promoting interdisciplinary research across a wide range of related fields. Based on this concept, we have successfully organized international symposia for Interface Oral Health Science four times, in 2005, 2007, 2009, and 2011, including inspiring special lectures, symposium sessions, poster presentations, and other discussions. These presentations from the four international symposia were published in a series of English monographs under the title *Interface Oral Health Science*.

These achievements were praised, and, in 2007, “Highly Functional Interface Science: Innovation of Biomaterials with Highly Functional Interface to Host and Parasite” was adopted as a program for Research and Education Funding for the Inter-University Research Project 2007–2011, Ministry of Education, Culture, Sports, Science and Technology (MEXT), Japan. Subsequently, we have been

developing the project with a broader and deeper concept: “Biosis–Abiosis Intelligent Interface,” which also was adopted as a program for a Research Promotion Project 2012–2015, MEXT, Japan. It is aimed at creating a highly functional and autonomic intelligent interface by combining the highly functional interface science established by the Tohoku University Graduate School of Dentistry and the Institute for Materials Research, Tohoku University, with the technology of evaluation and control at the interface which was offered by the Graduate School of Biomedical Engineering, Tohoku University. We firmly believe that the Biosis–Abiosis Intelligent Interface project can contribute to solving various problems not only in dentistry and medicine but also in other disciplines.

Therefore, the 5th International Symposium for Interface Oral Health Science was held as the Innovative Research for Biosis–Abiosis Intelligent Interface Symposium, organized by the Tohoku University Graduate School of Dentistry with the aid of a Research Promotion Project Grant, MEXT, Japan. The symposium was composed of four focus sessions and 90 poster presentations. We had 18 distinguished invited/keynote speakers for the focus sessions.

I hope that our project, including the symposium and the book, will accelerate the progress of dental science and point the way for dental research for future generations. Finally, I would like to thank all members of our school and participants of the symposium for their contributions. Our thanks go especially to the authors of the excellent review papers for this book.

Keiichi Sasaki

President, The 5th International Symposium for Interface Oral Health Science  
Innovative Research for Biosis–Abiosis Intelligent Interface Symposium  
Director, Tohoku University Graduate School of Dentistry  
Dean, Tohoku University School of Dentistry  
Sendai, Japan

# Acknowledgments

The Editors wish to acknowledge the following members of the Tohoku University Graduate School of Dentistry, Institute for Materials Research, Tohoku University and Tohoku University Graduate School of Biomedical Engineering, all of whom have contributed their valued expertise and time to hold the symposium, and to edit manuscripts submitted to *Interface Oral Health Science 2014*. These colleagues have provided essential assistance, without which it wouldn't have been possible to publish this monograph in a timely manner.

## Tohoku University Graduate School of Dentistry

Hidetoshi Shimauchi  
Tetsu Takahashi  
Satoshi Fukumoto  
Haruhiko Takada  
Teruko Yamamoto  
Minoru Wakamori  
Yoshimi Niwano  
Shunji Sugawara  
Masahiko Kikuchi  
Takeyoshi Koseki  
Yasuyuki Sasano  
Yutaka Henmi  
Kiyoshi Matsuda  
Takuro Kisara  
Kaori Inoue  
Tatsuya Onodera  
Shinji Kameya  
Hiroaki Oyamada  
Satsuki Horita  
Kumiko Oba

Aya Machita  
Kaori Sato  
Takako Sato  
Shunichi Yuki  
Eri Ono  
Genki Fukaya  
Naoko Miura  
Daisuke Haneda  
Yuriko Kimura  
Hidetomo Kawauchi  
Masayuki Kagi  
Teruko Ando  
Kouki Hatori  
Yasuhsisa Takeuchi  
Guang Hong  
Keiichi Saito  
Naoko Sato  
Azusa Fukushima  
Risa Ishiko  
Mayumi Oikawa  
Takehiko Mito  
Kazuko Ishiguro  
Kenta Takahashi  
Yoshiki Matsudate  
Tomoko Ishiguro  
Aya Shibamoto  
Makiko Miyashita  
Jun Takahira  
Naoya Saito  
Kuniyuki Izumita

**Institute for Materials Research, Tohoku University**

Takashi Goto  
Takayuki Narushima  
Hirokazu Katsui

**Tohoku University Graduate School of Biomedical Engineering**

Yoshifumi Saijo  
Tetsu Tanaka  
Ryoichi Nagatomi

# Contents

## Part I Symposium I: Biosis–Abiosis Interface of Dental Implants

<b>1 Biological Events Occuring on the Biosis–Abiosis Interface: Cellular Responses Induced by Implantable Electrospun Nanofibrous Scaffolds . . . . .</b>	<b>3</b>
Xuliang Deng, Yan Wei, Xuehui Zhang, Ying Huang, and Mingming Xu	
<b>2 Updates in Treatment Modalities and Techniques on Compromised Alveolar Ridge Augmentation for Successful Dental Implant Therapy . . . . .</b>	<b>17</b>
Myung-Jin Kim	
<b>3 Surface Modification of Dental Implant Improves Implant–Tissue Interface . . . . .</b>	<b>33</b>
Takashi Inoue and Kenichi Matsuzaka	
<b>4 Oral Microbiota in Crevices Around Dental Implants: Profiling of Oral Biofilm . . . . .</b>	<b>45</b>
Takuichi Sato, Yoshiaki Kawamura, Keiko Yamaki, Naoko Ishida, Lingyang Tian, Yasuhisa Takeuchi, Kazuhiro Hashimoto, Yuki Abiko, Gen Mayanagi, Jumpei Washio, Junko Matsuyama, and Nobuhiro Takahashi	

## Part II Symposium II: Biomaterials in Interface Science

<b>5 Biofunctionalization of Metallic Materials: Creation of Biosis–Abiosis Intelligent Interface . . . . .</b>	<b>53</b>
Takao Hanawa	

<b>6</b>	<b>Evaluation of Photocatalytic Activity of the TiO<sub>2</sub> Layer Formed on Ti by Thermal Oxidation . . . . .</b>	65
	Takayuki Narushima, Shota Sado, Natsumi Kondo, Kyosuke Ueda, Mitsuko Kawano, and Kouetsu Ogasawara	
<b>7</b>	<b>Enhancing Functionalities of Metallic Materials by Controlling Phase Stability for Use in Orthopedic Implants . . . . .</b>	79
	Masaaki Nakai, Mitsu Niinomi, Ken Cho, and Kengo Narita	
<b>8</b>	<b>Surface Improvement for Biocompatibility of Ti-6Al-4V by Dealloying in Metallic Melt . . . . .</b>	93
	Yuichi Fukuzumi, Takeshi Wada, and Hidemi Kato	
<b>9</b>	<b>Chemical Vapor Deposition of Ca-P-O Film Coating . . . . .</b>	103
	Takashi Goto and Hirokazu Katsui	

### **Part III Symposium III: Biomedical Engineering Interface**

<b>10</b>	<b>Importance of Visual Cues in Hearing Restoration by Auditory Prostheses . . . . .</b>	119
	Tetsuaki Kawase, Yoko Hori, Takenori Ogawa, Shuichi Sakamoto, Yōiti Suzuki, and Yukio Katori	

### **Part IV Symposium IV: Cell Manipulation and Tissue Regeneration**

<b>11</b>	<b>Designer Supersurfaces via Bioinspiration and Biomimetics for Dental Materials and Structures . . . . .</b>	131
	David W. Green and Han-Sung Jung	
<b>12</b>	<b>Feeder Cell Sources and Feeder-Free Methods for Human iPS Cell Culture . . . . .</b>	145
	Guannan Yu, Yuya Kamano, Fangfang Wang, Hiroko Okawa, Hirofumi Yatani, and Hiroshi Egusa	
<b>13</b>	<b>Hydrogel-Based Biomimetic Environment for In Vitro Cell and Tissue Manipulation . . . . .</b>	161
	Takuya Matsumoto	
<b>14</b>	<b>Trends in Periodontal Regeneration Therapy: Potential Therapeutic Strategy of Extracellular Matrix Administration for Periodontal Ligament Regeneration . . . . .</b>	169
	Masahiro Saito	

**Part V Poster Presentation Award Winners**

- 15 Histochemical Characteristics of Glycoproteins During Rat Palatine Gland Development . . . . .** 183  
Zaki Hakami, Hideki Kitaura, Shiho Honma,  
Satoshi Wakisaka, and Teruko Takano-Yamamoto
- 16 The Role of NFIC in Regulating Odontoblastic Differentiation of Human Molar Stem Cells from Apical Papilla . . . . .** 193  
Yuming Zhao, Shuo Gao, and Lihong Ge
- 17 Microbicidal Activity of Artificially Generated Hydroxyl Radicals . . . . .** 203  
Hong Sheng, Keisuke Nakamura, Taro Kanno,  
Keiichi Sasaki, and Yoshimi Niwano
- 18 High Levels of Saturated Fatty Acids may Exacerbate the Pathogenesis of Primary Sjögren's Syndrome . . . . .** 217  
Yosuke Shikama, Naozumi Ishimaru, Yasusei Kudo,  
Rieko Arakaki, Yukiko Bando, Nanako Aki, Yoshio Hayashi,  
and Makoto Funaki
- 19 Effects of Carbon Addition on Mechanical Properties and Microstructures of Ni-Free Co-Cr-W-Based Dental Alloys . . . . .** 225  
Kenta Yamanaka, Manami Mori, and Akihiko Chiba
- 20 Periodontal Disease as a Possible Risk Factor for Alzheimer's Disease . . . . .** 237  
Naoyuki Ishida, Yuichi Ishihara, Kazuto Ishida,  
Hiroyuki Tada, Yoshiko Kato, Ryutaro Isoda,  
Makoto Hagiwara, Makoto Michikawa, Toshihide Noguchi,  
and Kenji Matsushita
- 21 Measurement of Skin Elasticity Using High Frequency Ultrasound Elastography with Intrinsic Deformation Induced by Arterial Pulsation . . . . .** 245  
Ryo Nagaoka, Kazuto Kobayashi, and Yoshifumi Saijo

**Part VI Poster Presenters**

- 22 Effect of Macrophage Colony-Stimulating Factor Receptor c-Fms Antibody on Lipopolysaccharide-Induced Pathological Osteoclastogenesis and Bone Resorption . . . . .** 259  
Keisuke Kimura, Hideki Kitaura, Masahiko Ishida,  
Zaki Hakami, Jafari Saeed, Haruki Sugisawa,  
and Teruko Takano-Yamamoto

<b>23 The Role of Th1 Cytokines on Mechanical Loading-Induced Osteoclastogenesis and Bone Resorption . . . . .</b>	269
Hideki Kitaura, Keisuke Kimura, Masahiko Ishida, Zaki Hakami, Jafari Saeed, Haruki Sugisawa, Haruka Kohara, Masako Yoshimatsu, and Teruko Takano-Yamamoto	
<b>24 The Ventral Primary Somatosensory Cortex of the Primate Brain: Innate Neural Interface for Dexterous Orofacial Motor Control . . . . .</b>	281
Takashi Toda and Tada-aki Kudo	
<b>25 Possible Roles of IL-33 in Periodontal Diseases: <i>Porphyromonas gingivalis</i> Induced IL-33 in Human Gingival Epithelial Cells . . . . .</b>	293
Hiroyuki Tada, Hidetoshi Shimauchi, Haruhiko Takada, and Kenji Matsushita	
<b>26 Prospects for Liposome-Encapsulated Nisin in the Prevention of Dental Caries . . . . .</b>	305
Hideaki Tsumori, Yoshitaka Shimizu, Kohei Nagatoshi, Yutaka Sakurai, and Kazuo Yamakami	
<b>27 Clinical Chipping of Zirconia All-Ceramic Restorations . . . . .</b>	317
Shoko Miura, Shin Kasahara, Momoko Kudo, Yayoi Okuyama, Akio Izumida, Masanobu Yoda, Hiroshi Egusa, and Keiichi Sasaki	
<b>28 Dentin Hypersensitivity: Etiology, Prevalence and Treatment Modalities . . . . .</b>	325
M. Kanehira, H. Ishihata, and M. Saito	
<b>29 Preventing Aspiration Pneumonia Among the Elderly: A Review Focused on the Impact of the Consistency of Food Substances . . . . .</b>	335
Reiko Sakashita, Miho Takami, Hiroshi Ono, Tomoko Nishihira, Takuichi Sato, and Misao Hamada	

**Part I**

**Symposium I: Biosis–Abiosis Interface  
of Dental Implants**

# **Chapter 1**

## **Biological Events Occuring on the Biosis–Abiosis Interface: Cellular Responses Induced by Implantable Electrospun Nanofibrous Scaffolds**

**Xuliang Deng, Yan Wei, Xuehui Zhang, Ying Huang, and Mingming Xu**

**Abstract** Electrospun nanofibers have tremendous potential as novel scaffolds for tissue engineering of various soft and hard tissues because of their high surface area, surface functional groups, interconnected pores, and nano-scaled size. In this chapter, we reviewed the types of the nanofibrous scaffolds that have been used as implantable biomedical devices and used electrospun nanofibrous guided tissue regeneration membrane as an example to illustrate how the physicochemical properties of nanofibrous scaffolds influenced the biological events occurring on the scaffolds-host interface. It could be concluded that physical and chemical stimuli caused by nanofibrous scaffold would support in vivo-like three-dimensional cell adhesion and activate cell-signaling pathways. In terms of physical stimulus, the process of mechanotransduction may play an important role in influencing cellular behaviors. As a result, biological events such as cell-interface recognition, cell proliferation, and cell differentiation are altered. Nevertheless, the cellular and molecular mechanisms by which cells sense and respond to nanofibrous scaffolds remain poorly understood. More evidences are needed to reveal the underlying mechanisms whereby environmental cues alternated the cellular responses to the

---

X. Deng (✉)

Department of Geriatric Dentistry, Peking University School and Hospital of Stomatology, Beijing, P. R. China

National Engineering Laboratory for Digital and Material Technology of Stomatology, Beijing, P. R. China

e-mail: [kqdengxuliang@bjmu.edu.cn](mailto:kqdengxuliang@bjmu.edu.cn)

Y. Wei • Y. Huang • M. Xu

Department of Geriatric Dentistry, Peking University School and Hospital of Stomatology, Beijing, P. R. China

X. Zhang

Department of Dental Materials, Peking University School and Hospital of Stomatology, Beijing 100081, P. R. China

Department of Geriatric Dentistry, Peking University School and Hospital of Stomatology, Beijing, P. R. China

physiochemical properties of nanofibrous scaffolds. These future studies may help to design may help to design new generations of implantable biomedical devices that possess controllable cellular responses.

**Keywords** Biosis–abiosis interface • Electrospun nanofibrous scaffolds • Mechanotransduction • Mesenchymal stem cells

## 1.1 Electrospun Nanofibrous Scaffolds as Implantable Biomedical Devices

The electrospinning technique is being used to fabricate fibrous scaffolds for tissue engineering, with the aim of restoring and maintaining the biological function lost in host tissues [1]. The electrospun fibrous matrices can provide an ultrahigh surface for cell attachment with high porosity [2] for the exchange of nutrients, ions, and regulatory molecules between cells. The electrospun fibrous matrix holds great promise for tissue regeneration based on its morphology, which favors to support and guide cell growth [3].

Formhals first introduced electrospinning or e-spinning in 1938 [4]. Recently, numerous research groups have explored its use to generate fibrous scaffolds for tissue regeneration. A typical electrospinning apparatus includes a polymer solution/melt in a syringe, charged through a high voltage supply, and a grounded plate positioned at a predetermined distance from the tip of the needle. The potential difference overcomes the surface tension of the fluid droplet at the tip of the metal needle, which in turns results in the formation of the so-called Taylor cone. The fluid jet experience whipping instabilities and tends to dry and form fibers with an average diameter ranging from several microns to tens of nanometers. Processing parameters including voltage, distance from tip to collector, collector type (rotating or static), solution properties (e.g., concentration, viscosity and conductivity) and flow rate have significant influences on fiber formation and morphology. The solution must be sufficiently concentrated so that the polymer chains are continuous and entangled and of suitable viscosity to maintain a droplet and be pumped through the syringe. The resultant materials comprise biocompatible and degradable natural or synthetic polymers or blends and normally resemble the arrangement of the native extracellular matrix (ECM). The fibers can be collected at a random orientation when using a static collector or with high degree of alignment by using a rotating mandrel.

Maintenance of wound stability is a key factor for a successful outcome in regenerative periodontal surgery. Essentially, the three-dimensional (3D) structure shown by these e-spun membranes, with a high surface area of improved hydrophilicity and wettability, endow the structure with mechanical support and cell regulation functions that guide new bone formation into the defect. Li et al. have cultured different cells such as fibroblasts, cartilage cells, and mesenchymal stem cells on poly (lactic-co-glycolic acid) (PLGA) and poly-(caprolactone) (PCL) nanofibrous scaffolds and demonstrated the ability of the nanofiber structure to support cell attachment and proliferation.

### ***1.1.1 Categories of Electrospun Nanofibrous Scaffolds: Classified by Chemical Components***

#### **1.1.1.1 Single Component Nanofibers**

The choice of material for tissue engineering applications depends upon the type of scaffold required. The correct material to fulfill the requirement of specific mechanical properties and degradation times required for the particular application [5]. Polymer are the main source materials of electrospun nanofibers. Certain of the synthetic and natural polymers have been introduced widely to electrospinning technique for regenerative medicine. Aliphatic polyesters, such as PCL, poly (lactide) (PLA), and their copolymers and blends, are some of the many biodegradable synthetic polymers that have been electrospun. By adjusting electrospinning parameters such as voltage, distance between the electrodes, and flow rate of the solution during electrospinning, and polymer solution properties, such as viscosity and conductivity, most of the biocompatible polymers can be electrospun (e.g. Poly (L-lactic acid) (PLLA), PLGA).

Compared with synthetic polymers, natural biopolymers have good biocompatibility and provide many of the instructive cues required by the cells for attachment and proliferation; however, they tend to display poor processability, which needs to be modified for better electrospinnability. For instance, Zhang et al. have tried to improve the electrospun processability of gelatin by modifying the solubility of gelatin at elevated temperature and the degree of cross-linking of the resultant gelatin fibers [6].

Besides polymer nanofibers, ceramic nanofibers were also fabricated using electrospinning. For example, Zhang et al. developed woven-bone-like  $\beta$ -TCP fibers by sol–gel electrospinning [7]. Optimization studies were conducted in terms of sol–gel synthesis and the electrospinning process, to fabricate electrospun nanofibrous scaffolds with pure  $\beta$ -TCP fibers that mimic the mineralized collagen fibrils in woven bone in size [7].

#### **1.1.1.2 Composite Nanofibers**

##### **Organic/Organic Composite Nanofibers**

The combination of synthetic and natural polymers is considered advantageous not only for tuning the solubility of natural polymers but also for easy surface modification. Many synthetic (e.g. aliphatic polyester) and natural polymers (e.g. proteins and polysaccharides) have been reported to possess the tissue regenerative potential [8]. However, the innate concerns associated with synthetic polymers are their poor cell affinity [9], while biopolymers are rarely considered as scaffold materials for tissue engineering applications without any special treatment (e.g. cross-linking, or hydrophobic modification) [10, 11]. Mixing synthetic and natural polymers is a

feasible approach to theoretically circumvent the shortcomings of the individual materials and produce new biomaterials with good performances for tissue engineering applications. Jiang et al. firstly reported the preparation of co-electrospun composite membranes composed of PLGA and dextran [12]. After that, different synthetic/natural polymer pairs were coelectrospun, including Poly(L-lactic acid) (PLLA)/gelatin (GE), polycaprolactone (PCL)/GE and cellulose acetate/polyurethane, exhibiting desired cell behaviors and degradation properties [13–15].

### Organic/Inorganic Composite Nanofibers

Recent efforts have focused on the development of composite nanofiber scaffolds which can better mimic the composition and mechanical properties of natural bone. Incorporating inorganic phase material (e.g. hydroxyapatite (HA) or  $\beta$ -tricalcium phosphate ( $\beta$ -TCP)), which is one of the compositions of natural bone or bone precursors, into an organic phase material (e.g. biodegradable polymeric nanofibers) is generally used to enhance the mechanical property and osteoconductivity of nanofiber scaffolds in recent years. Sui et al. developed a kind of electrospun membranes composed of HA and PLLA and reported their applications for periodontal tissue regeneration and guided bone regeneration [16, 17]. More recently, Mei et al. developed a novel electrospinning nanofibrous membrane which contained ceramic nano-HA, carbon nanotubes (CNTs), and PLLA matrix [18]. Zhang et al. have fabricated gelatin/ $\beta$ -TCP composite nanofibers using electrospinning technique, which could regulate Ca ions release by altering the content of  $\beta$ -TCP nanoparticles in gelatin matrix [19]. These composite membranes exhibited excellent biocompatibility, biodegradability, and mechanical properties.

### **1.1.2 Categories of Electrospun Nanofibrous Scaffolds: Classified by Electrospinning Techniques**

#### **1.1.2.1 Coaxial Electrospinning**

The formation of core/shell nanofibers by coaxial electrospinning was first reported by [20]. This technique proved to be very versatile not only for the encapsulation of biorelevant molecules and nanocomposites but also for modifying the surfaces of electrospun fibers. The effect of nanofiber surface coatings on the cell-proliferation behavior was studied by Zhang et al. studied the effect of nanofiber surface coatings on cell-proliferation behavior the coaxial electrospinning technique [21]. They produced collagen coated PCL nanofibers. Coatings of collagen on PCL were shown to favor proliferation of human dermal fibroblasts and also encouraged cell migration inside the scaffolds. Using a similar approach, biodegradable fibrous scaffolds composed of gelatin coated PCL were prepared by Zhao et al. by coaxial

electrospinning [22]. More recently, Sun et al. developed core–shell PAN–PMMA nanofibers by coaxial electrospinning [23].

### 1.1.2.2 Coaxial or Emulsion Electrospray

Bioactive factors-loaded microparticles can generally be achieved by two different electrospray approaches: coaxial or emulsion electrospray. Coaxial electrospray was first reported by Loscertales et al. [24]. Two immiscible solutions are coaxially and simultaneously electrosprayed through two separate feeding channels into one nozzle. The eventual jet, by which the outer polymeric solution encapsulates the inner proteinaceous liquid, breaks into droplets to generate microparticles with core–shell structure. This technique is preferred for preparing protein-loaded microcapsules, because it totally eliminates the emulsion step that is basically unsuitable for sensitive biomacromolecules [25, 26]. Coaxial electrospray is envisioned a promising approach to prepare biomacromolecule-loaded microcapsules for controlled drug delivery applications.

Emulsion electrospray involves mixing of an aqueous solution containing proteins with immiscible polymeric solution by ultrasonication [27, 28]. Compared with other conventional manufacture methods, the second emulsion or high temperature is omitted in emulsion electrospray. It increases the drug-loading efficiency and is suited for encapsulation of thermosensitive bioactive compounds.

### 1.1.3 Biofunctionalization of Nanofibrous Scaffolds

Electrospun nanofibrous membranes are considered to have great potential in the field of tissue engineering because they can closely mimic the ECM architecture [29, 30]. However, for some polymer nanofibers with the relative hydrophobicity and surface inertia, such as poly (methyl methacrylate) (PMMA) and PLLA, bioactive treatment will usually be needed to improve their cellular affinity and facilitate osteogenesis.

#### 1.1.3.1 Plasma Treatment

Low-temperature plasma treatment has been shown to be a convenient and effective way to modify surfaces to improve the hydrophilicity of biomaterials, thus increasing their biocompatibility and facilitate cell attachment [31, 32]. Wan et al. reported that ammonia plasma treatment significantly increased the hydrophilicity of PLA scaffolds and resulted in enhanced cell adhesion and proliferation of mouse 3T3 fibroblasts [33]. D’Sa et al. reported that improved hydrophilicity of PMMA surfaces by plasma treatment increased adsorption of proteins and promoted actin stress fiber formation [34]. Moreover, plasma technique was found to modify levels

of chemical groups, such as  $-COOH$ ,  $-OH$ , or  $-NH_2$  on scaffold surfaces, thereby influencing the cell–substrate interactions. For example, human umbilical vein endothelial cell (HUVEC) adhesion was improved by plasma treatment of PLA through the control of carbon and oxygen concentration [35], and human embryonic palatal mesenchyme (HEPM) cell proliferation was increased by plasma-treated poly(ether ether ketone) (PEEK) through assembling amino groups on the surface [36]. Amino-rich PLA surfaces created by plasma treatment were also reported to promote osteogenic differentiation of MC3T3-E1 cells [32]. More recently, Liu et al. investigated the effects of plasma treatment on the surface of PLLA nanofibrous membranes, and the subsequent dose-dependent cellular response and osteogenesis of MSCs were clarified preliminary [37]. These results support the feasibility of plasma technology to regulate the biological functions of biomaterials.

### 1.1.3.2 Biominerization

In addition to encapsulation of inorganic materials to improve the properties of fibrous materials, depositing inorganic phase materials i.e. biominerization on the surface of polymeric nanofibers to form uniform coatings is an alternative methods. Biominerization on the nanofiber surface can not only enhance its mechanical properties, but also provide a favorable substrate for cell proliferation and osteogenic differentiation. Ramakrishna and co-workers mineralized electrospun PLGA/collagen fibrous scaffolds, and the presence of the functional groups of collagen significantly hastened n-HA deposition in comparison with pure PLGA fibrous scaffolds [38]. The use of simulated body fluid (SBF), a kind of solution with ionic concentration closely resembling human blood plasma to biomimetically coat the composite fibers with apatite layers should be a good choice.

In principle, the morphology and grain size of minerals deposited on the nanofibers can be tailored by controlling the composition of the mineralized solution, the surface charge of substrate and the surface chemical properties. Recently, Cai et al. reported biominerization of electrospun poly(L-lactic acid)/gelatin composite fibrous scaffold by using a supersaturated simulated body fluid with continuous  $CO_2$  bubbling [39]. They found that the mineralites could be formed heterogeneously in the 5× SBF with  $CO_2$  bubbling.

### 1.1.3.3 Biomagnetism

Nature is a source of inspiration for scientists and engineers to design advanced functional materials. Very weak local magnetic fields exist in living organisms and various organs in humans. Earlier clinical research showed that the magnetic field might be beneficial for enhancing bone tissue regeneration though mechanisms that have not yet been clarified.

In recent years, interest in magnetic biomimetic scaffolds for tissue engineering has increased considerably. Magnetic nanoparticles are of great interest owing to

their potential biomedical applications [40, 41], such as cell expansion, cell sheets construction, magnetic cell seeding, as drug delivery vehicles and for hyperthermia treatment. For bone regenerative research, electrospinning technique has been used successfully to fabricate magnetic fibrous scaffolds, including  $\text{Fe}_3\text{O}_4/\text{PVA}$  nanofibers [42],  $\text{Fe}_3\text{O}_4/\text{CNF}$ , and  $\text{FePt}/\text{PCL}$  nanofibers. More recently, Wei et al. fabricated magnetic biodegradable  $\text{Fe}_3\text{O}_4/\text{CS}/\text{PVA}$  nanofibrous membranes, which promoted MG63 cells adhesion and proliferation on these membranes [43]. These results support the feasibility of incorporating magnetic nanoparticles into polymer nanofibers to regulate the biological functions of biomaterials.

## 1.2 Cellular Responses Influenced by Electrospun Nanofibrous Scaffolds

Electrospun nanofibrous scaffolds are able to recapitulate both the topographical features of the ECM, and biochemical cues via various modifications to the fiber material or surface. This type of artificial scaffold with enhanced biofunctionality would comprise a more biomimetic microenvironment for ex vivo stem cell culture. The cell/nanofibers interface exerts considerable influence on MSC functions and differentiation.

### 1.2.1 *Biological Events Occuring on the Biosis–Abiosis Interface: The Role of Chemical Cues*

The chemical matrix of nanofibers may create and maintain specialized functional properties in the local microenvironment for cell function. Hybrid scaffolds comprising synthetic and natural organic polymers take advantage of the physical properties of the synthetic components and the bioactivity of the natural constituents while minimizing the disadvantages of both, resulting in more favorable biocompatibility than those with a single component [16, 44]. The incorporated nanoparticles in nanofibers could provide multiple binding-ligands for amino and carboxyl groups of serum proteins to facilitate cell attachment [44] and bone matrix deposition [16, 43], and introduce magneto-electrical effect ( $\text{Fe}_3\text{O}_4$ ,  $\text{r}-\text{Fe}_2\text{O}_3$ ,  $\text{BeTiO}_3$ , ...) to benefit cell proliferation [43, 45]. The simultaneously incorporation of multi-walled carbon nanotubes (MWCNTs) and HA nanoparticles in PLLA nanofibers selectively increased adhesion of osteoblast cells and decreased the adhesion of osteoblast competitive cell lines, which was a valuable feature for GBR application [17]. The small trace amount of Mg [46, 47], Si [48–50], and Zn ions [51, 52] integrated in nanofibrous scaffolds have been proved to accelerate cell adhesion and proliferation by delivering the mitogenic stimuli and enhancing channel sensitivity. In addition, chemical signal molecules in the form of growth

and differentiation factors [53, 54] or plasmid DNA [55, 56] incorporated in the nanofibers in a spatially defined manner could achieve corresponding bioactivity in promoting specific differentiation to orchestrate the growth of new tissue.

Surface modification, including chemically grafted surface-functional-groups and microcontact printed peptides or proteins, could initiate specialized cell-nanofibers interactions. The enrichment of specific -OH, -NH<sub>3</sub> or -COOH chemical groups on nanofibers may lead to improved hydrophilicity and reversible albumin adsorption, facilitating focal adhesion assembly and matrix deposition [57–59]. Attachment of adhesion-promoting peptides, such as RGD, 52 GRGDS, and GEFYFDLRLKGDK could increase the selective interactions between nanofibers and cells in terms of adhesion, spreading, and proliferation [60, 61]. The coated structural ECM proteins of collagen, fibronectin and laminin may present cells with a myriad of recognition sites for binding integrins, heparin sulfate proteoglycans, growth factors and cytokines, these biologically active nanofibers can better support cell attachment and growth [24, 25]. Interaction of these modified cell-nanofibers interaction could in turn exert a considerable influence on the osteogenic differentiation of mesenchymal stem cells (MSCs).

### ***1.2.2 Biological Events Occuring on the Biosis–Abiosis Interface: The Role of Topographical Features***

Topography cues of electrospun nanofibers have been demonstrated to provide actual osteogenic niches in various aspects. Their fibrous structure could mimic the structure of ECM-derived scaffolds [50]. And, their dimension seems to simulate the structure of woven bone, which is the initial bone phenotype formed in the healing procedure after a fracture [49]. The apparent porosity of nanofibers was considered to favor efficient mass transportation of nutrients, oxygen, and waste products [48]. Recent studies have indicated a powerful role of the nanotopographic cues from nanofibers in regulating the osteogenic behavior of stem cells [51, 52].

#### **1.2.2.1 Temporal Changes in the Osteogenic Behaviors on Diversely Arranged Nanofibrous Scaffolds**

Phenotype observation showed that the cell shape, nuclear morphology and focal adhesion were modulated by nanofiber orientation; all these three aspects are considered to be closely correlated with the differentiation state of stem cells [62, 63]. The relatively isotropic random nanofibers may favor the growth of human bone mensenchymal stem cells with a highly branched morphology with spherical nuclei and large focal adhesion, while the aligned nanofibers result in a polarized morphology with elongated oval nuclei and small focal adhesion. Such a highly branched cell shape is thought to have an “osteocyte-like” morphology to

push hBMSCs toward an osteogenic lineage [62]. The small and immature focal adhesion (FA) of MSCs on aligned nanofibers was considered to represent a migratory cell status, while the large and super-mature FA of MSCs on random nanofibers indicated the cell status of sensing the mechanical properties to act on cell lineage [54, 64]. The more osteogenic-specific fate of MSCs on random nanofibers than those on aligned ones was corroborated by many studies. Hu et al. reported that MSCs cultured on random PLLA nanofibers exhibit an enhanced osteogenic differentiation phenotype involving higher bone sialoprotein (BSP) and osteocalcin expression and increased alkaline phosphatase (ALP) activity [53]. Yin et al. reported that randomly oriented nanofibers induce higher ALP activities and more calcium deposition, which is related to integrin- and myosin-mediated mechanotransduction [56]. Wang showed that ALP activity and the production of collagen type I and osteocalcin all increased in MG63 cells cultured on random PLLA nanofibers [55]. These observations demonstrated that the nanotopographic features of electrospun nanofibers might provide essential niches to guide MSCs osteogenic behavior.

To explore the biological mechanisms underlying the osteogenic behavior of MSCs in response to nanofibrous scaffolds, full-scale, high-throughput and high-efficient global microarray analyses were carried out [37]. The temporal gene expression profiles demonstrated that the dynamic cellular behaviors of MSCs on nanofibers occur in a time-dependent pattern. At day 4, genes representing in cell adhesion molecules, extracellular matrix receptors, and integrin-mediated signaling pathways were up-regulated. At day 7, expression of genes associated with cytoskeletal organization and mechanical stimulation was observed to notably increased. At day 14, osteogenic pathways, including TGF- $\beta$ /BMP, MAPK, and Wnt, were up-regulated. At day 21, genes associated with skeleton development, ossification and mineralization were up-regulated. Taken together, a lower extent but similar rhythm of dynamic cellular behavior was induced on random nanofibers when compared with the osteogenic supplement condition. Furthermore, this temporal dynamic rhythm suggested that mechanotransduction might be the underlying mechanism of nanofibrous topography driven osteogenic differentiation of MSCs.

### 1.2.2.2 Mechanisms of Electrospun Nanofibrous Scaffolds-Induced Cellular Responses

#### The Nanometer Effects of Nanofibrous Scaffolds on Cellular Responses

Nanofibers have distinct advantages over conventional scaffolds as its topographic structure mimics the *in vivo* extracellular milieus. For example, the fiber diameters of electrospun nanofibers are in the range about 100 nm. The mineralized type I collagen fibrils, constituting ~90 % of the bone structure, are nano-sized (50–500 nm in diameter) [65], and may thus be well mimicked by the synthetic nanofibers. In previous studies, it was demonstrated that the nanometer effects of

nanofibrous scaffolds could induce up-regulated focal adhesion kinase signaling and increased cellular elastic modulus for osteoblastic cells and enhanced fate direction into osteogenesis for hBMSCs.

### The Role of Focal Adhesion Formation and Cellular Cytoskeleton Arrangement

Knowledge of cells-ECM interactions might help to understand the various cellular responses to the diversely arranged electrospinning nanofibrous scaffolds (aligned or randomly distributed). It is well known that cells anchored to the extracellular matrix through focal adhesions, which allow the cells to “communicate” with the ECM [66]. Thus, the properties of the ECM, including its mechanical character, are transmitted via focal adhesions to the cytoskeletal network of a cell [67]. In general, the cytoskeleton is composed of three distinct components: actin microfilaments, microtubules, and intermediate filaments [68]. The organization of the cell cytoskeleton actively participate in the ability of cells to sense and convert mechanical cues into biological responses. It cells display highly elongated cell morphologies when growing on aligned nanofibers and spread cell morphologies when growing on randomly distributed nanofibers [37, 65]. These phenomena might be associated with the spatial distribution of the focal adhesion formation of the attached cells which arises from the “communication” between cells and diversely arranged nanofiber scaffolds. Cells on fiber networks, developed longer and more concentrated focal adhesion clusters compared with cells on flat control substrates [69]. In addition, the highly elongated cell morphology also means the greater cytoskeletal tension, and relevant signaling such as ROCK may be up-regulated in cells on aligned nanofibers [65].

### The Role of Mechanotransduction

Mechanotransduction describes the molecular mechanisms by which cells respond to changes in their physical environment. Cells can sense mechanical stimulation and changes in their physical environment through force-induced conformational changes at the molecular level; however, of the molecular mechanisms are still incompletely understood. Kris et al. [68] summarized that the underlying mechanisms as: extracellular forces might stimulate stretch sensitive ion channels and force-driven activation of transcription factors might stimulate the downstream cellular pathways. For instance, opening of these ion channels could result in changes in intracellular ion concentrations, which would have different downstream effects including activation of signaling pathways that leading to changes in gene transcription [70]. Moreover, transcription factors, such as nuclear factor NF-κB, translocate from the cytoplasm to the nucleus on mechanical stimulation, and protein cascades such as the mitogenactivated protein kinase (MAPK) cascade could be activated following molecular events.

### 1.3 Future Prospective

In this review, we discussed the biochemical and biophysical cues given by the nanofibrous scaffolds that could influence cellular behaviors on the biosis–abiosis interface. These cues include the chemical composition of the nanofibers, the surface biofunctionalization of the nanofiber scaffolds and the arrangement of the nanofibers in three-dimension. Future studies are needed to fully understand the molecular and biophysical basis of this direct form of nuclear mechanotransduction and to understand how these processes are integrated with chemical diffusion-based signaling mechanisms [68].

**Open Access** This chapter is distributed under the terms of the Creative Commons Attribution Noncommercial License, which permits any noncommercial use, distribution, and reproduction in any medium, provided the original author(s) and source are credited.

## References

1. Langer R, Vacanti JP. Tissue engineering. *Science*. 1993;260:920–6.
2. Li WJ, Laurencin CT, Caterson EJ, Tuan RS, Ko FK. Electrospun nanofibrous structure: a novel scaffold for tissue engineering. *J Biomed Mater Res*. 2002;60:613–21.
3. Stevens MM, George JH. Exploring and engineering the cell surface interface. *Science*. 2005;310:1135–8.
4. Bottino MC, Thomas V, Schmidt G, et al. Recent advances in the development of GTR/GBR membranes for periodontal regeneration—a materials perspective. *J Dental Mater*. 2012;28(7):703–21.
5. Agarwal S, Wendorff JH, Greiner A. Progress in the field of electrospinning for tissue engineering applications. *Adv Mater*. 2009;21:3343–51.
6. Zhang S, Huang Y, Yang X, Mei F, Ma Q, Chen G, et al. Gelatin nanofibrous membrane fabricated by electrospinning of aqueous gelatin solution for guided tissue regeneration. *J Biomed Mater Res A*. 2009;90:671–9.
7. Zhang S, Zhang X, Cai Q, Wang B, Deng X, Yang X. Microfibrous beta-TCP/collagen scaffolds mimic woven bone in structure and composition. *Biomed Mater*. 2010;5:065005.
8. Ma PX. Biomimetic materials for tissue engineering. *Adv Drug Deliv Rev*. 2008;60:184–98.
9. Zong X, Bien H, Chung CY, Yin L, Fang D, Hsiao BS, et al. Electrospun fine-textured scaffolds for heart tissue constructs. *Biomaterials*. 2005;26:5330–8.
10. Dawson JI, Wahl DA, Lanham SA, Kanczler JM, Czernuszka JT, Oreffo RO. Development of specific collagen scaffolds to support the osteogenic and chondrogenic differentiation of human bone marrow stromal cells. *Biomaterials*. 2008;29:3105–16.
11. Sisson K, Zhang C, Farach-Carson MC, Chase DB, Rabolt JF. Evaluation of cross-linking methods for electrospun gelatin on cell growth and viability. *Biomacromolecules*. 2009;10:1675–80.
12. Jiang H, Fang D, Hsiao BS, Chu B, Chen W. Optimization and characterization of dextran membranes prepared by electrospinning. *Biomacromolecules*. 2004;5:326–33.
13. Ciardelli G, Chiono V, Vozzi G, Pracella M, Ahluwalia A, Barbani N, et al. Blends of poly-(epsilon-caprolactone) and polysaccharides in tissue engineering applications. *Biomacromolecules*. 2005;6:1961–76.
14. Sarasam AR, Krishnaswamy RK, Madihally SV. Blending chitosan with polycaprolactone: effects on physicochemical and antibacterial properties. *Biomacromolecules*. 2006;7:1131–8.

15. Ghasemi-Mobarakeh L, Prabhakaran MP, Morshed M, Nasr-Esfahani MH, Ramakrishna S. Electrospun poly(epsilon-caprolactone)/gelatin nanofibrous scaffolds for nerve tissue engineering. *Biomaterials*. 2008;29:4532–9.
16. Sui G, Yang X, Mei F, Hu X, Chen G, Deng X, et al. Poly-L-lactic acid/hydroxyapatite hybrid membrane for bone tissue regeneration. *J Biomed Mater Res A*. 2007;82:445–54.
17. Deng XL, Sui G, Zhao ML, Chen GQ, Yang XP. Poly(L-lactic acid)/hydroxyapatite hybrid nanofibrous scaffolds prepared by electrospinning. *J Biomater Sci Polym Ed*. 2007;18:117–30.
18. Mei F, Zhong J, Yang X, Ouyang X, Zhang S, Hu X, et al. Improved biological characteristics of poly(L-lactic acid) electrospun membrane by incorporation of multiwalled carbon nanotubes/hydroxyapatite nanoparticles. *Biomacromolecules*. 2007;8:3729–35.
19. Zhang X, Cai Q, Liu H, Zhang S, Wei Y, Yang X, et al. Calcium ion release and osteoblastic behavior of gelatin/beta-tricalcium phosphate composite nanofibers fabricated by electrospinning. *Mater Lett*. 2012;73:172–5.
20. Sun Z, Zussman E, Yarin AL, et al. Compound core-shell polymer nanofibers by co-electrospinning. *J Adv Mater*. 2003;15(22):1929–32.
21. Zhang YZ, Venugopal J, Huang ZM, Lim CT, Ramakrishna S. Characterization of the surface biocompatibility of the electrospun PCL-collagen nanofibers using fibroblasts. *Biomacromolecules*. 2005;6:2583–9.
22. Zhao P, Jiang H, Pan H, Zhu K, Chen W. Biodegradable fibrous scaffolds composed of gelatin coated poly(epsilon-caprolactone) prepared by coaxial electrospinning. *J Biomed Mater Res A*. 2007;83:372–82.
23. Sun W, Cai Q, Li P, Deng X, Wei Y, Xu M, et al. Post-draw PAN-PMMA nanofiber reinforced and toughened Bis-GMA dental restorative composite. *Dental Mater*. 2010;26:873–80.
24. Loscertales IG, Barrero A, Guerrero I, Cortijo R, Marquez M, Ganan-Calvo AM. Micro/nano encapsulation via electrified coaxial liquid jets. *Science*. 2002;295:1695–8.
25. Xie J, Ng WJ, Lee LY, Wang CH. Encapsulation of protein drugs in biodegradable microparticles by co-axial electrospray. *J Colloid Interface Sci*. 2008;317:469–76.
26. Wu Y, Yu B, Jackson A, Zha W, Lee LJ, Wyslouzil BE. Coaxial electrohydrodynamic spraying: a novel one-step technique to prepare oligodeoxynucleotide encapsulated lipoplex nanoparticles. *Mol Pharm*. 2009;6:1371–9.
27. Xu Y, Hanna MA. Electrospray encapsulation of water-soluble protein with polylactide. Effects of formulations on morphology, encapsulation efficiency and release profile of particles. *Int J Pharm*. 2006;320:30–6.
28. Xie J, Wang CH. Encapsulation of proteins in biodegradable polymeric microparticles using electrospray in the Taylor cone-jet mode. *Biotechnol Bioeng*. 2007;97:1278–90.
29. Powell HM, Supp DM, Boyce ST. Influence of electrospun collagen on wound contraction of engineered skin substitutes. *Biomaterials*. 2008;29:834–43.
30. Ma J, He X, Jabbari E. Osteogenic differentiation of marrow stromal cells on random and aligned electrospun poly(L-lactide) nanofibers. *Ann Biomed Eng*. 2011;39:14–25.
31. Wang H, Kwok DT, Xu M, Shi H, Wu Z, Zhang W, et al. Tailoring of mesenchymal stem cells behavior on plasma-modified polytetrafluoroethylene. *Adv Mater*. 2012;24:3315–24.
32. Barradas AM, Lachmann K, Hlawacek G, Frieling C, Truckenmoller R, Boerman OC, et al. Surface modifications by gas plasma control osteogenic differentiation of MC3T3-E1 cells. *Acta Biomater*. 2012;8:2969–77.
33. Wan Y, Tu C, Yang J, Bei J, Wang S. Influences of ammonia plasma treatment on modifying depth and degradation of poly(L-lactide) scaffolds. *Biomaterials*. 2006;27:2699–704.
34. D'Sa RA, Burke GA, Meenan BJ. Protein adhesion and cell response on atmospheric pressure dielectric barrier discharge-modified polymer surfaces. *Acta Biomater*. 2010;6:2609–20.
35. Shah A, Shah S, Mani G, Wenke J, Agrawal M. Endothelial cell behaviour on gas-plasma-treated PLA surfaces: the roles of surface chemistry and roughness. *J Tissue Eng Regen Med*. 2011;5:301–12.

36. Briem D, Strametz S, Schroder K, Meenen NM, Lehmann W, Linhart W, et al. Response of primary fibroblasts and osteoblasts to plasma treated polyetheretherketone (PEEK) surfaces. *J Mater Sci Mater Med.* 2005;16:671–7.
37. Liu W, Wei Y, Zhang X, Xu M, Yang X, Deng X. Lower extent but similar rhythm of osteogenic behavior in hBMSCs cultured on nanofibrous scaffolds versus induced with osteogenic supplement. *ACS Nano.* 2013;7:6928–38.
38. Ngiam M, Liao S, Patil AJ, Cheng Z, Chan CK, Ramakrishna S. The fabrication of nano-hydroxyapatite on PLGA and PLGA/collagen nanofibrous composite scaffolds and their effects in osteoblastic behavior for bone tissue engineering. *Bone.* 2009;45:4:16.
39. Cai Q, Xu QQ, Feng QF, Cao XY, Yang XP, Deng XL. Biominerization of electrospun poly (L-lactic acid)/gelatin composite fibrous scaffold by using a supersaturated simulated body fluid with continuous CO<sub>2</sub> bubbling. *Appl Surf Sci.* 2011;257:10109–18.
40. Wilhelm C, Billotey C, Roger J, Pons JN, Bacri JC, Gazeau F. Intracellular uptake of anionic superparamagnetic nanoparticles as a function of their surface coating. *Biomaterials.* 2003;24:1001–11.
41. Akiyama H, Ito A, Kawabe Y, Kamihira M. Genetically engineered angiogenic cell sheets using magnetic force-based gene delivery and tissue fabrication techniques. *Biomaterials.* 2010;31:1251–9.
42. Wang H, Tang HZ, He JH, Wang QW. Fabrication of aligned ferrite nanofibers by magnetic-field-assisted electrospinning coupled with oxygen plasma treatment. *Mater Res Bull.* 2009;44:1676–80.
43. Wei Y, Zhang X, Song Y, Han B, Hu X, Wang X, et al. Magnetic biodegradable Fe<sub>3</sub>O<sub>4</sub>/CS/PVA nanofibrous membranes for bone regeneration. *Biomed Mater.* 2011;6:055008.
44. Yang X, Chen X, Wang H. Acceleration of osteogenic differentiation of preosteoblastic cells by chitosan containing nanofibrous scaffolds. *Biomacromolecules.* 2009;10:2772–8.
45. Zhang Z, Liu H, Lin Y, Wei Y, Nan C-W. Influence of La doping magnetic and optical properties of bismuth ferrite nanofibers. *J Nanomater.* 2012; doi:[10.1155/2012/238605](https://doi.org/10.1155/2012/238605).
46. Hussain A, Bessho K, Takahashi K, Yabata T. Magnesium calcium phosphate as a novel component enhances mechanical/physical properties of gelatin scaffold and osteogenic differentiation of bone marrow mesenchymal stem cells. *Tissue Eng Part A.* 2012;18:768–74.
47. Sun H, Wu C, Dai K, Chang J, Tang T. Proliferation and osteoblastic differentiation of human bone marrow-derived stromal cells on akermanite-bioactive ceramics. *Biomaterials.* 2006;27:5651–7.
48. Honda M, Kikushima K, Kawanobe Y, Konishi T, Mizumoto M, Aizawa M. Enhanced early osteogenic differentiation by silicon-substituted hydroxyapatite ceramics fabricated via ultrasonic spray pyrolysis route. *J Mater Sci Mater Med.* 2012;23:2923–32.
49. Nair MB, Bernhardt A, Lode A, Heinemann C, Thieme S, Hanke T, et al. A bioactive triphasic ceramic-coated hydroxyapatite promotes proliferation and osteogenic differentiation of human bone marrow stromal cells. *J Biomed Mater Res A.* 2009;90:533–42.
50. Amaral M, Costa MA, Lopes MA, Silva RF, Santos JD, Fernandes MH. Si(3)N(4)-bioglass composites stimulate the proliferation of MG63 osteoblast-like cells and support the osteogenic differentiation of human bone marrow cells. *Biomaterials.* 2002;23:4897–906.
51. Oh SA, Kim SH, Won JE, Kim JJ, Shin US, Kim HW. Effects on growth and osteogenic differentiation of mesenchymal stem cells by the zinc-added sol-gel bioactive glass granules. *J Tissue Eng.* 2011;2010:475260.
52. Luo X, Barbieri D, Davison N, Yan Y, de Bruijn JD, Yuan H. Zinc in calcium phosphate mediates bone induction: *in vitro* and *in vivo* model. *Acta Biomater.* 2014;10:477–85.
53. Aigner A. Nonviral *in vivo* delivery of therapeutic small interfering RNAs. *Curr Opin Mol Ther.* 2007;9:345–52.
54. Li C, Vepari C, Jin HJ, Kim HJ, Kaplan DL. Electrospun silk-BMP-2 scaffolds for bone tissue engineering. *Biomaterials.* 2006;27:3115–24.
55. Nie H, Wang CH. Fabrication and characterization of PLGA/HAp composite scaffolds for delivery of BMP-2 plasmid DNA. *J Control Release.* 2007;120:111–21.

56. Moreira JN, Santos A, Moura V, Pedroso de Lima MC, Simoes S. Non-viral lipidbased nanoparticles for targeted cancer systemic gene silencing. *J Nanosci Nanotechnol*. 2008;8:2187–204.
57. Liu W, Cai Q, Zhang F, Wei Y, Zhang X, Wang Y, et al. Dose-dependent enhancement of bone marrow stromal cells adhesion, spreading and osteogenic differentiation on atmospheric plasma-treated poly(L-lactic acid) nanofibers. *J Bioact Compat Polym*. 2013;28:453–67.
58. Chua KN, Chai C, Lee PC, Tang YN, Ramakrishna S, Leong KW, et al. Surface-aminated electrospun nanofibers enhance adhesion and expansion of human umbilical cord blood hematopoietic stem/progenitor cells. *Biomaterials*. 2006;27:6043–51.
59. Keselowsky BG, Collard DM, Garcia AJ. Surface chemistry modulates focal adhesion composition and signaling through changes in integrin binding. *Biomaterials*. 2004;25:5947–54.
60. Klinkhammer K, Bockelmann J, Simitzis C, Brook GA, Grafahrend D, Groll J, et al. Functionalization of electrospun fibers of poly(epsilon-caprolactone) with star shaped NCO-poly(ethylene glycol)-stat-poly(propylene glycol) for neuronal cell guidance. *J Mater Sci Mater Med*. 2010;21:2637–51.
61. Kim TG, Park TG. Surface functionalized electrospun biodegradable nanofibers for immobilization of bioactive molecules. *Biotechnol Prog*. 2006;22:1108–13.
62. Andersson AS, Backhed F, von Euler A, Richter-Dahlfors A, Sutherland D, Kasemo B. Nanoscale features influence epithelial cell morphology and cytokine production. *Biomaterials*. 2003;24:3427–36.
63. Kumar G, Tison CK, Chatterjee K, Pine PS, McDaniel JH, Salit ML, et al. The determination of stem cell fate by 3D scaffold structures through the control of cell shape. *Biomaterials*. 2011;32:9188–96.
64. Wang Y, Gao R, Wang PP, Jian J, Jiang XL, Yan C, et al. The differential effects of aligned electrospun PHBHHx fibers on adipogenic and osteogenic potential of MSCs through the regulation of PPAR gamma signaling. *Biomaterials*. 2012;33:485–93.
65. Andalib MN, Lee JS, Ha L, Dzenis Y, Lim JY. The role of RhoA kinase (ROCK) in cell alignment on nanofibers. *Acta Biomater*. 2013;9:7737–45.
66. Sheetz MP. Cell control by membrane-cytoskeleton adhesion. *Nat Rev Mol Cell Biol*. 2001;2:392–6.
67. Schellenberg A, Joussen S, Moser K, Hampe N, Hersch N, Hemeda H, et al. Matrix elasticity, replicative senescence and DNA methylation patterns of mesenchymal stem cells. *Biomaterials*. 2014;35:6351–8.
68. Dahl KN, Ribeiro AJ, Lammerding J. Nuclear shape, mechanics, and mechanotransduction. *Circ Res*. 2008;102:1307–18.
69. Sheets K, Wunsch S, Ng C, Nain AS. Shape-dependent cell migration and focal adhesion organization on suspended and aligned nanofiber scaffolds. *Acta Biomater*. 2013;9:7169–77.
70. Shah N, Morsi Y, Manasseh R. From mechanical stimulation to biological pathways in the regulation of stem cell fate. *Cell Biochem Funct*. 2014;32:309–25.

# **Chapter 2**

## **Updates in Treatment Modalities and Techniques on Compromised Alveolar Ridge Augmentation for Successful Dental Implant Therapy**

**Myung-Jin Kim**

**Abstract** Installation of dental implants is often hindered by compromised alveolar ridge which requires augmentation. Several methods including autogenous bone graft, guided bone regeneration, and distraction osteogenesis are implied to restore the compromised alveolar ridge. This chapter reviews treatment modalities and techniques of alveolar ridge augmentation. Recent development and updates in this field are also presented.

**Keywords** Alveolar ridge augmentation • Autogenous block bone grafting • Bone graft material • Distraction osteogenesis

### **2.1 Treatment Modalities for Augmentation of the Compromised Alveolar Ridge**

Edentulism often exists with concomitant alveolar ridge resorption. Consequently implant installation is very often complicated with severely atrophic alveolar ridge. Various efforts have been tried to overcome the problem of insufficient alveolar bone for ideal implant installation. Alveolar bone augmentation which restores the atrophic alveolar bone to its near intact state will exhibit ideal properties in both functional and esthetic means for implant installation.

Alveolar bone resorption occurs in either a horizontal or vertical direction. A composite defect is also common. Treatment options for the horizontal alveolar bone defect include guided bone regeneration (GBR), veneer bone graft, ridge splitting technique, and distraction osteogenesis. For the vertical defect, the options are GBR, onlay bone graft, interpositional bone graft, and distraction osteogenesis.

---

M.-J. Kim (✉)

Department of Oral and Maxillofacial Surgery, Seoul National University Dental Hospital,  
101, Daehak-ro, Jongno-gu, Seoul 110-768, Republic of Korea  
e-mail: [myungkim@snu.ac.kr](mailto:myungkim@snu.ac.kr)

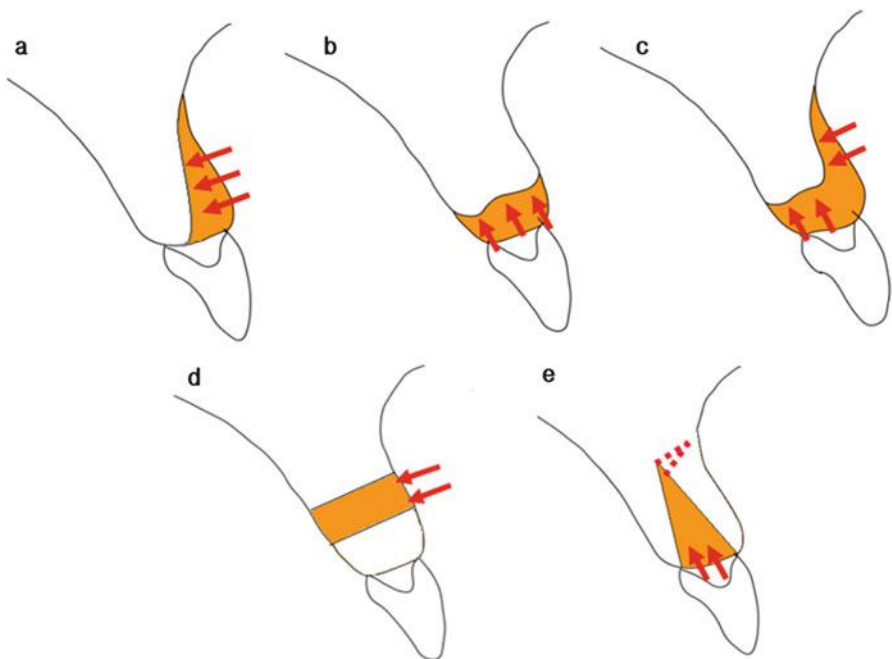


**Fig. 2.1** Schematic diagrams of alveolar ridge augmentation. (a) Veneer bone graft, (b) onlay bone graft, (c) saddle bone graft, (d) interpositional bone graft, (e) ridge splitting technique

The composite defects can be restored by GBR, saddle bone graft, or distraction osteogenesis (Fig. 2.1).

Bone restoration capability differs according to the method applied. Guided bone regeneration is restricted in terms of small feasible bone regain amount. When applied with resorbable membranes, the expected bone regeneration does not exceed 3–4 mm vertically and 4 mm horizontally. Titanium mesh may enhance the capability to 4–7 mm vertically and 5 mm horizontally. Onlay block bone graft has similar capability with the latter of GBR technique. Interpositional bone graft is capable of regaining 5–7 mm of vertical height. Distraction osteogenesis is the most capable modality in terms of feasible bone regain amount which may exceed 10 mm in vertical height and 6 mm in alveolar width.

## 2.2 Autogenous Block Bone Grafting

Autogenous bone graft had been the gold standard of bone grafting. It is the only graft material that is considered to have osteoconductive, osteoinductive, and osteogenetic properties all together. Furthermore when block bone is adapted properly, it may contribute to initial stability of the implant fixture installed

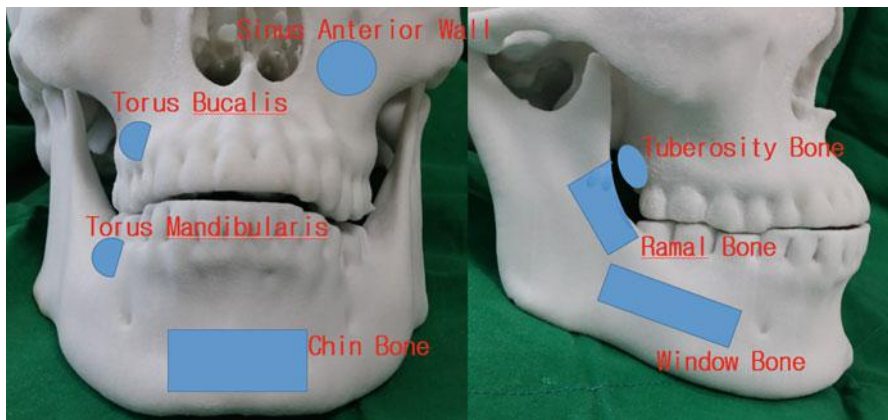


**Fig. 2.2** Schematic diagram of the intraoral donor sites of autogenous bone

simultaneously. This characteristic can increase the feasibility of simultaneous bone grafting and implant installation.

### **2.2.1 Autogenous Bone Donor Sites**

Autogenous bone is harvested from either an intraoral site or extraoral. Intraoral donor sites include the chin bone, the ramal bone, the mandibular body window bone, the mandibular torus bone, the maxillary torus bone, the sinus anterior wall and the maxillary tuberosity bone. The chin bone is the most abundant source among the listed (Figs. 2.2 and 2.3).

Extraoral donor sites include the anterior iliac crest bone, the proximal tibia bone, and the calvarial bone. These sites may suffice any amount of requisite for an alveolar augmentation.

### **2.2.2 Block Bone Grafting Techniques**

The most intuitive form of autogenous block bone grafting is the onlay or veneer grafting techniques (Fig. 2.4). These techniques directly replace the resorbed alveolar bone in a vertical or horizontal direction, respectively. Both vertical and horizontal augmentations are possible by the saddle bone graft technique. Khoury demonstrated the method and results of sinus floor augmentation with mandibular block bones where dental implants were installed simultaneously [1]. Cases with severely atrophic alveolar ridge may require additional bone grafting. In the atrophic maxilla, subnasal or subantral block bone graftings are applied in addition of the onlay bone graft for this purpose.

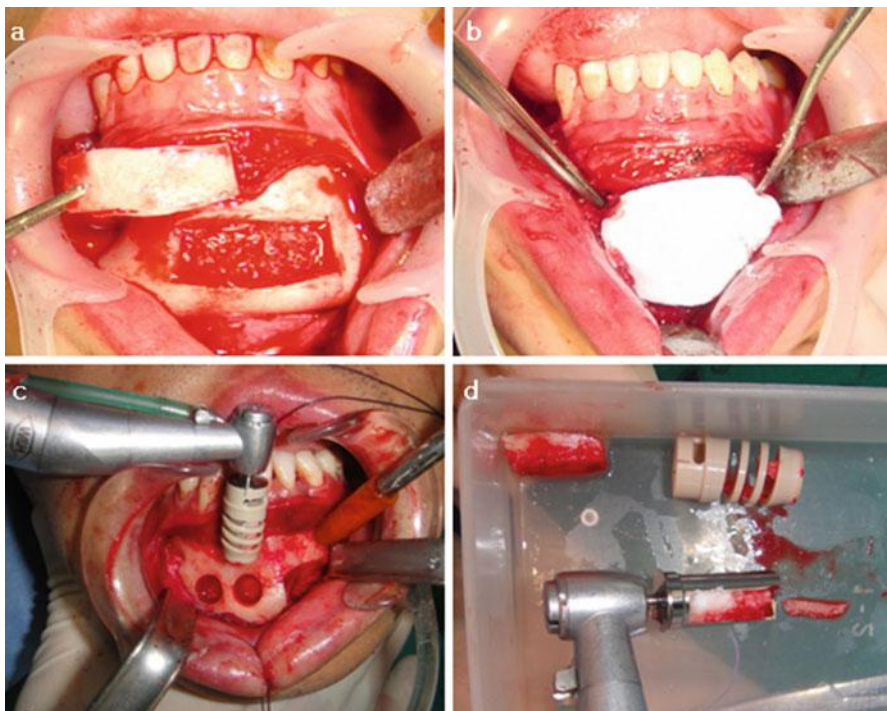


**Fig. 2.3** Chin bone harvesting. (a) Window type block bone harvesting, (b) Barrier membrane placed for bone healing of the donor site, (c and d) Mashed particulated bone block harvesting with bone mill bur (Neobiotech®)

Vertical interpositional bone graft is an alternative to the conventional methods described above, when the bone demand is large. This method has the advantage of preserving the alveolar crest with intact nourished bone. Soft tissue management and flap design is very important and should be done carefully with interpositional bone graft procedures for preserving the vascularity.

### 2.2.3 *The Fate of Autogenous Onlay Bone Graft*

Resorption of grafted autogenous bone is always a matter of concern. Cordaro et al. reported that when block bones harvested from the mandibular ramus or symphysis are grafted in an onlay style, mean resorption rates during a graft healing period of 6 months were 23.5 % for lateral grafts and 42 % for verticals [2]. Proussaefs et al. suggested that vertical augmentation of the alveolar ridge with autogenous block bone from the mandibular ramus is a viable treatment option. They reported a vertical resorption rate of 16.34 % from an initial 6.12 mm of augmentation after 4–6 months of healing period [3]. Widmark

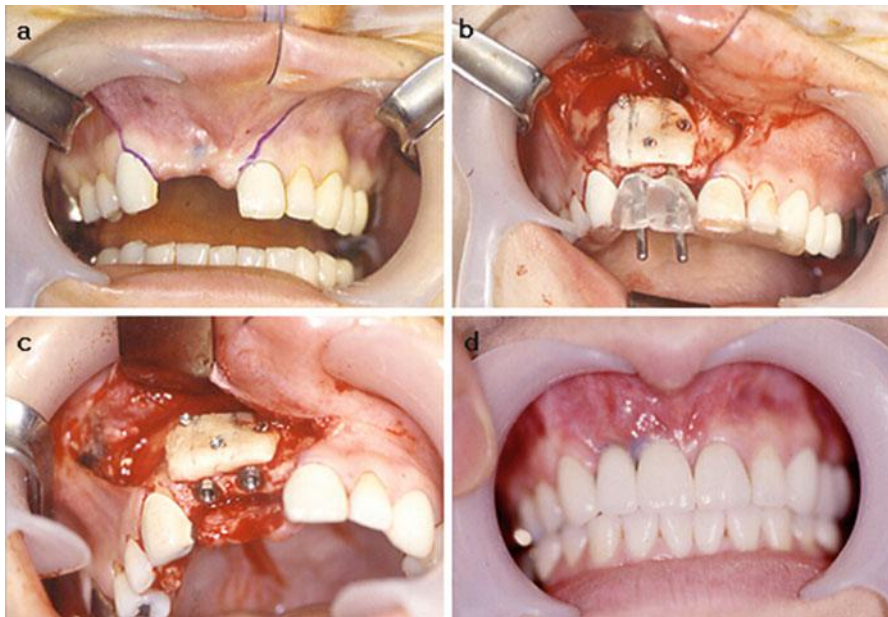


**Fig. 2.4** Case presentation of a veneer bone graft. (a) Edentulous state on the anterior maxilla with atrophic and narrow alveolar ridge and the flap design, (b) Veneer bone graft positioned and fixed with titanium screws, (c) Implant installation, (d) Final prosthetic outcome

et al. demonstrated that the horizontal resorption was 25 % after 4 months and 60 % at the time of abutment connection when symphyseal block bone was grafted to the anterior maxilla for single tooth implant installation [4].

In a clinical survey conducted in our department, 76 patients underwent simultaneous autogenous onlay bone graft and installation of total 256 dental implants from 2000 to 2006. The amount of bone augmentation was 5.42 mm in average. After a minimum follow up period of 2 years, average bone resorption at the mesial and distal site of implant collar was 1.48 mm. About 27.3 % of the augmented bone height was resorbed.

#### **2.2.4 Drawbacks of Autogenous Bone Grafting**

Although the autogenous bone is considered as the gold standard of bone grafting for its osteogenic potential, drawbacks exist which limits its application. Donor site morbidity is of the most concern. Bone harvesting procedures may put adjacent anatomical structures at a risk of damage. For instance during chin bone harvesting, the mental nerve may be pulled under undue traction and the incisive nerve may become interrupted when the harvesting depth is inordinate. Ramal bone harvesting can damage the inferior alveolar nerve.

In addition some patients may be reluctant to the harvesting procedures, especially when extraoral donor sites are concerned. General anesthesia is mandatory for these procedures. Gate problem could occur when autogenous bone is harvested from the tibia or the iliac crest.

## 2.3 Biomaterials for Guided Bone Regeneration

Guided bone regeneration utilizes the principle concept of guided tissue regeneration which is to separate a space from ingrowth of unintended tissues. Addition of bone graft materials in the space can secure the space from collapsing and promote the speed of bone regeneration. Bioengineering techniques may either enhance osteoinductive properties or mimic osteogenesis in non-autogenous graft materials (Fig. 2.5).

### 2.3.1 Bone Graft Materials

Bone graft materials can be classified according to their source of origin. Each class possesses different capability for regeneration of bone. The most ideal graft material in terms of regeneration potency is the autogenous bone graft which has osteogenetic properties. However application of autogenous bone graft may be restricted. Furthermore, in particular instances of graft material under constant

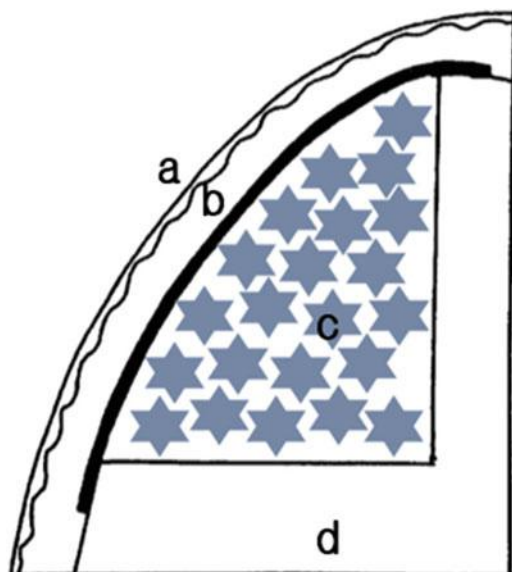


**Fig. 2.5** A schematic diagram of the guided bone regeneration technique, (a) Mucoperiosteal flap, (b) GBR membrane, (c) Bone graft material, (d) Host bone bed

pressure, the autogenous bone graft may fail to secure the graft space. The rapid turnover rate may be problematic. In summary, non-autogenous bone grafts are not simply alternatives to autogenous but may be the best option we have for specific cases.

In Korea, various non-autogenous graft materials are commercially available for clinical use. These allogenic, xenogenic and alloplastic bone graft materials are recommended for small minor bone defects in combination with the guided bone regeneration technique.

### **2.3.1.1 Allogenic Bone Graft**

Allogenic bone graft material originates from human individuals other than the recipient individual, genetically. Bone banks typically accumulate allogenic bone grafts from two donor sources, namely cadaveric and living donors who are undergoing bone removal procedures. Three forms of allogenic bone graft are available. Fresh or fresh-frozen allograft, freeze dried bone allograft and demineralized freeze dried bone allograft. When applying allografts for bone augmentation, the risk of disease transmission is of concern. Fortunately, according to the Centers for Disease Control and Prevention, there have been no reports of disease transmission when freeze-dried types of allograft are used for periodontal procedures.

Advantage of the allogenic grafts over the other bone graft materials is that these grafts can carry osteoinductive properties. Xenogenic and alloplastic bone graft materials are only osteoconductive at the best, unless they are enhanced by bioengineering techniques.

Allogenic bone graft materials available and currently in clinical use in Korea are as in the following. Demineralized freeze-dried form of allografts are Grafton®, Orthoblast II®, Tutoplast®, Regenafil®, and SureFuse®. Freeze-dried bones include Puros®, OraGraft® and ICB®.

### **2.3.1.2 Xenogenic Bone Graft**

Xenogenic bone grafts are harvested and processed from other species than human. Bovine bone is the most representative. This class of bone graft materials is accepted to have only osteoconductive properties. Commercially available products include Bio-Oss®, BioCera®, Biogen®, Osteoplant®, OSC-B®, and NuOss®.

Both allogenic and xenogenic bone graft materials can be applied for subantral augmentation. Regardless of the residual alveolar bone height, if it provides sufficient initial stability for the implant fixture, bone graft and implant installation can be performed simultaneously. If initial stability is not obtained, implant installation should be delayed for a recommended period of 9 to 12 months after subantral bone graft.

### 2.3.1.3 Alloplastic Bone Graft

Alloplastic bone graft materials are usually synthetic in its origin and are known to have only osteoconductive properties. Products consisting of sole or combinations of hydroxyapatite, calcium carbonate and beta tricalcium phosphate are available. Examples from Korean markets are Calcitite HA®, Osteon, Osteograft®, Frios®, Algipore®, OsteoGen®, HA Resorb® for sole hydroxyapatite, CeraSorb®, InduCera®, Biobase® for sole  $\beta$ -TCP, MBCP® for combination of hydroxyapatite and  $\beta$ -TCP, and Biocoral®, Interpore®, SIC nature bone® for sole calcium carbonate.

Alloplastic bone graft materials are often produced in combination with osteoinductive substances in Korea and sold in the market. Hydroxyapatite mixed with rhBMP-2 such as Novosis®,  $\beta$ -TCP mixed with rhBMP-2 such as Cowell BMP®, and products containing biphasic calcium phosphate lyophilized with rhBMP-2 materials are also available.  $\beta$ -TCP mixed with rhBMP-2 and bio-degradable Hydrogel is produced as an injectable putty with a trade name Exelos Inject®.

### 2.3.2 Bioengineering Techniques

Ideal bone graft materials should exhibit not only osteoconductive properties but as well osteoinductive. They should also provide a favorable environment for the invading blood vessels and bone forming cells. Recently various basic and clinical researches on the effect of recombinant human bone morphogenetic protein 2 (rhBMP-2) and potential use of human multipotent mesenchymal stromal/stem cells (MSC) are being reported and investigated.

#### 2.3.2.1 rhBMP-2

Bone morphogenetic protein was first introduced by Urist in 1965 as a consisting substance of a decalcified bone [5]. Several different types of the protein are classified now with approval of products containing bone morphogenetic protein 2 and 7 for orthopedic application by the FDA.

Current focus of investigation concerning rhBMP-2 is concentrated on the carrier of the growth factor. Carriers of rhBMP-2 are required to have properties that will make possible to control the release of rhBMP-2 to the bone defect. Uncontrolled release of rhBMP-2 not only diminishes its effectiveness but also may induce concentration related side effects. Currently in our institute, both combination of collagen hydrogel, nano-hydroxyapatite and rhBMP-2 coated on dental implant surface and poloxamer based hydrogel with rhBMP-2 are under investigation.

### 2.3.2.2 Autologous Bone Marrow Mesenchymal Stem Cells

Bone graft materials can be enhanced by addition of stem cells which may improve the rate and quality of defect repair. MSC can be isolated from the bone marrow or the periosteum and may be cultured for expansion. They can differentiate into several types of cell lines including fibroblast, chondroblast, endothelial cell, and of our most concern osteoblast which may accelerate bone regeneration. Derivation of mesenchymal stem cells from the bone marrow is the best characterized approach for osteogenic differentiation. The iliac spine is an easily manipulated, abundant store of autologous bone marrow MSC. Their use in combination with bone graft materials as a scaffold has produced promising clinical results (Fig. 2.6).

## 2.4 Alveolar Ridge Augmentation by Distraction Osteogenesis

In general, the available amount of soft tissue for wound closure restricts the capacity of bone grafting. Soft tissue coverage is crucial. Otherwise infection over the graft material may occur. Graft materials could be lost. At the best, the attained bone augmentation will be far behind than required.

Alveolar distraction osteogenesis (DO) is the most recent approach for alveolar ridge augmentation with promising results. Unlike any other approaches for alveolar ridge augmentation, DO is capable of lengthening both the hard and soft tissue. This method has the advantage of preserving the transport part of alveolar crest with intact vascularized nourished bone. This property permits the amount of alveolar augmentation attained by DO to surpass what the conventional methods of bone grafting would possibly do.

### 2.4.1 Distraction Techniques

Alveolar DO is capable to regenerate bone in both vertical and horizontal direction. Vertical distraction is achieved by placing the osteotomy line in a horizontal direction. By placing the osteotomy line at a more basal position of the alveolar ridge, a greater amount of width of regenerated bone is achievable. Horizontal distraction of the alveolar ridge utilizes the ridge splitting technique for the osteotomy. Takahashi et al. developed a novel method of applying a titanium mesh plate on the split transport segment and a rod for widening the gap which was known ‘Alveo Wider’ [6] (Fig. 2.7).

The span of the edentulous alveolar ridge should be at least two teeth wide in purpose to apply this technique. Otherwise the transport segment is under a risk of resorption during distraction. When the span of the alveolar ridge that requires

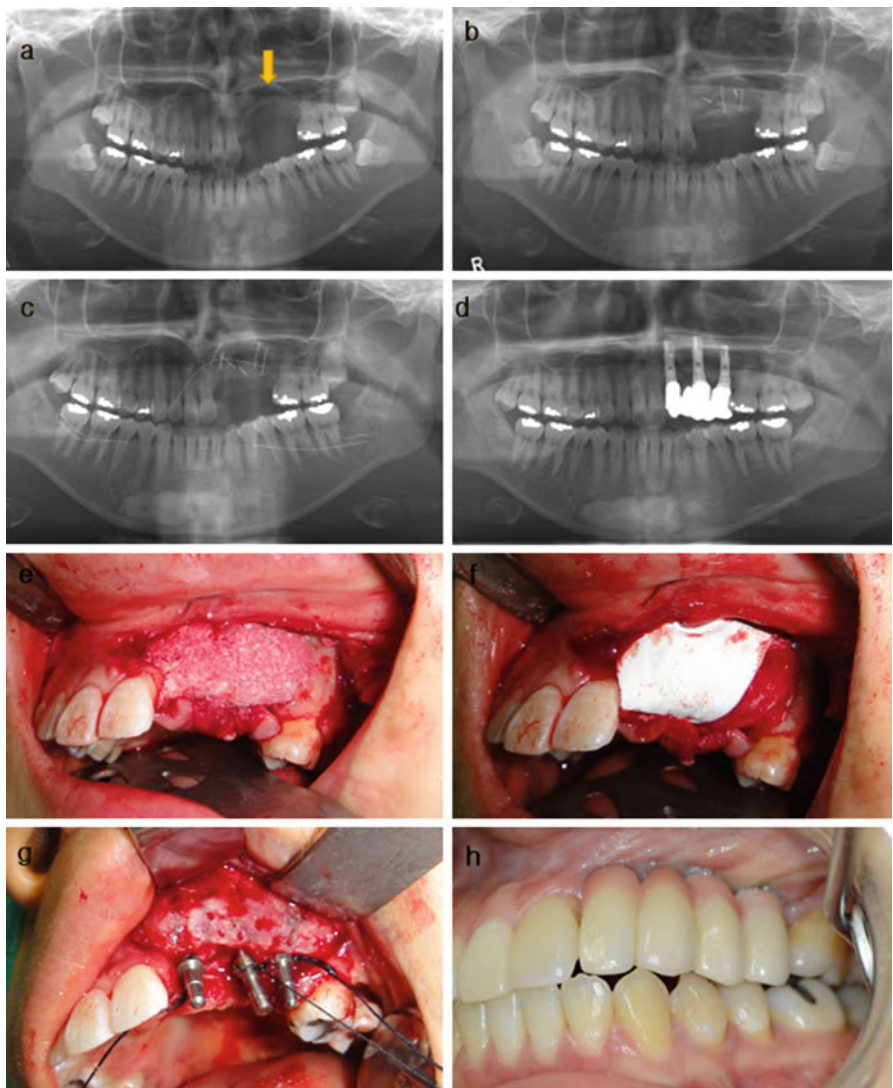


**Fig. 2.6** A case presentation of an alveolar basal bone reconstruction. (a) Severe alveolar bone defect following resection of adenomatous odontogenic tumor on the left anterior and pre-maxilla depicted by an arrow, (b) First stage operation was done for reconstruction of basal part of the alveolar bone defect by onlay bone graft, veneer bone graft, and xenogenic bone graft mixed with chin bone, (c) X-ray finding shows Xenogenic bone graft mixed with autologous MSC at second stage operation, (d) Implant installation 6 months after 2nd stage bone grafting procedure, (e) Second stage operation was done for the reconstruction of alveolar part of the bone defect by a combination of ramal bone graft and guided bone regeneration with xenogenic bone graft mixed with autologous bone marrow MSC, (f) Barrier membrane placed over the graft, (g) Augmented alveolar bone at the stage of implant installation, (h) Final outcome

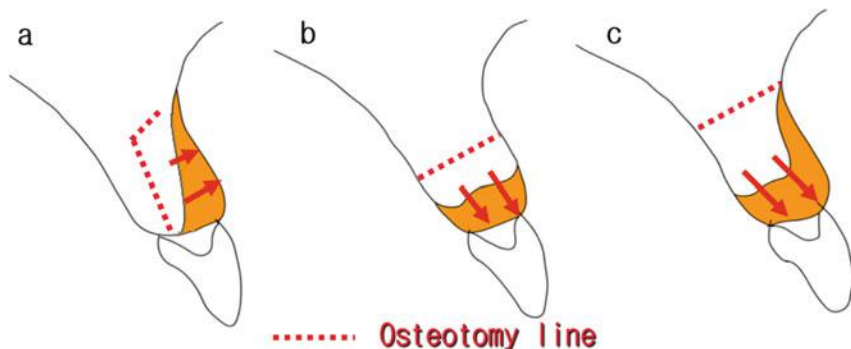


**Fig. 2.7** Schematic diagrams of alveolar DO. (a) Horizontal DO, (b) Vertical DO, (c) Vertical DO for vertical and horizontal bone augmentation

distraction becomes larger, it can be segmented according to the vector of distraction required.

The alveolar distraction timeline requires that the latency period be 3–5 days postoperatively. The distraction velocity should be adjusted according to the span of the transport segment. Short segments should be distracted slowly. This is intended to minimize the resorption of the transport segment. Two times of 0.3 mm distraction per day will satisfy this intention. With larger transport segments, three times of 0.3 mm distraction or two times of 0.5 mm distraction per day is allowed. After the distraction period, 3 months of consolidation period is required before implant installation (Figs. 2.8, and 2.9).

#### 2.4.2 Possible Amount of Bone Gain: Clinical Outcome

In a clinical study reported by Paeng et al. in 2006, 25 patients who have undergone alveolar ridge augmentation by DO and subsequent installation of total 84 dental implants were investigated. Average amount of augmentation was  $9.8 \pm 3.4$  mm. All of the implants installed survived for an average follow up period of 13.5 months. They suggested that DO may be acknowledged as a viable treatment option for alveolar augmentation so far [7]. In another case series of four patients who underwent alveolar distraction of the anterior atrophic mandible for dental implants, Yeom et al. reported that an average of  $11.38 \pm 1.38$  mm vertical gain was obtained by distraction [8]. DO can also be applied for augmentation of a reconstructed mandible with vascularized fibular free flap. Paeng et al. stressed that despite a tendency of surgical site infection during distraction of the fibular bone, undisturbed bone regeneration occurs for successful dental implant installation [9].

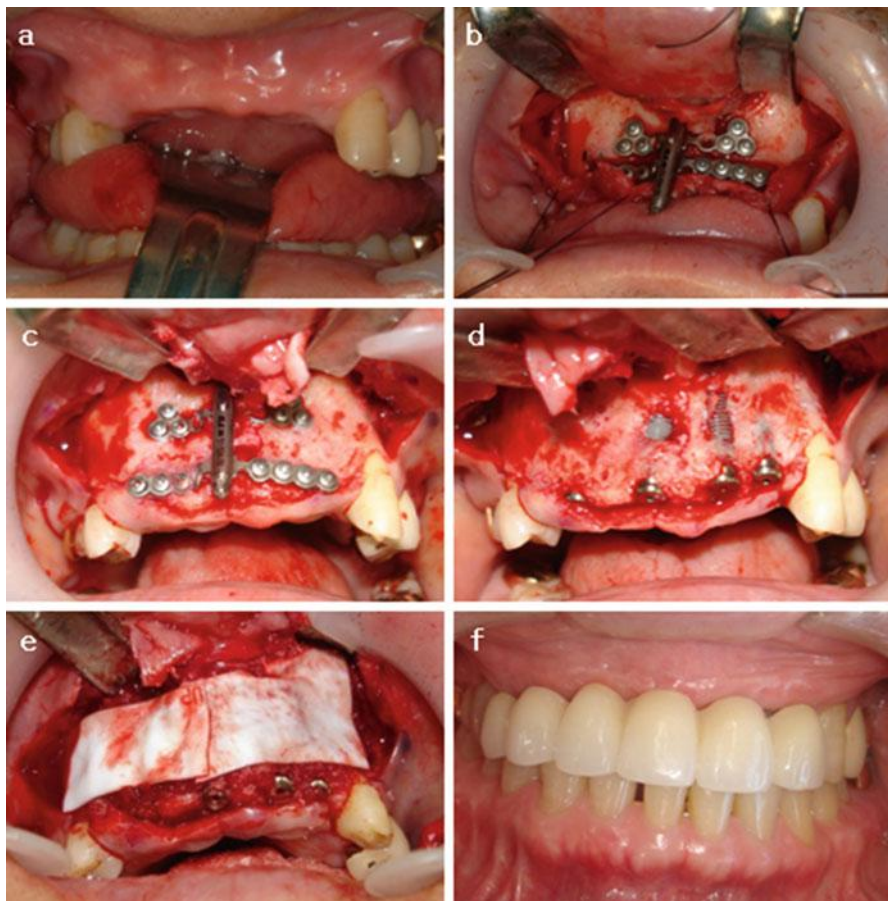


**Fig. 2.8** Case presentation of an alveolar DO of the anterior maxilla. (a) Preoperative atrophic edentulous state of the anterior maxilla, (b) Installation of the distraction device, (c) Regenerated bone by distraction osteogenesis after 4 months postoperatively, (d) After implant installation, (e) Guided bone regeneration technique applied for the repair of bony fenestrations, (f) Final outcome

#### 2.4.3 Consolidation Enhancement Factors

Current studies on DO of the alveolar bone are focused on the consolidation enhancement factors. The purpose of these studies is to develop a novel method to shorten the consolidation time and at the same time to enhance the mechanical property of the newly distracted bone. Both biological and mechanical stimulations are under research.

Kim et al. reported that significant amount of new bone volume was observed when human mesenchymal stromal cells were injected to the distraction site one day before distraction initiation in a rabbit mandibular distraction model. Human mesenchymal stromal cells also increased bone mineral density [10].

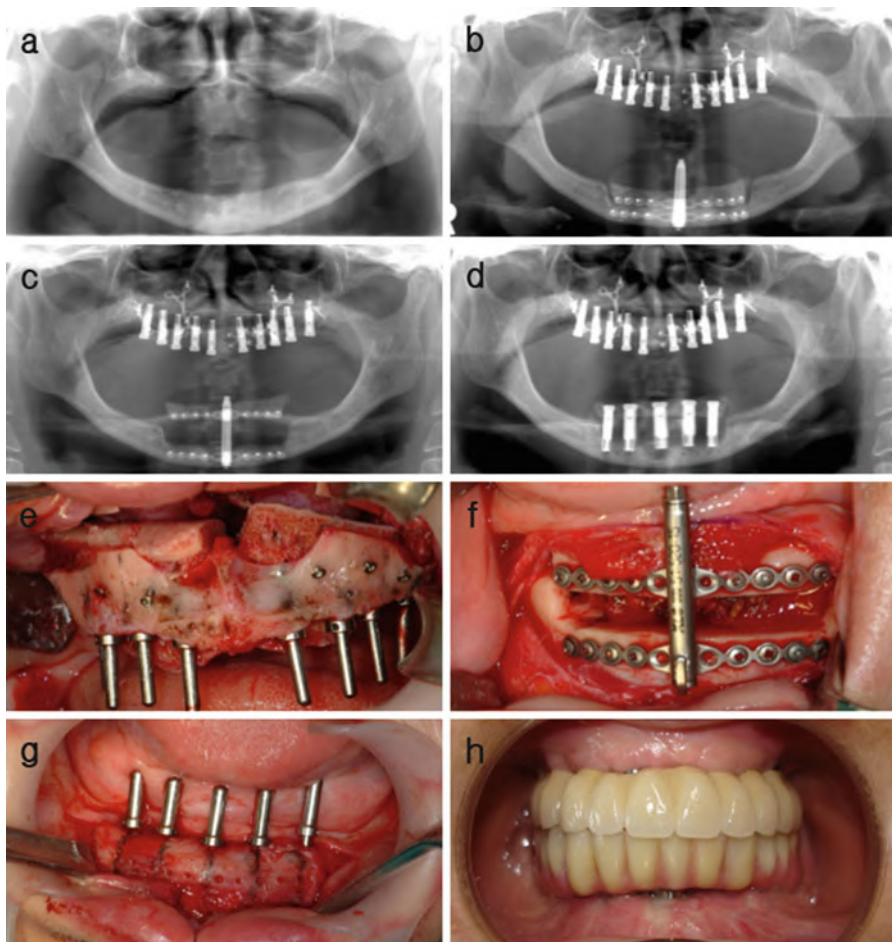


**Fig. 2.9** Case presentation of a severe maxillo-mandibular atrophy. (a) Radiograph representing severe atrophy of both the maxilla and the mandible, (b) After Le Fort 1 osteotomy and iliac bone graft with simultaneous implant installation of the maxilla and distraction device installation on the mandible, (c) After full activation of the distraction device, (d) After implant installation on the mandible, (e) Clinical photographs of the operation. Maxilla was down fractured and moved anteriorly and interpositional iliac bone graft was performed and fixed rigidly on the preplanned position and implant installation was done simultaneously, (f) Activation trial of the distraction device at the time of installation, (g) Regenerated bone on the distracted alveolar bone on the mandible and implants were installed, (h) Final prosthetic outcome

Growth factors are also candidates. Floerkemeier et al. demonstrated that percutaneous triple injection of rhBMP-2 improves trabecular microarchitecture of the regenerated bone and in turn contributes to advanced mechanical integrity [11]. Fugio et al. suggested that failure of high speed DO attributes to lack of bone marrow endothelial cells and endothelial progenitor cells into the gap formed by

distraction. In their study, stromal cell derived factor 1 showed possibility to overcome the resulting ischemic condition and facilitate acceleration of distraction speed [12].

Mechanical means of consolidation enhancement include electric, laser, and ultrasonic stimulations. Hwang et al. investigated the effect of pulsed electromagnetic field stimulation on consolidation of the distracted callus with results of enhanced bone formation. In their study, they applied the pulsed electromagnetic field stimulation for 5 days at the beginning of the consolidation period [13]. Miloro et al. studied the effect of low-level laser on DO. They found that lower-level laser when applied after each activations of distraction device accelerates bone regeneration [14]. The effect of low-intensity pulsed ultrasound when applied during the consolidation period had been reported by Shimazaki et al. They reported that not only normal distraction protocol but also a rapid distraction protocol may benefit from the application of low-intensity pulse ultrasound [15].

**Acknowledgement** The author would like to thank professor Jong-Ho Lee, Soon-Jung Hwang, Soung-Min Kim and doctor Kang-Mi Pang, Ju-Hyun Kim and Seung-Ki Min of the School of Dentistry, Seoul National University for their help provided in preparing this manuscript.

**Open Access** This chapter is distributed under the terms of the Creative Commons Attribution Noncommercial License, which permits any noncommercial use, distribution, and reproduction in any medium, provided the original author(s) and source are credited.

## References

1. Khoury F. Augmentation of the sinus floor with mandibular bone block and simultaneous implantation: a 6-year clinical investigation. *Int J Oral Maxillofac Implants*. 1999;14(4):557.
2. Cordaro L, Amade DS, Cordaro M. Clinical results of alveolar ridge augmentation with mandibular block bone grafts in partially edentulous patients prior to implant placement. *Clin Oral Implants Res*. 2002;13(1):103–11.
3. Proussaefs P, Lozada J, Kleinman A, Rohrer MD. The use of ramus autogenous block grafts for vertical alveolar ridge augmentation and implant placement: a pilot study. *Int J Oral Maxillofac Implants*. 2002;17(2):238.
4. Widmark G, Andersson B, Ivanoff C-J. Mandibular bone graft in the anterior maxilla for single-tooth implants: presentation of a surgical method. *Int J Oral Maxillofac Surg*. 1997;26(2):106–9.
5. Urist MR. Bone: formation by autoinduction. *Science*. 1965;150(3698):893–9.
6. Takahashi T, Funaki K, Shintani H, Haruoka T. Use of horizontal alveolar distraction osteogenesis for implant placement in a narrow alveolar ridge: a case report. *Int J Oral Maxillofac Implants*. 2004;19(2):291.
7. Paeng JY, Myoung H, Hwang SJ, Seo BM, Choi JY, Lee JH, et al. Clinical evaluation of alveolar distraction osteogenesis for implant installation. *J Korean Assoc Maxillofac Plast Reconstr Surg*. 2006;28(4):329–38.
8. Yeom HR, Jeon SH, Kim YT, Paeng JY, Ahn KM, Myung H, et al. Implant installation using vertical distraction osteogenesis at a severely atrophied edentulous mandible. *J Korean Assoc Maxillofac Plast Reconstr Surg*. 2006;28(2):154–65.

9. Paeng JY, Lee JY, Myoung H, Hwang SJ, Seo BM, Choi JY, et al. Vertical distraction osteogenesis for implant installation on the reconstructed mandible with free fibular flap. *J Korean Assoc Maxillofac Plast Reconstr Surg.* 2006;28(6):579–85.
10. Kim IS, Cho TH, Lee ZH, Hwang SJ. Bone regeneration by transplantation of human mesenchymal stromal cells in a rabbit mandibular distraction osteogenesis model. *Tissue Eng Part A.* 2013;19(1–2):66–78. doi:[10.1089/ten.TEA.2011.0696](https://doi.org/10.1089/ten.TEA.2011.0696).
11. Pastor MF, Floerkemeier T, Witte F, Nellesen J, Thorey F, Windhagen H, et al. Repetitive recombinant human bone morphogenetic protein 2 injections improve the callus microarchitecture and mechanical stiffness in a sheep model of distraction osteogenesis. *Orthop Rev.* 2012;4(1):e13. doi:[10.4081/or.2012.e13](https://doi.org/10.4081/or.2012.e13).
12. Fujio M, Yamamoto A, Ando Y, Shohara R, Kinoshita K, Kaneko T, et al. Stromal cell-derived factor-1 enhances distraction osteogenesis-mediated skeletal tissue regeneration through the recruitment of endothelial precursors. *Bone.* 2011;49(4):693–700. doi:[10.1016/j.bone.2011.06.024](https://doi.org/10.1016/j.bone.2011.06.024).
13. Hwang KK, Cho TH, Song YM, Kim DK, Han SH, Kim IS, et al. Effect of pulsed electromagnetic field stimulation on the early bone consolidation after distraction osteogenesis in rabbit mandible model. *J Korean Assoc Maxillofac Plast Reconstr Surg.* 2007;29(2):123–31.
14. Miloro M, Miller JJ, Stoner JA. Low-level laser effect on mandibular distraction osteogenesis. *J Oral Maxillofac Surg.* 2007;65(2):168–76. doi:[10.1016/j.joms.2006.10.002](https://doi.org/10.1016/j.joms.2006.10.002).
15. Shimazaki A, Inui K, Azuma Y, Nishimura N, Yamano Y. Low-intensity pulsed ultrasound accelerates bone maturation in distraction osteogenesis in rabbits. *J Bone Joint Surg.* 2000;82(7):1077–82.

# Chapter 3

## Surface Modification of Dental Implant Improves Implant–Tissue Interface

Takashi Inoue and Kenichi Matsuzaka

**Abstract** The implant material must have optimum surface compatibility with the host epithelial tissue, connective tissue, and bone tissue. Because, dental implants, which are partially exposed to the oral cavity, must have firm contact with tissues to prevent the bacterial infection. Such materials can be created under well-controlled conditions by modifying the surfaces that contact these tissues. The rough and grooved surfaced implant contributes to a more rapid cell migration and make osseointegration during wound healing. A number of chemical and physical methods for titanium and/or zirconium surface modification have already been established. Recently, plasma treatment can control surface physicochemical properties and affect protein adsorption for bioengineering. Moreover, the “motif-programming” methodology to “biologically” modify titanium and zirconium surfaces has created interfacing artificial proteins that endowed those surfaces with cell-binding activity. These technique should improve firm contact between tissue and dental implant.

**Keywords** Dental implant • Surface modification • Tissue interface

### 3.1 Dental Implant–Tissue Interface

Dental implant therapy creates an open wound, and an epithelium-implant interface which is always exposed to the possibility of inflammation is formed [1–3]. Peri-implantitis is a risk factor for a number of age-related diseases, including diabetes, arteriosclerosis, cardiac infarction and NASH (Fig. 3.1). It is important to create a firm implant–tissue interface from such a viewpoint.

Implant–tissue interface formation occurs during the process of wound healing [2, 3]. The oral mucosa is penetrated along the implant surface after the implantation and as a result, peri-implant epithelium is created (Fig. 3.2). Peri-implant epithelium lack the junctional epithelium that are normally formed by

---

T. Inoue (✉) • K. Matsuzaka

Department of Clinical Pathophysiology, Oral Health Science Center, Tokyo Dental College,  
2-9-18, Misaki, Chiyoda, Tokyo 101-0061, Japan  
e-mail: [inoue@tdc.ac.jp](mailto:inoue@tdc.ac.jp)

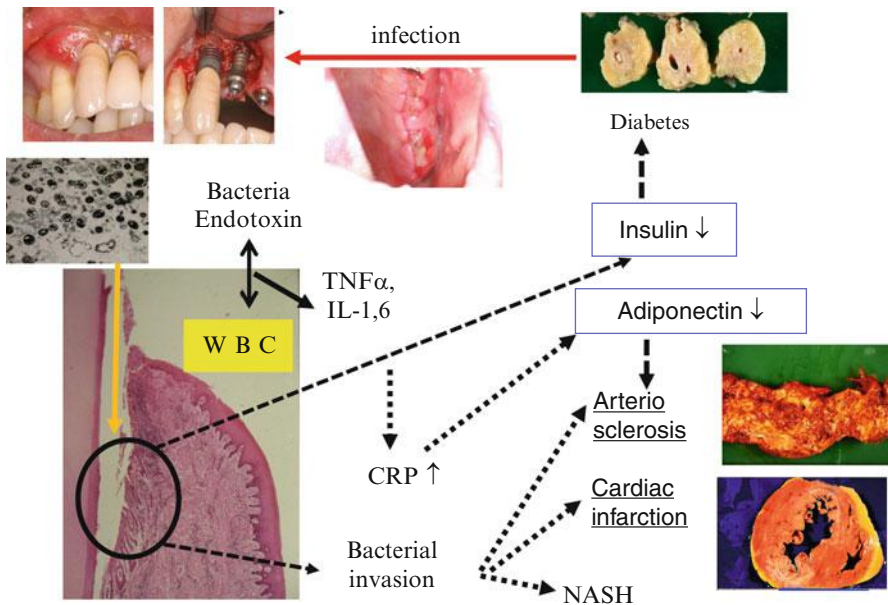
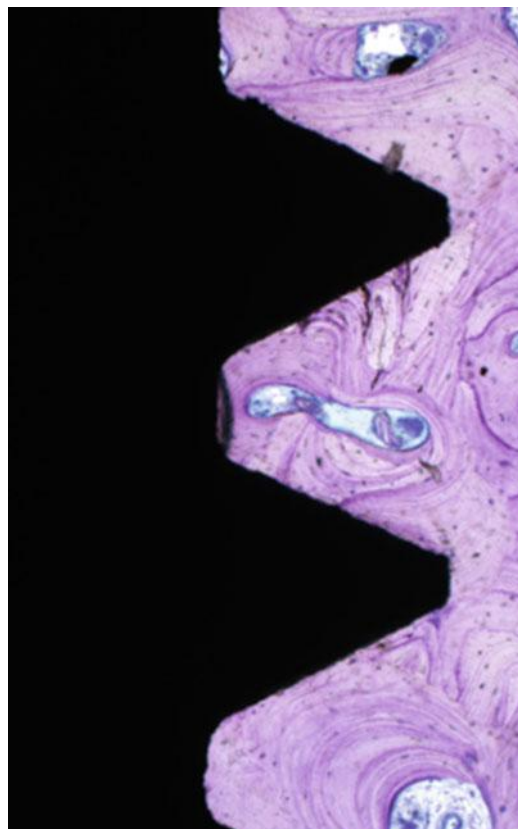


**Fig. 3.1** Peri-implantitis is a risk factor for a number of diseases

**Fig. 3.2** Ground section of the periimplant epithelium



**Fig. 3.3** Ground section of osseointegration



hemidesmosomes and the basal lamina, which connect enamel and epithelium of natural tooth [4].

Fibroblast face to the implant surface differentiates into osteoblasts also during the process of wound healing. The osteoblast deposits bone matrix on the implant surface, becomes calcified, and completes osseointegration which is complicatedly associated with the implant materials. It is known that a direct bond between implant and surrounding bone has been demonstrated with implants made of bioactive materials, i.e. bio-glasses and calcium phosphate ceramics [5, 6].

Titanium is known to have a greater ability than other metals to facilitate osseointegration, which is defined as a close contact between bone tissues and implant material such that there is no progressive relative motion of living bone and implant under functional levels and loading for the life of the patient (Fig. 3.3). Even when light microscopy confirms osseointegration of titanium implants, examination by electron microscope reveals that the bone and the implant are not crystallographically continuous (Fig. 3.4). The thin amorphous structures between the bone and the titanium implant, that is, there is no direct contact between titanium and bone was also observed [7].

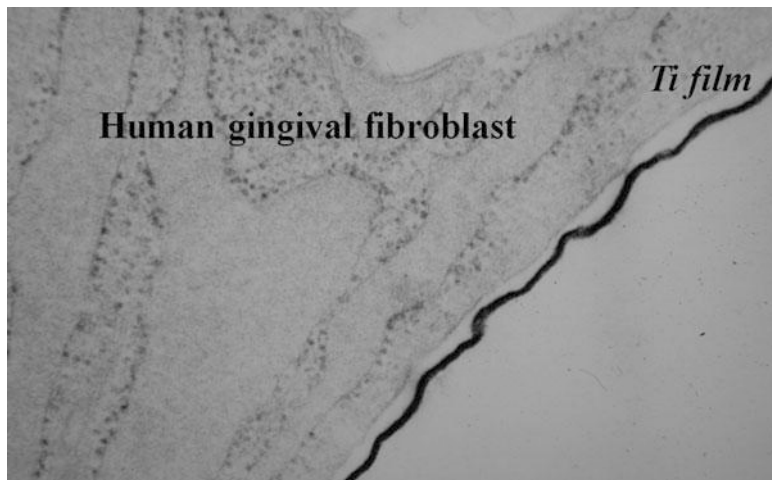
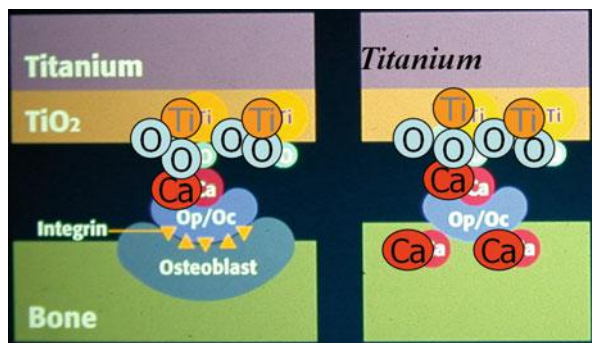


**Fig. 3.4** Ultrastructural feature of Human gingival fibroblast titanium film (Ti) interface in vitro

**Fig. 3.5** Hypothetical osseointegration on the titanium surface. *Ti* Titanium, *O* Oxygen, *Op* Osteopontin, *OC* Osteocalcin, *Ca* Calcium [2]



Generation of the titanium oxide film on the surface of titanium is one reason for this ability and its high level of corrosion resistance. In addition, the degree of the deposition of calcium phosphates in body fluid is greater on titanium than on other metals. Presently, adsorption of osteogenic proteins such as osteocalcin (Oc) and osteopontin (Op) to the titanium surface is a main function of the osseointegration of titanium [2, 3]. There are two mechanisms involved in the adsorption of osteogenic proteins. Titanium oxide has a similar number of isoelectric points (pI) at approximately pH = 5 as those of pH = 4.7–4.9 on osteogenic proteins. Accordingly, at around pH 7, both titanium oxide and osteogenic proteins are negatively charged. The calcium ion-mediated mechanism caused by the positively charged calcium ions,  $\text{Ca}^{2+}$ . The hydration effect of terminal OH radicals which are positively charged, is also considered as playing a role in protein adsorption (Fig. 3.5) [8].

In view of the direct bone-implant contact, it plays important roles of surface geometry and surface chemistry of the implant material, and cell behavior surrounding implant.

### 3.2 Effect of the Surface Geometry

Brunette et al. [9] discuss that the grooved surface changes the cytoplasm by offering a microenvironment and prepares a good condition for generating the calcifying tissue, and that cells which are arranged along the groove help the osteogenic cell differentiate to osteoblast (Fig. 3.6). Further, vinculins, which is one of the proteins of attaching to the substrate, are also oriented to the microgroove (Fig. 3.7). To support cellular attachment, spreading and growth, and improve cellular function, a lot of reports have been published about roughened implant surfaces (Fig. 3.8) [10–13], as well as on controlled microtopography [9, 13–19]. We also explored how the fibroblast originated from human gingiva reacts against the titanium discs of various surface geometries. In the phase-contrast microscopic view of titanium disc with mechanically polished grooves on the surface, it is observed that cells are surrounding the disc. In the scanning electron microscopic view, cells are arranged along the groove (Contact guidance (Fig. 3.9) [10]. On the other hand, in the phase-contrast microscopic view of titanium disc with rough surface, cells are arranged vertically to disc. In the scanning electron microscopic view, cells are arranged in free directions to disc, and cell bridge is geometryed (Two center effect: Fig. 3.10) [10].

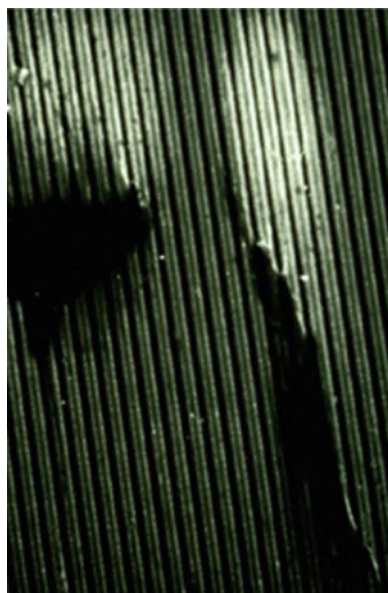


**Fig. 3.6** Scanning electron microscopic findings of fibroblast on microgrooved surface

**Fig. 3.7** Confocal scanning microscopic findings of osteoblast using vinculin on microgrooved surface

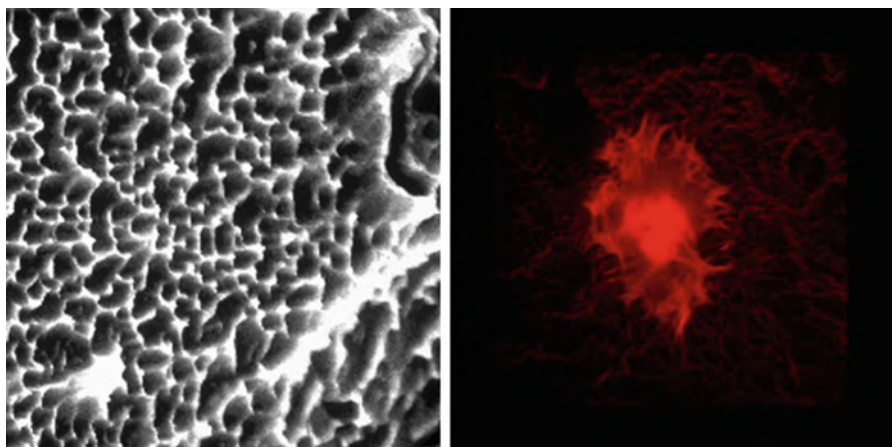
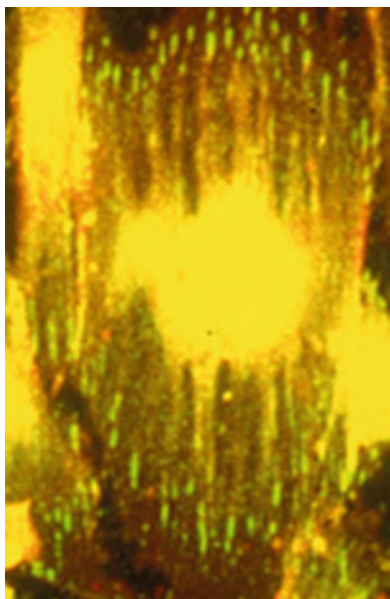


**Fig. 3.8** Scanning electron microscopic findings of rough surface implant (SLA: *Left*) and Immune-fluorescence microscopic findings of cells on the SLA

### 3.3 Control of Surface Chemistry

Surface chemistry involves the adsorption of proteins and cells on biomaterials. This adsorption reflects the affinity between two substances, and the strength of adsorption follows the order: chemical adsorption including covalent bonds and ionic bonds > electrostatic force found in electrokinetic potential or zeta

**Fig. 3.9** Numerous cellular bridges that extend from the multilayer to the oriented cell sheet and orientated parallel to the grooves (contact guidance)

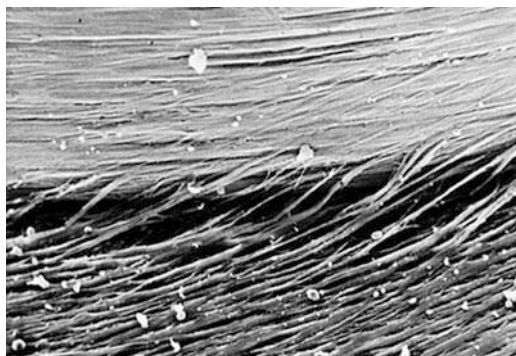
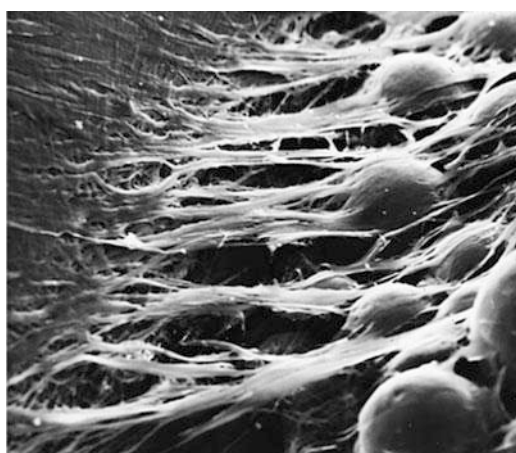


**Fig. 3.10** The migration of fibroblasts onto rough surface and numerous cellular bridges oriented at right angle to the rim of the disc (Two center effect)



potential > hydrogen bonds involved in hydrophilic groups such as  $-\text{OH}$ ,  $-\text{COOH}$ , and  $-\text{NH}_2$  > hydrophobic interaction (i.e., adsorption of hydrophobic substances in water) > van der Waals forces. Adsorption characteristics are primarily evaluated by hydrophobicity (wettability), which can be determined by measuring the surface energy (contact angle), and electrokinetic potential (zeta potential, isoelectric point), which reflects surface electric charges and these affect creation of firm integration between implant and cells.

### 3.4 Protein Application

As for the surface chemistry, methods of modifying the titanium surface using adhesive proteins such as osteonectin, fibronectin or laminin-5 compatible with the soft tissue/implant interface have been proposed. For the implant surface in contact with subepithelial connective tissues, tresyl chloride treatment is used to

adhere the selected proteins such as fibronectin to the amino residues [20]. Thus the gingival epithelium attached to dental implants through the formation of hemidesmosomes using laminin-5 [21]. However, a stable coating and prevention of protein denaturation at the time of implantation are necessary using motif-programming or plasma treatment.

### 3.5 Application of Motif-Programming

Motif-programming is a method for creating artificial proteins by combining functional peptide motifs in a combinatorial manner. This method is particularly well suited for developing liaison molecules that interface between cells and inorganic materials. Here we describe creation of artificial proteins through the programming of two motifs, a natural cell attachment motif (RGD) and an artificial Ti-binding motif (Fig. 3.11). Although the interaction with Ti was not covalent, the proteins recapitulated several functions of fibronectin, and thus, could serve as an artificial ECM on Ti materials. Because the motif-programming system could be easily extended to create artificial proteins having other biological functions and material specificities, it should be highly useful for application to dental implant and tissue

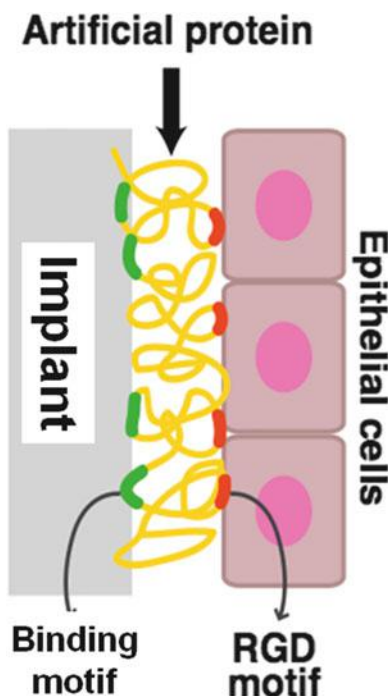


**Fig. 3.11** Schematic representation of an artificial protein intermediating between the surface of titanium and cells. Artificial proteins are shown as yellow containing Ti binding motif (TBP: green) and a cell binding motif (RGD: red) [22]

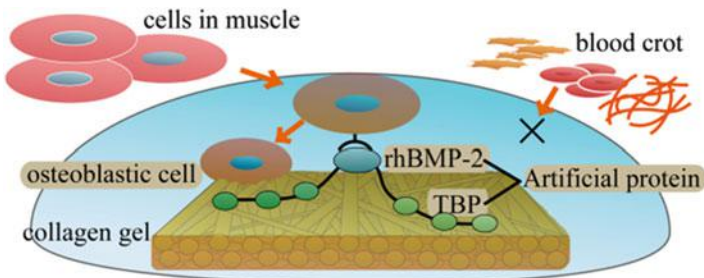


**Fig. 3.12** Schematic image of the AFT between BMP-2 and TBP [24]

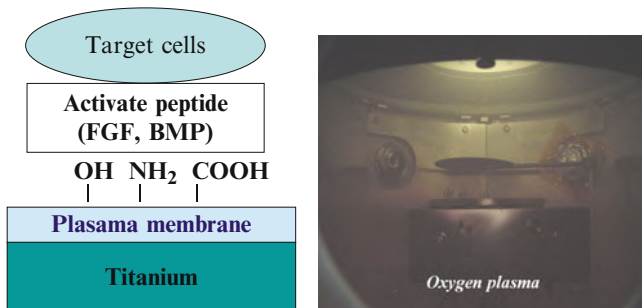


**Fig. 3.13** Plasma treatment was performed using the VEP-1000 system (right) and schematic image shows the attachment of cells on the plasma treatment titanium surface (left)

engineering [22, 23]. Yuasa et al. using an artificial fusion protein between bone morphogenetic protein 2 and titanium-binding peptide and reported that this artificial protein accelerates osteogenesis in the muscle tissue and suggests its possible use in dental implant for better osseointegration (Fig. 3.12) [24].

### 3.6 Plasma Treatment of Implant Surface

Plasma treatment is a well-established method of surface processing in the microelectronics industry for effective surface modification, exhibiting high surface energies, good wettability and cleaning (Fig. 3.13). This technique can control surface physicochemical properties and affect protein adsorption, and is of particular interest in biomedical engineering. Matsuzaka et al. reported that bone morphogenetic protein-2(BMP-2) and fibronectin could be immobilized using oxygen plasma treatment. Immobilization of FGF-2 on an implant using modified surface topography might allow proliferation of periodontal ligament cells around the implant [25, 26].

### 3.7 Calcium Phosphate (Ca-P) Coating by Plasma Spraying

Ca-P implants, including hydroxyapatite (HA), are well known for good osteoconductivity (the early stage of osteogenesis) as well as for direct binding to bone tissue *in vivo*. Alkaline phosphatase expression and parathyroid hormone response were higher in cultures grown in HA than in cultures grown in titanium [27] and the *in vitro* formation of extracellular matrices was greater on Ca-P coatings than on titanium.

In spite of their rapid and strong bonds to living bone tissues and favorable osteogenic ability, Ca-P ceramics alone cannot be used for implants because of their lack of strength. Accordingly, Ca-P coatings on Ti implants produced by the plasma spraying have frequently been used [28]. These Ca-P coated implants, however, often develop fractures in their coatings as well as at the titanium interface after implantation. The reason for this is thought to originate in the comparatively thick, porous, non-uniform (crystalline surrounded by an amorphous mass), and poorly adherent Ca-P layer produced by plasma spraying. These fragments of a certain size cause phagocytosis by macrophages, leading to inflammation. It is therefore desirable for the materials to be rapidly and completely absorbed in the host tissues and to be entirely replaced with bone tissue. When osteogenesis occurs at the site where old bones are absorbed (remodeling of bones), the Ca-P coatings should be no thicker than necessary.

### 3.8 Thin Ca-P Coatings

Attempts have recently been made to solve problems, the cold plasma, ion-plating [29] and the ion sputtering [28], which are a kind of physical vapor deposition (PVD), are used to produce implant materials consisting of a thin, homogeneous, and adherent Ca-P coating. Ion beam dynamic mixing (IBDM) was also introduced as a suitable technique for fabricating a thin and adherent ceramic layer [30]. This method is a combination of ion implantation and PVD, and has the advantages of a high deposition rate, producing defect-free transparent thin films, and excellent adhesion compared to conventional thin-film deposition techniques.

### 3.9 Future of Dental Implant

The next generation should be the surface modification of any of the materials for bio-functionalization of dental implants. Such materials can be created under well-controlled conditions by modifying the surfaces of metals that contact those tissues. “Tissue-compatible implants,” which are compatible with all host tissues, must integrate with bone tissue, easily form hemidesmosomes, and prevent biofilm accumulation.

**Acknowledgements** This study was supported by Oral Health Science Center Grant 5A10, 5A08 from Tokyo Dental College, by MEXT. HITEKU (2002–2006), and by a Grant-in-Aid for Scientific Research No. 07672123, 10671845, 10085839, 15592065 and 14207093 from The Ministry of Education, Culture, Sports, Science and Technology in Japan.

**Open Access** This chapter is distributed under the terms of the Creative Commons Attribution Noncommercial License, which permits any noncommercial use, distribution, and reproduction in any medium, provided the original author(s) and source are credited.

## References

1. Inoue T, Takeda T, Chan YL, Abiko Y, Ayukawa Y, Tanaka T, Yoshinari M, Shimono M. Immunolocalization of proliferating cell nuclear antigen in the peri-implant epithelium. *Bull Tokyo Dent Coll.* 1997;38:187–93.
2. Inoue T, Shimono M, Abiko Y, Kaku T. Dental implant-tissue interface (Endosseous titanium implant). *Bull Kanagawa Dent Coll.* 1994;22:125–38.
3. Inoue T, Matsuzaka K, Yoshinari M, Abiko Y, Shimono M. Implant-bone tissue interface. *Bull Kanagawa Dent Coll.* 1999;27:132–41.
4. Ikeda H, Yamaza T, Yoshinari M, Ohsaki Y, Ayukawa Y, Kido MA, Inoue T, Shimono M, Koyano K, Tanaka T. Ultrastructural and immunoelectron microscopic studies of the peri-implant epithelium-implant (Ti-6Al-4V) interface of rat maxilla. *J Periodontol.* 2000;71:961–73.
5. de Groot K. Implant materials in dentistry. *Med Prog Technol.* 1982;9:129–36.
6. de Groot K. Ceramics based on calciumphosphates. In: Vincenzini P, editor. *Ceramics in surgery*. Amsterdam: Elsevier; 1983. p. 79–90.
7. Yoshinari M, Oda Y, Inoue T, Shimono M. Dry-process surface modification for titanium dental implants. *Metall Mater Trans A.* 2002;33:511–9.
8. Hansson HA, Albrektsson T, Branemark PI. Structural aspects of interface between tissue and titanium implants. *J Prosthet Dent.* 1983;50:108–13.
9. Brunette DM. The effect of implant surface topography on the behavior of cells. *Int J Oral Maxillofac Implants.* 1988;3:231–46.
10. Inoue T, Cox JE, Pilliar RM, Melcher AH. Effect of the surface geometry of smooth and porous-coated titanium alloy on the orientation of fibroblasts in vitro. *J Biomed Mater Res.* 1987;21:107–26.
11. Boyan BD, Schwartz Z, Hambleton JC. Response of bone and cartilage cells to biomaterials in vivo and in vitro. *J Oral Implantol.* 1993;19:116–20.
12. Martin JY, Schwartz Z, Hummert TW, Schraub DM, Simpson J, Lankford D, Dean DD, Cochran DL, Boyan BD. Effect of titanium surface roughness on proliferation, differentiation, and protein synthesis of human osteoblast-like cells (MG63). *J Biomed Mater Res.* 1995;29:389–401.
13. Schwartz Z, Martin JY, Dean DD, Simpson J, Cochran DL, Boyan BD. Effect of titanium surface roughness on chondrocyte proliferation, matrix production, and differentiation depends on the state of cell maturation. *J Biomed Mater Res.* 1996;30:145–55.
14. Curtis A, Wilkinson C. Review, topographical control of cells. *Biomaterials.* 1997;18:1573–83.
15. Matsuzaka K, Walboomers XF, de Ruijter JE, Jansen JA. The effect of poly-L-lactic acid with parallel surface micro groove on osteoblast-like cells in vitro. *Biomaterials.* 1999;20:1293–301.
16. Matsuzaka K, Walboomers XF, de Ruijter JE, Jansen JA. Effect of microgrooved poly-L-lactic (PLA) surfaces on proliferation, cytoskeletal organization, and mineralized matrix formation of rat bone marrow cells. *Clin Oral Implants Res.* 2000;11:325–33.

17. den Braber ET, de Ruijter JE, Croes HJE, Ginsel LA, Jansen JA. Transmission electron microscopical study of fibroblast attachment to microtextured silicone rubber surfaces. *Cell Mater.* 1998;7:31–9.
18. den Braber ET, de Ruijter JE, Ginsel LA, von Recum AF, Jansen JA. Orientation of ECM protein deposition, fibroblast cytoskeleton, and attachment complex components on silicone microgrooved surfaces. *J Biomed Mater Res.* 1998;40:291–300.
19. Walboomers XF, Jansen JA. Cell and tissue behavior on micro-grooved surfaces (review). *Odontology.* 2001;89:2–11.
20. Hayakawa T, Yoshinari M, Nemoto K. Characterization and protein-adsorption behavior of deposited organic thin film onto titanium by plasma polymerization with hexamethyldisiloxane. *Biomaterials.* 2004;25:119–27.
21. Tamura RN, Oda D, Quaranta V, Plopper G, Lambert R, Glaser S, Jones JCR. Coating of titanium alloy with soluble laminin-5 promotes cell attachment and hemidesmosome assembly in gingival epithelial cells: potential application to dental implants. *J Periodontal Res.* 1997;32:287–94.
22. Kokubun K, Kashiwagi K, Yoshinari M, Inoue T, Shiba K. Motif-programmed artificial extracellular matrix. *Biomacromolecules.* 2008;9:3098–105.
23. Hashimoto K, Yoshinari M, Matsuzaka K, Shiba K, Inoue T. Identification of peptide motif that binds to the surface of zirconia. *Dent Mater J.* 2011;30:935–40.
24. Yuasa K, Kokubu E, Kokubun K, Matsuzaka K, Shiba K, Kashiwagi K, Inoue T. An artificial fusion protein between bone morphogenetic protein 2 and titanium-binding peptide is functional in vivo. *J Biomed Mater Res A.* 2014;102S:1180–6.
25. Kokubu E, Yoshinari M, Matsuzaka K, Inoue T. Behavior of rat periodontal ligament cells on fibroblast growth factor-2-immobilized titanium surfaces treated by plasma modification. *Biomed Mater Res A.* 2009;91A:69–75.
26. Kokubu E, Hamilton DW, Inoue T, Brunette DM. Modulation of human gingival fibroblast adhesion, morphology, tyrosine phosphorylation, and ERK1/2 localization on polished, grooved and SLA substratum topographies. *Biomed Mater Res A.* 2009;91A:663–70.
27. Massas R, Pitarui S, Weinreb MM. The effects of titanium and hydroxyapatite on osteoblastic expression and proliferation in rat parietal bone cultures. *J Dent Res.* 1993;72:1005–8.
28. Jansen JA, Wolke JGC, van der Waerden JPCM, de Groot K. Application of magnetron sputtering for producing ceramic coating on implant materials. *Clin Oral Implants Res.* 1993;4:28–34.
29. Yoshinari M, Ozeki K, Sumii T. Properties of hydroxyapatite-coated Ti-6Al-4V alloy produced by the ion-plating method. *Bull Tokyo Dent Coll.* 1991;32:147–56.
30. Yoshinari M, Ohtsuka Y, Dérand T. Thin hydroxyapatite coating produced by the ion beam dynamic mixing method. *Biomaterials.* 1994;15:529–35.

# **Chapter 4**

## **Oral Microbiota in Crevices Around Dental Implants: Profiling of Oral Biofilm**

**Takuichi Sato, Yoshiaki Kawamura, Keiko Yamaki, Naoko Ishida, Lingyang Tian, Yasuhisa Takeuchi, Kazuhiro Hashimoto, Yuki Abiko, Gen Mayanagi, Jumpei Washio, Junko Matsuyama, and Nobuhiro Takahashi**

**Abstract** Large numbers of bacteria ( $>10^6/\text{mm}^2$ ) generally inhabit the surface of the oral cavity, particularly at the interface between teeth and gingiva, as an oral biofilm (microbiota). The establishment of anaerobic bacterial culture and molecular biological techniques has enabled us to isolate and detect various bacterial species from oral biofilm. It has been estimated that more than 600 bacterial species

---

T. Sato (✉) • L. Tian • Y. Abiko • J. Washio • N. Takahashi

Division of Oral Ecology and Biochemistry, Tohoku University Graduate School of Dentistry, Sendai 980-8575, Japan

e-mail: [tak@m.tohoku.ac.jp](mailto:tak@m.tohoku.ac.jp)

Y. Kawamura

Department of Microbiology, Aichigakuin University School of Pharmacy, Nagoya 464-8650, Japan

K. Yamaki • K. Hashimoto

Division of Periodontology and Endodontology, Tohoku University Graduate School of Dentistry, Sendai 980-8575, Japan

N. Ishida

Division of Oral Ecology and Biochemistry, Tohoku University Graduate School of Dentistry, Sendai 980-8575, Japan

Division of Advanced Prosthetic Dentistry, Tohoku University Graduate School of Dentistry, Sendai 980-8575, Japan

Y. Takeuchi

Division of Advanced Prosthetic Dentistry, Tohoku University Graduate School of Dentistry, Sendai 980-8575, Japan

G. Mayanagi

Division of Oral Ecology and Biochemistry, Tohoku University Graduate School of Dentistry, Sendai 980-8575, Japan

Research Unit for Interface Oral Health Science, Tohoku University Graduate School of Dentistry, Sendai 980-8575, Japan

J. Matsuyama

Division of Pediatric Dentistry, Niigata University Graduate School of Medical and Dental Sciences, Niigata 951-8514, Japan

inhabit the oral cavity. Nevertheless, the oral cavity is considered healthy when the oral microbiota is composed of indigenous bacteria. Numerous environmental changes in the oral cavity may lead to accumulation of dental caries-associated or periodontitis-associated bacteria, resulting in the initiation of dental caries or periodontitis, respectively. The environment in crevices around dental implants is considered similar to that in subgingival sulcus, such as neutral pH, anaerobiosis and rich nutrition (e.g., amino acids and peptides). The environment may be supportive of anaerobic growth of the bacteria in microbiota in crevices around implants, particularly at the interface between histocompatible artificial material and mucosal epithelium. The microbiota may trigger inflammation in the tissue around the implants. In this article, the current topics on the profiling of oral microbiota in crevices around implants are reviewed.

**Keywords** Bacteria • Dental implant • Oral microbiota • Profiling

## 4.1 Introduction

Large numbers of bacteria ( $>10^6/\text{mm}^2$ ) generally inhabit the surface of the oral cavity, particularly at the interface between teeth and gingiva, as an oral biofilm (microbiota). The establishment of anaerobic bacterial culture and molecular biological techniques has enabled us to isolate and detect various bacterial species from oral biofilm. Currently, it has been estimated that more than 600 bacterial species inhabit the oral cavity. Nevertheless, the oral cavity is considered healthy when the oral microbiota is composed of indigenous bacteria.

### 4.1.1 Quantitative and Qualitative Analyses of Oral Biofilm

For the past several decades, with the development of techniques for culturing obligate anaerobes, in particular, adoption of the well-maintained anaerobic glove box system permitted the efficient recovery of obligate anaerobes from oral cavities and lesions. Importantly, all plates, media, buffer solutions and experimental instruments are kept in an anaerobic glove box for at least 24 h before use. To ensure strictly anaerobic conditions in the glove box, reduction of methyl viologen ( $-446\text{ mV}$ ) is carefully monitored whenever experimental procedures are carried out. By adopting these exacting anaerobic techniques, the microbiota of oral biofilm has been shown to consist mainly of obligate anaerobes [1–5].

At present, the identification of obligate anaerobes is generally performed utilizing molecular biological techniques [6–12]. For instance, the bacterial 16S ribosomal RNA gene sequences are amplified by PCR, and partial sequences are then compared with those from the GenBank database using the BLAST search program through the National Center for Biotechnology Information website. Bacterial species are determined by percent sequence similarity ( $>97\%$ ).

### ***4.1.2 Oral Ecology: Environmental Factors Affecting Oral Biofilm***

Numerous environmental changes in the oral cavity may lead to an accumulation of dental caries-associated or periodontitis-associated bacteria, resulting in the initiation of dental caries or periodontitis, respectively. The environment in crevices around dental implants is considered similar to that in subgingival sulcus, such as neutral pH, anaerobiosis and rich nutrition (e.g., amino acids and peptides). The environment may be supportive of anaerobic growth in the crevices around implants, particularly at the interface between histocompatible artificial material and mucosal epithelium. The microbiota may trigger inflammation in the tissue around the implants.

In this article, the current topics related to profiling of oral microbiota in crevices around implants are reviewed.

## **4.2 Nutritional and Environmental Aspects of Dental Implants**

Nutrition for bacteria are supplied by the fluids around implants (PICF; peri-implant crevicular fluids) and teeth (GCF; gingival crevicular fluids), thus, fluid volume and contents, as well as pH, are considered to be critical to the health of dental implants.

### ***4.2.1 Fluid Volume***

Fluid volume with healthy implants was  $2.17 \pm 2.09 \mu\text{L}$  (range of Periotron 22.6–35.2 units) and that with healthy teeth was  $3.49 \pm 2.26 \mu\text{L}$  (36.3–56.6 units) ( $n = 7$ , mean age, 54.2 years) [13]. Similarly, Apse et al. [14] reported that fluid volumes were Periotron  $57.1 \pm 37.5$  units and  $54.8 \pm 28.9$  units, for healthy implants ( $n = 28$ ) and healthy teeth ( $n = 19$ ), respectively. There were no significant differences between healthy implants and healthy teeth, suggesting similar conditions between healthy implants and healthy teeth.

### ***4.2.2 Fluid Constituents***

In terms of profile of crevicular fluid constituents such as inflammatory markers in healthy PICF and GCF are reportedly similar, e.g.,  $\alpha 2$ -macroglobulin (17 and 16 ng/ $\mu\text{g}$  albumin),  $\alpha 1$ -antitrypsin (33 and 48), transferrin (34 and 47), lactoferrin (17 and 40)

and immunoglobulin G against *Porphyromonas gingivalis* (82 and 102), respectively [15]. These trends were also observed in inflamed status (peri-implantitis and periodontitis), e.g.,  $\alpha 2$ -macroglobulin (20 and 15 ng/ $\mu$ g albumin),  $\alpha 1$ -antitrypsin (42 and 46), transferrin (35 and 31), lactoferrin (14 and 24) and immunoglobulin G against *Porphyromonas gingivalis* (47 and 43), respectively [15].

#### 4.2.3 Environmental Condition: Fluid pH

Fluid pH of healthy PICF was 6.82 (range 6.30–7.70) and that of healthy GCF was 6.90 (range 6.50–8.50). On the other hand, the ranges of fluid pH for peri-implantitis and periodontitis were 5.63–8.50 and 7.20–7.70, respectively [16].

### 4.3 Microbiota Around Implants

#### 4.3.1 Quantitative and Qualitative Analysis of Microbiota in PICF

Bacterial counts in healthy PICF ( $n = 10$ ) were  $(0.8 \pm 2.0) \times 10^6$  [17], while those in healthy GCF ( $n = 7$ ) were  $(7.6 \pm 8.6) \times 10^8$  [7]. In inflamed status,  $(7.5 \pm 9.8) \times 10^7$  bacteria were recovered from plate crevices ( $n = 3$ ) for orthodontic treatment [7], while  $(5.8 \pm 2.8) \times 10^6$  and  $(1.6 \pm 1.5) \times 10^7$  bacteria were found in periodontal pockets ( $n = 7$  and  $n = 5$  from [4] and [8], respectively).

The proportion of obligate anaerobes among the microbiota of healthy PICF was 21 % [17], and that of healthy GCF was 31 % [7]. With regard to bacterial composition, *Actinomyces* (17 %), *Campylobacter* (12 %), *Fusobacterium* (10 %), *Selenomonas* (10 %), *Streptococcus* (8.2 %), *Lepotrichia* (7.6 %), *Prevotella* (7.1 %), *Neisseria* (6.5 %), *Veillonella* (6 %), *Dialister* (3.3 %) and *Haemophilus* (2.7 %) were predominant in healthy plate crevices, while *Actinomyces* (37 %), *Streptococcus* (20 %), *Veillonella* (7.5 %), *Olsenella* (6.2 %), *Prevotella* (4.8 %), *Fusobacterium* (2.7 %), *Parvimonas* (2.7 %), *Selenomonas* (2.1 %), *Neisseria* (2.1 %), *Capnocytophaga* (2.1 %), *Gemella* (2.1 %), *Rothia* (2.1 %) and *Haemophilus* (1.4 %) were predominant in healthy GCF [7]. Under the viewpoint that major anaerobes were *Campylobacter*, *Fusobacterium*, *Selenomonas*, *Prevotella*, *Veillonella* and *Dialister*, and major facultative anaerobes were *Actinomyces*, *Streptococcus*, *Neisseria* and *Haemophilus*, a similarity were suggested between healthy plate crevices and healthy GCF.

This suggests that the microbiota around implants is similar to that of gingival sulcus with regard to bacterial density and proportion of anaerobes in microbiota. Therefore, similarly to the maintenance of the teeth with periodontal pockets, treatments with dental implants require strict self-oral care and regular professional plaque control in order to prevent infection.

### 4.3.2 Metagenome (Pyrosequencing) Analysis of Microbiota in PICF

In contrast, inflammatory and immune responses of peri-implant mucosa to microbiota around implants have not been reported in detail. Thus, it is possible that particular microbiota may be formed around dental implants. Indeed, recent pyrosequencing analyses have shown that microbiota in healthy PICF was distinct from that in healthy GCF, and that the currently accepted theory on the transmission from the tooth to the implant surface requires reexamination [18, 19]. More specifically, utilizing the pyrosequencing technique, Kumar et al. [18] reported that *Prevotella*, *Treponema*, *Leptotrichia*, *Streptococcus mutans*, *Butyrivibrio* and *Lactococcus* were significantly present in healthy PICF, while non-mutans streptococci, *Fusobacterium*, *Actinomyces*, *Granulicatella*, *Dialister*, *Veillonella*, *Neisseria*, *Corynebacterium*, *Synergistes* and *Arthrobacter* were significantly present in healthy GCF. In addition, Dabdoub et al. [19] reported that *Actinomyces gerencseriae*, *Actinomyces bovis*, *Veillonella dispar*, *Haemophilus influenza*, *Streptococcus minor*, *Mycoplasma faecium*, *Streptococcus macedonicus*, *Streptococcus pseudoporcinus*, Unclassified Bacillales, *Actinomyces radicidentis*, *Streptococcus infantis*, *Actinomyces meyeri*, *Streptococcus ursoris* and *Veillonella* spp. were significantly present in healthy PICF, while *Caulobacter* spp., *Peptostreptococcus anaerobius*, Unclassified Rs-045, *Desulfobulbus* spp. and *Bulleidia* spp. were significantly present in healthy GCF.

With the improvement of materials and techniques of dental implants, the environment around dental implants will possibly change markedly, and thus a comprehensive analysis of microbiota, as well as the development of novel markers in the environment, is required in order to elucidate the etiological role in peri-implant diseases.

**Acknowledgements** This study was supported in part by Grants-in-Aid for Scientific Research (25462945 to KY, 25463237 to JM, 25861785 to KH, 24390511, 25670777, 26462869 to TS) from the Japan Society for the Promotion of Science.

**Open Access** This chapter is distributed under the terms of the Creative Commons Attribution Noncommercial License, which permits any noncommercial use, distribution, and reproduction in any medium, provided the original author(s) and source are credited.

## References

1. Hoshino E. Predominant obligate anaerobes in human carious dentin. J Dent Res. 1985;64:1195–8.
2. Hoshino E, Sato M, Sasano T, Kota K. Characterization of bacterial deposits formed in vivo on hydrogen-ion-sensitive field-effect transistor electrodes and enamel surfaces. Jpn J Oral Biol. 1989;31:102–6.
3. Ando N, Hoshino E. Predominant obligate anaerobes invading the deep layers of root canal dentin. Int Endod J. 1990;23:20–7.

4. Uematsu H, Hoshino E. Predominant obligate anaerobes in human periodontal pockets. *J Periodontal Res.* 1992;27:15–9.
5. Sato T, Hoshino E, Uematsu H, Noda T. Predominant obligate anaerobes in necrotic pulps of human deciduous teeth. *Microb Ecol Health Dis.* 1993;6:269–75.
6. Washio J, Sato T, Koseki T, Takahashi N. Hydrogen sulfide-producing bacteria in tongue coating and their relationship with oral malodour. *J Med Microbiol.* 2005;54:889–95.
7. Sato R, Sato T, Takahashi I, Sugawara J, Takahashi N. Profiling of bacterial flora in crevices around titanium orthodontic anchor plates. *Clin Oral Implants Res.* 2007;18:21–6.
8. Hashimoto K, Sato T, Shimauchi H, Takahashi N. Profiling of dental plaque microflora on root caries lesions and the protein-denaturing activity of these bacteria. *Am J Dent.* 2011;24:295–9.
9. Komori R, Sato T, Takano-Yamamoto T, Takahashi N. Microbial composition of dental plaque microflora on first molars with orthodontic bands and brackets, and the acidogenic potential of these bacteria. *J Oral Biosci.* 2012;54:107–12.
10. Sato T, Yamaki K, Ishida N, Hashimoto K, Takeuchi Y, Shoji M, Sato E, Matsuyama J, Shimauchi H, Takahashi N. Cultivable anaerobic microbiota of infected root canals. *Int J Dent.* 2012;2012:609689.
11. Takeuchi Y, Nakajo K, Sato T, Koyama S, Sasaki K, Takahashi N. Quantification and identification of bacteria in acrylic resin dentures and dento-maxillary obturator-prostheses. *Am J Dent.* 2012;25:171–5.
12. Hasegawa A, Sato T, Hoshikawa Y, Ishida N, Tanda N, Kawamura Y, Kondo T, Takahashi N. Detection and identification of oral anaerobes from intraoperative bronchial fluids of patients with pulmonary carcinoma. *Microbiol Immunol.* 2014;58:375–81.
13. Murata M, Tatsumi J, Kato Y, Suda S, Nunokawa Y, Kobayashi Y, Takeda H, Araki H, Shin K, Okuda K, Miyata T, Yoshie H. Osteocalcin, deoxypyridinoline and interleukin-1 $\beta$  in peri-implant crevicular fluid of patients with peri-implantitis. *Clin Oral Implants Res.* 2002;13:637–43.
14. Apse P, Ellen RP, Overall CM, Zarb GA. Microbiota and crevicular fluid collagenase activity in the osseointegrated dental implant sulcus: a comparison of sites in edentulous and partially edentulous patients. *J Periodontal Res.* 1989;24:96–105.
15. Adonogianaki E, Mooney J, Wennström JL, Lekholm U, Kinane DF. Acute-phase proteins and immunoglobulin G against *Porphyromonas gingivalis* in peri-implant crevicular fluid: a comparison with gingival crevicular fluid. *Clin Oral Implants Res.* 1995;6:14–23.
16. Nyako EA, Watson CJ, Preston AJ. Determination of the pH of peri-implant crevicular fluid in successful and failing dental implant sites: a pilot study. *Arch Oral Biol.* 2005;50:1055–9.
17. Mombelli A, van Oosten MA, Schurch Jr E, Land NP. The microbiota associated with successful or failing osseointegrated titanium implants. *Oral Microbiol Immunol.* 1987;2:145–51.
18. Kumar PS, Mason MR, Brooker MR, O'Brien K. Pyrosequencing reveals unique microbial signatures associated with healthy and failing dental implants. *J Clin Periodontol.* 2012;39:425–33.
19. Dabdoub SM, Tsigarida AA, Kumar PS. Patient-specific analysis of periodontal and peri-implant microbiomes. *J Dent Res.* 2013;92(12 Suppl):168S–75.

**Part II**

**Symposium II: Biomaterials in Interface  
Science**

# **Chapter 5**

## **Biofunctionalization of Metallic Materials: Creation of Biosis–Abiosis Intelligent Interface**

**Takao Hanawa**

**Abstract** Osseointegration, the first concept of biosis–abiosis intelligent interface, is primarily explained, and researches on the elucidation of osseointegration mechanism and titanium-tissue interface observation are reviewed to understand a concept to create biosis–abiosis intelligent interface. In addition, current status of surface treatment of metallic materials is reviewed. In particular, a gap between research level progress and commercialization in surface treatments is focused. Mechanical property, durability, and manufacturing process of surface layer formed on titanium by surface treatment, are significant to commercialize the treatment, while most of researches focuses only evaluation of biocompatibility and biofunction.

**Keywords** Bone formation • Mechanical anchoring • Osseointegration • Surface treatment • Titanium

### **5.1 Introduction**

Excellent biocompatibility and biofunction of ceramics and polymers are expected to show excellent properties as biomaterials; in fact many devices consisting of metals have been substituted by those consisting of ceramics and polymers. In spite of this event, over 70 % of implant devices in medical field including dentistry, especially over 95 % in orthopedics, still consist of metals, and this share is currently maintained, because of their high strength, toughness, and durability.

On the contrary, a disadvantage of using metals as biomaterials is that they are typically artificial materials and have no biofunction. Therefore, metal surface naturally forms a clear interface against living tissue that works as a barrier to conduct biofunctions. To add biocompatibility and biofunction to metals, in other words, to create biosis–abiosis intelligent interface, surface treatment is essential,

---

T. Hanawa (✉)

Institute of Biomaterials and Bioengineering, Tokyo Medical and Dental University,  
2-3-10 Kanda-surugadai, Chiyoda-ku, Tokyo 101-0062, Japan  
e-mail: [hanawa.met@tmd.ac.jp](mailto:hanawa.met@tmd.ac.jp)

because biofunction cannot be added during manufacturing processes of metals such as melting, casting, forging, and heat treatment. Surface treatment is a process that changes a material's surface composition, structure, and morphology, leaving the bulk mechanical properties intact.

This chapter primarily reviews past researches on the interface between titanium and tissue and change in the research trend with era that much help us to understand a concept to create biosis–abiosis intelligent interface. In addition, current status of surface treatment of metallic materials is reviewed to enhance new and superior designs of biosis–abiosis intelligent interface.

## 5.2 Biosis–Abiosis Intelligent Interface

When a metallic material is implanted into a human body, immediate reaction occurs between its surface and the living tissues. In other words, immediate reaction at this initial stage straightaway determines and defines a metallic material's tissue compatibility. An artificial material usually makes clear interface against a biological system, such as cell, bacterial and tissue: The interface works as a barrier for transportation of molecules and conduction of biofunction, as shown in Fig. 5.1a. On the other hand, if we could create unclear and graded interface at which molecules smoothly transport, both material and tissue are integrated together, and biofunctions are conducted, this interface may be defined as biosis–abiosis

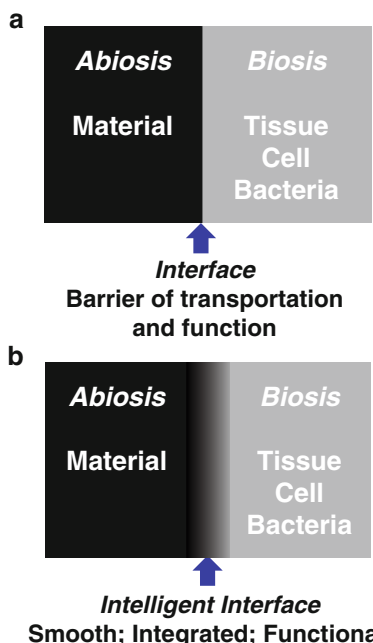


**Fig. 5.1** Clear interface against cell, bacterial and tissue: The interface works as a barrier for transportation of molecules and conduction of biofunction (a). Unclear and graded interface at which smooth transportation of molecules occurs, both material and tissue are integrated together, and biofunctions are conducted (b)

intelligent interface, as shown in Fig. 5.1b. In addition, this interface is expected to be a field not only for chemically biofunctional conduction, but also for mechanically stress conduction. If so, how to make this biosis–abiosis intelligent interface? Of course, one of the solutions is surface treatment of materials. With surface treatment, tissue compatibility of surface layer could be improved.

### 5.3 Osseointegration of Titanium

Osseointegration is the first definition of the interface between a metallic material and living tissue. The definition of osseointegration is as follows: The formation of a direct interface between an implant and bone, without intervening soft tissue. No scar tissue, cartilage or ligament fibers are present between the bone and implant surface. The direct contact of bone and implant surface can be verified microscopically [1]. This “osseointegration” concept was immediately accepted by dentists and dental materials researchers in the world to show biocompatible advantage of titanium among metals that makes it possible that titanium occupies major position in dental implant bodies. After percolating the concept of osseointegration, the elucidation of osseointegration mechanism including the investigation on microscopic interface structure between titanium and bone tissue has been actively studied.

### 5.4 Mechanism of Osseointegration in Titanium

From the viewpoint of the property of titanium surface, mechanism and process of osseointegration has been discussed. Titanium and some of its alloys are known to be among the best biocompatible materials, and commercially the materials have been successfully used for orthopedic and dental implants. The question is why titanium and its alloys show such good biocompatibility compared with other alloys. The explanation to the question is generally believed to be that titanium passivates in aqueous solutions and that passive film is stable even in a biological system. Therefore, it was first thought that good hard tissue compatibility of titanium is caused by its high corrosion resistance. This hypothesis was false. For example, electric plating of platinum on titanium makes delay bone formation on itself, while the corrosion resistance increased [2]. Therefore, good hard tissue compatibility of titanium is caused not only by its high corrosion resistance but also other causes.

In this regard, the surface layer of titanium is essentially  $\text{TiO}_2$  before and after autoclaving and anodic oxidation treatment [3, 4]. However, it is questionable whether titanium oxide is stable and does not react with any electrolyte even in biological system. In this question, the mechanisms of passive dissolution of titanium in a model physiological environment were revealed [5]. They explained that dissolution of titanium depends on solution ligands and the surface oxide characteristics. They also revealed preferential molecular adsorption on titanium [6].

**Fig. 5.2** Schematic model of reconstruction of the surface oxide film on metallic biomaterials

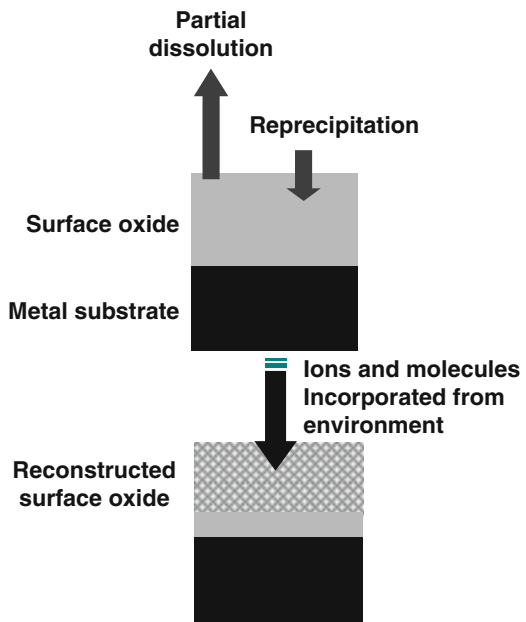
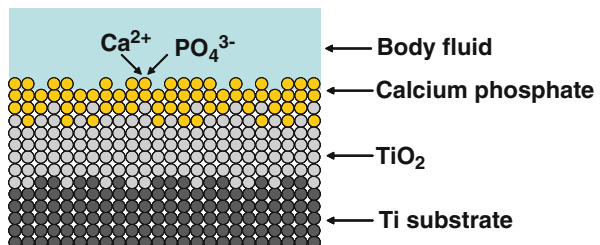


**Fig. 5.3** Calcium phosphate formation on titanium in a simulated body fluid such as Hanks' solution



Composition of surface oxide film varies according to environmental changes, though the film is macroscopically stable. Passive surfaces co-exist in close contact with electrolytes, undergoing a continuous process of partial dissolution and re-precipitation from the microscopic viewpoint. In this sense, surface composition is always changing according to the environment (Fig. 5.2). The composition and properties of the oxide film regenerated in a biological environment may be different from those in water. When titanium which has been surgically implanted into the human jaw is characterized using Auger electron spectroscopy, its surface oxide film reveals constituents of calcium, phosphorus, and sulfur [7, 8]. By immersing titanium and its alloys in Hanks' solution and other solutions [9–12] (Fig. 5.3), preferential adsorption of phosphate ions occurs. Even during cell culture on titanium, calcium phosphate is formed on it [13]. Extrapolating from here, it can be assumed that bone formation is faster on titanium implanted in hard tissue simply because the surface oxide film is titanium oxide. The surface oxide film

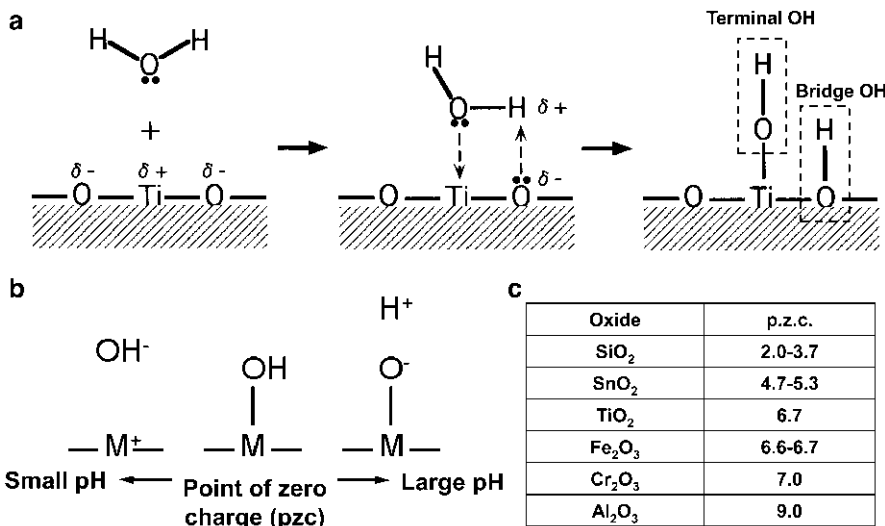


**Fig. 5.4** Formation of surface hydroxyl groups on titanium oxide by the adsorption of water molecules (a), dissociation of hydroxyl groups in aqueous solutions including body fluid and showing positive and negative charges according to the environmental pH (b), and point of zero charge (pzc) of various oxide (c)

on titanium is not completely oxidized and is relatively reactive; neither calcium nor phosphate stably exists alone on titanium, and calcium phosphate is naturally formed on it; calcium phosphate formed on titanium is stable and protective [14]. Surface oxide films as passive films on valve metals such as Ti are almost amorphous and different from titanium oxide bulk and crystalline ceramics with regard to its chemical property.

The surface oxide is always formed on conventional metallic biomaterials and the surface of the surface oxide is active. Therefore, the oxide surface immediately reacts with water molecules and hydroxyl groups are formed as shown in Fig. 5.4a. The surface hydroxyl groups contain both terminal OH and bridge OH in the equal amounts. Concentration of hydroxyl groups on the unit area of the surface is determined with various techniques. Active surface hydroxyl groups dissociates in aqueous solutions and forms electric charges as shown in Fig. 5.4b [15–18]. Positive or negative charge due to the dissociation is governed by pH of the surrounding aqueous solution: positive and negative charges are balanced and apparent charge is zero at a certain pH. This pH is the point of zero charge (pzc). The pzc is the unique value for an oxide and an indicator which the oxide shows acidic or basic property. For example, in the case of TiO<sub>2</sub>, the pzc of rutile is 5.3 and that of anatase is 6.2 [15] (Fig. 5.4c). In other words, anatase surface is acidic at smaller pH and basic at larger pH than 6.2. Active surface hydroxyl groups and electric charges formed by the dissociation of the groups play important roles for the bonding with polymers and immobilization of biomolecules. Therefore, the

concentration of surface hydroxyl group and pH is important factors for the bonding with polymeric materials and immobilization of biomolecules.

Proteins adsorption influences cells adhesion. Likewise, proteins denaturalization and fragmentation (which occur due to adsorption) may affect the function of the host body. To characterize proteins adsorbed to metals and metal oxides, various techniques can be used [19], especially that of ellipsometry [20]. To predict proteins adsorption, the wettability test is used where a liquid droplet is applied to the material [21]. Fibrinogen is much more naturally adsorbed on titanium surface than on gold surface, because the dielectric constant, the factor governing electrostatic force, of  $\text{TiO}_2$  is 80.1 and similar to that of water [22]. Therefore, fibrinogen remains its conformation even after the adsorption on titanium surface.

As described above, many researchers made their effort to elucidate the mechanism of osseointegration by characterization of titanium surface oxide (composition and change of it), surface hydroxyl groups, adsorption of proteins (amount, speed, change in the conformation, and denaturalization), and adhesion, proliferation and differentiation of cells. However, the true mechanism of osseointegration is still not clear.

## 5.5 Nanometer-Level Interface Structure

On the other hand, micrometer and nanometer-level observation of the interface between titanium and tissue has been studied. The intact bone-to-titanium interface consists of a fibrous tissue-free boundary zone with a 20–40 nm thick proteoglycan coat immediately adjacent to titanium oxide are revealed [23, 24]. Bundles of collagen appear at a minimum distance of 100–200 nm from the interface. Calcium deposits were sometimes seen in direct contacted (resolution level 30–50 nm) with the titanium oxide. The similar variation in interface ultrastructure within 50–100 nm of titanium surface [25]. The collagen fibrils did not reach the implant surface but were separated from it by an amorphous layer, being 300–500 nm thick which did not decrease in width with time [26]. An electron-dense lamina limitans-like line containing mineral was observed between the amorphous layer and the bone tissue. On the other hand, amorphous proteoglycan layer is not interposed at the interface between bone and titanium was observed [27]. In addition, this lamina limitans seems to consist of osteopontin and  $\alpha 2$  HS-glycoprotein [28]. Recently, osteoblast-like cells made direct contact with titanium via a 20–50 nm thin amorphous zone is shown [29]. A 20–50 nm thin amorphous zone, a slender cell layer, and/or a poorly mineralized zone were interposed between bone and titanium. There is apparently a 20–50 nm amorphous layer containing proteoglycan on titanium oxide according to the above studies. Relatively high-resolutioinal observation using transmission electron microscopy is feasible in the findings regarding structure of the interface. However, it is difficult to make a tissue specimen with metallic material for TEM observation. Therefore, a couple of studies [24, 25] employed a

foil and sputter-coated film of titanium instead of bulk material to be easily sectioned with a microtome. That is, the structure at the interface near titanium is unclear, while the observation of the interface is currently continued [30].

## 5.6 Surface Treatment

### 5.6.1 *Change of Research Trend*

The above researches on the elucidation of osseointegration mechanism and characterization of structure at the interface, now showed down and research trend moved to surface treatment for bone formation on titanium. Tremendous amount of surface treatment researches has been conducted, while some of the researches are left important matters behind somewhere. In these researches, the control is usually untreated titanium. Therefore, some researchers declare that “titanium is bioinert” to demonstrate the effective results of their surface treatment. Origin of this misunderstanding is that no apatite forms on titanium by SEM-level after immersion in Kokubo’s simulated body fluid (SBF) [31, 32]. Where has the initial definition of “osseointegration” of titanium gone? The true story is as follows: Titanium shows the best bone conduction among metallic materials, while the ability is much lower than bioactive ceramics.

### 5.6.2 *Surface Treatment*

Surface treatment is a process that changes a material’s surface composition, structure, and morphology, leaving the bulk mechanical properties intact. With surface treatment, the tissue compatibility of the surface layer can be improved, as shown in Fig. 5.5. Surface treatment techniques by both dry and wet processes used in research and industry are summarized in Fig. 5.6. Surface treatment techniques are reviewed elsewhere [33, 34].

### 5.6.3 *Surface Treatment for Bone Formation*

Titanium and its alloys, which show good hard tissue compatibility, are used for dental implants and artificial hip joints. However, the hard-tissue compatibility of these materials is lower than that of bioactive ceramics, such as hydroxyapatite and bioactive glasses. Therefore, numerous surface treatment techniques to improve the hard tissue compatibility of titanium have been developed, and some have been commercialized.

### **Properties required to surface of materials**

- Bone formation; Bone bonding
- Inhibition of bone formation
- Adhesion to soft tissue
- Blood compatibility
- Inhibition of biofilm formation

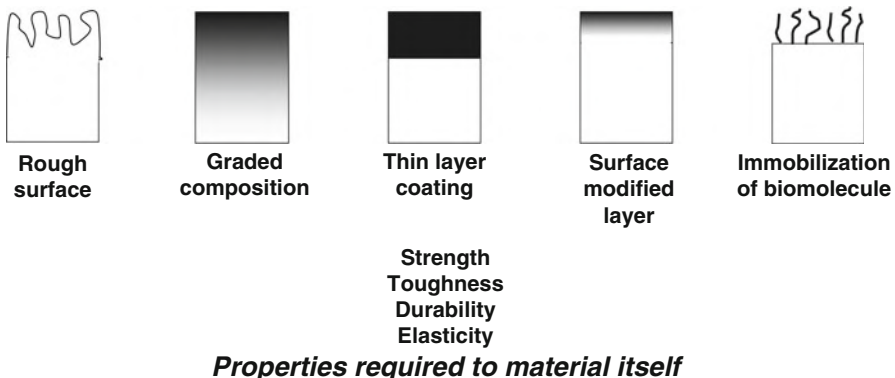


**Fig. 5.5** Category of surface treatment of metallic materials to add biocompatibility and biofunctions remaining good mechanical property

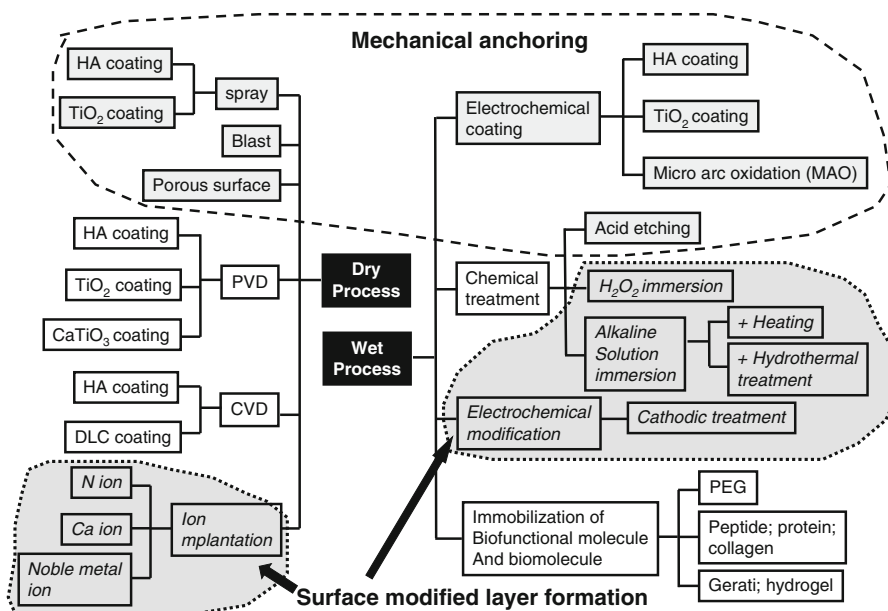


**Fig. 5.6** Surface treatment techniques by dry and wet processes attempted in researches. Some of them are commercialized

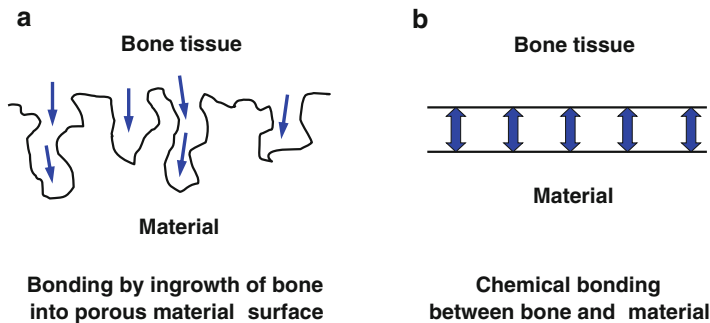


**Fig. 5.7** Mechanical anchoring (a) and chemical bonding (b) between bone and material

In the stems of artificial hip joints and dental implants, the chemical bonding of metal surfaces with bone is not expected. In other words, it is impossible for metals as typical artificial materials to chemically and naturally bond with bone as living tissue, especially in the human body with body fluid. Therefore, the surface morphology is sometimes controlled, and rough and porous surface is formed in titanium. Living tissue, such as bone, is expected to grow into the rough porous surface, and the materials and bone are strongly connected as a result of the so-called anchoring effect. Figure 5.7 shows chemical bonding and a mechanical anchoring connection between bone and material.

#### 5.6.4 Evolution of Surface Treatment for Bone Formation

Figure 5.8 shows the evolution of surface treatment techniques to improve hard tissue compatibility at the research level:

First generation: Grind machining of the surface.

Second generation: Grooving, blast, acid etching, anodic oxidation, and laser abrasion.

Third generation: Chemical treatment and hydroxyapatite coating.

Fourth generation: Immobilization of biofunctional molecules (collagen, bone morphogenetic protein, and peptide).

Fifth generation: Coating of stem cells and tissues?

The bone formation of the materials surface is accelerated when biomolecules concerning bone formation are immobilized on the material surface, such as in the fourth generation in Fig. 5.8. Therefore, many studies have achieved good results in this direction. However, to increase the popularity of the immobilization of biofunctional molecules, it is necessary to ensure the safety, quality maintenance during storage, and dry-conditioned durability of the immobilized layer. Therefore, it is difficult for manufacturers to commercialize those research results. Most of commercialized goods are categorized into the second generation, a few belong to

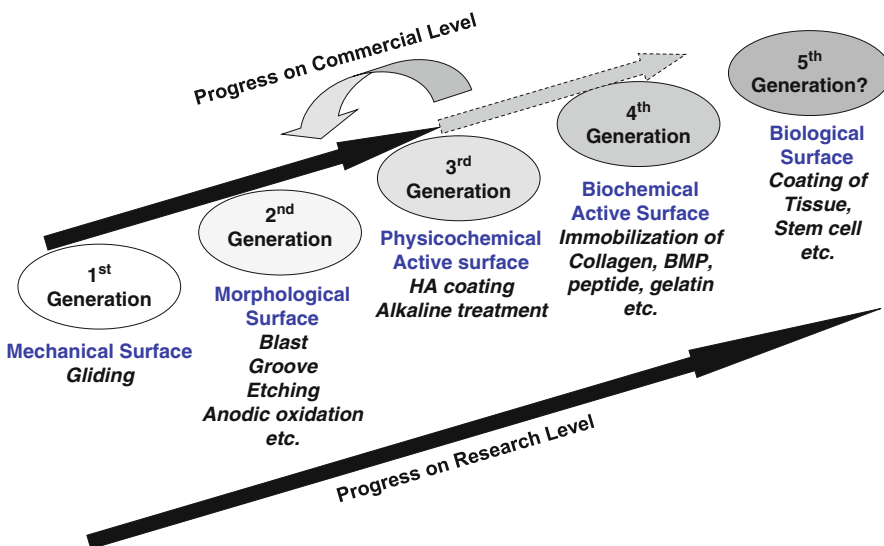


**Fig. 5.8** The evolution of surface treatment techniques to improve hard tissue compatibility at the research level

the third generation, and there is no prospect for the commercialization of the fourth generation, at present. The commercialization went faster for the second than third generation possibly because materials employing mechanical anchoring are more practical than materials employing chemical bonding with bone.

On researches developing new surface treatment techniques, biocompatibility and biofunction are usually focused, while sometimes mechanical properties, durability, and manufacturing process are left behind, that may delays the utilization of the technique. Most of researchers make the best effort to evaluate biological effects with cell culture and animal test; they hesitate conduct the evaluation of durability. They sometimes do not remember “materials engineering”, while remind only materials chemistry and biological evaluation.

However, immobilization of biomolecules and biofunctional molecules as shown as the fourth generation above is effective tool to add biofunction to metal surface. This subject is reviewed somewhere [35].

## 5.7 Conclusions

Metallic materials are widely used in medicine not only for orthopedic implants and dental implants, but also for cardiovascular devices and for other purposes. Metallic biomaterials are always used in close contact with living tissues. Therefore, interactions between material surfaces and living tissues must be well controlled. Metal surface may be biofunctionalized by various surface treatment techniques. These techniques make it possible to apply metals to a scaffold in tissue engineering.

**Open Access** This chapter is distributed under the terms of the Creative Commons Attribution Noncommercial License, which permits any noncommercial use, distribution, and reproduction in any medium, provided the original author(s) and source are credited.

## References

- Bränemark PI, Hansson BO, Adell R, Breine U, Lindström J, Hallén O, Ohman A. Osseointegrated implants in the treatment of the edentulous jaw. Experience from a 10-year period. *Scand J Plast Reconstr Surg Suppl.* 1977;16:1–132.
- Itakura Y, Tajima T, Ohkoh S, Matsuzawa J, Sudo H, Yamamoto S. Osteocompatibility of platinum-plated titanium assessed in vitro. *Biomaterials.* 1989;10:489–93.
- Lausmaa J, Kasemo B, Mattsson H. Surface spectroscopic characterization of titanium implant materials. *Appl Surf Sci.* 1990;44:133–46.
- Lausmaa J, Kasemo B, Mattsson H, Odellius H. Multi-technique surface spectroscopic characterization of electropolished and anodized Ti. *Appl Surf Sci.* 1990;45:189–200.
- Healy KE, Ducheyne P. Hydration and preferential molecular adsorption on titanium in vitro. *J Biomed Mater Res.* 1992;26:319–38.
- Healy KE, Ducheyne P. Hydration and preferential molecular adsorption on titanium in vitro. *Biomaterials.* 1992;13:553–61.
- Espostito M, Lausmaa J, Hirsch JM, Thomsen P. Surface analysis of failed oral titanium implants. *J Biomed Mater Res Appl Biomater.* 1999;48:559–68.
- Hanawa T, Ota M. Characterization of surface film formed on titanium in electrolyte. *Appl Surf Sci.* 1992;55:269–76.
- Hanawa T. Titanium and its oxide film: a substrate for formation of apatite. In: Davies JE, editor. *The bone-biomaterial interface.* Toronto: University of Toronto Press; 1991. p. 49–61.
- Hanawa T, Okuno O, Hamanaka H. Compositional change in surface of Ti-Zr alloys in artificial bioliquid. *J Jpn Inst Met.* 1992;56:1168–73.
- Bruesch P, Muller K, Atrens A, Neff H. Corrosion of stainless-steels in chloride solution—an XPS investigation of passive films bruesch. *Appl Phys.* 1985;38:1–18.
- Sundgren JE, Bodo P, Lundstrom I. Auger electron spectroscopic studies of the interface between human tissue and implants of titanium and stainless steel. *J Colloid Interface Sci.* 1986;110:9–20.
- Hiromoto S, Hanawa T, Asami K. Composition of surface oxide film of titanium with culturing murine fibroblasts L929. *Biomaterials.* 2004;25:979–86.
- Tsutsumi Y, Nishimura D, Doi H, Nomura N, Hanawa T. Difference in surface reactions between titanium and zirconium in Hanks' solution to elucidate mechanism of calcium phosphate formation on titanium using XPS and cathodic polarization. *Mater Sci Eng C.* 2009;29:1702–8.
- Parfitt GD. The surface of titanium dioxide. *Progr Surf Membr Sci.* 1976;11:181–226.
- Westall J, Hohl H. A comparison of electrostatic models for the oxide/solution interface. *Adv Colloid Interface Sci.* 1980;12:265–94.
- Healy TW, Fuerstenau DW. The oxide-water interface-Interaction of the zero point of charge and the heat of immersion. *J Colloid Sci.* 1965;20:376–86.
- Boehm HP. Acidic and basic properties of hydroxylated metal oxide surfaces. *Discuss Faraday Soc.* 1971;52:264–89.
- Ivarsson B, Lundström I. Physical characterization of protein adsorption on metal and metal oxide surfaces. *CRC Critic Rev Biocompat.* 1986;2:1–96.
- Elwing H. Protein absorption and ellipsometry in biomaterial research. *Biomaterials.* 1998;19:397–406.
- Bagnall RD, Arundel PA. A method for the prediction of protein adsorption on implant surfaces. *J Biomed Mater Res.* 1983;17:459–66.

22. Sundgren JE, Bodö P, Ivarsson B, Lundström I. Adsorption of fibrinogen on titanium and gold surfaces studied by ESCA and ellipsometry. *J Colloid Interface Sci.* 1986;113:530–43.
23. Albrektsson T, Hansson HA, Ivarsson B. Interface analysis of titanium and zirconium bone implants. *Biomaterials.* 1985;6:97–101.
24. Albrektsson T, Hansson HA. An ultrastructural characterization of the interface between bone and sputtered titanium or stainless steel surfaces. *Biomaterials.* 1986;7:201–5.
25. Linder L, Obrant K, Boivin G. Osseointegration of metallic implants. II. Transmission electron microscopy in the rabbit. *Acta Orthop Scand.* 1989;60:235–9.
26. Sennery L, Thomsen P, Ericson LE. Early tissue response to titanium implants inserted in rabbit cortical bone. *J Mater Sci Mater Med.* 1993;4:494–502.
27. Listgarten MA, Buser D, Steinemann SG, Donath K, Lang NP, Weber HP. Light and transmission electron microscopy of the intact interfaces between non-submerged titanium-coated epoxy resin implants and bone or gingiva. *J Dent Res.* 1992;71:364–71.
28. Nanci A, McCarthy GF, Zalzal S, Clokie CML, Warshawsky H, McKee MD. Tissue response to titanium implants in the rat tibia: ultrastructural immunocytochemical and lectin-cytochemical characterization of the bone-titanium interface. *Cell Mater.* 1994;4:1–30.
29. Murai K, Takeshita F, Ayukawa Y, Kiyoshima T, Suetsgu T, Tanaka T. Light and electron microscopic studies of bone-titanium interface in the tibiae of young and mature rats. *J Biomed Mater Res.* 1996;30:523–33.
30. Brunette DM, Tengvall P, Textor M, Thomsen P, editors. Titanium in medicine. Berlin: Springer; 2001.
31. ISO23317:2007. Implants for surgery. In vitro evaluation for apatite-forming ability of implant materials. Geneva: International Organization for Standardization; 2007.
32. Kokubo T, Takadama H. How useful is SBF in predicting in vivo bone bioactivity? *Biomaterials.* 2006;27:2907–15.
33. Hanawa T. An overview of biofunctionalisation of metals in Japan. *J R Soc Interface.* 2009;6: S361–9.
34. Hanawa T. Biofunctionalization of titanium for dental implant. *Jpn J Dent Sci Rev.* 2010;46:93–101.
35. Hanawa T. Metal-polymer composite biomaterials. In: Dumitriu S, Popa V, editors. Polymeric biomaterials Vol. 1, Structure and function. Boca Raton: CRC; 2013. p. 343–75.

# **Chapter 6**

## **Evaluation of Photocatalytic Activity of the TiO<sub>2</sub> Layer Formed on Ti by Thermal Oxidation**

**Takayuki Narushima, Shota Sado, Natsumi Kondo, Kyosuke Ueda,  
Mitsuko Kawano, and Kouetsu Ogasawara**

**Abstract** Two-step thermal oxidation was proposed for Ti and Ti alloys as a surface-treatment process for preparing an anatase-containing TiO<sub>2</sub> layer. This process consisted of treatment in a CO-containing atmosphere (first step) and subsequent treatment in air (second step). In this chapter, first, the current status of TiO<sub>2</sub> coating onto Ti and Ti alloys for biomedical applications is reviewed; then our recent work on the phase and microstructure of TiO<sub>2</sub> layers prepared on commercially pure (CP) Ti, Ti-25mass%Mo alloy, and Ti-25mass%Nb alloy by two-step thermal oxidation is described. The anatase fraction in the TiO<sub>2</sub> layer was controlled through process parameters such as the second-step temperature. Finally, photocatalytic activity of TiO<sub>2</sub> layers formed on the Ti and Ti alloys is evaluated, including: results of water contact angle, decomposition of methylene blue, and antibacterial effects.

**Keywords** Anatase • Antibacterial activity • Photocatalytic activity • Thermal oxidation • Ti and Ti alloys

---

T. Narushima (✉) • S. Sado • N. Kondo • K. Ueda

Department of Materials Processing, Tohoku University, Sendai 980-8579, Japan  
e-mail: [narut@material.tohoku.ac.jp](mailto:narut@material.tohoku.ac.jp)

M. Kawano

Department of Immunobiology, Institute of Development, Aging and Cancer,  
Tohoku University, Sendai 980-8575, Japan

K. Ogasawara

Department of Immunobiology, Institute of Development, Aging and Cancer,  
Tohoku University, Sendai 980-8575, Japan

Department of Intractable Diseases and Immunology,  
Tohoku University, Sendai 980-8575, Japan

## 6.1 Introduction

Ti and Ti alloys are important metallic biomaterials as well as stainless steels and Co-Cr alloys because of their excellent properties such as high specific strength, high corrosion resistance, and low allergenicity [1, 2]. Since they can be directly connected to living bone at an optical microscopic level, i.e., osseointegration [3, 4], they have been used as substitutes for hard tissues such as in the stems of artificial hip joints and in dental implants, where implantation in bones for the long-term is expected. However, a relatively long time is required for establishing osseointegration, and fixation between Ti implants and bones can be influenced by the state of the bones and by the implant/bone interfacial area. Surface modification is a promising way to improve bone compatibility of Ti implants [5], while leaving bulk mechanical properties intact.

Surface modification used to improve bone compatibility of Ti implants is conducted from the point of view of the morphology and phase/composition of their surfaces [6–8]. The aim of modifying surface morphology is to increase adhesion between bones and implants by an anchorage effect, while the purpose of phase/composition modification is to form either an apatite coating, or a non-apatite coating that enhances the formation of apatite [7].

We have reported amorphous calcium phosphate coating using RF magnetron sputtering [8–10], and  $\text{TiO}_2$  coating using thermal oxidation [11–13], as surface modifications of Ti and Ti alloys for biomedical applications. In this chapter, first, the current status of  $\text{TiO}_2$  coating of Ti and Ti alloys is reviewed, and then our recent work on preparation and evaluation of photocatalytic activity of  $\text{TiO}_2$  layers on Ti and Ti alloys formed by a two-step thermal oxidation process is described.

## 6.2 $\text{TiO}_2$ Layers on Ti and Ti Alloys for Biomedical Applications

$\text{TiO}_2$  layers on Ti and Ti alloys are reported to be effective for improving biological performance such as biomimetic growth of apatite [14], initial adhesion of osteoblast-like cells [15], bone-bonding ability [16], and bone growth [17]; in fact, Ti implants coated with a porous  $\text{TiO}_2$  layer through anodic oxidation are clinically used [18]. It is known that  $\text{TiO}_2$  can exhibit photocatalytic activity [19, 20]. Photo-induced superhydrophilicity and photocatalytic oxidation of organic compounds are closely related to biological phenomena on the  $\text{TiO}_2$  surface such as cell response, removal of hydrocarbons, and antibacterial properties [21–23].

$\text{TiO}_2$  has three polymorphic phases at atmospheric pressure: rutile, anatase, and brookite. Rutile is a thermodynamically stable phase on the macroscale, with the stability of these phases depending on particle size. Rutile and anatase are the most stable phase for particles above 35 nm and below 11 nm, respectively, and

brookite has been found to be the most stable for nanoparticles in the 11–35 nm range [20, 24]. Anatase is considered to possess excellent bone compatibility [14, 16, 25], and the photocatalytic activities of anatase [19, 26], anatase + rutile composite [27], and anatase + brookite composite [28] are reported to be high, although the precise reason for different photocatalytic activities has not been elucidated in detail [20].

Many processes for preparing TiO<sub>2</sub> layers on Ti and Ti alloys have been investigated including chemical vapor deposition [29], physical vapor deposition [30], anodic oxidation/micro arc oxidation (MAO) [31, 32], and sol–gel [33] methods. Thermal oxidation, which is based on the reaction between an oxidizing gas and Ti at elevated temperatures, is a simple and low-cost method to prepare TiO<sub>2</sub> layers on Ti with excellent adherence and high crystallinity, and can be applied to substrates with a complex geometry.

The thermal oxidation of commercially pure (CP) Ti in air and oxygen has been reported since the 1950s [34]. Recently, the oxide layer on Ti and/or the oxygen-dissolved and hardened layer of Ti prepared by thermal oxidation have been utilized for improving corrosion and wear resistance [35–37]. Browne and Gregson [38] showed that the air oxidation treatment at 673 K for 2.7 ks for Ti-6Al-4V implants reduced metal ion dissolution into bovine serum, particularly in the early stages.

The major product obtained in the thermal oxidation of Ti and Ti alloys has been reported to be the thermodynamically stable rutile [37]. A few reports show formation of the anatase phase in thermal oxidation of Ti and Ti alloys [39, 40]. Borgioli et al. [39] reported the formation of rutile + anatase in the oxide film on a Ti–6Al–4V alloy after glow-discharge processing in air at a total gas pressure of 0.01 atm. Lee and Park [40], using oxidation in a wet oxygen atmosphere for 10.8 ks at 683 K in combination with post-annealing in air at 773 K, showed formation of a Ti<sub>5</sub>O<sub>7</sub> + anatase layer on a magnetron-sputtered Ti thin film. In these reports, however, the main oxidation products were rutile and Ti<sub>5</sub>O<sub>7</sub> phases, namely, not an anatase-rich TiO<sub>2</sub> layer.

On the other hand, it is known that anatase is formed as a main product in thermal oxidation of TiC [41, 42] and TiN [43]. Shabalin et al. [42] presented an oxidation model of TiC, in which incorporation of carbon in TiO<sub>2</sub> stabilized the anatase phase. Meanwhile, Kao et al. [44] observed the reversible transformation between TiO having an NaCl-type structure and anatase. They pointed out the similarity between their structures: TiC and TiN exhibit NaCl type structure with a lattice constant close to TiO; the anatase formation on TiC and TiN in thermal oxidation would be related to this NaCl-type structure.

Based on the information on anatase formation on TiC and TiN under thermal oxidation, we proposed and investigated a two-step thermal oxidation process in which an anatase-rich TiO<sub>2</sub> layer is formed on Ti and Ti alloys [11–13]. The preparation and photocatalytic evaluation of TiO<sub>2</sub> layers formed on Ti and Ti alloys by two-step thermal oxidation are described in Sects. 6.3 and 6.4, respectively.

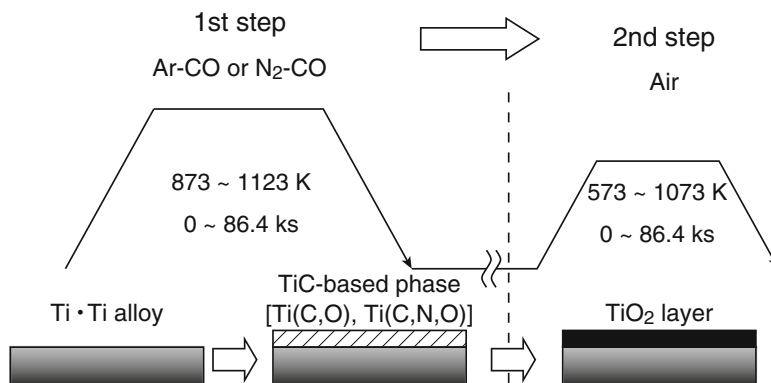
### 6.3 Preparation of Anatase-Rich TiO<sub>2</sub> Layer on Ti and Ti Alloys

Figure 6.1 schematically shows the process of two-step thermal oxidation. This process consists of treatment in CO-containing atmospheres such as Ar-CO [11] and N<sub>2</sub>-CO [12] gas mixtures (first step) and subsequent treatment in air (second step). A Ti(C,O) or Ti(C,N,O) phase is formed on the Ti and Ti alloys in the first step and converted to TiO<sub>2</sub> through air oxidation in the second step.

The  $\alpha$ -2θ XRD patterns ( $\alpha = 0.3^\circ$ , Cu K $\alpha$ ) of the reaction layer on CP Ti, Ti-25mass%Mo (Ti-25Mo) alloy, and Ti-25mass%Nb (Ti-25Nb) alloy after the first-step treatment in Ar-1%CO at 1,073 K for 3.6 ks are shown in Fig. 6.2. Reflections that are located close to but at a slightly higher angle than those of TiC are observed. It is known that oxygen substitution in a carbon site decreases the lattice parameter of TiC [42]; in fact, the reflections of the reaction layer are located between those of TiC and TiO as shown in Fig. 6.2. In addition, chemical composition analysis by X-ray photoelectron spectroscopy (XPS) revealed the presence of oxygen in the reaction layer as well as carbon and Ti [11]. From these results, the phase of the reaction layer is considered to be Ti(C,O). In the case of using an N<sub>2</sub>-CO gas atmosphere in the first step, a Ti(C,N,O) reaction layer was formed [12]. Figure 6.3a, b depict potential diagrams of Ti-C-O and Ti-C-N-O systems respectively, at 1,100 K [11, 12]. The chemical composition of Ti(C,O) and Ti(C,N,O) phases was arbitrarily chosen as TiC<sub>0.5</sub>O<sub>0.5</sub> because of the lack of reliable thermodynamic data for these phases. The relationship between carbon activity ( $a_C$ ) and oxygen partial pressure ( $P_{O_2}$ ) suggests that the TiC<sub>0.5</sub>O<sub>0.5</sub> phase is thermodynamically stable at a CO partial pressure ( $P_{CO}$ ) of 0.01 atm, which corresponds to Ar-1%CO and N<sub>2</sub>-1%CO.

Figure 6.4 shows cross-sectional SEM images of the Ti(C,O) and Ti(C,N,O) layers, which were formed in Ar-1%CO and N<sub>2</sub>-1%CO, respectively. From the images, it was confirmed that the films were dense and uniform.

The phase fraction in TiO<sub>2</sub> layers formed on CP Ti, Ti-25Mo alloy, and Ti-25Nb alloy at different second-step temperatures and holding times are summarized in



**Fig. 6.1** Schematic of the two-step thermal oxidation process

**Fig. 6.2**  $\alpha$ -2 $\theta$  XRD patterns of the reaction layers on CP Ti, Ti-25Mo alloy, and Ti-25Nb alloy after first-step treatment in Ar-1%CO at 1,073 K for 3.6 ks

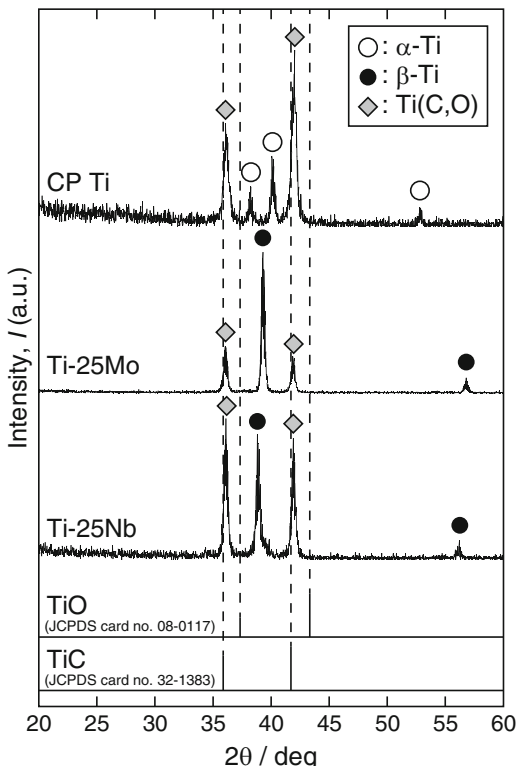


Fig. 6.5a–c, respectively [13]. The first-step treatment was carried out in Ar-1%CO at 1,073 K for 3.6 ks, and the reaction layer was confirmed to be Ti(C,O) single phase after the first-step. The phase fractions of anatase and rutile in TiO<sub>2</sub> layer were calculated using the equation given by Spurr and Myers [45]. The anatase-rich TiO<sub>2</sub> layers were formed for second-step temperatures between 673 and 873 K. At a lower temperature of 573 K, single-phase anatase was produced, but the Ti(C,O) phase remained, indicating that the oxidation reaction from Ti(C,O) to TiO<sub>2</sub> was not completed in the second step. On the other hand, thermodynamically stable rutile was a main phase in the TiO<sub>2</sub> layers for the higher second-step temperatures of 973 and 1,073 K. At these higher temperatures, rutile single phase was detected on CP Ti, while anatase was detected as a minor phase on Ti-25Mo and Ti-25Nb alloys. Moreover, the anatase fraction in the TiO<sub>2</sub> layer on Ti-25Mo and Ti-25Nb alloys was higher than on CP Ti at mid-level temperatures of 773 and 873 K. The formation window for anatase in two-step thermal oxidation of Ti alloys is wider than that of CP Ti.

Anatase irreversibly transforms to rutile at high temperatures, and the larger the valence number and ionic radius of dopants in TiO<sub>2</sub>, the more suppressed the anatase-to-rutile transformation: the transformation is enhanced by relaxation of the large oxygen sublattice through the increased presence of oxygen vacancies [46].

**Fig. 6.3** Potential diagrams for the (a) Ti-C-O system and (b) Ti-C-N-O system ( $N_2$  pressure: 0.1 MPa) at 1,100 K [11, 12]

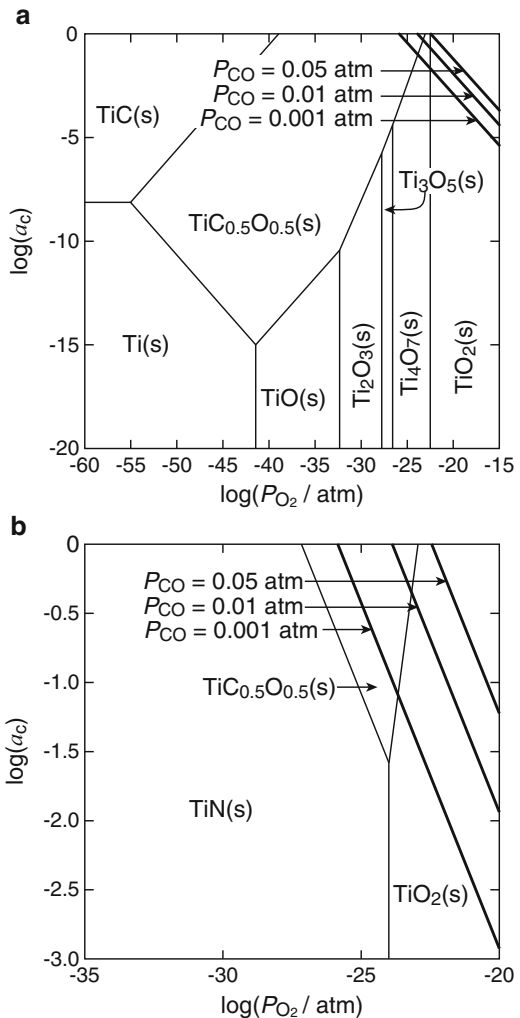
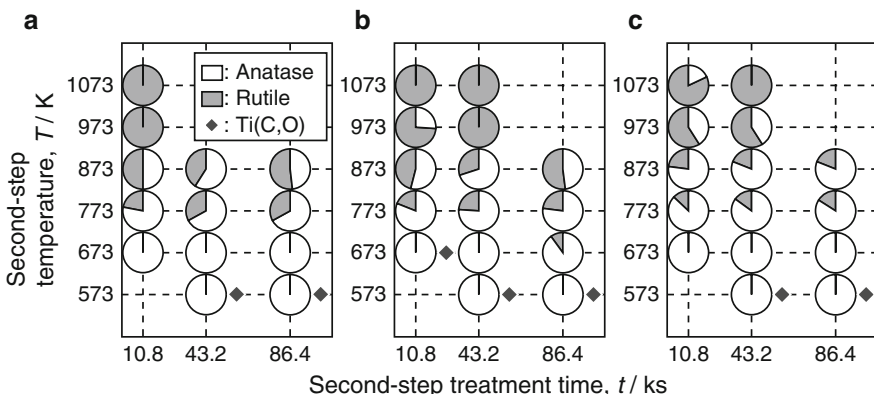
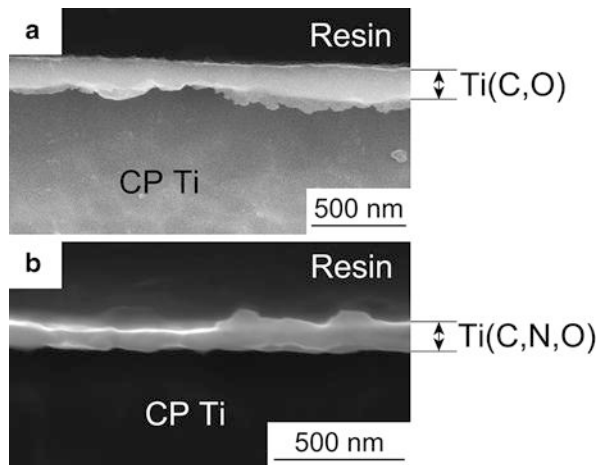


Figure 6.6 shows the comprehensive valence/radius plot of the anatase-to-rutile transformation, categorizing  $TiO_2$  dopants as inhibiting or promoting [46]. From this figure, Mo and Nb are likely inhibiting dopants. The incorporation of Mo and Nb into the  $TiO_2$  layer during two-step thermal oxidation process may have resulted in the presence of anatase on the Ti alloys at higher second-step temperatures and the higher anatase fraction at mid-level temperatures.

The formation of the  $Ti(C,O)$  or  $Ti(C,N,O)$  single phase during the first step and optimization of the second-step temperature are required for preparing an anatase-rich  $TiO_2$  layer on Ti and Ti alloys. We varied CO partial pressures in the first-step treatment between Ar- or  $N_2$ -0.1%CO and 20%CO. The rutile phase tended to form to a greater degree in the first-step treatment under higher partial pressures (up to 20 %) of CO gas, because of its high oxidizing potential.

**Fig. 6.4** Cross sections of (a) Ti(C,O) and (b) Ti(C,N,O) layers on CP Ti after the treatments in Ar-1%CO and N<sub>2</sub>-1%CO, respectively [11, 12]



**Fig. 6.5** Phase fraction of the reaction layer on (a) CP Ti, (b) Ti-25Mo alloy, and (c) Ti-25Nb alloy after the second-step treatment in air [13]. Grey and white parts in small circles show rutile and anatase fractions, respectively

Figure 6.7a, b show a cross-sectional TEM image and an electron diffraction pattern, respectively, of the anatase + rutile TiO<sub>2</sub> layer formed on CP Ti after a second-step treatment at 673 K that was preceded by a first-step treatment at 1,073 K in N<sub>2</sub>-1%CO [12]. Nanoscale crystallites of anatase and rutile are observed. The thickness of the TiO<sub>2</sub> layer formed in the second-step at 873 K was much greater than that formed in the 573–773 K range [12]. This result suggests that the formation of the rutile phase at higher second-step temperatures is also caused by direct oxidation of metallic Ti after completion of oxidation of the Ti(C,O) or Ti(C,N,O) layer.

Bonding strength of the anatase-rich TiO<sub>2</sub> layer to the CP Ti substrate was evaluated by a pulling test using an Al stud, and was greater than the strength of the epoxy glue (60–70 MPa) used for bonding between the TiO<sub>2</sub> layer and the Al stud [14]. The high bonding strength is an advantage of the thermal oxidation process over wet processes such as anodic oxidation.

**Fig. 6.6** Comprehensive valence/radius plot of anatase-to-rutile transformation, categorizing dopants as inhibiting or promoting [46]

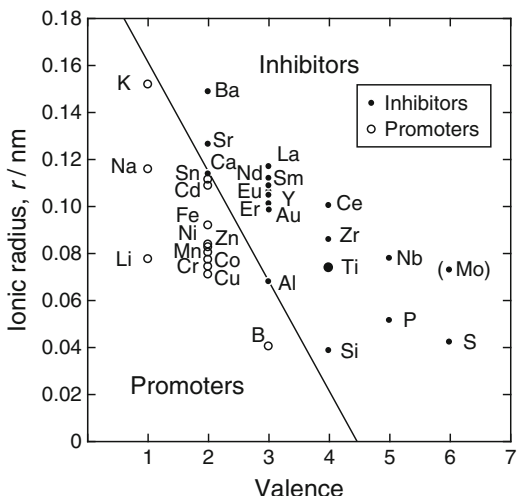
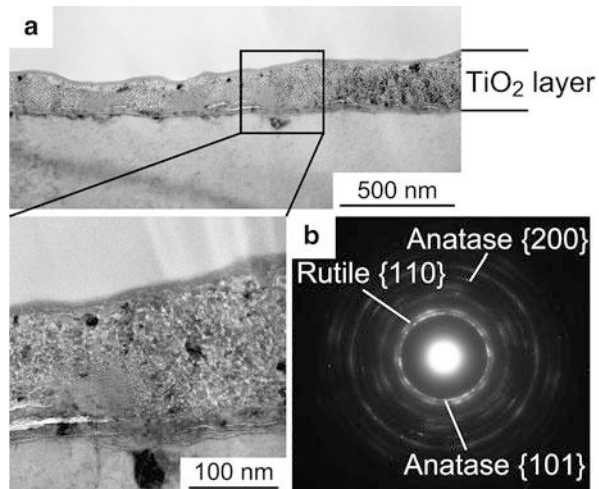


**Fig. 6.7** (a) Cross-sectional TEM image and (b) electron diffraction pattern of the  $\text{TiO}_2$  layer formed on CP Ti after two-step thermal oxidation [12]



## 6.4 Evaluation of Photocatalytic Activity of $\text{TiO}_2$ Layers Formed by Two-Step Thermal Oxidation

The photocatalytic activity of  $\text{TiO}_2$  layers prepared on CP Ti, Ti-25Mo alloy, and Ti-25Nb alloy was evaluated for water contact angle, decomposition of methylene blue (MB), and antibacterial effect under UV irradiation. Figure 6.8 shows the average water contact angle obtained for UV irradiation times of 3.6–7.2 ks with an irradiance of  $1 \text{ mW} \cdot \text{cm}^{-2}$  as a function of anatase fraction ( $f_A$ ) in  $\text{TiO}_2$  layers [13]. The water contact angle decreased with increasing  $f_A$ , and in particular, a water contact angle less than  $5^\circ$  was achieved on  $\text{TiO}_2$  layers for an  $f_A$  higher than 0.6.

**Fig. 6.8** Variation in water contact angle with anatase fraction ( $f_A$ ) of the TiO<sub>2</sub> layer under UV irradiation [13]

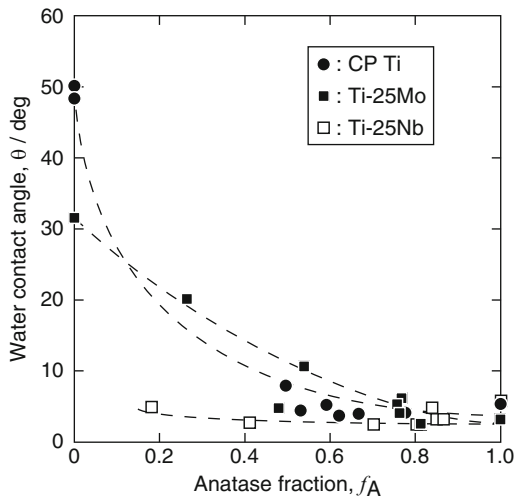
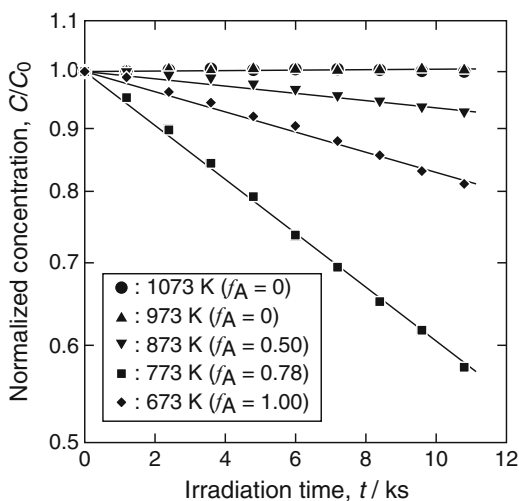


**Fig. 6.9** Degradation of methylene blue under UV irradiation on the TiO<sub>2</sub> layer with different anatase fractions ( $f_A$ ) formed on CP Ti



It is confirmed that anatase is effective for expression of superhydrophilicity. Meanwhile, in the case of Ti-25Nb alloy, a low water contact angle was observed even on TiO<sub>2</sub> layers with lower  $f_A$  values such as 0.2 and 0.4. The effect of Nb doping on the photocatalytic activity of TiO<sub>2</sub> was reported to be complex [47]. Further studies on the chemical state, concentration, and distribution of Nb in the TiO<sub>2</sub> layer are required. The water contact angle increased again under dark condition after UV irradiation; however, the hydrophobization rate was reduced in TiO<sub>2</sub> layers with high  $f_A$ .

Figure 6.9 shows the variation in concentration of MB with UV irradiation time on TiO<sub>2</sub> layers formed on CP Ti, Ti-25Mo alloy, and Ti-25Nb alloy. The values of

$f_A$  in the TiO<sub>2</sub> layers were controlled by varying the second-step temperature between 673 and 1,073 K. The rate constants for degradation of MB can be expressed by the gradients of the lines in Fig. 6.9. The anatase-containing TiO<sub>2</sub> layers exhibited higher decomposition rates compared to the rutile single-phase TiO<sub>2</sub> layers. The maximum rate constant was obtained at the  $f_A$  value of 0.78. Bickley et al. [48] proposed a synergistic effect between anatase and rutile in order to explain a greater photocatalytic activity of anatase + rutile + amorphous TiO<sub>2</sub> particles. Su et al. [49] reported that porous TiO<sub>2</sub> films with an  $f_A$  value of 0.6 exhibited optimal performance of photocatalytic activity and suggested a synergistic effect on photocatalytic activity: electrons excited in rutile can migrate to the conduction band of anatase, thereby effectively suppressing recombination of electrons and holes [49].

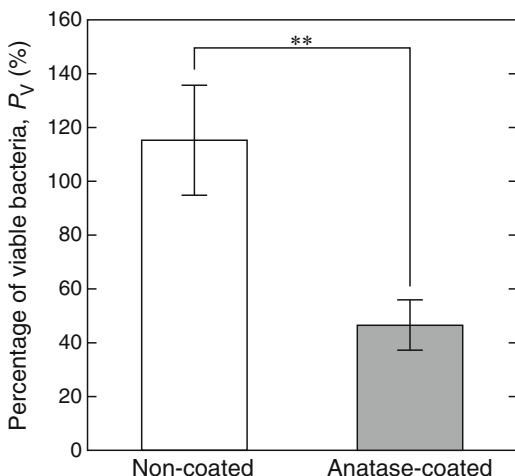
Antibacterial activities of a CP Ti plate coated with anatase single-phase TiO<sub>2</sub> layer by two-step thermal oxidation (Anatase-coated, 10 × 10 × 1 mm) and an as-polished CP Ti plate (Non-coated, 10 × 10 × 1 mm) were evaluated using gram-positive *E. coli* (DH 5α). All specimens were ultrasonically cleaned and sterilized in ethanol for 0.6 ks before the antibacterial tests. Solution (0.1 mL) containing the bacteria at a concentration of 10<sup>7</sup> CFU · mL<sup>-1</sup> diluted using 1/500 nutrient broth (NB) was dropped onto the specimen in a 24-well plate. The specimen was exposed to UV with an irradiance of 0.25 mW · cm<sup>-2</sup> at 298 ± 5 K in a dark room. After 10.8 ks incubation, the dropped bacterial solution was washed out from the specimen using 4.9 mL of phosphate buffered saline (PBS). The washed-out solution (0.1 mL) including bacteria was inoculated onto a standard NB agar culture plate ( $\phi = 90$  mm). The number of colonies resulting from the growth of viable bacteria was counted after incubation for 64.8 ks at 310 K, and the number of viable bacteria ( $N_{\text{sp}}$ ) was calculated. The same protocol was conducted with the well plate without specimen and the number of viable bacteria ( $N_{\text{well}}$ ) was also calculated. A percentage of viable bacteria ( $P_v$ ) was evaluated using a following equation.

$$P_v = N_{\text{sp}} / N_{\text{well}} \times 100 \quad (6.1)$$

Significant differences were statistically evaluated using Student's *t*-test.

Figure 6.10 shows the percentage of viable bacteria for the Non-coated and Anatase-coated specimens. The percentage of viable bacteria for Anatase-coated was significantly lower than for Non-coated. This result indicates that the anatase layer on Ti formed by two-step thermal oxidation is useful to improve the antibacterial activity of Ti implants. Many research groups have reported antibacterial activity of an anatase layer on Ti formed by anodic oxidation [50–52]. We have showed significant antibacterial activity of an anatase layer on Ti formed by a dry process: two-step thermal oxidation.

**Fig. 6.10** Percentage of viable bacteria of CP Ti plate coated with anatase single-phase TiO<sub>2</sub> layer (Anatase-coated) and as-polished CP Ti plate (Non-coated). (\*\*p < 0.01)



## 6.5 Summary

TiO<sub>2</sub> layers formed by thermal oxidation can improve the biological properties of Ti through their photocatalytic activity. Research and development of TiO<sub>2</sub> coatings on Ti implants for hard tissue replacement is continuing. In applications of TiO<sub>2</sub>-coated Ti implants, it would be preferable if the photocatalytic response of TiO<sub>2</sub> layers were to visible light. Theoretical and experimental studies are needed to further improve photocatalytic activity and clarify the detailed mechanism of photocatalytic activity of TiO<sub>2</sub> layers on Ti, which would relate to phase fraction, defect structure, and dopants. In particular, precise microscopic analyses of the structure and composition of TiO<sub>2</sub> thin layers on Ti are needed to aid in understanding their photocatalytic properties.

**Acknowledgements** This study was partially supported by a Grant-in-Aid for Scientific Research from the Ministry of Education, Culture, Sports, Science and Technology (MEXT), Japan.

**Open Access** This chapter is distributed under the terms of the Creative Commons Attribution Noncommercial License, which permits any noncommercial use, distribution, and reproduction in any medium, provided the original author(s) and source are credited.

## References

- Niinomi M, Hanawa T, Narushima T. Japanese research and development on metallic biomedical, dental, and healthcare materials. *JOM*. 2005;57(4):18–24.
- Niinomi M. Recent metallic materials for biomedical applications. *Metall Mater Trans A*. 2002;33:477–86.
- Bränemark P-I, Hansson BO, Adell R, Breine U, Lindström J, Hallén O, Öhman A. Osseointegrated implants in the treatment of the edentulous jaw, experience from a 10-year period. *Scand J Plast Reconstr Surg Suppl*. 1977;16:1–132.

4. Bränemark P-I. Osseointegration and its experimental background. *J Prosthet Dent.* 1983;50:399–410.
5. Goto T, Narushima T, Ueda K. Bio-ceramic coating on titanium by physical and chemical vapor deposition. In: Zhang S, editor. CRC handbook of biological and biomedical coatings. Boca Raton: CRC; 2011. p. 299–332.
6. Narushima T, Ueda K. Calcium phosphate coating on titanium by RF magnetron sputtering. In: Wu J, editor. Technological advancements in biomedicine for healthcare applications. Hershey: IGI Global; 2012. p. 223–33.
7. Hanawa T. Research and development of metals for medical devices based on clinical needs. *Sci Technol Adv Mater.* 2012;13:064102.
8. Narushima T, Ueda K, Goto T, Masumoto H, Katsume T, Kawamura H, Ouchi C, Iguchi Y. Preparation of calcium phosphate films by radiofrequency magnetron sputtering. *Mater Trans.* 2005;46:2246–52.
9. Ueda K, Narushima T, Goto T, Taira M, Katsume T. Fabrication of calcium phosphate films for coating on titanium substrates heated up to 773K by RF magnetron sputtering and their evaluations. *Biomed Mater.* 2007;2:S160–6.
10. Shiraishi N, Rong T, Uzuka R, Narushima T, Goto T, Niinomi M, Sasaki K, Suzuki O. Biomechanical evaluation of amorphous calcium phosphate coated TNTZ implants prepared using a radiofrequency magnetron sputtering system. *Mater Trans.* 2012;53:1343–8.
11. Okazumi T, Ueda K, Tajima K, Umetsu N, Narushima T. Anatase formation on titanium by two-step thermal oxidation. *J Mater Sci.* 2011;46:2998–3005.
12. Umetsu N, Sado S, Ueda K, Tajima K, Narushima T. Formation of anatase on commercially pure Ti by two-step thermal oxidation using N<sub>2</sub>-CO gas. *Mater Trans.* 2013;54:1302–7.
13. Narushima T, Ueda K, Sado S. Surface treatment of titanium using thermal oxidation for biomedical applications. *Corr Eng Jpn.* 2014;63:295–300.
14. Lin C-M, Yen S-K. Biomimetic growth of apatite on electrolytic TiO<sub>2</sub> coatings in simulated body fluid. *Mater Sci Eng C.* 2006;26:54–64.
15. Yang X-F, Chen Y, Yang F, He F-M, Zhao S-F. Enhanced initial adhesion of osteoblast-like cells on an anatase-structured titania surface formed by H<sub>2</sub>O<sub>2</sub>/HCl solution and heat treatment. *Dent Mater.* 2009;25:473–80.
16. Liang B, Fujibayashi S, Neo M, Tamura J, Kim H-M, Uchida M, Kokubo T, Nakamura T. Histological and mechanical investigation of the bone-bonding ability of anodically oxidized titanium in rabbits. *Biomaterials.* 2003;24:4959–66.
17. Hazan R, Brener R, Oron U. Bone growth to metal implants is regulated by their surface chemical properties. *Biomaterials.* 1993;14:570–4.
18. Degidi M, Nardi D, Piattelli A. 10-year follow-up of immediately loaded implants with TiUnite porous anodized surface. *Clin Implant Dent Relat Res.* 2012;14:828–38.
19. Fujishima A, Rao TN, Tryk DA. Titanium dioxide photocatalysis. *J Photochem Photobiol C Photochem Rev.* 2000;1:1–21.
20. Fujishima A, Zhang X, Tryk DA. TiO<sub>2</sub> photocatalysis and related surface phenomena. *Surf Sci Rep.* 2008;63:515–82.
21. Han Y, Chen D, Sun J, Zhang Y, Xu K. UV-enhanced bioactivity and cell response of micro-arc oxidized titania coatings. *Acta Biomater.* 2008;4:1518–29.
22. Aita H, Hori N, Takeuchi M, Suzuki T, Yamada M, Anpo M, Ogawa T. The effect of ultraviolet functionalization of titanium on integration with bone. *Biomaterials.* 2009;30:1015–25.
23. Sunada K, Watanabe T, Hashimoto K. Studies on photokilling of bacteria on TiO<sub>2</sub> thin film. *J Photochem Photobiol A Chem.* 2003;156:227–33.
24. Zhang H, Banfield JF. Understanding polymorphic phase transformation behavior during growth of nanocrystalline aggregates: insights from TiO<sub>2</sub>. *J Phys Chem B.* 2000;104:3481–7.
25. Cui X, Kim H-M, Kawashita M, Wang L, Xiong T, Kokubo T, Nakamura T. Preparation of bioactive titania films on titanium metal via anodic oxidation. *Dent Mater.* 2009;25:80–6.

26. Tanaka K, Capule MFV, Hisanaga T. Effect of crystallinity of TiO<sub>2</sub> on its photocatalytic action. *Chem Phys Lett.* 1991;187:73–6.
27. Kawahara T, Ozawa T, Iwasaki M, Tada H, Ito S. Photocatalytic activity of rutile–anatase coupled TiO<sub>2</sub> particles prepared by a dissolution–reprecipitation method. *J Colloid Interface Sci.* 2003;267:377–81.
28. Ozawa T, Iwasaki M, Tada H, Akita T, Tanaka K, Ito S. Low-temperature synthesis of anatase–brookite composite nanocrystals: the junction effect on photocatalytic activity. *J Colloid Interface Sci.* 2005;281:510–3.
29. Hirose F, Ito M, Kurita K. Low-temperature chemical vapor deposition of anatase TiO<sub>2</sub> with titanium tetraisopropoxide and H<sub>2</sub>O<sub>2</sub> vapor. *Jpn J Appl Phys.* 2008;47:5619–22.
30. Chaiyakun S, Pokaipisit A, Limsuwan P, Ngotawornchai B. Growth and characterization of nanostructured anatase phase TiO<sub>2</sub> thin films prepared by DC reactive unbalanced magnetron sputtering. *Appl Phys A.* 2009;95:579–87.
31. Diamanti MV, Pedeferri MP. Effect of anodic oxidation parameters on the titanium oxides formation. *Corr Sci.* 2007;49:939–48.
32. Ma C, Nagai A, Yamazaki Y, Toyama T, Tsutsumi Y, Hanawa T, Wang W, Yamashita K. Electrically polarized micro-arc oxidized TiO<sub>2</sub> coatings with enhanced surface hydrophilicity. *Acta Biomater.* 2012;8:860–5.
33. Arconada N, Durán A, Suárez S, Portela R, Coronado JM, Sánchez B, Castro Y. Synthesis and photocatalytic properties of dense and porous TiO<sub>2</sub>-anatase thin films prepared by sol-gel. *Appl Catal B Environ.* 2009;86:1–7.
34. Kofstad P, Anderson PB, Krudtaa OJ. Oxidation of titanium in the temperature range 800–1200°C. *J Less Common Met.* 1961;3:89–97.
35. Jamesh M, Kumar S, Narayanan TSNS. Effect of thermal oxidation on corrosion resistance of commercially pure titanium in acid medium. *J Mater Eng Perform.* 2012;21:900–6.
36. Güleyüz H, Çimenoglu H. Effect of thermal oxidation on corrosion and corrosion–wear behaviour of a Ti–6Al–4 V alloy. *Biomaterials.* 2004;25:3325–33.
37. Dong H, Li XY. Oxygen boost diffusion for the deep-case hardening of titanium alloys. *Mater Sci Eng A.* 2000;280:303–10.
38. Browne M, Gregson PJ. Surface modification of titanium alloy implants. *Biomaterials.* 1994;15:894–8.
39. Borgioli F, Galvanetto E, Fossati A, Pradelli G. Glow-discharge and furnace treatments of Ti-6Al-4V. *Surf Coat Technol.* 2004;184:255–62.
40. Lee K-S, Park I-S. Anatase-phase titanium oxide by low temperature oxidation of metallic Ti thin film. *Scr Mater.* 2003;48:659–63.
41. Shimada S, Kozeki M. Oxidation of TiC at low temperatures. *J Mater Sci.* 1992;27:1869–75.
42. Shabalin IL, Roach DL, Shabalina LI. Oxidation of titanium carbide–graphite hetero-modulus ceramics with low carbon content II. Physico-chemical interpretation of the ridge effect. *J Eur Ceram Soc.* 2008;28:3177–88.
43. Nishikiori H, Takei M, Oki K, Takano S, Tanaka N, Fujii T. Photocatalytic activity of titania layer prepared by oxidizing titanium compounds on titanium plate surface. *Appl Catal B Environ.* 2012;127:227–33.
44. Kao C-H, Yeh S-W, Huang H-L, Gan D, Shen P. Study of the TiO to anatase transformation by thermal oxidation of Ti film in air. *J Phys Chem C.* 2011;115:5648–56.
45. Spurr RA, Myers H. Quantitative analysis of anatase-rutile mixtures with an X-ray diffractometer. *Anal Chem.* 1957;29:760–2.
46. Hanaor DAH, Sorrell CC. Review of the anatase to rutile phase transformation. *J Mater Sci.* 2011;46:855–74.
47. Kaleji BK, Sarraf-Mamoory R, Fujishima A. Influence of Nb dopant on the structural and optical properties of nanocrystalline TiO<sub>2</sub> thin films. *Mater Chem Phys.* 2012;132:210–5.
48. Bickley RI, Gonzalez-Carreno T, Lees JS, Palmisano L, Tilley RJD. A structural investigation of titanium dioxide photocatalysts. *J Solid State Chem.* 1991;92:178–90.

49. Su R, Bechstein R, Sø L, Vang RT, Silllassen M, Esbjörnsson B, Palmqvist A, Besenbacher F. How the anatase-to-rutile ratio influences the photoreactivity of TiO<sub>2</sub>. *J Phys Chem C*. 2011;115:24287–92.
50. Li J, Zhao Y. Biocompatibility and antibacterial performance of titanium by surface treatment. *J Coat Technol Res*. 2012;9:223–8.
51. Joo H-C, Lim Y-J, Kim M-J, Kwon H-B, Han J-H. Characterization on titanium surfaces and its effect on photocatalytic bactericidal activity. *Appl Surf Sci*. 2010;257:741–6.
52. Baran N, Starosvetsky D, Starosvetsky J, Epshtein M, Armon R, Ein-Eli Y. Enhanced photo-efficiency of immobilized TiO<sub>2</sub> catalyst via intense anodic bias. *Electrochem Commun*. 2007;9:1684–8.

# Chapter 7

## Enhancing Functionalities of Metallic Materials by Controlling Phase Stability for Use in Orthopedic Implants

Masaaki Nakai, Mitsuo Niinomi, Ken Cho, and Kengo Narita

**Abstract** This chapter aims to review the recent trends pertaining to the enhanced functionalities, including low Young's modulus, self-tunable Young's modulus, and low magnetic susceptibility, of titanium and zirconium alloys for use in orthopedic implants. These value-added functionalities can be realized by controlling the type of crystal structure and their lattice structure stabilities, which are related to the phase stability of titanium and zirconium alloys.

**Keywords** Magnetic susceptibility • Metallic materials • Orthopedic implant • Phase stability • Young's modulus

### 7.1 Introduction

One of the most important factors concerning the use of orthopedic implants is to ensure safety in usage, which is often associated with their mechanical reliability to endure physiologically cyclic loading and unexpected large loads during treatment. Given these considerations, metallic materials are advantageous over ceramic and polymeric materials for use as implantable materials. Therefore, more than 80 % of the implant devices used till date are made of metallic materials [1]. Another important factor concerning the use of orthopedic implants is their toxicity toward living tissues. In general, the human body inherently resists any incoming toxic element. In other words, human body exhibits low permittivity to highly toxic elements eluted from orthopedic implants [2]. That is, the toxicity of orthopedic implants depends not only on the nature of the metallic elements but also on the amount of them, which, in turn, strongly depends on the corrosion resistance of each metallic material. Therefore, in the human body, a metallic material with high corrosion resistance is highly imperative to ensure their safe usage as orthopedic implants.

---

M. Nakai (✉) • M. Niinomi • K. Cho • K. Narita  
Institute for Materials Research, Tohoku University, 2-1-1 Katahira,  
Aoba-ku, Sendai 980-8577, Japan  
e-mail: [nakai@imr.tohoku.ac.jp](mailto:nakai@imr.tohoku.ac.jp)

Conventionally, industrial metallic materials with high corrosion resistance, such as stainless steels (SUS316L), titanium (Ti) alloys (CP Ti and Ti–6Al–4V ELI alloys), and cobalt (Co) alloys (Co–Cr alloys), have been widely used in biomedical applications [3]. Among these materials, Ti alloys have recently attracted considerable attention because of the feasibility of imparting improved functionalities to orthopedic implants. For instance, Ti undergoes allotropic transformation at 1,155 K, which is considered to be very important in terms of phase stability to obtain various functions. In simple terms, Ti alloys can be tuned to perform special functions by adept control of phase stability by varying the chemical composition. In addition, zirconium (Zr), which is one of the congeners of Ti, has also received considerable attention, and new Zr alloys for orthopedic implants have been developed on the basis of phase stability.

In this chapter, we have reviewed the latest trends in the development of Ti and Zr alloys for orthopedic implants with special functionalities, especially those obtained by controlling phase stability.

## 7.2 Low Young's Modulus

During orthopedic surgery, the use of metallic material with Young's modulus higher than that of the bone can lead to excess bone resorption due to the inhibition of load transfer to the bone (stress shielding effect) [4, 5]. Among the different metallic materials, Ti alloys exhibit high strength and relatively low Young's modulus. Furthermore, among the different Ti alloys,  $\beta$ -type Ti alloys consisting of bcc- $\beta$  phase generally exhibit Young's modulus lower than those of  $\alpha$ -type and ( $\alpha + \beta$ )-type Ti alloys consisting of hcp- $\alpha$  and (hcp- $\alpha$  + bcc- $\beta$ ) phases, respectively. This can be attributed specifically to their crystal structures, as shown in Fig. 7.1 [6]. Given this consideration, several studies have focused on the reduction of the Young's modulus of  $\beta$ -type Ti alloys closer to that of the bone [7–13].

The Young's modulus of  $\beta$ -type Ti alloys is considered to be closely related to the stability of the  $\beta$ -phase. For example, the Young's modulus of Ti–Nb alloys, which is quenched above the  $\beta$  transus temperature, depends on the niobium (Nb) content [14, 15]. Depending on the chemical composition, Ti alloys exhibit some intermediate phases, such as non-equilibrium hcp- $\alpha'$ , orthorhombic- $\alpha''$ , and hexagonal- or trigonal- $\omega$  phases between the equilibrium  $\alpha$  and  $\beta$  phases [17]. As a function of the chemical composition, the Young's modulus of Ti–Nb alloys shows local maximum at the chemical composition in which the  $\omega$  phase is formed by quenching (Ti–30Nb). Conversely, the Young's modulus of Ti–Nb alloys shows local minimum at the chemical composition in which the lowest Nb content in the range of the non- $\omega$  phase is formed by quenching (Ti–40Nb) [14, 15]. This implies that the formation of the  $\omega$  phase has to be suppressed in order to obtain low Young's modulus in  $\beta$ -type Ti alloys [16]. Furthermore, studies on the temperature dependence of the Young's moduli of Ti–Nb–Al [11] and Ti–Nb–Sn [9, 16] alloys show that their Young's moduli reduce close to their  $\alpha''$  martensitic transformation temperature. Figure 7.2 [11] shows a typical example of this case in Ti–24Nb–3Al

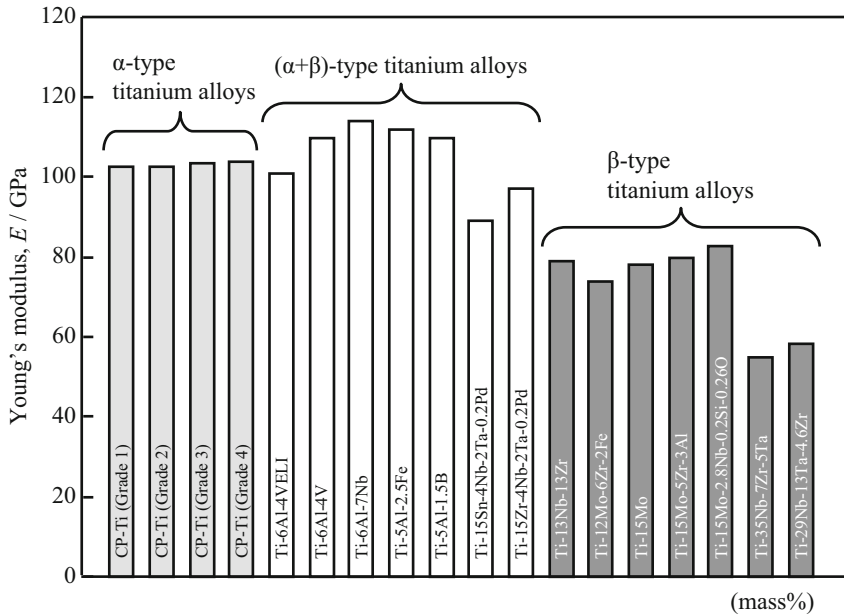
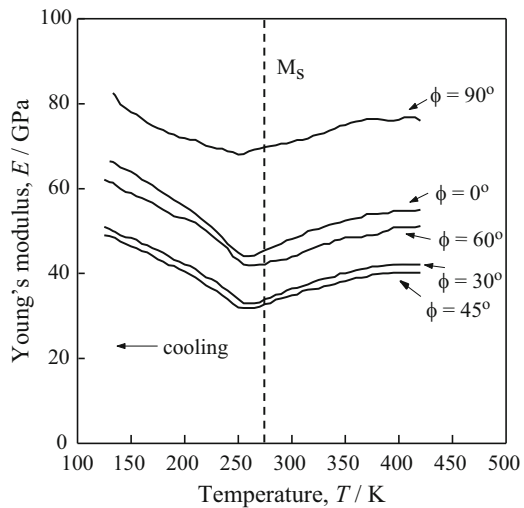


**Fig. 7.1** Young's moduli of  $\alpha$ -,  $(\alpha+\beta)$ -, and  $\beta$ -type titanium alloys [6]

**Fig. 7.2** Dependence of Young's modulus of a  $\beta$ -type titanium alloy with low Young's modulus (Ti-24Nb-3Al alloy (mol %)) on temperature.  $\phi$  is angles between longitudinal and rolling directions in specimen, and  $M_s$  is  $\alpha''$  martensitic transformation temperature [11]



alloys (only the chemical composition of this alloy is expressed using mol% in this chapter). Therefore, in order to obtain the lower Young's modulus of  $\beta$ -type Ti alloys closer to room temperature or body temperature, the chemical composition of the alloys should be determined to be their  $\alpha''$  martensitic transformation

temperatures just below these temperatures [16]. Newly developed  $\beta$ -type Ti alloys such as Ti–Nb–Ta–Zr [7, 8], Ti–Nb–Sn [16, 9, 15], Ti–Nb–Al [11, 17], Ti–Nb–Ta [18], and Ti–Nb–Zr–Sn [10] alloys are considered to satisfy the abovementioned requirements for obtaining low Young’s modulus of the order of 40–60 GPa, which is close to that of the bone (10–30 GPa) [19].

However, the mechanical reliability of these  $\beta$ -type Ti alloys with low Young’s modulus is typically lesser than that of a common ( $\alpha + \beta$ )-type Ti–6Al–4V ELI alloy. Therefore, improvement in the mechanical reliability of  $\beta$ -type Ti alloys with low Young’s modulus is currently under study [20, 21]. The static strength, namely, the tensile strength and 0.2 % proof strength of  $\beta$ -type Ti alloys with maintaining low Young’s modulus can be achieved to the level of those of Ti–6Al–4V ELI alloy by severe cold working such as severe cold rolling, swaging and forging, and severe plastic deformation such as high pressure torsion (HPT) [5, 22, 23]. However, the dynamic strength, namely, the fatigue strength with maintaining low Young’s modulus cannot be improved by severe cold working or severe plastic deformation [24]. Therefore, to improve fatigue strength of  $\beta$ -type Ti alloys, introducing the secondary phases such as  $\alpha$  and  $\omega$  phases, which are formed by aging, in the  $\beta$ -phase matrix is effective, but increases the Young’s modulus. Therefore, controlling the amount of the secondary phase should be considered to maintain the Young’s modulus as low as possible. One of the way to introduce a small amount of the secondary phase is short-time aging at a relatively low temperature. In this case, the  $\omega$  phase is attractive because it increases remarkably the strength of  $\beta$ -type Ti alloys although increasing the Young’s modulus. For example, as a result of introducing a small amount of the  $\omega$  phase by the sort-time aging, the fatigue strength of Ti–29Nb–13Ta–4.6Zr alloy, which is one of the  $\beta$ -type Ti alloys with low Young’s modulus for biomedical applications, increases to a level of that of Ti–6Al–4V ELI alloy while maintaining its Young’s modulus around 75 GPa [20]. Furthermore, introducing a small amount of ceramics such as TiB and  $\text{Y}_2\text{O}_3$  to the  $\beta$ -phase matrix is also effective to improve the fatigue strength of  $\beta$ -type Ti alloys [21, 25]. Figure 7.3 [21] shows maximum cyclic stress-fatigue life (the number of cycles to failure) curves, namely, S-N curves of Ti–29Nb–13Ta–4.6Zr alloys with different  $\text{Y}_2\text{O}_3$  additions obtained from fatigue tests where the amounts of  $\text{Y}_2\text{O}_3$  are expresses as Y concentrations. The fatigue strength is highly improved by  $\text{Y}_2\text{O}_3$  additions both in low- and high-cycle-fatigue life regions, where the number of cycles to failure is less than  $10^5$  cycles and exceeds  $10^5$  cycles, respectively. The fatigue limit of the alloy with 0.1mass% Y is the greatest among the alloys with different Y concentrations. Young’s moduli of Ti–29Nb–13Ta–4.6Zr alloys with different  $\text{Y}_2\text{O}_3$  additions are shown in Fig. 7.4 [21]. It indicates that Young’s moduli of Ti–29Nb–13Ta–4.6Zr alloys with different  $\text{Y}_2\text{O}_3$  additions are almost similar to that of Ti–29Nb–13Ta–4.6Zr alloy without  $\text{Y}_2\text{O}_3$  addition, which is around 60 GPa.

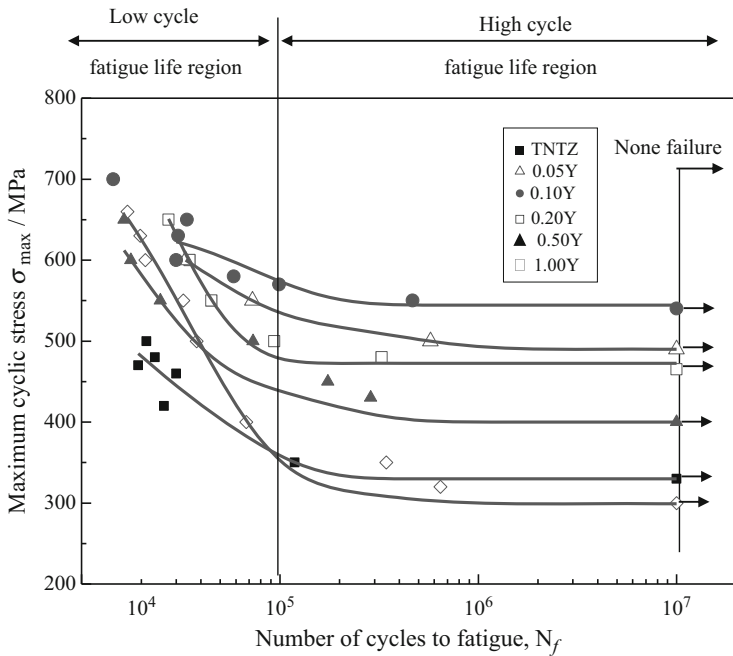
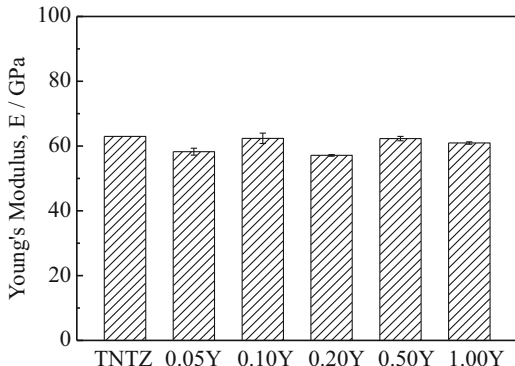


**Fig. 7.3** S-N curves of cold-rolled Ti-29Nb-13Ta-4.6Zr alloys (mass%) without and with different Y<sub>2</sub>O<sub>3</sub> additions which are shown as contents [21]

**Fig. 7.4** Young's moduli of cold-rolled Ti-29Nb-13Ta-4.6Zr alloys (mass%) without and with different Y<sub>2</sub>O<sub>3</sub> additions as a function of content [21]



### 7.3 Wear Properties of Low Young's Modulus Titanium Alloy

Some orthopedic implants consist of more than one component with metal-to-metal contacts such as spinal fixation devices so that the wear properties of materials is important for use in such the applications. A difference of wear behavior between

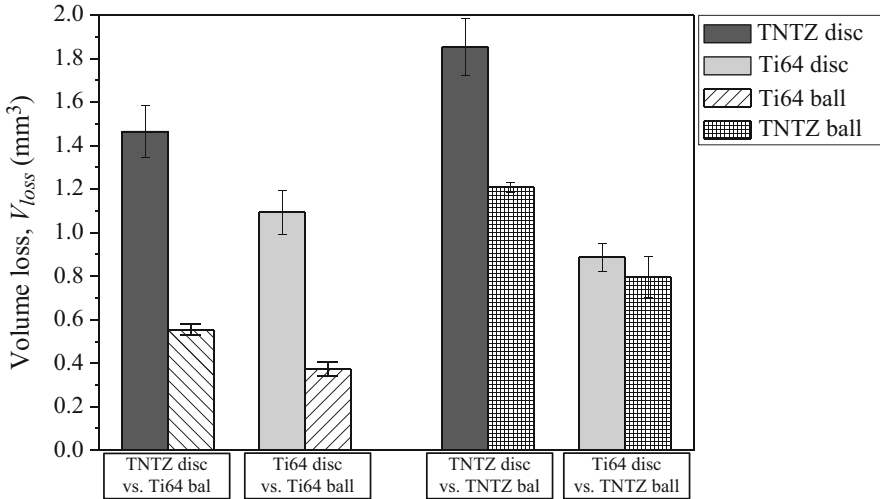


**Fig. 7.5** Volume losses of discs and balls made of Ti-6Al-4V ELI alloy (mass%) (Ti64) and Ti-29Nb-13Ta-4.6Zr alloy (mass%) (TNTZ) obtained from the frictional wear tests [26]

Ti-6Al-4V ELI alloy and Ti-29Nb-13Ta-4.6Zr alloy was investigated [26, 27]. Volume loss of Ti-29Nb-13Ta-4.6Zr alloy was larger than that of Ti-6Al-4V ELI alloy for both discs and balls (mating materials) in the ball-on-disc type wear testing as shown in Fig. 7.5 [26]. According to wear track observations shown in Fig. 7.6 [27], continuous uniform groove and micro cutting, indicative of abrasion, and oxide debris are observed on the worn surface of Ti-6Al-4V ELI alloy. On the other hand, severe plowing, massive surface deformation, many cracks, and some traces of spalling in the form of platelets, indicative of delamination, are observed on the worn surface of Ti-29Nb-13Ta-4.6Zr alloy. These observation results indicate that the resistance to plastic shearing of Ti-29Nb-13Ta-4.6Zr alloy is lower than that of Ti-6Al-4V ELI alloy, which is intrinsically related to low Young's modulus, resulting in different wear behaviors between these two alloys.

## 7.4 Self-Tunable Young's Modulus

In case of spinal fixation devices, high rigidity can increase the risks of stress shielding effect and adjacent segment degeneration. Therefore, materials with low Young's modulus are often preferred to realize healthy spine formation [28, 29]. However, these devices also require high Young's modulus as they are subjected to bending during surgery to obtain the physiological curvature of the spine [30]. In this case, the device must be bent within a limited space inside the patient's body. Therefore, it is often difficult for the surgeon to make an intended curvature if the spring-back of the spinal fixation devices is relatively large [31]. Furthermore, it has

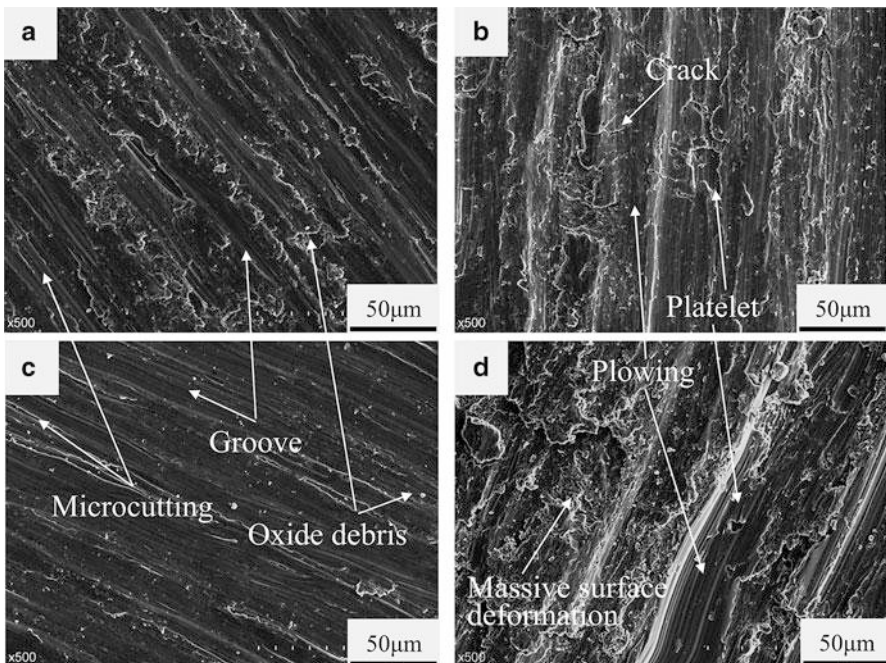
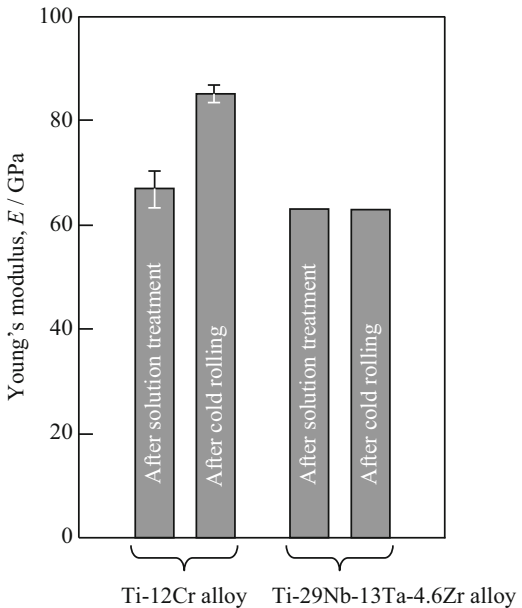


**Fig. 7.6** Scanning electron micrographs of worn surfaces of a  $\beta$ -type titanium alloy with low Young's modulus (Ti-29Nb-13Ta-4.6Zr alloy (mass%) (TNTZ)) and a conventional ( $\alpha + \beta$ )-type titanium alloy (Ti-6Al-4V ELI alloy (mass%) (Ti64)) after ball-on-disc wear tests; (a) Ti64 disc against Ti64 ball, (b) TNTZ disc against Ti64 ball, (c) Ti64 disc against TNTZ ball, and (d) TNTZ disc against TNTZ ball [27]

been reported that the bending tool used by a surgeon to bend the device often leads to scratches on the device surface during the surgery. This, in turn, decreases the mechanical reliability of the spinal fixation devices [32]. Large spring-back leads to difficulty in bending, resulting in the repetition of contouring during operation. This increases the risk of failure of spinal fixation devices [33]. The degree of spring-back depends on both the strength and Young's modulus of spinal fixation devices. Given the same strength, it is the spinal fixation devices with higher Young's modulus that will exhibit a smaller spring-back. That is, these devices are often preferred to suppress the spring-back [34]. Therefore, there is a conflicting requirement in Young's modulus from the viewpoint of patients and surgeons, which cannot be completely satisfied by  $\beta$ -type Ti alloys with low Young's modulus [31]. In order to overcome this issue, recent studies have proposed a novel concept using a deformation-induced  $\omega$ -phase transformation in  $\beta$ -type Ti alloys [31], such as Ti-Cr [35], Ti-Mo [36], Ti-Zr-Mo [37], Ti-Zr-Mo-Cr [38], and Ti-Cr-O [39] alloys. These materials exhibit novel functionality, wherein the deformed material possesses high Young's modulus, while the non-deformed part has low Young's modulus. This is made possible by the phenomenon of deformation-induced

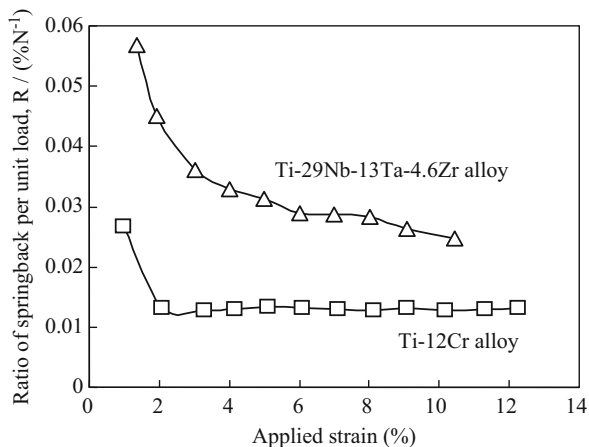
**Fig. 7.7** Young's moduli of  $\beta$ -type titanium alloys with self-tunable Young's modulus (Ti-12Cr alloy (mass%)) and low Young's modulus (Ti-29Nb-13Ta-4.6Zr alloy (mass%)) [31]



$\omega$ -phase transformation localized within the deformed part of the material, which provides an opportunity to satisfy the conflicting requirement in terms of Young's modulus.

Figure 7.7 [31] shows the Young's moduli of  $\beta$ -type Ti alloys, Ti-12Cr alloy with self-tunable Young's modulus and Ti-29Nb-13Ta-4.6Zr alloy with low Young's modulus, after being subjected to solution treatment and cold rolling. The Young's moduli of both Ti-12Cr and Ti-29Nb-13Ta-4.6Zr alloys subjected to solution treatment are almost similar of the order of 60–70 GPa. After being subjected to cold rolling, Ti-29Nb-13Ta-4.6Zr alloy, in which no phase transformation occurs during cold rolling, reveals Young's modulus almost similar to that subjected to solution treatment. Conversely, the Young's modulus of Ti-12Cr alloy is found to increase with cold rolling. The microstructure of Ti-12Cr alloy after cold rolling, as observed using a transmission electron microscope, indicates the formation of the  $\omega$  phase. In general, the formation of the  $\omega$  phase significantly increases the Young's modulus of  $\beta$ -type Ti alloys [24]. Therefore, the observed increase in Young's modulus of Ti-12Cr alloy as a result of cold rolling could be attributed to the deformation-induced  $\omega$  phase transformation [31, 35]. The increase in Young's modulus due to the deformation-induced  $\omega$  phase transformation was also confirmed experimentally, as shown in Fig. 7.8 [35], which indicates that the spring-back of Ti-12Cr alloy could be suppressed in comparison to that of Ti-29Nb-13Ta-4.6Zr alloy.

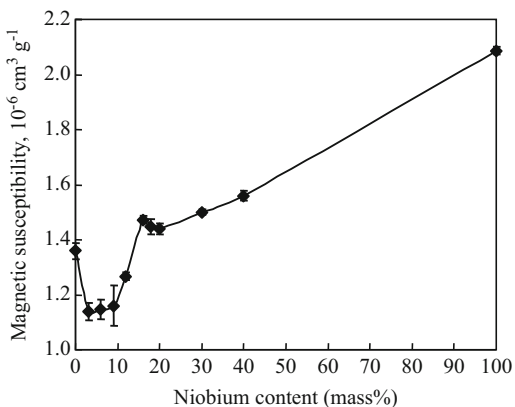
**Fig. 7.8** Springbacks of  $\beta$ -type titanium alloys with self-tunable Young's modulus (Ti-12Cr alloy (mass%)) and low Young's modulus (Ti-29Nb-13Ta-4.6Zr alloy (mass%)) [35]



## 7.5 Low Magnetic Susceptibility

Conventionally, magnetic resonance imaging (MRI) is used for the diagnosis of various diseases. However, when metallic orthopedic devices are implanted in the human body, deficits and distortions are formed in the images of organs and tissues around the implant (artifact), hindering the exact diagnosis performed using a MRI. The artifacts formed by the metallic materials could be ascribed mainly to the difference in magnetic susceptibilities between living tissues and metallic materials [2]. The magnetic susceptibility of living tissues reveals diamagnetism, while that of water being  $-9 \times 10^{-6} \text{ cm}^3 \text{ g}^{-1}$  [40]. On the other hand, Ti, being paramagnetic, has the magnetic susceptibility of  $3.2 \times 10^{-6} \text{ cm}^3 \text{ g}^{-1}$  [41]. This magnetic susceptibility of Ti is much lower than that of ferromagnetic iron (Fe) and Co, but still higher than that of water. Therefore, Zr, which is a congener of Ti, also exhibits a smaller magnetic susceptibility of  $1.3 \times 10^{-6} \text{ cm}^3 \text{ g}^{-1}$ , [41]. This property has gained significant attention, and it forms the genesis for the recent developments of Zr alloys, such as Zr–Nb [41, 42] and Zr–Mo [43, 44] alloys. The dependence of magnetic susceptibility on the Nb content in Zr–Nb alloys is shown in Fig. 7.9 [41]. As is seen, the magnetic susceptibility of Zr–Nb alloys varies as a function of Nb content, showing a local minimum for the Nb content of 3–9 mass% [41]. As Zr undergoes allotropic transformation similar to Ti, the concept of the phase stability in Zr alloys is similar to that of Ti alloys. Therefore, the phase stability of Zr alloys depends on the chemical composition. The allotropic transformation results in the formation of some intermediate phases, such as non-equilibrium  $\alpha'$  and  $\omega$  phases, in addition to the equilibrium  $\alpha$  and  $\beta$  phases [41–43]. In Zr–Nb alloys, the magnetic susceptibility of Zr–(3–9)Nb alloys reveals local minimum with Zr–3Nb, Zr–6Nb, and Zr–9Nb alloys consisting of single  $\alpha'$  phase, ( $\alpha' + \omega + \beta$ ) phases, and ( $\omega + \beta$ ) phases, respectively. However, given the volume fractions of each phase, the  $\omega$  phase is considered to have the lowest magnetic susceptibilities among these phases

**Fig. 7.9** Dependence of magnetic susceptibility of Zr–Nb alloys on niobium content [41]



[41]. Analogously, Zr–3Mo alloys consist of ( $\omega + \beta$ ) phases, revealing the lowest magnetic susceptibility of below  $1.1 \times 10^{-6} \text{ cm}^3 \text{ g}^{-1}$  among both Zr–Nb and Zr–Mo alloys [43].

## 7.6 Summary

Metallic materials used in orthopedic implants are required to have high mechanical reliability and corrosion resistance. In addition to these conventional properties, additional value-added functionalities are being considered beneficial for the successful use of metallic materials in orthopedic implants. Therefore, in this chapter, the authors have reviewed the recent topics pertaining to the improved functionalities (low Young's modulus, self-tunable Young's modulus, and low magnetic susceptibility) of titanium and zirconium alloys via controlling the phase stability, which imparts essential functionalities to the implants. This overview is expected to facilitate a better understanding of biomedical metallic materials in potential future applications.

**Acknowledgements** This work was partly supported by the inter-university cooperative research program “Innovative Research for Biosis–Abiosis Intelligent Interface” from Ministry of Sports, Culture, and Education, Japan, the Industrial Technology Research Grant Program in 2009 from the New Energy and Industrial Technology Development Organization (NEDO), and Grant-in-Aid for Scientific Research (A), Young Scientists (A), and Challenging Exploratory Research from the Japan Society for the Promotion of Science (JSPS), Japan.

**Open Access** This chapter is distributed under the terms of the Creative Commons Attribution Noncommercial License, which permits any noncommercial use, distribution, and reproduction in any medium, provided the original author(s) and source are credited.

## References

1. Hanawa T. Research and development of metals for medical devices based on clinical needs. *Sci Technol Adv Mater.* 2012;13(6):064102. doi:[10.1088/1468-6996/13/6/064102](https://doi.org/10.1088/1468-6996/13/6/064102).
2. Hanawa T. Metals for medicine. Sendai: Japan Institute of Metals; 2010.
3. Niinomi M. Recent metallic materials for biomedical applications. *Metall Mater Trans A.* 2002;33(3):477–86.
4. Sumitomo N, Noritake K, Hattori T, Morikawa K, Niwa S, Sato K, et al. Experiment study on fracture fixation with low rigidity titanium alloy. *J Mater Sci Mater Med.* 2008;19(4):1581–6. doi:[10.1007/s10856-008-3372-y](https://doi.org/10.1007/s10856-008-3372-y).
5. Niinomi M, Nakai M, Hieda J. Development of new metallic alloys for biomedical applications. *Acta Biomater.* 2012;8(11):3888–903.
6. Niinomi M. Mechanical properties of biomedical titanium alloys. *Mater Sci Eng A.* 1998;243 (1–2):231–6.
7. Ahmed T, Long M, Silvestri J, Ruiz C, Rack HJ. A new low modulus, biocompatible titanium alloy. In: Blenkinsop PA, Evans WJ, Flower HM, editors. Titanium '95: science and technology. Birmingham: The Institute for Materials; 1996. p. 1760–7.
8. Kuroda D, Niinomi M, Morinaga M, Kato Y, Yashiro T. Design and mechanical properties of new beta type titanium alloys for implant materials. *Mater Sci Eng A.* 1998;243(1–2):244–9.
9. Matsumoto H, Watanabe S, Hanada S. Beta TiNbSn alloys with low Young's modulus and high strength. *Mater Trans.* 2005;46(5):1070–8.
10. Hao YL, Li SJ, Sun SY, Yang R. Effect of Zr and Sn on Young's modulus and superelasticity of Ti-Nb-based alloys. *Mater Sci Eng A.* 2006;441(1–2):112–8. doi:[10.1016/j.msea.2006.09.051](https://doi.org/10.1016/j.msea.2006.09.051).
11. Inamura T, Hosoda H, Wakashima K, Miyazaki S. Anisotropy and temperature dependence of Young's modulus in textured TiNbAl biomedical shape memory alloy. *Mater Trans.* 2005;46 (7):1597–603.
12. Tane M, Akita S, Nakano T, Hagihara K, Umakoshi Y, Niinomi M, et al. Peculiar elastic behavior of Ti-Nb-Ta-Zr single crystals. *Acta Mater.* 2008;56(12):2856–63. doi:[10.1016/j.actamat.2008.02.017](https://doi.org/10.1016/j.actamat.2008.02.017).
13. Matsumoto H, Watanabe S, Hanada S. Microstructures and mechanical properties of metastable beta TiNbSn alloys cold rolled and heat treated. *J Alloys Compd.* 2007;439(1–2):146–55. doi:[10.1016/j.jallcom.2006.08.267](https://doi.org/10.1016/j.jallcom.2006.08.267).
14. Boyer R, Welsch G, Collings EW. Materials properties handbook: titanium alloys. Materials Park: ASM International; 1994.
15. Ozaki T, Matsumoto H, Watanabe S, Hanada S. Beta Ti alloys with low Young's modulus. *Mater Trans.* 2004;45(8):2776–9.
16. Hanada S. Materials properties of biomedical titanium alloys. *Mater Jpn.* 2008;47:242–8.
17. Fukui Y, Inamura T, Hosoda H, Wakashima K, Miyazaki S. Mechanical properties of a Ti-Nb-Al shape memory alloy. *Mater Trans.* 2004;45(4):1077–82.
18. Kim HY, Sasaki T, Okutsu K, Kim JI, Inamura T, Hosoda H, et al. Texture and shape memory behavior of Ti-22Nb-6Ta alloy. *Acta Mater.* 2006;54(2):423–33. doi:[10.1016/j.actamat.2005.09.014](https://doi.org/10.1016/j.actamat.2005.09.014).
19. Niinomi M. Mechanical biocompatibilities of titanium alloys for biomedical applications. *J Mech Behav Biomed Mater.* 2008;1(1):30–42. doi:[10.1016/j.jmbbm.2007.07.001](https://doi.org/10.1016/j.jmbbm.2007.07.001).
20. Nakai M, Niinomi M, Oneda T. Improvement in fatigue strength of biomedical beta-type Ti-Nb-Ta-Zr alloy while maintaining low Young's modulus through optimizing omega-phase precipitation. *Metall Mater Trans A.* 2012;43(1):294–302. doi:[10.1007/s11661-011-0860-3](https://doi.org/10.1007/s11661-011-0860-3).
21. Song X, Niinomi M, Nakai M, Tsutsumi H, Wang L. Improvement in fatigue strength while keeping low Young's modulus of a beta-type titanium alloy through yttrium oxide dispersion. *Mater Sci Eng C.* 2012;32(3):542–9. doi:[10.1016/j.msec.2011.12.007](https://doi.org/10.1016/j.msec.2011.12.007).
22. Niinomi M. Fatigue performance and cyto-toxicity of low rigidity titanium alloy, Ti-29Nb-13Ta-4.6Zr. *Biomaterials.* 2003;24(16):2673–83.

23. Narita K, Niinomi M, Nakai M, Hieda J, Oribe K. Development of thermo-mechanical processing for fabricating highly durable beta-type Ti-Nb-Ta-Zr rod for use in spinal fixation devices. *J Mech Behav Biomed Mater.* 2012;9:207–16. doi:[10.1016/j.jmbbm.2012.01.011](https://doi.org/10.1016/j.jmbbm.2012.01.011).
24. Akahori T, Niinomi M, Fukui H, Ogawa M, Toda H. Improvement in fatigue characteristics of newly developed beta type titanium alloy for biomedical applications by thermo-mechanical treatments. *Mater Sci Eng C.* 2005;25(3):248–54. doi:[10.1016/j.msec.2004.01.007](https://doi.org/10.1016/j.msec.2004.01.007).
25. Song X, Niinomi M, Tsutsumi H, Nakai M, Wang L. Effects of TiB on the mechanical properties of Ti-29Nb-13Ta-4.6Zr alloy for use in biomedical applications. *Mater Sci Eng A.* 2011;528(16–17):5600–9. doi:[10.1016/j.msea.2011.03.108](https://doi.org/10.1016/j.msea.2011.03.108).
26. Lee Y-S, Niinomi M, Nakai M, Hieda J, Cho K. Wear properties of Ti-6Al-4V/Ti-29Nb-13Ta-4.6Zr combination for spinal implants. *Adv Mater Res.* 2014;922:424–8. doi:[10.4028/www.scientific.net/AMR.922.424](https://doi.org/10.4028/www.scientific.net/AMR.922.424).
27. Nakai M, Niinomi M, Hieda J, Cho K, Lee Y-S. Difference of wear behavior between Ti-29Nb-13Ta-4.6Zr alloy and Ti-6Al-4V ELI alloy for biomedical applications. *TMS2014 annual meeting supplemental proceedings.* 2014. p. 217–20.
28. Shi L, Wang L, Guo Z, Wu Z-X, Liu D, Gao M-X, et al. A study of low elastic modulus expandable pedicle screws in osteoporotic sheep. *J Spinal Disord Tech.* 2012;25(2):123–8.
29. Wang Z, Fu S, Wu Z-X, Zhang Y, Lei W. Ti2448 Pedicle screw system augmentation for posterior lumbar interbody fusion. *Spine.* 2013;38(23):2008–15. doi:[10.1097/BRS.0b013e3182a76fec](https://doi.org/10.1097/BRS.0b013e3182a76fec).
30. Steib JP, Dumas R, Skalli W. Surgical correction of scoliosis by in situ contouring – a detorsion analysis. *Spine.* 2004;29(2):193–9.
31. Nakai M, Niinomi M, Zhao XF, Zhao XL. Self-adjustment of Young's modulus in biomedical titanium alloys during orthopaedic operation. *Mater Lett.* 2011;65(4):688–90. doi:[10.1016/j.matlet.2010.11.006](https://doi.org/10.1016/j.matlet.2010.11.006).
32. Lindsey C, Deviren V, Xu Z, Yeh RF, Puttlitz CM. The effects of rod contouring on spinal construct fatigue strength. *Spine.* 2006;31(15):1680–7. doi:[10.1097/01.brs.0000224177.97846.00](https://doi.org/10.1097/01.brs.0000224177.97846.00).
33. Noshchenko A, Yao XF, Armour GA, Baldini T, Patel VV, Ayers R, et al. Evaluation of spinal instrumentation rod bending characteristics for in-situ contouring. *J Biomed Mater Res B.* 2011;98(1):192–200. doi:[10.1002/jbm.b.31837](https://doi.org/10.1002/jbm.b.31837).
34. Niinomi M, Nakai M. Titanium-based biomaterials for preventing stress shielding between implant devices and bone. *Int J Biomater.* 2011. doi:[10.1155/2011/836587](https://doi.org/10.1155/2011/836587).
35. Zhao XF, Niinomi M, Nakai M, Hieda J, Ishimoto T, Nakano T. Optimization of Cr content of metastable beta-type Ti-Cr alloys with changeable Young's modulus for spinal fixation applications. *Acta Biomater.* 2012;8(6):2392–400. doi:[10.1016/j.actbio.2012.02.010](https://doi.org/10.1016/j.actbio.2012.02.010).
36. Zhao XF, Niinomi M, Nakai M, Hieda J. Beta type Ti-Mo alloys with changeable Young's modulus for spinal fixation applications. *Acta Biomater.* 2012;8(5):1990–7. doi:[10.1016/j.actbio.2012.02.004](https://doi.org/10.1016/j.actbio.2012.02.004).
37. Zhao XL, Niinomi M, Nakai M. Relationship between various deformation-induced products and mechanical properties in metastable Ti-30Zr-Mo alloys for biomedical applications. *J Mech Behav Biomed Mater.* 2011;4:2009–16. doi:[10.1016/j.jmbbm.2011.06.020](https://doi.org/10.1016/j.jmbbm.2011.06.020).
38. Zhao XL, Niinomi M, Nakai M, Miyamoto G, Furuhsara T. Microstructures and mechanical properties of metastable Ti-30Zr-(Cr, Mo) alloys with changeable Young's modulus for spinal fixation applications. *Acta Biomater.* 2011;7(8):3230–6. doi:[10.1016/j.actbio.2011.04.019](https://doi.org/10.1016/j.actbio.2011.04.019).
39. Liu H, Niinomi M, Nakai M, Hieda J, Cho K. Deformation-induced changeable Young's modulus with high strength in beta-type Ti-Cr-O alloys for spinal fixture. *J Mech Behav Biomed Mater.* 2014;30:205–13. doi:[10.1016/j.jmbbm.2013.11.001](https://doi.org/10.1016/j.jmbbm.2013.11.001).
40. Uyama E, Hamada K, Asaoka K. Magnetic susceptibility and mechanical property of non-magnetic AuPtNb alloys for biomedical application. *J J Dent Mater.* 2010;29(5):415.
41. Nomura N, Tanaka Y, Suyalatu, Kondo R, Doi H, Tsutsumi Y, et al. Effects of phase constitution of Zr-Nb alloys on their magnetic susceptibilities. *Mater Trans.* 2009;50(10):2466–72. doi:[10.2320/matertrans.M2009187](https://doi.org/10.2320/matertrans.M2009187).

42. Kondo R, Nomura N, Suyalatu, Tsutsumi Y, Doi H, Hanawa T. Microstructure and mechanical properties of as-cast Zr-Nb alloys. *Acta Biomater.* 2011;7(12):4278–84. doi:[10.1016/j.actbio.2011.07.020](https://doi.org/10.1016/j.actbio.2011.07.020).
43. Suyalatu, Nomura N, Oya K, Tanaka Y, Kondo R, Doi H et al. Microstructure and magnetic susceptibility of as-cast Zr-Mo alloys. *Acta Biomater.* 2010;6(3):1033–8. doi:[10.1016/j.actbio.2009.09.013](https://doi.org/10.1016/j.actbio.2009.09.013).
44. Suyalatu, Kondo R, Tsutsumi Y, Doi H, Nomura N, Hanawa T. Effects of phase constitution on magnetic susceptibility and mechanical properties of Zr-rich Zr-Mo alloys. *Acta Biomater.* 2011;7(12):4259–66. doi:[10.1016/j.actbio.2011.07.005](https://doi.org/10.1016/j.actbio.2011.07.005).

# Chapter 8

## Surface Improvement for Biocompatibility of Ti-6Al-4V by Dealloying in Metallic Melt

Yuichi Fukuzumi, Takeshi Wada, and Hidemi Kato

**Abstract** Dealloying is known to be a powerful method to produce porous materials mainly with noble metals because the mechanism involves the selective dissolution of specific element(s) by corrosion in acid/alkali aqueous solutions. Recently, an alternative dealloying method has been developed by our research group using a metallic melt in place of the corrosive aqueous solution. In this study, using the novel dealloying method using a metallic melt, toxic Al element, was successfully removed from the surface of Ti-6Al-4V, which has been used for biomedical applications, for improving their biocompatibility. The toxic ion release from the overall sample did not effectively decrease because of the substantial surface area that developed using the dealloying method. By optimizing the dealloying conditions to suppress surface area development, drastic improvement in the biocompatibility of this Ti alloy is expected.

**Keywords** Biocompatibility • Dealloying • Surface improvement • Ti-6Al-4V

### 8.1 Introduction

Biomaterials are becoming more important for our better quality of life. When a person temporally or permanently loses particular biofunction by illness or injury, biomaterials are required to compensate it. The properties required for biomaterials are mainly divided into mechanical conditions such as strength, toughness, elasticity and the biological conditions such as toxicity, biodegradation and carcinogenicity. The Ti-based alloys are promising biomedical material because they can combine excellent mechanical and biological properties [1]. Among the various Ti-based alloys, the Ti-6Al-4V alloy one of the most frequently used metallic biomaterials. This alloy is two-phase alloy in which Al element acts as an

---

Y. Fukuzumi

Graduate Student, Graduate School of Engineering, Tohoku University,  
Sendai 980-8579, Japan

T. Wada • H. Kato (✉)

Institute for Materials Research, Tohoku University, 2-1-1 Katahira,  
Aoba-ku, Sendai 980-8577, Japan  
e-mail: [hikato@imr.tohoku.ac.jp](mailto:hikato@imr.tohoku.ac.jp)

$\alpha$ -phase (hexagonal close packed phase) stabilizer and V acts as a  $\beta$ -phase (body-centered cubic phase) stabilizer. This two-phase alloy was originally developed as a material for aircraft, therefore, this alloy combines high strength, high toughness and low density. As for the biomedical use, the Ti-6Al-4V alloy is often used as a load-bearing components such as artificial bone and dental implant [2]. Despite excellent mechanical and biological properties from this alloy, the cytotoxicity problem due to the release of V and Al ion *in vivo* remains unsolved [3]. To make this alloy more biocompatible, extensive researches for developing two-phase alloy without using V and Al [4] and also the establishing surface improvement technology are ongoing [5]. Unlike these conventional works, our approach is to utilize a dealloying method to dissolve toxic elements from an alloy by immersion into a metallic melt [6–10]. In this study, we apply this dealloying method to remove toxic elements from the surface of biomedical alloys and then investigate the resulting effect on the biocompatibility.

## 8.2 Dealloying in a Metallic Melt

When we mix two elements, the free energy change due to this event is

$$\Delta G_{\text{mix}} = \Delta H_{\text{mix}} - T\Delta S_{\text{mix}} \quad (8.1)$$

where  $\Delta H_{\text{mix}}$  is the heat of mixing,  $\Delta S_{\text{mix}}$  is the entropy of mixing, and  $T$  is the absolute temperature. Usually, the entropy increases after mixing. Therefore, if  $\Delta H_{\text{mix}} < 0$ , the  $\Delta G_{\text{mix}} < 0$ , and the mixing reaction can occur spontaneously from a thermodynamic point of view. On the other hand, if  $\Delta H_{\text{mix}} > 0$  the sign (positive or negative) of  $\Delta G_{\text{mix}}$  depends on the temperature. If the temperature is adequately controlled to make the enthalpy term larger than the entropy term, then  $\Delta G_{\text{mix}} > 0$ , and we can avoid the mixture of the two elements. Here we dip an A-B binary alloy precursor into a metallic melt consisting of element C. If the heat of mixing between elements B and C is negative, i.e.,  $\Delta H_{\text{mix}, B-C} < 0$  and if the heat of mixing between elements A and C is positive, i.e.,  $\Delta H_{\text{mix}, A-C} > 0$ , then by controlling temperature adequately only element B dissolves from the precursor into the C melt; since element A is rejected from the C melt, it is expected to self-organize into a porous structure by surface diffusion in the same manner as that of the ordinary dealloying method in an aqueous solution [11]. Figure 8.1 shows a schematic of this novel dealloying method that involves the selective dissolution of B atoms (orange) in the C atom melt (pink) and surface diffusion of the remaining A atoms (yellowish green). Figure 8.2 summarizes this “triangle” relationship in terms of the heat of mixing among elements A, B, and C required for the dealloying reaction in a metallic melt. We have to calculate the accurate value for the heat of mixing by considering the temperature and chemical composition for designing the dealloying reaction. However, this is sometimes complicated. The heat of mixing between the transition metals, and the transition metals and metalloids can be obtained from the

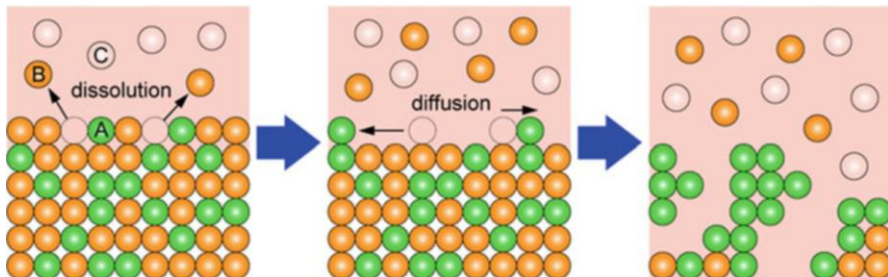


**Fig. 8.1** Schematic of the dealloying method using a metallic melt, where atom B (orange) dissolves into a melt composed of C atoms (pink), and the remaining atom A (yellowish green) self-organizes into a porous structure by surface diffusion

**Fig. 8.2** Triangle relationship of the enthalpies of mixing among elements A, B, and C for dealloying in a metallic melt

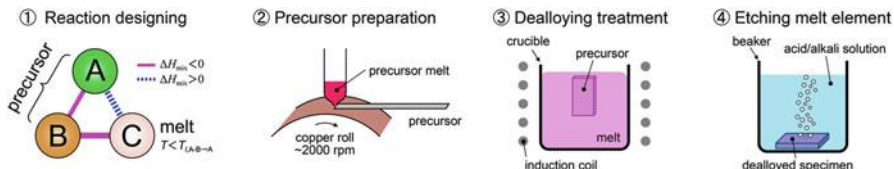
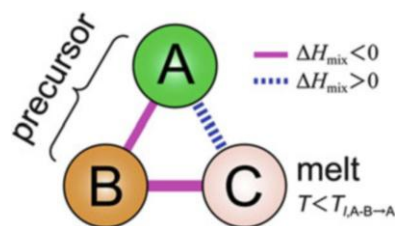


**Fig. 8.3** Schematic of the process of porous metal preparation using dealloying in a metallic melt

table in Boer and Perrifor [12], the values of which are approximately calculated by the Miedema model, and that of other metals can be obtained from the table constructed by Takeuchi et al. [13]. In our study, we first identify the candidates for elements A, B, and C from the tables in Boer and Perrifor [12] and Takeuchi and Inoue [13] and we then confirm the relationships A-B and B-C (mixture) and A-C (separation) by the related binary phase diagrams. Here, we summarize the preparation procedures for nanoporous metals by dealloying in a metallic melt, as they are schematically shown in Fig. 8.3.

1. Selection of A-B-C elements, which satisfy the triangle relationship of the heats of mixing. (tables of values of heat of mixing and equilibrium phase diagrams can be used).
2. Preparation of the A-B alloy precursor.

3. Selective dissolution of element B from the A–B precursor into the C metal melt (formation of the porous structure).
4. Removal of the C element by etching with an acid or alkaline solution (the remaining A component must be inert in the solution).

## 8.3 Surface Improvement of Ti-6Al-4V Alloy by Dealloying with a Metallic Melt [14]

### 8.3.1 Morphology and Composition Change by Dealloying

The Ti-6Al-4V alloy, which consists of both  $\alpha$ -Ti and  $\beta$ -Ti phases, is one of the promising biomedical materials among Ti alloys. However, the Al and V in this alloy are known to be cytotoxic elements. We attempted selective removal of the toxic element(s) from the surface of the Ti-6Al-4V alloy using dealloying with a metallic melt. In this section, we demonstrate the selected removal of Al as the first step for improving the biocompatibility of this alloy. Based on the triangle relationship of values of heat of mixing, the Mg melt can be used due to the negative enthalpy of mixing with Al and the positive enthalpy of mixing with both Ti and V. This relationship is illustrated in Fig. 8.4. Figure 8.5 and Table 8.1 exhibit SEM images and the corresponding results of EDX analysis of the Ti-6Al-4V surface dealloyed in a Mg melt at 1,148 K for 0.3–7.2 ks, respectively. An increasing immersion time resulted in the coarsening of the porous structure on the surface. Similarly, an increase in the immersion temperature from 1,048 to 1,148 K under the fixed immersion time of 1.2 ks resulted in the coarsening of the porous structure on the surface. It has been generally observed that the morphology and chemical composition of the dealloyed sample depend on the immersion time and temperature of the melt during dealloying treatment [10]. An increased immersion time up to 1.2 ks at 1,148 K resulted in a slight decrease in Al concentration. However, a further increase in the immersion time resulted in an increase of Al content. This is probably due to the dissolution of Ti into the Mg melt, which is suggested by the observed concentration decrease in Ti with immersion time that became dominant after 1.2 ks. To confirm dissolution of Ti, a cp-Ti rod was immersed into a Mg melt at 1,184 K for 1.8 ks in a carbon crucible. The mass loss, which is defined by (mass loss) = (mass of initial cp-Ti) – (mass of treated cp-Ti), was estimated to be ~6 mg (Fig. 8.6). Therefore, dissolution of Ti was confirmed to occur in the Mg melt,

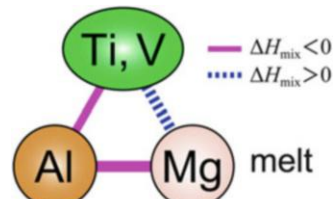


**Fig. 8.4** Triangle relationship of the enthalpies of mixing among Ti, V, Al, and Mg

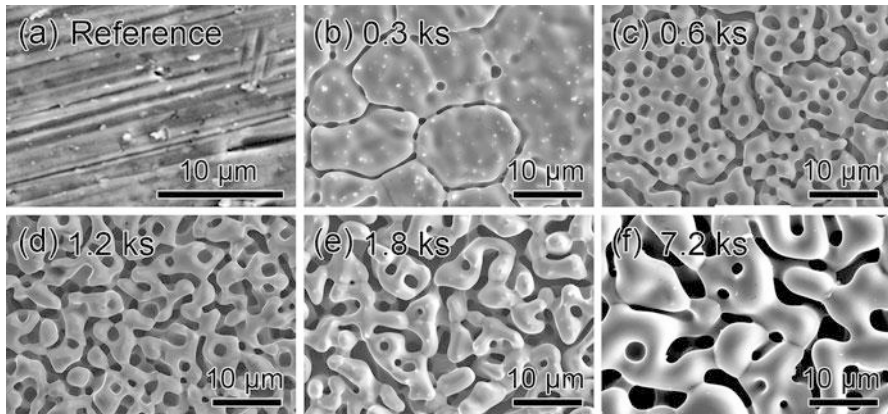
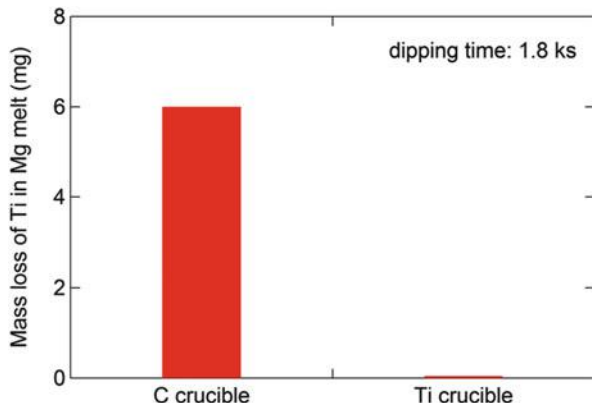


**Fig. 8.5** SEM images of the surface of Ti-6Al-4V disks immersed in a Mg melt at 1,148 K for 0 s (reference) (a), 0.3 ks (b), 0.6 ks (c), 1.2 ks (d), 1.8 ks (e), and 7.2 ks (f) followed by leaching of Mg phases in a nitric acid aqueous solution. *Scratches* shown in (a) are from the mechanical polishing process

**Table 8.1** EDX analysis results for Ti, Al, and V concentrations (wt.%) of the dealloyed samples shown in Fig. 8.5

	Ti	Al	V
Reference	90.9	6.5	4.4
0.3 ks	88.8	6.8	4.4
0.6 ks	85.4	5.1	9.8
1.2 ks	88.9	5.0	6.2
1.8 ks	90.1	5.7	4.21
7.2 ks	83.9	11.1	5.1

**Fig. 8.6** Dependence of crucible material (carbon and titanium) on mass loss of a cp-Ti rod immersed in a Mg melt at 1,148 K for 1.8 ks



although the heat of mixing between them is positive. Interestingly, it is found that the mass loss of cp-Ti is well suppressed when a Ti crucible is used, as shown in Fig. 8.6. These results suggest that the crucible material affects the morphology and composition. Here, we investigated effect of crucible materials composed of Mo, C,

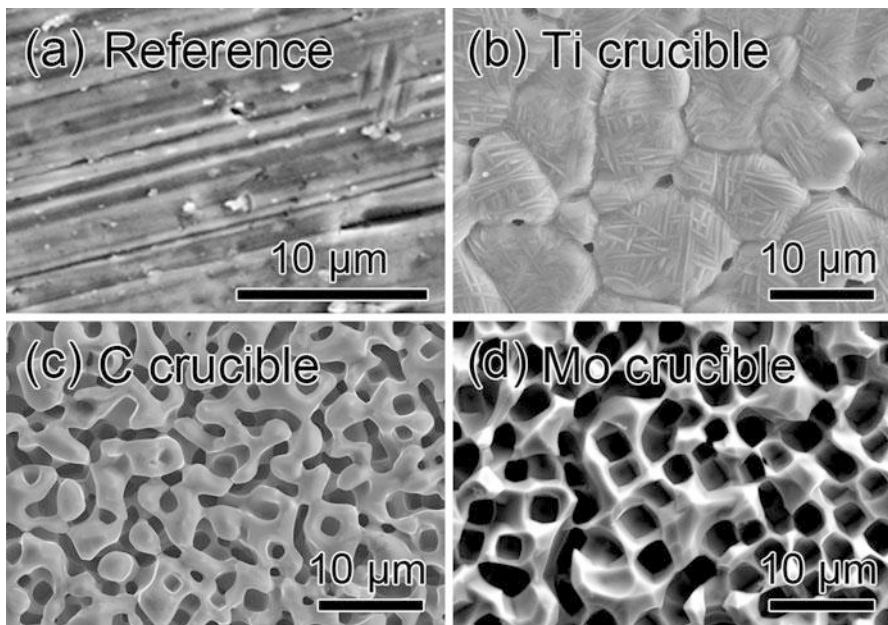


**Fig. 8.7** SEM images of the surface of Ti-6Al-4V dealloyed in a Mg melt at 1,148 K for 1.2 ks using various crucibles: Ti (b), C (c), and Mo (d). Nondealloyed Ti-6Al-4V is shown in (a) for a reference

**Table 8.2** EDX analysis results for Ti, Al, and V concentrations (wt.%) on the surface of the samples shown in Fig. 8.7

	Ti	Al	V
Reference	90.9	6.5	2.6
Ti crucible	93.1	3.4	3.6
C crucible	88.9	5.0	6.2
Mo crucible	93.1	4.2	5.2

and Ti, which are all immiscible with Mg according to the related phase diagrams. Figure 8.7 and Table 8.2 exhibit SEM images and the corresponding results of EDX analysis of the surface of Ti-6Al-4V dealloyed at 1,148 K for 1.2 ks using different crucibles, together with an untreated sample for comparison. On the surface of the untreated sample, only the linear scratches formed during the machining process are observed. However, the dealloyed samples using C and Mo crucibles show a well-developed porous structure on their surfaces. On the contrary, the sample dealloyed in a Ti crucible shows a small number of isolated pores at the grain boundary on the surface. Regardless of crucible materials, the Al concentration decreased after the dealloying treatment. This result indicates that when Ti-6Al-4V is immersed into Mg, a mass change occurs due to the dissolution of Ti, as schematically shown in Fig. 8.8. If the Ti crucible is used, dissolution of Ti from the crucible possibly occurs. The fact that the Al and V concentration on the surface decreased

**Fig. 8.8** Schematic of differences in the dealloying using C and Mo crucibles (left) and a Ti crucible (right)

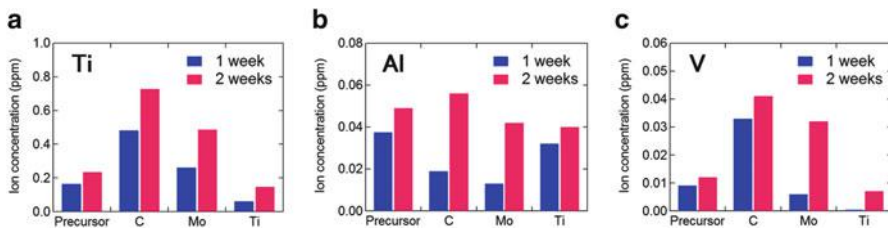
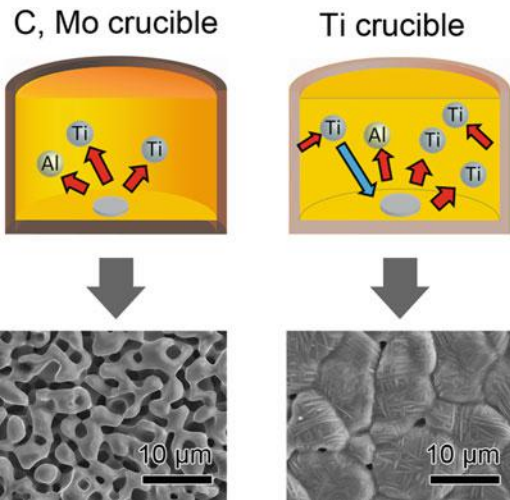


**Fig. 8.9** Influence of crucible material for dealloying treatment on the amount of Ti (a), Al (b), and V (c) ion release from the dealloyed Ti-6Al-4V disk in a simulated body fluid (SBF) after 1 and 2 weeks

without developing a nanoporous structure suggests that Ti atoms dissolved from Ti crucible into the Mg melt deposited onto the Ti-6Al-4V surface simultaneously with dealloying.

### 8.3.2 Effect of Crucible Material on Ion Release of Dealloyed Ti-6Al-4V

As described in the above section, the surface feature of the dealloyed Ti-6Al-4V sample strongly depends on the crucible material. Such effect is expected to significantly affect the ion release behavior of the dealloyed samples. Therefore, the effects of crucible material on ion release of dealloyed Ti-6Al-4V were studied. Figure 8.9 shows the results of ion release from Ti-6Al-4V dealloyed using crucibles made of C, Mo, and Ti after 1 and 2 weeks in simulated body fluid (SBF). The amount of Al ion release decreased for all cases because of the

dealloying effect. The amount of Ti and V ion release increased for the sample dealloyed using C and Mo crucibles due to the increase of surface area owing to the well-developed porous structure. In contrast, the amount of Ti and V ions released from Ti-6Al-4V dealloyed using a Ti crucible decreased due to the formation of a less porous surface composed of a Ti-rich phase. That the surface structure and composition might depend on the crucible material was beyond our expectations; however, this effect is potentially useful for controlling the ion release behavior as well as the surface structure of the dealloyed sample.

## 8.4 Summary

Using the dealloying method in a metallic melt, selective removal of toxic Al element from the surface of and Ti-6Al-4V alloys, which have been used as biomedical metals, was attempted in order to improve their biocompatibility.

1. By immersing a Ti-6Al-4V alloy into a Mg melt, the surface Al concentration of the Ti-6Al-4V alloy was successfully reduced.
2. The surface morphology and composition of the dealloyed Ti-6Al-4V was found to depend strongly on the crucible materials used during the dealloying treatment. When C and Mo crucibles were used, not only Al but Ti and V also dissolved into the Mg melt, resulting in a well-developed porous surface layer. On the other hand, when using a Ti crucible, the Al and V surface concentration was successfully reduced by means of a less porous Ti rich surface layer that was considered to have developed due to surface deposition of Ti dissolved from the Ti crucible into the Mg melt.

Considering the crucible material, more research is required to optimize the dealloying conditions that can realize a reduction of the surface concentration of a toxic element without increasing the surface area.

**Open Access** This chapter is distributed under the terms of the Creative Commons Attribution Noncommercial License, which permits any noncommercial use, distribution, and reproduction in any medium, provided the original author(s) and source are credited.

## References

1. Niinomi M, Nakai M, Hieda J. Development of new metallic alloys for biomedical applications. *Acta Biomater.* 2012;8:3888–903.
2. Geetha M, Singh AK, Asokamani R, Gogia AK. Ti based biomaterials, the ultimate choice for orthopaedic implants – a review. *Progr Mater Sci.* 2009;54:397–425.
3. Steinemann SG. Corrosion of surgical implants—in vivo and in vitro tests. In: Winter GD, Leray JL, de Groot K, editors. *Evaluation of biomaterials, advances in biomaterials.* New York: Wiley; 1980. p. 1–34.

4. Okazaki Y, Rao S, Ito Y, Tateishi T. Corrosion resistance, mechanical properties: corrosion fatigue strength and cytocompatibility of new Ti alloys without Al and V. *Biomaterials*. 1998;19:1197–215.
5. Liu X, Chu PK, Ding C. Surface modification of titanium, titanium alloys, and related materials for biomedical applications. *Mater Sci Eng R*. 2004;47:49–121.
6. Wada T, Yubuta K, Inoue A, Kato H. Dealloying by metallic melt. *Mater Lett*. 2011;65:1076–8.
7. Wada T, Setyawan AD, Yubuta K, Kato H. Nano- to submicro-porous beta-Ti alloy prepared from dealloying in a metallic melt. *Scripta Mater*. 2011;65:532–5.
8. Wada T, Kato H. Three-dimensional open-cell macroporous iron, chromium and ferritic stainless steel. *Scripta Mater*. 2013;68:723–6.
9. Kim JW, Wada T, Kim SG, Kato H. Sub-micron porous niobium solid electrolytic capacitor prepared by dealloying in a metallic melt. *Mater Lett*. 2014;116:223–6.
10. Tsuda M, Wada T, Kato H. Kinetics of formation and coarsening of nanoporous  $\alpha$ -titanium dealloyed with Mg melt. *J Appl Phys*. 2013;114(1–8):113503.
11. Forty AJ. Corrosion micromorphology of noble metal alloys and depletion gilding. *Nature*. 1979;282:597–8.
12. Boer FR, Perrifor DG. Cohesion in metals. Netherlands: Elsevier Science Publishers B.V; 1988.
13. Takeuchi A, Inoue A. Classification of bulk metallic glasses by atomic size difference, heat of mixing and period of constituent elements and its application to characterization of the main alloying element. *Mater Trans*. 2005;46:2817–29.
14. Fukuzumi Y. Surface modification of Ti-6Al-4V biomaterial by dealloying with metallic melt, Master Thesis. Tohoku University Japan; 2012.

# Chapter 9

## Chemical Vapor Deposition of Ca–P–O Film Coating

Takashi Goto and Hirokazu Katsui

**Abstract** Ca–P–O system bio-ceramic films were coated by chemical vapor deposition (CVD). CVD is a versatile technique for controlling crystal phase and microstructure, which significantly affect bio-compatibility. By introducing auxiliary energy, laser and plasma, in CVD, much wider range of Ca–P–O coatings can be synthesized. Hydroxyapatite regeneration of the Ca–P–O coatings prepared by CVD techniques were evaluated in a simulated body fluid (SBF).

**Keywords** Apatite regeneration • Calcium phosphate • Crystal structure • Laser and plasma CVD

### 9.1 Introduction

Metallic bio-materials, typically Ti and Ti alloys, can be used as artificial bones or dental implants because they are non-allergenic, have good corrosion resistance in the human body and possess comparable mechanical properties with bone. However, these metallic bio-materials do not have sufficient tissue compatibility; therefore, they require a few months for bone-regeneration. Since human bone is similar in makeup calcium hydroxyapatite ( $\text{Ca}_{10}(\text{PO}_4)_6(\text{OH})_2$ ) ceramics, materials of the Ca–P–O system are commonly used as bio-ceramic coatings on metallic bio-materials to accelerate the bone regeneration. Several coating techniques, such as plasma spray, sol–gel, alkaline treatment and magnetron sputtering, have been proposed [1]. Although chemical vapor deposition (CVD) has been widely used to prepare various forms of materials, i.e., films, powders and bulks as electric devices and anti-abrasive coatings [2], CVD has rarely been used to synthesize bio-ceramic coatings. However, CVD has advantages in controlling crystal phase and microstructure, providing well-adhered coatings even on complex-shaped metal substrates. CVD is a promising technique for the preparation of bio-ceramic coatings because it can optimize their microstructure to enhance bio-compatibility. The authors of this review have prepared Ca–Ti–O [3], Ca–Si–O [4] and Ca–P–O

---

T. Goto (✉) • H. Katsui  
Institute for Materials Research, Tohoku University, 2-1-1, Katahira, Aoba-ku,  
Sendai 980-8579, Japan  
e-mail: [goto@imr.tohoku.ac.jp](mailto:goto@imr.tohoku.ac.jp)

bio-ceramic coatings [5] by CVD. This review briefly describes the CVD preparation of Ca–P–O bio-ceramic coatings and their bone (hydroxyapatite) regeneration behavior in a simulated body fluid (SBF).

## 9.2 Chemical Vapor Deposition (CVD)

In CVD, various forms of materials (powder, amorphous, poly-crystalline, single-crystal, film and bulk) are prepared through chemical reactions, such as thermal decomposition, hydrolysis and hydrogen reduction. By controlling deposition parameters, i.e., source gases, deposition temperature, gas pressure, geometry of the CVD reaction chamber etc., wide-ranging oxide, nitride, carbide and boride materials with different microstructures (fine grains, cauliflower grains and columnar grains) can be prepared. Since source gases can be easily purified, deposited materials can also be highly pure and dense or intentionally porous. Chemical reactions in CVD take place usually by thermal energy. Therefore, conventional CVD is called thermal CVD. Substrate materials may be degraded and corroded by the high temperature of thermal CVD; auxiliary energy sources such as plasma and laser can be introduced to enhance the chemical reactions and lower the deposition temperature. These CVDs are called laser CVD (LCVD) [6] and plasma-enhanced CVD (PECVD) [7]. Figure 9.1a–c schematically depict thermal CVD, PECVD and LCVD, respectively. In thermal CVD, chemical reactions proceed on a substrate surface, forming films via nucleation and grain growth on the atomic/molecular level. The resulting films are generally well-adhered to the substrate with good step coverage. By optimizing deposition parameters, high deposition rates of 1–2 mm/h can be achieved, forming thick film or bulky materials [8]. Bio-ceramic oxide films are not usually deposited at high deposition rate because precursor vapors and oxygen gas are easily reacted in the gas phase to form powders and premature reactions take place on CVD chamber walls. The deposition rates of oxide films by thermal CVD are commonly around a few  $\mu\text{m}/\text{h}$  [9]. Thermal CVD can be performed close to thermal equilibrium. The films can be synthesized according to a phase diagram, producing thermally stable products.

PECVD (Fig. 9.1a) uses plasma as an auxiliary energy source. An electromagnetic field with radio frequency (RF: 13.5 MHz) or micro-wave (2.45 GHz) can be applied to a deposition zone to form the plasma. The gas can be discharged and dissociated to activate ions, radicals and electrons. These activated species are significantly reactive, even at low temperatures, forming non-equilibrium or quasi-equilibrium films [10]. The authors first utilized PECVD for preparing bio-ceramic coatings as shown later.

Lasers can be an auxiliary energy source of light and heat in CVD, and thus LCVD (Fig. 9.1c) can be categorized into two types: photolytic LCVD and pyrolytic LCVD [6]. Since a source gas may absorb a specific laser wavelength, photolytic LCVD can prepare films without substrate heating. The laser passes through a gas phase, directly decomposing source gases. Photolytic LCVD using a

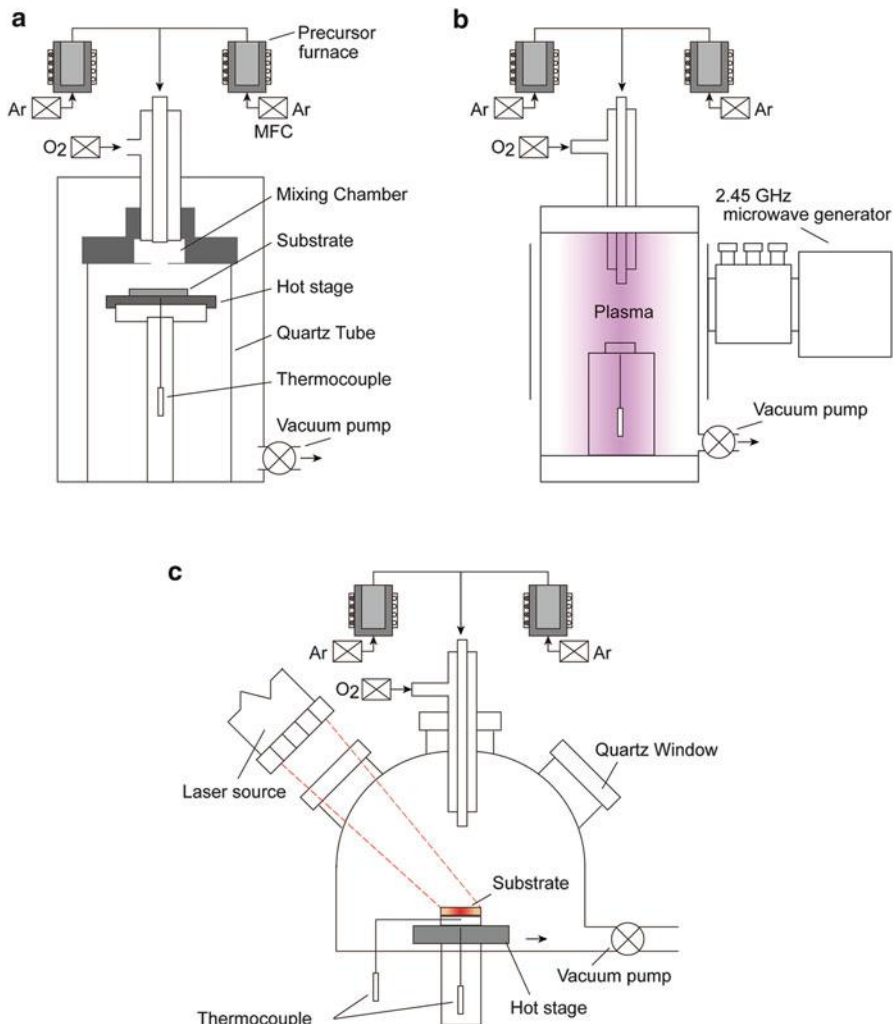


**Fig. 9.1** Schematic diagram of thermal CVD (a), plasma enhanced CVD (PECVD) (b) and laser CVD (LCVD) (c)

high energy laser, typically an ultra-violet or Excimer laser, has the advantage of low temperature deposition without thermal degradation of the substrate. However, photolytic LCVD cannot create a wide-area coating at a high deposition rate. In pyrolytic LCVD, infra-red lasers, such as CO<sub>2</sub> and Nd:YAG lasers, are generally used. Pyrolytic LCVD heats locally at a small area of the substrate by focusing the laser beam; thus, source gases can easily access the heated area. The deposition rate of pyrolytic LCVD can be significantly high, reaching several 100 m/h [6]. However, the deposition area is usually less than several mm<sup>2</sup>. Therefore, pyrolytic LCVD are generally understood to not make large-area coatings on substrates with

complicated shape. The authors first developed LCVD to prepare oxide and non-oxide films at high deposition speeds (more than several 100  $\mu\text{m}/\text{h}$ ) on wide-area substrates (around several  $\text{cm}^2$ ) by using a high power laser (several 100 W of  $\text{CO}_2$ , Nd:YAG and diode lasers), as shown later [11, 12].

### 9.3 CVD of Ca-P-O Films and Their Bio-Characteristics

Figure 9.2 depicts the phase diagram of a Ca-P-O system [13], which contains various bio-ceramic materials.  $\alpha$ - and  $\beta$ - $\text{Ca}_3\text{P}_2\text{O}_8$  (TCP: tricalcium phosphate) have been widely studied as bio-resorbable materials. Figure 9.3 depicts the crystal structures of  $\alpha$  and  $\beta$ -TCP. The structure of  $\alpha$ -TCP (Fig. 9.3a) is classified as a glaserite-type structure, where Ca ions exhibit coordination numbers ranging from five to nine and share edges with a  $\text{PO}_4$  group [14]. Ca and phosphate ions are packed in columns along the  $c$ -axis in two ways; one contains only cations and the other contains both cations and anions. While the  $\alpha$ -TCP is thermo-dynamically stable at 1,393–1,743 K and metastable at room temperature,  $\beta$ -TCP is stable below 1,393 K. The structure of  $\beta$ -TCP (Fig. 9.3b) is related to that of  $\text{Ba}_3(\text{VO}_4)_2$ , although  $\beta$ -TCP has lower symmetry due to site vacancies and distortions [15]. Ca ions coordinated to six, seven, eight and nine oxygen ions share edges with  $\text{PO}_4$  tetrahedra. The major difference in crystal structure between  $\alpha$ - and  $\beta$ -TCP is that

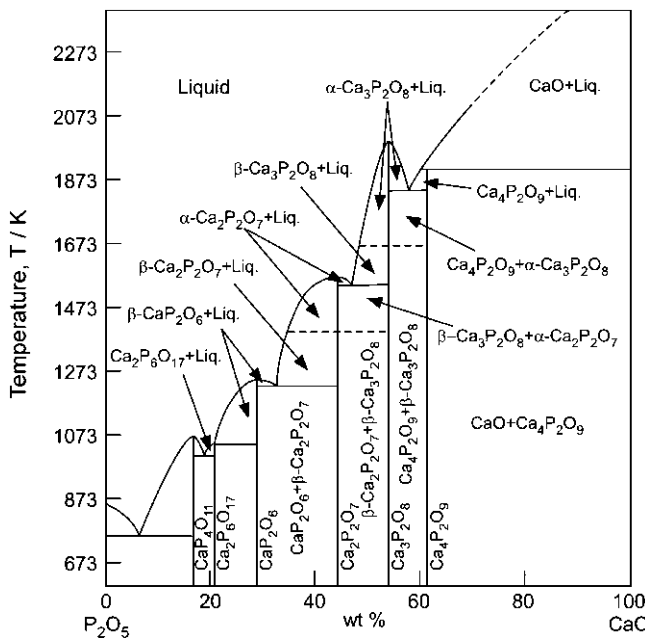


**Fig. 9.2** A phase diagram of Ca-P-O system

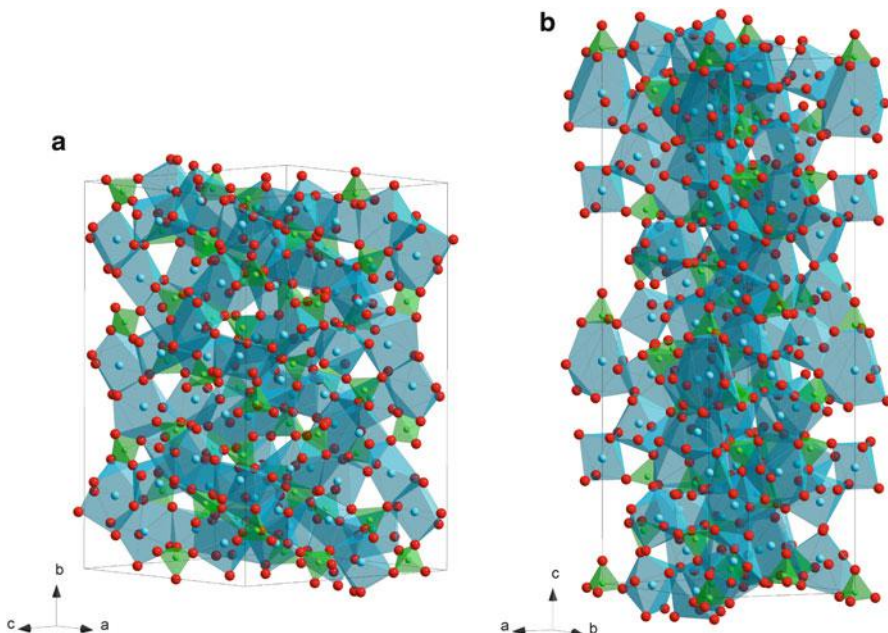


**Fig. 9.3** Crystal structures of  $\alpha$ - (a) and  $\beta$ -tricalcium phosphate (TCP) (b)

$\beta$ -TCP has no cation–cation columns. Additionally, compared to that of  $\beta$ -TCP,  $\alpha$ -TCP has a higher internal energy because of its higher volume per formula unit, which is consistent with  $\alpha$ -TCP being the high-temperature phase [14].

$\alpha$ - and  $\beta$ -Ca<sub>2</sub>P<sub>2</sub>O<sub>7</sub> (CPP: calcium pyrophosphate) have been scarcely studied. The crystal structures of  $\alpha$ - and  $\beta$ -CPP are illustrated in Fig. 9.4a, b, respectively. Structures of both  $\alpha$ - and  $\beta$ -CPP contain pyro-groups, P<sub>2</sub>O<sub>7</sub>, which consist of two corner-shared PO<sub>4</sub> tetrahedra with P–O–P angles of 130° for the  $\alpha$ -phase and angles of 131° and 135° for the  $\beta$ -phase [16, 17]. In  $\alpha$ -CPP, Ca ions coordinate with eight oxygen atoms and the chains of edge-shared Ca polyhedra form sheets parallel and perpendicular to the ac plane. The coordination numbers of Ca in  $\beta$ -CPP are seven, eight and nine; each pyrophosphate group is linked by commonly-shared Ca atoms, forming infinite pyrophosphate-Ca chelate-like chains [17]. Allen et al. prepared an  $\alpha$ -CPP film by thermal CVD using Ca(dpm)<sub>2</sub> (dpm: dipivaloylmethanate) and P<sub>2</sub>O<sub>5</sub> at a total pressure ( $P_{\text{tot}}$ ) of 1 kPa and a deposition temperature of 1,123 K. The  $\beta$ -CPP film was heat-treated at 1,623 K and transformed to a  $\beta$ -TCP film [18].

Ca<sub>4</sub>P<sub>2</sub>O<sub>9</sub> (TTCP: tetracalcium phosphate) would be more bio-resorbable than TCP because of its greater P<sub>2</sub>O<sub>5</sub> content. TTCP is also written as Ca<sub>4</sub>(PO<sub>4</sub>)<sub>2</sub>O (tetracalcium diphosphate monooxide) since its structure contains Ca ions coordinated with seven and eight oxygen atoms that share PO<sub>4</sub> edges, and oxygen ions strongly coordinated to four Ca ions, forming tetrahedra of OCa<sub>4</sub>, as oxide ions (Fig. 9.5a) [19]. The Ca and P atoms lie near four sheets that contain two cation–anion (Ca–PO<sub>4</sub>) columns and one cation–cation (Ca–Ca) column perpendicular

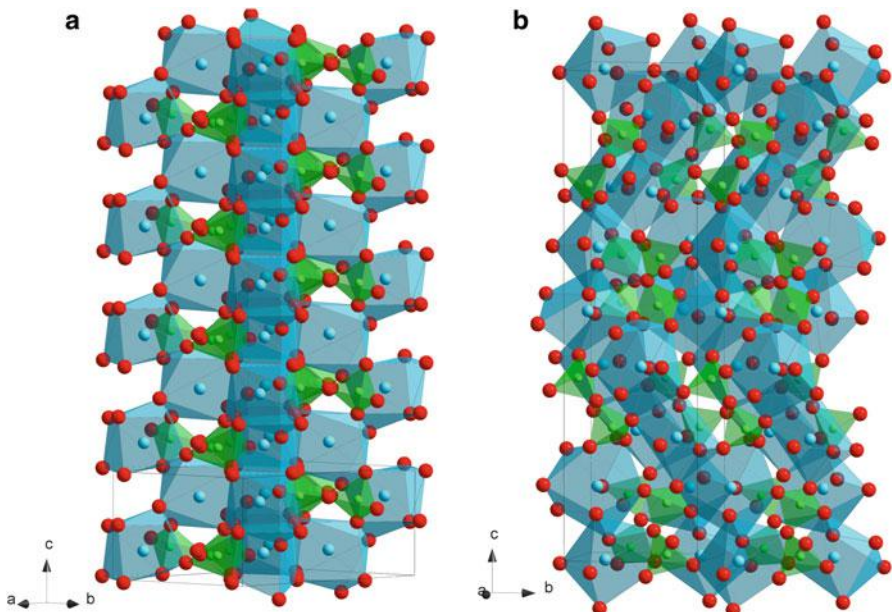


**Fig. 9.4** Crystal structures of  $\alpha$ - (a) and  $\beta$ -calcium pyrophosphate (CPP) (b)

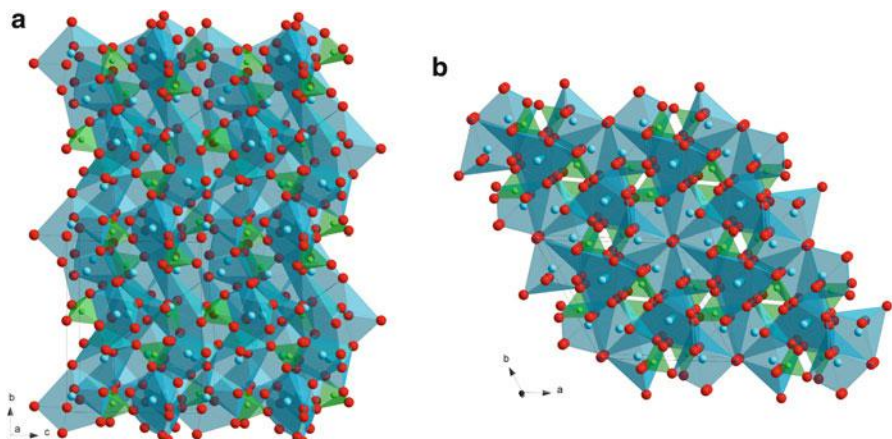


**Fig. 9.5** Crystal structure of tetracalcium phosphate (TTCP) (a) calcium hydroxyapatite (HAp) (b)

to the *b*-axis. Because of these so-called ‘apatitic layers’, TTCP has a close structural relationship with calcium hydroxyapatite (HAp:  $\text{Ca}_{10}(\text{PO}_4)_6(\text{OH})_2$ ) and its dehydration product, calcium oxyapatite (OAp:  $\text{Ca}_{10}(\text{PO}_4)_6\text{O}$ ) [19–22].

Figure 9.5b depicts a crystal structure of HAp, which is illustrated by tetrahedra of  $\text{PO}_4$  and polyhedra of Ca ions coordinated with seven and nine oxygen atoms.

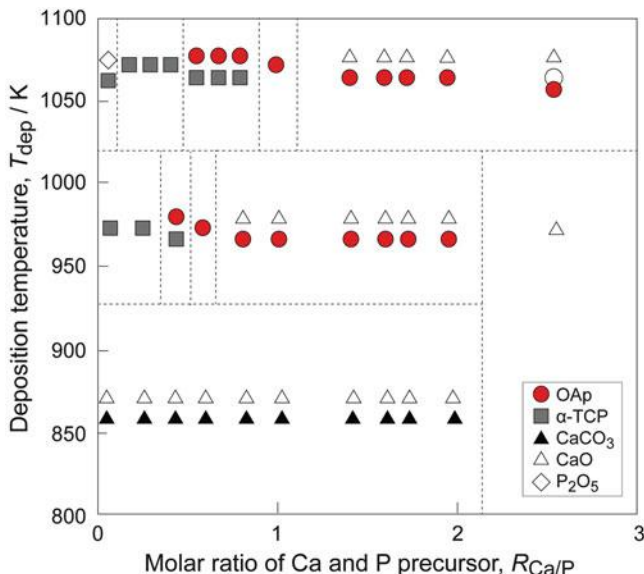


**Fig. 9.6** Relationship between deposition parameters and crystal phases by thermal CVD

HAp and OAp have ‘apatite layers’, composed of two Ca-PO<sub>4</sub> columns and one Ca-Ca column parallel to the *ac* plane, and hydroxyl ions in HAp and oxygen ions in OAp are located at the center of Ca hexagons parallel to the *ab* plane. HAp or OAp have been frequently studied because HAp is bio-active and similar to human bones. Although many techniques including solid-state sintering, sol-gel and magnetron sputtering [23] have been employed to prepare OAp or HAp, Darr et al. prepared fluorine-containing carbonated hydroxyapatite by thermal CVD using Ca(tmhd)<sub>2</sub> (where tmhd=2,2,6,6,-tetramethylheptane-3,5-dione) and P<sub>2</sub>O<sub>5</sub> [24]. The crystal structure of the film was not investigated, but the Ca/P content of the film was about 1.3 which is different from that of HAp (Ca/P=1.7). The bio-compatibility of this film was not reported. Since OH is easily evaporated in a vacuum, preparing OH-containing HAp by dry processes (vacuum processes), such as CVD and sputtering, is difficult. OAp film prepared by magnetron sputtering did not contain OH [25], whereas OAp film prepared by thermal CVD contained a small amount of OH. In this review, the OAp film prepared by CVD containing a small amount of OH is described as OAp film. The authors first prepared a crystalline OAp film in as-deposited form.

By controlling deposition parameters, various bio-ceramic films of TCP, TTCP and OAp films can be prepared by thermal CVD. Figure 9.6 represents the relationship between deposition parameters and crystal phases, i.e., the CVD phase diagram, by thermal CVD using Ca(dpm)<sub>2</sub> and (C<sub>6</sub>H<sub>5</sub>O<sub>3</sub>)PO as source materials [5]. α-TCP film in a single phase can be prepared at a high deposition temperature ( $T_{dep}$ ) and low Ca/P gas ratio ( $R_{Ca/P}$ ), while OAp film in a single phase can be prepared at a

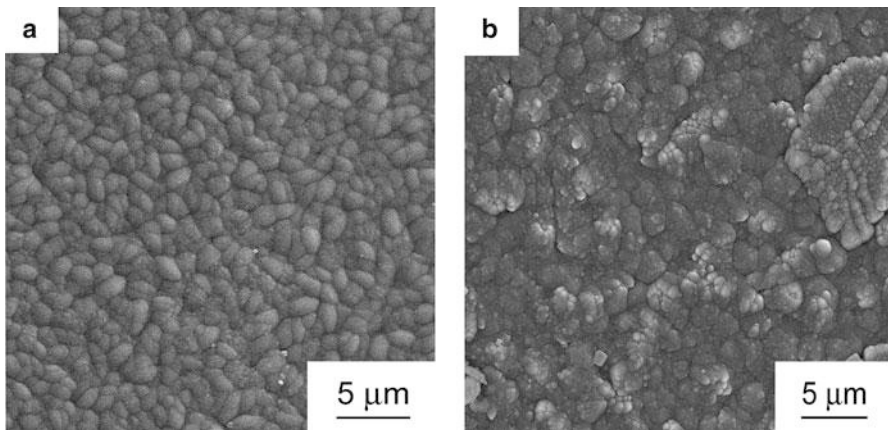


**Fig. 9.7** Surface morphology of  $\alpha$ -TCP (a) and OAp (b) films prepared by thermal CVD

high  $T_{\text{dep}}$  and intermediate  $R_{\text{Ca/P}}$  condition. Figure 9.7a, b depict the surface morphologies of  $\alpha$ -TCP and OAp films in a single phase, respectively. The  $\alpha$ -TCP film has uniform and smooth small grains, while the OAp film has a cauliflower structure. Figure 9.8 shows the HAp regeneration behavior in Hanks' solution on the  $\alpha$ -TCP film [26]. A small amount of HAp embryo starts to form after 1 day of immersion, and the whole surface of the  $\alpha$ -TCP film is covered by HAp after 14 days. Figure 9.9 shows the HAp regeneration behavior in Hanks' solution on the OAp film. The HAp embryo formed within a 1 h, and the whole surface is covered by HAp within 6 h. HAp regeneration is preferential at hollows in the cauliflower-like grains. HAp and OAp have hexagonal structures as shown in Fig. 9.5b. HAp regeneration is also preferred to  $c$ -axis on the  $c$ -plane. The preferential  $c$ -axis orientation of the OAp film can be obtained by controlling  $T_{\text{dep}}$  and  $R_{\text{Ca/P}}$  in thermal CVD. The highly  $c$ -axis oriented OAp film exhibited the highest regeneration of HAp in Hanks' solution [27]. Since a few months are needed for bone regeneration on Ti without bio-ceramic coatings, the OAp coating by thermal CVD is the effective strategy to regenerate HAp.

Since lasers can photolytically or thermally activate source gases, more kinds of Ca-P-O materials can be prepared by LCVD. Figure 9.10a, b depict the relationship between deposition parameters and the crystal phases (CVD phase diagram) by LCVD using  $\text{Ca}(\text{dpm})_2$  and  $(\text{C}_6\text{H}_5\text{O}_3)\text{PO}$  as source gases at a low (30 W) and high (200 W) laser power, respectively [28]. At relatively low  $T_{\text{dep}}$  of 750–950 K, a mixture film of OAp and  $\beta$ -TCP or OAp and TTCP can be obtained under a wide range of conditions. OAp films in a single phase can be obtained at  $R_{\text{Ca/P}} = 0.5$  to 0.6. At  $T_{\text{dep}}$  of 1,000–1,300 K, a mixture film of OAp and  $\alpha$ -TCP can be prepared by LCVD.  $\alpha$ -TCP films can be prepared by thermal CVD, whereas both  $\alpha$ - and  $\beta$ -TCP films can be prepared by LCVD.

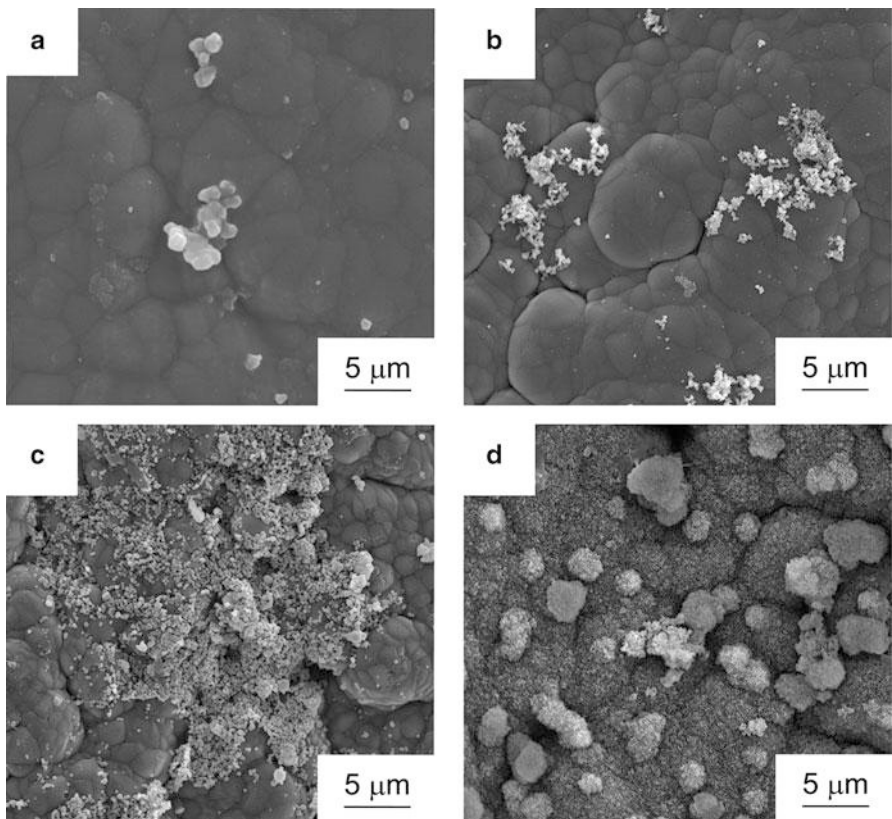


**Fig. 9.8** HAp regeneration behavior on  $\alpha$ -TCP film in Hanks' solution for 1 day (a), 3 days (b), 7 days (c) and 14 days (d)

Plasma can electromagnetically activate source gases, and a greater variety of Ca–P–O system materials can be synthesized by PECVD. Figure 9.11 depicts the relationship between deposition parameters and crystal phases (the CVD phase diagram) by PECVD using  $\text{Ca}(\text{dpm})_2$  and  $(\text{C}_6\text{H}_5\text{O}_3)\text{PO}$  as source gases.  $\alpha$ - and  $\beta$ -CPP films can both be prepared by PECVD. At a relatively high  $T_{\text{dep}}$ , a  $\beta$ -CPP film in a single phase or a mixture film of  $\beta$ -CPP and  $\alpha$ -TCP can be prepared. At a low  $T_{\text{dep}}$ , a mixture of  $\beta$ - and  $\alpha$ -TCP can be prepared. Figure 9.12 shows change in surface morphology of a  $\beta$ -CPP film prepared at micro-wave power of 4 kW and  $R_{\text{Ca/P}} = 0.7$  after immersion in Hanks' solution. A slightly smooth surface morphology can be seen after immersion for 3 days, suggesting that  $\beta$ -CPP is bio-resorbable. A small amount of HAp embryo can be observed after immersion for 7 days.

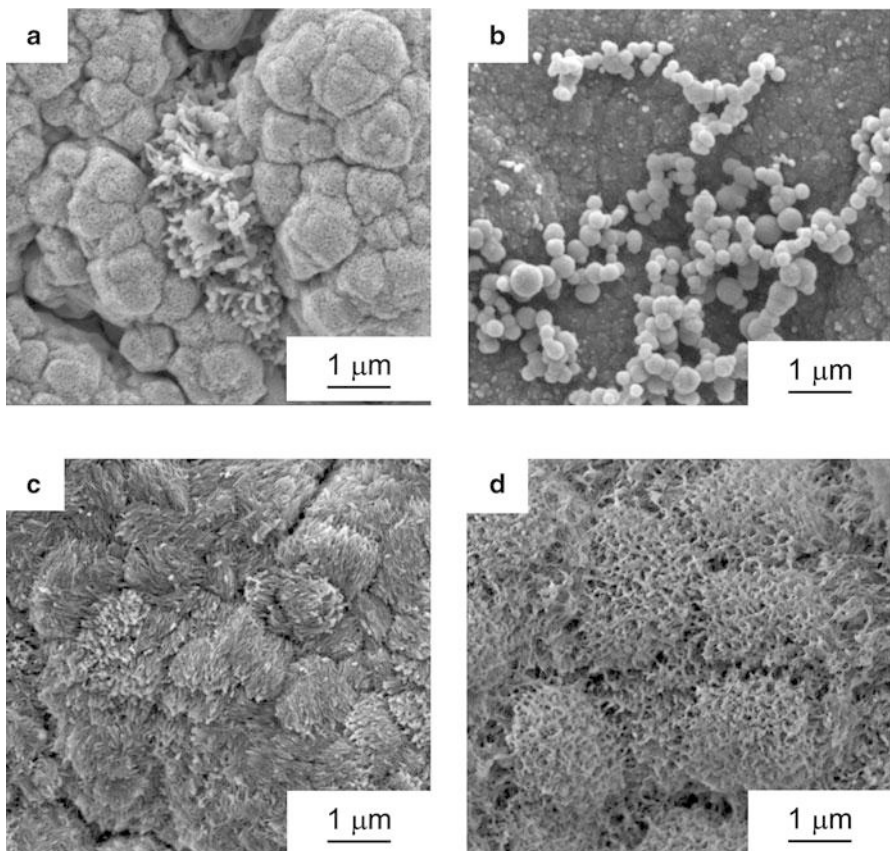


**Fig. 9.9** HAprec regeneration behavior on OAp film in Hanks' solution for 1 h (a), 3 h (b), 6 h (c) and 12 h (d)

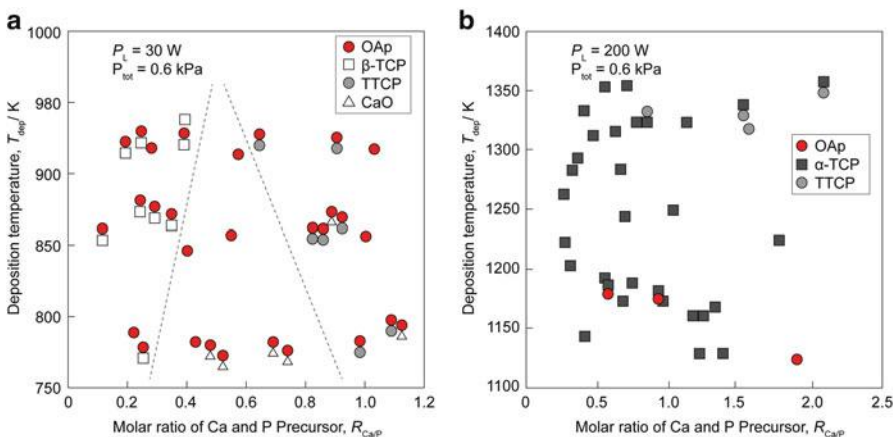


**Fig. 9.10** Relationship between deposition parameters and crystal phases by LCVD at a low (a) and high (b) laser power

**Fig. 9.11** Relationship between deposition parameters and crystal phases by PECVD

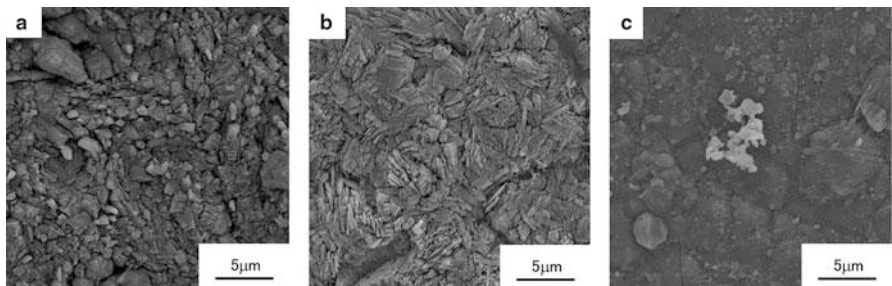
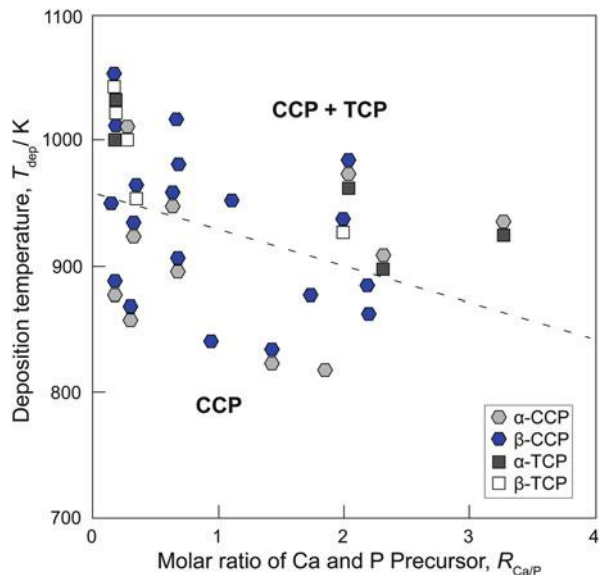


**Fig. 9.12** HAp regeneration behavior on CPP film in Hanks' solution for 1 day (a), 3 days (b), 7 days (c)

#### 9.4 Summary

CVD is a promising process for bio-ceramic coatings because it can provide well-defined crystal phases and microstructures through the control of process parameters. Auxiliary energy sources, such as laser and plasma, are particularly useful to fabricate materials that cannot be synthesized by conventional thermal CVD. The Ca–P–O system has many useful bio-ceramics, i.e., bio-inert, bio-active and bio-resorbable materials. CVD and in particular LCVD and PECVD are promising methods for the preparation of metastable or unstable bio-ceramic materials. Since CVD has many process parameters, CVD can prepare optimized microstructures, crystal phases and preferential orientations for HAp regeneration.

**Open Access** This chapter is distributed under the terms of the Creative Commons Attribution Noncommercial License, which permits any noncommercial use, distribution, and reproduction in any medium, provided the original author(s) and source are credited.

## References

1. Goto T, Narushima T, Ueda K. *Biological and biomedical coatings handbook-processing and characterization*. Boca Raton: CRC; 2011.
2. Powell CF. Chemical vapor deposition. In: Powell CF, Oxley JH, Blocher Jr JM, editors. *Vapor deposition*. New York: Wiley; 1966. p. 249–76.
3. Sato M, Tu R, Goto T. Preparation conditions of  $\text{CaTiO}_3$  film by metal-organic chemical vapor depositon. *Mater Trans*. 2006;47:1386–90.
4. Nath S, Tu R, Goto T. Preparation of  $\text{Ca-Si-O}$  films by chemical vapor deposition. *Surf Coating Tech*. 2010;205:2618–23.
5. Sato M, Tu R, Goto T. Preparation of hydroxyapatite and calcium phosphate films by MOCVD. *Mater Trans*. 2007;48:3149–53.
6. Duty C, Jean D, Lackey WJ. Laser chemical vapor deposition: materials, modeling, and process control. *Int Mater Rev*. 2001;46:271–87.
7. Preachat B, Drawin S. Properties of PECVD-deposited thermal barrier coatings. *Surf Coating Tech*. 2001;142–144:835–42.
8. Hirai T, Goto T, Kaiji T. Preparation of silicon carbide by chemical vapor deposition. *J Ceram Soc Jpn*. 1983;91:503–9.
9. Tu R, Goto T. High temperature stability of anastase films prepared by MOCVD. *Mater Trans*. 2008;49:2040–6.
10. Zhang W, Vargas R, Goto T, Someno Y, Hirai T. Preparation of epitaxial AlN films by electron cyclotron resonance plasma-assisted chemical vapor deposition on Ir- and Pt-coated sapphire substrates. *Appl Phys Lett*. 1994;64:1359–61.
11. Goto T, Banal R, Kimura T. Morphology and preferred orientation of  $\text{Y}_2\text{O}_3$  film prepared by high-speed laser CVD. *Surf Coating Tech*. 2007;201:5776–81.
12. Goto T. Thermal barrier coatings deposited by laser CVD. *Surf Coating Tech*. 2005;198:367–71.
13. Hill WL, Faust GT, Reynolds DS. The binary system  $\text{P}_2\text{O}_5-2\text{CaO}\cdot\text{P}_2\text{O}_5$ . *Am J Sci*. 1944;242:457–77.
14. Mathew M, Schroeder LW, Dickens B, Brown WE. The crystal structure of  $\alpha\text{-Ca}_3(\text{PO}_4)_2$ . *Acta Crystallogr*. 1977;B33:1325–33.
15. Dickens B, Schroeder LW, Brown WE. The crystal structure of pure  $\beta\text{-Ca}_3(\text{PO}_4)_2$ . *J Solid State Chem*. 1974;10:232–48.
16. Calvo C. The crystal structure of  $\alpha\text{-Ca}_2\text{P}_2\text{O}_7$ . *Inorg Chem*. 1968;7:1345–51.
17. Webb NC. The crystal structure of  $\beta\text{-Ca}_2\text{P}_2\text{O}_7$ . *Acta Crystallogr*. 1966;21:942–8.
18. Allen GC, Ciliberto E, Fragala I, Spoto G. Surface and bulk study of calcium phosphate bioceramics obtained by Metal Organic Chemical Vapor Deposition. *Nucl Instrum Methods B*. 1996;116:457–60.
19. Dickens B, Brown WE, Kruger GJ, Stewart JM.  $\text{Ca}_4(\text{PO}_4)\text{O}$ , tetracalcium diphosphate monoxide. Crystal structure and relationships to  $\text{Ca}_5(\text{PO}_4)_3\text{OH}$  and  $\text{K}_3\text{Na}(\text{SO}_4)_2$ . *Acta Crystallogr*. 1973;B29:2046–56.
20. Kay MI, Young RA. Crystal structure of hydroxyapatite. *Nature*. 1964;204:1050–2.
21. Henning PA, Landa-Canovas AR, Larsson A, Lidin S. Elucidation of the crystal structure of oxyapatite by high-resolution electron microscopy. *Acta Crystallogr*. 1999;B55:170–6.
22. Elliott JC. Structure and chemistry of the apatites and other calcium orthophosphates. Amsterdam: Elsevier; 1994.

23. Narushima T, Ueda K, Goto T, Masumoto H, Katsume T, Kawamura H, Ouchi C, Iguchi Y. Preparation of calcium phosphate films by radiofrequency magnetron sputtering. Mater Trans. 2005;46:2246–52.
24. Darr JA, Guo ZX, Raman V, Bououdina M, Rehman IU. Metal organic chemical vapour deposition (MOCVD) of bone mineral like carbonated hydroxyapatite coatings. Chem Commun. 2004;6:696–7.
25. Ueda K, Narushima T, Goto T, Katsume T, Nakagawa H, Kawamura H, Taira M. Evaluation of calcium phosphate coating films on titanium fabricated using RF magnetron sputtering. Mater Trans. 2007;48:307–12.
26. Sato M, Tu R, Goto T, Ueda K, Narushima T. Hydroxyapatite formation on Ca–P–O coating prepared by MOCVD. Mater Trans. 2008;49:1848–52.
27. Sato M, Tu R, Goto T, Ueda K, Narushima T. Apatite formation behavior on bio-ceramic films prepared by MOCVD. J Ceram Soc Jpn. 2009;117:461–5.
28. Sato M, Tu R, Goto T, Ueda K, Narushima T. Preparation behavior in a Hanks' solution on Ca–P–O films prepared by laser CVD. Mater Trans. 2009;50:2455–9.

**Part III**

**Symposium III: Biomedical Engineering  
Interface**

# Chapter 10

## Importance of Visual Cues in Hearing Restoration by Auditory Prosthesis

Tetsuaki Kawase, Yoko Hori, Takenori Ogawa, Shuichi Sakamoto, Yôiti Suzuki, and Yukio Katori

**Abstract** Auditory prostheses, such as cochlear implant and auditory brainstem implant, are used clinically to restore the hearing of patients with sensorineural hearing loss. These devices can considerably improve the auditory information conveyed to the auditory cortex, but proper rehabilitation process is usually necessary to restore auditory communication to an adequate level. Therefore, improvements in the auditory information provided by the prosthesis can be complemented by better rehabilitation process.

Moreover, the complementary role of visual cues is also important. The “lip-reading” phenomenon is well known in patients with degraded speech perception; i.e., reduced speech perception in the presence of poor auditory conditions, such as background noise and in patients with hearing loss, is improved by the combined presentation of visual speech. In addition to such conventional lip-reading, audio-visual speech has another beneficial role in the auditory rehabilitation process; i.e., the visual cue enhances the auditory adaptation process to the degraded speech sound.

In the present paper, these two aspects of audio-visual speech in auditory rehabilitation are reviewed.

**Keywords** Audio-visual speech • Auditory prosthesis • Lip-reading • Rehabilitation

---

T. Kawase (✉)

Laboratory of Rehabilitative Auditory Science, Tohoku University Graduate School of Biomedical Engineering, Sendai 980-8574, Japan

Department of Audiology, Tohoku University Graduate School of Medicine, Sendai 980-8574, Japan

Department of Otolaryngology-Head and Neck Surgery, Tohoku University Graduate School of Medicine, Sendai 980-8574, Japan  
e-mail: [kawase@orl.med.tohoku.ac.jp](mailto:kawase@orl.med.tohoku.ac.jp)

Y. Hori • T. Ogawa • Y. Katori

Department of Otolaryngology-Head and Neck Surgery, Tohoku University Graduate School of Medicine, Sendai 980-8574, Japan

S. Sakamoto • Y. Suzuki

Research Institute of Electrical Communication, Tohoku University, Sendai 980-8574, Japan

## 10.1 Introduction

Sound vibrations in the air are transmitted to the inner ear via the ear drum and ossicular chain. The hair cell system, located in the inner ear, converts the sound vibrations into the electrical spike signals of the cochlear nerves. Therefore, the hair cell system is very important in the mechanism of electrical transduction in the inner ear. However, this important transducer system never regenerates after damage. Consequently, various types of auditory prostheses have been developed to restore the hearing of patients with sensorineural hearing loss.

Generally speaking, auditory prostheses are classifiable into two types depending on the fundamental concept of the device: some devices such as hearing aids (HAs), bone-anchored hearing aids (BAHAs), and Vibrant SoundBridge middle ear implants (MEIs) increase the energy of the sound vibrations transmitted to the damaged inner ear; whereas other devices such as cochlear implants (CIs), auditory brainstem implants (ABIs), and auditory midbrain implants (AMIs) stimulate the auditory system electrically (Fig. 10.1). Usually these latter devices (CI, ABI, AMI, etc.) are used if the hearing loss is too severe to use the former

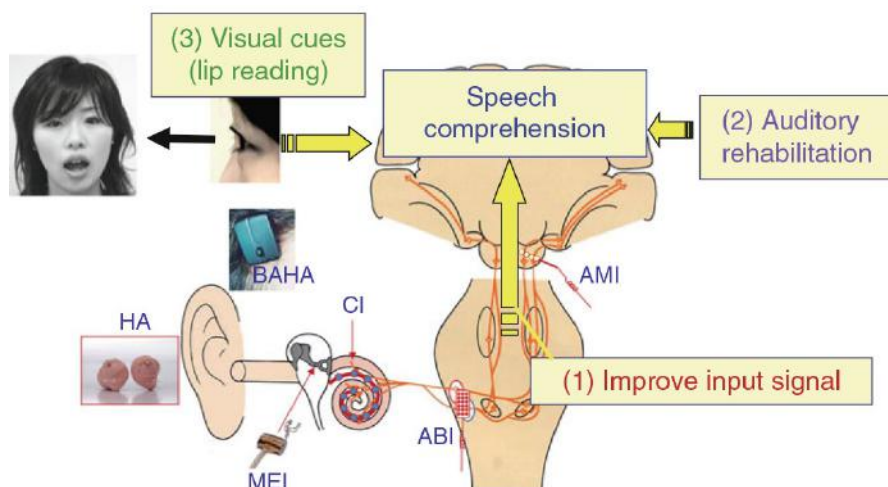


**Fig. 10.1** Basic strategy for better speech intelligibility in auditory rehabilitation. Devices such as the hearing aid (HA), bone-anchored hearing aid (BAHA, a type of HA based on bone conduction), and middle ear implant (MEI, a direct-drive, implantable middle ear device, which mechanically stimulates the ossicles, mimicking the natural hearing process) increase the energy of the sound vibrations transmitted to the damaged inner ear. In contrast, the cochlear implant (CI), auditory brainstem implant (ABI), and auditory midbrain implant (AMI) stimulate the auditory system electrically. The CI restores hearing by direct electrical stimulation of the cochlear nerve, whereas the ABI and AMI directly stimulate the auditory pathway at the cochlear nucleus and mid-inferior colliculus, respectively. Auditory information can be considerably improved by these electrical stimulation devices, but is usually insufficient. Therefore, rehabilitation and sometimes visual information known as the lip-reading effect are usually necessary to restore auditory communication to an adequate level

devices (HA, BAHA, MEI, etc.). All these devices can considerably improve auditory information conveyed to the auditory cortex, even in patients with severely degraded hearing loss requiring CI and/or ABI, however, a suitable rehabilitation process is usually necessary to restore a certain level of auditory communication. The basic strategy for improving speech intelligibility by auditory rehabilitation is presented in Fig. 10.1.

Therefore, it is important to improve both the quality of the auditory information that can be provided by each prosthesis ((1) in Fig. 10.1), and the rehabilitation process for individual patients ((2) in Fig. 10.1). Moreover, the complementary role of visual cues is also important ((3) in Fig. 10.1). The “lip-reading” phenomenon is well known in patients with degraded speech perception; i.e., reduced speech perception in the presence of poor auditory conditions, such as background noise and in patients with hearing loss, is improved by the combined presentation of visual speech [12, 15]. If the degraded speech can be perceived as bimodal audio-visual stimuli, the visual information from the speaker’s face can be effectively utilized to compensate for the inadequate auditory information [2, 9, 13]. In addition to such conventional lip-reading, audio-visual speech has another beneficial role in the auditory rehabilitation process; i.e., the visual cue enhances the auditory adaptation process to the degraded speech sound [10].

Here, these two aspects of audio-visual speech in auditory rehabilitation are reviewed.

## 10.2 Recruitment of Visual Cues in Degraded Speech Conditions

Perception of external signals is followed by integration of the information from multisensory modalities in the brain. Such multi-modal processing results in fast and accurate recognition of the perceived signals. Speech perception effectively utilizes the visual information from the speaker’s face not only in patients with hearing loss but also in healthy subjects; i.e., speech perception in degraded conditions such as background noise can be improved by visual information obtained from the speaker’s face [12, 15]. Therefore, visual cues (speaker’s face) presented with auditory cues (speech sound) will be utilized to complement the auditory information in every situation. However, the degree of recruitment of visual cues will depend on the degree of deterioration of speech perception [9].

Positron emission tomography (PET) was used to evaluate the effect of this recruitment of visual cues on the activation of additional brain areas caused by degradation of auditory input, as presented in Fig. 10.2. This PET study compared brain activation caused by the presentation of a visual cue (facial movement at speech) with control conditions (visual noise) under two different audio-conditions, normal speech and degraded speech. Lip-reading for degraded speech caused more activations than for normal speech in V2 and V3 of visual cortex as well as in the right fusiform gyrus of the temporal lobe (see [9] for details). The right fusiform

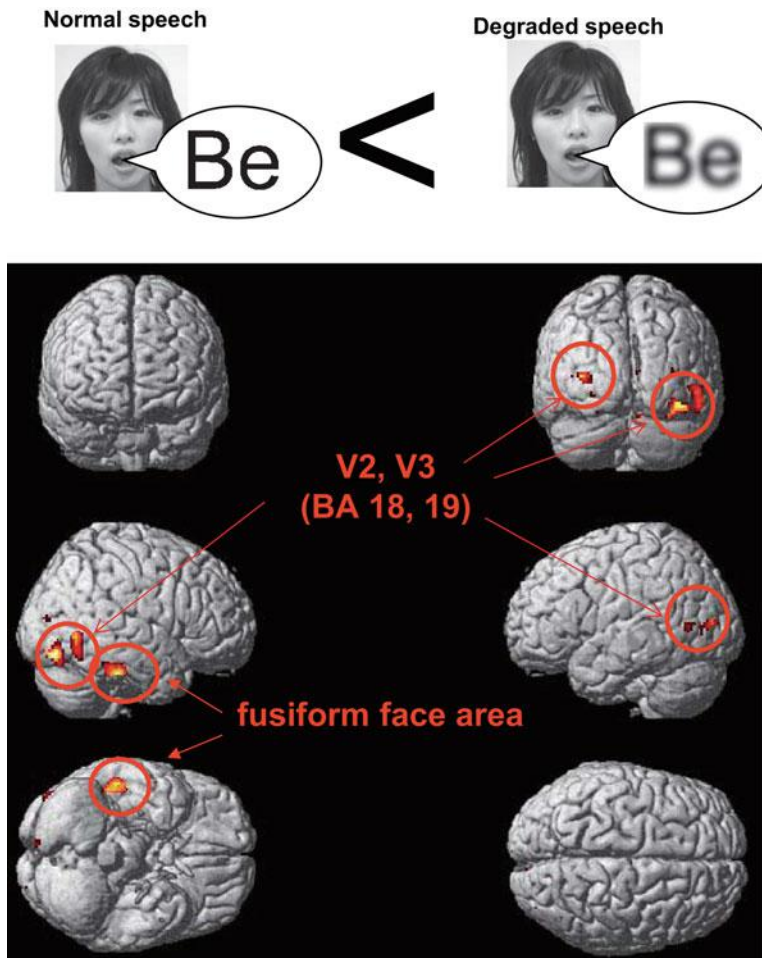


**Fig. 10.2** Additional recruitment of brain areas caused by degradation of auditory input (unpublished figure using our data published previously [9]). Positron emission tomography (PET) was used to compare brain activation caused by the presentation of a visual cue (facial movement at speech) with control conditions (visual noise) under two different audio-conditions, normal speech and degraded speech. Significant brain activation is presented during lip-reading under degraded speech compared with normal speech. Suprathreshold voxels ( $P < 0.001$ , uncorrected for multiple comparisons,  $k > 20$  voxels) superimposed on the 3D-rendered surface image. Lip-reading for degraded speech caused more activations than for normal speech in V2 and V3 of visual cortex as well as in the right fusiform gyrus of the temporal lobe (see Kawase et al. 2005 [9] for details)

gyrus of the temporal lobe is a well-known brain area known as the fusiform face area (FFA). The FFA, together with the inferior occipital gyri and the superior temporal sulcus, is one of the three important brain regions in the occipitotemporal visual extrastriate cortex related to human face perception [3–8, 11]. Therefore,

activation of the FFA during auditory-visual speech perception is very likely. The present study indicated that the degree of activation of FFA depends on the degree of the degradation of auditory cues. This observation is consistent with the hypothesis that more visual information than usual is recruited under conditions of degraded auditory information.

### 10.3 Auditory Training with Bimodal Audio-Visual Stimuli

These investigations of perception of bimodal audio-visual stimuli under degraded speech conditions show that visual information from the speaker's face can be effectively utilized to make up for inadequate auditory information. Therefore, combined presentation of visual speech information is important in speech communication in the presence of degraded auditory conditions, such as background noise and in patients with hearing loss.

On the other hand, audio-visual speech cues have another beneficial role in the auditory rehabilitation process; i.e., the visual cue enhances the auditory adaptation process to the degraded speech sound [10]. In that study, auditory training was examined in normal volunteers using highly degraded noise-vocoded speech sound (NVSS), which is often used as a simulation of the effects of cochlear implant on speech [1, 14]. NVSS is hardly intelligible at first listening, but adequate auditory training can improve the intelligibility of NVSS. After the initial assessment of auditory speech intelligibility (no visual cue), the subject underwent different training sessions with combinations of presence/absence of visual cue and presence/absence of feedback of the correct answer. The training sessions used two word lists consisting of the same 50 four-mora words in different orders which were alternately presented ten times (five times each). The effects of these different training sessions on auditory speech intelligibility (no visual cue) were assessed for the trained words (in different order from those used in the training session) as well as untrained words after the training session (see [10] for details).

The effects of the presence of visual cues during the training session on word intelligibility after the training session are presented in Fig. 10.3 (feedback (-) groups) and 4 (feedback (+) groups). Speech intelligibility after the training session was significantly improved in all training groups but was significantly different between the different training conditions. Visual cues simultaneously presented with auditory stimuli during the training session significantly improved auditory speech intelligibility compared to only auditory stimuli. Feedback during the training session also resulted in significantly better speech intelligibility for trained words (Fig. 10.4). In contrast, feedback resulted in lower scores compared to without feedback in the post-training test for untrained words (Fig. 10.4), showing over-training effects. However, facilitative visual effects on post-training auditory performance were also observed regardless of the over-training effects. These results indicate that combined audio-visual training has beneficial effects in auditory rehabilitation.

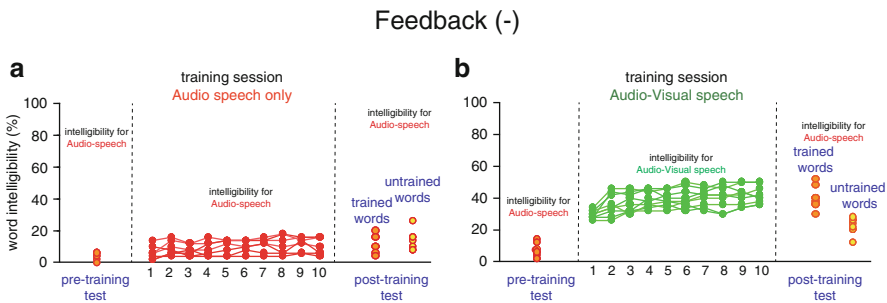


**Fig. 10.3** Effects of the presence of visual cues during the training session on word intelligibility after the training session (no feedback condition) (unpublished figure using our data published previously [10]). (a) Training with auditory cue only (without visual cues), (b) training with auditory + visual cues (lip-reading condition). Word intelligibilities (no visual cue) before and after training are presented along with those during the training (learning curves). Intelligibilities during the training are those for training modalities; i.e. for only auditory speech (a) and audio-visual speech (b), respectively. Intelligibilities after training are shown for trained words (intelligibility for words used in the training session) and for untrained words (intelligibility for words not used in the training session)

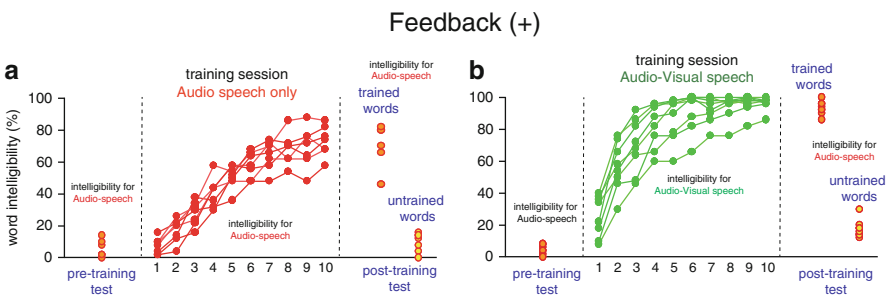


**Fig. 10.4** Effects of the presence of visual cues during the training session on word intelligibility after the training session (with feedback condition) (unpublished figure using our data published previously [10]). (a) Training with auditory cue only (without visual cues), (b) training with auditory + visual cues (lip-reading condition). Word intelligibilities (no visual cue) before and after training are presented along with those during the training (learning curves). Intelligibilities during the training are those for training modalities; i.e. for only auditory speech (a) and audio-visual speech (b), respectively. Intelligibilities after training are shown for trained words (intelligibility for words used in the training session) and for untrained words (intelligibility for words not used in the training session). In contrast with feedback (-) groups in Fig. 10.3, better speech intelligibilities were obtained for trained words. On the other hand, feedback resulted in lower scores compared to without feedback in the post-training test for untrained words, showing over-training effects. Facilitative visual effects on post-training auditory performance were also observed regardless of the over-training effects

The effects of different training sessions on the intelligibility are presented in Fig. 10.5, divided into each “mora” of the words. Basically, similar trends to those found based on word intelligibility were also observed by this “mora”-based analysis, although the intelligibility was different for the first, second, third, and fourth moras.

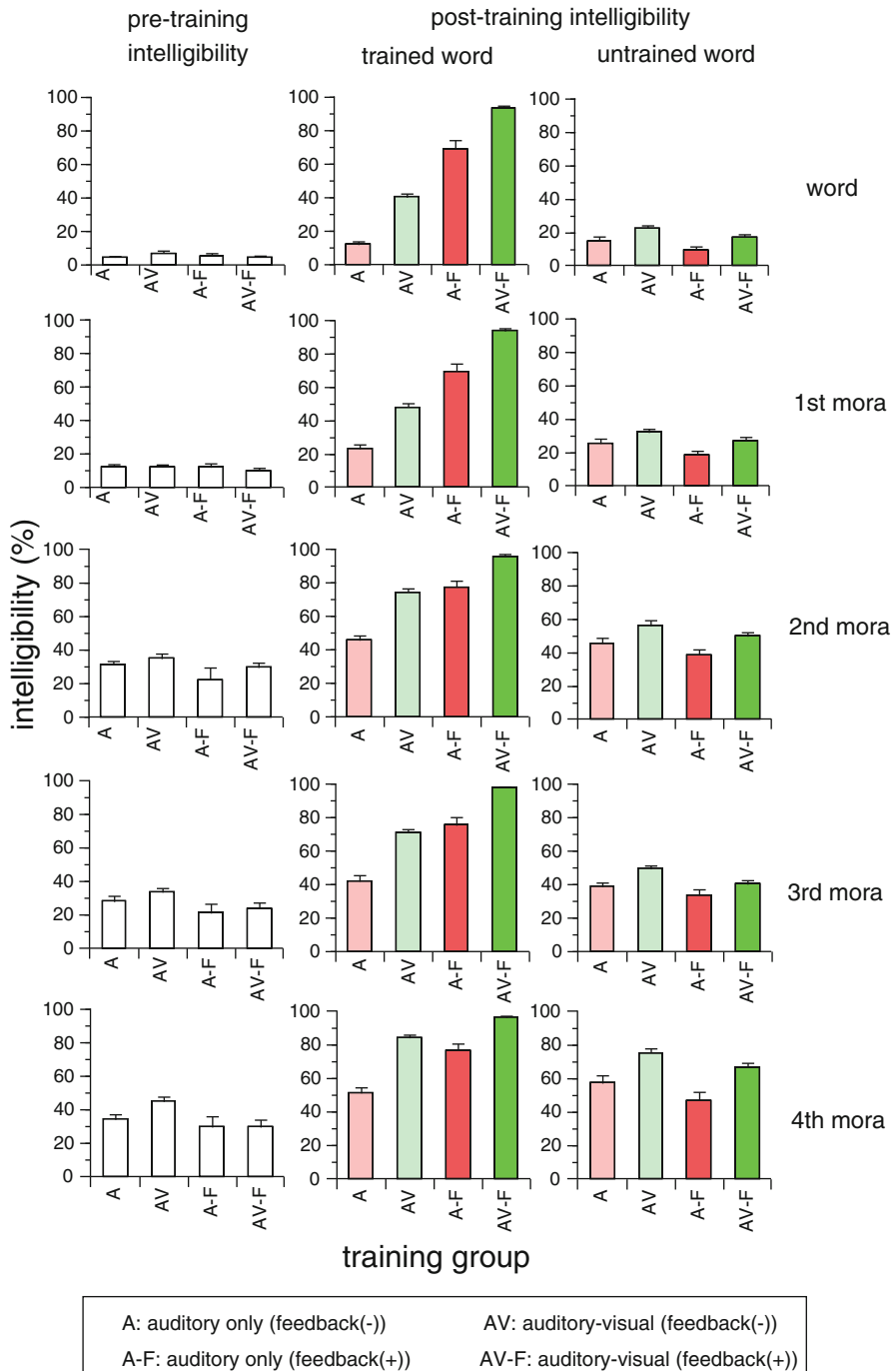


**Fig. 10.5** Effects of different training sessions on “mora” intelligibilities (unpublished figure using our data published previously [10]). In addition to word intelligibilities, the intelligibilities for the first, second, third, and fourth moras are presented for four training sessions. Although the intelligibilities for the first mora were significantly smaller, basically similar trends to those found based on word intelligibility were also observed

Visual information is generally considered to complement insufficient speech information in speech comprehension. However, the present results revealed another beneficial effect of audio-visual training; i.e., the visual cue enhances the auditory adaptation process to the degraded new speech sound. The present findings suggest that the correct use of audio-visual bimodal training would facilitate the auditory rehabilitation process of patients with auditory prostheses such as a CI or ABI.

## 10.4 Summary

Visual information of audio-visual speech is known to complement degraded speech information in rehabilitation after implantation of a CI or ABI. In addition to this basic effect, audio-visual speech may also enhance the auditory adaptation process, with as little as a few hours audio-visual training.

**Acknowledgements** This study was supported by a grant-in-aid from the Japanese Ministry of Education, Culture, Sports, Science and Technology for fiscal 2007–2009 (Grant-in-Aid for Scientific Research (C) 19591954). Most contents of the present proceedings are based on our previous publications [9, 10].

**Open Access** This chapter is distributed under the terms of the Creative Commons Attribution Noncommercial License, which permits any noncommercial use, distribution, and reproduction in any medium, provided the original author(s) and source are credited.

## References

1. Fu QJ, Nogaki G, Galvin 3rd JJ. Auditory training with spectrally shifted speech: implications for cochlear implant patient auditory rehabilitation. *J Assoc Res Otolaryngol*. 2005;6:180–9.
2. Giraud AL, Truy E. The contribution of visual areas to speech comprehension: a PET study in cochlear implants patients and normal-hearing subjects. *Neuropsychologia*. 2002;40:1562–9.
3. Halgren E, Dale AM, Sereno MI, Tootell RB, Marinkovic K, Rosen BR. Location of human face-selective cortex with respect to retinotopic areas. *Hum Brain Mapp*. 1999;7:29–37.
4. Haxby JV, Ungerleider LG, Clark VP, Schouten JL, Hoffman EA, Martin A. The effect of face inversion on activity in human neural systems for face and object perception. *Neuron*. 1999;22:189–99.
5. Haxby JV, Hoffman EA, Gobbini MI. The distributed human neural system for face perception. *Trends Cogn Sci*. 2000;4:223–33.
6. Hoffman EA, Haxby JV. Distinct representations of eye gaze and identity in the distributed human neural system for face perception. *Nat Neurosci*. 2000;3:80–4.
7. Ishai A, Ungerleider LG, Martin A, Schouten JL, Haxby JV. Distributed representation of objects in the human ventral visual pathway. *Proc Natl Acad Sci U S A*. 1999;96:9379–84.
8. Kanwisher N, McDermott J, Chun MM. The fusiform face area: a module in human extrastriate cortex specialized for face perception. *J Neurosci*. 1997;17:4302–11.
9. Kawase T, Yamaguchi K, Ogawa T, Suzuki K, Suzuki M, Itoh M, et al. Recruitment of fusiform face area associated with listening to degraded speech sounds in auditory-visual speech perception: a PET study. *Neurosci Lett*. 2005;382:254–8.

10. Kawase T, Sakamoto S, Hori Y, Maki A, Suzuki Y, Kobayashi T. Bimodal audio-visual training enhances auditory adaptation process. *Neuroreport*. 2009;20:1231–4.
11. McCarthy G, Puce A, Gore JC, Allison T. Face-specific processing in the human fusiform gyrus. *J Cogn Neurosci*. 1977;9:605–10.
12. Rosen SM, Fourcin AJ, Moore BC. Voice pitch as an aid to lipreading. *Nature*. 1981;291:150–2.
13. Sekiyama K, Kanno I, Miura S, Sugita Y. Auditory-visual speech perception examined by fMRI and PET. *Neurosci Res*. 2003;47:277–87.
14. Shannon RV, Zeng FG, Kamath V, Wygonski J, Ekelid M. Speech recognition with primarily temporal cues. *Science*. 1995;270:303–4.
15. Sumby WH, Pollack I. Visual contribution to speech intelligibility in noise. *J Acoust Soc Am*. 1954;26:212–5.

**Part IV**

**Symposium IV: Cell Manipulation and  
Tissue Regeneration**

# **Chapter 11**

## **Designer Supersurfaces via Bioinspiration and Biomimetics for Dental Materials and Structures**

**David W. Green and Han-Sung Jung**

**Abstract** The design of surfaces and interfaces gives rise to superior qualities and properties to materials and structures. The interface between biology and materials in nature is being closely examined at the smallest scales for a number of significant reasons. It is recognised that the properties of surfaces have definite biological effects that can be harnessed in clinical regeneration biology. Also the deeper understanding of surface interactions between cells and matrices in human biology is spurring the fabrication of biomimetic and bioinspired versions of these natural designs. The new emerging science of bioinspired surface engineering is helping to improve clinical performances for biomaterials and biostructures because it resolves the problems necessary to optimise integration of implant biomaterials and structures. One of the major developments is the use of surface topography, which is now being exploited for microbial control, steering stem cell behaviours in proliferation and differentiation and adhesive surfaces for better bonding with tissues. In this Chapter we will explore the status of these super surfaces and examine the possibilities for the next generation of dental biomaterials and implants.

**Keywords** Antibacterial surfaces • Bactericidal surfaces • Cell influencing surfaces • Microtopography • Surface nanotopography

---

D.W. Green

Oral Biosciences, Faculty of Dentistry, The University of Hong Kong, Hong Kong SAR, China

H.-S. Jung (✉)

Oral Biosciences, Faculty of Dentistry, The University of Hong Kong, Hong Kong SAR, China

Division in Anatomy and Developmental Biology, Department of Oral Biology, Oral Science Research Center, BK21 PLUS Project, Yonsei University College of Dentistry, 50 Yonsei-ro, Seodaemun-Gu, Seoul, South Korea

e-mail: [hsjung@yuhs.ac](mailto:hsjung@yuhs.ac)

## 11.1 Introduction

The structural and chemical details at surfaces of biomaterials and the meeting between surfaces is vitally important in the mechanical design of organisms, structural biomaterials, anti-wetting, self-cleaning properties, cell adhesion and migration. These superior and sophisticated properties are what can be termed super surfaces. Evolution has selected for adaptations that include various styles of physical structuring, chemical coatings and molecular patterning to create superior and sophisticated functions at surfaces. These are the best possible adaptations, in the design of surfaces that also apply to the same intrinsic problems faced in applications for biology and medicine. They have been tried, tested and optimized over millions of years of evolution. A result is that many of the adaptations discovered in nature are often new to science and technology. Hence this is the reason why biomimetic based researchers search across nature for new potent ideas in solving materials based problems. There are added advantages in following biomimetic approaches such as, learning how to reduce energy during the construction of materials and features at the surfaces [1]. There are now large catalogues where this kind of innovation information can be easily accessed, interpreted and used for the interrogators problem in hand [2]. An important distinction is to be made between biomimetic and bioinspired approaches. In biomimetics the objective is to simulate or copy a structure, process or mechanism directly from nature. Bioinspiration is the strategy where an influential component from biology is used in the problem solving and its eventual solution. So with bioinspiration there is a confluence of biological and human ingenuity. Each strategy has been used effectively in biomedicine.

In this chapter, we focus on two biomedically significant topics where the design of surfaces can be improved for better clinical outcomes. These topics are bacterial and human cell adhesion and detachment. Specifically, the clinical problem at biomaterial implant surfaces is to drive a strong yet stable biointegration and the second is an effective control of pathogenic microbes at the outer surface of implants. The construction and refinement by optimisation of the surfaces and interfaces of traditional restoration dental materials is a large topic of research but will not be included here. Material scientists are infact still grappling to control these phenomena and having the ability to programme their surfaces to work in tune with biology. The examples we will focus on in this chapter for developing biomedical supersurfaces are mainly studies in bioinspiration.

A major quest for regeneration scientists is the ability to control cell behaviour and activity for a variety of roles. Cell manipulation engineers have achieved some success in defining the mechanisms for influencing cells in predictable ways. Cells are influenced and guided by physical forces and contacts with surfaces. This environment conditions the cells future role. This means that cells in tissue organizing collectives are ultimately programmed outside in than inside out. Considerable research has been underway to develop surface features that can be used to sensitize and direct cell growth, proliferation and differentiation. More advanced

surface engineering employs changes in the characteristics of topography, symmetry, geometry, stiffness and elasticity of the underlying material all-together. It has been challenging to systematize all of these elements into cause and effect relationships. The desire is to produce a blueprint for designs that have predicted effects. Programmable biomaterials with influential topography are a realistic prospect for interplay with human cells and bacteria cells. There is tremendous array of data showing the diverse pairings of nanotopography arrays with fibroblasts, endothelial, epithelial, pluripotent, mesenchymal and embryonic [3–12]. There are numerous instances of conflicting results but there are strong trends emerging. For example, certain topographic structures induce clear differentiation responses within contacting cells. The best example is osteogenesis by Mesenchymal Stem Cells (MSCs) subject to disordered nanopits [13]. Significantly adding to this is evidence of the molecular pathways involved in this process, the main one being integrin-activated focal adhesion kinase (FAK). Another trend is that low aspect ratio structures are favourable to attachment and spreading phenomena whereas higher aspect ratio structures lead to cell sheets that self detach [14].

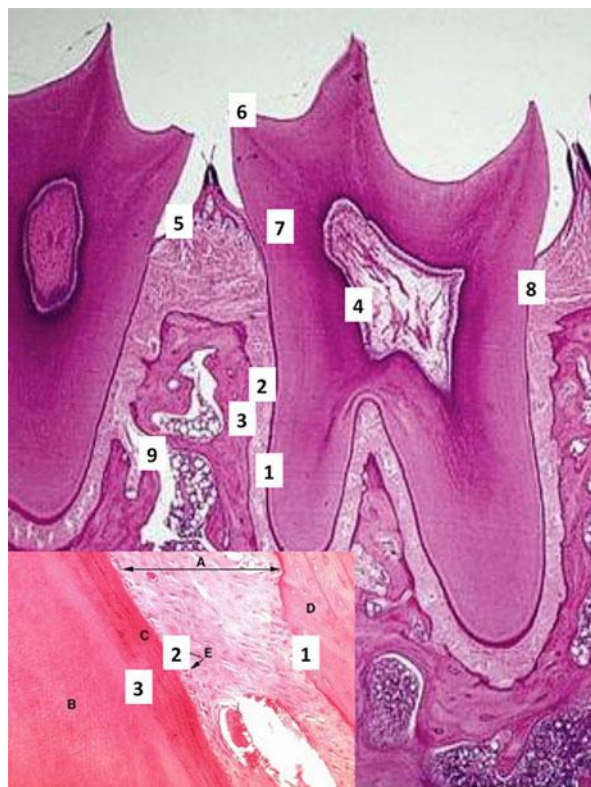
Eukaryotic and Prokaryotic cells are also influenced strongly by the chemistry of the surface. The chemistry aspect and the physical features are interlinked. Each influences the downstream effects of the other factor. A surface with a homogenous chemistry on a smooth surface once modified with surface topography redistributes the chemistry and introduces new heterogeneity. In the next section, we map the surfaces and boundaries in and around the tooth organ and describe briefly their biological and mechanical functions.

## 11.2 Materials Dentistry: A World of Surfaces and Interfaces

Restoration and replacement of dental structures is intensively focused on surfaces at boundaries and interfaces. The tooth organ is made up of a multiplicity of tissue layers and interfaces (Fig. 11.1). These are necessary for the intricate biomechanical functions of the tooth organ. Replacing them requires mastery of interface engineering. Graded interface is the key to integration between layers consisting of different compositions and structures. Many mechanisms are in play to stop or contain cracks from forming. In traditional restorative dentistry the question of bonding layers of different materials coherently has been studied in great depth. The better design of surface structures and chemistry is imperative for every material placed inside the body. Surfaces are also being used to control and manipulate biology in rational ways.

In the regenerative sciences precise control of cell proliferation and differentiation is unresolved and therefore remains of considerable future significance. In cell engineering surface structures over large surface areas have been developed to select, maintain, expand and invoke phenotype changes in cell populations with

**Fig. 11.1** A histological longitudinal slice through a human molar tooth with annotations to highlight surfaces and junctions or interfaces inside and around the tooth organ. (1) Dentine to Periodontal ligament interface; (2) PDL/cementum interface; (3) Cementum/bone junction; (4) Dentine/pulp junction; (5) Gingiva/boundary; (6) Enamel boundary; (7) Dentine/enamel junction; (8) Gingiva/enamel interface. Image reproduced from: <http://www.uky.edu/~brmacp/oralhist/module8/lab/imgshtml/image02.htm> and <http://www.am-medicine.com/2013/12/an-illustrative-note-powerpoint.html>



some important successes. Topography at the nanoscale is showing enormous promise as a device to influence cell behaviours in predictable and useful ways for benefits in cell therapy and tissue engineering. Research on surface continues to be a crux in materials dentistry and regenerative dentistry. The major areas would be surfaces for bacteria control and selectivity and surfaces for cell and tissue integration. The basic work on programmed surfaces for cell selection, growth and lineage specification also relate heavily to regenerative dentistry strategies and offer new therapeutic routes. In the next sections of this chapter we hone in on the programmed surfaces with topography for bacteria control, tissue adhesion and biointegration.

### 11.3 Bactericidal and Antibacterial Surfaces

Bacterial biofilms are notoriously difficult to eradicate from surfaces such as implants. There are different ways of preventing bacteria adhesion and colonisation. The first most extensively investigated is chemical and molecular engineering of surfaces. In these approaches surfaces are built with adjuncts such as dendrimers,

cationic peptides, photoactivation, lysostaphin, deactivators of quorum sensing and grafted antibiotics [15].

In dentistry, there is the added complexity by which the main aim is to selectively control different bacterial populations and not to eradicate everything. The mechanisms of attachment for bacteria are not fully understood. Surface roughness, wettability and surface energy are known to influence bacteria attachment and adhesion most profoundly. The range of limits for these properties has been difficult to measure precisely. Surface roughness above 0.2 µm is known to promote plaque formation. The influence of surface energy properties is complicated by the nature of the bacterial cell wall charge properties. Hydrophobic interactions in bacteria are common since adhesions located on pili are themselves hydrophobic. According to some evidence acquired in vitro hydrophobic processes drives attachment. However, the greatest task is to unravel the complexities of surface properties and bacteria adhesion in living biological environments. Of greatest prominence is the effect of serum proteins at the surface, which conditions all other biological responses.

### ***11.3.1 Controlling Oral Pathogens via Surface Structuring***

The oral cavity is colonised by a whole community of microbes that include bacteria, viruses and fungi. The ecology or interrelationships between the members of the various microbial communities are highly intricate and under constant investigation with new links in the network being uncovered regularly. It is thought that changes in community structure invoke degenerative diseases that cause tissue destruction of dentine, periodontal ligament, gingiva and bone. Once the environment and conditions favour the acceleration of pathogenic growth the disease and tissue destruction is highly likely to occur. Effective ways must be sought to control and eradicate pathogenic microbes from the mouth. A degree of control is often required to reset the community structure of bacteria. There has been voluminous research to effectively kill pathogenic outright. Antibiotics are the most effective altogether. However, there is increasing evolved resistance to antibiotics and the targeted delivery of antibiotics remains imperfect. Other main treatments implement chemical toxins, photodynamic elements and nanoparticles to destroy bacterial biofilms and kill bacteria. There is also renewed interest in prospecting for new antibacterial compounds from sessile invertebrates renowned for the complex defensive chemistry, e.g. Marine sponges and Ascidiens. As such there are many examples in nature where evolution has selected for sophisticated adaptations to kill microbes or prevent contact with the organism. A significant adaptation that has emerged is structural devices at surfaces.

Nature has evolved countless interfaces precisely with anti-bacterial defences using specific Nano topographies alone. And this is independent of the effects from chemical secretions. Probably the first application of patterned surfaces of diamond shaped micro-protuberances to hinder bacterial contamination is Sharklet inspired

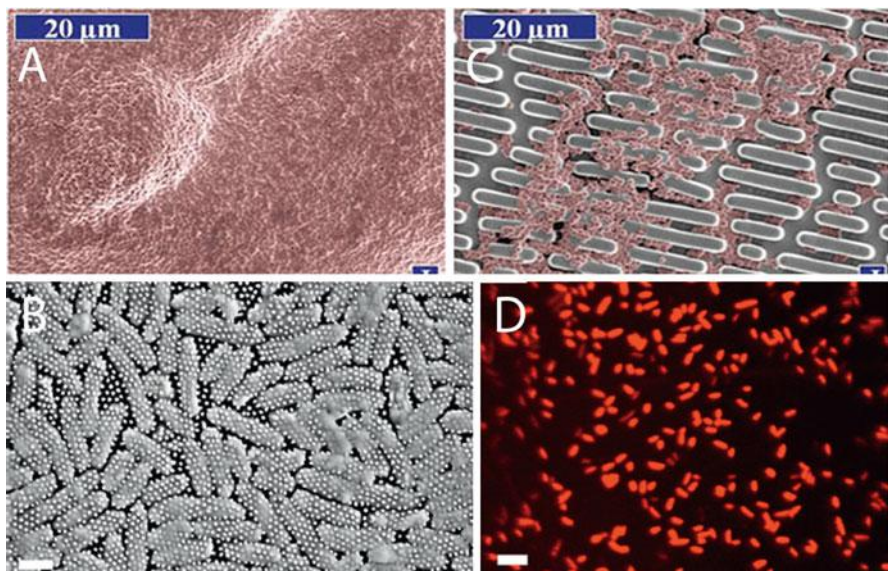


**Fig. 11.2** Anti-bacterial and Bactericidal surfaces based on microstructure and nanostructure. (a) Smooth surface covered in bacteria after 2 days; (b) Bacteria colonisation on a patterned micro-structure surface translated from shark skin; (c) SEM of “skewered” bacteria; (d) Confocal image showing dead bacteria sitting on top of Cicada nanopillar structure [18]

from the micron structure of scales or dermal denticles from shark-skin [16, 17]. The synthetically replicated surface hinders growth of a range of biomedically significant bacteria species such as, *Staphylococcus aureus* and *Escherichia coli* [16, 17]. The special nanostructure at the surface are deleterious to *Pseudomonas aeruginosa* and lead to the shredding of other pathogenic species including: *B. catarrhalis*, *E. coli*, *P. aeruginosa*, and *P. fluorescens*. Another recently discovered bactericidal surface imported directly from nature is the Cicada wing surface (Fig. 11.2).

The structure consists of nanometric pillars 200 nm tall, 100 nm in diameter at the base and 60 nm at the tip spaced 170 nm apart in a highly regular and tight pattern. This precision piece of Nano architecture being ten times smaller than the cell itself punctured settling bacterial cells and killed them with 60 min from attachment (Fig. 11.2). The killing power has been measured for this wing surface and was described as being efficient with  $6 \times 10^6$  bacterial cells made inoperable in every square centimeter after 30 min [18]. These initial results represent are of supreme usefulness for control of clinical infections anchored onto biomaterial and implant surfaces. However, the topography did not kill gram-positive species of bacteria: *B. subtilis*, *P. maritimus*, and *S. aureus* species of bacteria. Other wing topographies are being actively pursued as potential antibacterial and bactericidal devices. It has been reported that Dragonfly wings *Diplacodes bipunctata* have strong and rapid bactericidal effects on a broader range of bacteria classes-both

gram negative and gram-positive types as well as bacterial spores. A synthetically created surface with the exact same features of densely packed protruding nanospikes as the Dragonfly wing demonstrated the same bactericidal effects. It was estimated that 45,000 bacterial cells every minute in every cm squared were killed. Black silicon is this equivalent and is generated using ion beam technology. This is costly and cannot be transferred onto just any surface and specifically onto the type of materials useful in biomedicine [19].

Surface roughness and structure influences human cells more acutely than bacterial cells. This is because eukaryotic cells have a much more complicated sensory apparatus than prokaryotes. It was first evidenced that human cells can sense, detect and “react” to structures of  $>5$  nm at very small distances of 3–15 nm [20]. Physical attachments between cells and extracellular matrix (ECM) molecules can only be made at such close distance. There is broad remit to harness the sensory apparatus of the cell and influence their behaviour in many important aspects such as, migration, alignment, polarity, differentiation and proliferation. Such governability opens up many biotechnological and therapeutic avenues from tissue regeneration to biosensing.

## 11.4 Cell Adhesive Surfaces Using Nanotopography

Material surfaces with higher and more potent capacities to encourage cell attachment are required in a range of biomedical applications. This is achieved by modulating the type of nanostructure and its dimensions. Nanopillars have recently shown a degree of success in selectively adhering cells onto its structure with clear effects on phenotype and proliferation (Fig. 11.3a, b). In many applications adhesion and separation of different cell types is a desirable biological event (Fig. 11.3c). For example in one study nanopillar structures of a specified aspect ratio would favour endothelial cell adhesion while concomitantly preventing adhesion of fibroblastic cells. This duality is ideal for vascular implants in, which endothelial association is needed for coating and the fusion with existing vessels without interference of fibroblasts involved in clotting reactions [4] (Fig. 11.3c). Strong cell attachment on specialised cell adhesive nanotopographies is a vital outcome that can promote tissue formation, remodelling and bonding at the biomaterial surface.

## 11.5 Tissue Adhesive Surfaces

Materials with surfaces that can adhere to living tissue and participate in regeneration, development and repair are important. In surgery tough, stretchable and tear resistant tapes able to stick rigidly to tissues would be broadly revolutionary in the treatment of wounds, reducing surgery and complications. Conceivably such a

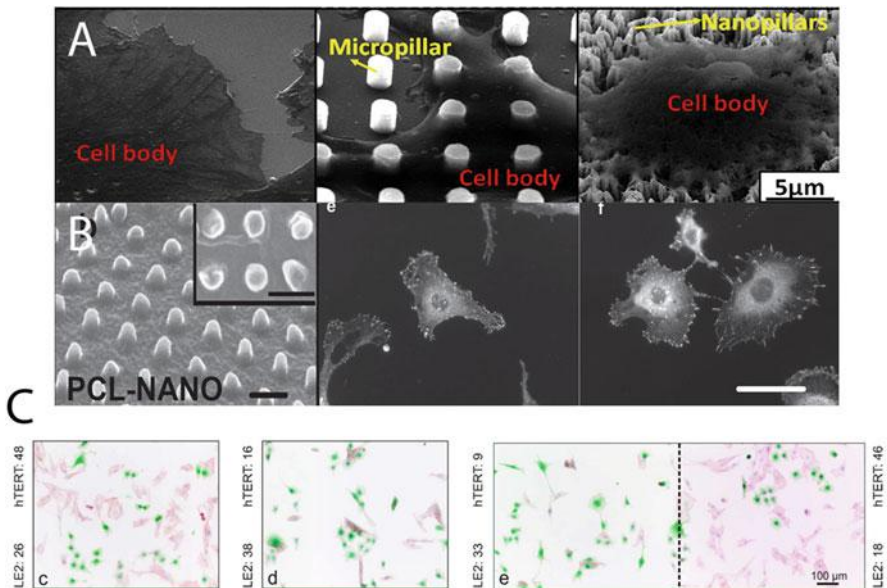


**Fig. 11.3** Cell responses to nanopillar topography. Variations are apparent in responses regarding different cell types and dimensions of the nanotopography. **(a)** MSCs growing on top of nanopillars did not spread and the shape governing stress distribution increased production of osteogenic matrix molecules; **(b)** Vinculin staining to highlight the focal adhesion portion inside hTERT (fibroblasts) cells at cell periphery on flat and nanopillar array. The low count of focal adhesions on nanopillars decreased proliferation; **(c)** Co-staining of hTERT and endothelial cells to show the different growth and proliferation responses with increasing pillar size (aspect ratio) from left to right. Endothelial cell growth and proliferation were preferentially selected on the high aspect ratio nanopillar surfaces [4, 5]

design could be used to replace sutures and staples. Bioglues have been developed as potential candidates for wound closure and sealing. However, they have been dogged by inflammation susceptibility. The reason is that the toughening of these tissue adhesives requires strong chemical reactions to take place, and is the source of biological irritation. Another point is to develop effective glues that bond in wet conditions. In both cases natural ingenuity may offer prospects for success. Adhesives derived from nature may offer a chemistry of bonding which is more favourable to biological systems and less inflammatory. In this vein, analogues (e.g. polydopamine) of the main active ingredient of mussel adhesive proteins, 3,4-dihydroxyphenylalanine (DOPA) have been broadly investigated.

The topic of bioadhesives is large and is focused upon chemical compounds assimilated with potent chemical reactions—a necessity in making tough and resilient materials for the task. This has the unintended consequence of eliciting inflammation. In a bioinspired approach the idea has been to harness naturally occurring surface structures for adhesion such as the Gecko foot pads; reproducing them in a biocompatible elastomer in the role of a self-adhesive tissue tape (Fig. 11.4a). Along these lines it was proposed that adhesion is largely based on

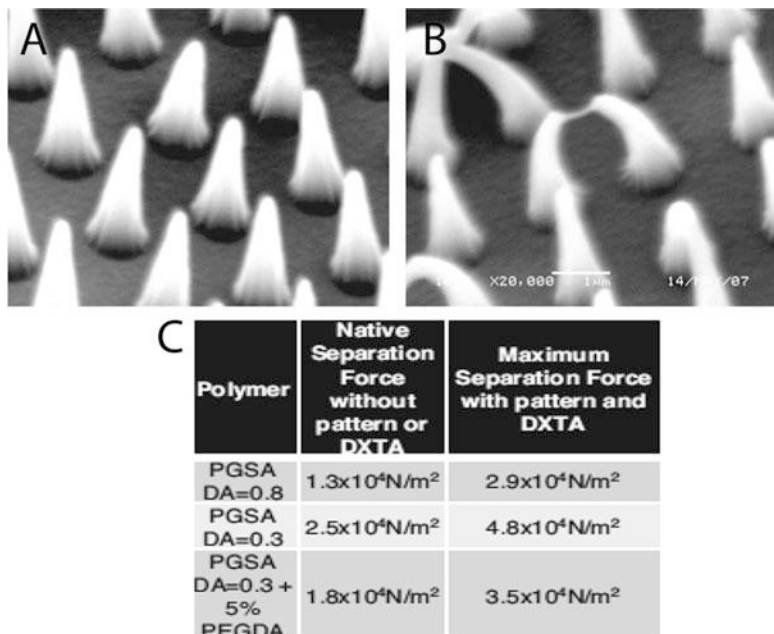


**Fig. 11.4** Nanotopography copied from the design of Gecko footpad setae were used to produce an self-adhesive tape material. (a) High power SEM of nanoprotrusions made from elastomer; (b) High power SEM of nanoprotrusions coated with a dextran coating to enhance tissue adhesion; (c) Table showing the strength of attachment to porcine intestine tissue between non nanotextured and textured with and without oxidised dextran [22]

physical structure. The problem of wet adhesion has been solved in nature by Tree frogs for example. The design blueprint has been unravelled in this organism and is therefore accessible for technology transfer into a useful product [21]. In the Gecko example wet adhesion property had to be introduced by additional chemical coating (Fig. 11.4b). The bioinspired engineers developed a strongly adherent tissue tape copied from the structure design of gecko foot pad surfaces. In tests the tape performed well on porcine intestine tissue and rat abdominal subfascial *in vivo* with strong forces of resistance to its separation from the living wet tissue (Fig. 11.4c) [22].

## 11.6 Surfaces for Cell Proliferation and Differentiation

Structures at surfaces that elicit proliferation and/or differentiation responses are in high demand especially those with high potency and precise reactions [11, 12]. A principal property of the surface with biological implications is wettability feature [23]. Still more information is needed to completely understand the effects of wettability on cell attachment and tissue integration. Surprisingly for dental

implants the wettability is usually not measured or considered in biological evaluation. The topic has been scrutinised most widely for implant osseointegration [23]. Generally wettabilities of intermediate values can optimise favourable cell interactions. An important contribution of wettability to biodynamics at the surface is protein adsorption. Proteins are the first biomolecule to arrive at the surface taking milliseconds. The nature of the protein assembly at the surface directs the cell response. This has been studied mainly with osteoblasts as well as fibroblasts and keratinocytes. Synergism between topography and chemical properties occurs but the interrelationship is unpredictable.

One of the purposes is to discover and develop the most efficient platform of expanding the numbers of stem cells in vitro into the population numbers needed for therapeutic tissue regeneration. In addition the ability to specify cell lineages of the expanded populations is another necessity to generate desired tissue types. Once again platform cell-scale microgauged technologies that can achieve this accurately and with high specificity are still needed. These base technologies are useful for the study of basic processes and in modelling responses to new drugs and to build phenotypically accurate populations of cells for tissue regeneration. Much work has been carried out to unravel the mechanisms involved in surface contact and gene expression. The principal contact point is the subcellular macromolecular focal adhesion, which is joined between the cell cytoskeleton and extracellular matrices [7]. The association and clustering of these objects with the matrix is an important effect that allows sensing of mechanical forces. Others have discovered the molecular circuits directly involved in transmitting topography influences into the cell nucleus where it impinges on gene expression patterns.

To be truly biomimetic with the totality of biological functions the surface patterns and design should ideally relate directly to the surfaces of the extracellular matrix and structural biomaterials (Fig. 11.5). Cell function is strongly influenced by active structures at nanometric sizes. Going beyond this, introduced nanoobjects such as rods, particles and fibres interplay with cells at the nanoscale by influencing extracellular micro-physiological events including protein adsorption and receptor-ligand binding. In one good example the ultrastructure details of the extracellular matrices were used to plan the design of synthetic topographies [24]. Thus this strategy has a strong biological basis to it. Many ECM structures possess nanogauged groove structures for example. In this study the researchers used the structural density of nanofeatures whose features were replicated from model tissues bone, nerve and skin. They found that processes such as adhesion, migration and differentiation could be controlled directly via the spacing and density of nanotopographic grooves [24]. The geometries of natural surface structures are being increasingly assessed as potential platforms for MSC differentiation and maintenance [13]. In nature the geometrical patterns are often more intricate than regular grooves, pillars or pits [25]. In the first report of its kind disordered arrangement of nanopits was found to stimulate osteogenic differentiation of MSC's. Recent similarity has been drawn between this geometry for MSC's and the nanofeature of collagen X on endochondral ossification because it shows a hexagonal pattern (Fig. 11.5) [26].

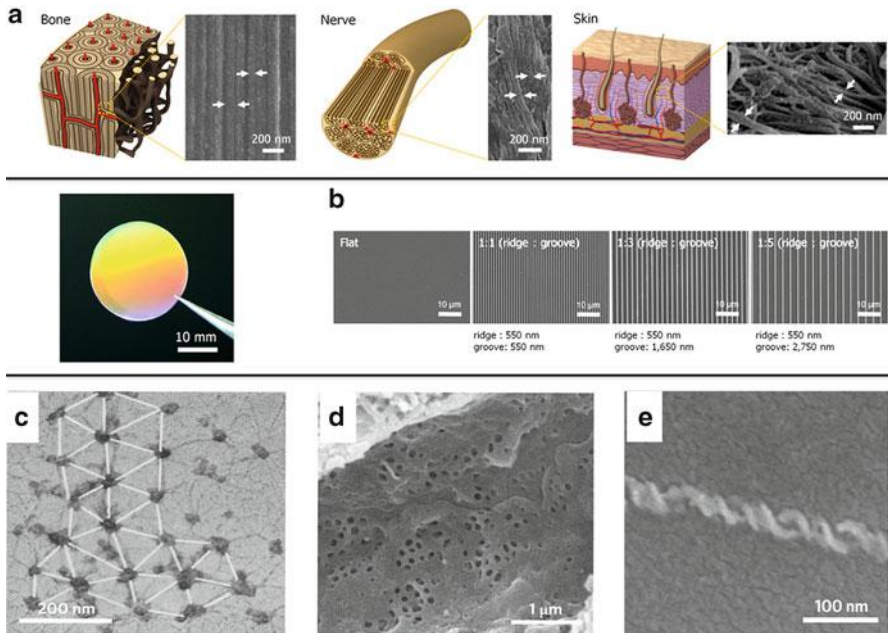


**Fig. 11.5** Selection of biological models for nanotopography in new synthetic materials. (a) Natural ECMs of bone, nerve and skin possess regular nanogroove architectures as shown in the SEM images [24]; (b) In this highlighted study nanogrooves with similar dimensions to groove structures in native tissues were printed onto artificial surfaces and tested for stem cell responses [24]; (c–e) Native 2D surface environments are often disordered and not regular, or show chiral patterns. (c) Periodicity in Type X collagen [26]; (d) Sinusoidal capillary with disordered pore arrangement [13]; (e) An artificial helical fibre with the same 63 nm periodicity of natural collagen, which was discovered to induce osteogenesis in mesenchymal stem cells

## 11.7 Conclusion

The interplay between cells and surfaces directs the future activity and behaviour of the contacting cell population. This interaction can be designed or programmed by physical and chemical patterning using sophisticated machines. Originally the patterning geometries did not have equivalents in biological systems. Increasingly cell engineering via surfaces is being lead by mimicking the patterned features on ECM supramolecules and other structures. The physical characteristics used to influence cells on contact include: topography, stiffness and elasticity. A lot of promising results have emerged through the different shaping of nanotopography, which cells can sense. We interpret this sensing feature to result from adaptations to sense features of extracellular matrices that are constructed from nanogauge objects and display nanofeatures in the final ECM product. We highlighted how nanotopography is helping to control bacteria populations and to stimulate stem and pluripotent cells into deliberate actions using natural Cicada wing structures. Construction of a systematic order is needed to connect a feature by shape or

dimension with a single or collective response by a cell. We also highlighted the utility of topography design on the physical attachment and biointegration with different tissues. In one instance a group of bioengineers successfully demonstrated the strong tissue attachment of a polymer membrane patterned with nanopillars, and augmented with oxidised dextran, but inspired from the structure and adhesive properties of small hairs on the Gecko footpad. Thus, bioinspiration methodology could be the guide for the next design of plaster for wound healing inside the oral cavity. Biomimetic and bioinspired nanotopographies mined from nature are largely unexplored in these areas of dentistry.

**Acknowledgements** We thank our lab members both Oral Biosciences at HKU and Jung's lab at YUCD for helpful discussion and comments on the manuscript.

**Open Access** This chapter is distributed under the terms of the Creative Commons Attribution Noncommercial License, which permits any noncommercial use, distribution, and reproduction in any medium, provided the original author(s) and source are credited.

## References

1. Benyus JM. *Biomimicry: innovation inspired by nature*. New York: Morrow; 1997.
2. Vincent JF, Bogatyreva OA, Bogatyrev NR, Bowyer A, Pahl AK. Biomimetics: its practice and theory. *J R Soc Interface*. 2006;3:471–82. doi:[10.1098/rsif.2006.0127](https://doi.org/10.1098/rsif.2006.0127).
3. Chen W, Villa-Diaz LG, Sun Y, Weng S, Kim JK, Lam RH, et al. Nanotopography influences adhesion, spreading, and self-renewal of human embryonic stem cells. *ACS Nano*. 2012;6:4094–103. doi:[10.1021/nn3004923](https://doi.org/10.1021/nn3004923).
4. Csaderova L, Martines E, Seunarine K, Gadegaard N, Wilkinson CD, Riehle MO. A biodegradable and biocompatible regular nanopattern for large-scale selective cell growth. *Small*. 2010;6(23):2755–61. doi:[10.1002/smll.201000193](https://doi.org/10.1002/smll.201000193).
5. Dalby MJ, Lee LC, Yang J, MacIntyre A, McCullly M. Endothelial coculture with mesenchymal stem cells on nanotopography to direct osteogenesis. *Nanomedicine*. 2013;8:1743–4.
6. Guvendik S, Trabzon L, Ramazanoglu M. The effect of Si nano-columns in 2-D and 3-D on cellular behaviour: nanotopography-induced CaP deposition from differentiating mesenchymal stem cells. *J Nanosci Nanotechnol*. 2011;11:8896–902.
7. Kato RB, Roy B, De Oliveira FS, Ferraz EP, De Oliveira PT, Kemper AG, et al. Nanotopography directs mesenchymal stem cells to osteoblast lineage through regulation of microRNA-SMAD-BMP-2 circuit. *J Cell Physiol*. 2014. doi:[10.1002/jcp.24614](https://doi.org/10.1002/jcp.24614).
8. Kim J, Kim HN, Lim KT, Kim Y, Pandey S, Garg P, et al. Synergistic effects of nanotopography and co-culture with endothelial cells on osteogenesis of mesenchymal stem cells. *Biomaterials*. 2013;34:7257–68. doi:[10.1016/j.biomaterials.2013.06.029](https://doi.org/10.1016/j.biomaterials.2013.06.029).
9. Pennisi CP, Zachar V, Fink T, Gurevich L, Fojan P. Patterned polymeric surfaces to study the influence of nanotopography on the growth and differentiation of mesenchymal stem cells. *Methods Mol Biol*. 2013;1058:77–88. doi:[10.1007/7651\\_2013\\_10](https://doi.org/10.1007/7651_2013_10).
10. Shi Z, Neoh KG, Kang ET, Poh CK, Wang W. Enhanced endothelial differentiation of adipose-derived stem cells by substrate nanotopography. *J Tissue Eng Regen Med*. 2014;8:50–8. doi:[10.1002/term.1496](https://doi.org/10.1002/term.1496).
11. Yim EK, Darling EM, Kulangara K, Guilak F, Leong KW. Nanotopography-induced changes in focal adhesions, cytoskeletal organization, and mechanical properties of human mesenchymal stem cells. *Biomaterials*. 2010;31:1299–306. doi:[10.1016/j.biomaterials.2009.10.037](https://doi.org/10.1016/j.biomaterials.2009.10.037).

12. Teo BK, Wong ST, Lim CK, Kung TY, Yap CH, Ramagopal Y, et al. Nanotopography modulates mechanotransduction of stem cells and induces differentiation through focal adhesion kinase. *ACS Nano*. 2013;7(6):4785–98. doi:[10.1021/nn304966z](https://doi.org/10.1021/nn304966z).
13. Dalby MJ, Gadegaard N, Oreffo RO. Harnessing nanotopography and integrin-matrix interactions to influence stem cell fate. *Nat Mater*. 2014;13:558–69. doi:[10.1038/nmat3980](https://doi.org/10.1038/nmat3980).
14. Bucaro MA, Vasquez Y, Hatton BD, Aizenberg J. Fine-tuning the degree of stem cell polarization and alignment on ordered arrays of high-aspect-ratio nanopillars. *ACS Nano*. 2012;6:6222–30. doi:[10.1021/nn301654e](https://doi.org/10.1021/nn301654e).
15. Campoccia D, Montanaro L, Arciola CR. A review of the biomaterials technologies for infection-resistant surfaces. *Biomaterials*. 2013;34(34):8533–54. doi:[10.1016/j.biomaterials.2013.07.089](https://doi.org/10.1016/j.biomaterials.2013.07.089).
16. Chung KK, Schumacher JF, Sampson EM, Burne RA, Antonelli PJ, Brennan AB. Impact of engineered surface microtopography on biofilm formation of *Staphylococcus aureus*. *Biointerphases*. 2007;2:89–94. doi:[10.1116/1.2751405](https://doi.org/10.1116/1.2751405).
17. Reddy ST, Chung KK, McDaniel CJ, Darouiche RO, Landman J, Brennan AB. Micropatterned surfaces for reducing the risk of catheter-associated urinary tract infection: an in vitro study on the effect of sharklet micropatterned surfaces to inhibit bacterial colonization and migration of uropathogenic *Escherichia coli*. *J Endourol*. 2011;25:1547–52. doi:[10.1089/end.2010.0611](https://doi.org/10.1089/end.2010.0611).
18. Hasan J, Webb HK, Truong VK, Pogodin S, Baulin VA, Watson GS, et al. Selective bactericidal activity of nanopatterned superhydrophobic cicada *Psaltoda claripennis* wing surfaces. *Appl Microbiol Biotechnol*. 2013;97:9257–62. doi:[10.1007/s00253-012-4628-5](https://doi.org/10.1007/s00253-012-4628-5).
19. Ivanova EP, Hasan J, Webb HK, Gervinskas G, Juodkazis S, Truong VK, et al. Bactericidal activity of black silicon. *Nat Commun*. 2013;4:2838. doi:[10.1038/ncomms3838](https://doi.org/10.1038/ncomms3838).
20. Curtis A, Wilkinson C. Nantotechniques and approaches in biotechnology. *Trends Biotechnol*. 2001;19:97–101. doi:[10.1016/S0167-7799\(00\)01536-5](https://doi.org/10.1016/S0167-7799(00)01536-5).
21. Majumder A, Ghatak A, Sharma A. Microfluidic adhesion induced by subsurface microstructures. *Science*. 2007;318:258–61. doi:[10.1126/science.1145839](https://doi.org/10.1126/science.1145839).
22. Mahdavi A, Ferreira L, Sundback C, Nichol JW, Chan EP, Carter DJ, et al. A biodegradable and biocompatible gecko-inspired tissue adhesive. *Proc Natl Acad Sci U S A*. 2008;105:2307–12. doi:[10.1073/pnas.0712117105](https://doi.org/10.1073/pnas.0712117105).
23. Gittens RA, Scheideler L, Rupp F, Hyzy SL, Geis-Gerstorfer J, Schwartz Z, et al. A review on the wettability of dental implant surfaces II: biological and clinical aspects. *Acta Biomater*. 2014. doi:[10.1016/j.actbio.2014.03.032](https://doi.org/10.1016/j.actbio.2014.03.032).
24. Kim J, Kim HN, Lim KT, Kim Y, Seonwoo H, Park SH, et al. Designing nanotopographical density of extracellular matrix for controlled morphology and function of human mesenchymal stem cells. *Sci Rep*. 2013;3:3552. doi:[10.1038/srep03552](https://doi.org/10.1038/srep03552).
25. Bettinger CJ, Langer R, Borenstein JT. Engineering substrate topography at the micro- and nanoscale to control cell function. *Angew Chem Int Ed*. 2009;48:5406–15. doi:[10.1002/anie.200805179](https://doi.org/10.1002/anie.200805179).
26. Kwan AP, Cummings CE, Chapman JA, Grant ME. Macromolecular organization of chicken type X collagen in vitro. *J Cell Biol*. 1991;114(3):597–604.

# **Chapter 12**

## **Feeder Cell Sources and Feeder-Free Methods for Human iPS Cell Culture**

**Guannan Yu, Yuya Kamano, Fangfang Wang, Hiroko Okawa, Hirofumi Yatani, and Hiroshi Egusa**

**Abstract** Induced pluripotent stem cells (iPSCs) hold great promise for regenerative medicine and disease modeling. The original methods to grow human iPSCs utilized methods developed for human embryonic cells (ESCs), in which mitotically inactivated mouse-derived fibroblasts are mainly used as a “feeder” cell layer to maintain the undifferentiated status of pluripotent stem cells. However, these methods still require further consideration to facilitate cell expansion and to maintain the undifferentiated state of human iPSCs and/or ESCs for a longer period of time. In addition, the use of animal-derived feeders should be avoided for eventual clinical application of iPSC therapies. Therefore, human-derived feeder culture systems or feeder-free culture systems are currently being developed to prevent exposure to animal pathogens. In this review, existing mouse and human feeder culture systems for human ESCs and iPSCs are first introduced, and then previously reported feeder-free culture methods using extracellular matrix-associated products or synthetic biomaterials are outlined to discuss an appropriate culture system for clinical application of iPSCs.

**Keywords** Embryonic stem cells (ESCs) • Feeder cells • Feeder-free culture • Induced pluripotent stem cells (iPSCs) • Pluripotent stem cells • Xeno-free culture

---

G. Yu • F. Wang • H. Okawa • H. Yatani

Department of Fixed Prosthodontics, Osaka University Graduate School of Dentistry, Osaka, Japan

Y. Kamano • H. Egusa (✉)

Department of Fixed Prosthodontics, Osaka University Graduate School of Dentistry, Osaka, Japan

Division of Molecular and Regenerative Prosthodontics, Tohoku University Graduate School of Dentistry, 4-1 Seiryo-machi, Aoba-ku, Sendai-City, Miyagi 980-8575, Japan  
e-mail: [egu@dent.tohoku.ac.jp](mailto:egu@dent.tohoku.ac.jp)

## 12.1 Introduction

Human induced pluripotent stem cells (iPSCs) generated by the introduction of defined factors from somatic cells exhibit pluripotency similar to that of human embryonic stem cells (ESCs) [1]. The iPSC technology offers great promise for regenerative therapies and disease modeling in both the medical and dental fields [2]. iPSCs have pluripotency to differentiate into almost all cell types and superior self-renewal capacity that enables unlimited expansion [3], which has prompted researchers to apply them as a cell source for transplantation therapies to regenerate various types of missing, diseased, or defective tissues/organs. However, before iPSCs can be used in the transplantation therapy, several technical limitations of the culture methods must be addressed. For instance, human ESCs and iPSCs cannot sustain their original characteristics in monoculture on standard tissue culture plates without supporting factors. In an in vitro culture system, human ESCs/iPSCs typically require “feeder cells”, which produce specific stemness-supporting factors, to prevent spontaneous differentiation [4, 5]. Feeder cells also produce adhesion molecules and extracellular matrix (ECM) to improve ESC/iPSC attachment, thereby supporting the growth and survival of ESCs/iPSCs. The most commonly used feeder cells are mitotically inactivated mouse-derived fibroblasts [4, 6–8]; however, these animal-derived feeder cells pose an increased risk of transferring unknown viruses and zoonotic pathogens in addition to immune rejection. Alternatively, human-derived cells have also been shown to effectively function as feeder cells for ESCs/iPSCs. Furthermore, “feeder-free” culture systems, such as culture using cell-free ECM proteins or synthetic biomaterials as substrates, have recently received increasing attention. This review assesses various ESC/iPSC culture methods with regard to feeder cells and feeder-free methods to help identify an appropriate culture condition for future clinical applications of iPSCs.

## 12.2 Feeder Cells for ESC/iPSC Culture

### 12.2.1 *Mouse-Derived Feeder Cells*

Since mouse ESCs were first established in 1981 [9, 10], mitotically inactivated fetal mouse fibroblasts have been used as feeder cells for mouse ESC culture. This feeder culture method developed for mouse ESCs was applied to human ESCs when Thomson group first established human ESC lines in 1998 [4], showing that mouse feeder cells could be used to facilitate proliferation and prevent differentiation of human ESCs. Subsequently, several types of mouse-derived feeder cells have been used in human ESC/iPSC studies, such as mouse embryonic fibroblasts (MEFs), STO cells, and SNL 76/7 cells.

MEFs are the most commonly used feeder cells used to support the pluripotent status of human ESC cultures [4, 11, 12]. Primary MEFs are not homogeneous, as

they contain several types of cells other than fibroblasts [13]. To maintain ESC proliferation and pluripotency, MEFs produce various proteins, including transforming growth factor beta 1 (TGF- $\beta$ 1), activin A, bone morphogenetic protein (BMP)-4 [14], and pleiotrophin (heparin-binding growth factor) [15]. When used as in feeder cell layers, MEFs are proliferation-inactivated by chemical (mitomycin C) treatment or gamma irradiation prior to seeding of ESCs/iPSCs. It should be noted that the mitotic inactivation or irradiation of MEFs stimulates the expression of several signaling proteins, such as Wnt-3 [16], which may participate in the molecular mechanisms underlying the maintenance of pluripotency in co-cultured human ESCs/iPSCs. The outbred mouse CF-1 strain may be the most widely used donor for MEF feeder cells for ESC and iPSC culture [13, 17], as CF-1 MEFs have been shown to produce TGF- $\beta$ 1, activin A, BMP-4, gremlin, and noggin [14, 18, 19] but not bFGF [14]. One disadvantage of using primary MEFs is their limited proliferation capacity, which requires repeated isolation from embryonic mice to supply feeder cells [20]. In addition, repeated passaging causes MEFs to lose their capacity to support the proliferation of ESCs/iPSCs [21]. To solve this problem, Choo et al. [22] generated an immortalized primary MEF line ( $\Delta E$ -MEF) through infection with retrovirus vectors encoding the E6 and E7 genes from human papillomavirus (DNA tumor virus) and demonstrated the consistent and reproducible feeder capacity of these cells for hESC culture.

STO cells were isolated by Bernstein from Sandoz inbred mouse (SIM)-derived fibroblasts as a thioguanine- and ouabain-resistant sub-line [13]. STO cells are more easily maintained than MEFs for preparation of feeder layers because STO cells are a spontaneously transformed cell line. In 1998, Shambrott et al. [23] showed that STO cells can be used in a feeder layer for establishing of human embryonic germ cells. In 2003, Park et al. [20] first demonstrated that STO cells have the potential to support the establishment and maintenance of human ESC lines. Thereafter, STO cells have been widely used as feeder cells for human ESC and iPSC culture [24, 25]. Proteome analyses have revealed that STO cells produce unique protein species, such as insulin-like growth factor binding protein 4 (IGFBP-4), pigment epithelium-derived factor (PEDF) and secreted protein acidic and rich in cysteine (SPARC, also known as osteonectin), which may be associated with differentiation and cell growth [26]. Talbot et al. [17] showed from quantitative immunoassays that STO cells express lower levels of activin A, interleukin-6, IGFBP-2, IGFBP-3, IGFBP-4, and IGFBP-5 than CF-1 cells but higher levels of hepatocyte growth factor (HGF) and stem cell factor (c-kit ligand). The difference in the growth factor production among feeder cell types may result in different abilities to support the growth of undifferentiated human ESCs/iPSCs. Indeed, conditioned media from primary MEF cultures but not STO cell cultures support the undifferentiated status of human ESCs on Matrigel- or laminin-coated culture plates [27]. One of the main mechanisms by which STO cells support ESC/iPSC pluripotency appears to be laminin expression because laminin on the STO cell surface interacts with specific receptors (integrin  $\alpha$ 6,  $\beta$ 1 dimer) on human ESCs to maintain their undifferentiated status [20]. Therefore, compared to MEFs, STO feeder cells may require more direct cell contact with human ESCs/iPSCs to support pluripotency.

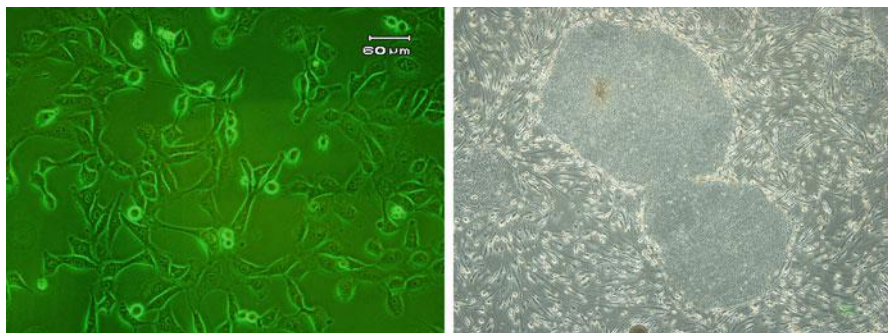


**Fig. 12.1** (Left) Mouse-derived SNL76/7 cells. (Right) Undifferentiated human iPSC colonies on the SNLP76/7-4 feeder cells

SNL76/7 cells were clonally derived by Bradley [28] from STO cells transformed with neomycin resistance and murine leukemia inhibitory factor (LIF) genes. SNL76/7 cells abundantly express the pleiotropic cytokine LIF, which promotes long-term maintenance of mouse ESCs by suppressing spontaneous differentiation [29]. In contrast to the case with mouse ESCs, LIF does not satisfactorily support the self-renewal of human ESCs [4]. Nonetheless, SNL76/7 cells basically inherit the nature of STO cells; therefore, SNL 76/7 cells can be used as feeder cells for both mouse [6, 30, 31] and human [1, 28, 30] ESCs/iPSCs. Bradley also established a puromycin-resistant derivative of SNL76/7 cells (SNLP76/7-4 cell line: Fig. 12.1) that is useful for drug selection of transfected ESCs/iPSCs [32]. An immortalized mouse fetal liver stromal cell line (KM3 cells) was also reported to support the growth and maintenance of human ESCs when co-cultured in with the ESCs in a feeder cell layer [33].

These feeder cell lines may be useful for laboratory experiments because they enable large-scale expansion of human ESCs/iPSCs at low cost; however, it is important to note that mouse feeder methods are associated with a high possibility of contamination by the feeder cells during human ESC/iPSC isolation. Kim et al. [34] described a unique and less labor-intensive method to reduce contamination by feeder cells by culturing human ESCs on porous membranes of transwell inserts that have mouse feeder cells attached to the other side of the membrane.

### 12.2.2 Human-Derived Feeder Cells

Although mouse feeder systems are convenient for laboratory experiments, such xenobiotic support systems are associated with the risk of cross-transfer of animal pathogens and are thus not favorable for future clinical application of iPSCs. To solve this problem, many studies to date have demonstrated the utility of human-derived cells as feeders for human ESCs and iPSCs (Table 12.1).

**Table 12.1** Summary of human feeder cells for human ESC/iPSC culture

Feeder cell sources	Cells	Culture medium	References
Foreskin fibroblasts	iPSCs	KSR medium	[35, 36]
	ESCs	KSR medium	[35–42]
	ESCs	HEScGRO	[43]
	ESCs	FBS-hES/KSR medium	[44]
Bone marrow-derived MSCs	ESCs	KSR medium	[37, 39, 45]
Adipose-derived stromal cells	iPSCs	mTeSR1	[46]
	ESCs	KSR medium	[47]
	iPSCs		
Amniotic MSCs	ESCs	—	[48]
Amniotic epithelial cells	ESCs	KSR medium	[49]
	ESCs	DMEM	[50]
	iPSCs	DMEM-F12 medium	[51]
Placental fibroblasts	ESCs	KSR medium	[37]
	ESCs	X-VIVO 10	[52]
Umbilical cord stromal cells	ESCs	KSR medium	[53]
Transgenic fetal fibroblasts	ESCs	KSR medium	[54]
Fetal muscle cells	ESCs	H1/H2 medium	[55]
Fetal skin cells	ESCs	H1/H2 medium	[55, 56]
Fetal liver stromal cells	ESCs	KSR medium	[57]

*MSCs* mesenchymal stem cells, *ESCs* embryonic stem cells, *iPSCs* induced pluripotent stem cells, *KSR KnockOut™ Serum Replacement*, *HEScGRO medium* animal-component-free medium (Millipore), *FBS* fetal bovine serum, *hES medium* standard human ESC culture medium, *mTeSR1* chemically defined xeno-free human ESC culture medium (Stemcell Technologies), *DMEM* Dulbecco's modified Eagle medium, *X-VIVO 10* chemically defined and serum-free medium (Lonza)

Primary human foreskin fibroblasts (FFs), which can easily be prepared from infant foreskin, are among the most frequently used human feeder cells for ESCs and iPSCs [35, 37–44]. Similar to primary MEF cells, human FF feeder cells show limited expansion in culture; therefore, fresh batches of FFs have to be prepared on a routine basis. To overcome this drawback, Unger et al. [36] established a conditionally immortalized human FF line that secreted bFGF and showed that the generated cells could support the culture of both human ESCs and iPSCs.

Mesenchymal stem cells (MSCs) are easily accessible postnatal human cells that include bone marrow-derived MSCs (BMSCs) [3]. Culture-expanded BMSCs can support prolonged expansion of human ESCs in culture [37, 39, 45]. Adipose-derived stromal cells (ASCs), which are another type of MSCs, also have the ability to serve as feeder cells for human ESCs/iPSCs [46, 47]. Sugii et al. [58] showed that ASCs express high levels of bFGF, TGF $\beta$ , fibronectin, and vitronectin and can thus serve as feeder cells for both autologous and heterologous human iPSCs. Because ASCs can be easily isolated by surgery or lipoaspiration from adults, their use as feeder cells is expected to provide an important step toward establishing safe, clinical-grade human iPSC lines.

The amniotic fluid contains MSCs that are easily obtained and relatively exempt from ethical problems. Zhang et al. [48] reported that human amniotic MSCs can be used as feeder cells for effective growth of human ESCs. Human amniotic epithelial cells (AECs) can be isolated from the surface membrane of fresh placentas, and they express many growth factors including EGF, bFGF, TGF- $\beta$ , and BMP-4 [49, 59, 60] in addition to stem cell markers such as Oct-4 and Nanog [50]. Additionally, Liu et al. [51] recently showed that microRNA-145-mediated regulation of Sox2 expression in human AECs maintains the self-renewal and pluripotency of human iPSCs. Human placental fibroblasts also showed comparable or superior efficacy to MEFs as feeder cells for human ESCs [37, 52]. Because the human placenta and amnion are discarded as medical waste, they may be promising tissue sources for human feeder cells for iPSCs. Umbilical cord stromal cells, which can be obtained through noninvasive procedures, also support the self-renewal of human ESCs in serum-free conditions [53]; therefore, they may be still another promising source of human feeder cells for iPSC culture.

Other previously reported human feed cells for ESC/iPSC culture include dermal fibroblasts [61], adult fallopian tube epithelial cells [55], adult lung cells [56], transgenic (puromycin resistant) fetal fibroblasts [54], fetal muscle cells [55], fetal skin cells [55, 56], and fetal liver stromal cells [57]. However, although these human feeder cells can be used in laboratory experiments, they are not suitable for clinical use because the harvesting of the source tissue is invasive and may pose ethical issues.

Nearly all human feeder cells require supplementation with bFGF to sustain human ESC/iPSC potential; therefore a bFGF-dependent pathway may be crucial for maintaining the pluripotency of human pluripotent stem cells. Park et al. [37] evaluated the feeder ability of several types of human feeder cells (placental cells, BMSCs, and FFs) and showed that these cells support the undifferentiated growth of human ESCs through bFGF synthesis. In contrast, Bendall et al. [62] demonstrated that human ESCs autologously produce fibroblast-like cells around their colonies that act as a supportive niche for the survival and self-renewal of human ESCs through IGF-II production in response to bFGF.

## 12.3 Feeder-Free Methods for ESC/iPSC Culture

To achieve reliable and safe production of human iPSCs, it is desirable to use reagents that are defined, qualified, and preferably derived from a non-animal source. Although the use of human feeder cells circumvents the use of animal-derived feeder cells, the function of the feeder cells in the human iPSC co-culture system is still not fully understood. In addition, the preparation of the feeder cells is highly laborious, which limits the large-scale production of human iPSCs for future clinical applications. Therefore, development of feeder-free human iPSC culture systems has been an important focus of recent iPSC research.

**Table 12.2** Summary of extracellular matrix-related biomaterials for feeder-free human ESC/iPSC culture

Matrix/biomaterial	Cells	Culture medium	References
Matrigel™	ESCs	hES medium	[27, 63, 64]
		MEF-CM	
Human MSC-derived matrix	ESCs	SBX medium	[65]
Human serum	ESCs	hES-dF-CM	[66]
Laminin	ESCs	hES medium	[27, 67]
		MEF-CM	
		NC-SFM	
Recombinant laminin E8 fragments	ESCs/iPSCs	mTeSR1	[68]
Fibronectin	ESCs	KSR medium	[69]
Vitronectin	ESCs	mTeSR1	[70]
Collagen (type 1)	ESCs	mTeSR1	[71]
Hyaluronic acid hydrogels	ESCs	MEF-CM	[72]

*MSCs* mesenchymal stem cells, *ESCs* embryonic stem cells, *iPSCs* induced pluripotent stem cells, *hES medium* standard human ESC culture medium, *MEF-CM* mouse embryonic fibroblast-derived conditioned medium, *SBX medium* chemically defined xeno-free medium, *hES-dF-CM* conditioned medium of fibroblasts derived from differentiated human ESCs, *NC-SFM* non-conditioned serum-free medium, *KSR KnockOut™ Serum Replacement*, *mTeSR1* chemically defined xeno-free human ESC culture medium (Stemcell Technologies)

### 12.3.1 ECM-Related Materials

The ECM is a uniquely assembled three-dimensional (3-D) molecular complex that varies in composition and diversity, and consists of basic components such as laminin, fibronectin, vitronectin, collagen, cadherin, elastin, hyaluronic acid, and proteoglycans. In the absence of feeder cells, human ESCs/iPSCs require attachment factors to promote their survival and proliferation. In this regard, the ECM and its soluble factors support the adhesion, growth, and maintenance of ESCs/iPSCs. To date, various ECM-related materials have been evaluated as a substitute for feeder cells for human pluripotent stem cell culture (Table 12.2).

#### 12.3.1.1 ECM Components

Matrigel™ [27, 63, 64], which is a commercially available protein mixture extracted from the Engelbreth-Holm-Swarm mouse tumor [73], is one of the most frequently used matrices for feeder-free growth of undifferentiated human pluripotent stem cells. Matrigel™ contains a complex and poorly defined mixture of fibronectin, laminin, type IV collagen, entactin, and heparan sulfate proteoglycans, in addition to various growth factors such as bFGF, EGF, PDGF, NGF, and TGF-β. To maintain human ESCs/iPSCs in an undifferentiated state, Matrigel™-coating requires soluble stemness-supporting factors produced by MEFs or other feeder cells (conditioned medium) [27]. Despite its availability and ease of use, Matrigel™

is not ideal for potential clinical application of human iPSCs because it is animal-derived and xenogenic pathogens can be transmitted through culture even though no feeder cells are present. However, Peiffer et al. [65] demonstrated that matrices derived from human MSCs could advantageously replace MEF or hMSC feeder cells. Furthermore, human serum can be also used as a matrix to support the undifferentiated growth of human ESCs [66].

### 12.3.1.2 Recombinant ECM Products

Human ESCs express integrin receptors for major ECM proteins (laminin, fibronectin, collagen, and vitronectin) and all of these receptors functionally mediate cell adhesion [70]. Laminin, which is a major component of the ECM of all basal laminae in vertebrates, can support the pluripotency of human ESCs when used together with the conditioned medium of MEFs [27]. The MEF conditioned medium can also be replaced, however, as the combination of a human laminin coating with defined medium supplements, such as recombinant bFGF and the additional growth factors flt3-L, SCF, and LIF, was shown to support the growth and maintenance of undifferentiated human ESCs [67]. It has also been shown that recombinant laminin E8 fragments (LM-E8s), which are truncated peptides composed of the C-terminal regions of the  $\alpha$ ,  $\beta$ , and  $\gamma$  chains of laminin, enable robust propagation of human ESCs and iPSCs in an undifferentiated state in cultures with defined and xeno-free media [68]. We have confirmed that human gingiva-derived iPSCs [30] can be maintained in an undifferentiated state on LM-E8-coated plates after dissociation and passaging (Fig. 12.2).

Fibronectin, vitronectin, and gelatin (a hydrolyzed product of collagen) are rich in arginine-glycine-aspartate (RGD) peptide sequences that are required for integrin-mediated cell adhesion and growth through activation of cellular signaling pathways [74]. Amit and Itskovitz-Eldor [69] reported that a human fibronectin coating and medium supplementation with TGF $\beta$  and bFGF provide a feeder-free and serum-free culture system for human ESCs. Vitronectin is the major ECM protein but is not present in Matrigel<sup>TM</sup>; thus, Braam et al. [70] reported that recombinant vitronectin was a defined functional alternative to Matrigel<sup>TM</sup> for supporting sustained self-renewal and pluripotency of human ESC lines. Liu et al. [75] also demonstrated that nanofibrous gelatin substrates can provide an alternative to Matrigel<sup>TM</sup> for long-term expansion of human ESCs.

Type 1 collagen is the most abundant structural protein of the human body. Furue et al. [71] reported that a substrate composed only of type I collagen could be combined with a defined medium supplemented with heparin, bFGF, insulin, transferrin, and fatty acid-free albumin conjugated with oleic acid for culture of human ESCs. E-cadherin, a cell adhesion molecule, is essential for intercellular adhesion [76] and colony formation among mouse ESCs [77]. Nagaoka et al. [78] generated a fusion protein consisting of human E-cadherin and the IgG Fc domain and demonstrated that this protein could be substituted for Matrigel<sup>TM</sup> and could support the pluripotency of human ESCs and iPSCs under completely defined

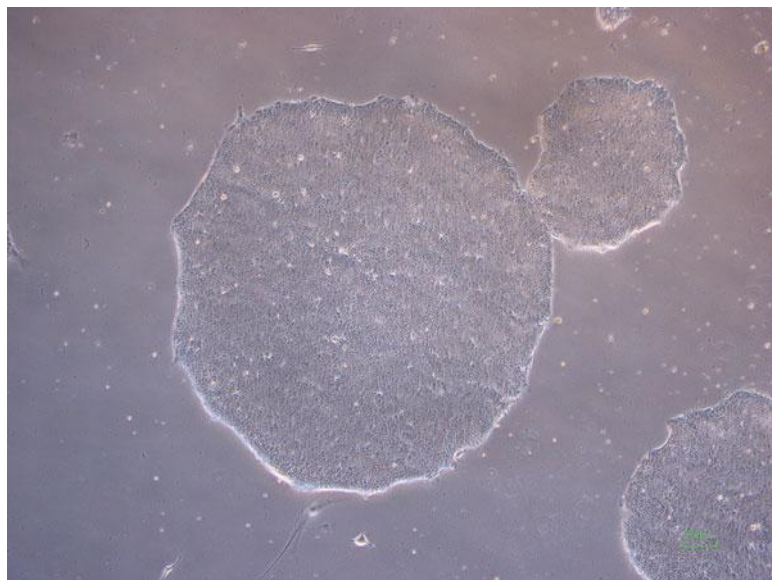


**Fig. 12.2** Undifferentiated human gingiva-derived iPSC colonies on a recombinant laminin E8 fragment-coated plate (feeder-free culture)

culture conditions. Hyaluronic acid (HA) is an anionic, nonsulfated glycosaminoglycan that is distributed widely throughout connective, epithelial, and neural tissues. Gerecht et al. [72] demonstrated that HA-based hydrogels maintain the undifferentiated state of human ESCs in the presence of conditioned medium from MEFs.

### 12.3.2 Synthetic Materials

Although human-sourced and recombinant ECM materials can be used in animal-component-free and effective culture systems for human ESCs/iPSCs, they are still associated with high product cost and possible batch-to-batch variation. In contrast, synthetic biomaterials and chemical coating technologies (Table 12.3) may offer a fully defined culture system with lower cost and higher consistency.

Because most cells are cultured on tissue culture-treated polystyrene, the development of a chemical treatment for standard tissue culture-treated polystyrene is desirable for a 2-dimensional culture system for ESCs/iPSCs. Along these lines, Mahlstedt et al. [79] demonstrated that oxygen plasma-etched tissue culture-treated polystyrene could maintain the pluripotency of human ESCs in MEF conditioned medium.

However, the 3-D microenvironment has recently been appreciated for its ability to influence the behavior of pluripotent stem cells. For example, a 3-D porous

**Table 12.3** Summary of synthetic materials for feeder-free human ESC/iPSC culture

Synthetic materials	Cells	Culture medium	References
Oxygen plasma-etched tissue culture-treated polystyrene	ESCs	MEF-CM	[79]
		hES medium	
Trimethyl ammonium-coated polystyrene microcarriers	ESCs	hES medium	[80]
Calcium alginate hydrogels	ESCs	hES medium	[81]
Chitosan and alginate scaffolds	ESCs	hES medium	[82]
Polymer scaffolds/poly-D-lysine	ESCs	mTeSR1	[83]

*ESCs* embryonic stem cells, *iPSCs* induced pluripotent stem cells, *MEF-CM* mouse embryonic fibroblast-derived conditioned medium, *hES medium* standard human ESC culture medium, *mTeSR1* chemically defined xeno-free human ESC culture medium (Stemcell Technologies)

natural polymer scaffold prepared from a chitosan and alginate complex was reported to sustain the self-renewal of human ESCs without the support of feeder cells or conditioned medium [82]. Similarly, Carlson et al. [83] reported the combination of poly-D-lysine, which is a synthetic positively charged amino acid chain commonly used as a coating to enhance cell adhesion, with synthetic polymer scaffolds with a 3-D fibrous architecture promote the adhesion, proliferation, and self-renewal of human ESCs. Additionally, microcarrier particles have also been used as substrates to amplify various types of adherent cells [84]. In particular, Phillips et al. [80] showed that seeding on trimethyl ammonium-coated polystyrene microcarriers enabled feeder-free 3-D suspension and-single cell culture for human ESCs, thus providing a low-cost, practical feeder-free method for large-scale human ESC/iPSC production. Furthermore, Siti-Ismail et al. [81] demonstrated that human ESCs encapsulated in calcium alginate hydrogels could be maintained in an undifferentiated state for more than 260 days without requiring feeder cells or passaging.

## 12.4 Conclusions

Feeder methods and ECM-related/synthetic materials for human ESC culture are relatively well established in the literature as outline above; however, the appropriate methods and materials for human iPSC culture, especially for clinical use, still need to be established. Most previous ESC/iPSC studies of animal-component-free methods focused on the growth and maintenance of iPSCs; however, few studies have focus on the generation and expansion of human iPSCs. Because iPSCs are generated from one reprogrammed somatic cell, xeno-free methods to efficiently promote the clonal growth of single human ESCs are necessary. Bigdeli et al. [85] reported that human ESC lines can be adapted to matrix-independent growth, even on plastic plates, by using a specified conditioned medium derived from human embryonic fibroblasts. This finding implies that it may be possible to develop a more effective defined culture medium that eliminates the need for a

substrate and thus achieves a feeder-free and xeno-free culture system for iPSCs. Investigators should therefore accumulate fundamental data for feeder- and xeno-free culture technologies by using both synthetic substrates and defined culture medium components. The establishment of cost-effective, easy-to-handle synthetic, defined, and stable xeno-free culture systems for human iPSCs will expedite the use of iPSCs in biomedical applications.

**Open Access** This chapter is distributed under the terms of the Creative Commons Attribution Noncommercial License, which permits any noncommercial use, distribution, and reproduction in any medium, provided the original author(s) and source are credited.

## References

1. Takahashi K, Tanabe K, Ohnuki M, Narita M, Ichisaka T, Tomoda K, et al. Induction of pluripotent stem cells from adult human fibroblasts by defined factors. *Cell.* 2007;131(5):861–72.
2. Egusa H. iPS cells in dentistry. *Clin Calcium.* 2012;22(1):67–73.
3. Egusa H, Sonoyama W, Nishimura M, Atsuta I, Akiyama K. Stem cells in dentistry—part I: stem cell sources. *J Prosthodont Res.* 2012;56(3):151–65.
4. Thomson JA, Itskovitz-Eldor J, Shapiro SS, Waknitz MA, Swiergiel JJ, Marshall VS, et al. Embryonic stem cell lines derived from human blastocysts. *Science.* 1998;282(5391):1145–7.
5. Reubinoff BE, Pera MF, Fong CY, Trounson A, Bongso A. Embryonic stem cell lines from human blastocysts: somatic differentiation in vitro. *Nat Biotechnol.* 2000;18(4):399–404.
6. Takahashi K, Okita K, Nakagawa M, Yamanaka S. Induction of pluripotent stem cells from fibroblast cultures. *Nat Protoc.* 2007;2(12):3081–9.
7. Yu JY, Vodyanik MA, Smuga-Otto K, Antosiewicz-Bouget J, Frane JL, Tian S, et al. Induced pluripotent stem cell lines derived from human somatic cells. *Science.* 2007;318(5858):1917–20.
8. Amit M, Carpenter MK, Inokuma MS, Chiu CP, Harris CP, Waknitz MA, et al. Clonally derived human embryonic stem cell lines maintain pluripotency and proliferative potential for prolonged periods of culture. *Dev Biol.* 2000;227(2):271–8.
9. Evans MJ, Kaufman MH. Establishment in culture of pluripotential cells from mouse embryos. *Nature.* 1981;292(5819):154–6.
10. Martin GR. Isolation of a pluripotent cell line from early mouse embryos cultured in medium conditioned by teratocarcinoma stem cells. *Proc Natl Acad Sci U S A.* 1981;78(12):7634–8.
11. Hoffman LM, Carpenter MK. Characterization and culture of human embryonic stem cells. *Nat Biotechnol.* 2005;23(6):699–708.
12. Pera MF, Reubinoff B, Trounson A. Human embryonic stem cells. *J Cell Sci.* 2000;113(1):5–10.
13. Furue MK. Standardization of human embryonic stem (ES) cell and induced pluripotent stem (iPS) cell research in Japan. *Tiss Cult Res Commun.* 2008;27:139–47.
14. Eiseleova L, Peterkova I, Neradil J, Slaninova I, Hampl A, Dvorak P. Comparative study of mouse and human feeder cells for human embryonic stem cells. *Int J Dev Biol.* 2008;52(4):353–63.
15. Soh BS, Song CM, Vallier L, Li P, Choong C, Yeo BH, et al. Pleiotrophin enhances clonal growth and long-term expansion of human embryonic stem cells. *Stem Cells.* 2007;25(12):3029–37.
16. Xie CQ, Lin G, Luo KL, Luo SW, Lu GX. Newly expressed proteins of mouse embryonic fibroblasts irradiated to be inactive. *Biochem Biophys Res Commun.* 2004;315(3):581–8.

17. Talbot NC, Sparks WO, Powell AM, Kahl S, Caperna TJ. Quantitative and semiquantitative immunoassay of growth factors and cytokines in the conditioned medium of STO and CF-1 mouse feeder cells. *In Vitro Cell Dev Biol Anim.* 2012;48(1):1–11.
18. Xu RH, Peck RM, Li DS, Feng X, Ludwig T, Thomson JA. Basic FGF and suppression of BMP signaling sustain undifferentiated proliferation of human ES cells. *Nat Methods.* 2005;2(3):185–90.
19. Greber B, Lehrach H, Adjaye J. Fibroblast growth factor 2 modulates transforming growth factor beta signaling in mouse embryonic fibroblasts and human ESCs (hESCs) to support hESC self-renewal. *Stem Cells.* 2007;25(2):455–64.
20. Park JH, Kim SJ, Oh EJ, Moon SY, Roh SI, Kim CG, et al. Establishment and maintenance of human embryonic stem cells on STO, a permanently growing cell line. *Biol Reprod.* 2003;69(6):2007–14.
21. Pan CY, Hicks A, Guan X, Chen H, Bishop CE. SNL fibroblast feeder layers support derivation and maintenance of human induced pluripotent stem cells. *J Genet Genomics.* 2010;37(4):241–8.
22. Choo A, Padmanabhan J, Chin A, Fong WJ, Oh SK. Immortalized feeders for the scale-up of human embryonic stem cells in feeder and feeder-free conditions. *J Biotechnol.* 2006;122(1):130–41.
23. Shambrott MJ, Axelman J, Wang S, Bugg EM, Littlefield JW, Donovan PJ, et al. Derivation of pluripotent stem cells from cultured human primordial germ cells. *Proc Natl Acad Sci U S A.* 1998;95(23):13726–31.
24. Park SP, Lee YJ, Lee KS, Shin HA, Cho HY, Chung KS, et al. Establishment of human embryonic stem cell lines from frozen-thawed blastocysts using STO cell feeder layers. *Hum Reprod.* 2004;19(3):676–84.
25. Yoshida Y, Takahashi K, Okita K, Ichisaka T, Yamanaka S. Hypoxia enhances the generation of induced pluripotent stem cells. *Cell Stem Cell.* 2009;5(3):237–41.
26. Lim JWE, Bodnar A. Proteome analysis of conditioned medium from mouse embryonic fibroblast feeder layers which support the growth of human embryonic stem cells. *Proteomics.* 2002;2(9):1187–203.
27. Xu CH, Inokuma MS, Denham J, Golds K, Kundu P, Gold JD, et al. Feeder-free growth of undifferentiated human embryonic stem cells. *Nat Biotechnol.* 2001;19(10):971–4.
28. McMahon AP, Bradley A. The Wnt-1 (int-1) proto-oncogene is required for development of a large region of the mouse brain. *Cell.* 1990;62(6):1073–85.
29. Williams RL, Hilton DJ, Pease S, Willson TA, Stewart CL, Gearing DP, et al. Myeloid leukaemia inhibitory factor maintains the developmental potential of embryonic stem cells. *Nature.* 1988;336(6200):684–7.
30. Egusa H, Okita K, Kayashima H, Yu GN, Fukuyasu S, Saeki M, et al. Gingival Fibroblasts as a promising source of induced pluripotent stem cells. *PLoS One.* 2010;5(9):e12743.
31. Egusa H, Kayashima H, Miura J, Uraguchi S, Wang F, Okawa H, et al. Comparative analysis of mouse-induced pluripotent stem cells and mesenchymal stem cells during osteogenic differentiation in vitro. *Stem Cells Dev.* (in press).
32. Cadinanos J, Bradley A. Generation of an inducible and optimized piggyBac transposon system. *Nucleic Acids Res.* 2007;35(12):e87.
33. Hu JB, Hu SQ, Ma QH, Wang XH, Zhou ZW, Zhang W, et al. Immortalized mouse fetal liver stromal cells support growth and maintenance of human embryonic stem cells. *Oncol Rep.* 2012;28(4):1385–91.
34. Kim S, Ahn SE, Lee JH, Lim DS, Kim KS, Chung HM, et al. A novel culture technique for human embryonic stem cells using porous membranes. *Stem Cells.* 2007;25(10):2601–9.
35. Pekkanen-Mattila M, Ojala M, Kerkela E, Rajala K, Skottman H, Aalto-Setala K. The effect of human and mouse fibroblast feeder cells on cardiac differentiation of human pluripotent stem cells. *Stem Cells Int.* 2012;2012:875059.

36. Unger C, Gao SP, Cohen M, Jaconi M, Bergstrom R, Holm F, et al. Immortalized human skin fibroblast feeder cells support growth and maintenance of both human embryonic and induced pluripotent stem cells. *Hum Reprod.* 2009;24(10):2567–81.
37. Park Y, Kim JH, Lee SJ, Choi IY, Park SJ, Lee SR, et al. Human feeder cells can support the undifferentiated growth of human and mouse embryonic stem cells using their own basic fibroblast growth factors. *Stem Cells Dev.* 2011;20(11):1901–10.
38. Lu ZY, Zhu WW, Yu Y, Jin D, Guan YQ, Yao RQ, et al. Derivation and long-term culture of human parthenogenetic embryonic stem cells using human foreskin feeders. *J Assist Reprod Genet.* 2010;27(6):285–91.
39. Zhu WW, Li N, Wang F, Fu LL, Xu YL, Guan YQ, et al. Different types of feeder cells for maintenance of human embryonic stem cells. *Zhongguo Yi Xue Ke Xue Yuan Xue Bao Acta Academiae Medicinae Sinicae.* 2009;31(4):468–72.
40. Illic D, Giritharan G, Zdravkovic T, Caceres E, Genbacev O, Fisher SJ, et al. Derivation of human embryonic stem cell lines from biopsied blastomeres on human feeders with minimal exposure to xenomaterials. *Stem Cells Dev.* 2009;18(9):1343–9.
41. Nieto A, Cabrera CM, Catalina P, Cobo F, Barnie A, Cortes JL, et al. Effect of mitomycin-C on human foreskin fibroblasts used as feeders in human embryonic stem cells: Immunocytochemistry MIB1 score and DNA ploidy and apoptosis evaluated by flow cytometry. *Cell Biol Int.* 2007;31(3):269–78.
42. Ellerstrom C, Strehl R, Moya K, Andersson K, Bergh C, Lundin K, et al. Derivation of a xeno-free human embryonic stem cell line. *Stem Cells.* 2006;24(10):2170–6.
43. Meng GL, Liu SY, Krawetz R, Chan M, Chernos J, Rancourt DE. A novel method for generating xeno-free human feeder cells for human embryonic stem cell culture. *Stem Cells Dev.* 2008;17(3):413–22.
44. Choo ABH, Padmanabhan J, Chin ACP, Oh SKW. Expansion of pluripotent human embryonic stem cells on human feeders. *Biotechnol Bioeng.* 2004;88(3):321–31.
45. Cheng LZ, Hammond H, Ye ZH, Zhan XC, David G. Human adult marrow cells support prolonged expansion of human embryonic stem cells in culture. *Stem Cells.* 2003;21(2):131–42.
46. Sugii S, Kida Y, Berggren WT, Evans RM. Feeder-dependent and feeder-independent iPS cell derivation from human and mouse adipose stem cells. *Nat Protoc.* 2011;6(3):346.
47. Hwang ST, Kang SW, Lee SJ, Lee TH, Suh W, Shim SH, et al. The expansion of human ES and iPS cells on porous membranes and proliferating human adipose-derived feeder cells. *Biomaterials.* 2010;31(31):8012–21.
48. Zhang KH, Cai Z, Li Y, Shu J, Pan L, Wan F, et al. Utilization of human amniotic mesenchymal cells as feeder layers to sustain propagation of human embryonic stem cells in the undifferentiated state. *Cell Reprogram.* 2011;13(4):281–8.
49. Lai DM, Cheng WW, Liu TJ, Jiang LZ, Huang Q, Liu T. Use of human amnion epithelial cells as a feeder layer to support undifferentiated growth of mouse embryonic stem cells. *Cloning Stem Cells.* 2009;11(2):331–40.
50. Miki T, Lehmann T, Cai H, Stoltz DB, Strom SC. Stem cell characteristics of amniotic epithelial cells. *Stem Cells.* 2005;23(10):1549–59.
51. Liu T, Chen Q, Huang YY, Huang Q, Jiang LZ, Guo LH. Low microRNA-199a expression in human amniotic epithelial cell feeder layers maintains human-induced pluripotent stem cell pluripotency via increased leukemia inhibitory factor expression. *Acta Biochim Biophys Sin.* 2012;44(3):197–206.
52. Genbacev O, Krtolica A, Zdravkovic PDUT, Zdravkovic T, Brunette E, Powell S, et al. Serum-free derivation of human embryonic stem cell lines on human placental fibroblast feeders. *Fertil Steril.* 2005;83(5):1517–29.
53. Cho M, Lee EJ, Nam H, Yang JH, Cho J, Lim JM, et al. Human feeder layer system derived from umbilical cord stromal cells for human embryonic stem cells. *Fertil Steril.* 2010;93(8):2525–31.

54. Sidhu KS, Lie KHD, Tuch BE. Transgenic human fetal fibroblasts as feeder layer for human embryonic stem cell lineage selection. *Stem Cells Dev.* 2006;15(5):741–7.
55. Richards M, Fong CY, Chan WK, Wong PC, Bongso A. Human feeders support prolonged undifferentiated growth of human inner cell masses and embryonic stem cells. *Nat Biotechnol.* 2002;20(9):933–6.
56. Richards M, Tan S, Fong CY, Biswas A, Chan WK, Bongso A. Comparative evaluation of various human feeders for prolonged undifferentiated growth of human embryonic stem cells. *Stem Cells.* 2003;21(5):546–56.
57. Xi JF, Wang YF, Zhang P, He LJ, Nan X, Yue W, et al. Human fetal liver stromal cells that overexpress bFGF support growth and maintenance of human embryonic stem cells. *PLoS One.* 2010;5(12):e14457.
58. Sugii S, Kida Y, Kawamura T, Suzuki J, Vassena R, Yin YQ, et al. Human and mouse adipose-derived cells support feeder-independent induction of pluripotent stem cells. *Proc Natl Acad Sci U S A.* 2010;107(8):3558–63.
59. Liu T, Cheng WW, Liu TJ, Guo LH, Huang Q, Jiang LZ, et al. Human amniotic epithelial cell feeder layers maintain mouse embryonic stem cell pluripotency via epigenetic regulation of the c-Myc promoter. *Acta Biochim Biophys Sin.* 2010;42(2):109–15.
60. Liu T, Guo LH, Liu ZX, Cheng WW. Human amniotic epithelial cells maintain mouse spermatogonial stem cells in an undifferentiated state due to high leukemia inhibitor factor (LIF) expression. *In Vitro Cell Dev Biol Anim.* 2011;47(4):318–26.
61. Takahashi K, Narita M, Yokura M, Ichisaka T, Yamanaka S. Human induced pluripotent stem cells on autologous feeders. *PLoS One.* 2009;4(12):e8067.
62. Bendall SC, Stewart MH, Menendez P, George D, Vijayaragavan K, Werbowetski-Ogilvie T, et al. IGF and FGF cooperatively establish the regulatory stem cell niche of pluripotent human cells in vitro. *Nature.* 2007;448(7157):1015–U3.
63. Rosler ES, Fisk GJ, Ares X, Irving J, Miura T, Rao MS, et al. Long-term culture of human embryonic stem cells in feeder-free conditions. *Dev Dynam.* 2004;229(2):259–74.
64. Carpenter MK, Rosler ES, Fisk GJ, Brandenberger R, Ares X, Miura T, et al. Properties of four human embryonic stem cell lines maintained in a feeder-free culture system. *Dev Dynam.* 2004;229(2):243–58.
65. Peiffer I, Barbet R, Zhou YP, Li ML, Monier MN, Hatzfeld A, et al. Use of xenofree matrices and molecularly-defined media to control human embryonic stem cell pluripotency: effect of low physiological TGF-center dot concentrations. *Stem Cells Dev.* 2008;17(3):519–33.
66. Stojkovic P, Lako M, Przyborski S, Stewart R, Armstrong L, Evans J, et al. Human-serum matrix supports undifferentiated growth of human embryonic stem cells. *Stem Cells.* 2005;23(7):895–902.
67. Li Y, Powell S, Brunette E, Lebkowski J, Mandalam R. Expansion of human embryonic stem cells in defined serum-free medium devoid of animal-derived products. *Biotechnol Bioeng.* 2005;91(6):688–98.
68. Miyazaki T, Futaki S, Suemori H, Taniguchi Y, Yamada M, Kawasaki M, et al. Laminin E8 fragments support efficient adhesion and expansion of dissociated human pluripotent stem cells. *Nat Commun.* 2012;3.
69. Amit M, Itskovitz-Eldor J. Feeder-free culture of human embryonic stem cells. *Methods Enzymol.* 2006;420:37–49.
70. Braam SR, Zeinstra L, Litjens S, Ward-van Oostwaard D, van den Brink S, van Laake L, et al. Recombinant vitronectin is a functionally defined substrate that supports human embryonic stem cell self-renewal via alpha V beta 5 integrin. *Stem Cells.* 2008;26(9):2257–65.
71. Furue MK, Na J, Jackson JP, Okamoto T, Jones M, Baker D, et al. Heparin promotes the growth of human embryonic stem cells in a defined serum-free medium. *Proc Natl Acad Sci U S A.* 2008;105(36):13409–14.
72. Gerecht S, Burdick JA, Ferreira LS, Townsend SA, Langer R, Vunjak-Novakovic G. Hyaluronic acid hydrogen for controlled self-renewal and differentiation of human embryonic stem cells. *Proc Natl Acad Sci U S A.* 2007;104(27):11298–303.

73. Kleinman HK, McGarvey ML, Liotta LA, Robey PG, Tryggvason K, Martin GR. Isolation and characterization of type IV procollagen, laminin, and heparan sulfate proteoglycan from the EHS sarcoma. *Biochemistry*. 1982;21(24):6188–93.
74. Barczyk M, Carracedo S, Gullberg D. Integrins. *Cell Tissue Res*. 2010;339(1):269–80.
75. Liu L, Yoshioka M, Nakajima M, Ogasawara A, Liu J, Hasegawa K, et al. Nanofibrous gelatin substrates for long-term expansion of human pluripotent stem cells. *Biomaterials*. 2014;35 (24):6259–67.
76. Gumbiner BM. Regulation of cadherin-mediated adhesion in morphogenesis. *Nat Rev Mol Cell Biol*. 2005;6(8):622–34.
77. Dang SM, Gerecht-Nir S, Chen J, Itskovitz-Eldor J, Zandstra PW. Controlled, scalable embryonic stem cell differentiation culture. *Stem Cells*. 2004;22(3):275–82.
78. Nagaoka M, Si-Tayeb K, Akaike T, Duncan SA. Culture of human pluripotent stem cells using completely defined conditions on a recombinant E-cadherin substratum. *BMC Dev Biol*. 2010;10.
79. Mahlstedt MM, Anderson D, Sharp JS, McGilvray R, Munoz MDB, Buttery LD, et al. Maintenance of pluripotency in human embryonic stem cells cultured on a synthetic substrate in conditioned medium. *Biotechnol Bioeng*. 2010;105(1):130–40.
80. Phillips BW, Horne R, Lay TS, Rust WL, Teck TT, Crook JM. Attachment and growth of human embryonic stem cells on microcarriers. *J Biotechnol*. 2008;138(1–2):24–32.
81. Siti-Ismail N, Bishop AE, Polak JM, Mantalaris A. The benefit of human embryonic stem cell encapsulation for prolonged feeder-free maintenance. *Biomaterials*. 2008;29(29):3946–52.
82. Li Z, Leung M, Hopper R, Ellenbogen R, Zhang M. Feeder-free self-renewal of human embryonic stem cells in 3D porous natural polymer scaffolds. *Biomaterials*. 2010;31 (3):404–12.
83. Carlson AL, Florek CA, Kim JJ, Neubauer T, Moore JC, Cohen RI, et al. Microfibrous substrate geometry as a critical trigger for organization, self-renewal, and differentiation of human embryonic stem cells within synthetic 3-dimensional microenvironments. *FASEB J*. 2012;26(8):3240–51.
84. Varani J, Inman DR, Fligiel SE, Hillegas WJ. Use of recombinant and synthetic peptides as attachment factors for cells on microcarriers. *Cytotechnology*. 1993;13(2):89–98.
85. Bigdeli N, Andersson M, Strehl R, Emanuelsson K, Kilimare E, Hyllner J, et al. Adaptation of human embryonic stem cells to feeder-free and matrix-free culture conditions directly on plastic surfaces. *J Biotechnol*. 2008;133(1):146–53.

# Chapter 13

## Hydrogel-Based Biomimetic Environment for In Vitro Cell and Tissue Manipulation

Takuya Matsumoto

**Abstract** A biomimetic environment fabricated with synthetic material would be an effective tool for reproducing the tissue-developmental process and even for achieving tissue engineering in vitro. A hydrogel material is one candidate for this tool, because a hydrogel normally shows harmless properties in regard to cells and tissue, and it can be tuned chemically and physically to obtain the desired form. Accordingly, fibrin gel was utilized to reproduce the 3D cellular orientations found in muscle tissue, fabricate tendon-like mineralized tissue, and regulate vascular formation. In this context, cell and tissue manipulations within the gel were led by in vitro physical and chemical stimulations. In this chapter, the approach used for manipulating cells and tissues using the designed hydrogel is discussed.

**Keywords** Biomimetic environment • Cell manipulation • Hydrogel • In vitro tissue engineering

### 13.1 Introduction

Thanks to recent advances in cell and molecular biology, researchers have gradually started to understand how molecules are concerned with the expression of cellular functions. They have also started to understand how the surrounding molecules guide cellular behavior. Engineers and chemists have also started to participate in this in-vitro cellular guidance, develop methods for so-called “in-vitro cellular guidance,” since they can design and construct an environment that is suitable for manipulating cell functions. For example, Chen et al. used a microprinting system that can control the cell-adhesion shape by applying the patterned coating of fibronectin on two-dimensional tissue-culture substrates. They indicated that the mesenchymal stem cells (MSCs) shape regulates the switch in lineage commitment by modulating endogenous RhoA activity. Expressing dominant-negative RhoA committed MSCs to become adipocytes, while constitutively active RhoA caused

---

T. Matsumoto (✉)  
Department of Biomaterials, Okayama University, 2-5-1 Shikata-cho, Kita-ku,  
Okayama 700-8558, Japan  
e-mail: [tmatsu@md.okayama-u.ac.jp](mailto:tmatsu@md.okayama-u.ac.jp)

osteogenesis [1]. Discher and Mooney indicated that hydrogel with different mechanical stiffnesses regulate cell proliferation, cell differentiation, and even the uptakes of non-viral vectors [2–4]. Since the environment surrounding a cell can be easily tuned by materials and devices according to our favorable design, a newly developed research methodology (integrative biology) is now recognized as a newcomer to find something new that cannot be found by conventional biological methods [5, 6]. Here, we consider that reproducing the tissue-development process in vitro is investigated as a robust tool for understanding cellular behavior in the tissue-developmental stage so that in vitro tissue engineering becomes possible.

## 13.2 Cell and Matrix Patterning Using Hydrogel with Static Mechanical Stimulation

Specific cellular and matrix patterning can be found in biological tissue development and growth. For example, skeletal muscle tissue consists of cells aligned parallel to the long axis of the muscle tissue. Osteoblasts adhered to the surface of bone matrix align in a similar direction to the bone-tissue growth direction in longitudinal bone. Reproduction of parallel cell alignment in three-dimensional (3D) matrices is thus one of the interesting targets for in-vitro tissue engineering. Hydrogel contains more than 80 % water, which is crucial for exchange of nutrition between cells and has similar mechanical properties to those of biological tissue. Fibrin, which is formed by mixing fibrinogen and thrombin purified from peripheral blood, is found in wound-healing regions. Not only is it used therapeutically as surgical glue but fibrin has also been investigated for its use as a biocompatible and biodegradable material in biomedical-engineering applications (e.g., drug delivery systems [7–9] and tissue engineering [10–12]). Fibrin gels, which are comprised of hydrophilic cross-linked fibrils, are considered suitable for 3D cell culture. To obtain 3D matrices having uniformly aligned fibrin fibers, surgical sutures fabricated from poly (lactic-co-glycolic acid) (PLGA) were used to tether the fibrin gels. Each fibrin gel was formed in a cylindrical silicone mold (length: 10 mm, diameter: 6 mm) with sutures inserted at both ends. The sutures were then clamped to a custom-made device for generating continuous tensile strain (up to 200 %) (Fig. 13.1a). The suture material possessed a highly rough texture due to its woven structure, and it firmly attached to the fibrin matrices. Scanning electron microscopy (SEM) images indicated that bundle-like structures were formed in the strained gels; this structure comprised fibrin fibrils that were oriented parallel to the strain direction (Fig. 13.1b, c). Highly magnified SEM images indicated that the fibril alignment in the bundle-like structure depend on the amount of strain applied. The fibrils were torn at the border of each bundle, suggesting that the displacement of each set of fibrils in the strain direction facilitated the formation of bundle-like structures in the fibrin gel. The cross-section of the generated bundle-like structures exhibited a polygonal shape, not a complete circular shape, which is similar to the cross-section of natural skeletal muscle tissue. The estimated diameter of each bundle-like structure decreased with increasing strain [13].

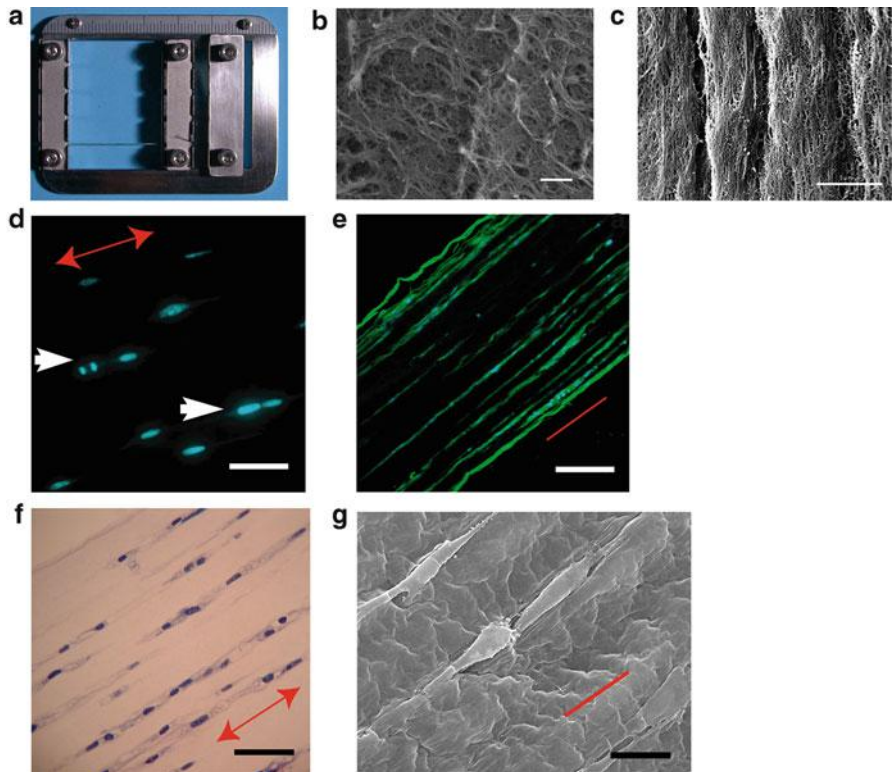


**Fig. 13.1** (a) Custom made device fabricated for tethering the strained fibrin gel. (b) The representative SEM image of microstructure of fibrin gel without strain (Bar: 1  $\mu\text{m}$ ). (c) The representative SEM image of strained fibrin gel (Bar: 5  $\mu\text{m}$ ). (d) The direction of cell proliferation was also identical with strain direction of hydrogel (Bar: 100  $\mu\text{m}$ ). (e) Three-dimensionally aligned cell groups formed in the strained fibrin gel (Green; actin, Blue; nucleus) (Bar: 400  $\mu\text{m}$ ). (f) Three-dimensionally aligned cell groups formed in the strained fibrin gel (Hematoxylin–Eosin staining) (Bar: 200  $\mu\text{m}$ ). (g) SEM images of aligned cells in the strained fibrin gel (Bar: 100  $\mu\text{m}$ )

### 13.3 Three-Dimensional Patterning of Mineralized Cell Groups in Hydrogel

The cell dynamics within the strained fibrin gel were investigated. The fibrinogen solution containing myoblast (C2C12) was used to form a gel, which was continuously subjected to 25 % strain. The cells in the fibrin gel display a specific alignment, that is, parallel to the strain direction. Interestingly, the direction of cell proliferation was identical to that of cell alignment (Fig. 13.1d). A single seeded cell therefore divided multiple times, and the oriented cells subsequently formed linear groups aligned parallel to the strain direction (Fig. 13.1e, f), in a similar manner to the cellular organization found in a longitudinal section of native

skeletal muscle tissue. It is assumed that the positions of the cells in the fibrin gel are restricted to the spaces between the fibrin bundles such that they align and proliferate parallel to the strain direction. This assumption is supported by a typical SEM image (Fig. 13.1g), which shows cells positioned in the spaces between the bundle-like structures of the fibrin gel.

In light of the above-described results, bone-marrow stromal cells (BMSCs) were used instead of myoblasts to fabricate the aligned mineralized tissue. In a similar manner to the cells in the above-described myoblast study, the cells in the strained gel displayed a specific alignment, namely, parallel to the strain direction in the gel. The direction of cell proliferation was identical to that of cell alignment. Consequently, the oriented cells formed a number of linear cell groups aligned parallel to the strain direction in the strained gel. In the strained fibrin gel, type-I collagen deposition showed a specific orientation, namely, parallel to the strain direction (Fig. 13.2a, b). The merged images with nuclear-stained cells in the figure indicate that the matrix was deposited in identical positions to the cell positions in the gel. When BMSCs were cultured in an osteogenic differentiation medium, mineralization derived from the cells was observed in the fibrin gel. Similar to the matrix deposition, mineral deposition was localized according to the cell position and showed a specific alignment in the strained gel. X-ray-diffraction (XRD) peak profiles revealed that the obtained mineral in the fibrin gel was hydroxyapatite (HAp) (Fig. 13.2c). Additionally, a specific orientation of the HAp crystals (namely, parallel to the strain direction) was confirmed from the relative intensity of the (002) to (211) planes in the XRD profiles (Fig. 13.2c). SEM images indicate that compared to those in the control gel, the mineralized matrix vesicles were concatenated serially parallel to the strain direction in the strained gel (Fig. 13.2d). EDS analysis revealed that the mineralized matrix vesicles contain both calcium and phosphorus. The concentrations of phosphorus in the mineralized vesicle regions are much higher than those of calcium in that region.

To investigate the alterations of cellular functions in strained fibrin gel, the cells were cultured in gels with different strain rates. At day eight, the gel subjected to a higher strain rate had enhanced cell proliferation compared to the gel subjected to a lower strain rate. The mRNA expressions of Opn and Oc, namely, osteogenic differentiation markers, were investigated at day four. Both Opn and Oc expressions decreased with the increasing strain rate from up to 50 %. These results suggest that cell functions in the strained fibrin gel are regulated by the alteration of strain rate. To confirm this suggestion, cell-derived mineralization in the gel (subjected to varied strain rate during the culture period) was investigated. Mineralization caused by cell differentiation was detected only in the sample that was subjected to strain rate decreased from 50 to 0 % at day 21 (III). In contrast, mineral deposition was not detected in the gel that was subjected to strain rate reduced from 50 to 0 % at day 28 (II) or in the gel that was subjected to 50 % strain maintained for 50 days (I) (Fig. 13.2e) [14].

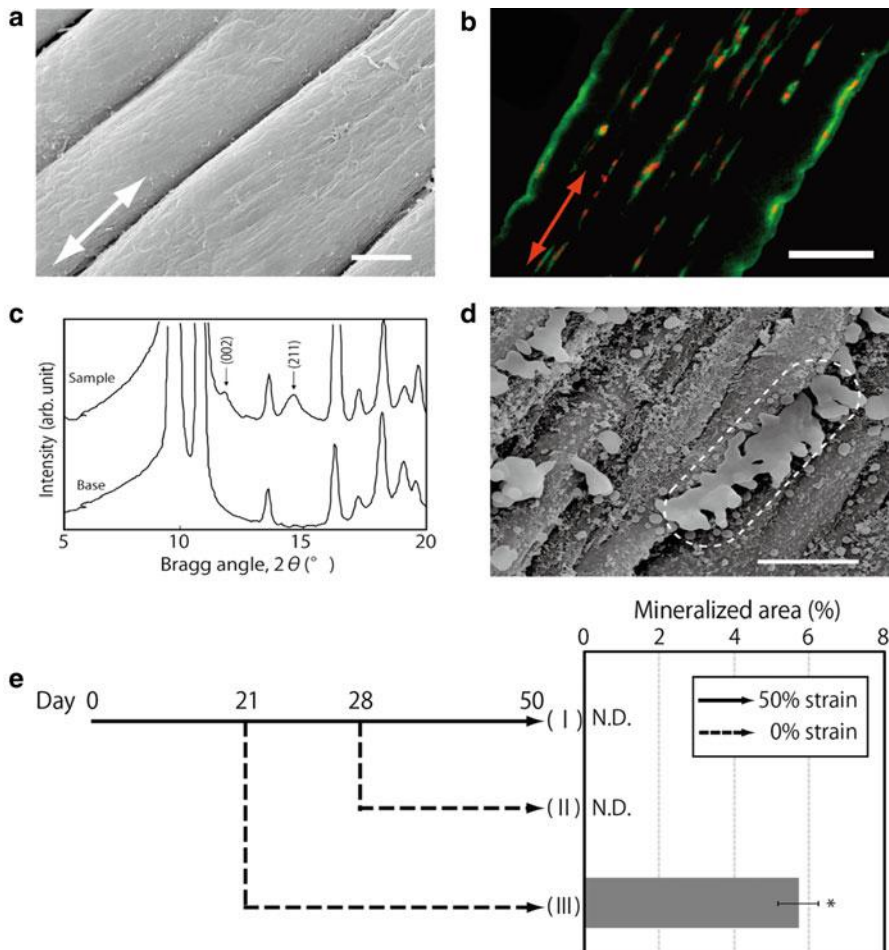


**Fig. 13.2** (a) SEM images of bundle-like structure formed in the strained fibrin gel (Bar: 20 μm). (b) Aligned cell groups and precipitated type I collagen according to the cell group presence (Bar: 250 μm). (c) X-ray diffraction analysis of precipitated minerals within the strained fibrin gel. (d) Connected minerals on aligned cells and fibers (Bar: 10 μm). (e) Mineralized area in strained fibrin gel cultured with different strain conditions. (I) 50 % strain for 50 days, (II) 50 % strain for 28 days reduced to 0 % strain for another 22 days, and (III) 50 % strain for 21 days reduced to 0 % strain for another 29 days (\*:  $p < 0.05$ )

### 13.4 Microvessel Patterning Using Fibrin Gel with Dynamic Mechanical Stimulation

By here, the cells were cultured in the strained condition; however, the strain was static and continuous. A device for applying dynamic strain against to cells in 3D hydrogel was also designed. The device was used to investigate the formation of

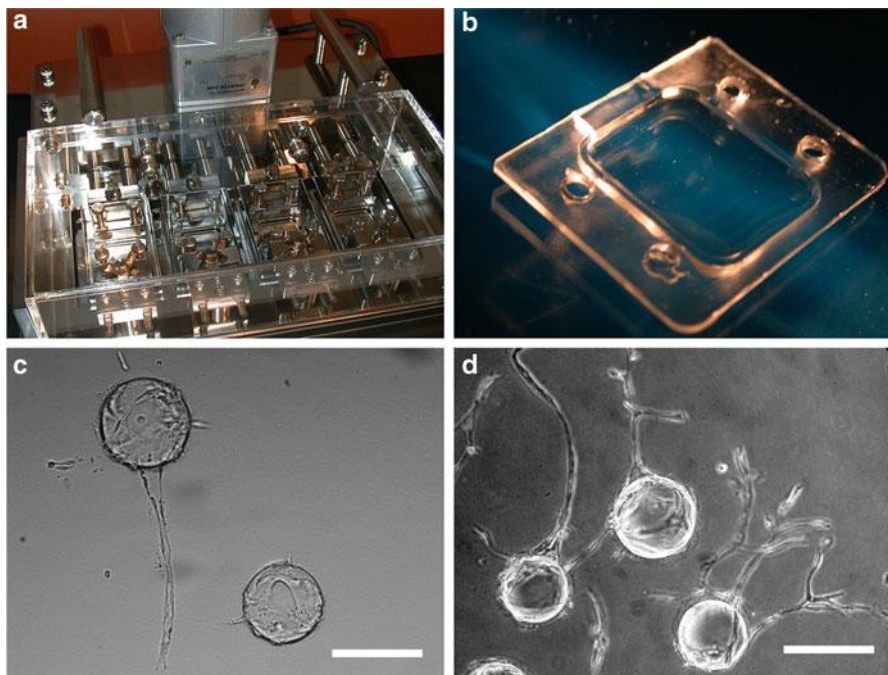


**Fig. 13.3** (a) Original device for applying mechanical strain to cells in the 3D gel. (b) Chamber for cell culture in 3D gel with strained condition. (c) Newly formed sprouts with well defined lumens elongated perpendicular to the strain direction when subjected to cyclic strain (Bar: 100  $\mu\text{m}$ ). (d) Cells in static culture sprouted in all directions equally (Bar: 100  $\mu\text{m}$ )

vascular tissue under cyclic mechanical stimulations. Dextran beads coated with human umbilical endothelial cells (HUVECs) were embedded in fibrin gels within a custom 3D chamber and subjected to cyclic strain (Fig. 13.3a, b). HUVECs on the beads started to invade the gels in a direction perpendicular to the strain direction and formed sprout-like structures within 5 days (Fig. 13.3c). Each bead formed only one or two of these structures, and they were aligned in a direction predominantly perpendicular to the direction of strain application. There were no branches in these structures formed in the strained condition. In contrast, single cells migrated, proliferated, and formed multiple sprouts per bead in the static condition. These sprouts had no consistent orientation, and the sprouts formed in this condition were branched (Fig. 13.3d). Structures formed in the presence of cyclic strain were also significantly thicker than those formed in the static condition. The structures formed under cyclic strain contained wall cells with nuclei located toward the some alternatives lumens, but the lumens also contain aligned cells. These cells were likely proliferated inside the structures, while the wall cells migrated and proliferated to form the structures [15].

### 13.5 Conclusion

As mentioned here, the hydrogel system can be physically tuned by applying mechanics. The cultured cells used in the physical stimulations show different behavior according to the surrounding architectures or stimulation conditions. Conventionally, the cell behavior was regulated only to confirm the effect of soluble factors that were newly-cloned. However, recent studies aiming to modulate cells and tissue to fabricate cell-based functional materials, or even to achieve biological tissue synthesis *in vitro*, have been performed [16–21]. In the present study, as well as chemical stimulation, physical stimulation is also considered as a promising candidate to modulate cell and tissue functions. Moreover, the trials on these cell and tissue manipulations would be valuable to help understanding of the biological unknown during the tissue-developmental process.

**Open Access** This chapter is distributed under the terms of the Creative Commons Attribution Noncommercial License, which permits any noncommercial use, distribution, and reproduction in any medium, provided the original author(s) and source are credited.

## References

1. McBeath R, Pirone DM, Nelson CM, Bhadriraju K, Chen CS. Cell shape, cytoskeletal tension, and RhoA regulate stem cell lineage commitment. *Dev Cell.* 2004;6:483–95.
2. Engler AJ, Sen S, et al. *Cell.* 2006;126:677–89.
3. Kong HJ, Polte TR, Alsberg E, Mooney DJ. FRET measurements of cell-traction forces and nano-scale clustering of adhesion ligands varied by substrate stiffness. *Proc Natl Acad Sci U S A.* 2005;102:4300–5.
4. Kong HJ, Matsumoto T, et al. *Nat Mater.* 2005;4:460–4.
5. Lutolf MP. Integration column: artificial ECM: expanding the cell biology toolbox in 3D. *Integr Biol (Camb).* 2009;1:235–41.
6. Beebe D, Cheran L. Introducing a new method section for integrative biology. *Integr Biol (Camb).* 2009;1:445.
7. Lu X, Le Noble F, Yuan L, Jiang Q, De Lafarge B, Sugiyama D, et al. The netrin receptor UNC5B mediates guidance events controlling morphogenesis of the vascular system. *Nature.* 2004;432:179–86.
8. Weinstein BM. Vessels and nerves: marching to the same tune. *Cell.* 2005;120:299–302.
9. Alon T, Hemo I, Itin A, Pe'er J, Stone J, Keshet E. Vascular endothelial growth factor acts as a survival factor for newly formed retinal vessels and has implications for retinopathy of prematurity. *Nat Med.* 1995;1:1024–8.
10. Senger DR, Ledbetter SR, Claffey KP, Papadopoulos-Sergiou A, Peruzzi CA, Detmar M. Stimulation of endothelial cell migration by vascular permeability factor/vascular endothelial growth factor through cooperative mechanisms involving the alphavbeta3 integrin, osteopontin, and thrombin. *Am J Pathol.* 1996;149:293–305.
11. Grunstein J, Masbad JJ, Hickey R, Giordano F, Johnson RS. Isoforms of vascular endothelial growth factor act in a coordinate fashion to recruit and expand tumor vasculature. *Mol Cell Biol.* 2000;20:7282–91.
12. Gerhardt H, Golding M, Fruttiger M, Ruhrberg C, Lundkvist A, et al. VEGF guides angiogenic sprouting utilizing endothelial tip cell filopodia. *J Cell Biol.* 2003;161:1163–77.

13. Matsumoto T, Sasaki J, Alsberg E, Egusa H, Yatani H, Sohmura T. Three-dimensional cell and tissue patterning in a strained fibrin gel system. *PLoS One.* 2007;2:e1211.
14. Sasaki JI, Matsumoto T, Egusa H, Nakano T, Ishimoto T, Sohmura T, et al. In vitro engineering of transitional tissue by patterning and functional control of cells in fibrin gel. *Soft Matter.* 2010;6:1662–7.
15. Matsumoto T, Yung YC, Fischbach C, Kong HJ, Nakaoka R, Mooney DJ. Mechanical strain regulates endothelial cell patterning in vitro. *Tissue Eng.* 2007;13:207–17.
16. Matsumoto T, Mooney DJ. Cell instructive polymers. In: Kaplan D, editor. *Tissue engineering, Advances in biochemical engineering/biotechnology series*, vol. 102. Berlin: Springer; 2006. p. 113–37.
17. Eiraku M, Takata N, Ishibashi H, Kawada M, Sakakura E, Okuda S, et al. Self-organizing optic-cup morphogenesis in three-dimensional culture. *Nature.* 2011;472:51–6.
18. Sasaki J, Matsumoto T, Egusa H, Matsusaki M, Nishiguchi A, Nakano T, et al. In vitro reproduction of endochondral ossification using a 3D mesenchymal stem cell construct. *Integr Biol (Camb).* 2012;4:1207–14.
19. Miyajima H, Matsumoto T, Sakai T, Yamaguchi S, An SH, Abe M, et al. Hydrogel-based biomimetic environment for in vitro modulation of branching morphogenesis. *Biomaterials.* 2011;32:6754–63.
20. Higgins CA, Chen JC, Cerise JE, Jahoda CA, Christiano AM. Microenvironmental reprogramming by three-dimensional culture enables dermal papilla cells to induce de novo human hair-follicle growth. *Proc Natl Acad Sci U S A.* 2013;110:19679–88.
21. Ogawa M, Oshima M, Imamura A, Sekine Y, Ishida K, Yamashita K, et al. Functional salivary gland regeneration by transplantation of a bioengineered organ germ. *Nat Commun.* 2013;4:2498.

# **Chapter 14**

## **Trends in Periodontal Regeneration Therapy: Potential Therapeutic Strategy of Extracellular Matrix Administration for Periodontal Ligament Regeneration**

**Masahiro Saito**

**Abstract** Current strategy for the treatment of periodontal disease is to application of stem cells or functional molecules that can reorganize tissue integrity, cellular activities and extracellular matrix framework to recover periodontal tissue function. The approach to be regeneration of periodontal ligament (PDL) that is a tooth supporting connective tissue has made a progress for consideration of strategies in regeneration therapy of periodontal tissue damaged by periodontitis. To realize the achieving functional PDL regeneration, the application of stem cells and functional molecules which are essential for PDL regeneration/development must be developed. The identification of stem cells/progenitors and functional molecules that contribute PDL regeneration will substantial contribution for realization of the regeneration therapy as a novel treatment of connective tissue disease. This review describes current strategy of functional PDL regeneration based on development, stem cell biology and tissue engineering after pathological degradation by periodontitis. The present status of the hurdles to this technology are also described and discussed.

**Keyword** Extracellular matrix • Marfan syndrome • Microfibril • Periodontal ligament • Regeneration therapy

### **14.1 Introduction**

The current advances in future regenerative therapies have been influenced by many previous studies of embryonic development, stem cell biology, and tissue engineering technologies [1, 2]. To restore the partial loss of organ functions and to repair damaged tissues, attractive concepts that have emerged in regenerative therapy is stem cell transplantation into various tissues and organs [3] and cytokine

---

M. Saito, D.D.S., Ph.D. (✉)

Division of Operative Dentistry, Department of Restorative Dentistry, Graduate School of Dentistry, Tohoku University, 4-1 Seiryo-machi, Aoba-ku, 980-8575, Sendai, Japan  
e-mail: [mssaito@dent.tohoku.ac.jp](mailto:mssaito@dent.tohoku.ac.jp)

therapy, which has the potential to induce the activation and differentiation of tissue stem/progenitor cells [4]. PDL stem cells and the cytokine network that involved PDL formation and dental follicle cell growth and differentiation, have been well characterized at the molecular level [5–7]. Based on these results, regeneration of periodontal tissues is being made clinically possible by the transplantation of mesenchymal stem cells which can differentiate into PDL cells, cementoblasts and osteoblasts, or through the local application of cytokines to stimulate the proliferation and differentiation of these stem cells [8–10]. Although these therapies are effective and contribute to periodontal tissue repair, these interventions will likely be improved by an enhanced understanding of the development of periodontal tissues, particularly those involved in the formation of PDL, cementum and alveolar bone.

Fibrillin-1 comprises one of the major insoluble extracellular matrix components in connective tissue microfibrils and provides limited elasticity to tissues through microfibril formation [11]. Various mouse models revealed that Marfan syndrome (MFS) is a severe, systemic disorder of connective tissue formation and can lead to aortic aneurysms, ocular lens dislocation, emphysema, bone overgrowth and severe periodontal disease [12]. MFS have been established via gene targeting or missense mutations, with germline mutations in fibrillin-1 leading to progressive connective tissue destruction due to fibrillin-1 fragmentation in association with an insufficiency of fibrillin-1 microfibril formation [13]. Hence, it is largely accepted that MFS is caused by insufficient fibrillin-1 microfibril formation in various connective tissues [14]. Fibrillin-1 has been shown to contribute to the formation and maintenance of periodontal ligament. An abnormal PDL structure in association with the progressive destruction of microfibrils has been observed in a Marfan's syndrome mouse model. These findings have strongly suggested that microfibril formation through fibrillin-1 assembly provides a novel therapeutic strategy for the treatment of periodontal disease.

We here review the present status of the periodontal tissue regeneration technologies that focus on the molecular mechanisms underlying development, regeneration and tissue engineering of periodontal tissue, and also discuss the potential of ECM administration therapy through the promotion of microfibril assembly as a novel therapeutic strategy for the essential functional recovery of periodontal tissue.

## 14.2 Periodontal Ligament Development

The PDL has essential roles in tooth support, homeostasis, and repair, and is involved in the regulation of periodontal cellular activities such as cell proliferation, apoptosis, the secretion of extracellular matrices, resorption and repair of the root cementum, and remodeling of the alveolar bone [15]. To develop future methods to regenerate damaged PDL, it will be important to understand the molecular basis of PDL development and also how the destruction of the PDL occurs during periodontal disease.

### ***14.2.1 Developmental Process of Dental Follicle***

The PDL is derived from the dental follicle (DF), which is located within the outer mesenchymal cells of the tooth germ and can generate a range of periodontal tissues including the PDL, cementum and alveolar bone [21]. The DF is formed during the cap stage of tooth germ development by an ectomesenchymal progenitor cell population originating from the cranial neural crest cells [16]. Given the critical role that the progenitor cell population in the DF appears to play in the development of periodontal tissue, the developmental processes in this tissue are of considerable interest in terms of further understanding the biology of these cells [17]. The differentiation of the DF proceeds as follows: (1) during the tooth root forming stage, the Hertwig's epithelial root sheath (HERS) comprising the inner- and outer-dental epithelia that initiate tooth root dentin formation is fragmented into the Mallasez epithelium resting on the tooth root surface; (2) the DF migrates to the surface of the tooth root and differentiates into cementoblasts to form the cementum matrix [18, 19]; (3) at almost the same time, the DF differentiates into the PDL on the cementoblasts in order to insert collagen fibers, known as Sharpey's fibers, into the cementum matrix. Fiber insertion also takes place along the alveolar bone; and (4) both bone- and PDL-derived fibers finally coalesce in the PDL to form the intermediate plexus, which resembles tendinous tissue [20].

### ***14.2.2 Tendon/Ligament Related Molecules Involved in DF Development***

Although the molecular mechanisms of DF development and differentiation remain to be determined, previous gene expression studies of mouse molar root development have suggested that some growth factors, including bone morphogenetic protein 4, growth and differentiation factors (GDFs)-5, 6, and 7 [21, 22], epidermal growth factors [23], Shh [24], and insulin-like growth factor-1 [25], are involved in the growth or differentiation of the DF. Transcriptional factors such as Scleraxis, Gli, Msx1, Msx2 and Runx2 have also been shown to be involved in the differentiation of the DF into cementoblasts and in the mineralization of cementum [20, 26]. Among these factors, GDFs and scleraxis are the most well characterized that are involved in tendon/ligament morphogenesis, suggesting that PDL development shares similar molecular mechanisms to those of tendon/ligament morphogenesis [20, 27]. These observations strongly suggest that the tendon/ligament related cytokines regulate induction of extracellular matrix (ECM) component to the formation of the tendinous structure of the PDL. The mechanisms involving fibrous ECM network formation may also have a role in formation of the DF development.

### 14.3 Microfibril is Essential for PDL Maintenance and Formation

The ECM is a biologically active molecule composed of a complex mixture of macromolecules that, in addition to serving a structural function, profoundly affect the tendon/ligament formation [28]. Global gene expression analysis of PDL forming stage have revealed that ECM components including type I collagen, type III collagen, lumican, decorin, periostin, f-spondin, tenascin-N, fibrillin-1 and PLAP1/aspirin are highly expressed during PDL formation [29, 30].

#### 14.3.1 *Fibrillin-1 Regulate PDL Formation and Maintenance*

Among the ECM formations in the PDL, fibrillin-1, a major component of the microfibrils that regulate tissue integrity and elasticity, has been shown to contribute to the formation and maintenance of PDL [31]. Various mouse models of Marfan's syndrome (MFS) have been established via gene targeting or missense mutations, with germline mutations in *fibrillin-1* leading to progressive connective tissue destruction due to fibrillin-1 fragmentation in association with an insufficiency of fibrillin-1 microfibril formation [32–35]. Hence, it is largely accepted that MFS is caused by insufficient fibrillin-1 microfibril formation in various connective tissues. MFS have been shown to increase the susceptibility to severe periodontal disease due to a dysfunction of the PDL through a microfibril insufficiency, suggesting that fibrillin-1 microfibril formation plays a central role in PDL formation [36]. MFS patient have been shown that periodontal disease is progressed severely compared with non MFS patient [37]. These findings have strongly suggested that microfibril formation through fibrillin-1 assembly plays an important role in PDL formation and function. However, the molecular mechanisms of fibrillin-1 microfibril assembly remain unclear as the microfibril-associated molecule that regulates or stabilizes fibrillin-1 microfibril formation has not yet been identified.

#### 14.3.2 *Strategy of MFS Treatment*

MFS is a severe, systemic disorder of connective tissue formation and can lead to aortic aneurysms, ocular lens dislocation, emphysema, bone overgrowth and severe periodontal disease. A variety of MFS therapies have been developed, including surgical therapy for aortic root aneurysms that are life-threatening, traditional medical therapies such as  $\beta$ -adrenergic receptor blockade for slow aortic growth and to decrease the risk of aortic dissection [14]. It has been demonstrated also that

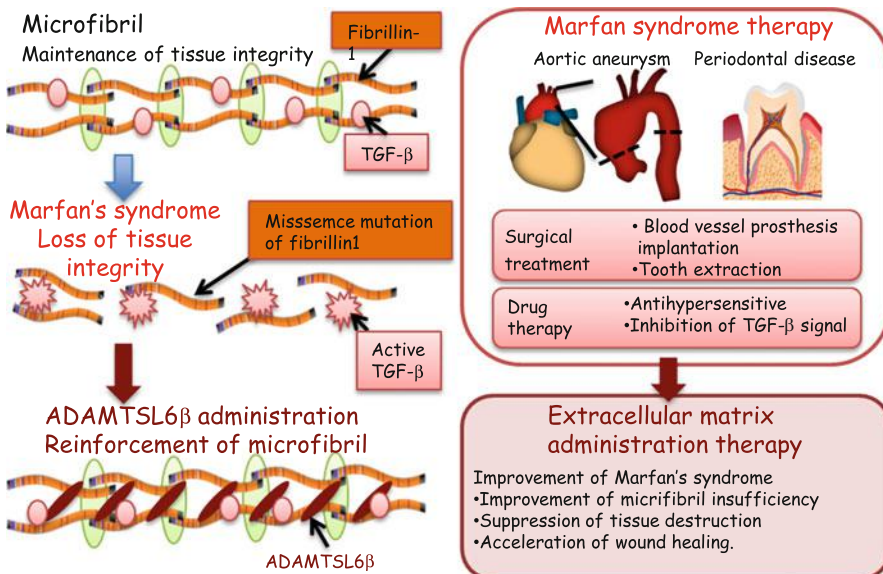


**Fig. 14.1** Schematic representation of the MFS and ECM administration therapy as a novel therapeutic strategy for the treatment of MFS. *Left panel:* Fibrillin-1 comprises insoluble extracellular matrix components in connective tissue microfibrils and provides limited elasticity to tissues through fibrillin-1 microfibril formation. Missense mutations of fibrillin-1 leading to progressive connective tissue destruction due to fibrillin-1 fragmentation in association with an insufficiency of fibrillin-1 microfibril formation. ADAMTS6 $\beta$  is essential for fibrillin-1 microfibril formation and suggest a novel therapeutic approach to the treatment of MFS through the promotion of ADAMTS6 $\beta$ -mediated fibrillin-1 microfibril assembly. *Right Panel:* A variety of MFS therapies have been developed, including surgical therapy for aortic root aneurysms that are life-threatening, traditional medical therapies such as  $\beta$ -adrenergic receptor blockade for slow aortic growth and to decrease the risk of aortic dissection, and novel approaches based on new insights such as the deregulation of TGF- $\beta$  activation. ECM reinforcement therapy which induces restoration of properly formed microfibrils by ADAMTS6 $\beta$  is essential not only for improvement of the predominant symptoms of MFS, but also for the suppression of excessive TGF- $\beta$  signaling induced by microfibril disassembly. Image from published paper [39]

systemic antagonism of Transforming Growth Factor-type beta (TGF- $\beta$ ) signaling through the administration of a TGF- $\beta$  neutralizing antibody or losartan, an angiotensin II type 1 receptor blocker, has been shown to have a beneficial effect on alveolar septation and muscle hypoplasia in MFS [33, 38]. However, another potential therapeutic strategy which remains to be investigated is the reconstruction of the microfibril in connective tissues through the expression or administration of a microfibril-associated molecule that regulates or stabilizes fibrillin-1 microfibril formation. To investigate this concept, it will be necessary to identify molecular mechanisms of microfibril formation and an appropriate fibrillin-1 microfibril associated molecule (Fig. 14.1).

## 14.4 Novel Approaches to Periodontal Tissue Regeneration Using ECM Administration Therapy

ECM components organized in the PDL not only reflect the functional requirements of this matrix such as mechanical stress and storage of signaling molecules, but also regulate the tissue framework during development and regeneration [30]. In addition, a new therapeutic concept has proposed that a fibrillin-1 microfibril insufficiency can be corrected by the administration of ECM components.

### 14.4.1 ADAMTSL6 $\beta$ Serves as a Novel Molecules that Regulate Microfibril Assembly

A disintegrin-like metalloprotease domain with thrombospondin type I motifs (ADAMTS)-like, ADAMTSL, is a subgroup of the ADAMTS superfamily that shares particular protein domains with the ADAMTS protease, including thrombospondin type I repeats, a cysteine-rich domain, and an ADAMTS spacer, but lacks the catalytic and disintegrin-like domains [40]. A recent study has demonstrated that ADAMTSL2 mutations cause geleophysic dysplasia, an autosomal recessive disorder similar to MFS, through the dysregulation of TGF- $\beta$  signaling [41]. A homozygous mutation in ADAMTSL4 also causes autosomal-recessive isolated ectopia lentis, another disease similar to MFS which is characterized by the subluxation of the lens as a result of disruption of the zonular fibers [42]. The novel ADAMTSL family molecules ADAMTSL6 $\alpha$  and 6 $\beta$  were recently identified by in silico screening for novel ECM proteins produced from a mouse full-length cDNA database (FANTOM). These proteins are localized in connective tissues, including the skin, aorta and perichondrocytes. Among ADAMTSL6, ADAMTSL6 $\beta$  has shown to associate with fibrillin-1 microfibrils through its direct interaction with the N-terminal region of fibrillin-1 and promotes fibrillin-1 matrix assembly in vitro and in vivo [43]. These findings suggest a potential clinical application of ADAMTSL6 $\beta$  as a novel MFS therapy by promoting fibrillin-1 microfibril assembly and regulating TGF- $\beta$  activation.

It is also suggested that the administration of fibrillin-1 microfibrils provides a novel therapeutic strategy for the treatment of periodontal disease.

### 14.4.2 ADAMTSL6 $\beta$ Regulates Microfibril Assembly

To investigate whether ADAMTSL6 $\beta$  plays a critical role in microfibril assembly in connective tissues, we generated ADAMTSL6 $\beta$  transgenic mice (TSL6 $\beta$ -TG mice) in which the transgene is expressed in the whole body. Since ADAMTSL6 $\beta$  has shown to be expressed in the aorta and skin, we investigated microfibril assembly of these tissues in the TSL6 $\beta$ -TG mice. Immunohistochemical analysis revealed that

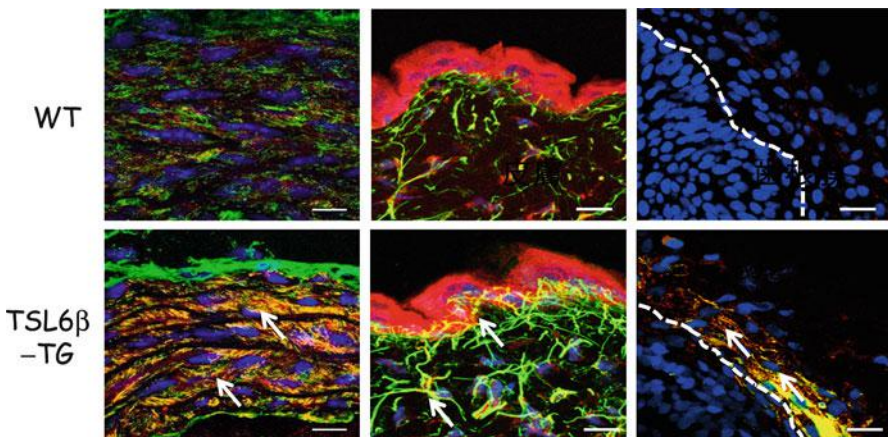


**Fig. 14.2** Immunohistochemical analysis of TSL6 $\beta$ -TG mice. Cryosections were prepared from the aortas (left), skin (middle) or PDL (right) of wild type (*upper panel*) or TSL6 $\beta$  TG (*lower panel*) littermates and subjected to double immunostaining with antibodies against ADAMTS6 $\beta$  (red) and fibrillin-1 (green). ADAMTS6 $\beta$  and fibrillin-1-positive microfibrils (green yellow) was markedly increased in the aorta and skin of TSL6 $\beta$  TG mice compared with WT mice. Bar = 50  $\mu$ m  
Image from published paper [39]

ADAMTS6 $\beta$  positive microfibril assembly was barely detectable in WT mice but strongly induced in the aorta of TSL6 $\beta$ -TG mice (Fig. 14.2). Histological analysis revealed that microfibrils are clearly increased in the aorta and that microfibril assembly is also induced in the skin and PDL of TSL6 $\beta$  – TG mice. This confirmed that ADAMTS6 $\beta$  induces fibrillin-1 microfibril assembly in connective tissue such as the aorta, skin and PDL.

#### 14.4.3 ADAMTS6 $\beta$ Involved in PDL Formation and Repair

To investigate whether ADAMTS6 $\beta$  contributes to PDL formation, we first examined its expression patterns during PDL forming stage of DF in the developing tooth germ. In situ hybridization analysis revealed that ADAMTS6 $\beta$  was strongly expressed in the PDL forming stage of the DF however ADAMTS6 $\beta$  expression was significantly downregulated in the adult PDL. Immunohistochemical analysis further revealed that ADAMTS6 $\beta$  is detectable in assembled microfibril-like structures during the PDL forming stage of the DF, and in organized microfibrils in the adult PDL. Because developmental processes involve similar mechanisms to wound healing, we next determined whether ADAMTS6 $\beta$  is involved in PDL microfibril assembly during wound healing using a tooth replantation model. Histochemical analysis revealed that both fibrillin-1 and ADAMTS6 $\beta$  expressions were found to be clearly induced during wound healing of PDL, but to decrease again after healing. These findings suggested that ADAMTS6 $\beta$  was involved in microfibril formation during PDL formation/regeneration.

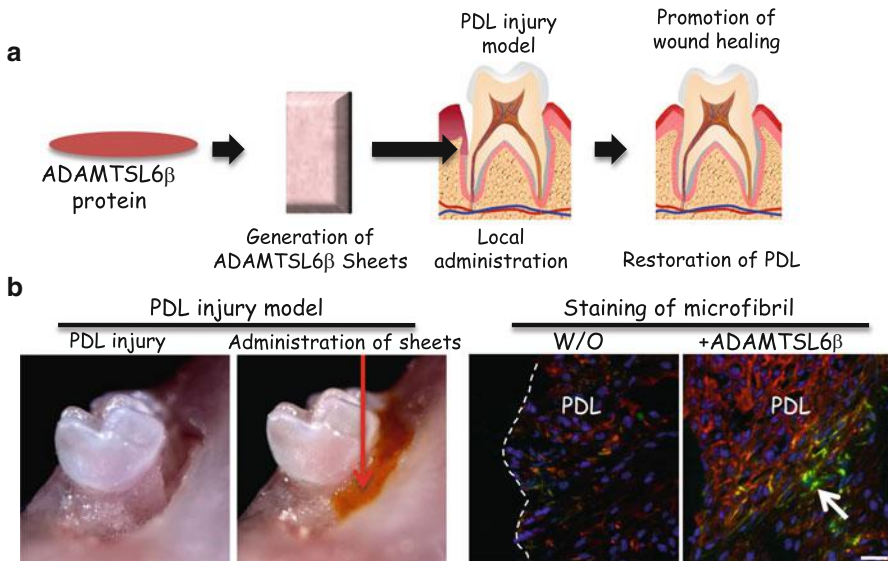


**Fig. 14.3** ADAMTSL6 $\beta$  improves microfibril disorder in PDL from an MFS model. (a) Schematic representation of the local administration of recombinant ADAMTSL6 $\beta$  into a PDL injury model (b) After injury of PDL by dislocation, collagen gel-containing recombinant ADAMTSL6 $\beta$  was then injected into the injured PDL (left). Immunohistochemical analysis showed an improvement in fibrillin-1 microfibril assembly (arrowheads) induced by the injection of recombinant ADAMTSL6 $\beta$ . W/O: Without treatment of ADAMTSL6 $\beta$ . Image from published paper [17]

Since oxytalan fiber, a principal elastic fiber system of PDL is composed of fibrillin-1 microfibrils and does not contain significant amounts of elastin [44, 45], this composition suggests that PDL will have an increased susceptibility to breakdown in MFS compared with other elastic tissues composed of both elastin and fibrillin-1 [46]. We demonstrated that ADAMTSL6 $\beta$  is highly expressed in DF during PDL forming stage. In addition, intense expression of ADAMTSL6 $\beta$  can be seen in wound healing process of PDL, indicating that this protein involved in recovery of damaged PDL. Using an animal model of MFS, we demonstrate that local administration of ADAMTSL6 $\beta$  can rescue fibrillin-1 microfibril formation through the promotion of fibrillin-1 microfibril assembly in PDL (Fig. 14.3). These results strongly indicate that ADAMTSL6 $\beta$  is essential for fibrillin-1 microfibril formation and suggest a novel therapeutic approach to the treatment of periodontal disease with MFS.

## 14.5 Conclusion

Regenerative therapy for the periodontal disease has been attempted to use of patient's own cells to recover periodontal defect. Predictable treatment for partial regeneration of PDL damaged by local application of cytokines or stem cell trans

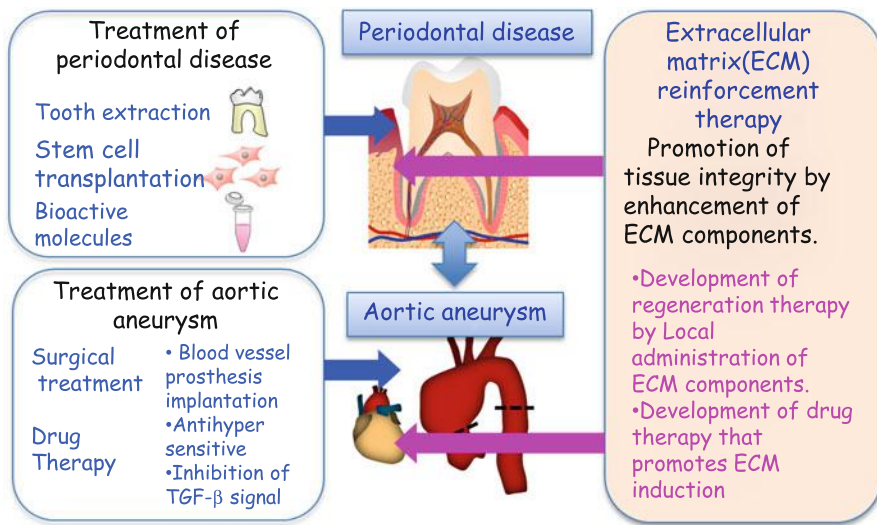


**Fig. 14.4** ECM administration therapy as a novel therapeutic strategy of MFS syndrome. ECM administration therapy using ADAMTSL6 $\beta$  which induces microfibril assembly, should be considered in the development of future mechanism-based therapeutics for the improvement of connective tissue disorders such as MFS. Image from published paper [17]

plantation has been established, thus regenerative medicine for PDL has made the most useful study model and is feasible clinical study for the planning of stem cell- and cytokine- therapies [47]. Although partial regeneration of the periodontal tissue has been established, novel treatment must be developed corresponding to regenerate large defect destroyed by severe periodontal disease. To approach this criticism, it is essential to understand the molecular mechanisms of PDL development to identify the appropriate functional molecules of inducing differentiation of stem cells into periodontal lineage cells for successful reconstruction of periodontal tissue [17, 48, 49].

In this review, we proposed that fibrillin-1 associated protein such as ADAMTSL6 $\beta$ , which induces microfibril assembly, should be considered as an ECM administration agent for the treatment of periodontal disease and improvement of connective tissue disorders such as MFS. The exogenous application of recombinant ADAMTSL6 $\beta$  improves fibrillin-1 microfibril assembly, indicating the reinforcement of fibrillin-1 microfibrils by ADAMTSL6 $\beta$  may represent a new treatment for periodontal disease which is accessible from oral cavity in MFS patients. Since elastolysis occurs continuously in aortic aneurysms arising in MFS cases, the chronic administration of ADAMTSL6 $\beta$  may be required for the stabilization of microfibrils to prevent progressive tissue destruction. It will also be necessary to develop methodologies for the systemic administration of ADAMTSL6 $\beta$  to induce fibrillin-1 microfibril assembly in connective tissue for the treatment of life-threatening conditions such as an aortic aneurysm (Fig. 14.4).

Hence, an ECM administration therapy involving ADAMTSL6 $\beta$  has the capacity to facilitate drug discovery for treating periodontal diseases, and MFS-associated disorders.

**Open Access** This chapter is distributed under the terms of the Creative Commons Attribution Noncommercial License, which permits any noncommercial use, distribution, and reproduction in any medium, provided the original author(s) and source are credited.

## References

1. Brockes JP, Kumar A. Appendage regeneration in adult vertebrates and implications for regenerative medicine. *Science*. 2005;310(5756):1919–23.
2. Watt FM, Hogan BL. Out of Eden: stem cells and their niches. *Science*. 2000;287(5457):1427–30.
3. Korbliog M, Estrov Z. Adult stem cells for tissue repair – a new therapeutic concept? *N Engl J Med*. 2003;349(6):570–82.
4. Gurther GC, Werner S, Barrandon Y, Longaker MT. Wound repair and regeneration. *Nature*. 2008;453(7193):314–21.
5. Liu Y, Zheng Y, Ding G, Fang D, Zhang C, Bartold PM, et al. Periodontal ligament stem cell-mediated treatment for periodontitis in miniature swine. *Stem Cells*. 2008;26(4):1065–73.
6. Seo BM, Miura M, Gronthos S, Bartold PM, Batouli S, Brahim J, et al. Investigation of multipotent postnatal stem cells from human periodontal ligament. *Lancet*. 2004;364(9429):149–55.
7. Murakami S. Periodontal tissue regeneration by signaling molecule(s): what role does basic fibroblast growth factor (FGF-2) have in periodontal therapy? *Periodontol 2000*. 2011;56(1):188–208.
8. Kitamura M, Nakashima K, Kowashi Y, Fujii T, Shimauchi H, Sasano T, et al. Periodontal tissue regeneration using fibroblast growth factor-2: randomized controlled phase II clinical trial. *PLoS One*. 2008;3(7):e2611.
9. Ishikawa I, Iwata T, Washio K, Okano T, Nagasawa T, Iwasaki K, et al. Cell sheet engineering and other novel cell-based approaches to periodontal regeneration. *Periodontol 2000*. 2009;51:220–38.
10. Sonoyama W, Liu Y, Fang D, Yamaza T, Seo BM, Zhang C, et al. Mesenchymal stem cell-mediated functional tooth regeneration in swine. *PLoS One*. 2006;1:e79.
11. Kiely CM, Sherratt MJ, Shuttleworth CA. Elastic fibres. *J Cell Sci*. 2002;115(Pt 14):2817–28.
12. Ramirez F, Sakai LY. Biogenesis and function of fibrillin assemblies. *Cell Tissue Res*. 2010;339(1):71–82.
13. Judge DP, Dietz HC. Therapy of Marfan syndrome. *Annu Rev Med*. 2008;59:43–59.
14. Ramirez F, Dietz HC. Marfan syndrome: from molecular pathogenesis to clinical treatment. *Curr Opin Genet Dev*. 2007;17(3):252–8.
15. Cho MI, Garant PR. Development and general structure of the periodontium. *Periodontol 2000*. 2000;24:9–27.
16. Chai Y, Jiang X, Ito Y, Bringas Jr P, Han J, Rowitch DH, et al. Fate of the mammalian cranial neural crest during tooth and mandibular morphogenesis. *Development*. 2000;127(8):1671–9.
17. Saito M, Tsuji T. Extracellular matrix administration as a potential therapeutic strategy for periodontal ligament regeneration. *Expert Opin Biol Ther*. 2012;12(3):299–309.
18. Saito M, Iwase M, Maslan S, Nozaki N, Yamauchi M, Handa K, et al. Expression of cementum-derived attachment protein in bovine tooth germ during cementogenesis. *Bone*. 2001;29(3):242–8.
19. Handa K, Saito M, Yamauchi M, Kiyono T, Sato S, Teranaka T, et al. Cementum matrix formation in vivo by cultured dental follicle cells. *Bone*. 2002;31(5):606–11.

20. Yokoi T, Saito M, Kiyono T, Iseki S, Kosaka K, Nishida E, et al. Establishment of immortalized dental follicle cells for generating periodontal ligament in vivo. *Cell Tissue Res.* 2007;327(2):301–11.
21. Morotome Y, Goseki-Sone M, Ishikawa I, Oida S. Gene expression of growth and differentiation factors-5, -6, and -7 in developing bovine tooth at the root forming stage. *Biochem Biophys Res Commun.* 1998;244(1):85–90 [published erratum appears in *Biochem Biophys Res Commun* 1998;246(3):925].
22. Sena K, Morotome Y, Baba O, Terashima T, Takano Y, Ishikawa I. Gene expression of growth differentiation factors in the developing periodontium of rat molars. *J Dent Res.* 2003;82(3):166–71.
23. Vaahtokari A, Aberg T, Thesleff I. Apoptosis in the developing tooth: association with an embryonic signaling center and suppression by EGF and FGF-4. *Development.* 1996;122(1):121–9.
24. Huang X, Xu X, Bringas Jr P, Hung YP, Chai Y. Smad4-Shh-Nf1c signaling cascade-mediated epithelial-mesenchymal interaction is crucial in regulating tooth root development. *J Bone Miner Res.* 2010;25(5):1167–78.
25. Fujiwara N, Tabata MJ, Endoh M, Ishizeki K, Nawa T. Insulin-like growth factor-I stimulates cell proliferation in the outer layer of Hertwig's epithelial root sheath and elongation of the tooth root in mouse molars in vitro. *Cell Tissue Res.* 2005;320(1):69–75.
26. Saito Y, Yoshizawa T, Takizawa F, Ikegami M, Ishibashi O, Okuda K, et al. A cell line with characteristics of the periodontal ligament fibroblasts is negatively regulated for mineralization and Runx2/Cbfa1/Osf2 activity, part of which can be overcome by bone morphogenetic protein-2. *J Cell Sci.* 2002;115(Pt 21):4191–200.
27. Nakamura T, Yamamoto M, Tamura M, Izumi Y. Effects of growth/differentiation factor-5 on human periodontal ligament cells. *J Periodontal Res.* 2003;38(6):597–605.
28. Daley WP, Peters SB, Larsen M. Extracellular matrix dynamics in development and regenerative medicine. *J Cell Sci.* 2008;121(Pt 3):255–64.
29. Yamada S, Murakami S, Matoba R, Ozawa Y, Yokokoji T, Nakahira Y, et al. Expression profile of active genes in human periodontal ligament and isolation of PLAP-1, a novel SLRP family gene. *Gene.* 2001;275(2):279–86.
30. Nishida E, Sasaki T, Ishikawa SK, Kosaka K, Aino M, Noguchi T, et al. Transcriptome database KK-Periome for periodontal ligament development: expression profiles of the extracellular matrix genes. *Gene.* 2007;404(1–2):70–9. Epub 2007 Sep 19.
31. Shiga M, Saito M, Hattori M, Torii C, Kosaki K, Kiyono T, et al. Characteristic phenotype of immortalized periodontal cells isolated from a Marfan syndrome type I patient. *Cell Tissue Res.* 2008;331(2):461–72.
32. Pereira L, Lee SY, Gayraud B, Andrikopoulos K, Shapiro SD, Bunton T, et al. Pathogenetic sequence for aneurysm revealed in mice underexpressing fibrillin-1. *Proc Natl Acad Sci U S A.* 1999;96(7):3819–23.
33. Neptune ER, Frischmeyer PA, Arking DE, Myers L, Bunton TE, Gayraud B, et al. Dysregulation of TGF-beta activation contributes to pathogenesis in Marfan syndrome. *Nat Genet.* 2003;33(3):407–11.
34. Carta L, Pereira L, Arteaga-Solis E, Lee-Arteaga SY, Lenart B, Starcher B, et al. Fibrillins 1 and 2 perform partially overlapping functions during aortic development. *J Biol Chem.* 2006;281(12):8016–23.
35. Habashi JP, Judge DP, Holm TM, Cohn RD, Loeys BL, Cooper TK, et al. Losartan, an AT1 antagonist, prevents aortic aneurysm in a mouse model of Marfan syndrome. *Science.* 2006;312(5770):117–21.
36. Straub AM, Grahame R, Scully C, Tonetti MS. Severe periodontitis in Marfan's syndrome: a case report. *J Periodontol.* 2002;73(7):823–6.
37. Suzuki J, Imai Y, Aoki M, Fujita D, Aoyama N, Tada Y, et al. Periodontitis in cardiovascular disease patients with or without Marfan syndrome -a possible role of *Prevotella intermedia*. *PLoS One.* 2014;9(4):e95521.

38. Holm TM, Habashi JP, Doyle JJ, Bedja D, Chen Y, van Erp C, et al. Noncanonical TGFbeta signaling contributes to aortic aneurysm progression in Marfan syndrome mice. *Science*. 2011;332(6027):358–61.
39. Saito M, et al. *J Biol Chem*. 2011;286(44):38602–13.
40. Hirohata S, Wang LW, Miyagi M, Yan L, Seldin MF, Keene DR, et al. Punctin, a novel ADAMTS-like molecule, ADAMTSL-1, in extracellular matrix. *J Biol Chem*. 2002;277(14):12182–9. *Epub 2002 Jan 22*.
41. Le Goff C, Morice-Picard F, Dagorneau N, Wang LW, Perrot C, Crow YJ, et al. ADAMTSL2 mutations in geleophysic dysplasia demonstrate a role for ADAMTS-like proteins in TGF-beta bioavailability regulation. *Nat Genet*. 2008;40(9):1119–23.
42. Ahram D, Sato TS, Kohilan A, Tayeh M, Chen S, Leal S, et al. A homozygous mutation in ADAMTSL4 causes autosomal-recessive isolated ectopia lentis. *Am J Hum Genet*. 2009;84(2):274–8.
43. Tsutsui K, Manabe R, Yamada T, Nakano I, Oguri Y, Keene DR, et al. ADAMTSL-6 is a novel extracellular matrix protein that binds to fibrillin-1 and promotes fibrillin-1 fibril formation. *J Biol Chem*. 2010;285(7):4870–82.
44. Staszyk C, Gasse H. Oxytalan fibres in the periodontal ligament of equine molar cheek teeth. *Anat Histol Embryol*. 2004;33(1):17–22.
45. Sawada T, Sugawara Y, Asai T, Aida N, Yanagisawa T, Ohta K, et al. Immunohistochemical characterization of elastic system fibers in rat molar periodontal ligament. *J Histochem Cytochem*. 2006;54:1095.
46. Ganburged G, Suda N, Saito M, Yamazaki Y, Isokawa K, Moriyama K. Dilated capillaries, disorganized collagen fibers and differential gene expression in periodontal ligaments of hypomorphic fibrillin-1 mice. *Cell Tissue Res*. 2010;341(3):381–95.
47. Pellegrini G, Seol YJ, Gruber R, Giannobile WV. Pre-clinical models for oral and periodontal reconstructive therapies. *J Dent Res*. 2009;88(12):1065–76.
48. Saito M, Nishida E, Sasaki T, Yoneda T, Shimizu N. The KK-Periome database for transcripts of periodontal ligament development. *J Exp Zool B Mol Dev Evol*. 2009;312B(5):495–502.
49. Morsczeck C, Schmalz G. Transcriptomes and proteomes of dental follicle cells. *J Dent Res*. 2010;89(5):445–56.

**Part V**

**Poster Presentation Award Winners**

# **Chapter 15**

## **Histochemical Characteristics of Glycoproteins During Rat Palatine Gland Development**

**Zaki Hakami, Hideki Kitaura, Shiho Honma, Satoshi Wakisaka,  
and Teruko Takano-Yamamoto**

**Abstract** Lectin histochemistry has been used to investigate glycosylation modification and glycoprotein expression that occurs during development and under different physiological and pathological conditions. Several lectin histochemical studies have been performed on the palatine gland of different species, which have described the heterogeneity of complex glycoconjugates present in these structures. However, no study has been conducted with regard to the relationship between glycoproteins and palatine gland development in mammals. Therefore, we conducted a study to test the hypothesis that a considerable modification in the expression of carbohydrates occurs in the palatine gland during developmental differentiation and maturation. Histochemical changes of glycoconjugates were observed during prenatal and postnatal development of the rat palatine gland. Qualitative and quantitative differences for the binding of lectins to palatal epithelium sections were determined. All lectins showed general progressive staining during development that was basally extended from the apical cytoplasm of mucous cells. The distribution of glycoproteins during palatine gland development and the heterogeneous distribution of glycoproteins observed between posterior and anterior sides expand our knowledge of the role of salivary glands in oral function. In

---

Z. Hakami

Division of Orthodontics and Dentofacial Orthopedics, Department of Translational Medicine,  
Tohoku University Graduate School of Dentistry, 4-1 Seiryo-machi, Aoba-ku,  
Sendai 980-8575, Japan

Department of Oral Anatomy and Developmental Biology, Osaka University  
Graduate School of Dentistry, Osaka 565-0871, Japan

H. Kitaura • T. Takano-Yamamoto (✉)

Division of Orthodontics and Dentofacial Orthopedics, Department of Translational Medicine,  
Tohoku University Graduate School of Dentistry, 4-1 Seiryo-machi, Aoba-ku,  
Sendai 980-8575, Japan

e-mail: [t-yamamo@m.tohoku.ac.jp](mailto:t-yamamo@m.tohoku.ac.jp)

S. Honma • S. Wakisaka

Department of Oral Anatomy and Developmental Biology, Osaka University  
Graduate School of Dentistry, Osaka 565-0871, Japan

this review, we describe and discuss glycohistochemical observations of the developing rat palatine gland.

**Keywords** Glycoprotein • Lectin • Palatine gland • Rat

## 15.1 Introduction

In humans, the oral cavity and oropharynx are lined by around 600–1,000 minor salivary glands [1, 2]. These glands are distributed throughout the mouth except in the gingiva and along the midline and in the anterior part of the hard palate. They consist predominantly of mucous cells that release their secretions through a short ductal system into the oral cavity [3]. Palatine glands are mixed glands of predominantly mucus acini and a few serous demilunes. They are located at the deep termination of secretory units that irregularly grow by pouching [4–6]. In humans they develop from the 11th week of gestation from solid epithelial cord arising from the epithelium lining the soft palate. Thereafter, they undergo lumenization, branching and acinar differentiation [7]. In rats, several thickenings in the palatal epithelium appear at embryonic day 17 (E17). At E18 these have extended as epithelial cords that progressively lumenize and branch to form acini at E20 [8].

Minor salivary glands function semi-continuously throughout the day and night, but only contribute up to 10 % of saliva produced [9]. In addition, they play a major role in the physiological defense mechanism of oral cavity structures by producing of up to two-thirds of mucus and half of the secretory IgA in the oral cavity [10, 11]. In addition, the most common site of minor salivary gland tumor occurrence is the oral cavity [12–20]. Salivary mucus glycoproteins are numerous and have a tremendous diversity of carbohydrate side chains that are linked to a polypeptide backbone. The advent of lectin histochemistry has allowed such carbohydrate moieties to be characterized. Lectins, which are proteins of plant or animal origin, have been used to visualize glycosylation modification and glycoprotein expression during development or under different physiological and pathological conditions [21–28].

Conventional histochemical methods have revealed that the mucins of rat palatine glands are rich in both acid and neutral glycoconjugates [29], and can incorporate [<sup>35</sup>S]-sulfate [30]. Several lectin histochemical studies have been reported for palatine glands of different species. These emphasize the heterogeneity of the complex glycoconjugates present in these glands, for example α-fucose is abundant in mammals, but is scarce or absent in birds [3, 31, 32]. Lectin histochemistry has shown the quantity of glycoproteins to progressively increase during postnatal development of the Magellanic penguin [31]. However, there is a scarcity of information regarding the relationship between glycoproteins and palatine gland development in mammals. Therefore, we hypothesized that a considerable modification in the expression of carbohydrates could occur in the palatine glands during developmental differentiation and maturation, which might coincide with the

change in diet from milk to solid feeding. In this review, we describe and discuss glycohistochemical observations of the developing rat palatine gland, according to our previous report [33].

## 15.2 Palatine Gland During Developmental Differentiation and Maturation

### 15.2.1 Prenatal Stage

Sprague–Dawley rats were used. The animals were deeply anesthetized with chloral hydrate (600 mg/kg body weight, i.p.) and perfused transcardially with 0.02 M phosphate-buffered saline (PBS; pH 7.2) followed by 4 % paraformaldehyde in 0.1 M phosphate buffer (PB; pH 7.4). For prenatal experiments, the day on which a vaginal plug was recognized was considered as “embryonic day (E) 0”. Pregnant mothers at E18, and E20 were sacrificed by an overdose injection of chloral hydrate (800 mg/kg), and the fetuses were extracted by caesarian surgery. The whole heads were fixed in 4 % paraformaldehyde in 0.1 M PB (pH 7.4) for 3 days. All postnatal pups were decalcified with 7.5 % ethylene diamine tetraacetic acid (EDTA) for 1–4 weeks at 4 °C. After decalcification, the head was cut into exact halves along the medial plane. For frozen sections two heads from each group were transferred to PBS containing 20 % sucrose. For paraffin sections, two heads from each group were post-fixed in 4 % paraformaldehyde in 0.1 M PB (pH 7.4) overnight or for longer. Specimens were then dehydrated by ethanol, cleared in xylene and embedded in paraffin. In accordance with previous reports [7, 8], at E18, gland buds and epithelial cords with a terminal bulb at the distal end were elongated from the epithelial basement membrane (ectoderm) into the stromal connective tissue (mesenchyme). At E20, branching and lumenization had taken place, and immature acini and ducts were formed. We applied lectin histochemistry to frozen sections to avoid false-negative errors. Parasagittal frozen sections were prepared at a thickness of 14 µm, and mounted on MS-coated glass slides (Matsunami, Osaka, Japan), rinsed with PBS, dried and processed for lectin histochemistry. For the identification of specific carbohydrate residues, tissue sections were incubated for 30 min with 0.3 % H<sub>2</sub>O<sub>2</sub> in methanol to block endogenous peroxidase activity. The sections were then incubated for 12–14 h with one of seven different biotinylated lectins, Glycine max (SBA), Dolichos biflorus (DBA), Vicia villosa (VVA), Ulex europaeus (UEA-1), Triticum vulgare (WGA), Succinyl WGA (sucWGA) or Arachis hypogaea (PNA). Sections were then washed three times in PBS, followed by incubation with ABC (Vector Laboratories) for 60 min and then washed again three times with PBS. The horseradish peroxidase was visualized by incubating slides with 0.05 M Tris–HCl buffer (pH 7.5) containing 0.08 % diaminobenzidine and 0.003 % H<sub>2</sub>O<sub>2</sub>. Sections were then lightly counterstained with methyl blue,

dehydrated and cover slips were mounted using Permount (Fisher, NJ, USA). Sections were examined by light microscopy.

At the prenatal stage, particularly at E18, lectin histochemistry showed considerable variety in the extent or presence of staining among different animals and even among different buds in the same gland. In general, at E18, N-acetylgalactosamine residues visualized by DBA, SBA and VVA showed heterogeneous staining that was negative to weakly positive in the terminal buds. At E21 this staining became progressively more moderate, in the cytoplasm and lumen of ducts, but VVA staining was confined to apical cytoplasm. PNA showed a heterogeneously positive reaction to cell membranes in the epithelial cord but little or no reaction to cells in the terminal buds. At E20, the PNA reaction was located near the lumen. At E18, UEA staining was similar to that of PNA; however, at E20 UEA staining was moderate in the apical cytoplasm and cell membrane as well as on the lumen surface of ducts. WGA reacted strongly at E18, while at E20 staining was moderate on cell membranes and in apical cytoplasm. sucWGA did not show any reaction at E18, but at E20 it stained the cell membrane but not the apical cytoplasm, where secretory granules reside.

In prenatal developmental differentiation, our data showed the importance of terminal sialic acid rather than N-acetylglucosamine, as indicated by intense binding of WGA to the cell membrane and stromal cells and the lack of sucWGA binding [34]. sucWGA labeling appeared largely during postnatal development. Other lectins showed heterogeneous patterns of staining with high affinity of PNA and UEA-1 observed in the epithelial cord at the bud stage. This pattern of reaction is similar to that of developing human labial and lingual minor salivary glands [35]. The varieties in the reactivity of lectins during epithelial budding and bud migration are indicative of a differentiation-dependent alteration in cell surface carbohydrates [36].

### 15.2.2 Suckling Stage

Sprague–Dawley rats aged PN 0–7 were used. We used the same methods for histological analysis and lectin histochemistry as for postnatal animals. The classification of the developmental periods used in this study is based upon the physiological and nutritional stages of animal development [37]. Histological analysis of suckling stage rats showed that the acini of newborns had the general overall appearance of the adult; they contained basophilic nuclei located basally within basal eosinophilic cytoplasm, and pale apical cytoplasm underlined by clear lumen. At day 0, the secretory units of palatine glands consisted of immature acini and ducts sparsely distributed in the connective tissue, and no extending epithelial cord was observed. The nuclei were round in shape and flattened progressively with age. Gradually with maturation, the glands arranged into lobules, and the number and size of acini increased. Lectin histochemistry at the suckling stage showed that all lectins examined, except PNA, bound to the luminal border and showed generally

similar reaction patterns. The staining tended to be diffuse or reticular in the apical cytoplasm and apical membrane, as well as in the basolateral membrane of acini in newborns. Moreover, SBA and to a lesser extent PNA showed more positive reactions at supranuclear membranes. The staining by all lectins progressively increased to become moderately distributed. UEA reacted in a similar pattern but was more intense and diffuse, particularly in the acini located on the anterior area of the soft palate where the mother's nipple sits during suckling.

Palatine glands of newborns exhibited the same general overall appearance as those of the adult; therefore, unlike the parotid gland [37], and to a lesser extent the submandibular gland [38], no dramatic histological or morphological changes occurred during postnatal development. Lectin labeling in the newborn was located in the apical portion of the cytoplasm, with slight variation, and with maturation progressively increased and spread out basally corresponding with the progressive enlargement of the apical eosinophilic cytoplasm where secretory granules exist.

### ***15.2.3 Transitional Stage***

Sprague–Dawley rats aged PN 10–14 were used. In this stage, both suckling and feeding on solid food occur after eruption of teeth and before weaning. The histological sections showed enlargement of the glandular lobules, while the interlobular connective tissue was slightly reduced. Some acini had formed the tubuloacinar and a few scattered serous cells were observed. Histochemically, the distribution of lectin staining remained similar to that in the first week, although the extent of reactions was slightly increased and a granular pattern of staining was noticed in most acini. In addition to mucous cells, UEA showed high affinity to serous cells. sucWGA, however, rarely reacted to serous cells.

### ***15.2.4 Weaning Stage***

Sprague–Dawley rats aged PN 21–28 were used. Histological analysis showed that the general appearance of the gland remained unchanged at the weaning stage; however, the whole gland at 4 weeks appeared more compact, the eosinophilic cytoplasm of the mucous cells was enlarged and nuclei were further flattened and displaced basally. Serous acinar cells were observed along the soft palate, predominantly in the posterior part. Some were capped in the mucous acini and others were isolated. Lectin histochemistry at the third week showed heterogeneous staining among different animals; however, overall patterns similar to those of the preceding stage were seen for WGA, sucWGA, UEA and PNA. SBA, sucWGA and UEA-1 showed affinity to serous cells, and the reactivity of DBA and VVA was expanded to cover the basal region and supranuclear membrane of some acinar cells. Some cells exhibited a similar pattern to that found in the adult. At the fourth week, the

lectin staining patterns were mostly similar to those found in the adult, in which reactivity was extended basally from the apical cytoplasm along the lateral surface of acinar cells. DBA staining was strong, covering the entire cytoplasm. Staining for VVA, WGA and UEA was weaker but there was no significant difference between anterior and posterior regions. Surprisingly, the reactivity of PNA and sucWGA was reduced by more than one-third and focal, moderate cytoplasmic staining was observed more in the posterior glands. At the third week, strong, broad distribution of lectin binding was observed; in particular, PNA and sucWGA reached their peaks of reactivity. These additional mucous secretions might be required as a lubricant for both chewing and swallowing solid food and may provide a protective coating for the soft palate [39–41], and are thus consistent with forced weaning.

### **15.2.5 Adult Stage**

Sprague–Dawley rats aged PN 42 were used. The histological analysis of the adult stage showed that the thickness of the glandular layer was increased, but the thickness of the posterior portion was clearly smaller than the anterior oral one. Glands appeared more dilated, and the faint apical cytoplasm was enlarged and pressed the spindle-shaped nuclei against the basement membrane. Serous cells with round nuclei and basophilic cytoplasm were observed along the soft palate, mainly in the posterior portion, some of which were isolated while others were capped with mucous cells. Lectin histochemistry at the adult stage showed a dramatic heterogeneity of glycoproteins between the anterior and posterior portions. DBA, VVA and WGA showed high affinity to all mucous cells, but their staining patterns were more broadly and intensely distributed in the posterior portion. The reactivity of SBA, however, was located in the apical cytoplasm in the anterior portion and was more intense and broad in the posterior region. Furthermore, less than one-third of cells showed binding to PNA and sucWGA, most of which were located in the posterior portion. Finally, UEA-1 reacted strongly and was evenly distributed along the palatine gland.

This study showed that the 4th week was the appropriate time for weaning, when the histochemical distribution of lectins among mucous cells of palatine glands behaved mostly like that of the adult. Our study showed that the mucins secreted from the palatine gland changed in quality and quantity during growth. Moreover, in the adult stage, a spectacular heterogeneous distribution of glycoconjugates was observed in the soft palate between palatine glands located in the anterior and posterior portions; the posterior side was rich in N-acetylglucosamine and galactose compared with the anterior side as demonstrated by its positive reactivity with sucWGA and PNA, respectively. N-acetylgalactosamine was also more abundant in the posterior side as demonstrated by intense and broad distribution of DBA, VVA and SBA. Heterogeneous distribution of glycoconjugates within an organ has been previously described for the kidney of JDS mice; distal tubules showed binding to

DBA, whereas proximal tubules did not [22]. Also, in the human large bowel, UEA-1 bound to mucous goblet cells proximally but not distally [42]. Generally, glycoproteins secreted by mucous cells contain both O-linked oligosaccharides, which contribute to the protective physiochemical properties of the mucus coat, and N-linked oligosaccharides. In the present study, N-linked oligosaccharides, as indicated by mannose directed ConA lectin binding, were evenly distributed throughout the soft palate. However, dramatic distinguishable differences were revealed between anterior and posterior regions, where O-linked oligosaccharides were highly expressed in the latter as indicated by DBA, VVA, SBA and PNA staining [22]. An apocrine mechanism of secretion by mucous cells in the salivary gland has been excluded [43]; therefore, two reasons may be speculated to explain the abovementioned heterogeneity in the soft palate. First, the epithelium covering the soft palate has fewer layers in the posterior portion, and the thickness of the glandular layer of the palatine gland is obviously smaller, which strikingly correlated with presence of more abundant glycoproteins in that area. This suggests that palatine glands located in the posterior portion, as a functional compensation, produce expanded and elongated mucin by over-secretion of glycoproteins with O-linked oligosaccharides that change the physiochemical properties of the mucin by making it more viscous, with lower solubility and higher elasticity and adhesiveness. This in turn provides additional integrity to the soft palate mucosa from any mechanical or chemical injury [44, 45]. The second speculation is inspired from the suggestion that serous demilunar and central acinar cells might be the phenotype of a single secretory-cell type [46]. Accordingly, we observed that SBA, PNA and sucWGA sometimes reacted to serous cells in addition to mucous cells during the stages examined, while in the adult samples they showed higher affinity to serous cells of the von Ebner gland. Therefore, the more abundant serous cells in the posterior portion probably could have contributed to the production of glycoproteins and were subsequently expressed by lectin binding in the main acinar cells due to glycosylation continuation of demilunes to main mucous cells.

### 15.3 Conclusions

Lectin histochemistry has the ability of identifying oligosaccharide-specific residues in histological sections and delineating information about the structure of carbohydrate-rich macromolecules. The method is useful for the analysis of palatal gland development. The present observations revealed that glycoprotein distribution during palatine gland development varies with age. This variation in staining properties could be related to the maturation process in the secretory cycle of the palatine mucous glands. Moreover, the heterogeneous distribution of glycoconjugates between posterior and anterior glands, which is probably due to different functional demands, expands our understanding of the role of salivary glands in oral function. Further studies are needed to elaborate further physiochemical and rheological differences.

**Open Access** This chapter is distributed under the terms of the Creative Commons Attribution Noncommercial License, which permits any noncommercial use, distribution, and reproduction in any medium, provided the original author(s) and source are credited.

## References

1. Kitagawa K, Hayasaka S, Matsunou H, Nagaki Y. Presumed minor salivary gland secretion in a patient with a history of oral mucous membrane graft. *Am J Ophthalmol.* 2003;136(2):374–5.
2. Sivarajasingam V, Drummond JR. Measurements of human minor salivary gland secretions from different oral sites. *Arch Oral Biol.* 1995;40(8):723–9.
3. Hand AR, Pathmanathan D, Field RB. Morphological features of the minor salivary glands. *Arch Oral Biol.* 1999;44 Suppl 1:S3–S10.
4. Leeson CR, Leeson TS. Fine structure and possible secretory mechanism of rat palatine glands. *J Dent Res.* 1968;47(4):653–62.
5. Nakamura S, Takahashi S, Wakita M, Morita M. Postnatal growth of the rat palatine gland. *Tissue Cell.* 2001;33(6):614–20.
6. Srivastava HC, Vyas DC. Postnatal development of rat soft palate. *J Anat.* 1979;128 (Pt 1):97–105.
7. Nielsen G, Westergaard E. The development of the palatine glands in human foetuses with a crown-rump length of 32–145 mm. *Acta Odontol Scand.* 1971;29(2):231–50.
8. Shinzato K, Takahashi S, Wakita M, Morita M. Prenatal development of the palatine gland of rats. *Tissue Cell.* 2004;36(2):115–20.
9. Eliasson L, Carlen A. An update on minor salivary gland secretions. *Eur J Oral Sci.* 2010;118 (5):435–42.
10. Crawford JM, Taubman MA, Smith DJ. Minor salivary glands as a major source of secretory immunoglobulin A in the human oral cavity. *Science.* 1975;190(4220):1206–9.
11. Dawes C, Wood CM. The contribution of oral minor mucous gland secretions to the volume of whole saliva in man. *Arch Oral Biol.* 1973;18(3):337–42.
12. Buchner A, Merrell PW, Carpenter WM. Relative frequency of intra-oral minor salivary gland tumors: a study of 380 cases from northern California and comparison to reports from other parts of the world. *J Oral Pathol Med.* 2007;36(4):207–14.
13. Carrillo JF, Maldonado F, Carrillo LC, Ramirez-Ortega MC, Pizano JG, Melo C, et al. Prognostic factors in patients with minor salivary gland carcinoma of the oral cavity and oropharynx. *Head Neck.* 2011;33(10):1406–12.
14. Chiuwa H, Sakamoto K, Umeno H, Nakashima T, Suzuki G, Hayafuchi N. Minor salivary gland carcinomas of oral cavity and oropharynx. *J Laryngol Otol Suppl.* 2009;31:52–7.
15. Hyam DM, Veness MJ, Morgan GJ. Minor salivary gland carcinoma involving the oral cavity or oropharynx. *Aust Dent J.* 2004;49(1):16–9.
16. Kakarala K, Bhattacharyya N. Survival in oral cavity minor salivary gland carcinoma. *Otolaryngol Head Neck Surg.* 2010;143(1):122–6.
17. Lee SY, Shin HA, Rho KJ, Chung HJ, Kim SH, Choi EC. Characteristics, management of the neck, and oncological outcomes of malignant minor salivary gland tumours in the oral and sinonasal regions. *Br J Oral Maxillofac Surg.* 2013;51(7):e142–7.
18. Matsuzaki H, Yanagi Y, Hara M, Katase N, Asaumi J, Hisatomi M, et al. Minor salivary gland tumors in the oral cavity: diagnostic value of dynamic contrast-enhanced MRI. *Eur J Radiol.* 2012;81(10):2684–91.
19. Spiro RH. Salivary neoplasms: overview of a 35-year experience with 2,807 patients. *Head Neck Surg.* 1986;8(3):177–84.
20. Spiro RH, Thaler HT, Hicks WF, Kher UA, Huvos AH, Strong EW. The importance of clinical staging of minor salivary gland carcinoma. *Am J Surg.* 1991;162(4):330–6.

21. Rademacher TW, Parekh RB, Dwek RA. Glycobiology. *Annu Rev Biochem.* 1988;57:785–838.
22. Spicer SS, Schulte BA. Diversity of cell glycoconjugates shown histochemically: a perspective. *J Histochem Cytochem.* 1992;40(1):1–38.
23. Ferrari MC, Parini R, Di Rocco MD, Radetti G, Beck-Peccoz P, Persani L. Lectin analyses of glycoprotein hormones in patients with congenital disorders of glycosylation. *Eur J Endocrinol.* 2001;144(4):409–16.
24. Goodarzi MT, Turner GA. A lectin method for investigating the glycosylation of nanogram amounts of purified glycoprotein. *Glycoconj J.* 1997;14(4):493–6.
25. Hayes CA, Doohan R, Kirkley D, Leister K, Harhen B, Savage AV, et al. Cross validation of liquid chromatography-mass spectrometry and lectin array for monitoring glycosylation in fed-batch glycoprotein production. *Mol Biotechnol.* 2012;51(3):272–82.
26. Kottgen E, Hell B, Muller C, Tauber R. Demonstration of glycosylation variants of human fibrinogen, using the new technique of glycoprotein lectin immunosorbent assay (GLIA). *Biol Chem Hoppe Seyler.* 1988;369(10):1157–66.
27. Patwa TH, Zhao J, Anderson MA, Simeone DM, Lubman DM. Screening of glycosylation patterns in serum using natural glycoprotein microarrays and multi-lectin fluorescence detection. *Anal Chem.* 2006;78(18):6411–21.
28. Zhou Y, Lu K, Pfefferle S, Bertram S, Glowacka I, Drosten C, et al. A single asparagine-linked glycosylation site of the severe acute respiratory syndrome coronavirus spike glycoprotein facilitates inhibition by mannose-binding lectin through multiple mechanisms. *J Virol.* 2010;84(17):8753–64.
29. Okamoto K, Takada K, Ikeda R, Aiyama S. Changes in the properties of secretory granules in the palatine gland acinar cells of the postnatally developing rat. *Okajimas Folia Anat Jpn.* 2008;85(2):49–56.
30. Green DR, Embrey G. Isolation, chemical and biological characterization of sulphated glycoproteins synthesized by rat buccal and palatal minor salivary glands in vivo and in vitro. *Arch Oral Biol.* 1987;32(6):391–9.
31. Samar ME, Avila RE, De Fabro SP, Porfirio V, Esteban FJ, Pedrosa JA, et al. Histochemical study of magellanic penguin (*Spheniscus magellanicus*) minor salivary glands during postnatal growth. *Anat Rec.* 1999;254(2):298–306.
32. Samar ME, Avila RE, Esteban FJ, Olmedo L, Dettin L, Massone A, et al. Histochemical and ultrastructural study of the chicken salivary palatine glands. *Acta Histochem.* 2002;104(2):199–207.
33. Hakami Z, Kitaura H, Honma S, Wakisaka S, Takano-Yamamoto T. Lectin histochemistry of palatine glands in the developing rat. *Acta Histochemica.* 2014;116(4):596–605.
34. Monsigny M, Roche AC, Sene C, Maget-Dana R, Delmotte F. Sugar-lectin interactions: how does wheat-germ agglutinin bind sialoglycoconjugates? *FEBS.* 1980;104(1):147–53.
35. Adi MM, Chisholm DM, Waterhouse JP. Histochemical study of lectin binding in the human fetal minor salivary glands. *J Oral Pathol Med.* 1995;24(3):130–5.
36. Sato M, Yonezawa S, Uehara H, Arita Y, Sato E, Muramatsu T. Differential distribution of receptors for two fucose-binding lectins in embryos and adult tissues of the mouse. *Differentiation.* 1986;30(3):211–9.
37. Redman RS, Sreebny LM. Morphologic and biochemical observations on the development of the rat parotid gland. *Dev Biol.* 1971;25(2):248–79.
38. Jacoby F, Leeson CR. The postnatal development of the rat submaxillary gland. *J Anat.* 1959;93(2):201–16.
39. Tabak LA. In defense of the oral cavity: structure, biosynthesis, and function of salivary mucins. *Annu Rev Physiol.* 1995;57:547–64.
40. Klein PB, Weilemann WA, Schroeder HE. Structure of the soft palate and composition of the oral mucous membrane in monkeys. *Anat Embryol.* 1979;156(2):197–215.
41. Lambert R, Pansu D, Berard A, Vitani C, Dechelette MA. Histochemical studies on human mucous secreting glands in the soft palate, uvula and esophagus. *Digestion.* 1973;8(2):110–9.

42. Yonezawa S, Nakamura T, Tanaka S, Sato E. Glycoconjugate with *Ulex europaeus* agglutinin-I-binding sites in normal mucosa, adenoma, and carcinoma of the human large bowel. *J Natl Cancer Inst.* 1982;69(4):777–85.
43. Tandler B. Structure of mucous cells in salivary glands. *Microsc Res Tech.* 1993;26(1):49–56.
44. Tabak LA, Levine MJ, Mandel ID, Ellison SA. Role of salivary mucins in the protection of the oral cavity. *J Oral Pathol.* 1982;11(1):1–17.
45. Amerongen AV, Bolscher JG, Veerman EC. Salivary mucins: protective functions in relation to their diversity. *Glycobiology.* 1995;5(8):733–40.
46. Triantafyllou A, Fletcher D, Scott J. Glycosylations in demilunar and central acinar cells of the submandibular salivary gland of ferret investigated by lectin histochemistry. *Arch Oral Biol.* 2004;49(9):697–703.

## Chapter 16

# The Role of NFIC in Regulating Odontoblastic Differentiation of Human Molar Stem Cells from Apical Papilla

Yuming Zhao, Shuo Gao, and Lihong Ge

**Abstract Objective:** The objective of this study was to investigate the regulating role of NFIC in odontoblastic differentiation of human stem cells from apical papilla (hSCAPs).

**Materials and methods:** The expression of NFIC in young permanent tooth was observed by immunohistochemical (IHC) staining and its expression levels both in young and mature permanent teeth were detected by western blot. hSCAPs were transplanted into the dorsum of immunocompromised mice, and immunohistochemical analysis was performed after 8 weeks. Real-time polymerase chain reaction and western blot were used to explore the expression pattern of NFIC and other odontogenic related genes during *in vitro* hSCAPs osteogenic differentiation.

**Results:** During molar root formation, NFIC expression was restricted within the odontoblasts and preodontoblasts of human molars. The expression of NFIC in apical papilla was at a very low level, and the amounts of NFIC protein in coronal pulp were more than that in root pulp in both young and mature permanent teeth. Odontoblast-like cells were positive to NFIC immunohistochemistry staining in dentin-pulp complexes formed after hSCAPs transplantation. NFIC expression was concomitant to dentin sialoprotein (DSP) at early stage of osteogenic differentiation of hSCAPs.

**Conclusion:** Our results suggest that NFIC is involved in the regulation of hSCAPs differentiation into odontoblasts during root development of the young permanent teeth and could be used as an early marker of odontoblast differentiation.

**Keywords** Dentin sialoprotein • Differentiation • NFIC • Odontoblast • Stem cells from apical papilla

---

Y. Zhao • S. Gao • L. Ge (✉)

Department of Pediatric Dentistry, Peking University Hospital and School of Stomatology,  
22 Zhongguancun Nandajie, Haidian District, Beijing 100081, China  
e-mail: [gelh0919@126.com](mailto:gelh0919@126.com)

## 16.1 Introduction

The formation of a dental root is the result of the interaction between the epithelial root sheath, dental papilla and dental follicle. Dental ectomesenchymal cells from the dental papilla differentiate into odontoblasts to produce a dentin layer that forms the bulk of the tooth. However, the molecular mechanisms underlying ectomesenchymal cells differentiation into odontoblast are not well understood.

The nuclear factor I (NFI) family of transcription-replication factors [1] encodes four members (*Nfia*, *Nfib*, *Nfic*, *Nfix*) in mammals, which are expressed in almost every tissue and organ [2]. However, mice with disruptions in each of the *NFI* genes have been found to display distinct phenotypes and developmental defects primarily in the nervous system (*Nfia*) [3], lung and brain (*Nfib*) [4, 5], and brain and skeleton (*Nfix*) [6], indicating different functions for each NFI subtype. Specifically, loss of *Nfic* is the first mouse mutation to affect the development of dental roots. Studies have demonstrated that *Nfic* null mice exhibit abnormal roots of molar teeth containing aberrant odontoblasts and abnormal formation of dentin, but normal crowns. NFIC should be necessary for root development [7–10]. However, the mechanism by which disruption of the *Nfic* gene leads to abnormal root formation remains unclear. Also, the relationship between NFIC and the formation of human dental roots has not been reported.

In present study, we focused on the root development of human molars and the differentiation of stem cells from the apical papilla (SCAPs). We sought to determine NFIC expression in young permanent human teeth and in the mineralization of human SCAPs.

## 16.2 Materials and Methods

### 16.2.1 Ethical Approval of the Study Protocol and Acquisition of Samples

The procedure to obtain healthy extracted teeth was approved by the Ethical Committee of the Health Science Center of Peking University (Beijing, China) (IRB00001052-11060). Patients provided written informed consent. Normal human impacted third molars with an open apical foramen and closed apical foramen were collected at a clinic in Peking University School and Hospital of Stomatology. The study protocol of animal experimentation was approved by the Animal Ethics Committee of Peking University (LA2012-58).

### ***16.2.2 Cell Culture and Induction of Mineralization***

Apical papilla tissues separated gently from the end of human teeth were digested in a solution of 3 mg/mL collagenase type I (Sigma-Aldrich, USA) and 4 mg/mL dispase (Sigma-Aldrich) for 1 h at 37 °C. Cultures were maintained in  $\alpha$ -modified Eagle's minimum essential medium ( $\alpha$ -MEM; Gibco, USA) supplemented with 10 % fetal bovine serum (FBS; Hyclone, USA) in 5 % carbon dioxide at 37 °C. The cells used were at passages 1–4.

Seventy to eighty percent confluent hSCAPs were cultured in differentiation medium supplemented with 10 % FBS, 10 mmol/L  $\beta$ -glycerolphosphate, 50 mg/mL ascorbate phosphate, 10 nmol/L dexamethasone, and 10 nmol/L 1,25-dihydroxyvitamin D3 for 3 weeks. Cultures were fixed in 4 % paraformaldehyde. Calcium deposition of the extracellular matrix was evaluated by staining with 1 % alizarin red-S (Sigma-Aldrich).

### ***16.2.3 Transplantation***

Approximately  $2.0 \times 10^6$  in vitro-expanded hSCAPs mixed with 40 mg hydroxyapatite ceramic particles (Bio Osteon, China) were transplanted subcutaneously into the dorsal surfaces of 10-week-old immunodeficient mice (CB-17/SCID; Vitalriver, China) according to a method reported previously [11]. Transplants were harvested 8 weeks after transplantation.

### ***16.2.4 Immunohistochemical Staining and Immunocytochemistry***

Samples were fixed in 4 % paraformaldehyde, then decalcified in 10 % EDTA and processed for embedding in paraffin. Immunohistochemical staining was undertaken on 4  $\mu$ m-thick tissue sections, which were deparaffinized and subsequently hydrated to water, then quenched endogenous peroxidase activity. Sections were incubated with anti-NFIC primary antibody (1:400 dilution. Abcam, UK), following by consecutive incubations with a Polymer Detection System for IHC Staining kit (Zhongshan Golden Bridge Biotechnology, China). Subsequently, sections were visualized with a 3,3'-diaminobenzidine tetrahydrochloride substrate kit (Zhongshan Golden Bridge Biotechnology). The same passage of hSCAPs grown to 80 % confluence on slides were immunocytochemically stained as described above.

**Table 16.1** Real-time PCR primer sequences

Gene symbol	Primer sequence
<i>GAPDH</i>	<i>Forward 5'-GGAGCGAGATCCCTCCAAAAT-3'</i> <i>Reverse 5'-GGCTGTTGTCATACTTCTCATGG-3'</i>
<i>NFIC</i>	<i>Forward 5'-ACCTGGCATA CGACCTGAAC-3'</i> <i>Reverse 5'-TCCATCGAGCCCCGATTGTG-3'</i>
<i>DMP1</i>	<i>Forward 5'-CACTCAAGATT CAGGTGGCAG-3'</i> <i>Reverse 5'-TCTGAGAT GCGAGACT CCTAAA-3'</i>
<i>ALP</i>	<i>Forward 5'-ATGGGATGGGTGTCTCCACA-3'</i> <i>Reverse 5'-CCACGAAGGGGAAC TTGTC-3'</i>
<i>OCN</i>	<i>Forward 5'-CACTCCTCGCCCTATTGGC-3'</i> <i>Reverse 5'-CCCTCCTGCTGGACACAAAG-3'</i>
<i>COLLA1</i>	<i>Forward 5'-GTGCGATGACGTGATCTGTGA-3'</i> <i>Reverse 5'-CGGTGGTTCTTGGTCGGT-3'</i>

### 16.2.5 RT-PCR Analysis

Tissues and cells were harvested and total RNA was isolated using TRIzol reagent (Invitrogen), according to the manufacturer's protocol. Isolated RNA was purified by removing genomic DNA with a DNase I, RNase-free kit (Fermentas, Glen Burnie, MD, USA). One microgram of total RNA from each group was used for synthesis of cDNA using the AMV Reverse Transcriptase kit (Fermentas), according to the manufacturer's protocol. Semiquantitative real-time PCR was performed using the ABI Prism 7000 Sequence Detection System (Applied Biosystems, Carlsbad, CA, USA) with SYBR Green (Roche). All samples were run in triplicate in 96-well plates, with each well containing 1.0 µL of cDNA diluted 1 in 20 to give a total reaction volume of 20 µL. Reactions were performed at 50 °C for 2 min and then at 95 °C for 10 min, followed by 40 cycles of 15 s at 95 °C and 1 min at 60 °C. Primers were designed (Table 16.1). For data analysis, the levels of target gene expression in samples relative to the level of expression in the control samples were calculated using the comparative cycle threshold method ( $\Delta\Delta CT$ ). The expression levels of target gene expression were normalized to the expression of the reference gene GAPDH.

### 16.2.6 Western Blotting

The expression level of NFIC and DSP proteins were measured by western blot. Total protein was extracted from tissues and cells using radioimmunoprecipitation assay (RIPA) lysis buffer containing a protease inhibitor cocktail (Applygen, Beijing, China), according to the manufacturer's instructions. Protein levels were calculated using a bicinchoninic acid (BCA) protein assay kit (Thermo Scientific,

Beijing, China). Equal amounts of protein samples were separated by electrophoresis through a 12 % SDS polyacrylamide gel and transferred onto polyvinylidene difluoride (PVDF) membranes (Millipore, Billerica, MA, USA). Blots were blocked with 5 % skim milk, followed by incubation with the following primary antibodies: mouse anti-NFIC (Abcam, Cambridge, UK), goat anti-DSP (Santa Cruz Biotechnology, CA), and mouse anti-GAPDH (Abmart, Shanghai, China). Blots were then incubated with goat anti-mouse or anti-goat secondary antibodies conjugated to horseradish peroxidase (Origene, Beijing, China) and visualized by enhanced chemiluminescence (Applygen).

## 16.3 Results

### 16.3.1 NFIC Expression in Tooth Tissue

To determine the expression pattern of NFIC during molar root formation, we conducted immunohistochemical staining for human molar root. NFIC expression was restricted within odontoblasts and preodontoblasts of the developing root (Fig. 16.1).

In order to quantify NFIC expression in different parts of human dental pulp, the coronal pulp, root pulp and apical papilla of young permanent teeth, as well as crown pulp and root pulp of mature permanent teeth were isolated and western blot was performed. The results showed that NFIC expressed in apical papilla at a very low level, and the amounts of NFIC protein in coronal pulp were more than that in root pulp in both young and mature permanent teeth. The expression of NFIC in coronal pulp of young permanent teeth was extremely strong (Fig. 16.2).

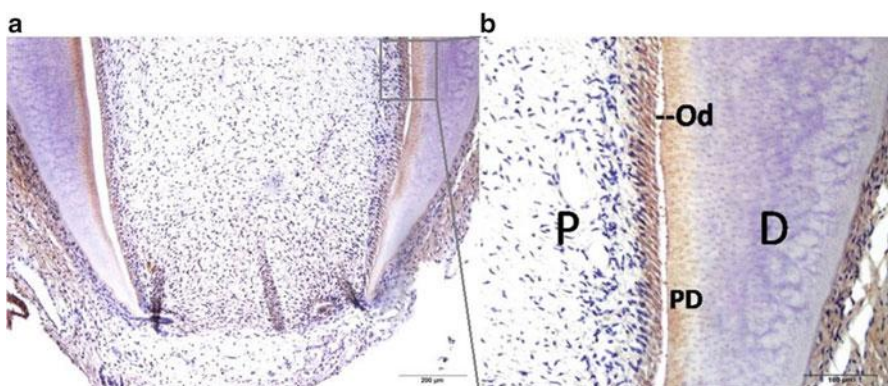


**Fig. 16.1** Immunohistochemistry shows NFIC expression in developing root of a human third molar (a). Figure (b) is a higher magnification of the boxed region of Fig (b). D dentin, Od odontoblasts, PD predentin, P pulp

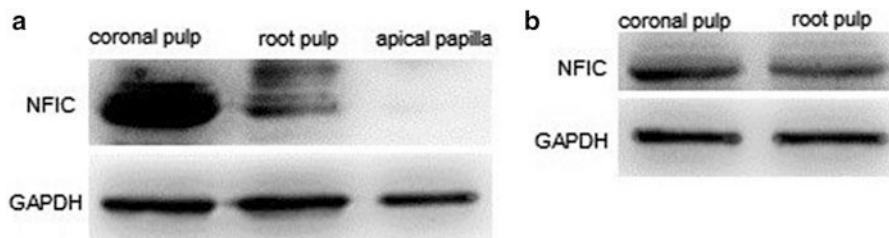


**Fig. 16.2** Quantification of NFIC expression in coronal pulp, root pulp and apical papilla by western blot. (a) Young permanent teeth. (b) Mature permanent teeth

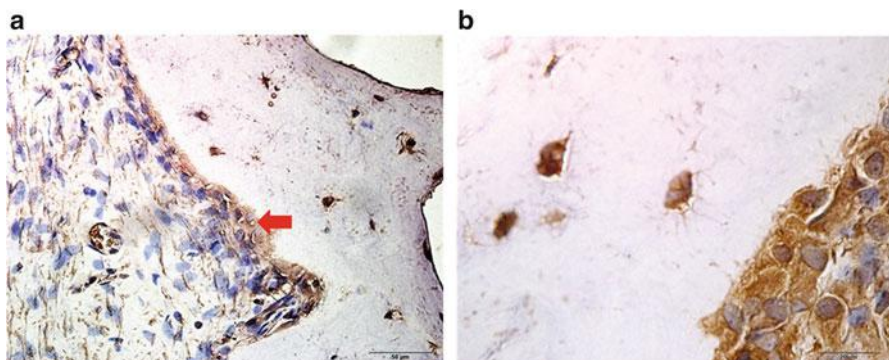


**Fig. 16.3** Immunohistochemical straining of NFIC in dentin-pulp complex ex vivo at 8 weeks after hSCAPs transplantation into the dorsum of immunocompromised mice (brown indicated positive staining). (a) The dentin-like structure (d) surfaces are lined with a layer of odontoblast-like cells (od), surrounding pulp-like tissue with blood vessels (bv). (b) Odontoblast-like cells displayed protruding cytoplasmic processes into the dentinal matrix

### 16.3.2 NFIC Expression in hSCAPs Transplantation

To study the expression of NFIC during odontoblast differentiation *in vivo*, the hSCAPs with hydroxyapatite carrier were transplanted into immunocompromised mice. Eight weeks after transplantation, the hSCAPs generated dentin-like structures. The odontoblast-like cells lined a layer along the surface of dentin-like structures and displayed protruding cytoplasmic processes into the dentinal matrix, which interfaced with a pulp-like interstitial tissue infiltrated with blood vessels. Odontoblast-like cells were positive to NFIC immunohistochemistry straining in dentin-pulp complex formed *ex vivo* (Fig. 16.3).

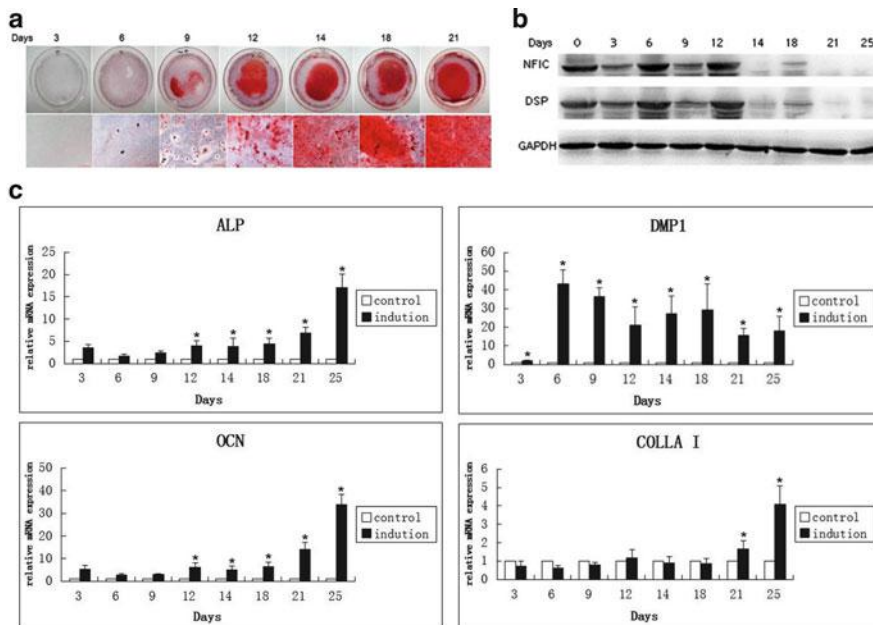


**Fig. 16.4** Osteogenic differentiation of hSCAPs. **(a)** Alizarin red-S staining showed mineralized nodule formation from days 6 to 21 after the induction of differentiation. **(b)** The expression of NFIC and DSP were evaluated by western blot analysis. **(c)** The expression of *ALP*, *OCN*, *COLLA I* and *DMP1* were evaluated by real-time PCR. \*P < 0.05. GAPDH used as a loading control

### 16.3.3 The Expression of NFIC and Odontogenic Related Genes During Osteogenic Differentiation of hSCAPs

During tooth development, SCAPs differentiate into odontoblasts and form root dentin. In order to determine how the related genes express when hSCAPs differentiate in vitro and gain insight into the mechanism of differentiation, the cells were cultured in mineralization medium for up to 3 weeks and the expression of odontoblast differentiation markers were analyzed by western blot and real-time polymerase chain reaction (PCR). The formation of mineralized nodules was evaluated by alizarin red-S staining.

Alizarin red-S staining revealed the presence of small, round mineralized nodules from days 6 to 21 after the induction of differentiation (Fig. 16.4a). Expression of NFIC increased from days 6 to 12 then decreased at day 14, and the expression of dentin sialoprotein (DSP) showed similar pattern as NFIC by western blot (Fig. 16.4b). The results of our real-time PCR analysis revealed that the expression levels of ALP, OCN increased significantly from days 12 and continued to increase through day 25. The expression of DMP-1 increased significantly at day 6 and kept at high level throughout the process, while the expression level of COLLA I increased significantly after days 21 (Fig. 16.4c).

## 16.4 Discussion

Previous studies showed that disruption of *Nfic* caused major defects in postnatal murine tooth development, the most striking defect being loss of molar root formation. It is generally believed that NFIC is one of the molecules known to be required for root formation—the key late event in tooth morphogenesis [12–14]. However most studies obtained conclusions based on experiments with other non-molar root tissues (such as jaw, incisor) or cell lines of mice [11]. In order to further explore the function of *Nfic* on root development, we use human young molar stem cells from apical papilla (SCAPs) as our research objectives, which can differentiate into the odontoblasts located in root portion to generate root dentin.

In this study, we found that NFIC *in situ* expression in tooth tissues showed interesting pattern. NFIC expression appeared most strongly within the odontoblasts and preodontoblasts though can be seen in a wide range of tissues, including ameloblasts, periodontal ligament and weakly in the pulp. Moreover the level of NFIC protein in coronal pulp was higher than in root pulp. However it is well known that the main tooth defect of *Nfic* null mice existed not in the crown but in abnormal roots of molar teeth. Therefore, we speculate that developmental mechanism maybe different between root and crown in human molar, and NFIC is probably essential for root development even though it is not the site of the highest NFIC expression. Moreover, it was predicted that osteodentin formation during dentin repair may be the result of pulp cells that do not express *Nfic* gene, given the morphological similarities of repair dentin with the abnormal roots dentin found in *Nfic*-deficient mice [13]. Thus, we proposed that primary dentin and secondary or reparative dentin may have different formational mechanisms.

To study the expression of NFIC during odontoblast differentiation *ex vivo*, hSCAPs with hydroxyapatite carriers were transplanted into immunocompromised mice. After eight weeks the hSCAPs generated dentin-like structures. Odontoblast-like cells aligned in a layer along the surface of dentin-like structures were positive to NFIC immunohistochemical staining, which conceivably imply that NFIC participates in the hSCAPs differentiation *ex vivo* and the generation of osteodentin. It's well established that HERS regulates the formation of organized root dentin through epithelial-mesenchymal interactions. The absence of HERS during the formation of dentin-like structures would cause odontoblast progenitor cells to form osteodentin without organized dentinal tubules, that resembled repair dentin [15]. The mechanisms behind the osteodentin formation and odontoblast-like cells differentiation remain uncertain. In summary, NFIC may work in the common molecular regulation mechanism sharing by the development and repair of dentin. Further research will be required to identify these different pathways at various stages of dentin formation and the relationship between the expression and function of NFIC.

It has previously been reported that *Nfic*-deficient mice showed abnormal odontoblasts with a round shape, no odontoblastic processes and no polarity [16] and the ectomesenchymal cells (EM) near the abnormal root showed no expression

of DSPP mRNA [13]. The odontoblasts of mice incisors exhibited a decreased level of DSP expression that is a product of DSPP-a dentin-specific gene. In the present study, NFIC and DSP had consistent expression pattern, both increased at early stage of hSCAPs osteogenic differentiation, and decreased at late stage. While the expression of osteogenic differentiation markers Alp, OCN and the main component of the dentin collagenous protein framework COLLA I, were gradually increased during later period of differentiation. The marker gene of odontoblast differentiation DMP-1 showed sustained high expression. Based on these findings, we suggest that NFIC and DSPP are likely to have a more compact expression and functional relationship, and NFIC may be another dentin-specific marker during human odontoblast differentiation.

In conclusion, NFIC expression was restricted to the odontoblasts, pre-odontoblasts and predentin of human molars. NFIC is involved in the regulation of hSCAPs differentiation into odontoblasts during root development of the young permanent teeth in a stage- and tissue-specific manner and could be regarded as an early marker of odontoblast differentiation.

**Open Access** This chapter is distributed under the terms of the Creative Commons Attribution Noncommercial License, which permits any noncommercial use, distribution, and reproduction in any medium, provided the original author(s) and source are credited.

## References

1. Nagata K, Guggenheim RA, Enomoto T, et al. Adenovirus DNA replication in vitro identification of a host factor that stimulates synthesis of the preterial protein-dCMP complex. *Proc Natl Acad Sci.* 1982;79(21):6438–42.
2. Gronostajski RM. Roles of the NFI/CTF gene family in transcription and development. *Gene.* 2000;249:31–45.
3. Shu T, Butz KG, Plachez C, Gronostajski RM, Richards LJ. Abnormal development of forebrain midline glia and commissural projections in Nfia knock-out mice. *J Neurosci.* 2003;23:203–12.
4. Steele-Perkins G, Plachez C, Butz KG, Yang G, Bachurski CJ, et al. The transcription factor gene Nfib is essential for both lung maturation and brain development. *Mol Cell Biol.* 2005;25:685–98.
5. Grunder A, Ebel TT, Mallo M, Schwarzkopf G, Shimizu T, et al. Nuclear factor I-B (Nfib) deficient mice have severe lung hypoplasia. *Mech Dev.* 2002;112:69–77.
6. Driller K, Pagenstecher A, Uhl M, Omran H, Berlis A, et al. Nuclear factor I X deficiency causes brain malformation and severe skeletal defects. *Mol Cell Biol.* 2007;27:3855–67.
7. Steele-Perkins G, Butz KG, Lyons GE, et al. Essential role for NFI-C/CTF transcription replication factor in tooth root development. *Mol Cell Biol.* 2003;23(3):1075–84.
8. Xing X, Deng Z, Yang F, et al. Determination of genes involved in the early process of molar root development initiation in rat by modified subtractive hybridization. *Biochem Biophys Res Commun.* 2007;363(4):994–1000.
9. Deryck R, Chen RH, Ebner R, Filvaroff EH, Lawler S. An emerging complexity of receptors for transforming growth factor-beta. *Princess Takamatsu Symp.* 1994;24:264–75.
10. Massague J. How cells read TGF- $\beta$  signals. *Nat Rev Mol Cell Biol.* 2000;1:169–78.

11. Lee DS, Yoon WJ, Cho ES, Kim HJ, Gronostajski RM, Cho MI, Park JC. Crosstalk between nuclear factor I-C and transforming growth factor- $\beta$ 1 signaling regulates odontoblast differentiation and homeostasis. *PLoS One*. 2011;6(12):e29160.
12. Lee DS, Park JT, Kim HM, et al. Nuclear factor I-C is essential for odontogenic cell proliferation and odontoblasted differentiation during tooth root development. *J Biol Chem*. 2009;254(25):17293–303.
13. Park JC, Herr Y, Kim HJ, et al. Nfic gene disruption inhibits differentiation of odontoblasts responsible for root formation and results in formation of short and abnormal roots in mice. *J Periodontol*. 2007;78(9):1795–802.
14. Kim MY, Reyna J, Chen LS, Zeichner-David M. Role of the transcription factor NFIC in odontoblast gene expression. *J Calif Dent Assoc*. 2009;37(12):875–81.
15. Xu L, Tang L, Jin F, et al. The apical region of developing tooth root constitutes a complex and maintains the ability to generate root and periodontium-like tissues. *J Periodontal Res*. 2009;44:275–82.
16. Lee TY, Lee DS, Kim HM. Disruption of Nfic causes dissociation of odontoblasts by interfering with the formation of intercellular junctions and aberrant odontoblast differentiation. *J Histochem Cytochem*. 2009;57(5):469–76.

# Chapter 17

## Microbicidal Activity of Artificially Generated Hydroxyl Radicals

Hong Sheng, Keisuke Nakamura, Taro Kanno, Keiichi Sasaki,  
and Yoshimi Niwano

**Abstract** The hydroxyl radical, one of the reactive oxygen species, has one unpaired electron in the structure, so that it tends to deprive other substances of an electron which is so-called oxidation. It is known that hydroxyl radicals produced by immunological response kill invading microorganisms by the oxidation. Besides the immune system, it has been demonstrated that hydroxyl radicals play an important role in the bactericidal action of antibiotics. In this context, we have conducted a research to develop disinfection techniques utilizing artificially generated hydroxyl radicals. We adopted photolysis of  $\text{H}_2\text{O}_2$ , sonolysis of water and the other photo-chemical reaction as generators of hydroxyl radicals. A series of studies demonstrated that the microbicidal activity of hydroxyl radicals was sufficient to kill bacteria in an experimental biofilm as well as planktonic bacteria and fungi within a short-treatment time. In addition, the safety aspect is confirmed by an *in vivo* study and a literature review. Thus, it is suggested that disinfection treatment utilizing artificially generated hydroxyl radicals can be applicable to medical/dental therapy as novel disinfection treatments.

**Keywords** Antimicrobial activity •  $\text{H}_2\text{O}_2$  • Hydroxyl radicals • Oxidation • Photolysis • Sonolysis

---

H. Sheng • K. Sasaki

Division of Advanced Prosthetic Dentistry, Tohoku University Graduate School of Dentistry,  
Seiryo-machi 4-1, Aoba-ku, Sendai 980-8575, Japan

K. Nakamura (✉) • Y. Niwano

Laboratory for Redox Regulation, Tohoku University Graduate School of Dentistry,  
Seiryo-machi 4-1, Aoba-ku, Sendai 980-8575, Japan  
e-mail: [keisuke@m.tohoku.ac.jp](mailto:keisuke@m.tohoku.ac.jp)

T. Kanno

Division of Molecular and Regenerative Prosthodontics, Tohoku University  
Graduate School of Dentistry, Seiryo-machi 4-1, Aoba-ku, Sendai 980-8575, Japan

## 17.1 Introduction

Dental caries and periodontitis, two major dental diseases, are infectious diseases caused by pathogenic bacteria found in dental plaque [1, 2]. Thus, effective removal of the dental plaque (i.e. bacterial biofilm) and maintaining oral hygiene are the keys in prevention and treatment. In dental practice, mechanical removal of dental plaque from the lesion site is the primary treatment modality because the effect of chemical disinfection is rather weak against biofilm in which bacteria are protected from such chemicals by a matrix [3, 4]. However, it is sometimes difficult to mechanically remove the dental plaque properly at narrow or anatomically complex lesion sites in oral cavity. Thus, an adjunctive treatment with antiseptics as well as local and systemic antimicrobial chemotherapy is performed in some cases. However, these treatments possess a risk of adverse effect caused by e.g. leakage of chemical solution and induction of bacterial drug resistance [5, 6]. Therefore, it is expected to develop a novel disinfection treatment which can be used in combination with conventional mechanical treatment with minimum adverse effect.

Application of antibiotics and antiseptics to the treatment and the prevention of dental infectious diseases has been studied. For example, it has been reported that systemic administration of metronidazole and amoxicillin together with scaling and root planing (SRP) improves the periodontal condition than SRP alone [7, 8]. However, the systemic administration of antibiotics is limited to a treatment of severe periodontitis because of the risk of adverse effect. Local application of antibiotics known as local drug delivery system (LDDS) has also been studied to treat periodontitis. The antibiotics in the form of gel, such as doxycycline and minocycline, are delivered to periodontal pockets after SRP. However, since there is a contradiction in the clinical benefit of LDDS [9–13], the clinical application is also limited to specific cases.

Besides the antibiotics, antiseptics have also been studied for periodontal therapy. For instance, mouthrinse with chlorhexidine (CHX) is a most widely studied as an adjunctive treatment for periodontitis [14]. It has been reported that CHX can effectively prevent plaque accumulation [15]. However, repeated use of CHX results in the discoloration of the teeth as well as the tongue, and in the taste perturbation [16, 17]. Thus, mouthrinse with CHX is limited to the case where meticulous plaque control is required, such as plaque control during treatment of severe periodontitis or after periodontal surgery [18]. Accordingly, although CHX has been proven effective as a preventive agent, it has not been recommended as a therapeutic agent in periodontal therapy [14]. The other example of disinfectant used as a mouthrinse is hydrogen peroxide ( $H_2O_2$ ) which is widely used as a disinfectant for skin wound at a concentration of  $\leq 3\%$ . Based on the clinical studies, mouthrinse with  $H_2O_2$  apparently prevents plaque accumulation [19–21] though its plaque prevention effect is weaker than that of CHX [22]. Thus, mouthrinse with  $H_2O_2$  is rarely used in dental therapy.

Photodynamic therapy (PDT), a newly developed chemical disinfection treatment, has been applied to the treatment of periodontitis over the last decade

[23]. The PDT consists of light, oxygen and a photosensitizer. Once the photosensitizer is irradiated with light of a specific wavelength, it absorbs photons and transfers the excitation energy to molecular oxygen which is in turn metamorphosed to its diamagnetic form, singlet oxygen [24]. Since singlet oxygen is unstable and has high reactivity, it oxidizes bacterial cell components resulting in cell death [23, 25]. The advantage of PDT is that it exerts bactericidal activity only when a photosensitizer is irradiated with light. Without irradiation, photosensitizer does not exert cytotoxic effect, indicating that residual toxicity after the treatment is negligible. Furthermore, it is suggested that the PDT does not induce bacterial resistance because singlet oxygen oxidize bacterial cell components non-selectively [26, 27]. This is a major advantage in comparison with antibiotics. Based on the bactericidal activity of PDT demonstrated by in vitro studies [28–31], the therapeutic effect of PDT following SRP has been studied expecting an additional effect. However, the clinical results are controversial between the studies [32–35]. Thus, clinical benefit of using PDT as an adjunctive treatment in periodontal therapy is still unclear.

To solve the problems of chemical disinfection treatment, novel disinfection treatment techniques in which artificially generated hydroxyl radicals kill bacteria have been developed in our laboratory. Our recent study demonstrated that hydroxyl radicals would not induce bacterial resistance as singlet oxygen does not [36]. In addition, hydroxyl radicals have higher oxidation power than singlet oxygen [25], resulting in higher antimicrobial activity. In this chapter, the generation systems of hydroxyl radicals and their microbicidal activity are discussed based on our recent works.

## 17.2 Application of Hydroxyl Radicals to Disinfection Treatment

The hydroxyl radical is one of the reactive oxygen species (ROS). Since the hydroxyl radical has one unpaired electron in the structure, it tends to deprive other substances of an electron which is so-called oxidation [37]. It is well-known that hydroxyl radicals are involved in various biochemical reactions, and hydroxyl radical-induced oxidative damage on cells and tissues leads to specific diseases if hydroxyl radicals are generated chronically [38, 39]. On the other hand, the cytotoxic effect of hydroxyl radicals is also used in a positive way. For instance, hydroxyl radicals are produced by immunological response to kill invading microorganisms [40, 41]. Besides the immune system, it has been demonstrated that ROS, especially hydroxyl radicals would play an important role in the mechanism of bacterial cell death induced by antibiotics via the reaction with primary target followed by Fenton like reaction [42, 43]. In this context, we have conducted research to develop novel disinfection techniques utilizing artificially generated hydroxyl radicals.

**Table 17.1** Hydroxyl radical generation systems [37]

One-electron reduction of H <sub>2</sub> O <sub>2</sub>	
Fenton reaction	Fe <sup>2+</sup> + H <sub>2</sub> O <sub>2</sub> → Fe <sup>3+</sup> + ·OH + OH <sup>-</sup>
Harber–Weiss reaction	O <sub>2</sub> <sup>·-</sup> + H <sub>2</sub> O <sub>2</sub> → (metal catalyst) → O <sub>2</sub> + ·OH + OH <sup>-</sup>
Reaction with semiquinone	tetrachlorosemiquinone + H <sub>2</sub> O <sub>2</sub> → tetrachloroquinone + ·OH + OH <sup>-</sup>
Homolytic fission	
Radiolysis of water	H <sub>2</sub> O + γ-ray → H + ·OH
Photolysis of H <sub>2</sub> O <sub>2</sub>	H <sub>2</sub> O <sub>2</sub> + UV → 2·OH
Sonolysis of water	H <sub>2</sub> O + ultrasound → H + ·OH

·OH hydroxyl radical, O<sub>2</sub><sup>·-</sup> superoxide anion radical, UV ultraviolet light

The key for the use of hydroxyl radicals as a disinfectant *in vivo* is to control the yield and the exposure time. Otherwise hydroxyl radicals will kill not only bacteria but also normal cells causing adverse reactions to the body. These factors are largely dependent on the generation systems of hydroxyl radicals. Hydroxyl radicals are generated basically by either one-electron reduction of H<sub>2</sub>O<sub>2</sub> or homolytic fission of chemical bond [37]. Representative examples are summarized in Table 17.1.

To control the yield of hydroxyl radicals, the reaction of hydroxyl radical generation system should be terminated appropriately when necessary. From this viewpoint, reaction involving homolytic fission is advantageous because the reaction can be terminated by cessation of irradiation of γ-ray, ultraviolet light or ultrasound. Since hydroxyl radicals have a very short lifetime (approximately 10<sup>-9</sup> s) [44, 45, 25], residual toxicity would be negligible after the termination of reaction. On the other hand, it might be difficult to control the reaction of one-electron reduction of H<sub>2</sub>O<sub>2</sub> during the disinfection treatment. The chemicals involved in the reaction of homolytic fission are basically safe because they are only H<sub>2</sub>O and H<sub>2</sub>O<sub>2</sub>. Indeed, a subcommittee of the US Food and Drug Administration concluded that H<sub>2</sub>O<sub>2</sub> as a disinfectant is safe at concentrations of up to 3 % [46]. Although H<sub>2</sub>O<sub>2</sub> is also one of ROS, it is expected that hydroxyl radicals can kill bacteria more effectively than H<sub>2</sub>O<sub>2</sub> because hydroxyl radicals have much higher reactivity and oxidative power [47]. Considering the safety aspect of reaction energy, exposure of normal tissue to γ-ray should be avoided. Thus, radiolysis of H<sub>2</sub>O cannot be applied to disinfection treatment *in vivo*. The irradiation of ultraviolet light (UV), which is electromagnetic wave with a wavelength of <400 nm, to normal tissue would also cause adverse effect especially when UV light with a short wavelength known as UVB (280–315 nm) and UVC (100–280 nm) is used [48]. Besides UV light, we have found that visible blue light (wavelength: around 400 nm) can also photolyze H<sub>2</sub>O<sub>2</sub> and it will probably be used without adverse effects as long as the treatment time is not so long. As for ultrasound irradiation, ultrasound device with a frequency of <5 MHz has been utilized in medical diagnostic imaging. Thus, the frequency of ultrasound itself is supposed to be safe. Therefore, we have been studying photolysis of H<sub>2</sub>O<sub>2</sub> and sonolysis of H<sub>2</sub>O to develop new disinfection techniques to treat infectious diseases.

### 17.2.1 Photolysis of $H_2O_2$

In dental and medical fields, the bactericidal activity of 3 %  $H_2O_2$  is well recognized and used as a disinfectant. However, the bactericidal effect is not sufficient to treat periodontal diseases as discussed above. To improve the bactericidal activity, we studied the effect of visible blue light irradiation of  $H_2O_2$  (i.e. photolysis of  $H_2O_2$ ). Ikai et al. used a laser with a wavelength of 405 nm at an irradiance of 940 mW/cm<sup>2</sup> and demonstrated that the yield of hydroxyl radicals generated by photolysis of  $H_2O_2$  increased with laser irradiation time [49]. The laser irradiation of bacterial suspensions in 1 M  $H_2O_2$  (corresponds to approximately 3 %  $H_2O_2$ ) resulted in a >4-log reduction of the viable counts of bacteria, such as *Staphylococcus aureus*, *Aggregatibacter actinomycetemcomitans*, *Streptococcus mutans* and *Enterococcus faecalis*, within 3 min of treatment [49]. Furthermore, treatment of *S. mutans* in an experimental biofilm also resulted in a >5-log reduction of viable counts within 3 min [49]. Concerning the periodontal pathogens other than *A. actinomycetemcomitans*, Ikai et al. also investigated the bactericidal effect of photolysis of  $H_2O_2$  on *Porphyromonas gingivalis*. It was demonstrated that photolysis of 500 mM  $H_2O_2$  killed *P. gingivalis* in an experimental biofilm with a >5-log reduction of viable counts within 30 s [50]. As for  $H_2O_2$  solution, Oyamada et al. compared the bactericidal activity of photoysis of oxydol products (2.5–3.0 %  $H_2O_2$  solution), which is an over-the-counter drug with quality guaranteed by Japanese Pharmacopoeia, to substitute them for  $H_2O_2$  of reagent grade [51]. It was demonstrated that any of the oxydol products that have been already approved by an authority can be used for the disinfection technique in terms of bactericidal activity. Thus, based on these findings, we have been developing a therapeutic device for the treatment of periodontitis, and a clinical trial will be conducted in the near future. In the therapeutic device,  $H_2O_2$  is released from the forefront of scalar tip of the device to the lesion site concomitantly with laser irradiation through an optical fiber during ultrasound scaling (Fig. 17.1).

Nakamura et al. conducted a kinetic analysis and demonstrated that hydroxyl radicals generated by photolysis of  $H_2O_2$  directly reacted with microorganisms [52]. In addition, it was demonstrated that the catalase activity of microorganisms influenced the microbial resistance to oxidative stress induced by photolysis of  $H_2O_2$ . Nonetheless, *Candida albicans*, a catalase positive yeast-like fungus whose catalase activity is more potent than that of catalase positive bacteria such as *S. aureus* could also be killed with a >4-log reduction of viable counts within 10 min when treated with the photolysis of 250 mM  $H_2O_2$  using LEDs at an irradiance of 80 mW/cm<sup>2</sup>. This finding suggests that photolysis of  $H_2O_2$  can effectively kill not only bacteria but also fungi. Shirato et al. evaluated the effect of thermal energy on the yield of and the bactericidal action of hydroxyl radicals generated by photolysis of  $H_2O_2$  [53]. The results demonstrated that thermal energy accelerated the generation of hydroxyl radicals by photolysis of  $H_2O_2$ , which in turn resulted in a synergistic bactericidal effect of hydroxyl radicals and thermal energy. When photolysis of  $H_2O_2$  was performed at 55 °C, *S. aureus* and *E. faecalis* were

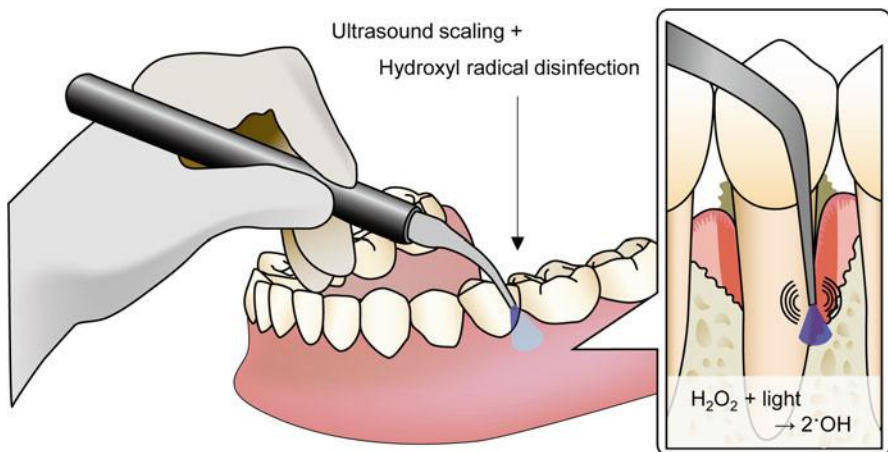


**Fig. 17.1** Schematic illustration of the therapeutic device for the treatment of periodontitis. Mechanical removal of dental plaque by ultrasound scaling and chemical disinfection by hydroxyl radical generated by photolysis of 3 %  $\text{H}_2\text{O}_2$  are performed at the same time

killed with a >5-log reduction of viable counts within 1 min even though the irradiance of light was  $110 \text{ mW/cm}^2$  and the concentration of  $\text{H}_2\text{O}_2$  was  $500 \text{ mM}$ . This synergistic effect will be beneficial especially when it comes to cleaning of medical instruments or dental prostheses which can tolerate the temperature of  $55^\circ\text{C}$ . Based on these findings, Kanno et al. applied photolysis of  $\text{H}_2\text{O}_2$  to cleaning of removable dentures and conducted a clinical test [54]. They demonstrated that microorganisms in denture plaque were reduced by approximately 7-log within 20 min. In addition to the in vitro tests, in vivo antibacterial effect of photolysis of  $\text{H}_2\text{O}_2$  was proven effective. Hayashi et al. evaluated antibacterial activity of photolysis of  $\text{H}_2\text{O}_2$  on skin infection [55]. Infection of *S. aureus* was established in the full-thickness skin wounds of immunosuppressed rats. Then, the wound was treated by photolysis of  $1 \text{ M H}_2\text{O}_2$ . Two minutes treatment resulted in significant reduction in viable counts in comparison with the treatment by  $\text{H}_2\text{O}_2$  alone. Thus, the disinfection technique based on photolysis of  $\text{H}_2\text{O}_2$  is expected to be applied to a wide range of fields other than treatment for periodontitis.

Besides the bactericidal activity, it was demonstrated that photolysis of  $\text{H}_2\text{O}_2$  caused lag of regrowth of the surviving bacteria after the disinfection treatment, known as the postantibiotic effect (PAE). Odashima et al. demonstrated that photolysis of  $250 \text{ mM H}_2\text{O}_2$  with a treatment time of 10 s significantly delayed the regrowth of *S. aureus* colony on agar plate [56]. The PAE would be beneficial because it contributes to giving time for host immune defense system to overcome the infection. More importantly, it has been demonstrated that repeated treatment by photolysis of  $\text{H}_2\text{O}_2$  does not induce bacterial resistance to this disinfection technique. Ikai et al. evaluated the risk of inducing bacterial resistance to disinfection treatment with photolysis of  $\text{H}_2\text{O}_2$  using *S. aureus*, *E. faecalis*, *Escherichia coli*, *Streptococcus salivarius*, *Pseudomonas aeruginosa*, *S. mutans*, and

*A. actinomycetemcomitans* [36]. The antibacterial activity against any of the bacterial species tested was not affected by repeated exposure to the disinfection treatment up to 40 times suggesting that the repeated treatment does not induce bacterial resistance.

Regarding the safety aspect of the disinfection system, Yamada et al. conducted an animal study in which histological analyses of oral mucosa and the full-thickness skin wounds in rats treated by the disinfection technique with photolysis of 1 M H<sub>2</sub>O<sub>2</sub> were performed [57]. Since topical treatment had no detrimental effect on the oral mucosa and the healing process of full thickness skin wounds, it is expected that the acute locally injurious property of the disinfection technique is low. Moreover, Kanno et al. assessed the risk of carcinogenicity by using the hydroxyl radical for the treatment of oral infections by reviewing the literatures [58]. The reviewed studies reported possible involvement of hydroxyl radicals in some sort of chemically-induced mutagenicity and carcinogenicity. However, manifestation of carcinogenicity requires chronic exposure to the carcinogens that generate hydroxyl radicals, such as heavy metals. Thus, it was concluded that there is little or no risk of carcinogenicity as long as the hydroxyl radical is used as a disinfectant for the short-term treatment of oral cavity. Therefore, the disinfection treatment with photolysis of H<sub>2</sub>O<sub>2</sub> is expected to be a novel alternative to antiseptics and antibiotics.

### 17.2.2 Sonolysis of Water

The antimicrobial effect of ultrasound has been studied in various fields, such as water treatment, food decontamination and medical disinfection [59]. The mechanism of killing microorganisms is mainly due to cavitation effect in which tiny gas bubbles formed in liquid medium by alternating compression and expansion collide violently, creating shock waves in a localized region with high temperature (5,500 °C) and pressure (50 MPa) [60]. When water is used as a liquid medium, the shock wave produced by the cavitation effect fragments the molecules of H<sub>2</sub>O into hydroxyl radicals and hydrogen atoms, which is so-called sonolysis of water [61]. Then, the localized heating and pressure together with the free radicals damage microorganisms resulting in cell death [60].

In this context, we examined fungicidal effect of ultrasound irradiation at a frequency of 1.6 MHz [62] to develop a treatment of onychomycosis (i.e. fungal nail infections). It was demonstrated that the ultrasound irradiation killed the dermatophytes, such as *Trichophyton mentagrophytes* and *Trichophyton rubrum*, with a yield of hydroxyl radicals that is proportion to ultrasound duration. In particular, when the treatment was performed at 50 °C, the fungi were killed with a 5-log of viable counts within 10 min. Thus, it is suggested that the ultrasound irradiation and heat treatment exerted a combination effect in fungicidal activity. This finding was in accordance with previous studies which evaluated the combination effect of heat and ultrasound on bactericidal activity [63, 64].

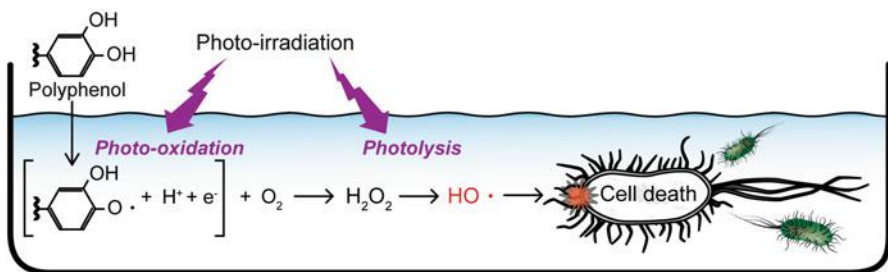


**Fig. 17.2** Schematic illustration of the mechanism of bacterial cell death induced by photo-irradiation of polyphenolic compound

As for application of sonolysis of water to dentistry, other research groups have conducted studies. For instance, it has been demonstrated that ultrasound irradiation of 1.5 % (450 mM) H<sub>2</sub>O<sub>2</sub> using a device for endodontic treatment generates hydroxyl radicals resulting in killing of *E. faecalis* [65]. However, the reduction of bacterial number within the treatment time of 90 s was less than 1-log. Thus, the clinical benefit of this treatment is still unclear. The other example is the ultrasonic scaler used for periodontal therapy. It has been reported that hydroxyl radicals are generated during scaling around ultrasonic scaler tip [66–68]. However, the role of hydroxyl radicals generated by ultrasonic scaler is still unknown.

The microbicidal activity of ultrasound irradiation varies dependently on the type of microorganisms treated (i.e. Gram-positive or negative bacteria, spore forming bacteria, and fungi). In addition, it has been reported that the microbicidal activity of ultrasound irradiation alone is relatively low (<1-log) and/or requires extended irradiation time (~60 min) unless it is used at high intensity [69]. Therefore, as suggested by Piyasena et al. [60], it would be beneficial to use ultrasound in conjunction with other disinfection techniques, such as heat treatment, antiseptics and antibiotics.

### 17.2.3 Other Hydroxyl Radical Generation Systems

More recently, we found that photo-irradiated polyphenolic compounds could generate hydroxyl radicals as well as H<sub>2</sub>O<sub>2</sub>. Since it has been reported that polyphenolic compounds exert antimicrobial effect via production of H<sub>2</sub>O<sub>2</sub> by auto-oxidation in a liquid medium [70, 71], we tried to enhance the antimicrobial activity by means of exposure of polyphenolic compounds to blue light, which enhances the H<sub>2</sub>O<sub>2</sub> production through photo-oxidation of the compounds resulting in hydroxyl radical production via photolysis of the resultant H<sub>2</sub>O<sub>2</sub> (Fig. 17.2). Nakamura et al. demonstrated that hydroxyl radicals were generated when gallic acid, a polyphenolic compound, was irradiated with blue light (wavelength: 400 nm) at an irradiance of 80 mW/cm<sup>2</sup> [72]. It was also demonstrated that *S. aureus*

was killed by the photo-irradiation of gallic acid with a >5-log reduction of viable counts within 15 min. Since the bactericidal activity was attenuated by adding hydroxyl radical scavengers, such as dimethyl sulfoxide and sodium formate, it is suggested that the hydroxyl radical is the main contributor to the bactericidal effect. Later, they showed similar bactericidal activity of photo-irradiated proanthocyanidin which is also a type of polyphenolic compounds [73]. The advantage of this disinfection technique is that polyphenols are supposed to be safe for humans because they are edible compounds naturally occurring in fruits, vegetables, nuts, seeds, and flowers. In addition, since those polyphenolic compounds are noteworthy for its antioxidative activity [74, 75], they might alleviate the oxidative damage in the tissue after the disinfection treatment. Therefore, it is expected that this disinfection technique is applicable to the fields of medical and food sanitation.

Based on the findings described above, we studied the combination effect of photolysis of H<sub>2</sub>O<sub>2</sub> and photo-irradiation of proanthocyanidin. Since both disinfection techniques utilize the same light source (wavelength: around 400 nm), they can be performed at once if the liquid contains H<sub>2</sub>O<sub>2</sub> and proanthocyanidin. Ikai et al. demonstrated that combination of H<sub>2</sub>O<sub>2</sub> and proanthocyanidin worked synergistically to kill *S. mutans* when photo-irradiated [76]. This synergistic effect would probably contribute to shortening the treatment time and/or to reducing the concentration of H<sub>2</sub>O<sub>2</sub> for more safety.

### 17.3 Summary

In the present review, we described our recent works on microbicidal effect of the artificially generated hydroxyl radicals. As discussed above, the microbicidal activity of hydroxyl radicals is sufficient to kill bacteria in an experimental biofilm as well as planktonic bacteria and fungi within a short-treatment time. At the same time, the safety aspect is also confirmed by an in vivo study and a literature review. Therefore, they can be applicable as novel disinfection treatments in medical/dental therapy. Further studies are in progress to understand the bactericidal mechanism of each disinfection system and also of a combination of each system for the more sophisticated medical devices.

**Open Access** This chapter is distributed under the terms of the Creative Commons Attribution Noncommercial License, which permits any noncommercial use, distribution, and reproduction in any medium, provided the original author(s) and source are credited.

## References

1. Marsh PD, Nyvad B. The oral microflora and biofilms on teeth. In: Fejerskov O, Kidd E, editors. *Dental caries. The disease and its clinical management*. Oxford: Blackwell Munksgaard; 2003. p. 49–70.

2. Socransky SS, Haffajee AD. Microbiology of periodontal disease. In: Lindhe J, Karring T, Lang NP, editors. Clinical periodontology and implant dentistry. 4th ed. Oxford: Blackwell; 2003. p. 106–49.
3. Costerton JW, Lewandowski Z, Caldwell DE, Korber DR, Lappin-Scott HM. Microbial biofilms. Annu Rev Microbiol. 1995;49:711–45. doi:[10.1146/annurev.mi.49.100195.003431](https://doi.org/10.1146/annurev.mi.49.100195.003431).
4. Cargill KL, Pyle BH, Sauer RL, McFeters GA. Effects of culture conditions and biofilm formation on the iodine susceptibility of *Legionella pneumophila*. Can J Microbiol. 1992;38 (5):423–9. doi:[10.1139/m92-071](https://doi.org/10.1139/m92-071).
5. Russell AD. Antibiotic and biocide resistance in bacteria: introduction. J Appl Microbiol. 2002;92(Suppl):1S–3. doi:[10.1046/j.1365-2672.92.5s1.14.x](https://doi.org/10.1046/j.1365-2672.92.5s1.14.x).
6. Tenover FC. Mechanisms of antimicrobial resistance in bacteria. Am J Med. 2006;119:S3–S10. doi:[10.1016/j.amjmed.2006.03.011](https://doi.org/10.1016/j.amjmed.2006.03.011).
7. Winkel EG, Van Winkelhoff AJ, Timmerman MF, Van der Velden U, Van der Weijden GA. Amoxicillin plus metronidazole in the treatment of adult periodontitis patients. A double-blind placebo-controlled study. J Clin Periodontol. 2001;28:296–305. doi:[10.1034/j.1600-051x.2001.028004296.x](https://doi.org/10.1034/j.1600-051x.2001.028004296.x).
8. Berglundh T, Krok L, Liljenberg B, Westfelt E, Serino G, Lindhe J. The use of metronidazole and amoxicillin in the treatment of advanced periodontal disease. A prospective, controlled clinical trial. J Clin Periodontol. 1998;25:354–62.
9. Tomasi C, Wennstrom JL. Locally delivered doxycycline as an adjunct to mechanical debridement at retreatment of periodontal pockets: outcome at furcation sites. J Periodontol. 2011;82:210–8. doi:[10.1902/jop.2010.100308](https://doi.org/10.1902/jop.2010.100308).
10. Tomasi C, Koutouzis T, Wennstrom JL. Locally delivered doxycycline as an adjunct to mechanical debridement at retreatment of periodontal pockets. J Periodontol. 2008;79:431–9. doi:[10.1902/jop.2008.070383](https://doi.org/10.1902/jop.2008.070383).
11. Wennstrom JL, Newman HN, MacNeill SR, Killoy WJ, Griffiths GS, Gillam DG, et al. Utilisation of locally delivered doxycycline in non-surgical treatment of chronic periodontitis. A comparative multi-centre trial of 2 treatment approaches. J Clin Periodontol. 2001;28:753–61.
12. Novak MJ, Dawson 3rd DR, Magnusson I, Karpinia K, Polson A, Ryan ME, et al. Combining host modulation and topical antimicrobial therapy in the management of moderate to severe periodontitis: a randomized multicenter trial. J Periodontol. 2008;79:33–41. doi:[10.1902/jop.2008.070237](https://doi.org/10.1902/jop.2008.070237).
13. Tonetti MS, Cortellini P, Carnevale G, Cattabriga M, de Sanctis M, Pini Prato GP. A controlled multicenter study of adjunctive use of tetracycline periodontal fibers in mandibular class II furcations with persistent bleeding. J Clin Periodontol. 1998;25:728–36. doi:[10.1111/j.1600-051X.1998.tb02514.x](https://doi.org/10.1111/j.1600-051X.1998.tb02514.x).
14. Addy M. The use of antiseptics in periodontal therapy. In: Lindhe J, Karring T, Lang NP, editors. Clinical periodontology and implant dentistry. Oxford: Blackwell; 2003.
15. Loe H, Schiott CR. The effect of mouthrinses and topical application of chlorhexidine on the development of dental plaque and gingivitis in man. J Periodontal Res. 1970;5:79–83. doi:[10.1111/j.1600-0765.1970.tb00696.x](https://doi.org/10.1111/j.1600-0765.1970.tb00696.x).
16. Watts A, Addy M. Tooth discolouration and staining: a review of the literature. Br Dent J. 2001;190:309–16. doi:[10.1038/sj.bdj.4800959a](https://doi.org/10.1038/sj.bdj.4800959a).
17. Lang NP, Catalanotto FA, Knopfli RU, Antczak AA. Quality-specific taste impairment following the application of chlorhexidine digluconate mouthrinses. J Clin Periodontol. 1988;15:43–8. doi:[10.1111/j.1600-051X.1988.tb01553.x](https://doi.org/10.1111/j.1600-051X.1988.tb01553.x).
18. Addy M, Moran JM. Clinical indications for the use of chemical adjuncts to plaque control: chlorhexidine formulations. Periodontol 2000. 1997;15:52–4. doi:[10.1111/j.1600-0757.1997.tb00104.x](https://doi.org/10.1111/j.1600-0757.1997.tb00104.x).
19. Wennstrom J, Lindhe J. Effect of hydrogen peroxide on developing plaque and gingivitis in man. J Clin Periodontol. 1979;6:115–30.

20. Boyd RL. Effects on gingivitis of daily rinsing with 1.5% H<sub>2</sub>O<sub>2</sub>. *J Clin Periodontol.* 1989;16:557–62.
21. Hasturk H, Nunn M, Warbington M, Van Dyke TE. Efficacy of a fluoridated hydrogen peroxide-based mouthrinse for the treatment of gingivitis: a randomized clinical trial. *J Periodontol.* 2004;75:57–65. doi:[10.1902/jop.2004.75.1.57](https://doi.org/10.1902/jop.2004.75.1.57).
22. Gusberti FA, Sampathkumar P, Siegrist BE, Lang NP. Microbiological and clinical effects of chlorhexidine digluconate and hydrogen peroxide mouthrinses on developing plaque and gingivitis. *J Clin Periodontol.* 1988;15:60–7. doi:[10.1111/j.1600-051X.1988.tb01556.x](https://doi.org/10.1111/j.1600-051X.1988.tb01556.x).
23. Konopka K, Goslinski T. Photodynamic therapy in dentistry. *J Dent Res.* 2007;86:694–707. doi:[10.1177/154405910708600803](https://doi.org/10.1177/154405910708600803).
24. Soukos NS, Goodson JM. Photodynamic therapy in the control of oral biofilms. *Periodontol 2000.* 2011;55:143–66. doi:[10.1111/j.1600-0757.2010.00346.x](https://doi.org/10.1111/j.1600-0757.2010.00346.x).
25. Redmond RW, Kochevar IE. Spatially resolved cellular responses to singlet oxygen. *Photochem Photobiol.* 2006;82:1178–86. doi:[10.1562/2006-04-14-IR-874](https://doi.org/10.1562/2006-04-14-IR-874).
26. Pedigo L, Gibbs A, Scott R, Street C. Absence of bacterial resistance following repeat exposure to photodynamic therapy. *Proc SPIE.* 2009;7380:73803H1–7. doi:[10.1117/12.822834](https://doi.org/10.1117/12.822834).
27. Tavares A, Carvalho CM, Faustino MA, Neves MG, Tome JP, Tome AC, et al. Antimicrobial photodynamic therapy: study of bacterial recovery viability and potential development of resistance after treatment. *Mar Drugs.* 2010;8:91–105. doi:[10.3390/md8010091](https://doi.org/10.3390/md8010091).
28. Burns T, Wilson M, Pearson G. Mechanism of killing of *Streptococcus mutans* by light-activated drugs. *Proc SPIE.* 1996;2625:288–97.
29. Wood S, Nattress B, Kirkham J, Shore R, Brookes S, Griffiths J, et al. An in vitro study of the use of photodynamic therapy for the treatment of natural oral plaque biofilms formed in vivo. *J Photochem Photobiol B.* 1999;50:1–7. doi:[10.1016/S1011-1344\(99\)00056-1](https://doi.org/10.1016/S1011-1344(99)00056-1).
30. Zanin IC, Lobo MM, Rodrigues LK, Pimenta LA, Hofling JF, Goncalves RB. Photosensitization of in vitro biofilms by toluidine blue O combined with a light-emitting diode. *Eur J Oral Sci.* 2006;114:64–9. doi:[10.1111/j.1600-0722.2006.00263.x](https://doi.org/10.1111/j.1600-0722.2006.00263.x).
31. Ishiyama K, Nakamura K, Ikai H, Kanno T, Kohno M, Sasaki K, et al. Bactericidal action of photogenerated singlet oxygen from photosensitizers used in plaque disclosing agents. *PLoS One.* 2012;7:e37871. doi:[10.1371/journal.pone.0037871.g001](https://doi.org/10.1371/journal.pone.0037871.g001).
32. Bassir SH, Moslemi N, Jamali R, Mashmouly S, Fekrazad R, Chiniforush N, et al. Photoactivated disinfection using light-emitting diode as an adjunct in the management of chronic periodontitis: a pilot double-blind split-mouth randomized clinical trial. *J Clin Periodontol.* 2013;40:65–72. doi:[10.1111/jcpe.12024](https://doi.org/10.1111/jcpe.12024).
33. Pourabbas R, Kashefimehr A, Rahmanpour N, Babaloo Z, Kishen A, Tenenbaum HC, et al. Effects of photodynamic therapy on the clinical and gingival crevicular fluid inflammatory biomarkers in chronic periodontitis: a split-mouth randomized clinical trial. *J Periodontol.* 2014. doi:[10.1902/jop.2014.130464](https://doi.org/10.1902/jop.2014.130464).
34. Alwaeli HA, Al-Khateeb SN, Al-Sadi A. Long-term clinical effect of adjunctive antimicrobial photodynamic therapy in periodontal treatment: a randomized clinical trial. *Lasers Med Sci.* 2013. doi:[10.1007/s10103-013-1426-y](https://doi.org/10.1007/s10103-013-1426-y).
35. Theodoro LH, Silva SP, Pires JR, Soares GH, Pontes AE, Zuza EP, et al. Clinical and microbiological effects of photodynamic therapy associated with nonsurgical periodontal treatment. A 6-month follow-up. *Lasers Med Sci.* 2012;27:687–93.
36. Ikai H, Odashima Y, Kanno T, Nakamura K, Shirato M, Sasaki K, et al. In vitro evaluation of the risk of inducing bacterial resistance to disinfection treatment with photolysis of hydrogen peroxide. *PLoS One.* 2013;8:e81316. doi:[10.1371/journal.pone.0081316](https://doi.org/10.1371/journal.pone.0081316).
37. Halliwell B, Gutteridge JM. The chemistry of free radicals and related ralactive species. Free radicals in biology and medicine. 4th ed. Oxford: Oxford University Press; 2007. p. 30–78.
38. Clark IA, Cowden WB, Hunt NH. Free radical-induced pathology. *Med Res Rev.* 1985;5:297–332.

39. Cross CE, Halliwell B, Borish ET, Pryor WA, Ames BN, Saul RL, et al. Oxygen radicals and human disease. *Ann Intern Med.* 1987;107:526–45.
40. Badwey JA, Karnovsky ML. Active oxygen species and the functions of phagocytic leukocytes. *Annu Rev Biochem.* 1980;49:695–726. doi:[10.1146/annurev.bi.49.070180.003403](https://doi.org/10.1146/annurev.bi.49.070180.003403).
41. Clifford DP, Repine JE. Hydrogen peroxide mediated killing of bacteria. *Mol Cell Biochem.* 1982;49:143–9.
42. Kohanski MA, Dwyer DJ, Hayete B, Lawrence CA, Collins JJ. A common mechanism of cellular death induced by bactericidal antibiotics. *Cell.* 2007;130:797–810. doi:[10.1016/j.cell.2007.06.049](https://doi.org/10.1016/j.cell.2007.06.049).
43. Wright GD. On the road to bacterial cell death. *Cell.* 2007;130:781–3. doi:[10.1016/j.cell.2007.08.023](https://doi.org/10.1016/j.cell.2007.08.023).
44. Pryor WA. Oxy-radicals and related species: their formation, lifetimes, and reactions. *Annu Rev Physiol.* 1986;48:657–67. doi:[10.1146/annurev.ph.48.030186.003301](https://doi.org/10.1146/annurev.ph.48.030186.003301).
45. Sies H, Stahl W, Sundquist A. Antioxidant functions of vitamins. Vitamins E and C, beta-carotene, and other carotenoids. *Ann N Y Acad Sci.* 1992;669:7–20.
46. FDA. Oral health care drug products for over-the-counter human use; Antigingivitis/antiplaque drug products; Establishment of a monograph. *Fed Regist.* 2003;68:32232–86.
47. Augusto O, Miyamoto S. Chapter 2. Oxygen radicals and related species. In: Pantopoulos K, Schipper H, editors. *Principles of free radical biomedicine*, vol. 1. New York: Nova; 2012. p. 19–41.
48. Maverakis E, Miyamura Y, Bowen MP, Correa G, Ono Y, Goodarzi H. Light, including ultraviolet. *J Autoimmun.* 2010;34:J247–57. doi:[10.1016/j.jaut.2009.11.011](https://doi.org/10.1016/j.jaut.2009.11.011).
49. Ikai H, Nakamura K, Shirato M, Kanno T, Iwasawa A, Sasaki K, et al. Photolysis of hydrogen peroxide, an effective disinfection system via hydroxyl radical formation. *Antimicrob Agents Chemother.* 2010;54:5086–91. doi:[10.1128/AAC.00751-10](https://doi.org/10.1128/AAC.00751-10).
50. Ikai H, Nakamura K, Shirato M, Kanno T, Iwasawa A, Niwano Y, et al. Bactericidal effect of hydroxyl radical generated by photolysis of hydrogen peroxide. In: Sasaki K, Suzuki O, Takahashi N, editors. *Interface Oral Health Science* 2011. Tokyo: Springer; 2012.
51. Oyamada A, Ikai H, Nakamura K, Hayashi E, Kanno T, Sasaki K, et al. In vitro bactericidal activity of photo-irradiated oxydol products via hydroxyl radical generation. *Biocontrol Sci.* 2013;18:83–8. doi:[10.4265/bio.18.83](https://doi.org/10.4265/bio.18.83).
52. Nakamura K, Kanno T, Mokudai T, Iwasawa A, Niwano Y, Kohno M. Microbial resistance in relation to catalase activity to oxidative stress induced by photolysis of hydrogen peroxide. *Microbiol Immunol.* 2012;56:48–55. doi:[10.1111/j.1348-0421.2011.00400.x](https://doi.org/10.1111/j.1348-0421.2011.00400.x).
53. Shirato M, Ikai H, Nakamura K, Hayashi E, Kanno T, Sasaki K, et al. Synergistic effect of thermal energy on bactericidal action of photolysis of  $H_2O_2$  in relation to acceleration of hydroxyl radical generation. *Antimicrob Agents Chemother.* 2012;56:295–301. doi:[10.1128/AAC.05158-11](https://doi.org/10.1128/AAC.05158-11).
54. Kanno T, Nakamura K, Ikai H, Hayashi E, Shirato M, Mokudai T, et al. Novel denture cleaning system based on hydroxyl radical disinfection. *Int J Prosthodont.* 2012;25:376–80.
55. Hayashi E, Mokudai T, Yamada Y, Nakamura K, Kanno T, Sasaki K, et al. In vitro and in vivo anti-Staphylococcus aureus activities of a new disinfection system utilizing photolysis of hydrogen peroxide. *J Biosci Bioeng.* 2012;114:193–7. doi:[10.1016/j.jbiosc.2012.03.020](https://doi.org/10.1016/j.jbiosc.2012.03.020).
56. Odashima Y, Nakamura K, Ikai H, Kanno T, Meirelles L, Sasaki K, et al. Postantibiotic effect of disinfection treatment by photolysis of hydrogen peroxide. *J Chemother.* 2014;26:92–100. doi:[10.1179/1973947813Y.0000000114](https://doi.org/10.1179/1973947813Y.0000000114).
57. Yamada Y, Mokudai T, Nakamura K, Hayashi E, Kawana Y, Kanno T, et al. Topical treatment of oral cavity and wounded skin with a new disinfection system utilizing photolysis of hydrogen peroxide in rats. *J Toxicol Sci.* 2012;37:329–35. doi:[10.2131/jts.37.329](https://doi.org/10.2131/jts.37.329).
58. Kanno T, Nakamura K, Ikai H, Kikuchi K, Sasaki K, Niwano Y. Literature review of the role of hydroxyl radical in chemically-induced mutagenicity and carcinogenicity for the risk assessment of disinfection system utilizing photolysis of hydrogen peroxide. *J Clin Biochem Nutr.* 2012;51:9–14. doi:[10.3164/jcbn.11-105](https://doi.org/10.3164/jcbn.11-105).

59. Erriu M, Blus C, Szmukler-Moncler S, Buogo S, Levi R, Barbato G, et al. Microbial biofilm modulation by ultrasound: current concepts and controversies. *Ultrason Sonochem.* 2014;21:15–22. doi:[10.1016/j.ultsonch.2013.05.011](https://doi.org/10.1016/j.ultsonch.2013.05.011).
60. Piyasena P, Mohareb E, McKellar RC. Inactivation of microbes using ultrasound: a review. *Int J Food Microbiol.* 2003;87:207–16. doi:[10.1016/S0168-1605\(03\)00075-8](https://doi.org/10.1016/S0168-1605(03)00075-8).
61. Riesz P, Kondo T. Free radical formation induced by ultrasound and its biological implications. *Free Radic Biol Med.* 1992;13:247–70. doi:[10.1016/0891-5849\(92\)90021-8](https://doi.org/10.1016/0891-5849(92)90021-8).
62. Iwasawa A, Saito K, Mokudai T, Kohno M, Ozawa T, Niwano Y. Fungicidal action of hydroxyl radicals generated by ultrasound in water. *J Clin Biochem Nutr.* 2009;45:214–8. doi:[10.3164/jcbn.08-261](https://doi.org/10.3164/jcbn.08-261).
63. Ordonez JA, Sanz B, Hernandez PE, Lopez-Lorenzo P. A note on the effect of combined ultrasonic and heat treatments on the survival of thermoduric streptococci. *J Appl Bacteriol.* 1984;56:175–7. doi:[10.1111/j.1365-2672.1984.tb04711.x](https://doi.org/10.1111/j.1365-2672.1984.tb04711.x).
64. McClements DJ. Advances in the application of ultrasound in food analysis and processing. *Trends Food Sci Technol.* 1995;6:293–9. doi:[10.1016/S0924-2244\(00\)89139-6](https://doi.org/10.1016/S0924-2244(00)89139-6).
65. Kobayashi Y, Hayashi M, Yoshino F, Tamura M, Yoshida A, Ibi H, et al. Passive ultrasonic irrigation in the presence of a low concentration of hydrogen peroxide enhances hydroxyl radical generation and bactericidal effect against *Enterococcus faecalis*. *J Oral Sci.* 2014;56:35–9. doi:[10.2334/josnusd.56.35](https://doi.org/10.2334/josnusd.56.35).
66. Felver B, King DC, Lea SC, Price GJ, Damien WA. Cavitation occurrence around ultrasonic dental scalers. *Ultrason Sonochem.* 2009;16:692–7. doi:[10.1016/j.ultsonch.2008.11.002](https://doi.org/10.1016/j.ultsonch.2008.11.002).
67. Walmsley AD, Lea SC, Felver B, King DC, Price GJ. Mapping cavitation activity around dental ultrasonic tips. *Clin Oral Investig.* 2013;17:1227–34. doi:[10.1007/s00784-012-0802-5](https://doi.org/10.1007/s00784-012-0802-5).
68. Price GJ, Tiong TJ, King DC. Sonochemical characterisation of ultrasonic dental descalers. *Ultrason Sonochem.* 2014. doi:[10.1016/j.ultsonch.2013.12.029](https://doi.org/10.1016/j.ultsonch.2013.12.029).
69. Iqbal K, Ohl SW, Khoo BC, Neo J, Fawzy AS. Effect of high-intensity focused ultrasound on *Enterococcus faecalis* planktonic suspensions and biofilms. *Ultrasound Med Biol.* 2013;39:825–33. doi:[10.1016/j.ultrasmedbio.2012.12.006](https://doi.org/10.1016/j.ultrasmedbio.2012.12.006).
70. Arakawa H, Maeda M, Okubo S, Shimamura T. Role of hydrogen peroxide in bactericidal action of catechin. *Biol Pharm Bull.* 2004;27:277–81. doi:[10.1248/bpb.27.277](https://doi.org/10.1248/bpb.27.277).
71. Taguri T, Tanaka T, Kouno I. Antibacterial spectrum of plant polyphenols and extracts depending upon hydroxyphenyl structure. *Biol Pharm Bull.* 2006;29:2226–35. doi:[10.1248/bpb.29.2226](https://doi.org/10.1248/bpb.29.2226).
72. Nakamura K, Yamada Y, Ikai H, Kanno T, Sasaki K, Niwano Y. Bactericidal action of photo-irradiated gallic acid via reactive oxygen species formation. *J Agric Food Chem.* 2012;60:10048–54. doi:[10.1021/jf303177p](https://doi.org/10.1021/jf303177p).
73. Nakamura K, Shirato M, Ikai H, Kanno T, Sasaki K, Kohno M, et al. Photo-irradiation of proanthocyanidin as a new disinfection technique via reactive oxygen species formation. *PLoS One.* 2013;8:e60053. doi:[10.1371/journal.pone.0060053](https://doi.org/10.1371/journal.pone.0060053).
74. Kondo K, Kurihara M, Miyata N, Suzuki T, Toyoda M. Scavenging mechanisms of (−)-epigallocatechin gallate and (−)-epicatechin gallate on peroxy radicals and formation of superoxide during the inhibitory action. *Free Radic Biol Med.* 1999;27:855–63. doi:[10.1016/S0891-5849\(99\)00133-1](https://doi.org/10.1016/S0891-5849(99)00133-1).
75. Yilmaz Y, Toledo RT. Major flavonoids in grape seeds and skins: antioxidant capacity of catechin, epicatechin, and gallic acid. *J Agric Food Chem.* 2004;52:255–60. doi:[10.1021/jf030117h](https://doi.org/10.1021/jf030117h).
76. Ikai H, Nakamura K, Kanno T, Shirato M, Meirelles L, Sasaki K, et al. Synergistic effect of proanthocyanidin on the bactericidal action of the photolysis of H<sub>2</sub>O<sub>2</sub>. *Biocontrol Sci.* 2013;18:137–41. doi:[10.4265/bio.18.137](https://doi.org/10.4265/bio.18.137).

## Chapter 18

# High Levels of Saturated Fatty Acids may Exacerbate the Pathogenesis of Primary Sjögren's Syndrome

**Yosuke Shikama, Naozumi Ishimaru, Yasusei Kudo, Rieko Arakaki, Yukiko Bando, Nanako Aki, Yoshio Hayashi, and Makoto Funaki**

**Abstract** Obesity and type 2 diabetes (T2D) are characterized by decreased insulin sensitivity and higher concentrations of free fatty acids (FFAs) in the serum. Among FFAs, saturated fatty acids, such as palmitate, have been reported to play a role in obesity-associated inflammation. Primary Sjögren's syndrome (SS) is an autoimmune disease characterized by infiltration of inflammatory mononuclear cells and destruction of epithelial cells in salivary and lacrimal glands. Although epidemiological studies have suggested a link between primary SS and dyslipidemia or T2D, little is known about the clinical significance of elevated serum level of FFAs in primary SS. In salivary gland epithelial cells of patients with primary SS, interleukin (IL)-6 production and  $\alpha$ -fodrin degradation are increased. IL-6 is one of the pro-inflammatory cytokines, and the cleaved  $\alpha$ -fodrin serves as an auto-antigen. In this study, we demonstrate that palmitate, but not unsaturated fatty acids, induces IL-6 production and  $\alpha$ -fodrin degradation in human salivary gland epithelial cell lines. However, palmitate did not induce these responses in keratinocytes. Taken together, these results suggest that higher levels of saturated fatty acids may promote the severity of primary SS.

**Keywords** Apoptosis • Interleukin-6 • Lipids • Palmitate • Sjögren's syndrome •  $\alpha$ -fodrin

---

Y. Shikama (✉) • Y. Bando • N. Aki • M. Funaki

Clinical Research Center for Diabetes, Tokushima University Hospital, 2-50-1

Kuramoto-cho, Tokushima 770-8503, Japan

e-mail: [shikama@tokushima-u.ac.jp](mailto:shikama@tokushima-u.ac.jp)

N. Ishimaru • Y. Kudo • R. Arakaki • Y. Hayashi

Department of Oral Molecular Pathology, Institute of Health Biosciences,

The University of Tokushima Graduate School, 3-18-15 Kuramoto-cho,

Tokushima 770-8504, Japan

## 18.1 Introduction

Obesity is rapidly prevailing and is one of the major threats to global health these days. The epidemic of obesity has resulted in dramatic increases in the prevalence of obesity-associated diseases including type 2 diabetes (T2D) [1]. It has been known that the level of free fatty acids (FFAs) in the blood is elevated in T2D patients as well as animal models of T2D [2], which is attributable to enhanced lipolysis in adipocytes and increased consumption of dietary lipids [3]. It has been demonstrated that saturated fatty acids (SFAs), such as palmitate and stearate, induce inflammatory responses presumably activation of Toll-like receptor (TLR) 4 and its downstream signaling pathway [4–6]. TLRs are one of the pattern recognition receptors that play a key role in induction of innate and adaptive immune response through recognition of pathogen-associated molecular patterns (PAMPs) of microbes [7]. Furthermore, excess amount of FFAs in the blood can lead to proinflammatory response and intracellular lipid accumulation, which could also result in cellular dysfunction, so-called ‘lipotoxicity’. Lipotoxicity has been reported in pancreatic  $\beta$  cells, hepatocytes, cardiomyocytes, and skeletal muscle cells [8], but hardly reported in epithelial cells such as epithelial cells in exocrine glands.

Primary Sjögren’s syndrome (SS) is an autoimmune disorder that is characterized by chronic dysfunction and destruction of exocrine glands, mainly the salivary and lacrimal glands associated with chronic lymphocytic infiltrating lesions, that leads to persistent dryness of eyes and mouth. Emerging evidence suggests that salivary gland epithelial cells also actively participate in the inflammatory process of SS [9]. For instance, interleukin (IL)-6, which is one of proinflammatory cytokines known to serve as a B cell growth factor and a vital factor for plasma cell survival [10], is upregulated in salivary gland epithelial cells of SS patients [11–13]. IL-6 production is induced by activation of intracellular signaling cascades including the mitogen-activated protein kinase (MAPK) pathways and the nuclear factor- $\kappa$ B (NF- $\kappa$ B) pathway [14]. It has been also reported that  $\alpha$ -fodrin, which is a ubiquitously-expressed heterodimeric calmodulin-binding protein, is cleaved during apoptosis by caspase-3 or  $\mu$ -calpain to produce 120 kDa fragments in salivary gland ductal epithelial cells. These  $\alpha$ -fodrin-derived 120 kDa fragments have been shown to serve as an auto-antigen in murine and human primary SS [15, 16].

An association between obesity-related metabolic disorders and SS was first reported in “pseudo-Sjögren syndrome” [17, 18], which was followed by an experimental study in mice that reported a link between SS and diabetes [19]. Moreover, it was recently reported that primary SS patients had significantly higher incidence of metabolic disorders, such as T2D [20, 21]. These observations described above led us to hypothesize that SFAs may induce IL-6 secretion, lipotoxicity, and  $\alpha$ -fodrin degradation in human salivary gland epithelial cells. In this report, we provide evidence that SFAs, but not unsaturated fatty acids, induce IL-6 secretion mediated by activation of p38 MAPK and NF- $\kappa$ B activation.

Palmitate also induces intracellular lipid accumulation and apoptosis, and  $\alpha$ -fodrin degradation. However, these SFAs-dependent responses observed in salivary gland epithelial cells are not common among epithelial cells in other type of tissues. These observations implicate that salivary gland epithelial cells are susceptible to palmitate-induced IL-6 secretion, lipotoxicity, and  $\alpha$ -fodrin degradation, which could exacerbate the pathogenesis of primary SS in salivary glands.

## 18.2 Materials and Methods

### 18.2.1 Reagents

Fetal bovine serum (FBS) and penicillin/streptomycin were purchased from Life Technologies (Carlsbad, CA). Dulbecco's modified Eagle's medium (DMEM), FFAs, SP600125, SB203580, and BAY11-7082 were obtained from Sigma-Aldrich (St. Louis, MO). FFA-free bovine serum albumin (BSA) was obtained from Merck (Darmstadt, Germany). A stock solution of FFA was prepared and conjugated with BSA as described previously [22] with slight modifications as follows; FFA was dissolved at a concentration of 100 mM in 0.1 mol/L NaOH at 90 °C for 20 min, which was then diluted 10-fold with 10 % BSA solution pre-incubated at 55 °C. The solution was vortexed for 10 s and incubated at 55 °C for additional 10 min. FFA solution of 10 mmol/L FFA with 10 % BSA and 10%BSA control solutions were prepared just before experiments. FFA preparations were checked for LPS contamination using Limulus Color KY Single Test (Wako).

### 18.2.2 Antibodies

Anti-glyceraldehyde-3-phosphate dehydrogenase (GAPDH), anti-I $\kappa$ B $\alpha$ , antiphospho-I $\kappa$ B $\alpha$  (Ser32/36), anti-p38 MAPK, antiphospho-p38 MAPK (Thr180/Tyr182), anti-SAPK/JNK, antiphospho-SAPK/JNK (Thr183/Tyr185), anti-caspase-3, and anti-calpain1 ( $\mu$ -type) antibodies were purchased from Cell Signaling Technology (Danvers, MA). Anti- $\alpha$ -fodrin was obtained from Enzo Life Sciences (Plymouth Meeting, PA).

### 18.2.3 Cells and Cell Culture

A human parotid gland ductal epithelial cell line HSY and a human submandibular gland ductal epithelial cell line HSG were developed as described previously [23, 24]. A human oral squamous carcinoma cell line HSC-2 was provided by

*Japanese Collection of Research Bioresources Cell Bank* (Osaka, Japan). An immortalized human keratinocyte cell line HaCaT was obtained from Dr. Norbert E. Fusenig (German Cancer Research Center, Heidelberg, Germany). Cells were cultured in DMEM supplemented with 10 % FBS, 100 U/mL penicillin and 100 µg/mL streptomycin at 37 °C with a humidified atmosphere of 5 % CO<sub>2</sub>. Cells were serum starved (0.1 % BSA) overnight for experiments.

#### **18.2.4 RNA Isolation and RT-PCR**

Cells were lysed in 1 mL of ISOGEN (Nippon Gene, Tokyo, Japan), and total RNA was extracted as described in the manufacturer's instructions. One µg of total RNA was reverse transcribed into cDNA with a first-strand cDNA synthesis kit (Roche Diagnostics, Indianapolis, IN). Primers used were as follows: TLR4 (forward) 5'-TGGATACGTTCTTATAAG-3' and (reverse) 5'-GAAATGGAGGCACCCCTTC-3'; IL-6 (forward) 5'-AAGCCAGAGCTGTG CAGATGAGTA-3' and (reverse) 5'-TGTCT GCAGCCACTGGTTC-3'; GAPDH (forward) 5'-GCCACATCGCTCAGACAC-3' and (reverse) 5'-CTCGC TCCTGGAAGATGG-3'. PCR products were then subjected to agarose gel electrophoresis and analyzed with an LAS-3000 UV Lumino-image analyzer (Fujifilm, Tokyo, Japan).

#### **18.2.5 Measurement of IL-6 Production**

Cells were seeded into 96-well plates at a concentration of 1 × 10<sup>5</sup> cells/well (Orange Scientific, Braine-l'Alleud, Belgium) and incubated overnight. After treating the cells as described in the figure legends, the medium was collected. The amount of IL-6 in the medium was determined using a human IL-6 ELISA kit (Thermo Scientific, Rockford, IL) according to the manufacturer's instructions.

#### **18.2.6 Immunoblotting**

After treating the cells as described in the figure legends, cells were rinsed three times with ice-cold phosphate-buffered saline (PBS) and lysed in radioimmunoprecipitation assay buffer [50 mM Tris, 150 mM NaCl, 1 % sodium deoxycholate, 1 % Triton X-100, 0.1 % sodium dodecyl sulfate, 1 mM sodium orthovanadate, and 1 % protease inhibitor cocktail (Sigma) (pH 7.5)]. Cell lysates obtained by centrifugation at 15,000 × g and 4 °C for 10 min were subjected to SDS-PAGE and transferred to polyvinylidene diflouride (PVDF) membranes as described previously [25]. In some experiments, antibodies were diluted in Can Get

Signal (Toyobo, Osaka, Japan). Immunoblotting was performed with an ECL PLUS system according to the manufacturer's instructions, and analyzed by a LAS-3000 UV Lumino-image analyzer (Fujifilm).

### ***18.2.7 Oil Red O Staining***

To evaluate intracellular lipid accumulation, cells were stained with Oil Red O as described previously [26]. Briefly, after treating the cells, cells were washed three times with iced PBS and fixed with 4 % paraformaldehyde. Fixed cells were washed again with PBS and stained with Oil Red O solution (1.8 mg/mL Oil Red O in 60 % ethanol) for 15 min at room temperature. After cells were washed again with PBS, cells were observed on a phase contrast microscope (Olympus, Tokyo, Japan).

### ***18.2.8 Cell Viability Assay***

Cell viability was assessed by measuring a mitochondrial activity in reducing 2-(2-methoxy-4-nitrophenyl)-3-(4-nitrophenyl)-5-(2,4-disulfophenyl)-2*H*-tetrazolium monosodium salt (WST-8) to formazan using a Cell Counting Kit-8 (Dojindo, Kumamoto, Japan) according to the manufacturer's instructions. The amount of formazan was quantified using a microplate reader (BioRad, Hercules, CA).

### ***18.2.9 Annexin V-FITC/Propidium Iodide (PI) Staining***

Palmitate-induced apoptosis of salivary gland cells was evaluated by an Annexin V-FITC/PI staining with a TACS Annexin V-FITC Apoptosis Detection Kit (R and D systems, Minneapolis, MN) according to the manufacturer's instructions. After treating the cells as described in the figure legends, fluorescent-positive cells were detected by FACSVersa and analyzed by FACSuite (BD Biosciences, San Diego, CA).

### ***18.2.10 DAPI Staining***

For detecting apoptosis in HSY cells, they were seeded on Lab-Tek chamber slides (Nunc, Thermo Fisher Scientific, Rochester, NY). After treating the cells as described in the figure legends, cells were washed three times with iced PBS and fixed with 4 % paraformaldehyde followed by staining with 4',6-diamidino-2-phenylindole (DAPI) (Invitrogen, Carlsbad, CA). Stained cells were visualized on

a laser scanning confocal microscope (Carl Zeiss, Gottingen, Germany). Apoptotic cells were morphologically defined as cells with nuclear shrinkage, condensation, and fragmentation.

### 18.2.11 Data Analysis

To confirm the reproducibility of the results, all experiments were conducted at least twice. Experimental values are given as mean  $\pm$  standard deviation (SD). The statistical significance of differences was evaluated using a Student's unpaired *t*-test or Dunnett's multiple-comparison test after an analysis of variance (ANOVA) with IBM SPSS Statistics software 19.0 (IBM, Armonk, NY). P values less than 0.05 were considered to be significant.

## 18.3 Results and Discussion

We obtained results as described below. (a) Palmitate treatment induces IL-6 secretion in HSY and HSG cells, but not HaCaT cells. (b) In salivary gland epithelial cells, saturated fatty acids, but not unsaturated fatty acids, induces IL-6 secretion presumably through activation of NF- $\kappa$ B and p38 MAPK. (c) It has been documented that lipotoxicity causes apoptosis, which is featured by some morphological changes such as cell shrinkage, cell rounding, and lipid accumulation [8, 27]. Thus, we investigated whether or not palmitate treatment induces morphological changes. Palmitate treatment induced morphological changes which are cell rounding and lipid accumulation in HSY and HSG cells. On the other hand, HSC-2 and HaCaT cells failed to accumulate lipid droplet after palmitate treatment despite their tendency to round up (Fig. 18.1). (d) Palmitate treatment increases apoptosis of HGY and HSG cells. (e) Palmitate induces a-fodrin degradation and caspase-3 activation in salivary gland epithelial cells. Details were already shown in our report [28]. Moreover, we recently confirmed that, when model mice of primary SS were fed with high-fat diet to elevate the serum level of saturated fatty acids, their salivary glands and lacrimal glands exhibited inflammation significantly more advanced than those observed in model mice fed with normal diet (data not shown). Taken together, these results suggest that higher levels of saturated fatty acids may promote the severity of primary SS.

In conclusion, our data indicate that palmitate may exacerbate the pathogenesis of primary SS. Results presented in this report should encourage further investigations on relationship between metabolic-related disorders and autoimmune diseases such as primary SS.

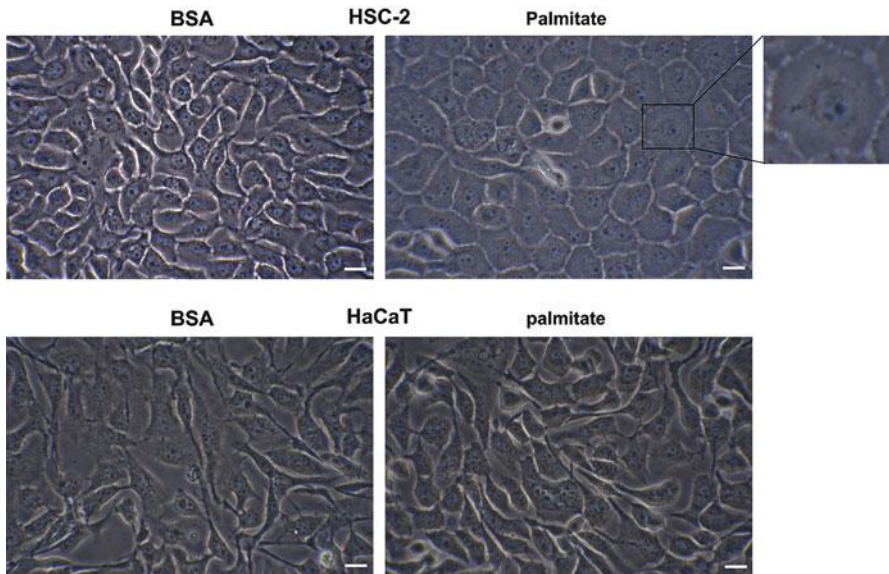


**Fig. 18.1** HSY cells and HSG cells, but not HSC-2 cells and HaCaT cells, exhibited palmitate-induced cell shape change and lipid accumulation. A representative image ( $\times 400$ ) of cells treated with control (BSA) or palmitate (500  $\mu$ M) for 24 h. Arrow heads indicate cytoplasmic lipid droplets. Scale bars = 20  $\mu$ m

**Open Access** This chapter is distributed under the terms of the Creative Commons Attribution Noncommercial License, which permits any noncommercial use, distribution, and reproduction in any medium, provided the original author(s) and source are credited.

## References

1. Hill JO. Understanding and addressing the epidemic of obesity: an energy balance perspective. *Endocr Rev.* 2006;27(7):750–61.
2. Boden G. Interaction between free fatty acids and glucose metabolism. *Curr Opin Clin Nutr Metab Care.* 2002;5(5):545–9.
3. Cnop M. Fatty acids and glucolipotoxicity in the pathogenesis of type 2 diabetes. *Biochem Soc Trans.* 2008;36(Pt 3):348–52.
4. Eguchi K, Manabe I, Oishi-Tanaka Y, Ohsugi M, Kono N, Ogata F, et al. Saturated fatty acid and TLR signaling link beta cell dysfunction and islet inflammation. *Cell Metab.* 2012;15(4):518–33.
5. Erridge C, Samani NJ. Saturated fatty acids do not directly stimulate Toll-like receptor signaling. *Arterioscler Thromb Vasc Biol.* 2009;29(11):1944–9.
6. Maloney E, Sweet IR, Hockenberry DM, Pham M, Rizzo NO, Tateya S, et al. Activation of NF-kappaB by palmitate in endothelial cells: a key role for NADPH oxidase-derived superoxide in response to TLR4 activation. *Arterioscler Thromb Vasc Biol.* 2009;29(9):1370–5.
7. Akira S, Uematsu S, Takeuchi O. Pathogen recognition and innate immunity. *Cell.* 2006;124(4):783–801.
8. Kusminski CM, Shetty S, Orci L, Unger RH, Scherer PE. Diabetes and apoptosis: lipotoxicity. *Apoptosis.* 2009;14(12):1484–95.

9. Manoussakis MN, Kapsogeorgou EK. The role of epithelial cells in the pathogenesis of Sjogren's syndrome. *Clin Rev Allergy Immunol*. 2007;32(3):225–30.
10. Minges Wols HA, Underhill GH, Kansas GS, Witte PL. The role of bone marrow-derived stromal cells in the maintenance of plasma cell longevity. *J Immunol*. 2002;169(8):4213–21.
11. Anaya JM, Talal N. Sjogren's syndrome comes of age. *Semin Arthritis Rheum*. 1999;28(6):355–9.
12. Fox RI, Kang HI, Ando D, Abrams J, Pisa E. Cytokine mRNA expression in salivary gland biopsies of Sjogren's syndrome. *J Immunol*. 1994;152(11):5532–9.
13. Sekiguchi M, Iwasaki T, Kitano M, Kuno H, Hashimoto N, Kawahito Y, et al. Role of sphingosine 1-phosphate in the pathogenesis of Sjogren's syndrome. *J Immunol*. 2008;180(3):1921–8.
14. Ajibade AA, Wang Q, Cui J, Zou J, Xia X, Wang M, et al. TAK1 negatively regulates NF- $\kappa$ B and p38 MAP kinase activation in Gr-1 + CD11b + neutrophils. *Immunity*. 2012;36(1):43–54.
15. Haneji N, Nakamura T, Takio K, Yanagi K, Higashiyama H, Saito I, et al. Identification of alpha-fodrin as a candidate autoantigen in primary Sjogren's syndrome. *Science*. 1997;276(5312):604–7.
16. Miyazaki K, Takeda N, Ishimaru N, Omotehara F, Arakaki R, Hayashi Y. Analysis of in vivo role of alpha-fodrin autoantigen in primary Sjogren's syndrome. *Am J Pathol*. 2005;167(4):1051–9.
17. Goldman JA, Julian EH. Pseudo-Sjogren syndrome with hyperlipoproteinemia. *JAMA*. 1977;237(15):1582–4.
18. Kaltreider HB, Talal N. Bilateral parotid gland enlargement and hyperlipoproteinemia. *JAMA*. 1969;210(11):2067–70.
19. Robinson CP, Yamachika S, Alford CE, Cooper C, Pichardo EL, Shah N, et al. Elevated levels of cysteine protease activity in saliva and salivary glands of the nonobese diabetic (NOD) mouse model for Sjogren syndrome. *Proc Natl Acad Sci U S A*. 1997;94(11):5767–71.
20. Kang JH, Lin HC. Comorbidities in patients with primary Sjogren's syndrome: a registry-based case-control study. *J Rheumatol*. 2010;37(6):1188–94.
21. Ramos-Casals M, Brito-Zeron P, Siso A, Vargas A, Ros E, Bove A, et al. High prevalence of serum metabolic alterations in primary Sjogren's syndrome: influence on clinical and immunological expression. *J Rheumatol*. 2007;34(4):754–61.
22. Cousin SP, Hugl SR, Wrede CE, Kajio H, Myers Jr MG, Rhodes CJ. Free fatty acid-induced inhibition of glucose and insulin-like growth factor I-induced deoxyribonucleic acid synthesis in the pancreatic beta-cell line INS-1. *Endocrinology*. 2001;142(1):229–40.
23. Shirasuna K, Sato M, Miyazaki T. A neoplastic epithelial duct cell line established from an irradiated human salivary gland. *Cancer*. 1981;48(3):745–52.
24. Yanagawa T, Hayashi Y, Nagamine S, Yoshida H, Yura Y, Sato M. Generation of cells with phenotypes of both intercalated duct-type and myoepithelial cells in human parotid gland adenocarcinoma clonal cells grown in athymic nude mice. *Virchows Arch B Cell Pathol Incl Mol Pathol*. 1986;51(3):187–95.
25. Shikama Y, Kuroishi T, Nagai Y, Iwakura Y, Shimauchi H, Takada H, et al. Muramyldipeptide augments the actions of lipopolysaccharide in mice by stimulating macrophages to produce pro-IL-1 $\beta$  and by down-regulation of the suppressor of cytokine signaling 1 (SOCS1). *Innate Immun*. 2011;17(1):3–15.
26. Lin CL, Huang HC, Lin JK. Theaflavins attenuate hepatic lipid accumulation through activating AMPK in human HepG2 cells. *J Lipid Res*. 2007;48(11):2334–43.
27. Maestre I, Jordan J, Calvo S, Reig JA, Cena V, Soria B, et al. Mitochondrial dysfunction is involved in apoptosis induced by serum withdrawal and fatty acids in the beta-cell line INS-1. *Endocrinology*. 2003;144(1):335–45.
28. Shikama Y, Ishimaru N, Kudo Y, Bando Y, Aki N, Hayashi Y, et al. Effects of free fatty acids on human salivary gland epithelial cells. *J Dent Res*. 2013;92(6):540–6.

## Chapter 19

# Effects of Carbon Addition on Mechanical Properties and Microstructures of Ni-Free Co–Cr–W-Based Dental Alloys

Kenta Yamanaka, Manami Mori, and Akihiko Chiba

**Abstract** We investigated the effects of carbon concentration on the microstructures and tensile properties of Ni-free Co–29Cr–9W–1Si–C (mass%) alloys used as disk materials in dental technology based on computer-aided design and computer-aided manufacturing (CAD/CAM). The alloy specimens, which contained carbon in different concentrations, were prepared by conventional casting. The precipitates changed from intermetallic compounds in the low-carbon alloys, e.g., the  $\sigma$  and Laves phases, to  $M_{23}C_6$ -type carbide ( $M$ : metal) with increasing bulk carbon concentration.  $M_{23}C_6$  dramatically enhanced the 0.2 % proof stress, which then gradually increased with increasing carbon content in the alloys. The elongation-to-failure also increased with increasing carbon content. The coarse  $M_{23}C_6$  particles formed by higher concentrations of carbon were detrimental to ductility, however, and a maximum elongation-to-failure was obtained at a carbon concentration of ~0.1 mass%. In addition, we applied hot-deformation processing to the cast-alloy specimens and revealed that compared to as-cast alloys, the hot-rolled alloys with added carbon showed an excellent combination of high strength and high ductility. The current study can thus aid in the design of biomedical, carbon-containing, Co–28Cr–9W–1Si-based alloys.

**Keywords** Biomedical Co–Cr–W alloy • Carbon addition • Mechanical properties • Microstructures • Precipitation

---

K. Yamanaka (✉) • A. Chiba

Institute for Materials Research, Tohoku University, 2-1-1 Katahira, Aoba-ku,  
Sendai 980-8577, Japan

e-mail: [k\\_yamanaka@imr.tohoku.ac.jp](mailto:k_yamanaka@imr.tohoku.ac.jp)

M. Mori

Department of Materials and Environmental Engineering, Sendai National College  
of Technology, 48 Nodayama, Medeshima-Shiote, Natori 981-1239, Japan

## 19.1 Introduction

Computer-aided design and computer-aided manufacturing (CAD/CAM) have been accepted in dentistry as advanced techniques that accelerate the production of dental restorations. Although several methods have been introduced, CAD/CAM facilitate rapid, low-cost, and precise fabrication of custom-made dental restorations for patients. In particular, CAD/CAM-based milling [1–3] produces dental restorations from block disks or pellets of ceramics, composite resins, or metallic materials. An all-ceramic system is currently a primary choice, although zirconia-based ceramic materials commonly used in restorative applications have poorer milling performance than metallic materials. In contrast, metal–ceramic systems show a good combination of aesthetics, mechanical rigidity, and machinability owing to the ceramic veneer and metallic framework [3, 4]. For example, Co–Cr alloys are suitable restorative materials because they have excellent corrosion resistance and their components are less expensive than those of conventionally used Au-based alloys.

Recently, extensive research and development have been conducted on high-strength Co–Cr-based dental alloys [5–7]. This may be partly because their higher strength basically yields higher fatigue strength, which then improves the mechanical reliability of restorations that are subjected to occlusal forces. In addition, materials used in this application should consist of small grains because chipping failure occurs in machined components with coarse grain structures, reducing the precision of the fit of a restoration. Thus, a grain-refinement process is necessary to improve the fatigue strength, mechanical reliability, and machinability. Although a high-strength Co–Cr–W-based alloy that meets ISO 22674 Type 5 (yield stresses higher than 500 MPa [8]) requirements has been commercialized, it is made by utilizing powder metallurgy, which is generally a high-cost process.

We have recently proposed a strategy for designing a new class of Ni-free Co–Cr–W-based alloys with excellent mechanical properties [9–14]. By employing thermodynamic calculations, we examined the alloying elements, namely, Si and C, to modify and further strengthen the commercial Co–28Cr–9W (mass%) alloy [9]. In particular, this review reports the effects of carbon on the relationship between the microstructures and mechanical properties of Ni-free Co–Cr–W-based alloys [9–12]. In addition to systematically investigating the carbon-concentration-dependence of the phase distributions, precipitates, and tensile properties of the alloys, we carried out a preliminary evaluation of the effects of thermomechanical processing to further improve the alloys' mechanical performance.

## 19.2 Effects of Carbon on Microstructural Evolution

### 19.2.1 Phase Diagram of Co–28Cr–9W–1Si–C System

The equilibrium constituent phases were investigated using Thermo-Calc software. Figure 19.1 shows a vertical section of the calculated phase diagram of the Co–28Cr–9W–1Si–xC ( $0 \leq x \leq 0.3$ , mass%) system [11]. The face-centered-cubic (fcc)  $\gamma$  phase is stable in the high-temperature region above  $\sim 1,150$  K, while the equilibrium-matrix phase at lower temperatures and ultimately room temperature is the  $\epsilon$  phase with hexagonal close-packed structures. The thermodynamic calculation also suggests that increasing carbon concentration suppresses the formation of the  $\sigma$  phase and replaces it with the Laves phase, while further carbon addition leads to the formation of  $M_{23}C_6$ -type carbide.

### 19.2.2 Refinement of Solidification Microstructures by Carbon Addition [10]

The changes in solidification microstructures resulting from carbon addition in the Co–Cr–W-based alloys were investigated experimentally for a wide range of carbon concentrations [10]. Four kinds of Co–28Cr–9W–1Si–xC (mass%) alloys, where  $x = 0.005$ – $0.33$ , were prepared in a high-frequency induction furnace in an argon atmosphere.

Figure 19.2 shows maps of the inverse pole figure (IPF) obtained by measuring the electron-backscatter diffraction (EBSD) of the as-cast Co–28Cr–9W–1Si–xC alloy specimens with different carbon content. The cellular dendritic microstructures were almost in the  $\gamma$  phase in all of the specimens, although the carbon

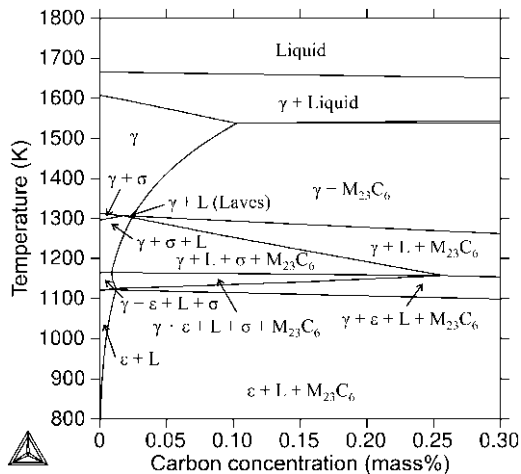


**Fig. 19.1** Vertical section of calculated phase diagram of Co–28Cr–9W–1Si–xC (mass%,  $0 \leq x \leq 0.3$ ) system obtained using Thermo-Calc software [11]

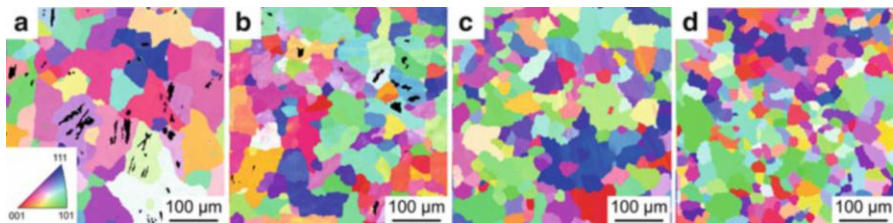
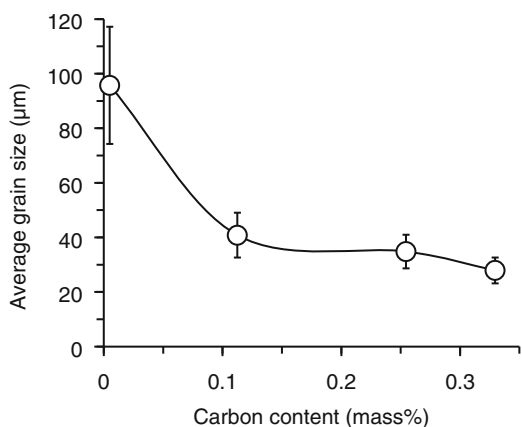


**Fig. 19.2** IPF maps of as-cast alloys with carbon concentrations of (a) 0.005, (b) 0.11, (c) 0.25, and (d) 0.33 mass% [10]

**Fig. 19.3** Average grain sizes of as-cast alloys as a function of carbon content [10]



addition stabilized the  $\gamma$  phase (the black area in Fig. 19.2 corresponds to the  $\epsilon$  phase). Increasing the carbon concentration from 0.005 to 0.33 mass% decreased the grain size from  $\sim 100 \mu\text{m}$  to  $\sim 30 \mu\text{m}$  (Fig. 19.3).

The mechanism of how carbon addition reduced the grain size of the cast microstructures was revealed by scanning electron microscopy (SEM) and electron probe microanalysis (EPMA). Figure 19.4 shows SEM backscattered-electron (SEM-BSE) images and the corresponding EPMA elemental maps of the as-cast alloy specimens. These figures clearly indicate solidification segregation of Cr, W, Si, and C, while Co was depleted in the interdendritic regions. The increase in bulk carbon concentration enhanced such inhomogeneous elemental distributions. Although the intermetallic compounds, in particular the  $\sigma$  phase, were identified in the low-carbon alloys [11], carbon-rich precipitates were clearly identified in the intergranular regions, especially when the carbon concentration was higher than 0.1 mass% (see the C maps in Fig. 19.4). The interdendritic precipitates in the high-carbon alloys corresponded to  $\text{M}_{23}\text{C}_6$  in the high-carbon alloys [10, 11], which agrees well with the calculated phase diagram (Fig. 19.1). Figure 19.5 shows the relationship between the area fraction of the precipitates, which was analyzed using the BSE maps in Fig. 19.4, and the bulk carbon concentration in each alloy; the amount of the precipitates increased with increasing carbon concentration.

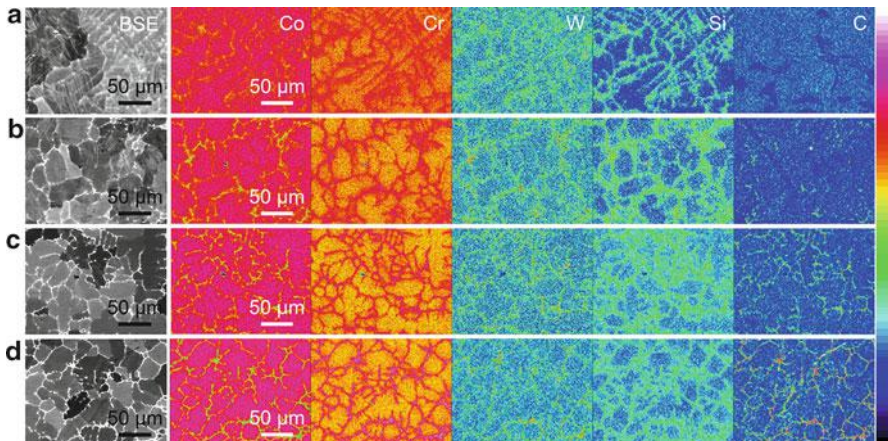
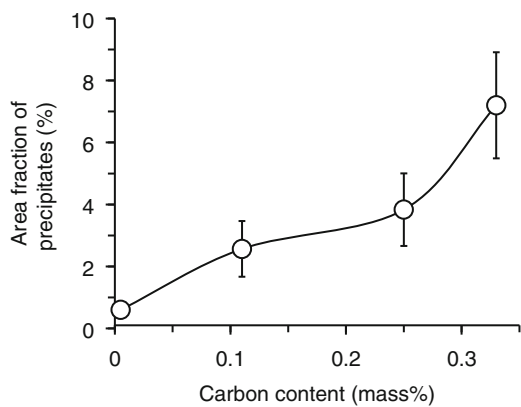


**Fig. 19.4** SEM-BSE images and corresponding EPMA elemental maps of as-cast alloys with carbon concentrations of (a) 0.005, (b) 0.11, (c) 0.25, and (d) 0.33 mass% [10]

**Fig. 19.5** Area fraction of precipitates of as-cast alloys as a function of carbon concentration [10]



These results indicate that the segregation and resulting precipitation of the carbide phase refined the solidification microstructures.

### 19.2.3 Effect of Hot-Deformation Processing on Microstructures [12]

We then prepared hot-rolled Co–28Cr–9W–1Si–C alloys with carbon concentrations up to 0.33 mass% to investigate the effect of hot-deformation processing on the microstructural evolution. The cast ingots were subjected to a homogenizing heat treatment at 1,473 K for 21.6 ks (6 h) and then directly processed by multi-pass

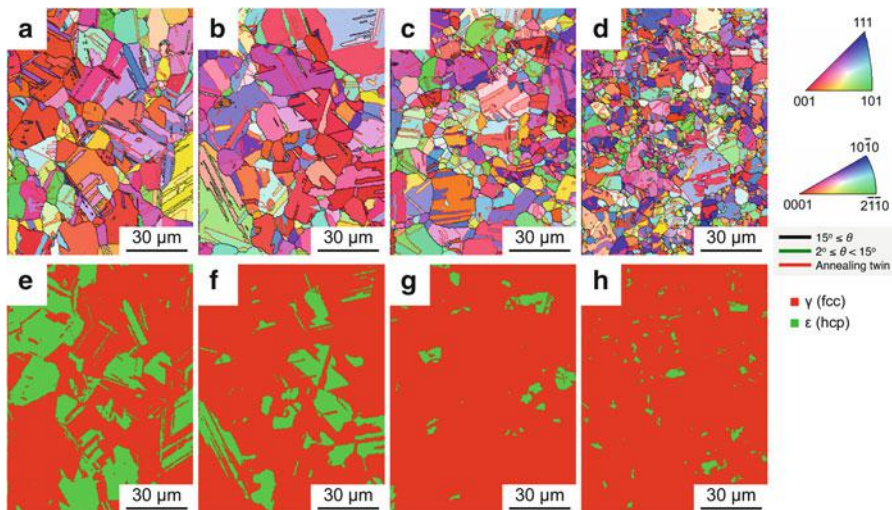


**Fig. 19.6** (a–d) IPF maps and (e–h) phase maps of hot-rolled alloys with carbon concentrations of (a, e) 0.02, (b, f) 0.05, (c, g) 0.11, and (d, h) 0.33 mass% [12]

**Table 19.1** Average  $\gamma$  grain sizes and fractions of  $\epsilon$  martensite of hot-rolled Co–28Cr–9W–1Si–C alloys with different carbon concentrations [12]

Carbon content (mass%)	$\gamma$ grain size ( $\mu\text{m}$ )	Fraction of $\epsilon$ martensite (%)
0.02	24.6	30.9
0.05	26.1	11.5
0.11	16.8	4.9
0.33	12.7	3.8

hot-caliber rolling (initial temperature: 1,473 K;  $\varphi$ : 15 mm → 9.6 mm), followed by water quenching.

The microstructures of the hot-rolled alloy specimens were investigated by EBSD analysis. The IPF maps in Fig. 19.6a–d reveal fully equiaxed  $\gamma$  grain structures with a considerable number of annealing twins. Table 19.1 shows that the average  $\gamma$  grain sizes decreased after hot rolling and further decreased as carbon was added. The phase maps in Fig. 19.6e–h suggest that these were duplex grain structures consisting of the  $\gamma$  and  $\epsilon$  phases (the fraction of the  $\epsilon$  phase is also shown in Table 19.1). We believe the plate-like  $\epsilon$  phase formed during cooling after hot rolling (i.e., athermal martensitic transformation), and its fraction decreased with increasing carbon concentration, as confirmed in the as-cast alloys.

Figure 19.7 shows the SEM-BSE images of the hot-rolled alloys. Very fine precipitates (0.01–1  $\mu\text{m}$  in diameter) were identified in all of the hot-rolled alloys; they were enriched with tungsten, as shown by their bright contrast in the SEM-BSE images. Figure 19.8a–d show transmission electron microscopy (TEM) bright-field images of the submicron-sized precipitates observed in the low-carbon

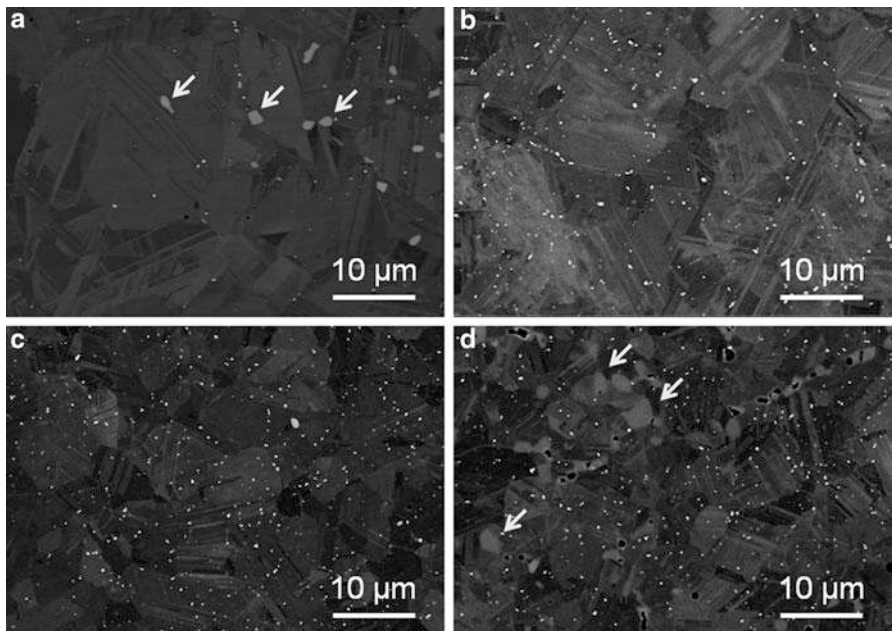


**Fig. 19.7** SEM-BSE images of hot-rolled alloys with carbon concentrations of (a, e) 0.02, (b, f) 0.05, (c, g) 0.11, and (d, h) 0.33 mass% [12]

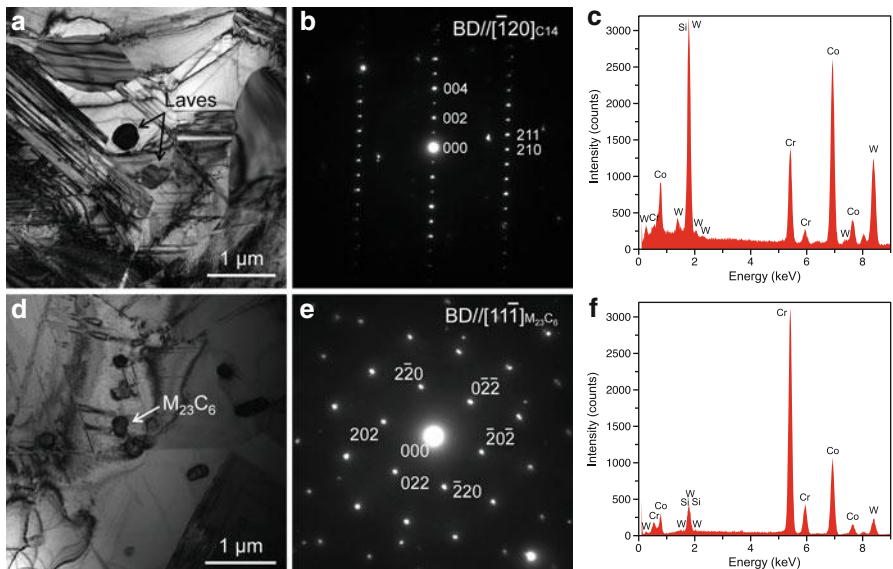


**Fig. 19.8** TEM bright-field image of hot-rolled (a) Co-28Cr-9W-1Si-0.02C alloy and (d) Co-28Cr-9W-1Si-0.33C alloy. The SAD patterns obtained from the precipitates in (a) and (d) are shown in (b) and (e), respectively. The corresponding EDS spectra of the precipitates in (a) and (b) are shown in (c) and (f), respectively [12]

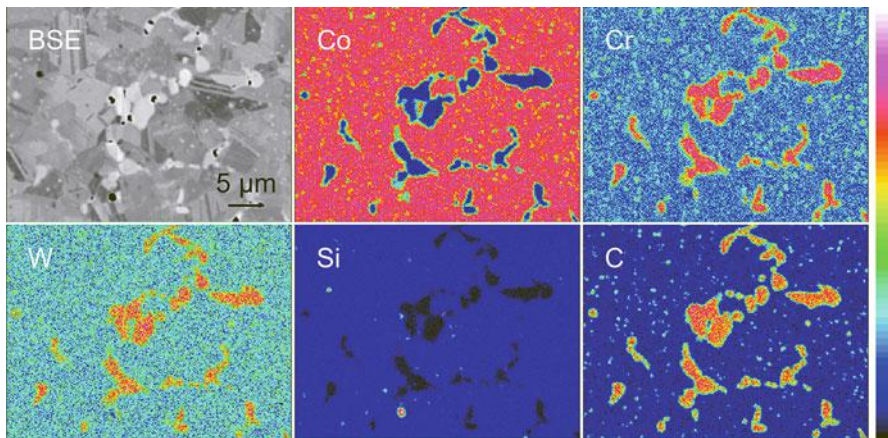


**Fig. 19.9** SEM-BSE image and EPMA elemental maps of hot-rolled Co–28Cr–9W–1Si–0.33C alloy [12]

(0.02 mass%) and high-carbon (0.33 mass%) alloys, respectively. The corresponding selected-area diffraction (SAD) pattern obtained for each precipitate, revealed to be the C14-Laves phase and  $M_{23}C_6$ , is shown in Fig. 19.8b, e, respectively. The TEM and energy-dispersive X-ray spectroscopy (TEM-EDS) analyses confirmed that both the Laves-phase and carbide particles were enriched with W and Si (Fig. 19.8c, f). In addition, the particles whose diameters were approximately 2–5  $\mu\text{m}$  are shown in Fig. 19.7a and coarse gray particles can also be seen in Fig. 19.7d (0.33 mass%), as indicated by arrows in each figure. Our previous study indicated that the particles formed in the low-carbon alloy are the  $\sigma$  phase [13]. On the other hand, Fig. 19.9 shows an SEM-BSE image and the corresponding EPMA elemental maps of the hot-rolled alloy with 0.33 mass% of carbon. The black particles in the image correspond to  $\text{SiO}_2$  or  $\text{Cr}_2\text{O}_3$  inclusions, which were also observed in other specimens and were not related to the carbon addition. The precipitates with diameters of a few micrometers were enriched with Cr, W, and C but were depleted of Co and Si. Therefore, we believe that these precipitates were  $M_{23}C_6$ . It should also be noted that the matrix phase exhibited a homogeneous elemental distribution similar to that obtained by powder metallurgy.

The obtained results indicate that the microstructures of the as-cast and hot-rolled, carbon-doped, Co–Cr–W-based dental alloys are in good agreement with those predicted by thermodynamic calculations. Adding carbon to this alloy system tended to stabilize the  $\gamma$  matrix and cause the precipitation of  $M_{23}C_6$ , effectively reducing their grain size.

### 19.3 Effect of Carbon Concentration on Tensile Properties [11, 12]

Finally, we investigated the effect of carbon on room-temperature tensile properties of the as-cast and hot-rolled Co–28Cr–9W–1Si–C alloys.<sup>1</sup> All of the stress–strain curves obtained in tensile testing for both types of alloys showed uniform elongation followed by sudden fractures without macroscopic necking [11, 12]. This type of tensile deformation is typically observed in Co–Cr–Mo-based alloys [15–18].

Figure 19.10 summarizes the tensile properties as functions of carbon concentration. The 0.2 % proof stress of the as-cast alloys gradually increased with increasing carbon concentration. The strengthening effect, which was deduced from the slope of the plot of 0.2 % proof stress versus carbon concentration, was determined to be 623 MPa/mass% for alloys containing >0.04 mass% C. The cast alloys with carbon concentrations of 0.17 and 0.27 mass% showed strengths that were standardized to the Type 5 criteria in ISO 22674 for dental restorations (>500 MPa [8]). On the other hand, the 0.2 % proof stress of the hot-rolled alloys did not change significantly when ≤0.05 mass% C was added, but it began to increase when the carbon concentration exceeded ~0.1 mass%. The strengthening effect of carbon in the hot-rolled alloys was determined to be 822 MPa/mass% for alloys with >0.05 mass% C. Accordingly, a much higher yield stress (851 MPa) was obtained by adding 0.33 mass% C.

Our previous studies [9, 19] showed that solid-solution strengthening of carbon was negligible, as theoretically predicted; therefore, the precipitates would have

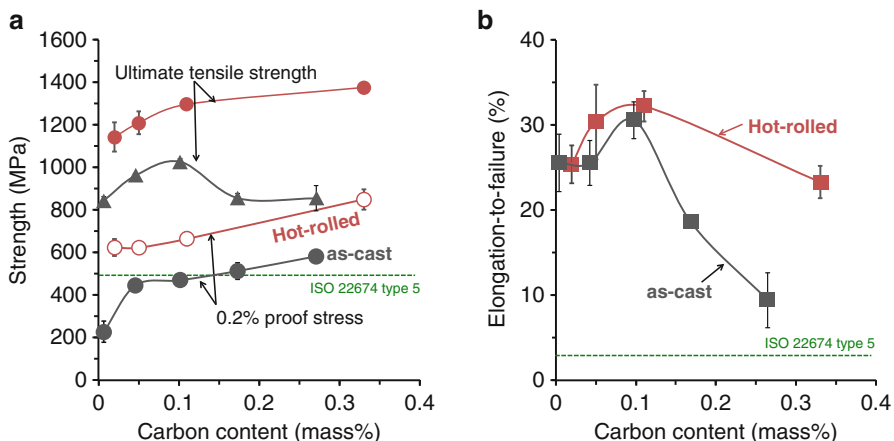


**Fig. 19.10** Tensile properties of Co–28Cr–9W–1Si–C alloys plotted as functions of carbon concentrations: (a) strength; (b) elongation-to-failure [11, 12]

<sup>1</sup> The casting and hot-rolling conditions are the same as those described in the previous sections.

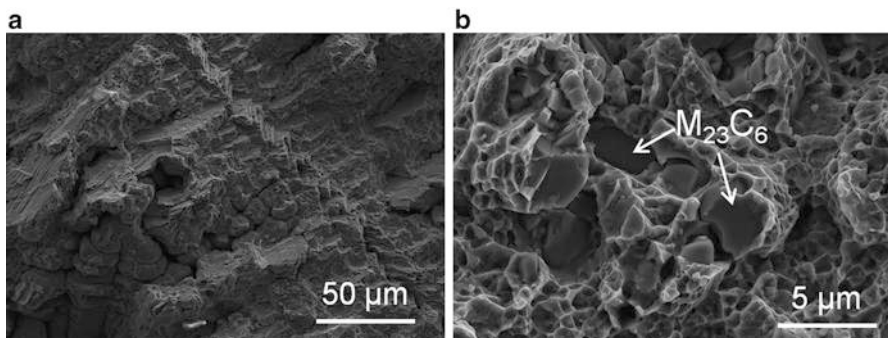


**Fig. 19.11** Fracture surfaces of (a) as-cast and (b) hot-rolled Co–28Cr–9W–1Si-based alloys with high carbon concentration (~0.3 mass%) [11, 12]

dominated the strengthening of the present alloys. The amount of  $M_{23}C_6$  precipitates that formed in the alloys, which varied with their carbon concentration (Fig. 19.5f), was actually consistent with the variations in the alloys' 0.2 % proof stress (Fig. 19.2a). Increasing the fraction of  $M_{23}C_6$  should have increased the strength of the alloys. The higher strength of the hot-rolled alloys than that of the as-cast counterparts partly originated from the precipitation size because finer precipitates dramatically increase the strength [20].

The elongation-to-failure of the as-cast and hot-rolled alloy specimens also showed similarly strong dependence on the carbon concentration (Fig. 19.10b): it increased initially, peaking at ~0.1 mass% C, and then gradually decreased with further increase in carbon concentration. Similar results were reported for Co–Cr–Mo-based alloys [19].

Figure 19.11 shows typical fracture surfaces of the tensile-tested specimens of the as-cast and hot-rolled alloys with high carbon content. The as-cast alloy (Fig. 19.11a) exhibited interdendritic fractures where carbide formed, and the  $\epsilon$ -martensite-related quasi-cleavage or intergranular fractures [15–18] were not dominant. The hot-rolled counterpart (Fig. 19.11b) showed  $M_{23}C_6$  particles on the fracture surface. Therefore, we conclude the fractures in the as-cast and hot-rolled tensile specimens were triggered by the coarse  $M_{23}C_6$  particles.

Until now, C-free Co–Cr–W-based alloys have been used for dental restorations. However, the current results revealed that the high-carbon-content alloys containing a considerable amount of  $M_{23}C_6$  still showed sufficient ductility even in the as-cast condition. Therefore, adding carbon to the alloys is a promising strategy for developing high-strength alloys that show acceptable tensile ductility. The hard Cr-rich  $M_{23}C_6$  carbide phase may deteriorate the milling properties and the corrosion resistance of the alloys, however. Thus, the optimal concentrations of carbon in the as-cast Co–28Cr–9W–1Si–C alloys were estimated to be just above 0.1 mass%. On the other hand, the hot-rolled alloys exhibited much better mechanical properties than those in the as-cast counterparts because homogeneous microstructures with fine precipitates were obtained. As the production cost is considered

to be not as significant as powder metallurgy, the hot-deformation processing is a potential route to fabricate disk materials for CAD/CAM-based milling applications.

## 19.4 Conclusions

We systematically investigated the effects of carbon on the room-temperature tensile properties and microstructures of dental Co–28Cr–9W–1Si alloys in as-cast condition and after thermomechanical processing. The microstructural development and tensile properties of alloys prepared under both processing conditions showed similar dependence on the carbon concentration, although the hot-rolled alloys showed much better mechanical properties. Adding carbon suppressed the formation of the hcp  $\epsilon$  martensite phase and stabilized the fcc  $\gamma$  phase. The  $\sigma$  phase was identified in the low-carbon-content alloys, but it was replaced by  $M_{23}C_6$  particles when the carbon concentration was increased. Adding carbon to the alloys dramatically strengthened them, and the 0.2 % proof stress of the alloys increased with increasing carbon concentration. However, the elongation-to-failure reached a maximum when the carbon concentration was ~0.1 mass% and then remarkably decreased with increasing carbon content thereafter. Therefore, the variation in tensile properties resulting from carbon addition to the alloys originated from the precipitation of  $M_{23}C_6$ .

**Acknowledgments** This research was financially supported by a Grant-in-Aid for JSPS Fellows; the Supporting Industry Program from the Ministry of Economy, Trade, and Industry (METI); and the Innovative Research for Biosis–Abiosis Intelligent Interface, Japan.

**Open Access** This chapter is distributed under the terms of the Creative Commons Attribution Noncommercial License, which permits any noncommercial use, distribution, and reproduction in any medium, provided the original author(s) and source are credited.

## References

1. Willer J, et al. Computer-assisted milling of dental restorations using a new CAD/CAM data acquisition system. *J Prosthet Dent.* 1998;80:346–53.
2. Beuer F, et al. High-strength CAD/CAM-fabricated veneering material sintered to zirconia copings—A new fabrication mode for all-ceramic restorations. *Dent Mater.* 2009;25:121–8.
3. Rekow ED. Dental CAD/CAM systems A 20-year success story. *J Am Dent Assoc.* 2006;137:5S–6S.
4. Roberts HW, et al. Metal–ceramic alloys in dentistry: a review. *J Prosthodont.* 2009;18:188–94.
5. Yoda K, et al. Effects of chromium and nitrogen content on the microstructures and mechanical properties of as-cast Co–Cr–Mo alloys for dental applications. *Acta Biomater.* 2012;8:2856–62.

6. Takaichi A, et al. Microstructures and mechanical properties of Co–29Cr–6Mo alloy fabricated by selective laser melting process for dental applications. *J Mech Behav Biomed Mater.* 2013;21:67–76.
7. Henriques B, et al. Microstructure, hardness, corrosion resistance and porcelain shear bond strength comparison between cast and hot pressed CoCrMo alloy for metal–ceramic dental restorations. *J Mech Behav Biomed Mater.* 2012;12:83–92.
8. ISO22674 (2006) Dentistry—Metallic materials for fixed and removable restorations and appliances. [http://www.iso.org/iso/home/store/catalogue\\_tc/catalogue\\_detail.htm?csnumber=36412](http://www.iso.org/iso/home/store/catalogue_tc/catalogue_detail.htm?csnumber=36412)
9. Yamanaka K, et al. Development of new Co–Cr–W-based biomedical alloys: effects of microalloying and thermomechanical processing on microstructures and mechanical properties. *Mater Des.* 2014;55:987–98.
10. Yamanaka K, et al. Refinement of solidification microstructures by carbon addition in biomedical Co–28Cr–9W–1Si alloys. *Mater Lett.* 2014;116:82–5.
11. Yamanaka K, et al. Effects of carbon concentration on microstructure and mechanical properties of as-cast nickel-free Co–28Cr–9W-based dental alloys. *Mater Sci Eng C.* 2014;40:127–34.
12. Yamanaka K, et al. Influence of carbon addition on mechanical properties and microstructures of Ni-free Co–28Cr–9W–1Si–C alloys subjected to thermomechanical processing. *J Mech Behav Biomed Mater.* 2014;37:274–85.
13. Yamanaka K, et al. Dynamic recrystallization of a biomedical Co–Cr–W-based alloy under hot deformation. *Mater Sci Eng A.* 2014;592:173–81.
14. Yamanaka K, et al. Effects of nitrogen on microstructural evolution of biomedical Co–Cr–W alloys during hot deformation and subsequent cooling. *Mater Des.* 2014;57:421–5.
15. Salinas-Rodriguez A, et al. Deformation behavior of low-carbon Co–Cr–Mo alloys for low-friction implant applications. *J Biomed Mater Res.* 1996;31:409–19.
16. Mori M, et al. Microstructures and mechanical properties of biomedical Co–29Cr–6Mo–0.14N alloys processed by hot rolling. *Metall Mater Trans A.* 2012;43:3108–19.
17. Yamanaka K, et al. Enhanced mechanical properties of as-forged Co–Cr–Mo–N alloys with ultrafine-grained structures. *Metall Mater Trans A.* 2012;43:5243–57.
18. Yamanaka K, et al. Effects of nitrogen addition on microstructure and mechanical behavior of Co–Cr–Mo alloys for orthopedic applications. *J Mech Behav Biomed Mater.* 2014;29:417–26.
19. Lee SH, et al. Effect of carbon addition on microstructure and mechanical properties of a wrought Co–Cr–Mo implant alloy. *Mater Trans.* 2006;47:287–90.
20. Asgar K, et al. Effect of microstructure on physical properties of cobalt-base alloys. *J Dent Res.* 1961;40:63–72.

# **Chapter 20**

## **Periodontal Disease as a Possible Risk Factor for Alzheimer's Disease**

**Naoyuki Ishida, Yuichi Ishihara, Kazuto Ishida, Hiroyuki Tada,  
Yoshiko Kato, Ryutaro Isoda, Makoto Hagiwara, Makoto Michikawa,  
Toshihide Noguchi, and Kenji Matsushita**

**Abstract** Periodontal disease is a localized infectious disease caused by periodontal disease-related bacteria, such as *Porphyromonas gingivalis*. Recently, Periodontal disease is known to cause systemic spread of chronic inflammation and exacerbate lifestyle-related diseases such as ischemic heart disease, diabetes mellitus, and obesity, while the inflammatory response plays a large role in the development of neurodegenerative conditions such as Alzheimer's disease (AD).

---

N. Ishida • Y. Kato

Department of Oral Disease Research, National Center for Geriatrics and Gerontology,  
35 Gengo Moriokamachi, Obu, Aichi 474-8511, Japan

Department of Periodontology School of Dentistry, Aichi-gakuin University,  
Aichi, Japan

Y. Ishihara • T. Noguchi

Department of Periodontology School of Dentistry, Aichi-gakuin University,  
Aichi, Japan

K. Ishida

Department of Physical Therapy, Graduate School of Medicine, Nagoya University,  
Aichi, Japan

H. Tada

Department of Oral Microbiology, Tohoku University Graduate School of Dentistry,  
Miyagi, Japan

R. Isoda • M. Hagiwara

Department of Oral Disease Research, National Center for Geriatrics and Gerontology,  
35 Gengo Moriokamachi, Obu, Aichi 474-8511, Japan

M. Michikawa

Department of Biochemistry, Graduate School of Medicine, Nagoya City University,  
Aichi, Japan

K. Matsushita (✉)

Department of Oral Disease Research, National Center for Geriatrics and Gerontology,  
35 Gengo Moriokamachi, Obu, Aichi 474-8511, Japan

Department of Geriatric Oral School, Tohoku University Graduate School of Dentistry,  
Miyagi, Japan

e-mail: [kmatsu30@ncgg.go.jp](mailto:kmatsu30@ncgg.go.jp)

Mild systemic inflammation has been reported to increase an individual's risk of AD. Inflammation has been thought to spread through the circulatory system and CNS. The increased amounts of inflammatory mediators in the blood are transmitted to the brain and may activate the microglia in the brain. Chronic inflammation in periodontal disease and periodontal disease-related bacteria are transmitted and spread to the brain via a certain mechanism, which might then exacerbate the AD. Periodontal infections are treatable, and thus this may be relevant for preventing and delaying the progression of AD. In this super-aging society, periodontal disease measures will become increasingly important.

**Keywords** Alzheimer's disease • Amyloid  $\beta$  protein • Chronic inflammation • Cognitive impairment • Lipopolysaccharide • *Porphyromonas gingivalis* • Proinflammatory cytokine • Senile plaque

## 20.1 Introduction

Rather than systemic diseases being the risk factors for periodontal disease, periodontal disease has been shown to cause systemic diseases, including lifestyle-related diseases. To date, periodontal disease has been reported as a risk factor for diabetes mellitus (DM), cardio- and cerebrovascular disease, aspiration pneumonia, premature and low birth weight infants, bacterial endocarditis, glomerulonephritis, arthritis, and palmoplantar pustulosis [1–5]. The following three pathways are assumed to be the mechanism of the systemic spread of periodontal disease: direct action of bacterial body and toxin of periodontal disease-related bacteria at the local periodontal site that spread to target organs through the hematogenous route or respiratory tract [4]; the action of inflammation-inducing substances such as cytokines, which are produced by the inflammatory response within periodontal tissue or immune response that spread hematogenously to the target organs [5]; and a pathway that results in intracerebral spread through the nervous system [6, 7]. There are various data on intravascular infiltration of periodontal disease-related bacteria and its spread to target organs thus far, but its mechanism of affecting diseases is not fully understood. On the other hand, the inflammatory response has been known to play a large role in the progression of cerebrovascular disorder and dementia, conditions that often occur in the elderly [8–10]; however, the effect of periodontal disease is not fully understood.

Taking other published studies into consideration, here we discuss our most recent analytical results of the correlation between periodontal disease and Alzheimer's disease (AD) in a mouse model in this study.

## 20.2 Current Status of AD in Japan

More than 30 million people in Japan are >65 years old. In a study group of the Ministry of Health, Labour and Welfare (2013), the number of patients with dementia was 4,620,000 people, while another four million people in the general population are estimated to have it. This number is expected to increase in the future. Among them, 60–70 % patients have AD, which becomes an urgent issue in an advancing aging society such as that in Japan. The current situation of AD involves the absence of an effective prevention method as well as a fundamental treatment method [11].

## 20.3 Inflammation and AD

In addition to aging and genetic mutation, AD is affected by accumulation of amyloid  $\beta$  protein ( $A\beta$ ) caused by intracerebral inflammation [12]. Further,  $A\beta$  deposits also cause inflammation, which results in the progression of synapse disorders and neuronopathy. In recent years, mutations of the *TREM2* gene, which controls the inflammatory response, has been found in patients with AD, renewing the importance of the inflammatory response in the development of AD [13]. Chronic inflammation is also thought to play an important role in the development of central nervous system (CNS) diseases. The long-term use of non-steroidal anti-inflammatory drugs is known to prevent the occurrence of neurodegenerative disease. Its effect in delaying the progression has been observed in an epidemiologic study and animal experiment [14]. The immune system of the CNS is extremely simple and is not acquired. Accordingly, the immune response is served by the innate immune system.

Microglia are cells of the macrophage system that possesses a phagocytic capacity that plays a central role in the intracerebral innate immune response. The microglia digest the accumulated  $A\beta$  in the brain and remove it from the brain. These cells produce cytokines such as active oxygen, interleukin (IL)-1, IL-6, tumor necrosis factor- $\alpha$  (TNF- $\alpha$ ), i.e., inflammatory response promoting molecules that are known to promote neurodegeneration in AD [15, 16]. On the other hand, they also produce anti-inflammatory molecules such as IL-4 and IL-10, which are thought to provide a neuroprotective role in addition to controlling the inflammatory response [17]. Therefore, microglia are important cells in the control of AD status.

Separately from the exacerbation of AD status due to intracerebral inflammation, mild systemic inflammation has been reported to reduce cognitive function and hippocampal capacity and increase the risk of AD [18–20]. Inflammation has been thought to spread through the circulatory system and CNS. The increased amounts of inflammatory mediators in the blood are transmitted to the brain and may activate the microglia in the brain. The TNF- $\alpha$  level is increased in the blood of patients with AD and reportedly correlates with reduced cognitive function [21, 22].

## 20.4 Periodontal Disease and AD

As mentioned earlier, chronic inflammation within peripheral organs might play a role in the exacerbation of the molecular pathogenesis of AD. One such inflammatory condition is periodontal disease. The inflammatory response that occurs in periodontal disease has been known to involve the development of various diseases, such as arteriosclerotic disease, DM, and obesity, and the incidence of premature and low birth weight infants [1–5, 23, 24]. In addition, periodontal disease has been reported to involve cerebral abscess formation [25]. Periodontal disease-related bacteria are spread systemically through the blood vessels and respiratory tract, suggesting its possible direct effect on the target organs. In addition, inflammatory mediators such as cytokines, which are produced in the local periodontal tissue, are carried hematogenously to the target organ and thought to worsen the inflammatory response.

There have been interesting reports on the correlation between AD and periodontal disease. *Porphyromonas gingivalis*, a periodontal disease-related bacteria, was found at high frequency in the autopsied brain tissue of patients who died of AD; however, it is not found in normal human brain tissue [26]. This result suggests that said bacteria spread hematogenously into the brain. *P. gingivalis* is a gram-negative anaerobic bacillus that possesses various toxins including lipopolysaccharide. Accordingly, it is known to cause a strong inflammatory response. In addition, the interesting finding is that a periodontal disease-related bacteria of the *Treponema* genus was found in the trigeminal ganglion, brainstem, and cerebral cortex; its frequency is said to be high in patients with AD in particular [6]. This finding suggests that periodontal disease-related bacteria can be directly transmitted into the brain and cause inflammation. The mechanism (hypothesis) of AD exacerbation due to periodontal disease is explained in Fig. 20.1. It will be important to analyze its detailed mechanism in the future. However, it is difficult to believe that AD is induced only by an inflammatory response due to periodontal disease and periodontal disease-related bacteria. Inflammatory responses are thought to aggravate the molecular level of AD, cause an earlier onset, worsen the degree of cognitive disorders, and cause faster progression, suggesting its action in modifying the disease status. The long-term use of anti-inflammatory drugs has been suggested to reduce the risk of AD onset [27].

Periodontal disease is the main cause of tooth loss; however, some reports have identified a correlation between tooth loss and AD. Tooth loss may be a risk factor for AD [28, 29]. Tooth loss reduces chewing function, which results in reduced cerebral blood flow and might lead to reduced cognitive function. However, tooth loss itself often does not accompany chronic inflammatory response, which suggests that the effects of tooth loss are not necessarily identical to those of periodontal disease. Oue et al. found that cognitive function was reduced by tooth removal in APP transgenic mice, but there was no effect on the molecular pathology of AD [30]. On the other hand, when we induced periodontal disease in the same mouse, we found that intracerebral A $\beta$  deposits increased and the intracerebral

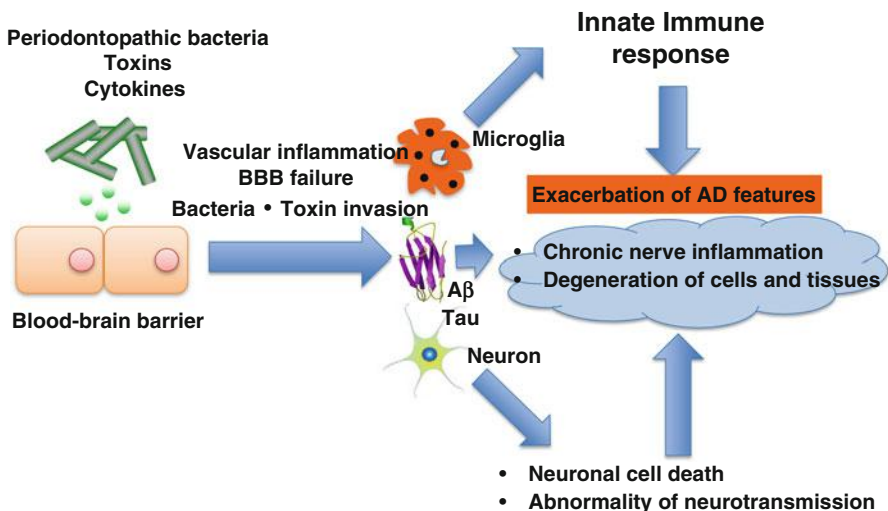


**Fig. 20.1** Possible mechanisms by which periodontitis induced by bacterial infection exacerbates features of Alzheimer's disease

inflammatory response was enhanced in addition to the reduced cognitive function. Both periodontal disease and tooth loss reduce cognitive function, but their molecular mechanisms are thought to differ.

## 20.5 Conclusion

All organisms survive by consuming food; the chewing function is therefore very important. This function not only supports life but could be important to the maintenance of cognitive function. In this modern aging society, preventing periodontal disease and maintaining oral cavity function will become increasingly more important.

**Open Access** This chapter is distributed under the terms of the Creative Commons Attribution Noncommercial License, which permits any noncommercial use, distribution, and reproduction in any medium, provided the original author(s) and source are credited.

## References

- Chapple IL, Genco R. Working group 2 of joint EFP/AAP. Diabetes and periodontal diseases: consensus report of the Joint EFP/AAP workshop on periodontitis and systemic diseases. *J Clin Periodontol*. 2013;40 Suppl 14:S106–12.
- Cullinan MP, Seymour GJ. Periodontal disease and systemic illness: will the evidence ever be enough? *Periodontol 2000*. 2013;62(1):271–86.

3. Linden GJ, Herzberg MC. Working group 4 of the joint EFPAAPW. Periodontitis and systemic diseases: a record of discussions of working group 4 of the Joint EFP/AAP workshop on periodontitis and systemic diseases. *J Periodontol.* 2013;84(4 Suppl):S20–3.
4. Reyes L, Herrera D, Kozarov E, Rolda S, Progulske-Fox A. Periodontal bacterial invasion and infection: contribution to atherosclerotic pathology. *J Periodontol.* 2013;84(4 Suppl):S30–50.
5. Schenck HA, Loos BG. Inflammatory mechanisms linking periodontal diseases to cardiovascular diseases. *J Clin Periodontol.* 2013;40 Suppl 14:S51–69.
6. Riviere GR, Riviere KH, Smith KS. Molecular and immunological evidence of oral Treponema in the human brain and their association with Alzheimer's disease. *Oral Microbiol Immunol.* 2002;17(2):113–8.
7. Kamer AR. Systemic inflammation and disease progression in Alzheimer disease. *Neurology.* 2010;84(14):1157. author reply –8.
8. Galea J, Brough D. The role of inflammation and interleukin-1 in acute cerebrovascular disease. *J Inflamm Res.* 2013;6:121–8.
9. Liu L, Chan C. The role of inflammasome in Alzheimer's disease. *Ageing Res Rev.* 2014;15C:6–15.
10. Serpente M, Bonsi R, Scarpini E, Galimberti D. Innate immune system and inflammation in Alzheimer's disease: from pathogenesis to treatment. *Neuroimmunomodulation.* 2014;21(2–3):79–87.
11. Fettelschoss A, Zabel F, Bachmann MF. Vaccination against Alzheimer disease: An update on future strategies. *Hum Vaccin Immunother.* 2014;10(4):847.
12. Shankar GM, Li S, Mehta TH, Garcia-Munoz A, Shepardson NE, Smith I, et al. Amyloid-beta protein dimers isolated directly from Alzheimer's brains impair synaptic plasticity and memory. *Nat Med.* 2008;14(8):837–42.
13. Jonsson T, Stefansson H, Steinberg S, Jónsdóttir I, Jonsson PV, Snaedal J, et al. Variant of TREM2 associated with the risk of Alzheimer's disease. *N Engl J Med.* 2013;368(2):107–16.
14. Cudaback E, Jorstad NL, Yang Y, Montine TJ, Keene CD. Therapeutic implications of the prostaglandin pathway in Alzheimer's disease. *Biochem Pharmacol.* 2014;88(4):565–72.
15. Akiyama H, Arai T, Kondo H, Tanno E, Haga C, Ikeda K. Cell mediators of inflammation in the Alzheimer disease brain. *Alzheimer Dis Assoc Disord.* 2000;14 Suppl 1:S47–53.
16. Ridolfi E, Barone C, Scarpini E, Galimberti D. The role of the innate immune system in Alzheimer's disease and frontotemporal lobar degeneration: an eye on microglia. *Clin Dev Immunol.* 2013;2013:939786.
17. Kloss CU, Kreutzberg GW, Raivich G. Proliferation of ramified microglia on an astrocyte monolayer: characterization of stimulatory and inhibitory cytokines. *J Neurosci Res.* 1997;49(2):248–54.
18. Marsland AL, Gianaros PJ, Abramowitch SM, Manuck SB, Hariri AR. Interleukin-6 covaries inversely with hippocampal grey matter volume in middle-aged adults. *Biol Psychiatry.* 2008;64(6):484–90.
19. Engelhart MJ, Geerlings MI, Meijer J, Kiliaan A, Ruitenberg A, van Swieten JC, et al. Inflammatory proteins in plasma and the risk of dementia: the rotterdam study. *Arch Neurol.* 2004;61(5):668–72.
20. Tobinick EL. Re: inflammatory markers and the risk of Alzheimer disease: the Framingham Study. *Neurology.* 2008;70(14):1222–3. author reply 3.
21. Alvarez A, Cacabelos R, Sanpedro C, Garcia-Fantini M, Aleixandre M. Serum TNF-alpha levels are increased and correlate negatively with free IGF-I in Alzheimer disease. *Neurobiol Aging.* 2007;28(4):533–6.
22. Holmes C, Cunningham C, Zotova E, Woolford J, Dean C, Kerr S, et al. Systemic inflammation and disease progression in Alzheimer disease. *Neurology.* 2009;73(10):768–74.
23. Genco RJ, Borgnakke WS. Risk factors for periodontal disease. *Periodontol 2000.* 2013;62(1):59–94.
24. Linden GJ, Lyons A, Scannapieco FA. Periodontal systemic associations: review of the evidence. *J Periodontol.* 2013;84(4 Suppl):S8–19.

25. Zijlstra EE, Swart GR, Godfroy FJ, Degener JE. Pericarditis, pneumonia and brain abscess due to a combined *Actinomyces*-*Actinobacillus actinomycetemcomitans* infection. *J Infect.* 1992;25(1):83–7.
26. Poole S, Singhrao SK, Kesavulu L, Curtis MA, Crean S. Determining the presence of periodontopathic virulence factors in short-term postmortem Alzheimer's disease brain tissue. *J Alzheimers Dis.* 2013;36(4):665–77.
27. Heneka MT, Kummer MP, Weggen S, Bulic B, Multhaup G, Munter L, et al. Molecular mechanisms and therapeutic application of NSAIDs and derived compounds in Alzheimer's disease. *Curr Alzheimer Res.* 2011;8(2):115–31.
28. Kondo K, Niino M, Shido K. A case-control study of Alzheimer's disease in Japan—significance of life-styles. *Dementia.* 1994;5(6):314–26.
29. Gatz M, Mortimer JA, Fratiglioni L, Johansson B, Berg S, Reynolds CA, et al. Potentially modifiable risk factors for dementia in identical twins. *Alzheimer's Dement.* 2006;2(2):110–7.
30. Oue H, Miyamoto Y, Okada S, Koretake K, Jung CG, Michikawa M, et al. Tooth loss induces memory impairment and neuronal cell loss in APP transgenic mice. *Behav Brain Res.* 2013;252:318–25.

# **Chapter 21**

## **Measurement of Skin Elasticity Using High Frequency Ultrasound Elastography with Intrinsic Deformation Induced by Arterial Pulsation**

**Ryo Nagaoka, Kazuto Kobayashi, and Yoshifumi Saito**

**Abstract** Mechanical property of the skin is one of the important factors for diagnosis of human skin diseases. In this paper, we proposed a novel method for estimation of shear wave velocity from deformation induced by an arterial pulsation. The induced deformation was measured by high frequency ultrasound. The elasticity of the *in vivo* human skin is evaluated based on the calculated parameters. P(VDF-TrFE) transducer with the central frequency of 100 MHz was used for imaging. The aperture diameter of the transducer was 2 mm, and the focal length was 4 mm. The repetition rate was 2,600 Hz. The sampling rate was 1 GS/s with 8 bit. The velocity induced by pulsation was measured by 1-D cross-correlation method at each depth. The shear wave velocity was estimated from the measured velocity. The shear wave velocity at the epidermis was 0.14 m/s, and the velocity at the dermis was 0.06 m/s. Because the stiffness of the skin was proportional to the shear wave velocity, the elasticity of the epidermis was higher than that of the dermis. These estimated elasticity well conformed to the histology of the skin and the past reports.

**Keywords** Elasticity • High frequency Ultrasound • Shear wave velocity • Skin

### **21.1 Introduction**

Mechanical properties of human skin are the important factors not only in medicine field but also in cosmetic field. Especially, viscoelasticity of human skin is closely related to collagen and elastin of human skin. Also, it's considered that the

---

R. Nagaoka (✉) • Y. Saito

Graduate School of Biomedical Engineering, Tohoku University, 2-1, Seiryo-machi,  
Aoba-ku, Sendai 980-8579, Japan

e-mail: [ryo@ecei.tohoku.ac.jp](mailto:ryo@ecei.tohoku.ac.jp)

K. Kobayashi

Division of Research and Development, Honda Electronics Co., Ltd.,  
Toyohashi 411-3193, Japan

viscoelasticity is linked to microstructures within the dermis, which are sebaceous glands, hair follicles, and capillary blood vessels. Flexibility and retractility of human skin may change with the changes in these combinations.

High frequency ultrasonography (HFUS) enables to achieve high-resolution measurement because the resolution is equal to one-half wavelength of ultrasound. An axial resolution of 20  $\mu\text{m}$  is acquired at 75 MHz, and a penetration depth of 75 MHz ultrasound is about 2.0 mm at most. HFUS with a center frequency of 100 MHz is much suitable for in vivo measurement of human skin because it's possible to observe not only the microstructures but also whole area of human skin. The microstructures of the human skin have been observed by HFUS at the central frequency of 100 MHz [1]. The hair follicles were reported as hypo echoic and the dermis was reported as echo-rich. Also, the human skin was observed using spherical focused single-element transducer with a center frequency of 20 MHz, [2] and the elasticity of the skin was assessed by applying suction to the skin surface with a stepwise increase in vacuum [3]. Additionally, the nevus inside the dermis was observed by strain imaging. In our previous study [4], the human skin structures, especially the sebaceous glands deeper in dermis, were observed by three-dimensional ultrasound microscopy with a central frequency of 120 MHz. This study revealed that the sebaceous glands also act as a cushion of the skin in addition to their classical role of secreting sebum and some hormones [5]. Additionally, viscoelasticity of the skin was estimated from displacements measured by Cutometer (MPA580, Courage and Khazaka, Köln, Germany) and Voigt model [6].

Elastography is a common technique that estimates mechanical properties of the tissue. Especially, viscoelasticity is a key parameter for a diagnosis of cancer and fibrosis. There are several kinds of elastography: strain elastography [7–11], acoustic radiation force impulse (ARFI) imaging [12–17], shear wave elastography [18–22] and transient elastography [23, 24]. The difference among these techniques is difference of what induces the deformation inside tissues. Recently, passive elastography [25, 26] has been attracted attention. This passive elastography is based on Green's function retrieval and utilize periodic physical motions, which are induced by heartbeats, breathing and so on. In our research group, deformations inside in vivo skin due to arterial pulsation were measured by HFUS with 100 MHz, and the viscoelasticity of human skin was evaluated based on measured deformation itself.

Our goal is to develop high frequency ultrasound elastography using intrinsic deformation induced by pulsation to reveal the origin of the skin viscoelasticity. In this paper, we proposed a novel method for estimation of elasticity the arterial pulsation as an intrinsic deformation. The induced deformation is measured by high frequency ultrasound, and the velocity is calculated from the displacements at several points. The elasticity of the in vivo human skin is evaluated based on the calculated parameters.

## 21.2 Method

### 21.2.1 Data Acquisition Setup

Figure 21.1 shows a schematic of an experiment system. An electric impulse was generated by a high speed switching semiconductor. The start of the pulse was within 400 ps, the pulse width was 2 ns and the pulse voltage was 40 V. The frequency of the impulse covered up to 500 MHz. The electric impulse was used to excite a vinylidene fluoride and trifluoroethylene P(VDF-TrFE) transducer. The aperture diameter of the transducer was 2.0 mm, and the focal length was 4 mm. The central frequency was 100 MHz, the bandwidth ( $-6$  dB) was 40–120 MHz, and the pulse repetition rate was 2,800 Hz. First, the transducer was mounted on the X-Y scanner with two linear servo motors that were controlled by X-Y scan controller connected to the serial port of the PC. The scan area was  $2 \times 2$  mm with  $100 \times 100$  pixels. Four pulse echo sequences with 4,096 sampling points along the depth z were averaged for each scan point in order to increase the S/N ratio. Consecutive 100 B-mode images were produced from the RF data by a conventional image processing algorithm of echography. Next, the measured positions were decided from the B-mode images. Figure 21.2 shows a schematic of an elasticity measurement. In this paper, a deformation induced by the pulsation was used as a source. With the position of the transducer fixed, the reflections from the skin in a forearm were received by the transducer and were introduced into a Windows-based personal computer (PC; Pentium 4, 3.40 GHz, 1 GB RAM, and 250 GB HDD) with a high-speed digitizer card (Acqiris DP 1400, Geneva, Switzerland). The sampling rate was 1 GS/s. The duration of the measurement was 2.5 s.

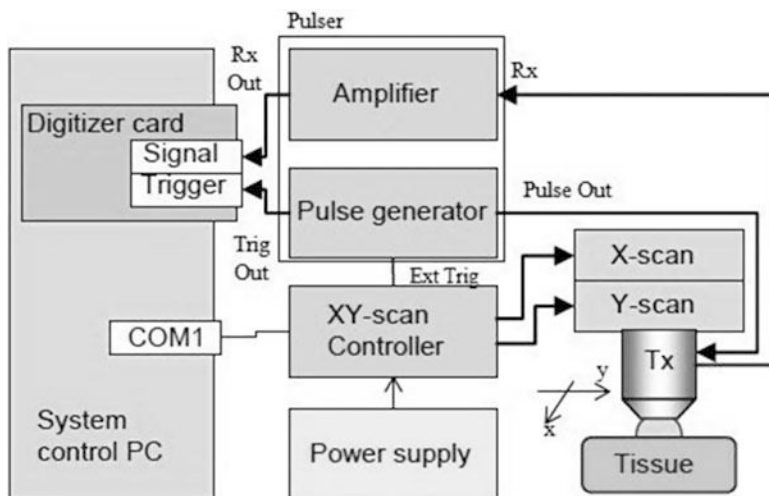


**Fig. 21.1** Block diagram of 3D ultrasound microscope system

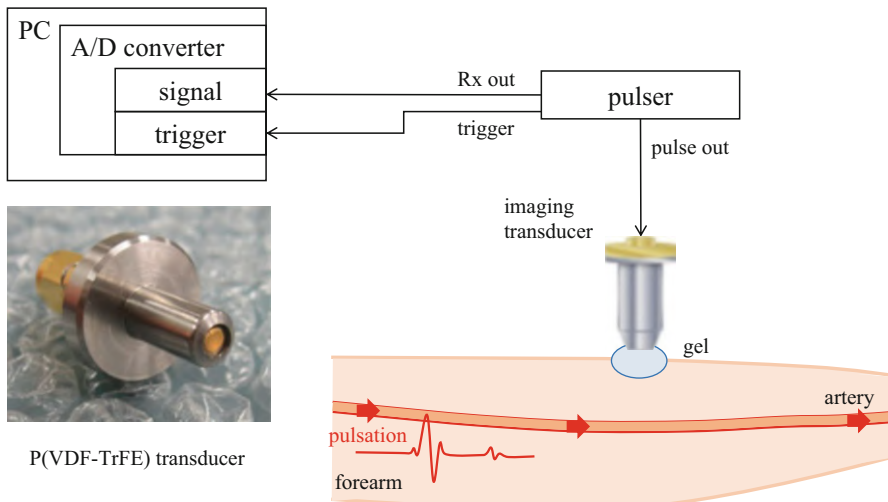


**Fig. 21.2** Schematic of elasticity measurement

The received data were converted to M-mode images. Obtained RF signals of each scanning line was converted to B-mode image by a conventional image processing algorithm of echography.

### 21.2.2 Subject

Subject is one 24-year-old healthy male. A measurement area is skin in his forearm.

### 21.2.3 Velocity Measurement

The velocity induced by the pulsation was measured from the RF echo data of the fixed position by implementing a 1-D cross correlation method. RF signal of time  $t$  at depth  $z$  was defined as  $r_t(z)$ . Analytical signal  $g_t(z)$  was obtained by applying the Hilbert transform to the RF signal  $r_t(z)$ . Pulse waves with angular frequency  $\omega_0 = 2\pi f_0$  were transmitted at a time interval of  $\Delta T$ . Analytical signal of time  $t$  and  $t + \Delta T$  at depth  $z$  can be modeled as

$$g_t(z) = u(z) \exp \left\{ -i \left( \omega_0 \frac{2f_s}{c_0} z - \theta_0 \right) \right\}, \quad (21.1)$$

$$g_{t+\Delta T}(z) = u(z) \exp \left[ -i \left\{ \omega_0 \frac{2f_s}{c_0} (z - z_\tau) - \theta_0 \right\} \right], \quad (21.2)$$

where  $u(z)$  was the envelope of the analytical signal,  $f_s$  was the sampling frequency,  $c_0$  was the sound speed,  $\theta_0$  was the initial phase, and  $z_\tau$  was the true displacement induced by the pulsation. The complex cross-correlation function  $\gamma(z_{lag})$  at lag  $z_{lag}$  was defined as

$$\gamma(z_{lag}) = \frac{\sum_{z=-\frac{N}{2}}^{\frac{N}{2}} g_t^*(z) g_{t+\Delta T}(z + z_{lag})}{\left| \sum_{z=-\frac{N}{2}}^{\frac{N}{2}} g_t^*(z) \right| \left| \sum_{z=-\frac{N}{2}}^{\frac{N}{2}} g_{t+\Delta T}(z + z_{lag}) \right|} \quad (21.3)$$

where  $N$  was 1-D cross correlation window of 256 pixels, corresponding to 195  $\mu\text{m}$  depth window with 91 % overlap using hamming window. An index at maximum value of the real part of the Eq. (21.3) corresponded to the index of  $\hat{z}_{lag}$ . In this paper,  $f_s$  was 1 GHz, and the temporal resolution was enough high to observe the deformation with HFUS of 100 MHz. Additionally, the received RF signal was up-sampled to 4 GHz before implementing the 1-D cross-correlation. Because of these reasons, the estimated displacement  $\hat{z}_{lag}$  was almost equal to the true displacement  $z_{lag}$ . The velocity, denoted by  $v_{t+\Delta T/2}(z)$ , of the skin in his forearm between the interval was given as follows:

$$v_{t+\Delta T/2}(z) = \frac{c_0 \hat{z}_{lag}}{2f_s \Delta T}. \quad (21.4)$$

The acceleration was calculated from the measured velocity. The acceleration was calculated by differentiating the measured velocity as

$$a_t(z) = \frac{v_{t+\Delta T/2}(z) - v_{t-\Delta T/2}(z)}{\Delta T}. \quad (21.5)$$

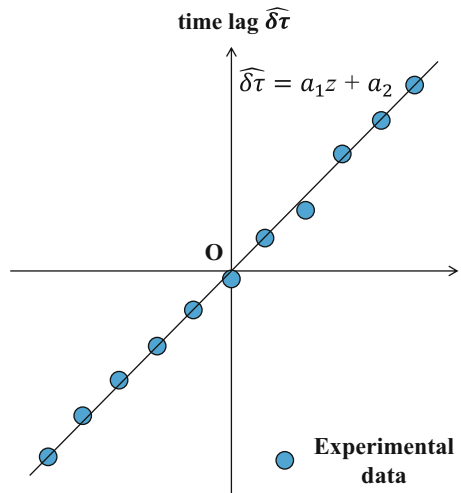
### 21.2.4 Shear Wave Measurement

By comparing an acceleration at reference depth with an acceleration at interest depth, a velocity of shear wave propagating from an artery toward a skin surface can be calculated from a relationship between the depth and the arrival time of shear wave at the depth. The relationship  $\varphi(z)$  can be expressed as

$$\varphi(z) = \frac{\sum_{t=-\frac{N_\alpha}{2}}^{t=\frac{N_\alpha}{2}} a_t^*(z_0) \cdot a_t(z)}{\left| \sum_{t=-\frac{N_\alpha}{2}}^{t=\frac{N_\alpha}{2}} a_t^*(z_0) \right| \left| \sum_{t=-\frac{N_\alpha}{2}}^{t=\frac{N_\alpha}{2}} a_t(z) \right|}, \quad (21.6)$$

where  $N_\alpha$  was an estimation window of 50 pixels, corresponding to a 50 ms time. A hamming window was used for the estimation. A variable  $z_0$  was a reference

**Fig. 21.3** Relationship between depth and time lag.  
Dots: experiments data, and  
line: regression line  
calculated by least square  
method



depth, and a variable  $z$  was an interest depth. A time lag between the reference depth and the interest depth was expressed as follows:

$$\delta\tau(z) = \frac{\varphi(z)}{2\pi f_c} \quad (21.7)$$

The center frequency  $f_c$  was obtained from the power spectrum calculated by applying the Fourier transform to the acceleration signals. Figure 21.3 shows the relationship between the depth  $z$  and the time lag. A regression line can be obtained by applying the least square method to the relationship. A slope  $a_1$  of the regression line can be obtained by minimizing a least mean square error  $e$  as follows:

$$e = \sum_{z=0}^{z=Z_N} |\delta\tau(z) - (a_1 z + a_2)|^2 \quad (21.8)$$

A variable  $Z_N$  is a total number of the region of interest. The velocity  $C_s$  of shear wave was given by dividing the depth distance  $\Delta z$  by the estimated slope value  $\hat{a}_1$ :

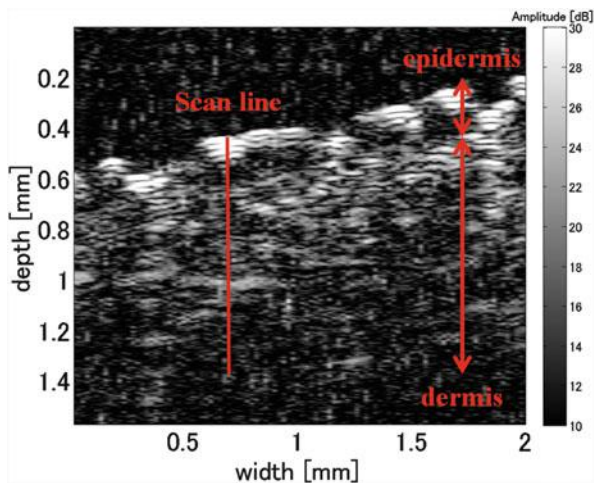
$$C_s = \frac{\Delta z}{\hat{a}_1} \quad (21.9)$$

## 21.3 Results

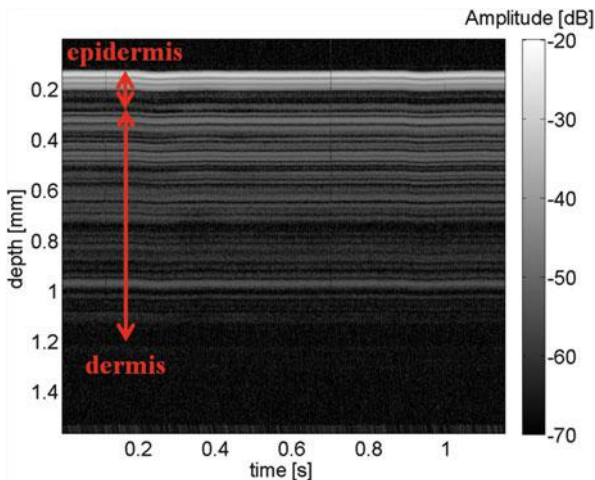
### 21.3.1 Measurement of Deformation

Figure 21.4 shows a B-mode image of the skin. In the B-mode image, an epidermis and a dermis were clearly distinguished. A scan line for an M-mode image was decided from the B-mode image (a red line). Figure 21.5 shows an M-mode image

**Fig. 21.4** B-mode image of human skin of forearm



**Fig. 21.5** M-mode image of scan line in human skin



of the scan line in the skin. In the M-mode image, each layer was slightly pulsating. Figure 21.6 shows a result of a velocity measurement. Figure 21.6a shows a velocity waveform, and Fig. 21.6b shows the velocity at each depth (surface, 0.20, 0.40, 0.60, and 0.80 mm). Figure 21.7 shows a result of an acceleration measurement. Figure 21.7a shows an acceleration waveform, and Fig. 21.7b shows the acceleration at each depth (surface, 0.20, 0.40, 0.60, and 0.80 mm).

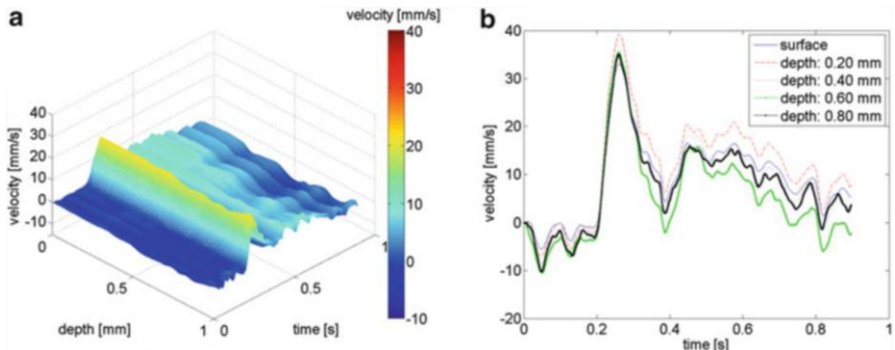


**Fig. 21.6** Measured velocity of scan line; (a) velocity waveform, and (b) velocity at each depth (skin surface, 0.20, 0.40, 0.60, and 0.80 mm, respectively)

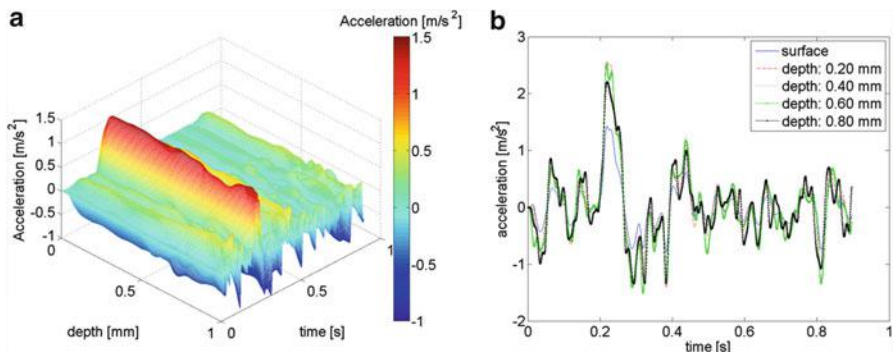
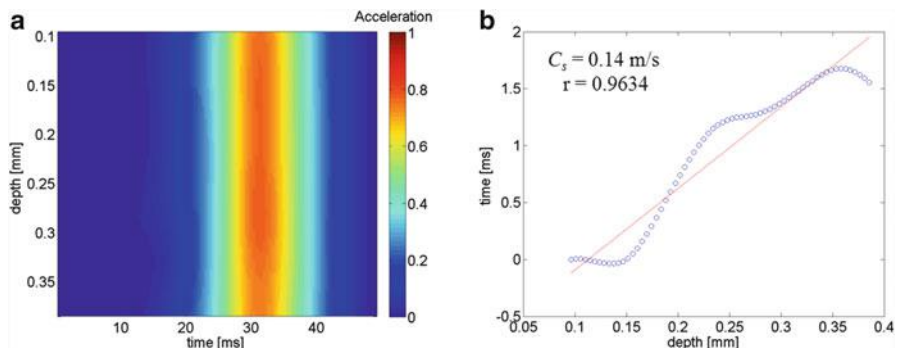
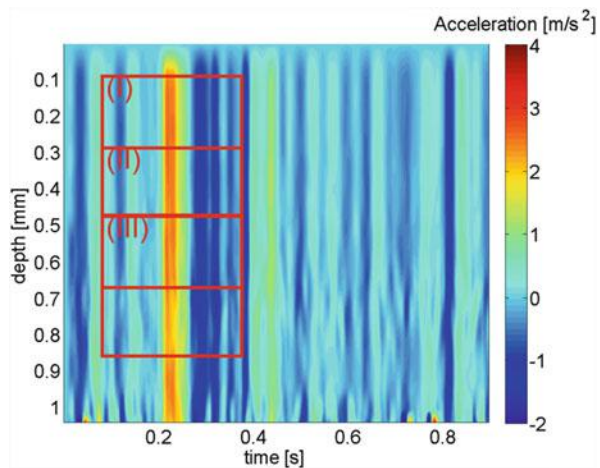


**Fig. 21.7** Measured acceleration of scan line; (a) acceleration waveform, and (b) acceleration at each depth (skin surface, 0.20, 0.40, 0.60, and 0.80 mm, respectively)

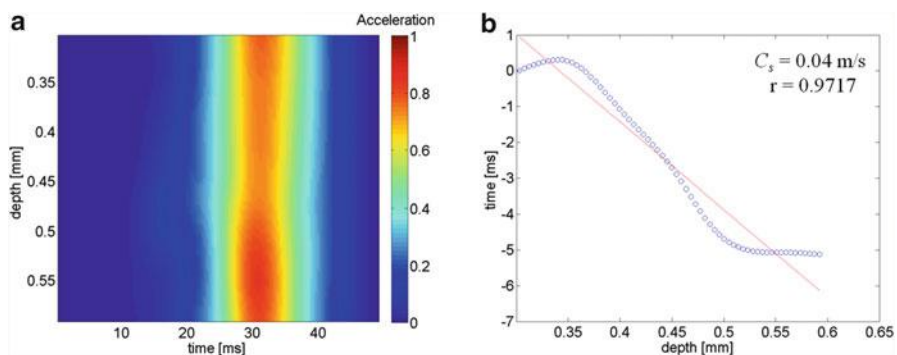
### 21.3.2 Estimated Shear Wave Velocity

Figure 21.8 shows the acceleration waveform map. 3 regions of interest (ROI I, II, and III) were set in the M-mode image. ROI I corresponded to an area of the epidermis, ROI II corresponded to an area of border between the epidermis and dermis, and ROI III corresponded to an area of the dermis. Figure 21.9a shows a close-up image of ROI I, and Fig. 21.9b shows a relationship between time and depth with a regression line. In the region of the epidermis, the shear wave velocity was 0.14 m/s. Figure 21.10a shows a close-up image of ROI II, and Fig. 21.10b shows a relationship between time and depth with a regression line. In the region of the border, the shear wave velocity was 0.04 m/s. Figure 21.11a shows a close-up image of ROI III, and Fig. 21.11b shows a relationship between time and depth with a regression line. In the region of the dermis, the shear wave velocity was 0.06 m/s.

**Fig. 21.8** Measured acceleration map. ROI I: area of epidermis, ROI II: area of border between epidermis and dermis, and ROI III: area of dermis



**Fig. 21.9** (a) Close-up image of ROI I, and (b) relationship between time and depth with regression line



**Fig. 21.10** (a) Close-up image of ROI II, and (b) relationship between time and depth with regression line

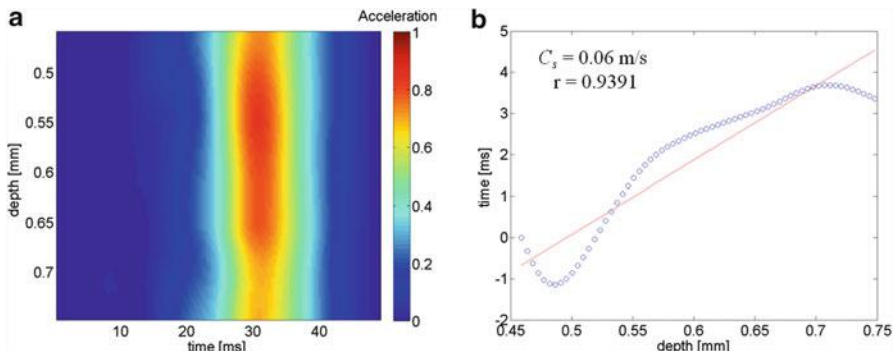


**Fig. 21.11** (a) Close-up image of ROI III, and (b) relationship between time and depth with regression line

## 21.4 Discussion

The measured shear wave velocity of ROI I was higher than that of ROI II, and this results conformed to the past researches that the elasticity of the epidermis is higher than that of the dermis. Due to use of low frequency in analysis of acceleration, the measured shear wave velocity was lower.

## 21.5 Conclusion

The deformation induced by arterial pulsation were measured with high frequency ultrasound. The acceleration and the shear wave velocity were calculated from the measured velocity. These estimated parameters well conformed to the histology of the skin and the past reports. We believe this proposed method is very useful to evaluate the elasticity of the human skin.

**Open Access** This chapter is distributed under the terms of the Creative Commons Attribution Noncommercial License, which permits any noncommercial use, distribution, and reproduction in any medium, provided the original author(s) and source are credited.

## References

1. Gammal SE, Gammal CE, Kaspar K, Pieck C, Altmeier P, Vogt M, Ermert H. J Invest Dermatol. 1999;113:821.
2. Vogt M, Ermert H. IEEE Trans Ultrason Ferroelectr Freq Control. 2008;55:1975.
3. Vogt M, Ermert H. IEEE Trans Ultrason Ferroelectr Freq Control. 2005;52:375.
4. Kumagai K, Koike H, Kudo Y, Nagaoka R, Kubo K, Kobayashi K, Saijo Y. Proceedings of the conference of 33rd IEEE EMBC; 2011, p. 7199.

5. Kumagai K, Koike H, Nagaoka R, Sakai S, Kobayashi K, Saijo Y. *Ultrasound Med Biol.* 2012;38:1838.
6. Nagaoka R, Kobayashi K, Saijo Y. Proceedings of the conference of 35th IEEE EMBC; 2013, p. 1112.
7. Krouskop TA, Doughtery DR, Levinson SF. *J Rehabil Res Dev.* 1987;24:1.
8. Yamakoshi Y, Sato J, Sato T. *IEEE Trans Ultrason Ferroelectr Freq Control.* 1990;37:45.
9. Ophir J, Cespedes I, Ponnekanti H, Yazdi Y, Li X. *Ultrason Imaging.* 1991;13:111.
10. Shiina T, Doyley MM, Bamber JC. Proceedings of the IEEE ultrasonics symposium; 1996, p. 1331.
11. Yamakawa M, Shiina T. *Jpn J Appl Phys.* 2001;40:3872.
12. Nightingale K, Soo MS, Nightingale R, Trahey G. *Ultrasound Med Biol.* 2002;28:227.
13. Nightingale K, McAleavy S, Trahey GE. *Ultrasound Med Biol.* 2003;29:1715.
14. Bercoff J, Tanter M, Fink M. *IEEE Trans Ultrason Ferroelectr Freq Control.* 2004;51:396.
15. Chen S, Fatemi M, Greenleaf JF. *J Acoust Soc Am.* 2002;112:884.
16. Hasegawa H, Takahashi M, Nishio Y, Kanai H. *J Appl Phys.* 2006;45:4706.
17. Yamaguchi J, Hasegawa H, Kanai H. *J Med Ultrasound.* 2012;39:279.
18. Sandrin L, Tanter M, Catheline S, Fink M. *IEEE Trans Ultrason Ferroelectr Freq Control.* 2002;49:426.
19. Tanter M, Bercoff J, Sandrin L, Fink M. *IEEE Trans Ultrason Ferroelectr Freq Control.* 2002;49:1363.
20. Montaldo G, Tanter M, Bercoff J, Benech N, Fink M. *IEEE Trans Ultrason Ferroelectr Freq Control.* 2009;56:489.
21. Chen S, Fatemi M, Greenleaf JF. *J Acoust Soc Am.* 2004;115:2781.
22. Chen S, Urban MW, Pislaru C, Kinnick R, Zheng Y, Yao A, Greenleaf JF. *IEEE Trans Ultrason Ferroelectr Freq Control.* 2009;56:55.
23. Sandrin L, Tanter M, Gennisson JL, Catheline S, Fink M. *IEEE Trans Ultrason Ferroelectr Freq Control.* 2002;49:436.
24. Sandrin L, Fourquet B, Hasquenoph JM, Yon S, Fournier C, Mal F, Christidis C, Zioli M, Poulet B, Kazemi F, Beaugrand M, Palau R. *Ultrasound Med Biol.* 2003;29:1705.
25. Brum J, Benech N, Negreira C, Catheline S, Callot T. Proceedings of the IEEE ultrasonics symposium; 2011 p. 1160.
26. Gallot T, Catheline S, Roux P, Brum J, Benech N, Negreira C. *IEEE Trans Ultrason Ferroelectr Freq Control.* 2002;58:1122.

**Part VI**  
**Poster Presenters**

## **Chapter 22**

# **Effect of Macrophage Colony-Stimulating Factor Receptor c-Fms Antibody on Lipopolysaccharide-Induced Pathological Osteoclastogenesis and Bone Resorption**

**Keisuke Kimura, Hideki Kitaura, Masahiko Ishida, Zaki Hakami, Jafari Saeed, Haruki Sugisawa, and Teruko Takano-Yamamoto**

**Abstract** Lipopolysaccharide (LPS) is a major component of Gram-negative bacteria cell walls and is a well-known potent inducer of inflammation and pathogens of inflammatory bone loss. Formation of osteoclasts is highly dependent on the presence of macrophage colony-stimulating factor (M-CSF) and receptor activator of nuclear factor kappa-B ligand (RANKL). Recent reports indicate that biological preparations, including anti-RANKL antibody and anti-tumor necrosis factor- $\alpha$  antibody, positively influence rheumatoid arthritis and osteoporosis. In this study, we aimed to investigate whether the M-CSF receptor c-Fms antibody would inhibit the formation of osteoclasts. C57BL6/J mice were injected with either LPS, LPS and anti-c-Fms antibody, anti-c-Fms antibody, or PBS into the supracalvariae. Animals were sacrificed and calvariae fixation and demineralization were performed. Histological sections of calvariae were stained for tartrate-resistant acid phosphatase (TRAP). In mice administered with both LPS and the anti-c-Fms antibody, osteoclast numbers were lower than those in mice administered with LPS alone. Moreover, levels of TRACP-5b, a bone resorption marker in mice serum, were lower in mice administered with both LPS and the anti-c-Fms antibody than in mice administered with LPS alone. These results suggest that M-CSF and its receptor are potential therapeutic targets in LPS-induced osteoclastogenesis, and that the anti-c-Fms antibody might be useful for inhibition of inflammation-induced bone erosion. In this study, we describe and discuss the effect the anti-c-Fms antibody has on pathological osteoclastogenesis and bone resorption.

**Keywords** LPS • M-CSF • Osteoclast

---

K. Kimura • H. Kitaura • M. Ishida • Z. Hakami • J. Saeed • H. Sugisawa

T. Takano-Yamamoto (✉)

Division of Orthodontics and Dentofacial Orthopedics, Department of Translational Medicine, Tohoku University Graduate School of Dentistry, 4-1 Seiryo-machi, Aoba-ku, Sendai 980-8575, Japan

e-mail: [t-yamamo@m.tohoku.ac.jp](mailto:t-yamamo@m.tohoku.ac.jp)

## 22.1 Biological Effect of Macrophage Colony-Stimulating Factor (M-CSF)

Macrophage colony-stimulating factor (M-CSF) is a known hematopoietic growth factor and regulator of key functions of macrophages and monocytes. M-CSF mediates the survival and proliferation of precursors of the monocyte and macrophage lineage and their differentiation into mature phagocytes [1, 2]. Macrophages, in relation to the immune response, exist as phagocytes and antigen-presenting cells [3, 4]. Furthermore, the activity of macrophages is associated with the regulation of many biological processes and is dependent on the actual macrophage phenotype induced under various inflammatory conditions [1]. Macrophages play an important role in homeostasis, autoimmunization, and first defense during infection. Macrophages react to tissue damage through non-specific activation followed by overproduction of proinflammatory factors within the pathological condition [5]. Furthermore, allergen or self-antigen presentation on macrophages induces a chronic inflammatory response and stultification of immunity. Primitive macrophages develop from hematopoietic cells and then differentiate into fetal macrophages. Monocytes are also differentiated from hematopoietic cells in the bone marrow and fetal hematopoietic organs. Macrophages contribute as effectors of metabolism and the host defense. When macrophages are depleted, bilirubin production and host resistance to infection are severely reduced. Macrophage growth factors induce macrophage differentiation and function. M-CSF-deficient mice are deficient in monocytes, tissue macrophages, and osteoclasts and show osteopetrosis phenotypes [6]. It has been reported that macrophages incorporate chemically modified, low-density lipoprotein (LDL) and differentiate into foam cells in the arterial wall [7]. When oxidized LDL binds to liver X receptor  $\alpha$ , this upregulates expression of its target genes and acts to remove cholesterol from macrophages. Inflammatory signals downregulate the expression of liver X receptor  $\alpha$  and enhance lipid accumulation [7]. Therefore, macrophages play a pivotal role in metabolism and host defense. Thus, the macrophage/monocyte growth factor, M-CSF, plays an important role in these events.

## 22.2 The Role of M-CSF in Osteoclast Formation and Bone Remodeling

Many cytokine contribute to osteoclast formation [8–12]. M-CSF is one of the essential cytokine for osteoclastogenesis. M-CSF plays an important role in bone remodeling and mediates osteoclast differentiation and the survival and proliferation of osteoclast precursors [13, 14]. The osteoclast, which is a unique bone resorptive cell, is a member of the macrophage family. Osteoclastogenesis is dependent on M-CSF and receptor activator of nuclear factor kappa-B ligand (RANKL) [15]. Osteoclasts play a role in bone resorption and maintain bone

homeostasis. This event was confirmed by the observation that osteopetrotic (*op/op*) mutant mice, deficient in expression of M-CSF, show an osteopetrotic phenotype [14]. Additionally, administration of soluble M-CSF to *op/op* mice rescues their osteoclast formation potential and occurrence of osteoporosis [6]. The functional relationship between M-CSF and its receptor is established in mice lacking c-fms, which display the same phenotype as the *op/op* mouse. These mice have decreased tissue macrophages and severe osteopetrosis owing to a lack of osteoclasts [16–19]. Mice homozygous for the osteopetrosis mutation are characterized by defective differentiation of osteoclasts, monocytes, and tissue macrophages, owing to the lack of M-CSF activity. It has been reported that the bone marrow cavities were filled with spongy bone in young *op/op* mice. Conversely, the bone marrow cavities were reconstructed and marrow hematopoiesis was increased in old *op/op* mice [7]. Osteoclast and bone marrow macrophage cell numbers were also increased in old *op/op* mice. However, many of the osteoclasts were mononuclear not multinuclear cells and showed insufficiently developed ruffled borders. Furthermore, in old *op/op* mice, lysosomes of bone marrow macrophages were laden with abundant crystalloid materials, which was not observed in young *op/op* mice. Although the number of Kupffer cells in the liver was not increased in the old *op/op* mice, cell ultrastructural maturation was absent and some crystalloid structures were observed [7]. M-CSF administration to old *op/op* mice increased the number of Kupffer cells and induced lysosome formation in the Kupffer cells. Furthermore, M-CSF administration reduced crystalloid structures in the lysosomes of the Kupffer cells and permitted development of atypical ruffled border in the osteoclasts [7]. These results suggest that the M-CSF-independent mechanisms for macrophage and osteoclast development in old *op/op* mice are restricted to the bone marrow. M-CSF plays important roles in the differentiation of macrophages and osteoclasts and the production and function of lysosomes. Binding of M-CSF to c-Fms activates the receptor tyrosine kinase and induces auto-phosphorylation of the dimer on selected tyrosine residues. The M-CSF/c-fms signaling pathway leads to activated phosphorylation of PI3K, cSrc, and ERK, which are critical for proliferation and survival of osteoclast precursors [20, 21].

Rheumatoid arthritis (RA) is a highly complex condition, the pathogenesis of which results from a host of cytokines produced by a variety of cells. While RANKL and interleukin (IL)-1 are important participants in the development of focal bone erosions, which eventuate in joint collapse, tumor necrosis factor (TNF)- $\alpha$  is the principal and rate-limiting culprit, whose blockade dampens both the inflammatory and osteoclastogenic components of the disease [22]. However, blockade of TNF- $\alpha$  alone is insufficient to optimize arrest of inflammatory joint disease, as coordinated treatment with IL-1 receptor antagonist (IL-1Ra) is more effective [23]. Added to the potential complications attending TNF- $\alpha$  inhibition, these observations underscore the importance of identifying new therapeutic candidates in this disease, a goal which can be achieved only by gaining insight into the means by which TNF- $\alpha$  impacts target cells.

While M-CSF is constitutively produced by a range of mesenchymal cells, its regulated secretion has pathological consequences in the context of the osteoclast.

Thus, absence of estrogen, the cause of postmenopausal osteoporosis, is because of enhanced bone resorption caused, at least in part, by increased production of M-CSF by bone marrow stromal cells [24]. Similarly, the enhanced osteoclastogenesis observed following deletion of the  $\beta 3$  integrin gene is due to stimulated M-CSF expression [25]. Regarding inflammatory osteolysis, the cytokine is increased in the serum of patients with RA [26] and those with severe ankylosing spondylitis [27], as well as in the synovial fluid around loose joint prostheses [28].

### **22.3 Biological Antibody Therapy for Bone Disease**

Recently, biological preparations, including anti-RANKL antibody and anti-TNF- $\alpha$  antibody, have been reported to positively influence RA, osteoporosis, and cancer bone metastasis [29]. These antibodies act as decoys to prevent receptor binding and therefore inhibit osteoclastogenesis. Denosumab, an anti-bone resorptive drug, is a complete human-type monoclonal antibody for RANKL [30, 31]. Denosumab has been shown to elicit an inhibitory effect on bone resorption in patients with osteoporosis and RA. However, in patients with massive renal dysfunction, denosumab administration increases the risk of hypocalcemia. Denosumab binds to a specific loop structure on the RANKL molecule and inhibits its interaction with its receptor, RANK [32]. When labeled with radioactivity, denosumab was detected in the lymph nodes and spleen after subcutaneous administration, indicating positive RANKL binding of the drug within those tissues. Therefore, researchers and clinicians are interested in the inhibitory effects of denosumab on bone resorption, as well as its mode of action. Biological therapy by blocking the TNF- $\alpha$  receptor is an efficacious RA treatment. TNF- $\alpha$  is produced primarily by activated macrophages and induces osteoclast formation via activated phosphorylation of P38, JNK, and AP-1. This cytokine likely plays a key role in RA pathogenesis [11, 32, 33]. Infliximab is a chimeric monoclonal IgG1 antibody against TNF- $\alpha$  [34]. It neutralizes TNF- $\alpha$  biological activity and inhibits bone distraction [35]. However, one side-effect of infliximab includes immunodeficiency, therefore it needs to be used cautiously.

### **22.4 The Inhibitory Effect of the Anti-c-Fms Antibody in Pathological Osteoclast Formation and Bone Resorption**

In this review, we describe and discuss the effect of the anti-c-Fms antibody on the pathology of osteoclastogenesis and bone resorption. M-CSF is produced by mesenchymal cells and its regulated secretion has physiological and pathological consequences for osteoclasts. M-CSF promotes the survival and longevity of

osteoclast precursors and organizes osteoclast cytoskeletons [15]. The absence of estrogen in post-menopausal osteoporosis is because of enhanced bone resorption caused by increased production of M-CSF by marrow stromal cells [24]. The level of M-CSF is increased in the serum of patients with RA who have severe ankylosing spondylitis [36] and in the synovial fluid around loose joint prostheses [28]. These observations suggest that stromal cell-produced M-CSF may be an important mediator of inflammation-induced osteoclastogenesis. Indeed, it has been reported that TNF- $\alpha$  induces M-CSF gene expression in stromal cells and increases the number of osteoclast precursors in vivo [37]. Stromal cell-produced M-CSF may be an important mediator of TNF-stimulated osteoclastogenesis. In fact, TNF- $\alpha$  has been shown to induce M-CSF gene expression in vivo and only in the presence of stromal cell-residing TNFRs. The capacity of TNF- $\alpha$  to increase osteoclast precursor numbers in vivo, corresponds with the pro-proliferative and pro-survival properties of abundant levels of M-CSF. The fact that TNF- $\alpha$  enhances osteoclast precursor numbers in the presence of only constitutive levels of M-CSF, suggests that, like its interaction with RANKL, this inflammatory cytokine synergizes with M-CSF to enhance osteoclast precursor numbers. In fact, mice treated with carrier or anti-c-Fms mAb developed equivalent periarticular inflammation, while those receiving the antibody were completely free of pathological osteoclastogenesis and bone resorption. This observation reflects, to a substantial degree, the arrest of TNF signaling, as similar results were obtained in TNF- $\alpha$ -injected mice also receiving the anti-c-Fms antibody.

Mechanical force loading exerts important effects on the skeleton by controlling bone mass and strength. Orthodontic tooth movement is a good model for exploring the mechanism of mechanical loading-induced bone remodeling. In a mouse model of orthodontic tooth movement, TNF- $\alpha$  was expressed and osteoclasts appeared on the compressed side of the periodontal ligament. In TNF-receptor-deficient mice, there was less tooth movement and osteoclast numbers were lower than in wild-type mice. These results suggest that osteoclast formation and bone resorption are caused by mechanical loading-induced TNF- $\alpha$  secretion and that TNF- $\alpha$  is concerned with orthodontic tooth movement [38]. However, the relationship between orthodontic movement and TNF- $\alpha$  is not fully understood as yet. Blocking M-CSF with an anti-c-Fms antibody was shown to inhibit osteoclast formation and tooth movement [39]. These results suggest that control of M-CSF could regulate osteoclast formation and subsequent orthodontic tooth movement. Root resorption often occurs following orthodontic treatment and is a serious problem for the orthodontist and patient. During one study, the anti-c-Fms antibody was locally injected adjacent to the first molar every other day during the experimental period. The anti-c-Fms antibody was found to inhibit odontoclastogenesis and root resorption during orthodontic tooth movement [39].

M-CSF and/or its receptor is therefore a potential therapeutic target in mechanical stress-induced odontoclastogenesis, and injection of the anti-c-Fms antibody might be useful for inhibition of mechanical stress-induced root resorption during orthodontic tooth movement.

Bacterial infection and lipopolysaccharide (LPS) are reported to induce osteoclast formation and inflammatory bone loss, as seen in periodontal diseases [40, 41]. LPS is major component of bacteria and is reported to be an inducer of inflammation and pathological bone resorption. We therefore, aimed to examine the effect of LPS on osteoclastogenesis and the anti-c-Fms antibody. We assumed that the M-CSF receptor c-Fms antibody would inhibit LPS-induced osteoclast formation. In our study, we showed that LPS induced M-CSF expression in vivo. The anti-c-Fms antibody has been previously reported to inhibit RANKL-induced osteoclastogenesis in vitro and completely block pathological osteoclastogenesis and bone resorption, induced by inflammatory arthritis and direct injection of TNF- $\alpha$  [42]. In the present study, we administered LPS with and without the anti-c-Fms antibody into mouse supracalvariae to analyze the effect of the anti-c-Fms antibody on LPS-induced osteoclastogenesis in vivo. In the LPS-administered group, increased numbers of osteoclasts were observed. In comparison, the number of osteoclasts was significantly reduced in the group administered with both LPS and the anti-c-Fms antibody, which was dependent on the concentration of the anti-c-Fms antibody. Levels of both cathepsin K and tartrate-resistant acid phosphatase mRNAs were also significantly lower in the group administered with both LPS and the anti-c-Fms antibody compared with the LPS-administered group. These results showed that anti-c-Fms antibody inhibited LPS-induced osteoclast formation [43]. To examine whether the anti-c-Fms antibody inhibited LPS-induced osteolysis, we used three-dimensional reconstruction images of calvariae obtained by microfocal computed tomography ( $\mu$ -CT). Many radiolucent spots on calvariae were observed in the  $\mu$ -CT images in the LPS-administered group but not in the group administered both LPS and the anti-c-Fms antibody. Furthermore, the level of TRACP-5b, a bone resorption marker, was lower in the serum of the group administered both LPS and the anti-c-Fms antibody compared with the LPS-administered group. The results suggest that the anti-c-Fms antibody can inhibit LPS-induced osteolysis by inhibition of osteoclast formation [43]. Our results showed that osteoclasts were induced in calvariae in the presence of LPS. Several previous studies have indicated that LPS induces the expression of inflammatory cytokines, such as TNF- $\alpha$ , IL-1, and IL-6, in vitro and in vivo. Furthermore, it has been reported that TNF- $\alpha$  induces M-CSF expression in stromal cells in vivo [42, 44]. In our study, we found that LPS induced M-CSF expression in vivo. It has been reported that M-CSF induces RANK expression by bone marrow macrophages in vitro [42]. We therefore investigated whether LPS-induced RANK expression in vivo was dependent on M-CSF. We found LPS-induced RANK gene and protein expression were inhibited by the anti-c-Fms antibody in vivo [43]. These results suggest that RANK expression induced by LPS in vivo might be dependent on LPS-induced M-CSF levels. Taken together, the inhibition of LPS-induced RANK expression might be one factor behind the inhibitory effect of the anti-c-Fms antibody on osteoclastogenesis.

## 22.5 Conclusions

M-CSF has an important role within the immune system and bone remodeling, representing one of many cytokines involved in the pathogenesis of inflammatory osteolysis. Although M-CSF-signaling is initiated at the induction of the arthritic process, the profundity of its effect on osteoclasts, as compared with macrophages, enhances its therapeutic appeal. The potential of M-CSF inhibition as a means of treating RA is underscored by the development of c-Fms-selective small molecules [45] and the capacity of the tyrosine kinase inhibitor drug, imatinib, to target the receptor [46]. Given the significant complications encountered with other forms of anti-cytokine therapy, however, the therapeutic targeting of M-CSF must be approached with caution [47]. M-CSF and/or its receptor are potential therapeutic targets for the treatment of bacterial infection-induced osteolysis caused by LPS. The injection of an anti-c-Fms antibody might be useful for the inhibition of pathological bone resorption during bacterial infection.

Taken together, these data indicate that M-CSF is a key cytokine that plays a central role in inflammatory osteolysis and might be a therapeutic target. However, M-CSF accelerates formation of osteoclasts by increasing their precursor pool, the majority of which fail to become bone resorptive polykaryons, but host defense mononuclear phagocytes. Thus, the coincident immunosuppressive effect of inhibiting macrophage proliferation and survival as a means of arresting inflammatory periarticular erosion, is a potential limitation of M-CSF blockade. Further studies are necessary to clarify this aspect.

**Open Access** This chapter is distributed under the terms of the Creative Commons Attribution Noncommercial License, which permits any noncommercial use, distribution, and reproduction in any medium, provided the original author(s) and source are credited.

## References

1. Li Y, Chen Q, Zheng D, Yin L, Chionh YH, Wong LH, et al. Induction of functional human macrophages from bone marrow promonocytes by M-CSF in humanized mice. *J Immunol*. 2013;191(6):3192–9.
2. Cecchini MG, Dominguez MG, Moccia S, Wetterwald A, Felix R, Fleisch H, et al. Role of colony stimulating factor-1 in the establishment and regulation of tissue macrophages during postnatal development of the mouse. *Development*. 1994;120(6):1357–72.
3. Calderon B, Carrero JA, Unanue ER. The central role of antigen presentation in islets of Langerhans in autoimmune diabetes. *Curr Opin Immunol*. 2014;26:32–40.
4. D’Souza AJ, Desai SD, Rudner XL, Kelly MN, Ruan S, Shellito JE. Suppression of the macrophage proteasome by ethanol impairs MHC class I antigen processing and presentation. *PLoS One*. 2013;8(2):e56890.
5. Nazimek K, Bryniarski K. The biological activity of macrophages in health and disease. *Postepy Hig Med Dosw* (Online). 2012;66:507–20.
6. Abboud SL, Woodruff K, Liu C, Shen V, Ghosh-Choudhury N. Rescue of the osteopetrosis defect in op/op mice by osteoblast-specific targeting of soluble colony-stimulating factor-1. *Endocrinology*. 2002;143(5):1942–9.

7. Naito M. Macrophage differentiation and function in health and disease. *Pathol Int.* 2008;58(3):143–55.
8. Kobayashi K, Takahashi N, Jimi E, Udagawa N, Takami M, Kotake S, et al. Tumor necrosis factor alpha stimulates osteoclast differentiation by a mechanism independent of the ODF/RANKL-RANK interaction. *J Exp Med.* 2000;191:275–86.
9. Kodama H, Nose M, Niida S, Yamasaki A. Essential role of macrophage colony-stimulating factor in the osteoclast differentiation supported by stromal cells. *J Exp Med.* 1991;173(5):1291–4.
10. Lacey DL, Timms E, Tan HL, Kelley MJ, Dunstan CR, Burgess T, et al. Osteoprotegerin ligand is a cytokine that regulates osteoclast differentiation and activation. *Cell.* 1998;93(2):165–76.
11. Redlich K, Hayer S, Ricci R, David JP, Tohidast-Akrad M, Kollias G, et al. Osteoclasts are essential for TNF-alpha-mediated joint destruction. *J Clin Invest.* 2002;110:1419–27.
12. Ross FP. M-CSF, c-Fms, and signaling in osteoclasts and their precursors. *Ann N Y Acad Sci.* 2006;1068:110–6.
13. Glantschnig H, Fisher JE, Wesolowski G, Rodan GA, Reszka AA. M-CSF, TNFalpha and RANK ligand promote osteoclast survival by signaling through mTOR/S6 kinase. *Cell Death Differ.* 2003;10(10):1165–77.
14. Yoshida H, Hayashi S, Kunisada T, Ogawa M, Nishikawa S, Okamura H, et al. The murine mutation osteopetrosis is in the coding region of the macrophage colony stimulating factor gene. *Nature.* 1990;345:442–4.
15. Teitelbaum SL. Bone resorption by osteoclasts. *Science.* 2000;289(5484):1504–8.
16. Dai XM, Zong XY, Sylvestre V, Stanley ER. Incomplete restoration of colony-stimulating factor 1 (CSF-1) function in CSF-1-deficient *Csf1op/Csf1op* mice by transgenic expression of cell surface CSF-1. *Blood.* 2004;103(3):1114–23.
17. Wiktor-Jedrzejczak W, Bartocci A, Ferrante Jr AW, Ahmed-Ansari A, Sell KW, Pollard JW, et al. Total absence of colony-stimulating factor 1 in the macrophagedeficient osteopetrotic (op/op) mouse. *Proc Natl Acad Sci U S A.* 1990;87(12):4828–32.
18. Wiktor-Jedrzejczak W, Ratajczak MZ, Ptasznik A, Sell KW, Ahmed-Ansari A, Ostertag W. CSF-1 deficiency in the op/op mouse has differential effects on macrophage populations and differentiation stages. *Exp Hematol.* 1992;20(8):1004–10.
19. Naito M, Hayashi S, Yoshida H, Nishikawa S, Shultz LD, Takahashi K. Abnormal differentiation of tissue macrophage populations in ‘osteopetrosis’ (op) mice defective in the production of macrophage colony-stimulating factor. *Am J Pathol.* 1991;139(3):657–67.
20. Long CL, Humphrey MB. Osteoimmunology: the expanding role of immunoreceptors in osteoclasts and bone remodeling. *Bonekey Rep.* 2012;1:59.
21. Bruzzaniti A, Baron R. Molecular regulation of osteoclast activity. *Rev Endocr Metab Disord.* 2006;7(1–2):123–39.
22. Smolen JS, Steiner G. Therapeutic strategies for rheumatoid arthritis. *Nat Rev Drug Discov.* 2003;2(6):473–88.
23. Zwerina J, Hayer S, Tohidast-Akrad M, Bergmeister H, Redlich K, Feige U, et al. Single and combined inhibition of tumor necrosis factor, interleukin-1, and RANKL pathways in tumor necrosis factor-induced arthritis: effects on synovial inflammation, bone erosion, and cartilage destruction. *Arthritis Rheum.* 2004;50(1):277–90.
24. Srivastava S, Weitzmann MN, Kimble RB, Rizzo M, Zahner M, Milbrandt J, et al. Estrogen blocks M-CSF gene expression and osteoclast formation by regulating phosphorylation of Egr-1 and its interaction with Sp-1. *J Clin Invest.* 1998;102(10):1850–9.
25. Faccio R, Takesita S, Zallone A, Ross FP, Teitelbaum SL. c-Fms and the alphavbeta3 integrin collaborate during osteoclast differentiation. *J Clin Invest.* 2003;111(5):749–58.
26. Kawaji H, Yokomura K, Kikuchi K, Somoto Y, Shirai Y. Macrophage colony-stimulating factor in patients with rheumatoid arthritis. *Nihon Ika Daigaku Zasshi.* 1995;62(3):260–70.
27. Yang C, Gu J, Rihl M, Baeten D, Huang F, Zhao M, et al. Serum levels of matrix metalloproteinase 3 and macrophage colony-stimulating factor 1 correlate with disease activity in ankylosing spondylitis. *Arthritis Rheum.* 2004;51(5):691–9.

28. Takei I, Takagi M, Ida H, Ogino T, Santavirta S, Kontinen YT. High macrophage-colony stimulating factor levels in synovial fluid of loose artificial hip joints. *J Rheumatol.* 2000;27(4):894–9.
29. Yasuda H. RANKL, a necessary chance for clinical application to osteoporosis and cancer-related bone diseases. *World J Orthop.* 2013;4(4):207–17.
30. Schwarz EM, Ritchlin CT. Clinical development of anti-RANKL therapy. *Arthritis Res Ther.* 2007;9 Suppl 1:S7.
31. Lipton A, Goessl C. Clinical development of anti-RANKL therapies for treatment and prevention of bone metastasis. *Bone.* 2011;48(1):96–9.
32. Miyazaki T, Tokimura F, Tanaka S. A review of denosumab for the treatment of osteoporosis. *Patient Prefer Adherence.* 2014;8:463–71.
33. Feldmann M, Maini RN. Anti-TNF alpha therapy of rheumatoid arthritis: what have we learned? *Annu Rev Immunol.* 2001;19:163–96.
34. Voloshyna I, Seshadri S, Anwar K, Littlefield MJ, Belilos E, Carsons SE, et al. Infliximab reverses suppression of cholesterol efflux proteins by TNF- $\alpha$ : a possible mechanism for modulation of atherogenesis. *Biomed Res Int.* 2014;2014:312647.
35. Feldman M, Taylor P, Paleolog E, Brennan FM, Maini RN. Anti-TNF $\alpha$  therapy is useful in rheumatoid arthritis and Crohn's disease: analysis of the mechanism of action predicts utility in other diseases. *Transplant Proc.* 1998;30(8):4126–7.
36. Azuma Y, Kaji K, Katogi R, Takeshita S, Kudo A. Tumor necrosis factor-alpha induces differentiation of and bone resorption by osteoclasts. *J Biol Chem.* 2000;275(7):4858–64.
37. Yang PT, Kasai H, Xiao WG, Zhao LJ, He LM, Yamashita A, et al. Increased expression of macrophage colony-stimulating factor in ankylosing spondylitis and rheumatoid arthritis. *Ann Rheum Dis.* 2006;65(12):1671–2.
38. Kitaura H, Zhou P, Kim HJ, Novack DV, Ross FP, Teitelbaum SL. M-CSF mediates TNF-induced inflammatory osteolysis. *J Clin Invest.* 2005;115(12):3418–27.
39. Yoshimatsu M, Shibata Y, Kitaura H, Chang X, Moriishi T, Hashimoto F, et al. Experimental model of tooth movement by orthodontic force in mice and its application to tumor necrosis factor receptor-deficient mice. *J Bone Miner Metab.* 2006;24(1):20–7.
40. Kitaura H, Yoshimatsu M, Fujimura Y, Eguchi T, Kohara H, Yamaguchi A, et al. An anti-c-Fms antibody inhibits orthodontic tooth movement. *J Dent Res.* 2008;87(4):396–400.
41. Slots J, Genco RJ. Black-pigmented *Bacteroides* species, *Capnocytophaga* species, and *Actinobacillus actinomycetemcomitans* in human periodontal disease: virulence factors in colonization, survival, and tissue destruction. *J Dent Res.* 1984;63(3):412–21.
42. Abu-Amer Y, Ross FP, Edwards J, Teitelbaum SL. Lipopolysaccharide-stimulated osteoclastogenesis is mediated by tumor necrosis factor via its P55 receptor. *J Clin Invest.* 1997;100(6):1557–65.
43. Kimura K, Kitaura H, Fujii T, Hakami ZW, Takano-Yamamoto T. Anti-c-Fms antibody inhibits lipopolysaccharide-induced osteoclastogenesis in vivo. *FEMS Immunol Med Microbiol.* 2012;64(2):219–27.
44. Kitaura H, Sands MS, Aya K, Zhou P, Hirayama T, Uthgenannt B, et al. Marrow stromal cells and osteoclast precursors differentially contribute to TNF-alpha-induced osteoclastogenesis in vivo. *J Immunol.* 2004;173(8):4838–46.
45. Murray LJ, Abrams TJ, Long KR, Ngai TJ, Olson LM, Hong W, et al. SU11248 inhibits tumor growth and CSF-1R-dependent osteolysis in an experimental breast cancer bone metastasis model. *Clin Exp Metastasis.* 2003;20(8):757–66.
46. Dewar A, Zannettino AC, Hughes TP, Lyons AB. Inhibition of c-fms by imatinib: expanding the spectrum of treatment. *Cell Cycle.* 2005;4(7):851–3.
47. Genovese MC, Cohen S, Moreland L, Liim D, Robbins S, Newmark R, et al. Combination therapy with etanercept and anakinra in the treatment of patients with rheumatoid arthritis who have been treated unsuccessfully with methotrexate. *Arthritis Rheum.* 2004;50(5):1412–9.

## Chapter 23

# The Role of Th1 Cytokines on Mechanical Loading-Induced Osteoclastogenesis and Bone Resorption

**Hideki Kitaura, Keisuke Kimura, Masahiko Ishida, Zaki Hakami, Jafari Saeed, Haruki Sugisawa, Haruka Kohara, Masako Yoshimatsu, and Teruko Takano-Yamamoto**

**Abstract** Mechanical loading exerts important effects on the skeleton by controlling bone mass and strength. Osteoclasts are required for bone resorption and remodeling. Two cytokines are required for osteoclast formation: macrophage colony-stimulating factor and receptor activator of nuclear factor kappa-B ligand (RANKL). Tumor necrosis factor- $\alpha$  (TNF- $\alpha$ ) has also been recognized as an important factor for osteoclastogenesis. It has previously been reported that interleukin (IL)-12 and IL-18, and interferon gamma (IFN- $\gamma$ ), which are type 1T helper cell (Th1) cytokines, inhibited RANKL- and TNF- $\alpha$ -mediated osteoclastogenesis. It also been reported that TNF- $\alpha$  plays an important role in mechanical loading-induced osteoclastogenesis and bone resorption. Orthodontic tooth movement is a good model for exploring the mechanism underlying mechanical loading-induced bone changes. Orthodontic tooth movement in a mouse model was established, and we investigated whether Th1 cytokines such as IL-12 and IFN- $\gamma$  inhibit osteoclastogenesis and bone resorption upon mechanical loading. The number of tartrate-resistant acid phosphatase (TRAP)-positive cells increased at the pressure side of the first molar. Conversely, the amount of tooth movement and the number of TRAP-positive cells at the pressure side in IL-12- and IFN- $\gamma$ -injected mice was less than that of non-injected mice. The results suggested that IL-12 and IFN- $\gamma$  might have an inhibitory effect on mechanical loading-induced osteoclastogenesis. In this review, we describe and discuss the effect of Th1 cytokines on mechanical loading-induced osteoclastogenesis and bone resorption.

---

H. Kitaura • K. Kimura • M. Ishida • Z. Hakami • J. Saeed • H. Sugisawa  
T. Takano-Yamamoto (✉)

Division of Orthodontics and Dentofacial Orthopedics, Department of Translational Medicine,  
Tohoku University Graduate School of Dentistry, 4-1 Seiryo-machi, Aoba-ku,  
Sendai 980-8575, Japan  
e-mail: [t-yamamo@m.tohoku.ac.jp](mailto:t-yamamo@m.tohoku.ac.jp)

H. Kohara • M. Yoshimatsu  
Department of Orthodontics and Dentofacial Orthopedics, Nagasaki University Graduate  
School of Biomedical Sciences, Nagasaki 852-8588, Japan

**Keyword** Bone resorption • Osteoclast • Th1 cytokines

### 23.1 Osteoclast Differentiation

Bone resorption is controlled by osteoclasts. Osteoclasts differentiate from hematopoietic stem cells [1]. Several important factors for osteoclast differentiation have been recognized. The receptor activator of nuclear factor kappa-B ligand (RANKL) [2], also known as osteoclast differentiation factor (ODF) [3], osteoprotegerin ligand (OPGL) [4], and tumor necrosis factor (TNF)-related activation-induced cytokine (TRANCE) [5] have been found to be essential in osteoclast differentiation. Macrophage colony-stimulating factor (M-CSF) is also identified as essential for the proliferation and differentiation of osteoclast precursors [6]. Op/op mice, which lack functional M-CSF, show osteopetrosis and have no osteoclasts. This deficiency can be cured by injection of M-CSF [7]. RANKL has been identified as a ligand of the receptor activator of nuclear factor kappa-B (RANK), which is an immunoresponsive receptor on dendritic cells [2]. RANKL-deficient mice have severe osteopetrosis and show a complete deficiency of osteoclasts [8]. Conversely, it has been reported that TNF- $\alpha$  also mediates osteoclast formation in vitro [9–11] and in vivo [12, 13]. TNF- $\alpha$  can also form osteoclasts independent of RANKL in the presence of transforming growth factor beta (TGF- $\beta$ ) [14]. However, it has been reported in another group that TNF- $\alpha$  failed to induce the differentiation of osteoclasts without RANKL [15]. They suggested that a constitutive level of RANKL was necessary for TNF- $\alpha$ -mediated osteoclast formation. Further studies are necessary to clarify this aspect.

### 23.2 TNF- $\alpha$ -Mediated Osteoclast Formation

TNF- $\alpha$  is pleiotropic and has a variety of biological effects in a cell-specific manner. TNF- $\alpha$  is known to play a major role in host defense, and exerts proinflammatory activities through various cells, including mononuclear phagocytes, in which it is responsible for the activation of bactericidal and cytoidal systems [16, 17]. It has been reported that TNF- $\alpha$  induces osteoclast formation from M-CSF-dependent bone marrow-derived macrophages in vitro [10]. TNF- $\alpha$  induced osteoclast recruitment might be central to the pathogenesis of inflammatory disorders [18]. TNF- $\alpha$  is a known contributor to rheumatoid arthritis [19], periodontal diseases [20, 21], and postmenopausal osteoporosis [22]. The findings that TNF- $\alpha$  recognizes two receptors on cell surfaces, type 1 or p55 (TNFR1) and type 2 or p75 receptors (TNFR2), and that each receptor is capable of distinct intracellular signaling [23], has substantially deepened our understanding of the complex activities of this cytokine. Analysis of TNFR1- and TNFR2-deficient mice revealed that TNFR1 induces osteoclast differentiation, while TNFR2 inhibits osteoclast

differentiation [24]. The role of TNF- $\alpha$  signaling in osteoclastogenesis remains poorly understood, and further studies are needed to clarify the relationship between TNF- $\alpha$  and osteoclast differentiation.

### 23.3 Mechanical Force Loading-Induced Osteoclast Formation and Bone Resorption

Mechanical loading force affects the skeleton by controlling bone mass and strength [25]. Several *in vivo* experimental models have been reported that evaluate the effect of mechanical loading on bone metabolism. The following experimental animal models have been established: jumping [26, 27], treadmill running [26, 28], squatting [29], and swimming [30]. Assessing an orthodontic tooth movement model *in vivo* is beneficial to understand the mechanism of mechanical loading-induced bone remodeling [31–34]. The animal models used for orthodontic tooth movement were usually rats and mice [35–43]. Opportunities for the use of various gene-mutated mice including those with genes that regulate bone metabolism have increased, because molecular biology techniques have progressed. Therefore, the mice tooth movement models can provide an understanding of the molecular mechanisms involved not only in tooth movement but also in mechanical loading-induced bone remodeling. A nickel-titanium (Ni-Ti) coil spring to obtain a continuous force for tooth movement is suitable for exerting continuous orthodontic force in mice models [44, 45]. The process of orthodontic tooth movement occurs by repeated alveolar bone resorption on the pressure side and bone formation on the tension side of teeth [46]. In orthodontic tooth movement, there is an association between osteoclasts and bone resorption on the pressure side [47]. In mice models, bone resorption was recognized on the pressure side and tartrate-resistant acid phosphatase (TRAP)-positive multinuclear cells also appeared on this side.

Mechanical force is relevant to tooth movement via the biological responses of cells in the periodontal ligament, alveolar bone, and other periodontal tissues [48]. Several factors, specifically cytokines and hormones, are related to this process. An increase in the level of TNF- $\alpha$  in the gingival sulcus during orthodontic tooth movement in humans has been reported [49, 50]. TNF- $\alpha$  has been shown to be expressed in rat periodontal tissue during excessive orthodontic force application [51]. When tooth movement was applied to TNFR1- and TNFR2-deficient mice, the amount of tooth movement observed in TNFR2-deficient mice was less than that in the wild-type mice [44]. These results suggested that TNFR2 is important for orthodontic tooth movement. However, it has been reported that the analysis of the reaction to TNF- $\alpha$  using TNFR1- or TNFR2-deficient mice showed the induction of osteoclastogenesis in TNFR1-deficient mice, whilst the inhibition of osteoclastogenesis was observed in TNFR2-deficient mice [20]. These results are controversial. In the evaluation of the role of TNFR1 in osteoclast formation during orthodontic tooth movement, the number of osteoclasts in TNFR1-deficient mice

was found to be lower than that in wild-type mice [52]. To further investigate the role of TNFRs, tooth movement experiments using double-mutated mice for both TNFR1 and TNFR2 were performed. The experiment showed significant decreases in the amount of tooth movement in the double-mutated mice [45]. These results suggested that TNF- $\alpha$  is associated with orthodontic tooth movement. However, the relationship between orthodontic movement and TNF- $\alpha$  is not yet completely understood.

### 23.4 Effect of Interleukin (IL)-12 on Osteoclast Formation

IL-12 is one of the type 1T helper cell (Th1) cytokines. IL-12 has been recognized as playing an important role in host defense. It induces differentiation of native T cells into IFN- $\gamma$ -producing Th1 cells that are resistant to infection [53]. IL-12 is a heterodimeric disulfide-linked 70-kDa protein consisting of 35- and 40-kDa subunits. It has previously been shown that IL-12 plays an important role in attaining the optimal level of cell-mediated immune response against intracellular pathogens [54]. IL-12 is produced by osteoblasts infected with *Staphylococcus aureus*, which is the most prevalent causative microorganism in osteomyelitis, a bone resorption disorder [55].

It has been shown that IL-12 inhibits osteoclast formation in the spleen cells of mice treated with M-CSF and RANKL [56]. It was found that the inhibitory effect of IL-12 depends on the presence of T cells among spleen cells. However, it has been reported that osteoclastogenesis induced by RANK/RANKL interaction decreased in the presence of IL-12 by a T-cell-independent mechanism in vitro [57], and TNF- $\alpha$ -induced osteoclastogenesis was also inhibited through induction of apoptosis mediated by the interaction of the IL-12-induced Fas ligand (FasL) and TNF- $\alpha$ -induced Fas in vitro [58]. IL-12 and IL-18 inhibited TNF- $\alpha$ -mediated osteoclastogenesis by up-regulating FasL synergistically [59]. IL-18 is also an important Th1 cytokine. It has been reported that IL-18 can also inhibit osteoclast formation in spleen cell cultures in vitro and that the IL-18-mediated inhibition of osteoclast formation is also T cell dependent [56].

The target cells of IL-12 have been shown to be T cells [54], natural killer (NK) cells [60], natural killer T cells, B cells [61], dendritic cells [62], and macrophages [63]. It has been reported that IL-12 influences non-adherent cells in bone marrow cell cultures and induces FasL expression in non-adherent cells. The results suggested that adherent cells, such as dendritic cells and macrophages, are not target cells [54]. In addition, when bone marrow macrophages were co-cultured with T cells isolated from among spleen cells in the presence of M-CSF, TNF- $\alpha$ , and IL-12 in vitro, apoptotic alterations were not observed [58]. In the study, when whole bone marrow cells from T-cell-deficient nude mice were cultured in the presence of M-CSF, TNF- $\alpha$ , and IL-12, the cells underwent apoptosis similar to those of wild-type mice [58]. These results also

suggest that T cells may not be target cells for IL-12 in this case. However, additional experiments are necessary to clarify the target cells for IL-12.

The effect of IL-12 on mechanical tooth movement in mice has been reported. Mechanical tooth movement, in which a Ni-Ti closed coil spring was inserted between the upper incisors and the first molar in mice, was used. IL-12 was injected into a local site adjacent to an upper molar during tooth movement. After 12 days, the distance of tooth movement was measured. The number of osteoclasts, which are TRAP-positive cells, were counted in a histological section. Tooth movement was inhibited when IL-12 was localized. The number of TRAP-positive cells was reduced in IL-12-treated mice [64].

Root resorption is a disagreeable phenomenon of orthodontic treatment, which may present at the dentinal and cemental areas of the tooth root surface, and is a serious problem for the orthodontist [65]. Even under normal conditions, it is possible to cause root resorption during orthodontic tooth movement [66–68]. Inhibition of root resorption is hopeful for orthodontists. In recent years, there have been studies investigating the use of medicine for future clinical application to prevent root resorption. It has been reported that bisphosphonates inhibit root resorption [69, 70]. In addition, it has been shown that osteoprotegerin inhibits root resorption more effectively than bisphosphonates [71]. Furthermore, the inhibitory effect on root resorption by amelogenin [72], bisphosphonates, and anti-c-Fms antibodies has also been reported [73, 74]. Root resorption was recognized in this tooth movement model. The root resorption area was measured using a scanning electron microscope. The root resorption area was reduced in IL-12-treated mice. In TdT-mediated dUTP-biotin nick end-labeling (TUNEL) assays, many apoptotic cells were seen on the pressure side in IL-12-treated mice. These findings indicate that IL-12 inhibits mechanical tooth movement and root resorption in orthodontic tooth movement. These results might be the outcome of apoptosis induced by IL-12.

### 23.5 Effect of IFN- $\gamma$ on Osteoclast Formation and Bone Resorption

IFN- $\gamma$  contributes to T-cell-mediated regulation of immune responses and is secreted by Th1 cells, cytotoxic T cells, dendritic cells, and NK cells [75]. In addition, IFN- $\gamma$  has been recognized as an activator of macrophages because of the induction both of nitric oxide production and major histocompatibility complex presentation in macrophages, and exhibits antiviral and antibacterial activity [76].

The effect of IFN- $\gamma$  has been recognized as suppression of osteoclast formation by inhibition of RANKL signaling via degradation of TNF receptor-associated factor 6 [77]. Furthermore, the bone resorption in collagen-induced arthritis was enhanced in IFN- $\gamma$ -deficient mice [78]. These data indicated that IFN- $\gamma$  inhibited osteoclast formation and bone resorption. However, it has been reported that IFN- $\gamma$

indirectly stimulates osteoclast formation via antigen-driven T-cell activation [79]. Therefore, the role of IFN- $\gamma$  in osteoclast formation is still unclear.

It has been reported that IFN- $\gamma$  directly inhibits osteoclastogenesis induced by TNF- $\alpha$  stimulation and accelerates apoptosis mediated by Fas/FasL signals. IFN- $\gamma$  directly interrupted TNF- $\alpha$ -induced osteoclast formation as revealed with a decreased number of osteoclasts and messenger ribonucleic acid (mRNA) levels of nuclear factor of activated T cells, cytoplasmic 1 (NFATc1), which is a gene essential for osteoclast formation, in cultured bone marrow macrophages. Apoptotic findings of cultured cells were evaluated by accelerated nuclear fragmentation in osteoclast precursor cells. Fas mRNA levels in bone marrow cells were stimulated by TNF- $\alpha$ . FasL mRNA levels in a bone marrow culture with IFN- $\gamma$  was increased. Furthermore, IFN- $\gamma$  inhibited osteoclastogenesis in response to TNF- $\alpha$  treatment in vivo. IFN- $\gamma$  inhibited TNF- $\alpha$ -induced osteoclastogenesis in mice with T cells blocked by anti-CD4 and anti-CD8 antibodies [80]. These results suggested that IFN- $\gamma$  directly inhibits osteoclastogenesis, and induces cell apoptosis by Fas/FasL signaling, leading to the indirect regulation of bone resorption. This might occur as a protective role against bone destruction at an inflammation site.

The cellular responses in periodontal tissue, including the alveolar bone, periodontal ligament, and other periodontal tissues, during mechanical force-driven tooth movement are mediated by interactions between various factors such as cytokines and hormones [48, 81]. In a rat tooth movement model, IFN- $\gamma$  is expressed on the pressure side of teeth [82]. IFN- $\gamma$ , which increases trabecular bone volume, has been evaluated histomorphometrically during orthodontic tooth movement in rats [83]. Therefore, these results suggest that IFN- $\gamma$  plays an important role in orthodontic tooth movement. However, there are few studies on the effect of IFN- $\gamma$  on tooth movement. The effect of IFN- $\gamma$  on mechanically loaded tooth movement in a mouse model has been reported. A Ni-Ti closed coil spring was inserted between the upper anterior alveolar bone and the upper left first molars in mice. The relationship between local IFN- $\gamma$  mRNA levels and orthodontic tooth movement was evaluated. In other experiments, IFN- $\gamma$  was injected to each first molar every other day during tooth movement. After 12 days, the amount of tooth movement was measured. The number of osteoclasts at the pressure side of each experimental tooth was assessed. Local IFN- $\gamma$  mRNA expression increased with orthodontic tooth movement in mice. The number of osteoclasts increased on the pressure side of the first molar. In contrast, the distance of tooth movement and the number of osteoclasts on the pressure side in IFN- $\gamma$ -injected mice were less than those of control mice. IFN- $\gamma$  expression was increased in experimental tooth movement. Furthermore, IFN- $\gamma$  could inhibit mechanical force-induced osteoclast formation and tooth movement. These results suggest that IFN- $\gamma$  might be useful in controlling orthodontic tooth movement, because IFN- $\gamma$  inhibited the action of progressive osteoclast formation during orthodontic tooth movement [84]. These results lead us to conclude that IFN- $\gamma$  induction is able to inhibit mechanical force-loaded osteoclast formation, consequently inhibiting orthodontic tooth movement.

## 23.6 Conclusions

It has been reported that many types of cytokines are expressed during mechanical loading of the periodontal ligament. TNF- $\alpha$  is an important molecule in mechanical loading force-induced osteoclast formation in the periodontal ligament during orthodontic tooth movement. Therefore, it is important to study the relationship between TNF- $\alpha$ -induced osteoclast formation and the cytokines expressed during mechanical loading. Th1 cytokines inhibited osteoclast and odontoclast formation during mechanical loading in the periodontal ligament. There is a possibility that local injection of Th1 cytokines might be a useful tool to enhance the anchorage site and control the rate of tooth movement during orthodontic treatment, as well as prevent relapse after orthodontic treatment. Moreover, local injection of Th1 cytokines might be a useful tool in reducing root resorption, particularly for high-risk teeth. However, further studies are required to fully understand the relationship between mechanical loading-induced osteoclast formation and the effect of cytokines.

**Open Access** This chapter is distributed under the terms of the Creative Commons Attribution Noncommercial License, which permits any noncommercial use, distribution, and reproduction in any medium, provided the original author(s) and source are credited.

## References

1. Suda T, Takahashi N, Martin TJ. Modulation of osteoclast differentiation. *Endocr Rev*. 1992;13(1):66–80.
2. Anderson DM, Maraskovsky E, Billingsley WL, Dougall WC, Tometsko ME, Roux ER, et al. A homologue of the TNF receptor and its ligand enhance T-cell growth and dendritic-cell function. *Nature*. 1997;390(6656):175–9.
3. Yasuda H, Shima N, Nakagawa N, Yamaguchi K, Kinoshita M, Mochizuki S, et al. Osteoclast differentiation factor is a ligand for osteoprotegerin/osteoclastogenesis-inhibitory factor and is identical to TRANCE/RANKL. *Proc Natl Acad Sci U S A*. 1998;95(7):3597–602.
4. Lacey DL, Timms E, Tan HL, Kelley MJ, Dunstan CR, Burgess T, et al. Osteoprotegerin ligand is a cytokine that regulates osteoclast differentiation and activation. *Cell*. 1998;93(2):165–76.
5. Wong BR, Rho J, Arron J, Robinson E, Orlinick J, Chao M, et al. TRANCE is a novel ligand of the tumor necrosis factor receptor family that activates c-Jun N-terminal kinase in T cells. *J Biol Chem*. 1997;272(40):25190–4.
6. Kodama H, Nose M, Niida S, Yamasaki A. Essential role of macrophage colony-stimulating factor in the osteoclast differentiation supported by stromal cells. *J Exp Med*. 1991;173(5):1291–4.
7. Begg SK, Radley JM, Pollard JW, Chisholm OT, Stanley ER, Bertonecello I. Delayed hematopoietic development in osteopetrotic (op/op) mice. *J Exp Med*. 1993;177(1):237–42.
8. Kong YY, Yoshida H, Sarosi I, Tan HL, Timms E, Capparelli C, et al. OPGL is a key regulator of osteoclastogenesis, lymphocyte development and lymph-node organogenesis. *Nature*. 1999;397(6717):315–23.
9. Azuma Y, Kaji K, Katogi R, Takeshita S, Kudo A. Tumor necrosis factor-alpha induces differentiation of and bone resorption by osteoclasts. *J Biol Chem*. 2000;275(7):4858–64.

10. Kobayashi K, Takahashi N, Jimi E, Udagawa N, Takami M, Kotake S, et al. Tumor necrosis factor alpha stimulates osteoclast differentiation by a mechanism independent of the ODF/RANKL-RANK interaction. *J Exp Med.* 2000;191(2):275–86.
11. Fuller K, Murphy C, Kirstein B, Fox SW, Chambers TJ. TNFalpha potently activates osteoclasts, through a direct action independent of and strongly synergistic with RANKL. *Endocrinology.* 2002;143(3):1108–18.
12. Kitaura H, Sands MS, Aya K, Zhou P, Hirayama T, Uthgenannt B, et al. Marrow stromal cells and osteoclast precursors differentially contribute to TNF-alpha-induced osteoclastogenesis in vivo. *J Immunol.* 2004;173(8):4838–46.
13. Kitaura H, Zhou P, Kim HJ, Novack DV, Ross FP, Teitelbaum SL. M-CSF mediates TNF-induced inflammatory osteolysis. *J Clin Invest.* 2005;115(12):3418–27.
14. Kim N, Kadono Y, Takami M, Lee J, Lee SH, Okada F, et al. Osteoclast differentiation independent of the TRANCE-RANK-TRAF6 axis. *J Exp Med.* 2005;202(5):589–95.
15. Lam J, Takeshita S, Barker JE, Kanagawa O, Ross FP, Teitelbaum SL. TNF-alpha induces osteoclastogenesis by direct stimulation of macrophages exposed to permissive levels of RANK ligand. *J Clin Invest.* 2000;106(12):1481–8.
16. Vassalli P. The pathophysiology of tumor necrosis factors. *Annu Rev Immunol.* 1992;10(411):411–52.
17. Tracey KJ, Cerami A. Tumor necrosis factor, other cytokines and disease. *Annu Rev Cell Biol.* 1993;9(317):317–43.
18. Wong M, Ziring D, Korin Y, Desai S, Kim S, Lin J, et al. TNFalpha blockade in human diseases: mechanisms and future directions. *Clin Immunol.* 2008;126(2):121–36.
19. Redlich K, Hayer S, Ricci R, David JP, Tohidast AM, Kollias G, et al. Osteoclasts are essential for TNF-alpha-mediated joint destruction. *J Clin Invest.* 2002;110(10):1419–27.
20. Abu AY, Ross FP, Edwards J, Teitelbaum SL. Lipopolysaccharide-stimulated osteoclastogenesis is mediated by tumor necrosis factor via its P55 receptor. *J Clin Invest.* 1997;100(6):1557–65.
21. Van Dyke TE, Serhan CN. Resolution of inflammation: a new paradigm for the pathogenesis of periodontal diseases. *J Dent Res.* 2003;82(2):82–90.
22. Kimble RB, Srivastava S, Ross FP, Matayoshi A, Pacifici R. Estrogen deficiency increases the ability of stromal cells to support murine osteoclastogenesis via an interleukin-1 and tumor necrosis factor-mediated stimulation of macrophage colony-stimulating factor production. *J Dent Res.* 1996;271(46):28890–7.
23. Goeddel DV. Signal transduction by tumor necrosis factor. *Chest.* 1999;116:69S.
24. Abu-Amer Y, Erdmann J, Alexopoulou L, Kollias G, Ross FP, Teitelbaum SL. Tumor necrosis factor receptors types 1 and 2 differentially regulate osteoclastogenesis. *J Biol Chem.* 2000;275(35):27307–10.
25. Frost HM. On our age-related bone loss: insights from a new paradigm. *J Bone Miner Res.* 1997;12(10):1539–46.
26. Notomi T, Okazaki Y, Okimoto N, Saitoh S, Nakamura T, Suzuki M. A comparison of resistance and aerobic training for mass, strength and turnover of bone in growing rats. *Eur J Appl Physiol.* 2000;83(6):469–74.
27. Kodama Y, Umemura Y, Nagasawa S, Beamer WG, Donahue LR, Rosen CR, et al. Exercise and mechanical loading increase periosteal bone formation and whole bone strength in C57BL/6 J mice but not in C3H/Hej mice. *Calcif Tissue Int.* 2000;66(4):298–306.
28. Iwamoto J, Yeh JK, Aloia JF. Differential effect of treadmill exercise on three cancellous bone sites in the young growing rat. *Bone.* 1999;24(3):163–9.
29. Westerlind KC, Fluckey JD, Gordon SE, Kraemer WJ, Farrell PA, Turner RT. Effect of resistance exercise training on cortical and cancellous bone in mature male rats. *J Appl Physiol.* 1998;84(2):459–64.
30. Hart KJ, Shaw JM, Vajda E, Hegsted M, Miller SC. Swim-trained rats have greater bone mass, density, strength, and dynamics. *J Appl Physiol.* 2001;91(4):1663–8.
31. Storey E. The nature of tooth movement. *Am J Orthod.* 1973;63(3):292–314.

32. Takano-Yamamoto T, Takemura T, Kitamura Y, Nomura S. Site-specific expression of mRNAs for osteonectin, osteocalcin, and osteopontin revealed by *in situ* hybridization in rat periodontal ligament during physiological tooth movement. *J Histochem Cytochem.* 1994;42(7):885–96.
33. Ohba Y, Ohba T, Terai K, Moriyama K. Expression of cathepsin K mRNA during experimental tooth movement in rat as revealed by *in situ* hybridization. *Arch Oral Biol.* 2000;45(1):63–9.
34. Kobayashi Y, Hashimoto F, Miyamoto H, Kanaoka K, Miyazaki-Kawashita Y, Nakashima T, et al. Force-induced osteoclast apoptosis *in vivo* is accompanied by elevation in transforming growth factor beta and osteoprotegerin expression. *J Bone Miner Res.* 2000;15(10):1924–34.
35. Hashimoto F, Kobayashi Y, Mataki S, Kobayashi K, Kato Y, Sakai H. Administration of osteocalcin accelerates orthodontic tooth movement induced by a closed coil spring in rats. *Eur J Orthod.* 2001;23(5):535–45.
36. Brudvik P, Rygh P. The initial phase of orthodontic root resorption incident to local compression of the periodontal ligament. *Eur J Orthod.* 1993;15(4):249–63.
37. Pavlin D, Dove SB, Zadro R, Gluhak-Heinrich J. Mechanical loading stimulates differentiation of periodontal osteoblasts in a mouse osteoinduction model: effect on type I collagen and alkaline phosphatase genes. *Calcif Tissue Int.* 2000;67(2):163–72.
38. Kaku M, Kohno S, Kawata T, Fujita I, Tokimasa C, Tsutsui K, et al. Effects of vascular endothelial growth factor on osteoclast induction during tooth movement in mice. *J Dent Res.* 2001;80(10):1880–3.
39. Tsuji Y, Yamaza T, Kido MA, Goto T, Nakata S, Akamine A, et al. Expression of cathepsin K mRNA and protein in odontoclasts after experimental tooth movement in the mouse maxilla by *in situ* hybridization and immunoelectron microscopy. *Cell Tissue Res.* 2001;303(3):359–69.
40. Gluhak-Heinrich J, Ye L, Bonewald LF, Feng JQ, MacDougall M, Harris SE, et al. Mechanical loading stimulates dentin matrix protein 1 (DMP1) expression in osteocytes *in vivo*. *J Bone Miner Res.* 2003;18(5):807–17. doi:[10.1359/jbmr.2003.18.5.807](https://doi.org/10.1359/jbmr.2003.18.5.807).
41. Kohno S, Kaku M, Tsutsui K, Motokawa M, Ohtani J, Tenjo K, et al. Expression of vascular endothelial growth factor and the effects on bone remodeling during experimental tooth movement. *J Dent Res.* 2003;82(3):177–82.
42. Chung CR, Tsuji K, Nifuji A, Komori T, Soma K, Noda M. Micro-CT evaluation of tooth, calvaria and mechanical stress-induced tooth movement in adult Runx2/Cbfα1 heterozygous knock-out mice. *J Med Dent Sci.* 2004;51(1):105–13.
43. Kuroda S, Balam TA, Sakai Y, Tamamura N, Takano-Yamamoto T. Expression of osteopontin mRNA in odontoclasts revealed by *in situ* hybridization during experimental tooth movement in mice. *J Bone Miner Metab.* 2005;23(2):110–3.
44. Yoshimatsu M, Shibata Y, Kitaura H, Chang X, Moriishi T, Hashimoto F, et al. Experimental model of tooth movement by orthodontic force in mice and its application to tumor necrosis factor receptor-deficient mice. *J Bone Miner Metab.* 2006;24(1):20–7.
45. Kitaura H, Yoshimatsu M, Fujimura Y, Eguchi T, Kohara H, Yamaguchi A, et al. An anti-c-Fms antibody inhibits orthodontic tooth movement. *J Dent Res.* 2008;87(4):396–400.
46. Storey E. Tissue response to the movement of bones. *Am J Orthod.* 1973;64(3):229–47.
47. Yokoya K, Sasaki T, Shibusaki Y. Distributional changes of osteoclasts and pre-osteoclastic cells in periodontal tissues during experimental tooth movement as revealed by quantitative immunohistochemistry of H(+)-ATPase. *J Dent Res.* 1997;76(1):580–7.
48. Krishnan V, Davidovitch Z. On a path to unfolding the biological mechanisms of orthodontic tooth movement. *J Dent Res.* 2009;88(7):597–608.
49. Lowney JJ, Norton LA, Shafer DM, Rossomando EF. Orthodontic forces increase tumor necrosis factor alpha in the human gingival sulcus. *Am J Orthod Dentofacial Orthop.* 1995;108(5):519–24.
50. Uematsu S, Mogi M, Deguchi T. Interleukin (IL)-1 beta, IL-6, tumor necrosis factor-alpha, epidermal growth factor, and beta 2-microglobulin levels are elevated in gingival crevicular fluid during human orthodontic tooth movement. *J Dent Res.* 1996;75(1):562–7.

51. Ogasawara T, Yoshimine Y, Kiyoshima T, Kobayashi I, Matsuo K, Akamine A, et al. In situ expression of RANKL, RANK, osteoprotegerin and cytokines in osteoclasts of rat periodontal tissue. *J Periodontal Res.* 2004;39(1):42–9.
52. Andrade Jr I, Silva TA, Silva GA, Teixeira AL, Teixeira MM. The role of tumor necrosis factor receptor type 1 in orthodontic tooth movement. *J Dent Res.* 2007;86(11):1089–94.
53. Berenson LS, Ota N, Murphy KM. Issues in T-helper 1 development–resolved and unresolved. *Immunol Rev.* 2004;202(157):157–74.
54. Scott P. IL-12: initiation cytokine for cell-mediated immunity. *Science.* 1993;260 (5107):496–7.
55. Bost KL, Ramp WK, Nicholson NC, Bento JL, Marriott I, Hudson MC. Staphylococcus aureus infection of mouse or human osteoblasts induces high levels of interleukin-6 and interleukin-12 production. *J Infect Dis.* 1999;180(6):1912–20.
56. Horwood NJ, Udagawa N, Elliott J, Grail D, Okamura H, Kurimoto M, et al. Interleukin 18 inhibits osteoclast formation via T cell production of granulocyte macrophage colony-stimulating factor. *J Clin Invest.* 1998;101(3):595–603.
57. Nagata N, Kitaura H, Yoshida N, Nakayama K. Inhibition of RANKL-induced osteoclast formation in mouse bone marrow cells by IL-12: involvement of IFN-gamma possibly induced from non-T cell population. *Bone.* 2003;33(4):721–32.
58. Kitaura H, Nagata N, Fujimura Y, Hotokezaka H, Yoshida N, Nakayama K. Effect of IL-12 on TNF-alpha-mediated osteoclast formation in bone marrow cells: apoptosis mediated by Fas/Fas ligand interaction. *J Immunol.* 2002;169(9):4732–8.
59. Kitaura H, Tatamiya M, Nagata N, Fujimura Y, Eguchi T, Yoshida N, et al. IL-18 induces apoptosis of adherent bone marrow cells in TNF-alpha mediated osteoclast formation in synergy with IL-12. *Immunol Lett.* 2006;107(1):22–31.
60. Yu Y, Hagiwara M, Ando K, Gansuvd B, Matsuzawa H, Tsuchiya T, et al. Enhancement of human cord blood CD34+ cell-derived NK cell cytotoxicity by dendritic cells. *J Immunol.* 2001;166(3):1590–600.
61. Airolidi I, Gri G, Marshall JD, Corcione A, Facchetti P, Guglielmino R, et al. Expression and function of IL-12 and IL-18 receptors on human tonsillar B cells. *J Immunol.* 2000;165 (12):6880–8.
62. Fukao T, Matsuda S, Koyasu S. Synergistic effects of IL-4 and IL-18 on IL-12-dependent IFN-gamma production by dendritic cells. *J Immunol.* 2000;164(1):64–71.
63. Puddu P, Fantuzzi L, Borghi P, Varano B, Rainaldi G, Guillemard E, et al. IL-12 induces IFN-gamma expression and secretion in mouse peritoneal macrophages. *J Immunol.* 1997;159 (7):3490–7.
64. Yoshimatsu M, Kitaura H, Fujimura Y, Eguchi T, Kohara H, Morita Y, et al. IL-12 inhibits TNF-alpha induced osteoclastogenesis via a T cell-independent mechanism in vivo. *Bone.* 2009;45(5):1010–6.
65. Terai K, Takano-Yamamoto T, Ohba Y, Hiura K, Sugimoto M, Sato M, Kawahata H, Inaguma N, Kitamura Y, Nomura S. Role of osteopontin in bone remodeling caused by mechanical stress. *J Bone Miner Res.* 1999;14(6):839–49.
66. Sameshima GT, Sinclair PM. Predicting and preventing root resorption: Part II. Treatment factors. *Am J Orthod Dentofacial Orthop.* 2001;119(5):511–5.
67. Chan E, Darendeliler MA. Physical properties of root cementum: Part 5. Volumetric analysis of root resorption craters after application of light and heavy orthodontic forces. *Am J Orthod Dentofacial Orthop.* 2005;127(2):186–95.
68. Wierzbicki T, El-Bialy T, Aldaghreer S, Li G, Doschak M. Analysis of orthodontically induced root resorption using micro-computed tomography (Micro-CT). *Angle Orthod.* 2009;79(1):91–6.
69. Komatsu K, Shimada A, Shibata T, Shimoda S, Oida S, Kawasaki K, et al. Long-term effects of local pretreatment with alendronate on healing of replanted rat teeth. *J Periodontal Res.* 2008;43(2):194–200.

70. Liu L, Igarashi K, Haruyama N, Saeki S, Shinoda H, Mitani H. Effects of local administration of clodronate on orthodontic tooth movement and root resorption in rats. *Eur J Orthod.* 2004;26(5):469–73.
71. Keles A, Grunes B, Difuria C, Gagari E, Srinivasan V, Darendeliler MA, et al. Inhibition of tooth movement by osteoprotegerin vs. pamidronate under conditions of constant orthodontic force. *Eur J Oral Sci.* 2007;115(2):131–6.
72. Yagi Y, Suda N, Yamakoshi Y, Baba O, Moriyama K. In vivo application of amelogenin suppresses root resorption. *J Dent Res.* 2009;88(2):176–81.
73. Fujimura Y, Kitaura H, Yoshimatsu M, Eguchi T, Kohara H, Morita Y, et al. Influence of bisphosphonates on orthodontic tooth movement in mice. *Eur J Orthod.* 2009;31(6):572–7.
74. Kitaura H, Fujimura Y, Yoshimatsu M, Eguchi T, Kohara H, Jang I, et al. An M-CSF receptor c-Fms antibody inhibits mechanical stress-induced root resorption during orthodontic tooth movement in mice. *Angle Orthod.* 2009;79(5):835–41.
75. Dunn GP, Koebel CM, Schreiber RD. Interferons, immunity and cancer immunoediting. *Nat Rev Immunol.* 2006;6(11):836–48.
76. Billiau A, Heremans H, Vermeire K, Matthys P. Immunomodulatory properties of interferon-gamma. An update. *Ann N Y Acad Sci.* 1998;856:22–32.
77. Takayanagi H, Ogasawara K, Hida S, Chiba T, Murata S, Sato K, et al. T-cell-mediated regulation of osteoclastogenesis by signalling cross-talk between RANKL and IFN-gamma. *Nature.* 2000;408(6812):600–5.
78. Vermeire K, Heremans H, Vandepitte M, Huang S, Billiau A, Matthys P. Accelerated collagen-induced arthritis in IFN-gamma receptor-deficient mice. *J Immunol.* 1997;158(11):5507–13.
79. Gao Y, Grassi F, Ryan MR, Terauchi M, Page K, Yang X, et al. IFN-gamma stimulates osteoclast formation and bone loss in vivo via antigen-driven T cell activation. *J Clin Invest.* 2007;117(1):122–32.
80. Kohara H, Kitaura H, Fujimura Y, Yoshimatsu M, Morita Y, Eguchi T, et al. IFN-gamma directly inhibits TNF-alpha-induced osteoclastogenesis in vitro and in vivo and induces apoptosis mediated by Fas/Fas ligand interactions. *Immunol Lett.* 2011;137(1–2):53–61.
81. Henneman S, Von den Hoff JW, Maltha JC. Mechanobiology of tooth movement. *Eur J Orthod.* 2008;30(3):299–306.
82. Alhashimi N, Frithiof L, Brudvik P, Bakhet M. Orthodontic movement induces high numbers of cells expressing IFN-gamma at mRNA and protein levels. *J Interferon Cytokine Res.* 2000;20(1):7–12.
83. Mermut S, Bengi AO, Akin E, Kurkcu M, Karacay S. Effects of interferon-gamma on bone remodeling during experimental tooth movement. *Angle Orthod.* 2007;77(1):135–41.
84. Kohara H, Kitaura H, Yoshimatsu M, Fujimura Y, Morita Y, Eguchi T, et al. Inhibitory effect of interferon-gamma on experimental tooth movement in mice. *J Interferon Cytokine Res.* 2012;32(9):426–31.

## Chapter 24

# The Ventral Primary Somatosensory Cortex of the Primate Brain: Innate Neural Interface for Dexterous Orofacial Motor Control

Takashi Toda and Tada-aki Kudo

**Abstract** Studies using nonhuman primates have made marked contributions to our understanding of the anatomy and function of the primary somatosensory cortex (SI). Its ventral or inferolateral part (vSI) represents orofacial structures, such as the lips, periodontium, tongue, palate, chewing musculature, etc. This brain region is neurally interconnected with the ventral part of the primary motor cortex that executes voluntary orofacial movements. Also within the vSI, regions representing different orofacial structures are interconnected with each other. Therefore, in self-generated actions, the vSI plays a crucial role in coordinating motor control of a set of structures that are functionally related: the vSI serves as an interface not only between orofacial structures and the external environment but also between the orofacial structures themselves. In this article, we will chiefly review the neuroanatomical and neurophysiological studies on the monkey vSI from the viewpoint of motor control or stereognostic ability. Future physiological studies that analyze the spatiotemporal spiking pattern of vSI neurons during various behaviors in monkeys should reveal the principles of information coding and might significantly benefit future applications of brain-machine-brain interface (BMBI) technology.

**Keywords** Monkey • Motor control • Neuronal receptive field • Primary somatosensory cortex • Tongue

### 24.1 Introduction

The primary somatosensory area (SI) of primates is located in the anterior-most part of the parietal lobe; i.e., the postcentral gyrus in Old World monkeys and humans. Its ventral or inferolateral part (vSI; Fig. 24.1a, b) represents orofacial structures and the larynx and plays a crucial role in the motor coordination of those structures. Its highly sophisticated form allows for speech motor control in humans.

---

T. Toda (✉) • T. Kudo

Division of Physiology, Tohoku University Graduate School of Dentistry, 4-1 Seiryo-machi, Aoba-ku, Sendai 980-8575, Japan  
e-mail: [ttoda@m.tohoku.ac.jp](mailto:ttoda@m.tohoku.ac.jp)

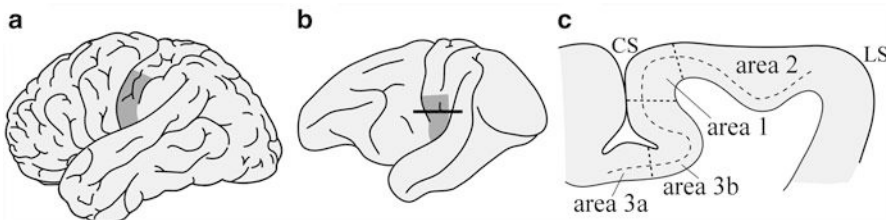


**Fig. 24.1** Overview of the ventral or inferolateral part of the primary somatosensory cortex (vSI). (a) (b) Lateral view of the cerebral hemisphere of humans (a) and macaques (b). The *dark-shaded* area roughly indicates the location of the vSI that represents the orofacial structures. The *solid line* in b corresponds to the section in c. (c) Cytoarchitectonic areas (Brodmann areas 3a, 3b, 1, 2) are shown in a parasagittal section. The *broken line* indicates layer IV. *Dotted lines* indicate the boundaries of cytoarchitectonic areas. CS central sulcus, LS lateral sulcus

Neuroimaging studies of voice and speech production have consistently reported activation of the vSI, as well as the primary motor cortex, in both hemispheres (for review see [1, 2]). For example, the vSI was activated bilaterally even in the simplest speech task, such as overt speaking of a single syllable [3]. Similar results were reported in singing, another sophisticated orofacial and laryngeal function in humans (for review see [4]): the vSI is activated bilaterally in a simple singing condition where subjects were asked to produce bisyllabic words melodically intoned at a certain pitch, and even during humming [5]. Moreover, several lines of evidence suggest that trained singers may rely more on somatosensory feedback than auditory feedback to make sure that notes are produced properly [4]. In one study, professional opera singers and vocal students showed increased activation in the bilateral vSI compared to laymen (medical students), but not in the auditory cortex [6]. The investigators interpreted this to mean that somatosensory feedback via the vSI towards the motor cortex might play a particularly important role in the development of classical singing skills. Chewing, a more vital orofacial function, was also reported to activate the vSI bilaterally [7, 8]. This suggests that chewing also requires information processing in the vSI to control or monitor a series of movements despite its semi-automatic nature.

Non-invasive brain imaging techniques have made significant contributions to our understanding of the brain mechanisms involved in orofacial functions, particularly those specific to humans. However, because of the limitation in spatial and temporal resolution, these techniques are unable to address finer anatomical and physiological details; e.g., the precise location of regions representing each orofacial structure and their neural interconnections, the principles of information coding by individual neurons, and populations of neurons, etc. Therefore, animal studies using nonhuman primates are also of tremendous value as complements to human brain imaging studies, and will continue to be so. In the following sections, we chiefly review the neuroanatomical and neurophysiological studies of the monkey vSI and some relevant neuroimaging studies in humans. Readers may also refer to a related review published recently by another group [9].

## 24.2 Representation of Orofacial Structures in Area 3b

The primary somatosensory area (SI) consists of three cytoarchitectonic areas, as shown in Fig. 24.1c: Brodmann areas 3 (3a, 3b), 1, and 2. Area 3 is regarded as the primary somatosensory area in a strict sense and is called the “SI proper”, because this area receives the densest projection from the specific somatosensory relay nuclei of the thalamus. Area 3b chiefly represents the contralateral body surface in a mediolaterally elongated band of the cortex. Along this mediolateral axis, the tail, lower limb (foot), trunk, upper limb (hand), face, and oral structures are represented in a somatotopical manner. Our current knowledge of the neuroanatomy of the vSI is based largely on studies performed by Professor Jon H. Kaas (see review [10]) and those of Professor Edward G. Jones. The representations of the hand and face are separated by a histologically visible border in both New [11, 12] and Old World monkeys [13–15]. This “hand-face border” can be detected as a myelin-light septum in brain sections cut parallel to the cortical surface. Further laterally, myelin-dense ovals were shown to indicate anatomical modules that correspond to representations of different orofacial structures in both New [16, 17] and Old World monkeys [13, 15]. In New World monkeys, the myelin-dense ovals are arranged in a rostrocaudal direction and extend to the ventral frontal lobe. There, the lips or chin, teeth (periodontal receptors), and tongue are represented in a caudorostral sequence. Further rostrally, the ipsilateral side of the teeth and tongue are represented. In Old World monkeys, the lips (cheek mucosa), teeth, and tongue are represented in a mediolateral sequence. Further anterolaterally, the ipsilateral side of the teeth and tongue are represented. The ipsilateral representation is a distinctive feature of oral structures, such as the teeth and tongue and each side of the oral structure is represented in area 3b of both hemispheres. This was confirmed in a wide range of primates: prosimian primates, such as the African galago [10], New World monkeys, such as the squirrel monkey and owl monkey [16, 18], Old World monkeys, such as macaques [15, 19, 20], and humans (see review [21]). Such corepresentation of the contralateral and ipsilateral sides of oral structures may facilitate the convergence of input from functionally related portions of both sides (bilateral integration described in the next section).

Dense neural interconnections between representations of different orofacial structures have been documented in both New [17] and Old World monkeys [15]. For example, a recent neuroanatomical study of macaques [15] demonstrated that the tongue representation received dense projections from regions representing the lower and upper teeth and tissue lining the inside of the cheek and lips. Such interconnections may partly explain the presence of neurons having composite receptive fields covering different orofacial structures (described later). In contrast, the hand representation, located medially to the orofacial representation, provided little to no input to either the face or mouth representations in both New [12] and Old World monkeys [14, 15] and it follows that the anatomical hand-face border mentioned earlier is also regarded as a functional border. Another interesting observation may be the relation between the tongue representation and the

gustatory related regions [15]: the tongue representation uniquely received projections from areas in the anterior upper bank of the lateral sulcus and anterior insula that may include the primary gustatory area (area G) and other taste-related areas. Also in that study, the tongue representation was likely to receive an additive projection from the lateral surface of the frontal operculum near the lateral sulcus, although the investigators did not particularly emphasize this. This region may presumably correspond to the precentral extension of area 3, which was also implicated in gustatory function [22, 23].

### 24.3 Neuronal Receptive Fields (RFs) as an Indicator of Hierarchical Information Processing in the vSI

Hierarchical information processing in the vSI was summarized in a previous review [24]. As shown in Fig. 24.2, spatial convergence of somesthetic information arising from orofacial structures proceeds across three cytoarchitectonic areas; i.e., areas 3, 1, and 2 [20, 25], in a manner established in the hand representation (see review [26]). Along this rostrocaudal stream, neuronal receptive fields (RFs) become larger and more complex so that the RFs cover functionally related portions of orofacial structures (composite RFs). The patterns of spatial convergence can be classified into three types (Fig. 24.2): bilateral convergence, intermaxillary convergence, and inter-structural convergence. Furthermore, the spatiotemporal integration also proceeds along this stream: the relative incidence of neurons exclusively responsive to light stroking stimuli (movement-specific neurons) increases moving caudally towards area 2 [27]. Of these, the majority responded with directional selectivity, that is, they responded exclusively to stimuli moving in a particular direction. Most of the movement-specific neurons had ordinally uninterrupted RFs and the remaining had composite RFs discretely covering different structures. The relative incidences of neurons with composite RFs in area 2 were significantly higher in movement-specific neurons than in other neurons, suggesting that the spatiotemporal integration for representing moving objects is accompanied by the convergence of inputs from discrete, but functionally related, oral portions. Such a hierarchical scheme in the vSI might be a prerequisite neural process for dexterous orofacial function and oral stereognosis. The spatial convergence found in awake macaque monkeys was indirectly supported in a subsequent human study using functional MRI [28]. Although neuronal RFs could not be studied in humans, the investigators inspected the degree of activation overlaps between the representations of different oral structures, such as the lips, teeth, and tongue. They showed that the overlap in the middle and caudal portions of the postcentral gyrus was significantly greater than in the rostral portion of the postcentral gyrus.

The SI receives not only somesthetic inputs arising from the periphery, but also signals from the frontal lobe related to motor command. It is therefore important to determine the activity of vSI neurons during self-generated orofacial movements.

The laboratory of Professor B.J. Sessle has played a pioneering role and is making tremendous contributions to this field (for review, see [9]). Their studies on the vSI (chiefly in areas 3b and 1) documented in a trilogy of papers revealed the relations between the neuronal RF properties and neuronal activity during self-generated movements [29–31]. In the first paper [29], monkeys were trained to perform a tongue-protrusion task and biting task. In the tongue protrusion task, a significant alteration of firing rate was observed in ~80 % of tongue RF neurons and 60 % of lip RF neurons. Of note here is that a substantial proportion of neurons did not change their activity during the task, despite apparent orofacial RFs. Moreover, among the task-related neurons, adaptation characteristics of RFs (slowly adapting or rapidly adapting) could not predict the patterns of neuronal activities during the task. For example, task-related neurons with a slowly adapting type of RF did not necessarily fire in a tonic manner during the task: rather, four types of activity patterns; i.e., phasic, tonic, phasic-tonic, and decreased, were detected during the task. In the second paper [30], the monkeys were required to protrude their tongue in each of three directions: the target was positioned at 0°, 30° to the left, or 30° to the right from the midsagittal plane. Again, laterality of a neuronal RF could not predict the preferred tongue-protrusion direction of the neuron. The results of these two papers strongly suggest that neurons with various RF properties are recruited simultaneously even in a simple self-generated orofacial movement. In the third paper [31], electrical or mechanical stimulations were applied to the RFs of each neuron (except to the lingual nerve for tongue RF neurons) when the monkeys were performing the task. Almost all of the neurons tested showed a decrease in evoked activity during the tongue-protrusion task. This finding indicates that disturbing somesthetic inputs arising from the periphery are gated out during self-generated movements. To summarize, the passive properties of neuronal RFs are indeed a reliable indicator for evaluating the flow of sensory information across different brain regions, but those properties alone cannot explain the actual neuronal behavior during self-generated movements.

The bidirectional neural interconnection between the vSI and the ventral primary motor area (vMI) was established in neuroanatomical studies of New [17] and Old World monkeys [15, 32]. In one study on the vMI, most neurons respond to light tactile stimulation rather than stimulation to deep tissues, such as the muscle and joint, which suggests the particular importance of tactile input in motor control [33]. Another important finding in this study was that neurons with RFs on different orofacial structures were intermingled. This may be partly explained by the presence of neurons with composite RFs in the aforementioned vSI and the direct neural projection from the vSI to the vMI. As has been suggested, such complex organization in the vMI may be a prerequisite neural basis for the motor coordination of various structures. The manner of neuroplastic changes in the vMI, as well as vSI, should also be addressed, because such changes permit the acquisition of new motor skills or adaptation to an altered orofacial environment. Studies on this subject were reviewed in detail by Professor B.J. Sessle and colleagues [9, 34].

From the viewpoint of dental pain, vSI neurons that receive input from the tooth-pulp are also important targets of study [35, 36]. In one study, monkeys were trained

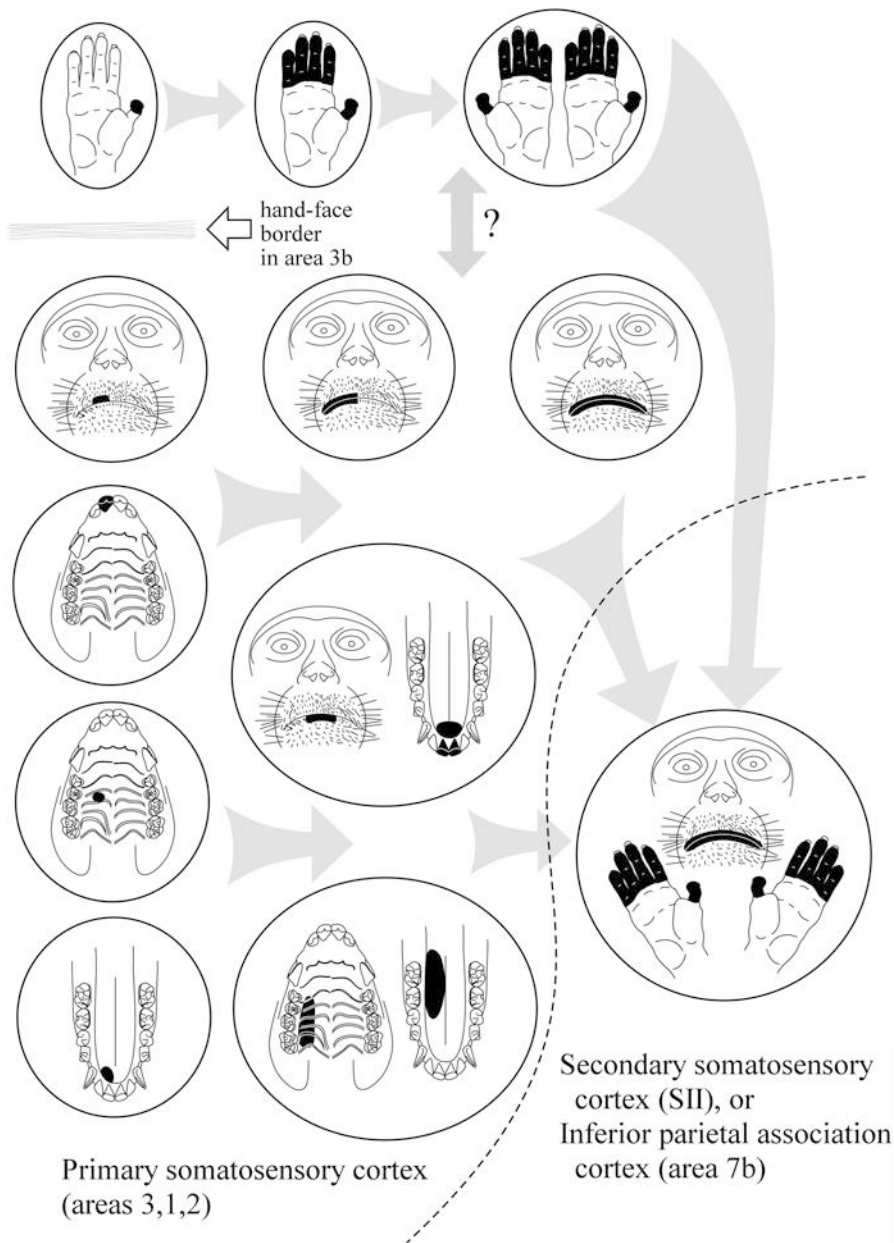


**Fig. 24.2** Schematic drawing showing the convergence of somesthetic information across areas of the vSI and adjacent somatosensory-related cortices. Each circle corresponds to a single neuron and its receptive field (RF, drawn in *black*). Neurons in area 3b are arranged on the *left side*. Hand, face, and oral structures are represented in a mediolateral sequence. In at least area 3b, the “hand-face border” limits the interconnection between the hand and orofacial representations. Note that actual RF sizes in area 3b neurons are often considerably smaller than depicted here. On moving

to detect changes in tooth-pulp stimulus intensity [36]. Some of the neurons examined were implicated in the sensory-discriminative aspect of tooth-pulp sensation, because their discharge rates were correlated with the detection latency of the monkey.

## 24.4 Hand-Mouth Motor Coordination in Self-Feeding Behavior

Motor coordination of the hand and mouth is essential for self-feeding behavior in primates. There should be neurons that integrate somesthetic information arising from both of the body parts somewhere in the brain; however, this subject is not currently well studied with regard to the vSI. In addition, at least in area 3b, such convergence is considered to be rare, because of the presence of the hand-face border. An earlier study of the vSI reported that several neurons in areas 3b or 1 had discrete RFs on both the radial hand and the lateral part of the face [37]. Since those neurons had face RFs that were remote from the oral slit, they are unlikely to relate to feeding behavior. Rather, neuronal activity related to hand-mouth coordination during self-feeding was documented in higher order cortical areas other than the vSI (Fig. 24.2). We review those articles for reference purposes, although this may be beyond the scope of the present paper regarding the SI. The laboratory of Professor A. Iriki has made important contributions to this field. In one study, they explored the inferior parietal cortex (area 7b), which is posteriorly adjacent to the vSI, and found “face-hand neurons” [38]. These neurons had discrete RFs on the lower face (mostly around the mouth or in the oral cavity) and hand, of which about half responded to the specific behavior with synergism between the face and hand movements. That is, these neurons responded more strongly when the animal executed face-hand coordinated behavior (e.g., self-feeding behavior) than when the monkey executed identical movements of the face and hand separately. Some neurons in their sample showed an especially strong response when pinching food or holding it with the mouth during self-feeding, which was suggestive of their role in monitoring a sequence of actions or an entire course of behavior. Based on these observations, they assumed that area 7b is related to the integration and construction of actions. In another study, they reported the presence of similar neurons



**Fig. 24.2** (continued) caudally from area 3b to area 2, neuronal RFs on the hand and orofacial structures become larger and more complex. The patterns of convergence in orofacial neurons can be classified into three types: bilateral convergence, intermaxillary convergence (e.g., upper and lower lips, palate and tongue dorsum), and inter-structural convergence (e.g., tongue tip and anterior teeth). Further caudally in the inferior parietal cortex (area 7b) or laterally in the secondary somatosensory cortex (SII), RFs often cover both the hand and orofacial structures. These neurons in higher-order brain regions are closely related to self-feeding behavior. For further explanation, see the text

(“hand-mouth neurons”) in the secondary somatosensory area (SII) lying laterally to the vSI in the upper bank of the lateral sulcus [39]. These neurons also showed activity during both food retrieval with the hand and eating. However, the investigators rarely encountered neurons that fired during self-generated feeding but were inactive during passive feeding separated from food retrieval with the hand: the synergism in area 7b neurons was not detected in SII neurons. Another interesting observation from this study was that the hand-mouth neurons showed activity irrespective of the hand used in retrieving food, which suggests the goal-coding nature of these neurons. In other words, it does not matter for these neurons which part of the body is used to bring food to the mouth.

## 24.5 Temporal Analysis of Spiking Activities in Neuronal Populations and Individual Neurons

The neural activity (the train of action potentials) of a single neuron is quite variable across trials even when the same stimulus is repeatedly applied. Therefore, simultaneous recording from different single neurons is necessary to analyze the functional neural circuits in a local brain locus or to study the dynamics of information coding by neuronal ensembles. The introduction of such a technique, especially in the past 10–15 years, has led to numerous achievements in various cortical regions. However, there are only a limited number of analogous studies in the vSI. In one study, we evaluated the difference in temporal profiles between spike trains recorded simultaneously from a pair of nearby vSI neurons [40]. A numerical method was adopted that evaluates the difference in the gross temporal profiles over several hundreds of milliseconds or more during sustained tactile stimulation [41]. There were significant temporal discrepancies in the activity of some pairs of putative pyramidal neurons. We speculated that this might help the brain to monitor the time course of stimulation, such as the onset, duration, and offset. Another recent study [42], using a much larger scale of data, examined whether the population activities of neurons in the vSI and vMI could represent the direction of tongue movement. The investigators adopted the mutual information as a measure of the strength in the relationship between spiking activity and direction of tongue protrusion. They showed that the direction of tongue protrusion was accurately predicted on a trial-by-trial basis from the spiking activity of populations of vSI and vMI neurons by using a discrete decoder.

In addition to the population activity of neurons, the temporal structure of spike trains (firing pattern) of individual neurons is an important subject of study. One of the metrics that evaluates firing pattern, the metric of local variation (LvR), is superior in that the temporal structures can be quantified independently of the firing rate [43]. In this study, the investigators clearly showed dissimilarities in firing-pattern across many cortical areas based on LvR scores: spiking patterns are regular in the motor areas, random in the visual areas, and bursty in the prefrontal area. Such numerical analysis is also needed in future studies of the vSI.

The temporal analysis of neural activities could conceivably lead to future improvement of a brain-machine-brain interface (BMBI). This technology, which was developed to restore normal sensorimotor function in the upper limb, consists of two major elements: one is the neural population recording from motor-related areas that permits subjects to move prosthetic arms or a virtual hand on a screen; the other is intracortical microstimulation (ICMS) of the SI giving rise to artificial tactile sensation [44, 45]. Neurophysiological studies of the monkey vSI will play an important role in determining the optimal ICMS conditions in BMBI for orofacial function and contribute to the future treatment of patients suffering from orofacial sensorimotor disorders.

**Open Access** This chapter is distributed under the terms of the Creative Commons Attribution Noncommercial License, which permits any noncommercial use, distribution, and reproduction in any medium, provided the original author(s) and source are credited.

## References

1. Indefrey P, Levelt WJM. The spatial and temporal signatures of word production components. *Cognition*. 2004;92:101–44.
2. Simonyan K, Horwitz B. Laryngeal motor cortex and control of speech in humans. *Neuroscientist*. 2011;17:197–208.
3. Ghosh SS, Tourville JA, Guenther FH. A neuroimaging study of premotor lateralization and cerebellar involvement in the production of phonemes and syllables. *J Speech Lang Hear Res*. 2008;51:1183–202.
4. Zarate JM. The neural control of singing. *Front Hum Neurosci*. 2013;7:237.
5. Özdemir E, Norton A, Schlaug G. Shared and distinct neural correlates of singing and speaking. *Neuroimage*. 2006;33:628–35.
6. Kleber B, Veit R, Birbaumer N, Gruzelier J, Lotze M. The brain of opera singers: experience-dependent changes in functional activation. *Cereb Cortex*. 2010;20:1144–52.
7. Onozuka M, Fujita M, Watanabe K, Hirano Y, Niwa M, Nishiyama K, Saito S. Mapping brain region activity during chewing: a functional magnetic resonance imaging study. *J Dent Res*. 2002;81:743–6.
8. Quintero A, Ichesco E, Myers C, Schutt R, Gerstner GE. Brain activity and human unilateral chewing: an fMRI study. *J Dent Res*. 2013;92:136–42.
9. Avivi-Arber L, Martin R, Lee JC, Sessle BJ. Face sensorimotor cortex and its neuroplasticity related to orofacial sensorimotor functions. *Arch Oral Biol*. 2011;56:1440–65.
10. Kaas JH, Qi HX, Iyengar S. Cortical network for representing the teeth and tongue in primates. *Anat Rec A Discov Mol Cell Evol Biol*. 2006;288:182–90.
11. Jain N, Catania KC, Kaas JH. A histologically visible representation of the fingers and palm in primate area 3b and its immutability following long-term deafferentations. *Cereb Cortex*. 1998;8:227–36.
12. Fang PC, Jain N, Kaas JH. Few intrinsic connections cross the hand-face border of area 3b of New World monkeys. *J Comp Neurol*. 2002;454:310–9.
13. Qi HX, Kaas JH. Myelin stains reveal an anatomical framework for the representation of the digits in somatosensory area 3b of macaque monkeys. *J Comp Neurol*. 2004;477:172–87.
14. Manger PR, Woods TM, Muñoz A, Jones EG. Hand/face border as a limiting boundary in the body representation in monkey somatosensory cortex. *J Neurosci*. 1997;17:6338–51.
15. Cerkevich CM, Qi HX, Kaas JH. Corticocortical projections to representations of the teeth, tongue, and face in somatosensory area 3b of macaques. *J Comp Neurol*. 2014;522:546–72.

16. Jain N, Qi HX, Catania KC, Kaas JH. Anatomic correlates of the face and oral cavity representations in the somatosensory cortical area 3b of monkeys. *J Comp Neurol.* 2001;429:455–68.
17. Iyengar S, Qi HX, Jain N, Kaas JH. Cortical and thalamic connections of the representations of the teeth and tongue in somatosensory cortex of New World monkeys. *J Comp Neurol.* 2007;501:95–120.
18. Manger PR, Woods TM, Jones EG. Representation of the face and intraoral structures in area 3b of the squirrel monkey (*Saimiri sciureus*) somatosensory cortex, with special reference to the ipsilateral representation. *J Comp Neurol.* 1995;362:597–607.
19. Manger PR, Woods TM, Jones EG. Representation of face and intra-oral structures in area 3b of macaque monkey somatosensory cortex. *J Comp Neurol.* 1996;371:513–21.
20. Toda T, Taoka M. Hierarchical somesthetic processing of tongue inputs in the postcentral somatosensory cortex of conscious macaque monkeys. *Exp Brain Res.* 2002;147:243–51.
21. Sakamoto K, Nakata H, Yumoto M, Kakigi R. Somatosensory processing of the tongue in humans. *Front Physiol.* 2010;1:136.
22. Ogawa H, Ito S, Nomura T. Oral cavity representation at the frontal operculum of macaque monkeys. *Neurosci Res.* 1989;6:283–98.
23. Hirata S, Nakamura T, Ifuku H, Ogawa H. Gustatory coding in the precentral extension of area 3 in Japanese macaque monkeys; comparison with area G. *Exp Brain Res.* 2005;165:435–46.
24. Toda T, Hayashi H. Functional organization in the orofacial region of the postcentral somatosensory cortex. *J Oral Biosci.* 2010;52:365–70.
25. Toda T, Taoka M. Converging patterns of inputs from oral structures in the postcentral somatosensory cortex of conscious macaque monkeys. *Exp Brain Res.* 2004;158:43–9.
26. Iwamura Y. Hierarchical somatosensory processing. *Curr Opin Neurobiol.* 1998;8:522–8.
27. Toda T, Taoka M. Hierarchical neural process to detect moving tactile stimuli in the postcentral oral representation of conscious macaque monkeys. *J Oral Biosci.* 2005;47:253–62.
28. Miyamoto JJ, Honda M, Saito DN, Okada T, Ono T, Ohyama K, Sadato N. The representation of the human oral area in the somatosensory cortex: a functional MRI study. *Cereb Cortex.* 2006;16:669–75.
29. Lin LD, Murray GM, Sessle BJ. Functional properties of single neurons in the primate face primary somatosensory cortex. I. Relations with trained orofacial motor behaviors. *J Neurophysiol.* 1994;71:2377–90.
30. Lin LD, Murray GM, Sessle BJ. Functional properties of single neurons in the primate face primary somatosensory cortex. II. Relations with different directions of trained tongue protrusion. *J Neurophysiol.* 1994;71:2391–400.
31. Lin LD, Sessle BJ. Functional properties of single neurons in the primate face primary somatosensory cortex. III. Modulation of responses to peripheral stimuli during trained orofacial motor behaviors. *J Neurophysiol.* 1994;71:2401–13.
32. Hatanaka N, Tokuno H, Nambu A, Inoue T, Takada M. Input–output organization of jaw movement-related areas in monkey frontal cortex. *J Comp Neurol.* 2005;492:401–25.
33. Huang CS, Hiraba H, Sessle BJ. Input–output relationships of the primary face motor cortex in the monkey (*Macaca fascicularis*). *J Neurophysiol.* 1989;61:350–62.
34. Sessle BJ. Face sensorimotor cortex: Its role and neuroplasticity in the control of orofacial movements. *Prog Brain Res.* 2011;188:71–82.
35. Biedenbach MA, Van Hassel HJ, Brown AC. Tooth pulp driven neurons in somatosensory cortex of primates: role in pain mechanisms including a review of the literature. *Pain.* 1979;7:31–50.
36. Iwata K, Tsuboi Y, Sumino R. Primary somatosensory cortical neuronal activity during monkey's detection of perceived change in tooth-pulp stimulus intensity. *J Neurophysiol.* 1998;79:1717–25.
37. Dreyer DA, Loe PR, Metz CB, Whitsel BL. Representation of head and face in postcentral gyrus of the macaque. *J Neurophysiol.* 1975;38:714–33.

38. Yokochi H, Tanaka M, Kumashiro M, Iriki A. Inferior parietal somatosensory neurons coding face-hand coordination in Japanese macaques. *Somatosens Mot Res.* 2003;20:115–25.
39. Taoka M, Tanaka M, Hihara S, Ojima H, Iriki A. Neural response to movement of the hand and mouth in the secondary somatosensory cortex of Japanese monkeys during a simple feeding task. *Somatosens Mot Res.* 2013;30:140–52.
40. Toda T, Hayashi H. The gross temporal correlation of nearby neuron activity in the macaque postcentral somatosensory cortex representing orofacial structures: with special reference to numerical methods for analysis. *J Oral Biosci.* 2011;53:170–81.
41. Fellous JM, Tiesinga PH, Thomas PJ, Sejnowski TJ. Discovering spike patterns in neuronal responses. *J Neurosci.* 2004;24:2989–3001.
42. Arce FI, Lee JC, Ross CF, Sessle BJ, Hatsopoulos NG. Directional information from neuronal ensembles in the primate orofacial sensorimotor cortex. *J Neurophysiol.* 2013;110:1357–69.
43. Shinomoto S, Kim H, Shimokawa T, Matsuno N, Funahashi S, Shima K, et al. Relating neuronal firing patterns to functional differentiation of cerebral cortex. *PLoS Comput Biol.* 2009;5:e1000433. doi:[10.1371/journal.pcbi.1000433](https://doi.org/10.1371/journal.pcbi.1000433).
44. O'Doherty JE, Lebedev MA, Ifft PJ, Zhuang KZ, Shokur S, Bleuler H, Nicolelis MA. Active tactile exploration using a brain-machine-brain interface. *Nature.* 2011;479:228–31.
45. Medina LE, Lebedev MA, O'Doherty JE, Nicolelis MA. Stochastic facilitation of artificial tactile sensation in primates. *J Neurosci.* 2012;32:14271–5.

## Chapter 25

# Possible Roles of IL-33 in Periodontal Diseases: *Porphyromonas gingivalis* Induced IL-33 in Human Gingival Epithelial Cells

Hiroyuki Tada, Hidetoshi Shimauchi, Haruhiko Takada,  
and Kenji Matsushita

**Abstract** In the oral mucosa, epithelial cells work not only as a physical barrier to pathogens, but also play a pivotal role in initiating immune responses to microbes. Interleukin (IL)-33, a member of the IL-1 family, is constitutively expressed in epithelial cells and amplifies Th2-type inflammatory immune responses. We found that IL-33 was detected in the inflamed gingival epithelium from chronic periodontitis patients, and periodontopathic *Porphyromonas gingivalis* strongly increased expressions of IL-33 mRNA and molecules in human gingival epithelial cells. In contrast, fimbriae, a lipopeptide and lipopolysaccharide derived from *P. gingivalis* were not active in this respect. Protease inhibitors specific for gingipains efficiently inhibited the induction of IL-33 mRNA by stimulation with *P. gingivalis*. Furthermore, *P. gingivalis* KDP136, a gingipains-null mutant, did not increase IL-33 mRNA expression. We also demonstrated that *P. gingivalis* upregulated IL-33 mRNA expression through protease-activated receptor-2, phospholipase C, mitogen-activated protein kinase p38 and NF- $\kappa$ B. IL-33 is suggested to negatively regulate antimicrobial peptide LL-37, resulting in attenuation of innate immune responses of gingival epithelial cells in chronic periodontitis. Possible roles of IL-33 in inflammation in the oral mucosa are discussed.

**Keywords** Gingipains • Gingival epithelial cells • Interleukin-33 • LL-37  
• *Porphyromonas gingivalis*

---

H. Tada (✉) • H. Takada

Division of Oral Microbiology, Department of Oral Biology, Tohoku University Graduate School of Dentistry, 4-1 Seiryo-machi, Aoba-ku, Sendai 980-8575, Japan  
e-mail: [htada@dent.tohoku.ac.jp](mailto:htada@dent.tohoku.ac.jp)

H. Shimauchi

Division of Periodontology and Endodontology, Department of Oral Biology, Tohoku University Graduate School of Dentistry, Sendai, Japan

K. Matsushita

Department of Oral Disease Research, National Center for Geriatrics and Gerontology, Obu, Japan

## 25.1 Introduction

In mucosal immune systems, including the oral mucosa, epithelial cells work not only as a physical barrier to bacterial pathogens, but also play a pivotal role in initiating and amplifying Th2-type immune responses in response to bacterial components [1, 2]. Epithelial cells produce interleukin (IL)-33, IL-25, and thymic stromal lymphopoietin, which may be involved in the development and regulation of Th2-type inflammatory responses. IL-33 is a member of the IL-1 cytokine family, and is constitutively expressed in epithelial cells, endothelial cells and fibroblasts [3]. IL-33 consists of two domains: a non-classical homeodomain-like helix-turn-helix DNA-binding domain, which consists of a chromatin-binding motif (CBM) and a nuclear localization sequence (NLS), and an IL-1-like domain [4] (Fig. 25.1a). IL-33 localizes in the nuclei of resting epithelial cells and acts as an alarmin when released from necrotic cells (Fig. 25.1b). IL-33 has a protective role in inflammatory bowel disease [7] and in the initiation of *Toxoplasma* infection that polarizes adaptive responses towards a Th2-biased response, which is protective in this disease [8]. In contrast, a lot of evidence suggests that IL-33 is also involved in the development of chronic inflammatory diseases such as arthritis [9]. IL-33 signals through the IL-33 receptor (IL-33R), which consists of heterodimers of ST2 and IL-1 receptor accessory protein (IL-1RAcP) [5, 6] (Fig. 25.2). IL-33 upon binding to ST2 induces the recruitment of IL-1RAcP and myeloid differentiation primary-response protein 88 (MyD88) to the Toll/IL-1R (TIR) domain in the

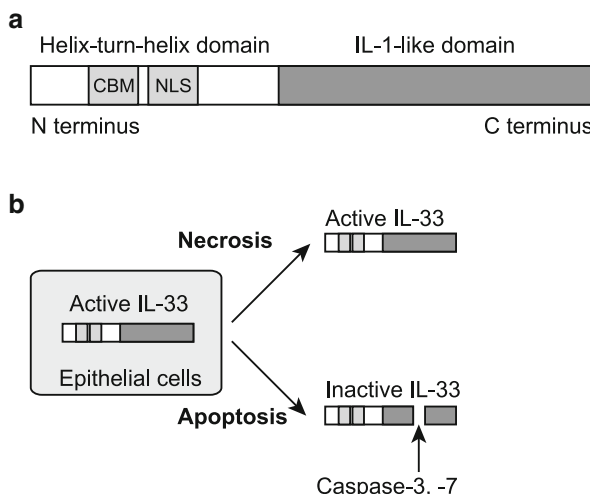


**Fig. 25.1** (a) Structure of IL-33 protein. IL-33 is a 30-kDa protein that consists of 270 amino acids. IL-33 consists of two domains: a helix-turn-helix domain and an IL-1-like domain. The helix-turn-helix domain contains a chromatin-binding motif (CBM) and a nuclear localization signal (NLS). (b) Release of IL-33. Active form of IL-33 is thought to be released by necrosis. IL-33 is inactivated by cleaving with caspase-3 or caspase-7 during apoptosis. Based on Martin, Oboki et al. and Palmer and Gabay [4–6]

**Fig. 25.2** IL-33 signaling pathways. IL-33 signaling through the IL-33 receptor (IL-33R), which consists ST2 and IL-1 receptor accessory protein (IL-1RAcP) dimers and myeloid differentiation primary-response protein 88 (MyD88) to the Toll/IL-1R (TIR) domain in the cytoplasmic region of ST2. The MyD88 and TRAF6 complex activates NF- $\kappa$ B- and MAP kinase-mediated signaling pathways. Based on Martin, Oboki et al. and Palmer and Gabay [4–6]

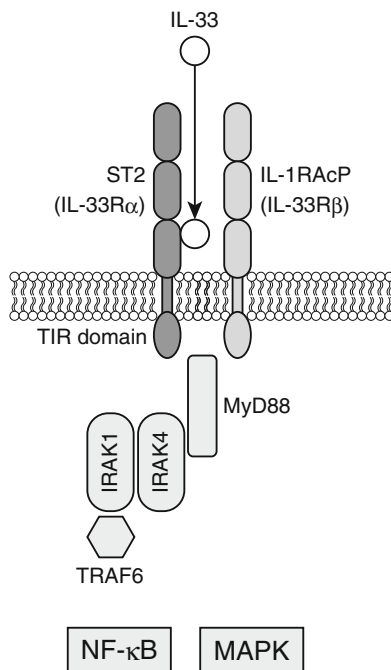


**Table 25.1** Articles on IL-33 in oral/dental science

Finding	Reference
IL-33 mRNA and protein expressions are enhanced by <i>P. gingivalis</i> LPS in human monocytes	Nile et al. 2010 [10]
IL-33 protein expressions are not differentiated from human gingival crevicular fluid, saliva, or plasma in chronic periodontitis	Buduneli et al. 2012 [11]
IL-33 protein expression is enhanced by TNF- $\alpha$ in human gingival fibroblasts	Beklen et al. 2013 [12]
IL-33 protein expression is not detected from human gingival crevicular fluid in gingivitis or periodontitis	Papathanasiou et al. 2014 [13]

cytoplasmic region of ST2. The MyD88 and TRAF6 complex activates NF- $\kappa$ B- and MAP kinase-mediated signaling pathways [5, 6].

*Porphyromonas gingivalis* is a periodontopathic pathogen in chronic periodontitis and has a variety of virulence factors that induce proinflammatory cytokines leading to chronic inflammation, resulting in destruction of periodontal tissues. In the dental/oral field, only limited information on IL-33 is available (see Table 25.1). TNF- $\alpha$  induces IL-33 expression in human gingival fibroblasts [12], although whether IL-33 expression is increased in the periodontal tissues in chronic periodontitis patients and the functions of IL-33 in the modulation of chronic periodontitis remain unelucidated. This review article shows possible regulation of IL-33

expression in human gingival epithelial cells in response to *P. gingivalis* based on our recent studies, and discusses possible roles of IL-33 expressed in gingival epithelial cells in relation to the pathogenesis of chronic periodontitis.

## 25.2 Expression of IL-33 in Periodontal Tissues from Chronic Periodontitis Patients

We first examined whether inflamed gingival tissues from chronic periodontitis patients expressed IL-33 by immunohistochemical studies using an anti-human IL-33 monoclonal antibody (mAb). As expected, IL-33 was strongly expressed in the cytoplasm of the inflamed gingival epithelium from chronic periodontitis patients, but only weakly detected in the normal gingival epithelium from healthy individuals. Unlike the expression of IL-33 in the gingival epithelium, IL-33 expression in the lamina propria of gingival tissues was only weakly observed. IL-33 expression is possibly upregulated in epithelial, mesenchymal, and myeloid cells in response to proinflammatory stimuli, pathogen-associated molecular patterns, and pathogens [5]. These findings suggest that gingival epithelial cells are capable of inducing IL-33 expression upon infection with periodontal pathogens.

## 25.3 Possible Induction of IL-33 by Gingipains from *P. gingivalis* in Gingival Epithelial Cells

### 25.3.1 *P. gingivalis* Induces IL-33 mRNA Expression in Human Gingival Epithelial Cells in Culture

As *P. gingivalis* is implicated as a major pathogenic bacteria for chronic periodontitis [14], we examined the effect of *P. gingivalis* infection on IL-33 mRNA expression in human gingival epithelial cells in culture. The IL-33 mRNA expression was increased 20-fold at 48 h after stimulation with *P. gingivalis* W83 in Ca9-22 cells, which is a human gingival epithelial cell line established from squamous cell carcinoma. Pretreatment of the cells with cycloheximide, a protein synthesis inhibitor, blocked the induction of IL-33 mRNA levels, suggesting that *de novo* protein synthesis was required for *P. gingivalis*-mediated IL-33 mRNA induction. Nile et al. [10] reported that *P. gingivalis* LPS induced IL-33 expression in human monocytes. Therefore, we examined the possible IL-33 mRNA-inducing capacity of *P. gingivalis*-related specimens; fimbriae (Toll-like receptor (TLR) 2 ligand [15]) and LPS (TLR2 and 4 ligand [16]) prepared from *P. gingivalis*, and synthetic *P. gingivalis*-type lipopeptide PGTP2-RL (TLR2/1 ligand [17]). Unlike *P. gingivalis* whole cells, fimbriae and lipopeptide were completely

inactive, and LPS specimens were only weakly active in this respect. These results suggest that gingival epithelial cells respond to *P. gingivalis* rather than TLR ligands for induction of IL-33 mRNA.

### **25.3.2 *Involvement of Gingipains in the Induction of IL-33 mRNA Expression in Human Gingival Epithelial Cells by P. gingivalis***

*P. gingivalis* produces two types of arginine-specific cysteine proteinases (Arg-gingipains, RgpA and RgpB) and a lysine-specific cysteine proteinase (Lys-gingipain, Kgp) [18]. Gingipains are localized to a cell-associated form, a soluble form, and released as outer membrane blebs [18]. We next examined whether enzymatic activities of gingipains are involved in the IL-33-inducing capacity in Ca9-22 cells and primary oral epithelial cells. The induction of IL-33 mRNA expression by *P. gingivalis* W83 in the two types was completely and significantly inhibited by FPR-cmk (Rgp inhibitor) and KYT-36 (Kgp inhibitor), respectively. Furthermore, *P. gingivalis* KDP136, a gingipains-null mutant, unlike *P. gingivalis* ATCC 33277, a wild-type parent strain of KDP136, did not induce IL-33 mRNA expression in either cell type. *P. gingivalis*-induced IL-33 mRNA expression was abolished by heat treatment (70 °C, 1 h) to inactivate enzymatic activities of *P. gingivalis*. We confirmed intact proteolytic activities for Rgps and Kgp in the whole cells of *P. gingivalis* W83 and ATCC 33277, but not in those of *P. gingivalis* KDP136. These observations suggest that the proteolytic activity of gingipains is essential for the induction of IL-33 mRNA expression by *P. gingivalis* in human gingival epithelial cells.

### **25.3.3 *Induction of the IL-33 Molecule by P. gingivalis in Human Gingival Epithelial Cells***

Next, we examined whether *P. gingivalis* induced IL-33 expression in human gingival epithelial cells using an immunoblot analysis. IL-33 expression in Ca9-22 cells was increased tenfold with a peak at 4 days by stimulation with whole cell preparations of *P. gingivalis*. Epithelial cells constitutively express IL-33 in their nuclei under resting conditions [19]. IL-33 is a nuclear protein that is also released into the extracellular environment. To further determine whether *P. gingivalis*-induced IL-33 was accumulated in the nuclei or the cytoplasm, we analyzed the location of IL-33 protein in Ca9-22 cells after stimulation with *P. gingivalis* using immunocytochemical analysis. Although IL-33 was constitutively expressed in the resting cells, IL-33 molecules accumulated in the cytoplasm of the cells when they were stimulated with *P. gingivalis* for 4 days. However, the

released IL-33 level was quite low (approximately 30 pg/mL), even after stimulation with *P. gingivalis* whole cells. IL-33 is not detected in viable human monocytic cells, even upon stimulation with *P. gingivalis* LPS [10]. Furthermore, IL-33 levels in gingival crevicular fluid (GCF) are not different between chronic periodontitis patients and healthy controls [11]. In fact, IL-33 is not detected in the GCF of inflamed regions from chronic periodontitis patients [13]. Further studies are required to elucidate the fate of IL-33 induced by *P. gingivalis* in gingival epithelial cells, which may modulate the innate immune functions of the cells in infected periodontal lesions.

## 25.4 PAR-2-p38/NF- $\kappa$ B-Mediated Signals in IL-33 Induction

### 25.4.1 Role of PAR-2 in the Induction of IL-33 by Gingipains

Proteinase-activated receptor-2 (PAR-2) is a seven-transmembrane domain receptor family which couples to G-proteins [20]. Rgps are capable of activating PAR-2 expressed on human gingival epithelial cells, which produce proinflammatory cytokines [21]. We examined the possible involvement of PAR-2 in *P. gingivalis*-induced IL-33 mRNA expression. Ca9-22 cells constitutively expressed PAR-1, -2, -3, and -4 mRNA. PAR-2 mRNA expression was increased upon stimulation with *P. gingivalis* W38 in Ca9-22 cells. Next, we performed inhibition of PAR-2 mRNA expression by RNA interference using a PAR-2-specific small interference RNA (siRNA). The induction of IL-33 mRNA by *P. gingivalis* W83 was partially inhibited in PAR-2 siRNA-transfected cells. PAR-2 is activated by a tethered ligand when cleaved by protease. A PAR-2 agonist peptide based on the tethered ligand sequences can activate PAR-2 in a proteolysis-independent manner. However, the PAR-2 agonist peptide was not able to induce IL-33 mRNA in Ca9-22 cells. Pretreatment of the cells with cytochalasin D, a particle internalization inhibitor, inhibited the IL-33 mRNA induction by *P. gingivalis*. These findings suggested that both proteolytic activation of PAR-2 by gingipains and the endocytosis of *P. gingivalis* are required for the up-regulation of IL-33 expression induced by *P. gingivalis* in oral epithelial cells. *P. gingivalis* enters gingival epithelial cells by endocytosis, which mediates binding of Rgp to the cells [22]. It must be noted that gingipains are required for maturation of *P. gingivalis* fimbriae [23], which is essential for internalization of the bacterium into epithelial cells [24]. However, endocytosis of both PAR-2 and *P. gingivalis* are probably required for the up-regulation of IL-33 in gingival epithelial cells.

### **25.4.2 Involvement of PLC in the Induction of IL-33 by Gingipains**

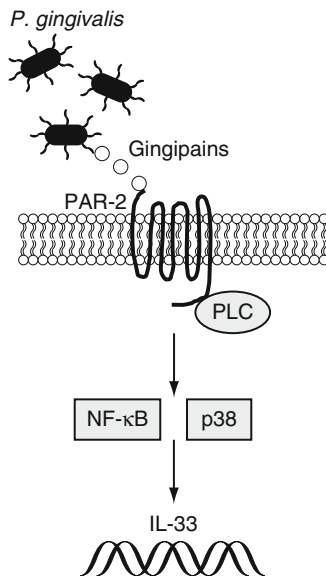
Because PAR-2 has been reported to be coupled to G protein, leading to activation of phospholipase C (PLC) [25, 26], we examined whether or not the PLC pathway is involved in *P. gingivalis*-induced IL-33 mRNA expression in Ca9-22 cells. The cells were pretreated with U-73122, a PLC inhibitor, and then stimulated *P. gingivalis* W83 for 48 h. The pretreatment significantly inhibited the *P. gingivalis*-induced IL-33 mRNA expression. In contrast, a protein kinase C (PKC) inhibitor, GF-109203X, did not inhibit either the basal level of IL-33 or the *P. gingivalis*-induced increase in IL-33. These findings suggest that *P. gingivalis*-induced up-regulation of IL-33 expression is mediated via a PAR-2-PLC-signaling pathway.

### **25.4.3 Involvement of p38 and NF-κB in the Induction of IL-33 by Gingipains**

As p38 and NF-κB are implicated in PAR-2 signaling [27], we first confirmed p38 phosphorylation in Ca9-22 cells stimulated with *P. gingivalis* W83. Then, we demonstrated that p38 signaling is involved in *P. gingivalis*-induced IL-33 mRNA expression using SB203580, a p38 inhibitor. In contrast, the *P. gingivalis* IL-33 mRNA expression was not inhibited by PD98059, an ERK1/2 inhibitor, or SP600125, a JNK inhibitor. Further, we demonstrated that gingipains are responsible for p38 activation caused by whole cells of *P. gingivalis* because p38 phosphorylation induced by *P. gingivalis* W83 was completely inhibited when *P. gingivalis* was treated with Rgp inhibitor FPR-cmk plus Kgp inhibitor KYT-36. In addition, p38 phosphorylation was not observed in the cells stimulated with *P. gingivalis* KDP136, a gingipains-null mutant.

Next, we demonstrated NF-κB activation in Ca9-22 cells stimulated with *P. gingivalis* W83 using a luciferase reporter assay. We demonstrated that NF-κB signaling is involved in *P. gingivalis*-induced IL-33 mRNA expression because pretreatment of cells with PDTC, an NF-κB inhibitor, significantly inhibited *P. gingivalis*-induced IL-33 mRNA expression. The NF-κB activities induced by *P. gingivalis* W83 were markedly diminished by FPR-cmk plus KYT-36, and the NF-κB activation was attenuated in the cells stimulated with *P. gingivalis* KDP136, indicating that gingipains are responsible for NF-κB activation caused by whole cells of *P. gingivalis*. Taken together, we demonstrated that the *P. gingivalis*-derived gingipain-mediated IL-33 increase was dependent on PAR-2-PLC-p38/NF-κB signaling (Fig. 25.3).

**Fig. 25.3** Role of gingipains in the induction of IL-33 via PAR-2-p38/NF- $\kappa$ B-mediated signals



## 25.5 Future Prospects: Possible Roles of IL-33 in Gingival Epithelial Cells in Chronic Periodontitis

Gingival epithelial cells play integral roles in innate immune defense by sensing periodontal pathogens, maintaining a physical barrier, and expressing antimicrobial peptides (AMPs) [28]. AMPs constitute an important component in the innate immune response. In humans, two main classes of cationic AMPs, the cathelicidins and the defensins, are expressed in a various type of cells, such as epithelial cells, neutrophils, and macrophages. LL-37, a 37-residue mature antimicrobial peptide with two leucine residues, is a 37 amino acid peptide derived from human cathelicidin, a cationic antimicrobial peptide of 18-kDa (CAP18). The peptide is mainly produced by epithelial cells and neutrophils [29] and detected in GCF [30]. Human  $\beta$ -defensin-2 (hBD-2), an antimicrobial peptide of the  $\beta$ -defensin family, is induced by gingipains through PAR-2 in gingival epithelial cells [31]. It has been reported that hBD-2 production is down-regulated by pretreatment with IL-33 in human foreskin keratinocytes [32]. Endogenous expression of LL-37 plays an important role in intracellular killing of mycobacteria in macrophages [33].

To address whether development of chronic periodontitis is attributable to IL-33, we examined the influence of *P. gingivalis*-mediated IL-33 production on the induction of LL-37 in human gingival epithelial cells. Indeed, we found that *P. gingivalis*-induced CAMP (LL-37 gene) mRNA expression was up-regulated in IL-33 siRNA-transfected Ca9-22 cells. LL-37 is capable of proteolytically degradation by gingipains secreted by *P. gingivalis*; however, the antibacterial activity of LL-37 is still intact in the presence of *P. gingivalis* proteases [34].

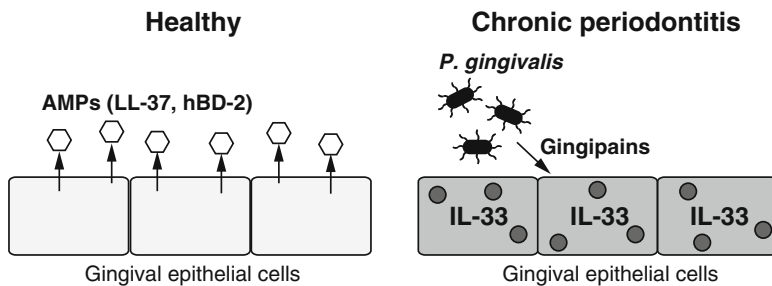


**Fig. 25.4** A hypothetical model for the role of IL-33 induced by *P. gingivalis* in the down-regulation of LL-37 expression in human gingival epithelial cells

These findings indicate that IL-33 may attenuate antimicrobial immune responses by epithelial cells against bacterial mucosal infections.

In this study, we revealed that *P. gingivalis* induced IL-33 via PAR-2-PLC-p38/NF- $\kappa$ B signaling pathways and that the IL-33 down-regulated LL-37 expression in human gingival epithelial cells. These findings suggest evasion of innate immune responses by *P. gingivalis* is due to inhibition of antimicrobial peptide expression (Fig. 25.4). Further studies are necessary to elucidate the role of intracellular IL-33 in maintaining host defense mechanisms in gingival epithelial cells against periodontal diseases.

**Open Access** This chapter is distributed under the terms of the Creative Commons Attribution Noncommercial License, which permits any noncommercial use, distribution, and reproduction in any medium, provided the original author(s) and source are credited.

## References

1. Saenz SA, Taylor BC, Artis D. Welcome to the neighborhood: epithelial cell-derived cytokines license innate and adaptive immune responses at mucosal sites. *Immunol Rev*. 2008;226:172–90.
2. Paul WE, Zhu J. How are T(H)2-type immune responses initiated and amplified? *Nat Rev Immunol*. 2010;10:225–35.
3. Schmitz J, Owyang A, Oldham E, Song Y, Murphy E, McClanahan TK, et al. IL-33, an interleukin-1-like cytokine that signals via the IL-1 receptor-related protein ST2 and induces T helper type 2-associated cytokines. *Immunity*. 2005;23:479–90.
4. Martin MU. Special aspects of interleukin-33 and the IL-33 receptor complex. *Semin Immunol*. 2013;25(6):449–57. doi:[10.1016/j.smim.2013.10.006](https://doi.org/10.1016/j.smim.2013.10.006).
5. Oboki K, Ohno T, Kajiwara N, Saito H, Nakae S. IL-33 and IL-33 receptors in host defense and diseases. *Allergol Int*. 2010;59:143–60.
6. Palmer G, Gabay C. Interleukin-33 biology with potential insights into human diseases. *Nat Rev Rheumatol*. 2011;7(6):321–9. doi:[10.1038/nrrheum.2011.53](https://doi.org/10.1038/nrrheum.2011.53).
7. Pastorelli L, Garg RR, Hoang SB, Spina L, Mattioli B, Scarpa M, et al. Epithelial-derived IL-33 and its receptor ST2 are dysregulated in ulcerative colitis and in experimental Th1/Th2 driven enteritis. *Proc Natl Acad Sci U S A*. 2010;107(17):8017–22. doi:[10.1073/pnas.0912678107](https://doi.org/10.1073/pnas.0912678107).

8. Jones LA, Roberts F, Nickdel MB, Brombacher F, McKenzie AN, Henriquez FL, et al. IL-33 receptor (T1/ST2) signalling is necessary to prevent the development of encephalitis in mice infected with *Toxoplasma gondii*. *Eur J Immunol.* 2010;40(2):426–36. doi:[10.1002/eji.200939705](https://doi.org/10.1002/eji.200939705).
9. Xu D, Jiang HR, Kewin P, Li Y, Mu R, Fraser AR, et al. IL-33 exacerbates antigen-induced arthritis by activating mast cells. *Proc Natl Acad Sci U S A.* 2008;105(31):10913–8. doi:[10.1073/pnas.0801898105](https://doi.org/10.1073/pnas.0801898105).
10. Nile CJ, Barksby E, Jitprasertwong P, Preshaw PM, Taylor JJ. Expression and regulation of interleukin-33 in human monocytes. *Immunology.* 2010;130:172–80.
11. Buduneli N, Ozcaka O, Nalbantsoy A. Interleukin-33 levels in gingival crevicular fluid, saliva, or plasma do not differentiate chronic periodontitis. *J Periodontol.* 2012;83(3):362–8. doi:[10.1902/jop.2011.110239](https://doi.org/10.1902/jop.2011.110239).
12. Beklen A, Tsao G. Interleukin-1 superfamily member, interleukin-33, in periodontal diseases. *Biotech Histochem.* 2013; doi:[10.3109/10520295.2013.832800](https://doi.org/10.3109/10520295.2013.832800).
13. Papathanasiou E, Teles F, Griffin T, Arguello E, Finkelman M, Hanley J, et al. Gingival crevicular fluid levels of interferon-gamma, but not interleukin-4 or –33 or thymic stromal lymphopoietin, are increased in inflamed sites in patients with periodontal disease. *J Periodontal Res.* 2014;49(1):55–61. doi:[10.1111/jre.12078](https://doi.org/10.1111/jre.12078).
14. Pathirana RD, O'Brien-Simpson NM, Reynolds EC. Host immune responses to *Porphyromonas gingivalis* antigens. *Periodontol 2000.* 2010;52(1):218–37. doi:[10.1111/j.1600-0757.2009.00330.x](https://doi.org/10.1111/j.1600-0757.2009.00330.x).
15. Ogawa T, Asai Y, Hashimoto M, Uchida H. Bacterial fimbriae activate human peripheral blood monocytes utilizing TLR2, CD14 and CD11a/CD18 as cellular receptors. *Eur J Immunol.* 2002;32:2543–50.
16. Darveau RP, Pham TT, Lemley K, Reife RA, Bainbridge BW, Coats SR, et al. *Porphyromonas gingivalis* lipopolysaccharide contains multiple lipid A species that functionally interact with both toll-like receptors 2 and 4. *Infect Immun.* 2004;72(9):5041–51. doi:[10.1128/IAI.72.9.5041-5051.2004](https://doi.org/10.1128/IAI.72.9.5041-5051.2004).
17. Hashimoto M, Asai Y, Ogawa T. Separation and structural analysis of lipoprotein in a lipopolysaccharide preparation from *Porphyromonas gingivalis*. *Int Immunol.* 2004;16:1431–7.
18. Potempa J, Sroka A, Imamura T, Travis J. Gingipains, the major cysteine proteinases and virulence factors of *Porphyromonas gingivalis*: structure, function and assembly of multidomain protein complexes. *Curr Protein Pept Sci.* 2003;4(6):397–407.
19. Moussion C, Ortega N, Girard JP. The IL-1-like cytokine IL-33 is constitutively expressed in the nucleus of endothelial cells and epithelial cells in vivo: a novel ‘alarmin’? *PLoS One.* 2008;3:e3331.
20. Rothmeier AS, Ruf W. Protease-activated receptor 2 signaling in inflammation. *Semin Immunopathol.* 2012;34:133–49.
21. Lourbakos A, Potempa J, Travis J, D'Andrea MR, Andrade-Gordon P, Santulli R, et al. Arginine-specific protease from *Porphyromonas gingivalis* activates protease-activated receptors on human oral epithelial cells and induces interleukin-6 secretion. *Infect Immun.* 2001;69:5121–30.
22. Boisvert H, Duncan MJ. Clathrin-dependent entry of a gingipain adhesin peptide and *Porphyromonas gingivalis* into host cells. *Cell Microbiol.* 2008;10(12):2538–52. doi:[10.1111/j.1462-5822.2008.01228.x](https://doi.org/10.1111/j.1462-5822.2008.01228.x).
23. Nakayama K, Yoshimura F, Kadokami T, Yamamoto K. Involvement of arginine-specific cysteine proteinase (Arg-gingipain) in fimbriation of *Porphyromonas gingivalis*. *J Bacteriol.* 1996;178(10):2818–24.
24. Amano A, Nakagawa I, Okahashi N, Hamada N. Variations of *Porphyromonas gingivalis* fimbriae in relation to microbial pathogenesis. *J Periodontal Res.* 2004;39(2):136–42.
25. Bohm SK, Kong W, Bromme D, Smeekens SP, Anderson DC, Connolly A, et al. Molecular cloning, expression and potential functions of the human proteinase-activated receptor-2. *Biochem J.* 1996;314(Pt 3):1009–16.

26. Böhm SK, Khitin LM, Grady EF, Aponte G, Payan DG, Bunnett NW. Mechanisms of desensitization and resensitization of proteinase-activated receptor-2. *J Biol Chem.* 1996;271:22003–16.
27. Belham CM, Tate RJ, Scott PH, Pemberton AD, Miller HR, Wadsworth RM, et al. Trypsin stimulates proteinase-activated receptor-2-dependent and -independent activation of mitogen-activated protein kinases. *Biochem J.* 1996;320(Pt 3):939–46.
28. Gorr SU. Antimicrobial peptides in periodontal innate defense. *Front Oral Biol.* 2012;15:84–98. doi:[10.1159/000329673](https://doi.org/10.1159/000329673).
29. Vandamme D, Landuyt B, Luyten W, Schoofs L. A comprehensive summary of LL-37, the factotum human cathelicidin peptide. *Cell Immunol.* 2012;280(1):22–35. doi:[10.1016/j.cellimm.2012.11.009](https://doi.org/10.1016/j.cellimm.2012.11.009).
30. Puklo M, Guentsch A, Hiemstra PS, Eick S, Potempa J. Analysis of neutrophil-derived antimicrobial peptides in gingival crevicular fluid suggests importance of cathelicidin LL-37 in the innate immune response against periodontogenic bacteria. *Oral Microbiol Immunol.* 2008;23(4):328–35. doi:[10.1111/j.1399-302X.2008.00433.x](https://doi.org/10.1111/j.1399-302X.2008.00433.x).
31. Chung WO, Hansen SR, Rao D, Dale BA. Protease-activated receptor signaling increases epithelial antimicrobial peptide expression. *J Immunol.* 2004;173(8):5165–70.
32. Alase A, Seltmann J, Werfel T, Wittmann M. Interleukin-33 modulates the expression of human beta-defensin 2 in human primary keratinocytes and may influence the susceptibility to bacterial superinfection in acute atopic dermatitis. *Br J Dermatol.* 2012;167(6):1386–9. doi:[10.1111/j.1365-2133.2012.11140.x](https://doi.org/10.1111/j.1365-2133.2012.11140.x).
33. Sonawane A, Santos JC, Mishra BB, Jena P, Progida C, Sorensen OE, et al. Cathelicidin is involved in the intracellular killing of mycobacteria in macrophages. *Cell Microbiol.* 2011;13(10):1601–17. doi:[10.1111/j.1462-5822.2011.01644.x](https://doi.org/10.1111/j.1462-5822.2011.01644.x).
34. Gutner M, Chaushu S, Balter D, Bachrach G. Saliva enables the antimicrobial activity of LL-37 in the presence of proteases of *Porphyromonas gingivalis*. *Infect Immun.* 2009;77(12):5558–63. doi:[10.1128/IAI.00648-09](https://doi.org/10.1128/IAI.00648-09).

# Chapter 26

## Prospects for Liposome-Encapsulated Nisin in the Prevention of Dental Caries

Hideaki Tsumori, Yoshitaka Shimizu, Kohei Nagatoshi, Yutaka Sakurai,  
and Kazuo Yamakami

**Abstract** Dental caries is a common oral bacterial infectious disease. Its prevention requires the control of the causative pathogens, such as *Streptococcus mutans*, that exist within dental plaque. Nisin is a proteinaceous bacteriocin produced by *Lactococcus lactis* that is used to suppress bacterial infections. It has an inhibitory mode of action on a wide range of gram-positive bacteria. Improvements in the medical benefits of antibacterial agents can be achieved if they can be retained in liposomes for a long period after administration. Liposome systems can increase the ability of the encapsulated compounds, which have been widely used to encapsulate many kinds of compounds in various scientific settings. Liposomes can release labile molecules at a moderate rate. Liposome technologies that effectively protect the encapsulated molecules from decomposition have the potential to improve their preventive and therapeutic effects. Therefore, the use of liposomes to administer antimicrobial agents has spurred research into their utility in preventive medicine. The encapsulation of nisin in liposomes can provide means of improving the stability of nisin and its antibacterial effect against *S. mutans*. The present chapter will review the prospects for liposome-encapsulated nisin for the prevention of oral infectious diseases.

**Keywords** Dental caries • Liposome • Nisin • Preventive medicine • *Streptococcus mutans*

---

H. Tsumori

Department of Chemistry, National Defense Medical College, Tokorozawa 359-8513, Japan  
e-mail: [htsumori@ndmc.ac.jp](mailto:htsumori@ndmc.ac.jp)

Y. Shimizu

Research and Development Division, BioMedCore Inc., Sapporo 001-0021, Japan  
e-mail: [shimizuy@bmcore.co.jp](mailto:shimizuy@bmcore.co.jp)

K. Nagatoshi

Eco Friendly Institute Ltd., Fukuoka 818-0013, Japan  
e-mail: [kona\\_bj5pp1@yahoo.co.jp](mailto:kona_bj5pp1@yahoo.co.jp)

Y. Sakurai • K. Yamakami (✉)

Department of Preventive Medicine and Public Health, National Defense Medical College,  
3-2 Namiki, Tokorozawa, Saitama 359-8513, Japan  
e-mail: [ysakurai@ndmc.ac.jp](mailto:ysakurai@ndmc.ac.jp); [yamakami@ndmc.ac.jp](mailto:yamakami@ndmc.ac.jp)

## 26.1 Introduction

Oral diseases related to cariogenic microorganisms, such as dental caries, affect majority of the world's populations [1]. Dental caries results from interaction of specific bacteria with dietary carbohydrates in the oral cavity. *Streptococcus mutans* is a key contributor to the formation of cariogenic glucan biofilms. Nisin is an effective bactericidal agent against gram-positive bacteria [2]. It is a bacteriocin with a molecular mass of 3,354 and is produced by certain strains of *Lactococcus lactis* subsp. *lactis* [3]. The bactericidal activity of nisin against cariogenic streptococci was investigated in vitro and the findings indicated that nisin acts as an inhibitor of typical cariogenic streptococci [4, 5]. It may be possible to use liposomes as a carrier for the effective administration of nisin. Liposomes are artificial spherical vesicles that can be created from lipids. They have been developed and evaluated as carriers to deliver encapsulated molecules to target organs and specific cells in vitro and in vivo [6–9]. Investigations on liposomes have led to their use with many substances, and the encapsulated agents are pharmacodynamically and pharmacokinetically much more efficient than the naked compounds. Liposome-encapsulated substances have been used in various applications such as to retain and control the release of antibacterial compounds [10, 11]. They have been used to deliver pharmaceuticals, and their recent application in the preservation of foods by the encapsulation of nisin has spurred further research into their use with food materials [12, 13]. With regard to liposome formulations, a variety of factors, such as lipid composition, cholesterol content, the presence of a charge on the lipid bilayer, and the size of the vesicle, affect the effectiveness of liposomes as preventive and therapeutic agents [6]. Oral delivery of liposomal bacteriocins is a useful for the treatment to prevent dental caries [5]. Encapsulation technologies, which may shield substances such as nisin from degradation by digestive enzymes, and effectively deliver the encapsulated contents at the same time, could be an advancement in the field of preventive medicine [10].

This review article provides brief background information on liposomal nisin and explores its possible applications with a focus on factors affecting its effectiveness and the advantages it offers for human health by preventing dental caries.

## 26.2 Cariogenic Microorganisms and Dental Caries

The oral cavity harbors many microorganisms that together constitute a complex micro-ecological environment [14]. Dental caries, a chronic infectious disease, is induced by cariogenic microorganisms such as *Streptococcus* spp. The key virulence factors of the microorganisms, insoluble glucans, can be identified when they colonize dental plaque on the surface of the teeth [4, 15]. *S. mutans* in particular has been recognized as a decisive factor in dental caries. Insoluble glucans provide specific binding sites for oral bacterial colonization of the tooth surface and confer

structural integrity on the extracellular matrix, and therefore they are essential for the formation and accumulation of dental glucan biofilms [16]. Because insoluble glucans are synthesized by glucosyltransferases of *S. mutans* and these glucans provide a matrix for dental plaque biofilm, the streptococcus is considered to contribute to the formation of cariogenic biofilms [16, 17]. The streptococcus tenaciously adheres to the glucan and is highly acidogenic and acid-tolerant; these are critical virulence properties in the pathogenesis of dental caries [18]. Therefore, dental caries results from the interaction of *S. mutans* with dietary carbohydrates in the oral cavity; the formation of insoluble glucan biofilms on the tooth surface is a key result of the diet-bacterium interaction [19].

### 26.3 Nisin as a Tool for Preventive Medicine

Nisin is approved for use in foods and is employed as a food preservative in more than 50 countries [20]. It belongs to a group of bactericidal peptides called type A lantibiotics [21]. Two main natural variants of nisin, nisin A and nisin Z, have been discovered [3]. Nisin Z is widely distributed and contains asparagine instead of histidine at position 27 of the amino acid sequence of nisin A. The two variants have nearly equal bactericidal activity, membrane insertion, and pore-forming ability. Nisin is bactericidal against a broad range of gram-positive microorganisms, such as *Staphylococcus aureus* and *Listeria monocytogenes*, and prevents the outgrowth of many *Clostridium* spp. and *Bacillus* spp. [11, 13]. However, stability issues such as proteolytic degradation and oxidation result in reduced bioactivity. It is soluble and stable at acidic pH, but at alkaline pH values its solubility decreases and it becomes biologically inactive [22]. Nisin is a peptide composed of 34 amino acids, including one lanthionine, four  $\beta$ -methyl-lanthionine, one dehydrobutyrine, and two dehydroalanine residues. The internal thioester rings formed by lanthionine are responsible for the conformation of nisin [23]. The lanthionine rings act as conserved binding motifs for the recognition of specific targets and create segments of defined spatial structures in the nisin molecule [24]. The bactericidal activity of nisin has been suggested to be a result of electrostatic interaction of the positively charged carboxylterminal end of the molecule with negatively charged bacterial membrane lipids [25].

Nisin antagonizes a broad spectrum of gram-positive bacteria [26, 27]. It has dual activity against spore-forming bacteria, it inhibiting the outgrowth of spores and killing cells in the vegetative state. The didehydro amino acid residues in nisin interact with the membrane sulphydryl groups of germinating spores [26]. Membrane disruption is considered to be the result of incorporation of nisin into the membrane and subsequent ion channel or pore formation [25]. Membrane potential is abolished in sensitive gram-positive cells as a result of the efflux of  $K^+$ , amino acids and ATP through the membrane pores [28]. Subsequent leakage of ions causes catastrophic changes in transmembrane potential and internal pH. Nisin interacts with high-affinity pyrophosphate binding sites on the membrane-bound

cell wall precursor Lipid II, leading to more effective formation of pores and inhibition of cell wall peptidoglycan biosynthesis [25, 29]. From these investigations, it is evident that nisin should be an effective antibacterial agent [30, 31].

## 26.4 Nisin Against Cariogenic Streptococci

Some antimicrobial agents, such as chlorohexidine, triclosan, xylitol, and cetylpyridinium chloride, have attracted interest as agents for prophylaxis against dental caries by inhibiting the multiplication of cariogenic microorganisms in the oral cavity [4]. However, these agents may cause some side effects such as discoloration of the teeth and tongue, drug resistance, and low solubility [4]. Because nisin is a lanthibiotic, unlike antibiotics, it does not produce drug resistance or chiasmatic resistance [21]. The bactericidal ability of nisin against cariogenic streptococci, such as *S. mutans*, has been investigated as a means of preventing dental caries [4]. Findings suggest that nisin has a potential to be used as a bactericidal agent to prevent dental caries. Liposomal nisin was shown to inhibit *S. mutans* [5]. In addition, nisin did not appear to be toxic to normal human gingival fibroblast and epithelial cells [32]. Therefore, nisin plays a role in inhibiting the viability of cariogenic streptococci.

## 26.5 Liposomes as a Tool for Preventive Medicine

Liposomes are formulated from phospholipid bilayers and consist of colloidal dispersions of lipids in aqueous buffers [33, 34]. Their formation is based on the interactions between phospholipids and water molecules in which the polar headgroups of phospholipids are exposed to the inner and outer aqueous phases and the hydrophobic carbohydrate tails are forced to face each other in a bilayer [12, 35]. Liposomal encapsulation has been shown to stabilize the encapsulated compound against enzymatic degradation and chemical modification [36]. Liposomes can encapsulate hydrophobic and hydrophilic molecules, prevent the decomposition of the encapsulated molecules, and release the compound at designated target organs [37, 38]. The bioactivity of encapsulated molecules can be maintained by the phospholipid vesicle until it is delivered to the target organ or cells, where the contents will be released [9, 39]. Liposomes can range in size from 40–50 nm to 1–2 µm, depending on the method of formulation, lipid components, and intended use [40]. One of the aims of liposome encapsulation in medicine is to increase the therapeutic index of the bioactive material [36, 41]. Encapsulation techniques have been developed in many fields because of the biocompatibility of liposomes, i.e., its ability to encapsulate both hydrophilic and lipophilic molecules, and its ability to deliver these molecules to target sites [42, 43]. In the food industry, liposomes have been used to deliver antibiotics, peptides, vitamins, and

flavors [44, 45]. The encapsulation of bacteriocins, such as nisin in liposomes represents an alternative to overcome problems related to the exploitation of bactericidal activities [5, 40]. Liposomes have been developed and used as carriers for therapeutic agents to improve the delivery of many anticancer and antibiotic compounds [46–48].

The usefulness of conservative therapeutics is restricted by their inability to deliver compounds to target sites. Attempts have been made to overcome this difficulty by providing selective delivery and release of encapsulated compounds. Hydrophobic compounds can be directly encapsulated into liposomes during vesicle formation, and retention is governed by interactions between the compound and lipid. Passive encapsulation of soluble compounds depends on the ability of liposomes to trap aqueous buffer containing dissolved compounds during vesicle formation [49]. The applications of liposomes in medicine and pharmacology can be divided into therapeutic and preventive uses of liposomes composed of various substances [9, 50, 51]. Advances in liposome design lead to applications for the delivery of new technology products such as nucleotides involved in numerous biological functions [48, 52]. There have been many studies on the viability of a range of conservative chemicals formulated in liposomes, frequently resulting in improved biological activity compared with that of the naked form. Many antibiotics are orally available and liposome encapsulation can be developed for labile chemicals with minimal loss of utility. Therefore, liposomes are used in pharmaceutical applications and the encapsulated substances have enhanced efficacy compared with the naked substances. Liposomes are achieving medical acceptance because of the effective shelf life of labile molecules, slow and steady release of the molecules, and delivery of the molecules to required locations [46]. In pharmaceutical applications, liposomes offer drug delivery systems for therapeutic and preventive strategies [53].

## 26.6 Characteristics of Liposomes

The design of liposomal delivery systems accelerates the treatment on human health [6]. The strategy for liposomes is the development of carrier systems with the ability to deliver and release encapsulated compounds [54]. The characteristics of liposomes in this regard depend on their lipid composition, surface charge, and vesicular size. Because bilayer fluidity and rigidity can affect the release of liposomal compounds, studies have been carried out on the effects of phospholipids of different phase transition temperatures on fluidity and the effects of lipid composition on rigidity of liposomes [55, 56]. Liposomes with many different lipid compositions exist, and those that include phospholipids provide efficient vesicles for individual applications [57].

The aim of lipid selection for liposomes is to provide stabilizing and encapsulation abilities. Phosphatidylcholines have been selected for the preparation of liposome vesicles in many settings. The amount of encapsulated content released

from vesicles is proportional to the acyl chain length of the phosphatidylcholine. Dimyristoylphosphatidylcholine (DMPC), dipalmitoylphosphatidylcholine (DPPC) and distearoylphosphatidylcholine (DSPC) have longer saturated acyl chains (14, 16, and 18 carbons, respectively) and their phase transition temperature increases with increasing chain length [58]. The trend in the release of encapsulated compounds from vesicles is in the order of DMPC > DPPC > DSPC, which reflects the fluidity of vesicles composed of DMPC, DPPC, and DSPC with a phase transition temperature of 23, 41, and 55 °C respectively [57]. For example, the configuration of DPPC is a highly ordered gel phase at room temperature; however, above 41 °C the lipid forms a liquid crystalline phase characterized by greater packing disorder because of temperature-induced changes in acyl chain composition [58]. Unsaturated phospholipid species show more permeable and fluidic bilayers, but saturated phospholipids with long acyl chains form a rigid, rather impermeable bilayer structure [33, 37].

The cholesterol in phosphatidylcholine-based liposomes can reduce liposome permeability, because membrane permeability is dependent on fluidity and rigidity [59]. Cholesterol interacts with fatty acids in liposomes by hydrogen bonding, increasing the cohesiveness and mechanical strength of the vesicular membrane [60]. For example, a comparison of nisin-containing phosphatidylcholine liposomes and phosphatidylcholine plus cholesterol showed that cholesterol reduced the release of nisin [38, 61]. The permeability of liposomes can be altered by modifying the cholesterol concentration according to the intended application of the liposomes [57, 62]. Sphingomyelin also increases the rigidity of the bilayer [6]. Therefore, the modification of liposomal composition enables the preparation of preferred kinds of liposomes for various scientific settings.

The effect of charge on lipid behavior is governed by the surface charge density of the liposomes, lipid head groups, and interactions between the encapsulated content and lipid [63, 64]. Liposomes composed of charged polar lipids with higher electrical charges are more stable than those composed of neutral polar lipids. A surface charge on liposomes increases repulsive interactions and reduces the frequency of liposome collisions [65]. With regard to control of the release of encapsulated compounds from liposomes, the charge has been observed to affect vesicle permeability [63]. The use of negatively charged liposomes containing phosphatidylglycerol led to greater effectiveness of the encapsulated molecules compared with the use of neutral or positively charged liposomes. Therefore, potency of the release of encapsulated compounds has been shown to be regulated by polymer size, lipid composition, and surface charge [65].

Liposomes can be used as carriers of many different kinds of compound, such as peptides and nucleotides, because liposomes are spherical vesicles whose membranes are composed of one or more phospholipid bilayers [66]. Phospholipid vesicles are capable of encapsulating labile molecules, and the lipids that they are composed are biodegradable and safe in vivo [67]. Liposome encapsulation of therapeutic and cosmetic agents can extend their activity by improving their stability and permeability and by providing targeted and timed release [68]. Labile compounds that are susceptible to proteolytic degradation, such as insulin,

calcitonin, parathyroid hormone, and erythropoietin, were shown to have improved pharmacological effects after oral administration when encapsulated in liposomes [69]. Oral delivery of liposomal compounds is useful for preventive and therapeutic treatments.

## 26.7 Characteristics of Liposome-Encapsulated Nisin

Nisin is a cationic, amphiphilic antimicrobial peptide that inhibits gram-positive bacteria [30]. The encapsulation efficacy of nisin is higher in liposomes composed of neutral zwitterionic phospholipids, such as phosphatidylcholine, compared with liposomes composed of anionic phospholipids, such as phosphatidylglycerol [40, 61]. The highest nisin encapsulation efficacy was achieved in liposomes having low contents of negatively charged phospholipids and high contents of zwitterionic phospholipids [70]. Encapsulation of positively charged nisin in anionic phospholipids should result in association because of attractive electrostatic interactions, whereas encapsulation in neutral liposomes should result in association because of hydrophobic interactions [71]. The electrostatic interaction of nisin with negatively charged membrane phospholipids is more pronounced than its interaction with neutral phospholipids [25]. Cationic vesicles containing stearylamine showed lower encapsulation efficiency when compared with other kind of vesicles, which could result from electrostatic repulsion between positively charged nisin and cationic vesicles [35]. The functional properties of liposomal nisin depend on the interaction of nisin with the liposome membrane and with the bacterial cell membrane. Such electrostatic interactions are considered to be the initial step in the series of events leading to membrane pore formation [72]. Nisin proved to have high penetration ability for anionic phospholipids and low penetration ability for neutral phospholipids [71]. Nisin in liposomes composed of phosphatidylcholine demonstrated the slowest release of nisin, whereas liposomes composed of phosphatidylcholine plus phosphatidylglycerol appeared to release efficiently [65]. Because nisin is positively charged at neutral pH, electrostatic interaction with negatively charged phosphatidylglycerol was attractive and should have led to the formation of unstable pores because of binding to the charged phospholipid head groups of phosphatidylglycerol [25]. The activity of the encapsulated nisin is expressed by providing relatively short-term effects by release of the encapsulated nisin and long-term effects by deposition of lipid-membrane-immobilized nisin, i.e., bactericidal activity [28]. Therefore, encapsulated nisin and membrane-immobilized nisin provide a tool for inhibiting pathogenic microbes.

Regarding the applications of nisin, various studies have shown the efficiency of liposome-encapsulated nisin in food models [12]. The encapsulation of nisin improves its antimicrobial activity as a food preservative and for the prevention of oral infectious diseases [73]. Liposomal nisin should be able to provide effective long-term inhibition of the target microbe, *S. mutans*, and therefore preventing dental caries [5]. The surface charge of the liposome influences the interaction

between liposomal nisin and bacteria [63]. As the bacterial cell has a negative charge, electrostatic repulsion is induced between the cell surface and liposomes composed of phosphatidylglycerol, preventing direct contact of the liposome with the microbes, and the subsequent release of nisin [61]. This assumption supports the idea that interaction between liposomes and microbes improves membrane fusion [73].

## 26.8 Liposome-Encapsulated Nisin as a Preventive Agent for Oral and Dental Health

There are relatively few published data regarding liposome-encapsulated nisin for the prevention of oral infectious diseases. There is a report that liposomal nisin inhibited the viability of *S. mutans* in vitro [5]. The inhibition of streptococcal viability led to the suppression of insoluble glucan formation by the streptococcus [5]. Previous studies have reported the synergistic antibacterial effects of combinations of antimicrobials, such as nisin plus ethylenediaminetetraacetic acid (EDTA), against gram-negative pathogens [74]. The ability of EDTA to destabilize the outer membrane of gram-negative bacteria by sequestering ions such as  $\text{Ca}^{2+}$  and  $\text{Mg}^{2+}$  is considered to enable nisin to access the cell membrane, thereby increasing its inhibitory effect [74]. The feasibility of encapsulating nisin plus EDTA in vesicles for the inhibition of *L. monocytogenes* and *Escherichia coli* O157:H7 was investigated [43, 65]. Coencapsulation of nisin plus EDTA increased the inhibitory potential of liposomes against gram-positive *S. mutans* and gram-negative *Porphyromonas gingivalis* [40, 74]. These findings indicate that the liposomal nisin plus EDTA can inhibit the both of which could prevent dental caries and periodontitis.

## 26.9 Prospects for Liposome-Encapsulated Nisin

Encapsulation of nisin in liposome carrier provides long-lasting inhibition of the oral pathogen *S. mutans*. The appropriate balancing of the lipid components of the vesicles allows the construction of stable liposomal nisin that provides predictable release of the bactericidal agent. The results obtained so far encourage the study of liposomal nisin with the aim of developing potential tools for the prevention of dental caries. We are focusing on the application of liposomal technology in order to ascertain the bactericidal potential of liposomes as an effective carrier of nisin for oral health in humans.

**Open Access** This chapter is distributed under the terms of the Creative Commons Attribution Noncommercial License, which permits any noncommercial use, distribution, and reproduction in any medium, provided the original author(s) and source are credited.

## References

1. Marsh PD. Are dental diseases examples of ecological catastrophe? *Microbiology*. 2003;149:279–94.
2. Field D, Connor PMO, Cotter PD, Hill C, Ross RP. The generation of nisin variants with enhanced activity against specific gram-positive pathogens. *Mol Microbiol*. 2008;69:218–30.
3. Suganthi V, Selvarajan E, Subathradevi C, Mohanasrinivasan V. Lantibiotic nisin: natural preservative from *Lactococcus lactis*. *Int Res J Pharm*. 2012;3:13–9.
4. Tong Z, Dong L, Zhou L, Tao R, Ni L. Nisin inhibits dental caries-associated microorganism *in vitro*. *Peptides*. 2010;31:2003–8.
5. Yamakami K, Tsumori H, Sakurai Y, Shimizu Y, Nagatoshi K, Sonomoto K. Sustainable inhibition efficacy of liposome-encapsulated nisin insoluble glucan-biofilm synthesis by *Streptococcus mutans*. *Pharm Biol*. 2013;51:267–70.
6. Katragadda A, Bridgman R, Betageri G. Effect of liposome composition and cholesterol on the cellular uptake of stavudine by human monocyte/macrophages. *Cell Mol Biol Lett*. 2000;5:483–93.
7. Jia Y, Joly H. Liposome as a carrier for gentamycin delivery: development and evaluation of the physicochemical properties. *Int J Pharm*. 2008;359:254–63.
8. Mozafari MR, Pardakhty A, Azarmi S, Jazayeri JA, Nokhodchi A, Omri A. Role of nanocarrier systems in cancer nanotherapy. *J Liposome Res*. 2009;19:310–21.
9. Shimizu Y, Takagi H, Nakayama T, Yamakami K, Tadakuma T, Yokoyama N, et al. Intraperitoneal immunization with oligomannose-coated liposome-entrapped soluble leishmanial antigen induces antigen-specific T-helper type 1 immune response in BALB/c mice through uptake by peritoneal macrophages. *Parasite Immunol*. 2007;29:229–39.
10. Trif M, Guillen C, Vaughan DM, Telfer JM, Brewer JM, Roseanu A, et al. Liposomes as possible carriers for lactoferrin in the local treatment of inflammatory diseases. *Exp Biol Med*. 2001;226:559–64.
11. Benech R-O, Kheadr EE, Lacroix C, Fliss I. Antibacterial activities of nisin Z encapsulated in liposomes or produced in situ by mixed culture during cheddar cheese ripening. *Appl Environ Microbiol*. 2002;68:5607–19.
12. Laridi R, Kheadr EE, Benech R-O, Vuillemaud JC, Lacroix C, Fliss I. Liposome encapsulated nisin Z: optimization, stability, and release during milk fermentation. *Int Dairy J*. 2003;13:325–36.
13. Cleveland J, Montville TJ, Nes IF, Chikindas ML. Bacteriocins: safe, natural antimicrobials for food preservation. *Int J Food Microbiol*. 2001;71:1–20.
14. Kuramitsu HK, He X, Lux R, Anderson MH, Shi W. Interspecies interactions within oral microbial communities. *Microbiol Mol Biol Rev*. 2007;71:653–70.
15. Nishikawara F, Katsumura S, Ando A, Tamaki Y, Nakamura Y, Sato K, et al. Correlation of cariogenic bacteria and dental caries in adults. *J Oral Sci*. 2006;48:245–51.
16. Selwitz RH, Ismail AI, Pitts NB. Dental caries. *Lancet*. 2007;369:51–9.
17. Paes Lame AF, Koo H, Bellato CM, Bedi G, Cury JA. The role of sucrose in cariogenic dental biofilm formation-new insight. *J Dent Res*. 2006;85:878–87.
18. Quivey Jr RG, Kuhnert WL, Hahn K. Genetics of acid adaptation in oral streptococci. *Crit Rev Oral Biol Med*. 2001;12:301–14.
19. Kreth J, Zhu L, Merritt J, Shi W, Qi F. Role of sucrose in the fitness of *Streptococcus mutans*. *Oral Microbiol Immunol*. 2008;23:213–9.
20. de Arauz LJ, Jozala AF, Mazzola PG, Penna TCV. Nisin biotechnological production and application: a review. *Trends Food Sci Technol*. 2009;20:146–54.
21. Willey JM, van der Donk WA. Lantibiotics: peptides of diverse structure and function. *Annu Rev Microbiol*. 2007;61:477–501.
22. Guerra NP, Pastrana L. Influence of pH drop on both nisin and pediocin production by *Lactococcus lactis* and *Pediococcus acidilactici*. *Lett Appl Microbiol*. 2003;37:51–5.

23. McAuliffe O, Ross RP, Hill C. Lantibiotics: structure, biosynthesis and mode of action. *FEMS Microbiol Rev.* 2001;25:285–308.
24. Hsu STD, Breukink E, Tischenko E, Lutters MAG, de Kruijff B, Kaptein R, et al. The nisin-lipid II complex reveals a pyrophosphate cage that provides a blueprint for novel antibiotics. *Nat Struct Mol Biol.* 2004;11:963–7.
25. Wiedemann I, Breukink E, van Kraaij C, Kuipers OP, Bierbaum G, de Kruijff B, et al. Specific binding of nisin to the peptidoglycan precursor lipid II combines pore formation and inhibition of cell wall biosynthesis for potent antibiotic activity. *J Biol Chem.* 2001;276:1772–9.
26. Hancock REW, Sahl H-G. Antimicrobial and host-defense peptides as new anti-infective therapeutic strategies. *Nat Biotechnol.* 2006;24:1551–7.
27. Jenssen H, Hamill P, Hancock REW. Peptide antimicrobial agents. *Clin Microbiol Rev.* 2006;19:491–511.
28. Were LM, Bruce BD, Davidson M, Weiss J. Size, stability, and entrapment efficiency of phospholipids nanocapsules containing polypeptide antimicrobials. *J Agric Food Chem.* 2003;51:8073–9.
29. Samuelson O, Haukland HH, Jenssen H, Kramer M, Sandvic K, Ulvatne H, et al. Induced resistance to the antimicrobial peptide lactoferricin B in *Staphylococcus aureus*. *FEBS Lett.* 2005;579:3421–6.
30. Kuwano K, Tanaka N, Shimizu T, Nagatoshi K, Nou S, Sonomoto K. Dual antibacterial mechanisms of nisin Z against gram-positive and gram-negative bacteria. *Int J Antimicrob Agents.* 2005;26:396–402.
31. Cotter PD, Hill C, Ross RP. Food microbiology: bacteriocins: developing innate immunity for food. *Nat Rev Microbiol.* 2005;3:777–88.
32. Akerey B, Le-Lay C, Fliss I, Subirade M, Rouabha M. *In vitro* efficacy of nisin Z against *Candida albicans* adhesion and transition following contact with normal human gingival cells. *J Appl Microbiol.* 2009;107:1298–307.
33. Lian T, Ho RJY. Trends and developments in liposome drug delivery systems. *J Pharm Sci.* 2001;90:667–80.
34. Samad A, Sultana Y, Aqil M. Liposomal drug delivery systems: an update review. *Curr Drug Deliv.* 2007;4:297–305.
35. Hsieh YF, Chen TL, Wang YT, Chang JH, Chang HM. Properties of liposomes prepared with various lipids. *J Food Sci.* 2002;67:2808–13.
36. Khosravi-Darani K, Pardakhty A, Honarpisheh H, Rao VS NM, Mozafari MR. The role of high-resolution imaging in the evaluation of nanovesicles for bioactive encapsulation and targeted nanotherapy. *Micron.* 2007;38:804–18.
37. Shehata T, Ogawara K, Higaki K, Kimura T. Prolongation of residence time of liposome by surface-modification with mixture of hydrophilic polymers. *Int J Pharm.* 2008;359:272–9.
38. Yamauchi M, Tsutsumi K, Abe M, Uosaki Y, Nakakura M, Aoki N. Release of drugs from liposomes varies with particle size. *Biol Pharm Bull.* 2007;30:963–6.
39. Hemanth KM, Spandana V. Liposomal encapsulation technology: a novel drug delivery system designed for ayurvedic drug preparation. *Int Res J Pharm.* 2011;2:4–6.
40. Taylor TM, Bruce BD, Weiss J, Davidson PM. *Listeria monocytogenes* and *Escherichia coli* O157:H7 inhibition *in vitro* by liposome-encapsulated nisin and ethylenediaminetetraacetic acid. *J Food Saf.* 2008;28:183–97.
41. Hofheinz RD, Gnad-Vogt SU, Beyer U, Hochhaus A. Liposomal encapsulated anti-carrier drugs. *Anticancer Drugs.* 2005;16:691–707.
42. Johnston MJ, Semple SC, Klimuk SK, Ansell S, Maurer N, Cullis PR. Characterization of the drug retention and pharmacokinetic properties of liposomal nanoparticles containing dihydrosphingomyelin. *Biochim Biophys Acta.* 2007;1768:1121–7.
43. Ikebara Y, Niwa T, Biao L, Kabata-Ikebara S, Ohashi N, Kobayashi T, et al. A carbohydrate recognition-based drug delivery and controlled release system using interperitoneal macrophages as a cellular vehicle. *Cancer Res.* 2006;66:8740–8.

44. Mozafari MR, Johnson C, Hatziantoniou S, Demetzos C. Nanoliposomes and their applications in food nanotechnology. *J Liposome Res.* 2008;18:309–27.
45. Taylor TM, Davidson PM, Bruce BD, Weiss J. Liposomal nanocapsules in food science and agriculture. *Crit Rev Food Sci Nutr.* 2005;45:587–605.
46. Matsui M, Shimizu Y, Kodera Y, Kondo E, Ikebara Y, Nakanishi H. Targeted delivery of oligomannose-coated liposome to the omental micrometastasis by peritoneal macrophages from patients with gastric cancer. *Cancer Sci.* 2010;101:1670–7.
47. Date AA, Joshi MD, Patravale VB. Polymeric parasitic disease: liposomes and polymeric nanoparticles versus lipid nanoparticles. *Adv Drug Deliv Rev.* 2007;59:505–21.
48. Ikegami S, Yamakami K, Ono T, Sato M, Suzuki S, Yoshimura I, et al. Targeting gene therapy for prostate cancer cells by liposomes complexed with anti-prostate-specific membrane antigen monoclonal antibody. *Hum Gene Ther.* 2006;17:997–1005.
49. Allen TM, Cullis PR. Drug delivery systems: entering the mainstream. *Science.* 2004;303:1818–22.
50. Kozako T, Hirata S, Shimizu Y, Satoh Y, Yoshimitsu M, White Y, et al. Oligomannose-coated liposomes efficiently induce human T-cell leukemia virus-1-specific cytotoxic T lymphocytes without adjuvant. *FEBS J.* 2011;278:1358–66.
51. Koning GA, Eggermont AMM, Lindner LH, ten Hagen TLM. Hyperthermia and thermosensitive liposomes for improved delivery of chemotherapeutic drugs to solid tumors. *Pharm Res.* 2010;27:1750–4.
52. Garбуzenko OB, Saad M, Pozharov VP, Reuhl KR, Mainelis G, Minko T. Inhibition of lung tumor growth by complex pulmonary delivery of drugs with oligonucleotides as suppressors of cellular resistance. *Proc Natl Acad Sci U S A.* 2010;107:10737–42.
53. Akbarzadeh A, Rezaei-Sadabady R, Davaran S, Joo SW, Zarghami N, Hanifehpour Y, et al. Liposome: classification, preparation, and applications. *Nanoscale Res Lett.* 2013;8:102–10.
54. Allon N, Saxena A, Chambers C, Doctor BP. A new liposome-based gene delivery system targeting lung epithelial cells using endothelin antagonist. *J Control Release.* 2010;160:217–24.
55. Volodkin DV, Ball V, Voegel JC, Mohwald H, Dimova R, Marchi-Artzner V. Control of the interaction between membranes or vesicles: adhesion, fusion and release of dyes. *Colloids Surf A Physicochem Eng Asp.* 2007;303:89–96.
56. Simoes S, Moreira JN, Fonseca C, Duzgunes N, de Lima MC. On the formulation of pH-sensitive liposomes with long circulation times. *Adv Drug Deliv Rev.* 2004;56:947–65.
57. Barenholz Y. Liposome application: problems and prospects. *Curr Opin Colloid Interface Sci.* 2001;6:66–77.
58. Bhardwaj U, Burgess DJ. Physicochemical properties of extruded and non-extruded liposomes containing the hydrophobic drug dexamethasone. *Int J Pharm.* 2010;388:181–9.
59. Daghestani KRP, Ferreira RB, Thedei GJ, Maggio B, Ciancaglini P. Lipid composition-dependent incorporation of multiple membrane proteins into liposomes. *Colloids Surf B.* 2004;36:127–37.
60. Anderson M, Omri A. The effect of different lipid components on the *in vitro* stability and release kinetics of liposome formulations. *Drug Deliv.* 2004;11:33–9.
61. Were LM, Bruce B, Davidson PM, Weiss J. Encapsulation of nisin and lysozyme in liposomes enhances efficacy against *Listeria monocytogenes*. *J Food Prot.* 2004;67:922–7.
62. Dhoot NO, Wheatley MA. Microencapsulated liposomes in controlled drug delivery: strategies to modulate drug release and eliminate the burst effect. *J Pharm Sci.* 2003;92:679–89.
63. Malheiros PS, Daroit DJ, Brandelli A. Food applications of liposome-encapsulated antimicrobial peptides. *Trends Food Sci Technol.* 2010;21:284–92.
64. Lu T, Wang Z, Ma Y, Zhang Y, Chen T. Influence of polymer size, liposomal composition, surface charge, and temperature on the permeability of pH-sensitive liposomes containing lipid-anchored(2-ethylacrylic acid). *Int J Nanomedicine.* 2012;7:4917–26.

65. Taylor TM, Gaysinsky S, Davidson PM, Bruce BD, Weiss J. Characterization of antimicrobial-bearing liposomes by  $\zeta$ -potential, vesicle size, and encapsulation efficacy. *Food Biophys.* 2007;2:1–9.
66. Takakura N, Wakabayashi H, Ishibashi H, Teraguchi S, Tamura Y, Yamaguchi H, et al. Oral lactoferrin treatment of experimental oral candidiasis in mice. *Antimicrob Agents Chemother.* 2003;47:2619–23.
67. Kisel MA, Kulik LN, Tsybovsky IS, Vlasov AP, Vorob'yov MS, Kholodova EA, et al. Liposomes with phosphatidylethanol as a carrier for oral delivery of insulin: studies in the rat. *Int J Pharm.* 2001;216:105–14.
68. Hayashida K, Kaneko T, Takeuchi T, Shimizu H, Ando K, Harada E. Oral administration of lactoferrin inhibits inflammation and nociception in rat adjuvant-induced arthritis. *J Vet Med Sci.* 2004;66:149–54.
69. Ishikado A, Imanaka H, Takeuchi T, Harada E, Makino T. Liposomalization of lactoferrin enhanced its anti-inflammatory effects via oral administration. *Biol Pharm Bull.* 2005;28:1717–21.
70. Teixeira ML, dos Santos J, Silveria NP, Brandelli A. Phospholipid nanovesicles containing a bacteriocin-like substance for control of *Listeria monocytogenes*. *Innov Food Sci Emerg Technol.* 2008;9:49–53.
71. Breukink E, Ganz P, de Kruijff B, Seelig J. Binding of nisin Z to bilayer vesicles as determined with isothermal titration calorimetry. *Biochemistry.* 2000;39:10247–54.
72. Deegan LH, Cotter PD, Hill C, Ross P. Bacteriocins: biological tools for bio-preservation and shelf-life extension. *Int Dairy J.* 2006;16:1058–71.
73. Mugabe C, Halwani M, Azghani AO, Lafrenie PM, Omri A. Mechanism of enhanced activity of liposome-encapsulated aminoglycosides against resistant strains of *Pseudomonas aeruginosa*. *Antimicrobial Agents Chemother.* 2006;50:2016–22.
74. Branen JK, Davidson PM. Environment of nisin, lysozyme, and monolaurin antimicrobial activities by ethylenediaminetetraacetic acid and lactoferrin. *Int J Food Microbiol.* 2004;90:63–74.

# Chapter 27

## Clinical Chipping of Zirconia All-Ceramic Restorations

**Shoko Miura, Shin Kasahara, Momoko Kudo, Yayoi Okuyama, Akio Izumida, Masanobu Yoda, Hiroshi Egusa, and Keiichi Sasaki**

**Abstract** Advancements in CAD/CAM systems employed in dentistry have made possible the application of yttria tetragonal zirconia polycrystal (Y-TZP) in zirconia-based all-ceramic restorations. Y-TZP has excellent flexural strength and fracture toughness and is used in molar crowns as well as frameworks of fixed partial dentures (FPDs). The use of Y-TZP in clinics has increased over the past several years, and it is now used in implant abutments and denture frameworks. While the demand for Y-TZP is increasing, chipping of porcelain used in the zirconia framework has been noted as a problem in zirconia-based all-ceramic restorations from a clinical point of view. We have previously used Cercon® smart ceramics with Y-TZP frames in clinics but have noticed the chipping of porcelain in a large number of cases over time. This review article focuses on the chipping of zirconia all-ceramic restorations by taking into account the following aspects: (1) clinical performance of zirconia all-ceramic restorations, (2) influence of frame thickness and porcelain firing schedules, and (3) reduction in porcelain chipping.

**Keywords** All-ceramic restoration • Chipping • Fracture toughness • Veneer porcelain • Zirconia

---

S. Miura (✉) • S. Kasahara • M. Kudo • Y. Okuyama • M. Yoda • H. Egusa

Division of Molecular and Regenerative Prosthodontics, Graduate School of Dentistry, Tohoku University, 4-1, Seiryō-machi, Aoba-ku, Sendai-City, Miyagi 980-8575, Japan  
e-mail: [miura@dent.tohoku.ac.jp](mailto:miura@dent.tohoku.ac.jp)

A. Izumida

Comprehensive Dentistry, Tohoku University Hospital,  
4-1, Seiryō-machi, Aoba-ku, Sendai-City, Miyagi 980-8575, Japan

K. Sasaki

Division of Advanced Prosthetic Dentistry, Graduate School of Dentistry, Tohoku University, 4-1, Seiryō-machi, Aoba-ku, Sendai-City, Miyagi 980-8575, Japan

## 27.1 Introduction

Porcelain fused to metal restorations, which in recent years have been commonly used in clinical practice as esthetic restorations show several problems caused by the metal [1]. The metal component used in porcelain fused to metal restorations may be eluted because of corrosive changes caused by saliva, food debris, and the like, triggering harmful biological effects such as metal allergies. Recovery of esthetics in porcelain fused to metal restorations also has limitations such as the occurrence of a black margin caused by gingival recession or when the labiobuccal gingiva is thin, or discoloration of the gingiva in the cervical region of the tooth due to metal elution. However, owing to the development of dental CAD/CAM systems, there has been implementation of all-ceramic restorations using yttrium-doped partially stabilized zirconia or yttria tetragonal zirconia polycrystal (Y-TZP). Y-TZP has excellent flexural strength and fracture toughness [2], and has been used as a framework for crowns and FPDs for the posterior teeth. Applications of Y-TZP for implant abutments as well as for denture frameworks have recently become possible, and the use of Y-TZP has become widespread in clinical practice [3]. It is regarded that zirconia all-ceramic restorations do not pose the problems caused by metal restorations owing to their excellent esthetics and biocompatibility. However, with the increasing demand for zirconia all-ceramic restorations, chipping of porcelain fired onto the zirconia frame has been noted as a clinical problem [4]. We therefore here discuss chipping of porcelain in zirconia all-ceramic restorations, and the prevention of the chipping, which is one of the challenges faced in clinical practice.

## 27.2 Clinical Performance of Zirconia All-Ceramic Restorations

Table 27.1 shows the clinical results for zirconia all-ceramic restorations as reported from 2010 to 2013. Reports based on implants are excluded here. Therapeutic methods for zirconia all-ceramic restorations have been established for the past 10 years or more. Further, reports with a follow-up period greater than 10 years have had widely ranging sample numbers in one compilation by Sax et al., at 11 to 1,132 cases, with few reports that have exceeded 100 cases. Numerous reports have made references to porcelain fracturing, with a rate of occurrence of 0.9–29.1 %.

Clinical reporting on porcelain fracturing in zirconia all-ceramic restorations has shown a high rate of occurrence of short-term cohesive failure of porcelain, a rate of occurrence that is significantly higher than that in the case of porcelain fused to metal restorations. In one report, a chipping rate of 0–88.9 % in a one- to eight-year follow-up period has been mentioned [28]. Moreover, the most common form of clinical failure is porcelain chipping [29], and prevention of the fracturing

**Table 27.1** Clinical performance of zirconia all-ceramic restorations

Authors [Ref] (Year)	Mean time (years)	Sample size	Type of restorations	Veneer porcelain fracture (%)
Rinke et al. [5] (2013)	7	80	3–4 unit FPDs	28.8
Burke et al. [6] (2013)	5	33	3–4 unit FPDs	24.2
Monaco et al. [7] (2013)	5	1,132	Single crowns	Unknown
Vavřičková et al. [8] (2013)	3	102	Single crowns	Unknown
Rinke et al. [9] (2013)	3	52	Single crowns	5.8
Raiqrodska et al. [10] (2012)	5	23	3 unit FPDs	21
Ortorp et al. [11] (2012)	5	143	Single crowns	3
Vigolo et al. [12] (2012)	5	39	Single crowns	7.7
Schmitter et al. [13] (2012)	5	30	4–7 unit FPDs	26.7
Schmitt et al. [14] (2012)	5	25	3–4 unit FPDs	28
Kern et al. [15] (2012)	5	20	3–4 unit FPDs	Unknown
Sorrentino et al. [16] (2012)	5	48	3 unit FPDs	6.3
Sagirkaya et al. [17] (2012)	4	107	Single crowns	0.9
Peláez et al. [18] (2012)	4	20	3 unit FPDs	10
Salido et al. [19] (2012)	4	17	4 unit FPDs	29.1
Ohlmann et al. [20] (2012)	2	11	3–4 unit FPDs	18.2
Poggio et al. [21] (2012)	1	102	Single crowns	2.0
Sax et al. [22] (2011)	10	57	3–5 unit FPDs	28.0
Tartaglia et al. [23] (2011)	3	463	Single or multiple-unit	Unknown
Roediger et al. [24] (2010)	4	99	3–4 unit FPDs	13
Beuer et al. [25] (2010)	3	68	Single or multiple-unit	7.4
Schmitt et al. [26] (2010)	3	17	Single crowns	5.9
Tsumita et al. [27] (2010)	2	21	3 unit FPDs	14.3

of porcelain fired onto the zirconia frame has become a clinical challenge. In particular, the parameters of occlusion are a factor and the usage of a night guard or press ceramics has been proposed [28, 29].

### 27.3 Influence of Frame Thickness and Porcelain Firing Schedules

It is thought that owing to differences in the physical properties of metal frames, zirconia frames might more readily experience chipping from thermal factors during porcelain firing. The reason for this is that the thermal conductivity of zirconia is about 1/100 that of gold [30]. Porcelain firing is thus thought to proceed gradually inward starting not from the frame side but rather from the porcelain surface layer, which more readily conducts heat, and the fired porcelain interior is possibly more susceptible to partially incomplete firing or distortion. In addition,

the heat capacity of the zirconia is about 3.5 times that of gold [30]. For this reason, a temperature gradient is believed to possibly occur in the process of cooling after firing, creating a shrinkage difference between the inner and outer surfaces of the sintered body and triggering cracking and other defects. The presence of the frame and thermal factors is thus expected to be a significant factor that triggers partially incomplete firing and defects. Modeling all-ceramic crowns mimicking clinical forms, Benetti et al. measured the temperature differences in porcelain interiors because of the differences between zirconia frames and metal frames and differences in cooling rates after firing. They noted that the specific heat, heat capacity, and thermal expansion rate of a material impacts early fracturing of all-ceramic crowns [31]. Nonetheless, though their research investigated temperature changes during sintering and cooling, there was no assessment of physical properties of porcelain caused by this. We have investigated how differences in the firing conditions of porcelain and frame material impact the fracture toughness of porcelain, in order to study how these factors impact the mechanical properties of porcelain. Our results showed that under conditions of faster heating rates, the fracture toughness decreases than that under manual conditions [32]. Regarding the thermal expansion coefficients of porcelain and zirconia, a zirconia frame has a slightly (about 10 %) greater thermal expansion coefficient than porcelain [33]. Owing to thermal expansion, the porcelain side experiences a compressive stress during the cooling process after porcelain firing and there is little possibility for cracking to occur.

## 27.4 Prevention of Porcelain Chipping

One factor causing chipping is the support of porcelain by a non-uniform frame thickness. In porcelain fused to metal restorations, which have been fully established, the metal frame is adjusted so that porcelain is given a uniform thickness by cutting back and waxing up, depending on the anatomical form [34]. A design with excessively thick porcelain or too thin frame is also a factor for errors, and porcelain supported by a frame with an anatomical form is reported to have little chipping [35]. It has also been reported that spontaneous cracking increases under conditions of firing with a higher cooling rate in a thicker layer of porcelain [36]. Accordingly, to prevent the occurrence of cracking in porcelain, it is desirable that the frame and porcelain have a favorable relationship of thermal expansion, the frame design results in the porcelain having a uniform thickness, and the cooling rate after firing is low.

If a restoration is considered structurally with a composite of porcelain and frame, however, then designing the frame with a color imparted to the lingual-side margin from the adjacent surface has been reported as being important for improving the strength of the restoration [37]. The molars in particular can possibly experience a large bite load in the lingual-side cervical region of the teeth. However, because this is a region that matters little in terms of esthetics, it seems best for

the lingual-side margin to be given a form where the zirconia frame is exposed, in order to prevent chipping. In our clinical studies, chipping did not occur in the front teeth area but did occur in bicuspids and molars [38], and mechanical problems such as occlusion could possibly be factors responsible for chipping. It seems important that the frame design also take occlusion factors, habits, and the like into consideration as well.

## 27.5 Conclusions

There are numerous reports that point to the prevention of porcelain chipping as a clinical challenge for zirconia all-ceramic restorations. Causes of chipping, clinically speaking, include occlusion factors; physically, they include the cooling rate after porcelain firing, excessively large porcelain thickness arising because of poor frame design, and the like. A prospective study should be carried out in the future that takes these factors into consideration.

**Open Access** This chapter is distributed under the terms of the Creative Commons Attribution Noncommercial License, which permits any noncommercial use, distribution, and reproduction in any medium, provided the original author(s) and source are credited.

## References

1. Komine F, Blatz MB, Matsumura H. Current status of zirconia-based fixed restorations. *J Oral Sci.* 2010;52:531–9.
2. Fischer H, Weber M, Marx R. Lifetime prediction of all-ceramic bridges by computational methods. *J Dent Res.* 2003;82:238–42.
3. Miyazaki T, Nakamura T, Matsumura H, Ban S, Kobayashi T. Current status of zirconia restoration. *J Prosthodont Res.* 2013;57:236–61.
4. Kimmich M, Stappert CF. Intraoral treatment of veneering porcelain chipping of fixed dental restorations: a review and clinical application. *J Am Dent Assoc.* 2013;144:31–44.
5. Rinke S, Gersdorff N, Lange K, Roediger M. Prospective evaluation of zirconia posterior fixed partial dentures: 7-year clinical results. *Int J Prosthodont.* 2013;26:164–71.
6. Burke FJ, Crisp RJ, Cowan AJ, Lamb J, Thompson O, Tulloch N. Five-year clinical evaluation of zirconia-based bridges in patients in UK general dental practices. *J Dent.* 2013;41:992–9.
7. Monaco C, Caldari M, Scotti R, AIOP Clinical Research Group. Clinical evaluation of 1,132 zirconia-based single crowns: a retrospective cohort study from the AIOP clinical research group. *Int J Prosthodont.* 2013;26:435–42.
8. Vavřičková L, Dostálová T, Charvát J, Bartoňová M. Evaluation of the three-year experience with all-ceramic crowns with polycrystalline ceramic cores. *Prague Med Rep.* 2013;114:22–34.
9. Rinke S, Schäfer S, Lange K, Gersdorff N, Roediger M. Practice-based clinical evaluation of metal-ceramic and zirconia molar crowns: 3-year results. *J Oral Rehabil.* 2013;40:228–37.
10. Raiqdroski AJ, Yu A, Chiche GJ, Hochstedler JL, Mancl LA, Mohamed SE. Clinical efficacy of veneered zirconium dioxide-based posterior partial fixed dental prostheses: five-year results. *J Prosthet Dent.* 2012;108:214–22.

11. Ortorp A, Kikl ML, Carlsson GE. A 5-year retrospective study of survival of zirconia single crowns fitted in a private clinical setting. *J Dent.* 2012;40:527–30.
12. Vigolo P, Mutinelli S. Evaluation of zirconium-oxide-based ceramic single-unit posterior fixed dental prostheses (FDPs) generated with two CAD/CAM systems compared to porcelain-fused-to metal single unit posterior FDPs: 5-year clinical prospective study. *J Prosthodont.* 2012;21:265–9.
13. Schmitter M, Mussotter K, Rammelsberg P, Gabbert O, Ohlmann B. Clinical performance of long-span zirconia frame works for fixed dental prostheses: 5-year results. *J Oral Rehabil.* 2012;39:552–7.
14. Schmitt J, Goellner M, Lohbauer U, Wichmann M, Reich S. Zirconia posterior fixed partial dentures: 5-year clinical results of a clinical trial. *Int J Prosthodont.* 2012;25:585–9.
15. Kern T, Tinschert J, Schley JS, Wolfart S. Five-year clinical evaluation of all-ceramic posterior FPDs made of In-Ceram Zirconia. *Int J Prosthodont.* 2012;25:622–4.
16. Sorrentino R, De Simone G, Teté S, Russo S, Zarone F. Five-year prospective clinical study of posterior three-unit zirconia-based fixed dental prostheses. *Clin Oral Investig.* 2012;16:977–85.
17. Sagirkaya E, Arikan S, Sadik B, Kara C, Karasoy D, Cehreli M. A randomized prospective open-ended clinical trial of zirconia fixed partial dentures on teeth and implants: interim results. *Int J Prosthodont.* 2012;25:221–31.
18. Peláez J, Coquillido PG, Serrano B, Suarez MJ. A four-year prospective clinical evaluation of zirconia and metal-ceramic posterior fixed dental prostheses. *Int J Prosthodont.* 2012;25:451–8.
19. Salido MP, Martinez-Rus F, del Rio F, Pradies G, Ozcan M, Suarez MJ. Prospective clinical study of zirconia-based posterior four-unit fixed dental prostheses: four-year follow-up. *Int J Prosthodont.* 2012;25:403–9.
20. Ohlmann B, Eiffler C, Rammelsberg P. Clinical performance of all-ceramic cantilever fixed dental prostheses: results of a 2-year randomized pilot study. *Quintessence Int.* 2012;43:643–8.
21. Poggio CE, Dosoli R, Ercoli C. A retrospective analysis of 102 zirconia single crowns with knife-edge margins. *J Prosthodont Res.* 2012;107:316–21.
22. Sax C, Hämmeler CH, Sailer I. 10-year clinical outcomes of fixed dental prostheses with zirconia frameworks. *Int J Comput Dent.* 2011;14:183–202.
23. Tartaglia GM, Sidoti E, Sforza C. A 3-year follow-up study of all-ceramic single and multiple crowns performed in a private practice: a prospective case series. *Clinics.* 2011;66:2063–70.
24. Roediger M, Gersdorff N, Huels A, Rinke S. Prospective evaluation of zirconia posterior fixed partial dentures: four-year clinical results. *Int J Prosthodont.* 2010;23:141–8.
25. Beuer F, Stimmelmayr M, Gernet W, Edelhoff D, Güh JF, Naumann M. Prospective study of zirconia-based restorations: 3-year clinical results. *Quintessence Int.* 2010;41:631–7.
26. Schmitt J, Wichmann M, Holst S, Reich S. Restoring severely compromised anterior teeth with zirconia crowns and feather-edged margin preparations: a 3-year follow-up of a prospective clinical trial. *Int J Prosthodont.* 2010;23:107–9.
27. Tsumita M, Kokubo Y, Ohkubo C, Sakurai S, Fukushima S. Clinical evaluation of posterior all-ceramic FPDs (Cercon): prospective clinical pilot study. *J Prosthodont Res.* 2010;54:102–5.
28. Koeing V, Vaheusden AJ, Le Goff SO, Mainjot AK. Clinical risk factors related to failures with zirconia-based restorations: An up to 9-year retrospective study. *J Dent.* 2013;41:1164–74.
29. Raigrodski AJ, Hillstead MB, Meng GK, Chung KH. Survival and complications of zirconia-based fixed dental prostheses: a systematic review. *J Prosthet Dent.* 2012;107:170–7.
30. Swain MV. Unstable cracking (chipping) of veneering porcelain on all-ceramic dental crowns and fixed partial dentures. *Acta Biomater.* 2009;5:1668–77.
31. Benetti P, Kelly JR, Bona AD. Analysis of thermal distributions in veneered zirconia and metal restorations during firing. *Dent Mater.* 2013;29:1166–72.

32. Kudo M, Miura S, Kikuchi M, Inagaki R, Kasahara S, Sasaki K, Toda M. Fracture toughness of Veneer Porcelain for zirconia all-ceramic restorations -influence of the frame materials and porcelain firing schedules. *Ann Jpn Prosthodont Soc* 2014; 6:291–99.
33. Miura S, Inagaki R, Yoda M, Kimura K. Thermal expansion of layering porcelains for the tetragonal stabilized zirconia. *J Jpn Prosthodon Soc.* 2007;51:556–62.
34. Donovan TE. Factors essential for successful all-ceramic restorations. *J Am Dent Assoc.* 2008;139(Suppl):14S–8.
35. Guess PC, Bonfante EA, Silva NR, Coelho PG, Thompson VP. Effect of core design and veneering technique on damage and reliability of Y-TZP-supported crowns. *Dent Mater.* 2013;29:307–16.
36. Guazzato M, Walton TR, Franklin W, Davis G, Bohl C, Klineberg I. Influence of thickness and cooling rate on development of spontaneous cracks in porcelain/zirconia structures. *Aust Dent J.* 2010;55:306–10.
37. Okabayashi S, Nomoto S, Sato T, Miho O. Influence of proximal supportive design of zirconia framework on fracture load of veneering porcelain. *Dent Mater J.* 2013;32:572–7.
38. Miura S, Kasahara S, Kudo M, Okuyama Y, Izumida A, Yoda M, Sasaki K. A retrospective study of Zirconia all-ceramic single crowns: 5-year clinical results. Innovative Research for Biosis-Abiosis Intelligent Interface Symposium. 2014; 86: Abstr. No. P3–10.

# **Chapter 28**

## **Dentin Hypersensitivity: Etiology, Prevalence and Treatment Modalities**

**M. Kanehira, H. Ishihata, and M. Saito**

**Abstract** Dentin hypersensitivity is a very common clinical symptom, which consists of sharp pain arising from exposed dentin in response to various types of stimuli and thus can cause considerable concern for patients. This condition is frequently encountered by periodontists, dentists and hygienists. The management of this condition requires good understanding of the complexity of the problem, as well as knowledge of the variety of treatment options available. Clinical trials on dentin hypersensitivity have been numerous and protocols varied. However, the entire body of clinical research literature is far from being unequivocal in suggesting one superior strategy. This paper reviews the etiology, prevalence and treatment modalities of dentinal hypersensitivity and describes a new approach to in-office treatment of dentin hypersensitivity using new biocompatible materials. Future treatment modalities for dentin hypersensitivity are currently under development that might combine the benefits of being both non-invasive and permanent, yet cost effective for both dentist and patients.

**Keywords** Dentin hypersensitivity • Etiology • Prevalence • Treatment modalities

### **28.1 Dentin Hypersensitivity**

#### **28.1.1 Definition**

The definition of dentin hypersensitivity is a “short, sharp pain arising from exposed dentin in response to stimuli typically thermal, evaporative, tactile, osmotic or chemical and which cannot be ascribed to any other form of dental defect or disease” according to the Canadian Advisory Board on Dentin Hypersensitivity [1].

---

M. Kanehira (✉) • M. Saito

Division of Operative Dentistry, Department of Restorative Dentistry, Tohoku University Graduate School of Dentistry, 4-1, Seiryo-machi, Aoba-ku, Sendai, Miyagi 980-8575, Japan  
e-mail: [kane@m.tohoku.ac.jp](mailto:kane@m.tohoku.ac.jp)

H. Ishihata

Division of Periodontology and Endodontology, Department of Oral Biology,  
Tohoku University Graduate School of Dentistry, 4-1, Seiryo-machi, Aoba-ku, Sendai,  
Miyagi 980-8575, Japan

### ***28.1.2 Diagnosis***

The diagnosis of this disease is often based on the subject's self-report of pain and requires exclusion of other dental and periodontal conditions that might cause pain [2]. Therefore, dentin hypersensitivity is characterized as a diagnosis of exclusion [3, 4]. Differential diagnosis is indispensable in order to exclude other conditions with similar symptoms where dentin is exposed and sensitive, such as chipped teeth, fractured cusps, cracked teeth, caries, and restorations with poor marginal adaptation [5, 6]. A correct differential diagnosis requires careful clinical and radiographic examinations and a complete dental history [5].

### ***28.1.3 Physiology***

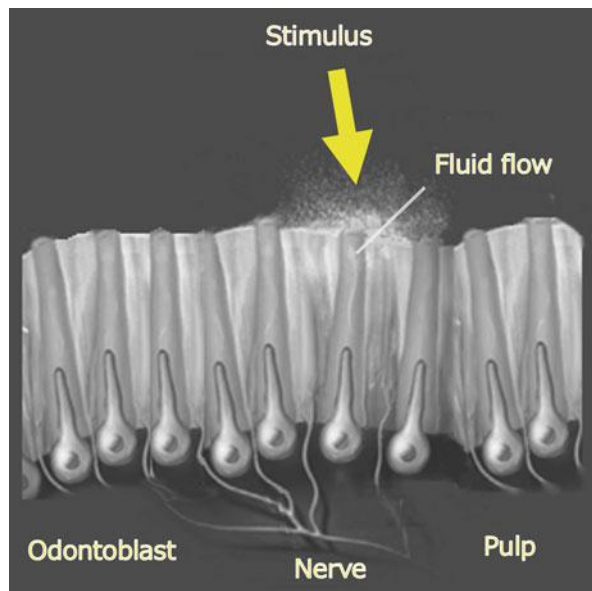
The number of tubules per unit area varies depending on location because the diameter of dentin tubule increases in pulpal direction. The presence of patent dentinal tubules renders dentin permeable to fluid movement [7]. Dentinal tubules follow a sinuous channel from the enamel dentin junction and from the cement-dentin junction. The tubules are conical and wider at the pulpal end than in the periphery.

Morphological changes occur in dentin as a result of age or injury. Secondary dentin is deposited throughout life, and the formation of peritubular dentin or deposition of intratubular crystals may result in partial or complete obturation of the dentinal tubules at last, producing dead tracts and areas of sclerotic dentin [8]. Traumatic injuries to the tooth such as cavity preparation may result in the deposition of an irregular layer of tertiary dentin that has fewer tubules [9]. As these newly deposited tubules are not continuous with those in primary dentin, they provide an effective barrier to rapid fluid movements and contribute to the reduction of dentin hypersensitivity [8].

The essential characteristics for appearance of dentin hypersensitivity are presence of exposed dentin surfaces, open tubule orifices on the exposed dentin surface and open tubules leading to a vital pulp [10]. The short, sharp pain arising from exposed dentin is a result of minute inward or outward movement of dentinal fluid inside tubules that stimulate pulpal nerve fibers.

Occlusion of dentin tubular orifices by a smear layer created during tooth brushing or by inorganic particles in a toothpaste results in reduction of fluid movements within the dentinal tubules. This physical blockade may partially account for the effectiveness of desensitizing toothpastes. On the other hand tooth-brushing is considered one of the main reasons for dentin wear and dentin hypersensitivity [11].

**Fig. 28.1** Brännström presumed that stimuli move fluid in or out of dentin and that this fluid activates intradental or pulpal nerves to cause pain



#### 28.1.4 Mechanism of Action

Brännström's hydrodynamic theory of pain is globally accepted for the mechanism of dentin hypersensitivity [12]. This theory assumes that stimuli applied on dentin tubules, patent at the pulp and the oral surface, cause rapid movements of the dentin fluid and excite mechanoreceptors, thus eliciting pain (Fig. 28.1). The hydrodynamic theory suggests that changes in the flow of the fluid present in the dentinal tubules can trigger receptors present on nerves located at the pulpal side thereby deriving a pain response. Dentin tubules can be exposed as a result of enamel loss due to mechanical attrition, erosion and abfraction or after gingival recession due to periodontal disease or surgery. When dentinal tubules in vital teeth are exposed due to erosion, abrasion, dental manipulation, or a tooth defect, fluid within the dentinal tubules may flow in either an inward or outward direction depending on pressure differences in the surrounding tissue. A cold stimulus causes the tubular fluid volume to shrink slightly, and heat causes it to expand. Strongly osmotic sugar or sour solutions cause fluid to be drawn out of the tubules. An air blast on the tooth evaporates a tiny portion of fluid at the end of the tubule, causing a significant outward flow of fluid in the tubule. Touching the tooth with a dental instrument or disinfectants forces a small amount of fluid into the tubule. The exact mechanism of dentin hypersensitivity is still under research.

### ***28.1.5 Etiology***

The most important factor in the etiology of dentin hypersensitivity is exposed dentin as a result of loss of enamel associated with tooth wear or trauma and/or as a result of gingival recession associated with exposure of root surfaces [13]. Tooth wear refers to the irreversible loss of tooth structure and includes conditions such as abrasion, erosion, attrition, and abfraction. Occurrence of wedge-shaped cervical lesions is often associated with abrasion and occlusal hyperfunction. Although there are many causes for non-carious cervical lesions of dentin, improper brushing is considered one of the major causes.

### ***28.1.6 Prevalence***

The prevalence of dentin hypersensitivity has been reported over the years in a variety of ways. Dentin hypersensitivity is a common condition with a reported prevalence between 4 and 69 % in the adult population [14]. Another research reported the prevalence of dentin hypersensitivity varies, but averages about 57 % and peaks between 20 to 40 years of age [15]. It has been reported that more than 40 million people in the U.S. are affected, 14.3 % of all dental patients, between 8 and 57 % of adult dentate population, and up to 30 % of adults at some time during their lifetime [16]. Among periodontal patients, the prevalence is even higher (60–98 %). Dentinal hypersensitivity occurs with a first peak in 20 to 30 year olds and then with another peak later in the 50s. The condition involves mainly the facial cervical surfaces of teeth and is mostly found in premolars and canines [17, 18]. Patients who have received periodontal treatment are particularly sensitive to this condition because of the loss of cementum following periodontal therapy. In addition periodontal disease and improper brushing can also cause gingival recession accompanied by sensitive teeth [17]. Dentinal hypersensitivity has been researched extensively through the years and many authors express an agreement that dentinal hypersensitivity is either under-reported by the dental patient population or misdiagnosed [19].

### ***28.1.7 Treatment***

Logical treatment regimens attempt (1) to occlude dentin tubules or (2) to block the pulpal nerve activity by increasing the potassium ion concentration, typically with potassium nitrate or potassium chloride. A variety of methods with tubule blocking agents is available for management of dentinal hypersensitivity comprising resins, glass-ionomers, primers, dentin adhesives, protein precipitants, oxalates and laser treatment [20–24]. According to a recent survey in the USA, 45 % of dental practitioners regularly use oxalates and approximately 60 % use glutaraldehyde/

HEMA as topically applied agents to treat dentinal hypersensitivity [21, 25]. Although the mechanisms of pain transmission across dentin are not fully understood, both dentin permeability and hypersensitivity are reduced when the dentinal tubules are occluded. Therefore, hypersensitivity treatment strategies have mainly focused on tubular occlusion.

### ***28.1.8 Permeability***

According to the hydrodynamic theory, dentinal hypersensitivity is related to the movement of intertubular fluid. Several studies have demonstrated the relationship between open tubules on the exposed cervical surface and hypersensitivity [12, 26]. In vitro studies investigating dentin desensitizers have focused on dentin permeability and hydraulic conductance as measures for effectiveness of these agents.

One of the laboratory methods that has been frequently used and that focuses directly on dentin fluid flow is a dentin disc model for assessment of permeability and hydraulic conductance [12, 27]. This model or modifications thereof have been used to assess both professional desensitizers and dentin adhesives [28–32], and the method is commonly considered a good and reliable model for in vitro screening and testing of the potential of desensitizing agents [33].

Ishihata et al. [34] have designed a modified split-chamber device using a chemiluminescence reaction to evaluate the liquid permeability of dentin discs. This test is also considered a suitable and reliable screening method for assessment of topical desensitizing agents efficacy in reducing or eliminating dentin permeability, irrespective of the tubular blocking mechanism used [35].

### ***28.1.9 Clinical Trials***

Clinical trials on dentin hypersensitivity should as a rule use randomized group assignments, be double-masked and contain a placebo product that is identical to the test product except that it does not contain the active ingredient [36, 37]. It is critical to evaluate the placebo effect, which can be very strong in such studies. Conclusions derived from early studies on dentin hypersensitivity using single-masked methods, or inappropriate stimuli should be viewed with caution.

Limited evidence indicates that tooth brushing without toothpaste decreases hypersensitivity scores while brushing with toothpaste increases dentin hypersensitivity scores unless the toothpaste contains a potassium-containing desensitizing agent. Although a recent meta-analysis of six clinical trials using potassium-containing desensitizing toothpaste demonstrated reductions in the symptoms of patients' dentin hypersensitivity compared to control toothpaste [38], the scientific evidence supporting the use of potassium salts to reduce nerve activity is based mostly on in vivo animal studies and one recent human in vivo trial [39].

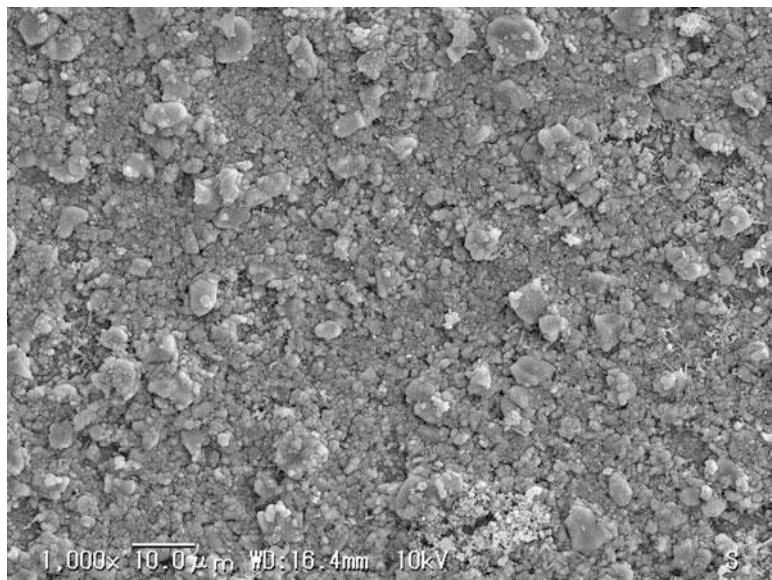


**Fig. 28.2** SEM photograph of dentin surface after application of calcium-phosphate containing compound. A layer of precipitated crystals (hydroxyapatite and other apatite species) covered the dentin surface and occluded the dentinal tubules

### 28.1.10 New Approach

Desensitizing products may be in the form of topically applied agents such as resins, primers, dentin bonding agents and others [40–43]. Recently there has been an increasing interest in calciumphosphate-containing materials [34, 44–48]. Such calcium phosphate-containing materials are potentially transformed to hydroxyapatite as a final product, which is the principal mineral in teeth. The proximity of hydroxyapatite to the natural tooth structure and its biocompatibility makes these materials useful in a variety of dental applications. The development of the next generation calcium phosphate cement materials is expected to have greater efficacy in a wide range of clinical applications.

A spin-off from calcium-phosphate cement developments is a topically applied desensitizer, claimed to precipitate hydroxyapatite as biocompatible mineral on dentin and inside the openings of dentinal tubules. This material showed outstanding characteristics in dentinal tubule occlusion and favorable reduction in dentin permeability (Fig. 28.2).

Human saliva contains an abundance of calcium and phosphate ions too. The supersaturation of salivary fluid is expected to contribute to further apposition and growth in size of hydroxyapatite crystals formed in the oral environment [49].

Petrou described a breakthrough technology based upon arginine and calcium carbonate that provides clinically proven benefits with respect to rapid and lasting relief of dentin hypersensitivity [50]. Arginine and calcium are found naturally in

saliva, and they work together to accelerate the natural mechanisms of occlusion to deposit a dentin-like mineral, containing calcium and phosphate, within the dentin tubules and in a protective layer on the dentin surface. Sodium calcium phosphosilicate has been shown in laboratory studies to rapidly occlude dentin tubules through the deposition of particles that react to form a protective layer on the dentin surface [51]. This material was originally developed as a bone regenerative material and is highly biocompatible.

Preliminary studies have shown that topical application of a combination of amorphous calcium phosphate (ACP) and casein phosphopeptide (CPP) can cause blockage of dentin tubules [52].

In this way the search for a natural desensitizing agent has led to the observation that calcium phosphate minerals obstruct dentinal tubule orifices mimicking the natural process of sclerosis.

## 28.2 Conclusion

Dentin hypersensitivity is a common and significant dental problem with the symptoms, measurement and oral factors that contribute to dentinal hypersensitivity having been well characterized. Several theories have been developed to explain the mechanisms with respect to the structure of the dentin and pulp. This has lead to the development of treatments that may be permanent and non-invasive in nature.

Future treatment modalities for dentin hypersensitivity are currently under development that might combine the benefits of being both non-invasive and permanent yet cost effective for both dentist and patients.

The authors acknowledge gratefully the support of Professor W.J. Finger (Tohoku University) and his valuable advice for editing of this manuscript.

**Open Access** This chapter is distributed under the terms of the Creative Commons Attribution Noncommercial License, which permits any noncommercial use, distribution, and reproduction in any medium, provided the original author(s) and source are credited.

## References

1. Canadian Advisory Board on dentin hypersensitivity. Consensus-based recommendations for the diagnosis and management of dentin hypersensitivity. *J Can Dent Assoc.* 2003;69:221–6.
2. Berman LH. Dentinal sensation and hypersensitivity. A review of mechanisms and treatment alternatives. *J Periodontol.* 1985;6:216–22.
3. Bränström M. A hydrodynamic mechanism in the transmission of pain producing stimuli through the dentine. In: Andersen DJ, editor. *Sensory mechanisms in dentine*. Oxford: Pergamon; 1963. p. 73–9.
4. Schmidlin PR, Sahrmann P. Current management of dentin hypersensitivity. *Clin Oral Investig.* 2013;17(Suppl1):55–9.

5. Gillam DG. Dentin hypersensitivity: an introduction to differential diagnosis. *Dent Pract.* 2010;48:34–5.
6. Gernhardt CR. How valid and applicable are current diagnostic criteria and assessment methods for dentin hypersensitivity? *Clin Oral Investig.* 2013;17(Suppl1):31–40.
7. Absi EG, Addy M, Adams D. Dentine hypersensitivity: a study of the patency of dentinal tubules in sensitive and non-sensitive cervical dentine. *J Clin Periodontol.* 1987;14:280–4.
8. Mjör IA. Dentin permeability: the basis for understanding pulp reactions and adhesive technology. *Braz Dent J.* 2009;20:3–16.
9. Mjör IA. Pulp-dentin biology in restorative dentistry. Part 2: initial reactions to preparation of teeth for restorative procedures. *Quintessence Int.* 2001;32:537–51.
10. Yoshiyama M, Masada J, Uchida A. Scanning electron microscopic characterization of sensitive vs. insensitive human radicular dentin. *J Dent Res.* 1989;68:1498–502.
11. Addy M. Tooth brushing, tooth wear and dentine hypersensitivity - are they associated? *Int J Dent.* 2005;55:261–7.
12. Greenhill JD, Pashley DH. The effects of desensitizing agents on the hydraulic conductance of human dentin in vitro. *J Dent Res.* 1981;60:686–98.
13. Embrey G, Edgar WM, Orchardson R, Addy M, editors. *Tooth wear and sensitivity.* London: Taylor and Francis; 2000. p. 39–51.
14. Gillam DG, Orchardson R. Advances in the treatment of root sensitivity: mechanisms and treatment principles. *Endod Topics.* 2006;13:13–33.
15. Flynn J, Galloway R, Orchardson R. The incidence of “hypersensitive” teeth in the West of Scotland. *J Dent.* 1985;13(3):230–6.
16. Chabanski MB, Gillam DG. Aetiology, prevalence and clinical features of cervical dentine sensitivity. *J Oral Rehabil.* 1997;24:15–9.
17. Splieth CH, Tachou A. Epidemiology of dentin hypersensitivity. *Clin Oral Investig.* 2013;17 Suppl 1:3–8.
18. Gillam DG, Aris A, Bulman JS, Newman NN, Ley F. Dentine hypersensitivity in subjects recruited for clinical trials: clinical evaluation, prevalence and intra-oral distribution. *J Oral Rehabil.* 2002;29:226–31.
19. Holland GR, Nähri MN, Addy M, Gangarosa L, Orchardson R. Guidelines for the design and conduct of clinical trials on dentine hypersensitivity. *J Clin Periodontol.* 1997;24:808–13.
20. Trowbridge HO, Silver DR. A review of current approaches to in-office management of tooth hypersensitivity. *Dent Clin North Am.* 1990;34:561–81.
21. Vora J, Mehta D, Meena N, Sushma G, Finger WJ, Kanehira M. Effect of two topical desensitizing agents and placebo on dentin hypersensitivity. *Am J Dent.* 2012;25:293–8.
22. Morris MF, Davis RD, Richardson BW. Clinical efficacy of two dentin desensitizing agents. *Am J Dent.* 1999;12:72–6.
23. Cunha-Cruz J, Stout JR, Heaton LJ, Wataha JC. Dentin hypersensitivity and oxalates: a systematic review. *J Dent Res.* 2011;90:304–10.
24. Sgolastra F, Petrucci A, Severino M, Gatto R, Monaco A. Lasers for the treatment of dentin hypersensitivity: a meta-analysis. *J Dent Res.* 2013;92:492–9.
25. Cunha-Cruz J, Wataha JC, Zhou L, Manning W, Trantow M, Bettendorf MM, Heaton LJ, Berg J. Treating dentin hypersensitivity: therapeutic choices made by dentists of the Northwest PRECEDENT network. *J Am Dent Assoc.* 2010;141:1097–105.
26. Ciucchi B, Bouillaguet S, Holz J, Pashley DH. Dentinal fluid dynamics in human teeth, *in vivo*. *J Endod.* 1995;21:191–204.
27. Pashley DH, Stewart FP, Galloway SE. Effects of air-drying *in vitro* on human dentine permeability. *Arch Oral Biol.* 1984;29:379–83.
28. Pashley DH, O'Meara JA, Kepler EE, Galloway SE, Thompson SM, Stewart FP. Dentin permeability. Effects of desensitizing dentifrices *in vitro*. *J Periodontol.* 1984;55:522–5.
29. Jain P, Reinhardt JW, Krell KV. Effect of dentin desensitizers and dentin bonding agents on dentin permeability. *Am J Dent.* 2000;13:21–7.
30. Kolker JL, Vargas MA, Armstrong SR, Dawson DV. Effect of desensitizing agents on dentin permeability and dentin tubule occlusion. *J Adhes Dent.* 2002;4:211–21.

31. Pashley DH, Agee K, Zhang Y, Smith A, Tavss EA, Gambogi RJ. The effects of outward forced convective flow on inward diffusion of potassium across human dentin. *Am J Dent.* 2002;15:256–61.
32. Pereira JC, Segala AD, Gillam DG. Effect of desensitizing agents on the hydraulic conductance of human dentin subjected to different surface pretreatments. An in vitro study. *Dent Mater.* 2005;21:129–38.
33. Mordan NJ, Barber PM, Gillam DG. The dentine disc. A review of its applicability as a model for the in vitro testing of dentine hypersensitivity. *J Oral Rehabil.* 1997;24:148–56.
34. Suge T, Ishikawa K, Kawasaki A, Yoshiyama M, Asaoka K, Ebisu S. Duration of dentinal tubule occlusion formed by calcium phosphate precipitation method: in vitro evaluation using synthetic saliva. *J Dent Res.* 1995;74:1709–14.
35. Ishihata H, Kanehira M, Nagai T, Finger WJ, Shimauchi H, Komatsu M. Effect of desensitizing agents on dentin permeability. *Am J Dent.* 2009;22:143–6.
36. Lin P-Y, Cheng Y-W, Chu C-Y, Lin C-P, Tu Y-K. In-office treatment for dentin hypersensitivity: a systematic review and network meta-analysis. *J Clin Periodontol.* 2013;40:53–64.
37. Addy M, West NX, Barlow A, Smith S. Dentine hypersensitivity: is there both stimulus and placebo responses in clinical trials? *Int J Dent Hyg.* 2007;5:53–9.
38. Poulsen S, Errboe M, Lescay Mevil Y, Glenny AM. Potassium containing toothpastes for dentine hypersensitivity. *Cochrane Database Syst Rev.* 2006;19:1–18.
39. Ajcharanukul O, Kraivaphan P, Wanachantararak S, Vongsavan N, Matthews B. Effects of potassium ions on dentine sensitivity in man. *Arch Oral Biol.* 2007;52:632–9.
40. Felton DA, Bergenholz G, Kanoy ED. Evaluation of the desensitizing effect of Gluma Dentin Bond on teeth prepared for complete-coverage restorations. *Int J Prosthodont.* 1991;4:292–8.
41. Duran I, Sengun A. The long-term effectiveness of five current desensitizing products on cervical dentin sensitivity. *J Oral Rehabil.* 2004;31:341–56.
42. Schüpbach P, Lutz F, Finger WJ. Closing of dentinal tubules by Gluma desensitizer. *Eur J Oral Sci.* 1997;105:414–21.
43. Qin C, Xu J, Zhang Y. Spectroscopic investigation of the function of aqueous 2-hydroxyethylmethacrylate/glutaraldehyde solution as a dentin desensitizer. *Eur J Oral Sci.* 2006;114:354–9.
44. Chow LC. Next generation calcium phosphate-based biomaterials. *Dent Mater J.* 2009;28:1–10.
45. Shetty S, Kohad R, Yeltiwar R. Hydroxyapatite as an in-office agent for tooth hypersensitivity: A clinical and scanning electron microscopic study. *J Periodontol.* 2010;81:1781–9.
46. Thanatvarakorn O, Nakashima S, Sadr A, Prasansuttiporn T, Ikeda M, Tagami J. In vitro evaluation of dentinal hydraulic conductance and tubule sealing by a novel calcium-phosphate desensitizer. *J Biomed Mater Res B.* 2013;101B:303–9.
47. Thanatvarakorn O, Nakashima S, Sadr A, Prasansuttiporn T, Thithaweerat S, Tagami J. Effect of a calcium-phosphate based desensitizer on dentin surface characteristics. *Dent Mater J.* 2013;32:615–21.
48. Imai Y, Akimoto T. A new method of treatment for dentin hypersensitivity by precipitation of calcium phosphate in situ. *Dent Mater J.* 1990;9:167–72.
49. Larsen MJ, Pearce EIF. Saturation of human saliva with respect to calcium salts. *Arch Oral Biol.* 2003;48:317–22.
50. Petrou I, Heu R, Stranick M, Lavender S, Zaidel L, Cummins D, Sullivan RJ, Hsueh C, Gimzewski JK. A breakthrough therapy for dentin hypersensitivity: how dental products containing 8% arginine and calcium carbonate work to deliver effective relief of sensitive teeth. *J Clin Dent.* 2009;20:23–31.
51. Litkowski L, Greenspan DC. A clinical study of the effect of calcium sodium phosphosilicate on dentin hypersensitivity—proof of principle. *J Clin Dent.* 2010;21:77–81.
52. Madhavan S, Nayak M, Shenoy A, Shetty R, Prasad K. Dentinal hypersensitivity: A comparative clinical evaluation of CPP-ACP F, sodium fluoride, propolis, and placebo. *J Conserv Dent.* 2012;15:315–8.

## **Chapter 29**

# **Preventing Aspiration Pneumonia Among the Elderly: A Review Focused on the Impact of the Consistency of Food Substances**

**Reiko Sakashita, Miho Takami, Hiroshi Ono, Tomoko Nishihira, Takuchi Sato, and Misao Hamada**

**Abstract** Aspiration pneumonia is the leading cause of death among the elderly. Modified-texture foods, i.e., foods with altered consistency, are recommended in order to maintain both normal swallowing and adequate nutrition, which is also expected to reduce aspiration pneumonia, when elderly people are suspected to suffer from disorders of eating and/or swallowing. However, it is reported that overly-restrictive diets have been provided to most residents given modified-texture diets. Furthermore, there is scant empirical evidence of the medical effectiveness of food texture-modification. Little attention has been paid to the effect of the consistency of food substances, as well as the ability of mastication, on general health. Our cross-sectional studies showed that eaters of regular foods have lower incidences of pneumonia and fever, while those eating modified-texture, i.e., softer and finer, foods have higher incidences of pneumonia and fever. In this review, the effects of interventions for prevention of aspiration pneumonia were overviewed then the impact of the consistency of food substances on the health of the elderly and the direction of further research was discussed.

**Keywords** Diet modification • Nutrition • Pneumonia • Prevention • Regular food

---

R. Sakashita (✉) • M. Takami • H. Ono • T. Nishihira

College of Nursing Art and Science, University of Hyogo, 13-71 Kitaouji-cho,  
Akashi, Hyogo 673-8588, Japan

e-mail: [sakashita@cnas.u-hyogo.ac.jp](mailto:sakashita@cnas.u-hyogo.ac.jp)

T. Sato

Division of Oral Ecology and Biochemistry, Tohoku University Graduate School of Dentistry,  
Sendai, Japan

M. Hamada

Social Welfare Corporation Lavita, Osaka, Japan

## 29.1 Pneumonia and its Causes in the Elderly

Pneumonia is the leading cause of death among the elderly in many countries including Japan [1, 2]. The overall mortality rate ranges from 20 to 50 %, with a rate as high as 80 % reported in some studies [3–6]. It is also the most serious common infection that occurs in nursing homes, with a high case-fatality rate and considerable mortality among survivors. The reported incidence of nursing home-acquired pneumonia has ranged from 0.3 to 2.5 episodes per 1,000 days of resident care [7, 8]. Pneumonia can be classified in several ways, most commonly by where it was acquired (hospital-acquired, nursing home-acquired and community-acquired pneumonia), but may also be classified by the cause (Bronchiolitis obliterans organizing, eosinophilic, aspiration, Dust pneumonia and so on) or the area of lung that is affected [9]. Among these causes, aspiration is an important pathogenic mechanism for pneumonia among the elderly and the management of patients with pneumonia with aspiration factors is a major medical problem [10].

## 29.2 Risk Factor Cause of Aspiration Pneumonia

A large number of studies of the bacteriology of aspiration pneumonia suggest that the combination of colonization of the oropharynx with bacterial pathogens and microaspiration of saliva containing these bacteria may be the most common source of aspiration pneumonia [11–13].

Mylotte [1] reviewed risk factors for pneumonia included poor functional status [14, 15], difficulties swallowing [15, 16], dementia and stroke [17, 18], poor oral hygiene or inadequate oral care [19, 20], presence of a nasogastric tube [14], use of sedatives [21], occurrence of an unusual event defined as confusion, agitation, falls, or wandering [15], chronic lung disease [22], tracheostomy [22], increasing age [16], and male sex [16]. Mitchell et al. [23] showed that advanced age and significant cognitive impairment increased the risk of aspiration. The most common causes of difficulties in swallowing among the elderly are dementia and stroke [24].

Logistic regression analyses identified the significant predictors of aspiration pneumonia. The best predictors, in one or more groups of subjects, were dependency for feeding, dependency for oral care, number of decayed teeth, tube feeding, more than one medical diagnosis, number of medications, and smoking [25]. Aspiration pneumonia is a multifactorial phenomenon and no single predictor can cause this disease. Langmore [19] concluded that dysphagia and aspiration are necessary but not sufficient conditions for development of pneumonia.

## 29.3 Interventions Aimed at Preventing Aspiration Pneumonia

### 29.3.1 Overview of Interventions

To reduce risk of aspiration pneumonia, several interventions have been tried clinically. However, a systematic review assessed the effectiveness of the following interventions for prevention of aspiration pneumonia in the elderly: compensatory strategy/positioning changes, dietary interventions, pharmacological therapies, oral hygiene and tube feeding, and it concluded that insufficient data exist to determine the efficacy of positioning strategies, modified-texture foods, oral hygiene, feeding tube placement, or delivery of food in preventing aspiration pneumonia [26]. Though meaningful studies have been carried out, it was suggested that larger, high-quality randomized controlled trials (RCTs) on the efficacy of preventive interventions are warranted [26].

Individuals with dementia often present feeding difficulties and are susceptible to aspiration pneumonia. Interventions can include behavioural strategies [27], modification of food consistencies [28], postural manoeuvres (for example, chin tuck) [29], pharmaceutical interventions [30], environmental modification [31] or enteral feeding [32]. Still insufficient data exist to determine the efficacy of those interventions. Popular interventions and studies are described below.

### 29.3.2 Oral Hygiene

Aspiration of oropharyngeal flora into the lung is the major route of pathogenesis of aspiration pneumonia [33], and colonization of dental plaque and oral mucosa represents a reservoir of potential pathogens that can reach the lung, so it was hypothesized that poor oral hygiene increases the rate of colonization of dental plaque and oral mucosa to cause aspiration pneumonia [34]. A study carried out in Japanese nursing homes demonstrated that residents randomly selected to follow an intensive oral care regimen had a significantly lower proportion of episodes of pneumonia than did residents following a standard oral care regimen [35]. A systematic review indicates three oral hygiene care intervention studies involving 470 participants resulted in improved oral hygiene in patients and reduced the incidence of pneumonia amongst the intervention group in a stroke ward [36].

### 29.3.3 Dietary Intervention

Since modifications in dietary textures and fluid viscosities are common dysphagia interventions, they are also expected to be effective in reducing aspiration pneumonia. Increasing the viscosity of a fluid can lead to a reduced rate of liquid bolus

transit and increased sensory awareness [37, 38]. It can also influence opening of the upper oesophageal sphincter [39]. This reduced rate of bolus movement and increase in sensory awareness may enhance the safety and efficiency of swallowing, thus reducing the risk of aspiration or penetration of fluid into the airway. It is believed that increasing the viscosity of the fluid bolus by altering its consistency allows individuals a better opportunity to swallow with a reduced risk of airway compromise.

Similarly, altering the consistency of foods is thought to lead to physiological changes which can reduce an individual's risk of aspiration. Foods are often modified according to a patient's oral motor control [20]. Reduced incidence of aspiration pneumonia was noted in a study where the participants were randomized to a soft mechanical diet and thickened liquids [40, 41]. However, it was summarized there is scant empirical evidence of its medical effectiveness by a systematic review [42]. This topic is discussed in later section (Sect. 29.5).

### ***29.3.4 Swallowing Therapy***

Most speech-language therapists have traditionally focused their therapy on teaching swallowing maneuvers, postural changes or instituting dietary alterations, so as to minimize pneumonia by making the swallow more effective. A systematic review of all RCTs with patients recovering from stroke and dysphagia [42] identify two RCTs which assessed the effectiveness of swallowing treatment programmes [43, 44]. Foley et al. [42] concluded that the evidence from these trials is weakened by small sample sizes, the lack of a control group, insufficient statistical comparisons, or inability to achieve clinically significant treatment effects.

### ***29.3.5 Controlling Gastroesophageal Reflux***

Gastroesophageal reflux has been estimated to occur in one-third of the elderly population. Aspiration of material from the stomach can damage the trachea in those with gastroesophageal reflux. Postural changes include the chin tuck position, upright position during and after meals to prevent gastroesophageal reflux, and semirecumbent position in bed. However, few data exist to support any of these strategies [26].

### ***29.3.6 Improvement of Nutrition***

The prevalence of malnutrition has been estimated to be between 40 and 60 % for patients aged 65 and older who are hospitalized in short-term units or convalescence and rehabilitation units and 13–50 % in institutions [45]. Infectious risk is

increased in the case of malnutrition [46], and hypoalbuminemia is associated with an increased risk of mortality [17]. Most studies on pneumonia have demonstrated a role of malnutrition in the development of the infection, but the results are somewhat contradictory [47]. Two RCTs evaluate that supplementation may improve survival rate [27, 48]. On the other hand, there was no difference for case fatality, or death or dependency, with fluid supplementation and nutritional supplementation, although nutritional supplementation was associated with reduced pressure sores, increased energy intake and protein intake [49]

### ***29.3.7 Enteral Tube Feeding***

One of the primary reasons given for the use of feeding tubes is to reduce the risk of aspiration among adults with swallowing disturbances. Non-oral feeding is believed to prevent aspiration pneumonia, improve function, promote physical comfort and prolong life. However, the evidence does not support (or refute) these assumptions. Several studies of tube-fed patients who are taking no foods or liquids by mouth have shown that tube feeding is associated with a higher rate of pneumonia than in patients who are eating [19, 50–57].

In one study, aspiration pneumonia was diagnosed in 44 % of the tube-fed patients with acute stroke [58]. Other studies showed incidence of aspiration pneumonia vary from 7 to 62 % in patients fed by feeding tube [59]. Nakajoh et al. [60] found that the incidence of pneumonia was significantly higher in post-stroke patients on oral feeding than in those with nasogastric tubes (NGT) feeding during a one-year follow-up period (54.3 % versus 13.2 %,  $p < 0.001$ ). As there are some evidence that patients with a very short life expectancy [61, 62], there appears to be a limited role for tube feeding among adults with swallowing disturbances, and some have suggested that their use should be discouraged [50].

### ***29.3.8 Pharmacologic Therapies***

From a systematic review [26], two RCTs were found to address pharmacological interventions. Use of amantadine prevented pneumonia in one trial among nursing home residents [63]. The antithrombotic agent cilostazol prevented aspiration pneumonia in another trial but resulted in excessive bleeding [64]. However the use of these agents (amantadine and cilostazol) for reducing aspiration pneumonia is unlikely to be accepted in practice. Amantadine is known to cause gastrointestinal and neurological side effects, and it has a propensity to interact with psychotropic medications [26]. Treatment with antibiotics can be difficult among the elderly because of an inability to identify the pathogen, altered drug metabolism, and associated medication side effects [65]. The efficacy of pneumococcal vaccine in the elderly population has been the subject of considerable debate as a result of

the lack of prospective, RCTs [66, 67]. Despite this limitation, experts recommend vaccination of all elderly people because the vaccine is safe, inexpensive, and cost effective [68, 69].

## 29.4 Benefits of Oral Ingestion

As mentioned in the previous paragraph, several studies have shown that a tube feeding is associated with a higher rate of pneumonia than that among patients who are eating [19, 50–57]. Some studies suggest that an enteral tube feeding may actually increase mortality and morbidity, and reduce QOL [70, 71]. It was shown by a study in animal models [72] and in children [73] that a gastrostomy tube placement may reduce lower oesophageal sphincter pressure and increase the risk of gastroesophageal reflux, with a change in the gastroesophageal angle as the suspected mechanism.

A tube feeding may worsen urinary and faecal incontinence, which is associated with an increased risk of pressure ulcers and also increase gastric secretions [74]. A percutaneous endoscopic gastrostomy (PEG) is an invasive surgical procedure with significant risks. Postoperative complications include aspiration pneumonia, oesophageal perforations, migrations of the tube, haemorrhage and wound infections [75]. Moreover, Leibovitz et al. [76] found that there is a high prevalence of oropharyngeal colonisation with gram-negative bacteria in patients with a tube feeding (both NGT and PEG) compared to orally-fed patients.

In addition, there are ethical issues. Low et al. [77] reported that 69 % of respondents would not agree to fed via a tube.

It is recommended that an artificial feeding should only be considered if dysphagia is thought to be a transient phenomenon and should not generally be used in people with severe dementia for whom dysphagia or disinclination to eat is a manifestation of disease severity [78, 79]. As a result of these guidelines, modified consistency food and fluids are used increasingly with people presenting with dysphagia due to dementia.

## 29.5 Food Modification and Pneumonia

### 29.5.1 Ways of Food Modification

Altering the consistency of foods is thought to lead to physiological changes which can reduce an individual's risk of aspiration. The consistency of foods can be altered from a regular texture to 'extensively modified-texture'

The terminology and definitions of different food and fluid consistencies vary and there is currently no international consensus regarding the terminology that

**Table 29.1** Reviewed studies about the impact of modified foods on pneumonia

Study	Study design	N of subjects
Flynn 2014 [80]	Protocol only	–
Karagiannis 2014 [82]	Quasi-experimental study	16
Steele 2013 [83]	Protocol only	–
Karagiannis 2011 [84]	RCT	76
Foley 2008 [42]	Systematic review	(4 studies)
Loeb 2003 [26]	Systematic review	(2 studies)
Whelan 2001 [85]	RCT	24
Goulding 2000 [86]	RCT	46
Garon 1997 [87]	RCT	17
Groher 1987 [40]	RCT	56

should be used for different consistencies of foods and fluids [80]. For instance, the National Dysphagia Diet is comprised of four levels of food modification with specific food items recommended at each level, namely (1) homogeneous, cohesive, and pudding like, (2) moist, semi-regular, (3) soft-solids, (4) regular [81]. Japan's Ministry of Health Labor and Welfare sets the following 6 levels. Level 0: Smooth jelly foods without protein, Level 1 Smooth jelly foods with protein, Level 2: Jelly foods with protein, Level 3: Paste containing meat/fish, Level 4: Soft foods, Level 5: Normal diet [80]. However, the International Dysphagia Diet Standardization Initiative (IDDSI) aims to develop global standardized terminology and definitions for modified-texture foods for individuals of all ages with dysphagia, in all care settings and for all cultures by December 2014 [37].

### 29.5.2 A Review of Food Modification and Pneumonia

The authors searched MEDLINE, the Cochrane Library and CINAHL, through April 2014, using the key words modification/modified, food/diet, consistency and pneumonia. The authors also hand-searched papers from *Dysphagia*, *Stroke*, *Physical Medicine and Rehabilitation*, *Clinical Infectious Diseases*, the *Journal of the American Geriatric Society* and *Age and Aging* from 1995 to 2014. Reference lists of relevant primary and review articles were searched. Among 59 citations identified, ten articles mentioned the relation between food modification and pneumonia in adults (Table 29.1), while others didn't provide any information about such relations. Of ten studies, five articles were RCTs, two were systematic review, one was quasi-experimental study, and two were just protocols without results.

The benefit of texture-modified foods and/or alteration of fluid viscosity was evaluated in five RCT [40, 84–87] and one quasi-experimental study [82]. Although four [40, 84, 85, 87] of five RCT studies evaluated pneumonia, it was difficult to meta-analyze the overall benefit due to heterogeneity of interventions, timing and duration of therapy and conditions of study population. Sample sizes across studies

were small, ranging from 20 [87] to 76 [84] and the event rates for pneumonia were low. In one trial [40], the simultaneous manipulation of solid textures and fluid viscosities makes it difficult to establish which component (solid or liquid) was associated with pulmonary benefit. In summary, although modifications in dietary textures and fluid viscosities are common interventions there is scant empirical evidence of their medical effectiveness.

## 29.6 Impact of the Consistency of Food Substances on Aspiration Pneumonia

### 29.6.1 A *Prompt Report from our Study*

The importance of oral intake versus enteral tube feeding is widely understood from the physical, mental, social and ethical aspects. It is recognized that oral intake can improve the organic response to stress and thus facilitate the recovery of patients after surgery [88]. Recently, clinicians have been attempting to promote oral intake. However, once oral intake is achieved, less attention has been paid to the consistency of food and to returning from modified-texture foods to regular solid food. It is hypothesized that regular food which requires mastication should promote masticatory function, salivary secretion and lower risk of dental diseases, and consequently promotes nutritional status and development of resistance against infections. Thus, a study considering the relationship between the consistency of food substances and the incidence of pneumonia in elderly people living in a welfare facility was conducted and presented briefly [89].

The subjects were 154 residents (29 males and 125 females; age, mean 87.9 years, range, 69–102 years). The following data were obtained from the facility's records: consistency of food substances, their caloric intake, their general health status (BMI and history of pneumonia), oral health (number of teeth, oral function, dental diseases, and amounts of ten specific microorganisms in the oral cavity). As results, solid food eaters were found to have a lower incidence of pneumonia (11.4 %) than paste food eaters (44.4 %) and those fed liquids through a gastrostomy tube (55.6 %) ( $\chi^2$ ,  $P < 0.001$ ). This may be because of the higher calorific intake (mean  $\pm$  SD;  $1513.0 \pm 135.3$  kcal) of regular food eaters compared to paste food eaters ( $1362.2 \pm 178.8$  kcal) and those receiving nutrition through a gastrostomy tube ( $9056.6 \pm 176.5$  kcal) (ANOVA,  $P < 0.001$ ). Regular food eaters had better oral function ( $\chi^2$ ,  $P < 0.001$ ) and fewer microorganisms (ANOVA,  $P < 0.001$ ). Since this was a cross-sectional study, it was not possible to ascertain causal relationships. However, the results suggest that the consistency of food substances which require mastication has some influence in lowering the incidence of aspiration pneumonia among the elderly.

## 29.6.2 *Advantage of Mastication of Food*

### 29.6.2.1 Promoting Physical Activity

**Saliva Production** Mastication promotes the production of saliva. Saliva plays a vital role in food oral processing and antimicrobial function [90]. Human saliva consists of electrolytes, mucus, glycoproteins, enzymes, and antibacterial compounds such as secretory IgA and lysozyme [91]. Functions are protection and lubricant (coating oral mucosa to protect from trauma), digestion (moistening foods and helping to create a food bolus, containing enzymes to digest starches and fats), antimicrobial function (a mechanical cleansing action and a specific, e.g., IgA, and a non-specific immunologic action e.g., lysozyme, lactoferrin and myeloperoxidase), pH maintenance (containing various ions which act as a buffer), remineralization of teeth, a taste mediation [91]. Promoting saliva production results in better oral hygiene and improvement of digestions.

**Oral Health** Physiologically, oropharyngeal colonization by pathogenic organisms is prevented by the mechanical clearance provided by chewing and swallowing [92].

**Helping Enzymes for Digestion** Mastication breaks the food into smaller pieces, increasing efficiency of the digestive enzymes by creating more surface area on food particles for attachment of enzymes.

**Oral Function** Using organs, disuse syndromes can be prevented. A physical can prevent disuse syndrome. Physical inactivity predictably leads to deterioration of many body functions. Regular food requires more chewing time than modified-texture foods, thus it is expected to activate related organs. Though there is insufficient evidence concerning the elderly, gum chewing decreases time to flatus and first defecation after surgery [93] and chewing and a fiber rich diet is suggested to help development in children [94].

**Cognitive Impairment** Although this theory is not confirmed in humans, the relationship between mastication and cognitive impairment has been studied in various animal models [95, 96]. Three mechanisms explaining these animal studies were proposed to relate to a neurogenesis in the part of the brain that is associated with cognition: an increase in corticosterone and a decrease of hippocampal glucocorticoid associated with stress, a disruption of cholinergic neurotransmitter system associated with learning ability, and spatial memory [97]. In humans, though several studies have been undertaken, there is insufficient substantial evidence to demonstrate the relationship [97].

### 29.6.2.2 Better Nutrition

Although it is widely believed that altering the consistency of foods and fluids can help individuals with dementia and swallowing difficulty more safely and more efficiently, the use of modified-texture foods, particularly pureed diets, has been implicated in the high prevalence of undernutrition [98]. There is little clinical evidence to explain how the use of modified-texture foods causes undernutrition, but previous studies have found that modified-texture foods, specifically pureed types, offer poor nutritional value compared with regular foods [99–101]. The modified-texture foods may also lead to dehydration and malnutrition. It can be unpalatable and the choice of food that is recommended may be limited [102, 103]. One study reported that if the consistency of food was changed from paste to soft solid food which requires mastication, people improved through the intervention ( $n = 13$ ) by gaining weight [104].

### 29.6.3 QOL

A result of satisfaction survey among residents in long-term care indicates that food is the topic with the most variability, reflecting not only a high level of interest in this important daily activity, but also a range in satisfactions [105]. They may resist consuming modified texture foods instead of appealing the texture and taste because they are often unappealing in their appearance, texture, and taste [106]. Some studies have shown that patients may be embarrassed eating pureed foods in front of other people, resulting in their social isolations [107]. Niezgoda et al. [108] reported several issues and challenges in relation to modified-texture foods.

### 29.6.4 Consideration of Modified-Texture Foods for the Elderly

Assessment of eating ability and adapting modified-texture foods has not been standardized in clinical settings [108]. One study indicated that among nursing home residents, 91 % of nursing home residents with modified-texture foods were placed on overly restrictive diets [109]. Only 5 % of these patients were identified to be on an appropriate diet level matching their swallowing ability and 4 % of patients were placed on diets above their clinically measured swallowing ability. Furthermore, low acceptability and resulting poor adherence to modified-texture food/liquids can contribute to increased risk of inadequate nutrition in elderly patients with dysphagia.

The phenomenon of elderly persons not eating is observed daily in clinical practice. However, assessment of the causes is highly complex and providing

proper care is difficult. If caused by dysphasia from stroke or dementia, the risk from diseases and comorbidity should be carefully taken into consideration and provide medical treatment. If caused by poor oral conditions such as losing teeth or edentulism [110, 111], dental treatment should be the first choice. If caused by the physiological changes that occur with aging, such as decreased sense of taste, hunger, and appetite, or fatigue after hospitalization, promoting functions may be taken into consideration to avoid disuse syndromes. Thus, it is important to keep personal history records and watch individuals carefully as well as to carry out further researches which will develop standardized care.

## 29.7 What Further Research Needs to be Done?

Review articles referred in this part concluded that there is a clear and pressing need for high-quality research to identify effective treatments. In the hierarchy of research designs [112], ‘high-quality research’ may indicate high-quality RCTs, which are considered to be evidence of the highest grade as “gold standard”. However, is sufficient evidences provided by RCTs for better clinical practice? The demerits of RCTs are well-known, as well as their advantages. Black [113] discussed many limitations and explained the necessity of observational studies. The issues of limitations of external validity is important. The RCTs are designed to maximize their internal validity to produce similar groups by random allocation. Usually, participants have been selected using strict inclusion and exclusion criteria, consequently characteristics of a study population were limited. In addition, other issues include difficulty in studying rare events, ethical problem, narrowing of the studied question, costs and time [113].

Two studies published in The New England Journal of Medicine in 2000 found that observational studies (with either a cohort or a case-control design) do not overestimate the magnitude of the effects of treatment as compared with those in RCTs [114, 115]. In addition, the range of the point estimates for the effect was wider for RCTs than for the observational studies, possibly due to the limitations of external validity.

As to compensate for the RCTs, comparative effectiveness research (CER) is proposed. CER is the direct comparison of existing health care interventions to determine which work best for which patients and which pose the greatest benefits and harms in the real world. Horn and Gassaway [116] extend the concept to develop practice-based evidence for clinical practice improvement (PBE-CPI) study methodology. PBE-CPI incorporates natural variation within data from routine clinical practice to determine what works, for whom, when, and at what costs. It uses the knowledge of front-line caregivers, who develop study questions and define variables as part of a transdisciplinary team. Its comprehensive measurement framework provides a basis for analyses of significant bivariate and multivariate associations between treatments and outcomes, incorporating patient differences, such as severity of illness [116]. PBE-CPI studies can uncover better

practices more quickly than RCTs or sophisticated statistical methods, while achieving many of the same advantages [116].

**Open Access** This chapter is distributed under the terms of the Creative Commons Attribution Noncommercial License, which permits any noncommercial use, distribution, and reproduction in any medium, provided the original author(s) and source are credited.

## References

1. Mylotte J. Nursing home-acquired pneumonia. *Clin Infect Dis.* 2002;35:1205–11.
2. Nakajima N, Aiba M, Fukuda Y, Boku S, Isonuma H, Tsuda H, Hayashida Y. *Nihon Ronen Igakkai Zasshi.* 2009;46(1):71–8.
3. Pugliese G, Lichtenberg DA. Nosocomial bacterial pneumonia: an overview. *Am J Infect Control.* 1987;15:249–65.
4. Garibaldi RA, Brodine S, Matsumiya S. Infections among patients in nursing homes: policies, prevalence, and problems. *N J Med.* 1981;305(13):731–5.
5. Bryan CS, Reynolds KL. Bacteremic nosocomial pneumonia: analysis of 172 episodes from a single metropolitan area. *Am Rev Respir Dis.* 1984;129:668–71.
6. Wenzel RP. Hospital-acquired pneumonia: overview of the current state of the art for prevention and control. *J Clin Microbiol Infect Dis.* 1989;8:56–60.
7. Muder RR. Pneumonia in residents of long-term care facilities: epidemiology, etiology, management, and prevention. *Am J Med.* 1998;105:319–30.
8. Medina-Walpole AM, Katz PR. Nursing home-acquired pneumonia. *J Am Geriatr Soc.* 1999;47:1005–15.
9. Dunn L. Pneumonia: classification, diagnosis and nursing management. *Nurs Stand.* 2005;19 (42):50–4. doi:[10.7748/ns2005.06.19.42.50.c3901](https://doi.org/10.7748/ns2005.06.19.42.50.c3901).
10. Sun T, Sun L, Wang R, Ren X, Sui DJ, Pu C, Ren Y, Liu Y, Yang Z, Li F. Clinical efficacy and safety of moxifloxacin versus levofloxacin plus metronidazole for community-acquired pneumonia with aspiration factors. *Chin Med J.* 2014;127(7):1201–5.
11. Verghese A, Berk SL. Bacterial pneumonia in the elderly. *Medicine.* 1983;62(5):271–85.
12. Finegold SM. Aspiration pneumonia. *Rev Infect Dis.* 1991;13:S737–42.
13. Terpenning M, Bretz W, Lopatin D, Langmore S, Dominguez B, Loesche W. Bacterial colonization of saliva and plaque in the elderly. *Clin Infect Dis.* 1993;16:S314–6.
14. Alvarez S, Shell CG, Woolley TW, Berk SL, Smith JK. Nosocomial infections in long-term care facilities. *J Gerontol.* 1988;43:M9–17.
15. Harkness GA, Bentley DW, Roghmann RJ. Risk factors for nosocomial pneumonia in the elderly. *Am J Med.* 1990;108:457–63.
16. Loeb M, McGeer A, McArthur M, Walter S, Simor AE. Risk factors for pneumonia and other lower respiratory tract infections in elderly residents of long-term care facilities. *Arch Intern Med.* 1999;159:2058–64.
17. Corti MC, Guralnik JM, Salive ME, et al. Serum albumin level and physical disability as predictors of mortality in older persons. *JAMA.* 1994;272:1036–42.
18. Naughton BJ, Mylotte JM, Tayara A. Outcome of nursing home-acquired pneumonia: derivation and application of a practical model to predict 30 day mortality. *J Am Geriatr Soc.* 2000;48:1292–9.
19. Langmore SE, Terpenning MS, Schork A, Chen Y, Murray JT, Lopatin D, Loesche WJ. Predictors of aspiration pneumonia: how important is dysphagia? *Dysphagia.* 1998;13 (2):69–81.
20. Garcia JM, Chambers E. Managing dysphagia through diet modifications. *Am J Nurs.* 2010;110(11):27–33.

21. Vergis EN, Brennen C, Wagener M, Muder RR. Pneumonia in longterm care: a prospective case-control study of risk factors and impact on survival. *Arch Intern Med.* 2001;161:2378-81.
22. Magaziner J, Tenney JH, DeForge B, Hebel JR, Muncie Jr HL, Warren JW. Prevalence and characteristics of nursing home-acquired infections in the aged. *J Am Geriatr Soc.* 1991;39:1071-8.
23. Mitchell SL, Kielley DK, Lipsitz LA. The risk factors and impact on survival of feeding tube placement in nursing home residents with severe cognitive impairment. *Arch Intern Med.* 1997;157:327-32.
24. Christmas C. Eating and feeding problems, Geriatric review syllabus. 5th ed. New York: Blackwell; 2002. p. 197-202.
25. Langmore SE, Terpenning MS, Schork A, Chen Y, Murray JT, Lopatin D, Loesche WJ. Predictors of aspiration pneumonia: how important is dysphagia? *Dysphagia.* 1998;13:69-81.
26. Loeb MB, Becker M, Eady A, Walker-Dilks C. Interventions to prevent aspiration pneumonia in older adults: a systematic review. *J Am Geriatr Soc.* 2003;51(7):1018-22.
27. Bisch EM, Logemann JA, Rademaker AW, Kahrlas PJ, Lazarus CL. Pharyngeal effects of bolus volume, viscosity, and temperature in patients with dysphagia resulting from neurologic impairment and in normal subjects. *J Speech Hear Res.* 1994;37(5):1041-59.
28. Logemann JA, Pauloski BR, Rademaker A, Cook B, Graner D, Milanti F, Beery Q, Stein D, Bowman J, Lazarus C, Heiser MA, Baker T. Impact of the diagnostic procedure on outcome measures of swallowing rehabilitation in head and neck cancer patients. *Dysphagia.* 1992;7:179-86.
29. Robbins J, Gensler G, Hind J, Logemann J, Lindblad A, Brand D, et al. Comparison of 2 interventions for liquid aspiration on pneumonia incidence a randomized trial. *Ann Intern Med.* 2008;148(7):509-18.
30. Wada H, Nakajoh K, Satoh-Nakagawa T, Suzuki T, Ohru T, Arai H, Sasaki H. Risk factors of aspiration pneumonia in Alzheimer's disease patients. *Gerontology.* 2001;47(5):271-6.
31. Koss E, Gilmore C. Environmental interventions and functional abilities of AD patients. In: Vellas B, Filten J, Frisoni G, editors. *Research and practice in Alzheimer's disease.* New York: Springer; 1998. p. 185-91.
32. Kuo S, Rhodes R, Mitchell S, Mor V, Teno J. Natural history of feeding tube use in nursing home residents with advanced dementia. *J Am Med Dir Assoc.* 2009;10(4):264-70.
33. Verghese A, Berk SL. Bacterial pneumonia in the elderly. *Medicine.* 1983;62:271-85.
34. Scannapieco FA, Mylotte JM. Relationships between periodontal disease and bacterial pneumonia. *J Periodontol.* 1996;67:1114-22.
35. Yoneyama T, Yoshida M, Ohru T, et al. Oral care reduces pneumonia in older patients in nursing homes. *J Am Geriatr Soc.* 2002;50:430-3.
36. Brady M, Furlanetto D, Hunter RV, Lewis S, Milne V. Staff-led interventions for improving oral hygiene in patients following stroke. *Cochrane Database Syst Rev.* 2006;4, CD003864.
37. International Dysphagia Diet Standardisation Initiative. International dysphagia diet standardisation initiative. 2012. <https://docs.google.com/file/d/0B1gDNrkHwLPcR25qMDJLSj3RG8/edit?pli=1>. Accessed 2 May 2014.
38. Troche MS, Sapienza CM, Rosenbek JC. Effects of bolus consistency on timing and safety of swallow in patients with Parkinson's disease. *Dysphagia.* 2008;23:26-32.
39. Bisch EM, Logemann JA, Rademaker AW, Kahrlas PJ, Lazarus CL. Pharyngeal effects of bolus volume, viscosity, and temperature in patients with dysphagia resulting from neurologic impairment and in normal subjects. *J Speech Lang Hear Res.* 1994;37(5):1041-59.
40. Groher ME. Bolus management and aspiration pneumonia in patients with pseudobulbar dysphagia. *Dysphagia.* 1987;1:215-6.
41. DePippo KL, Holas MA, Reding MJ, et al. Dysphagia therapy following stroke: a controlled trial. *Neurology.* 1994;44:1655-60.

42. Foley N, Teasell R, Salter K, Kruger E, Martino R. Dysphagia treatment post stroke: a systematic review of randomised controlled trials. *Age Ageing*. 2008;37(3):258–64. doi:[10.1093/ageing/afn064](https://doi.org/10.1093/ageing/afn064).
43. Carnaby G, Hankey GJ, Pizzi J. Behavioural intervention for dysphagia in acute stroke: a randomised controlled trial. *Lancet Neurol*. 2006;5:31–7.
44. DePippo KL, Holas MA, Reding MJ, Mandel FS, Lesser ML. Dysphagia therapy following stroke: a controlled trial. *Neurology*. 1994;44:1655–60.
45. Constans T, Alix E, Dardaine V. Protein-energy malnutrition. Diagnostic methods and epidemiology. *Presse Med*. 2000;16:2171–6.
46. Potter J, Klipstein K, Reilly JJ, et al. The nutritional status and clinical course of acute admissions to a geriatric unit. *Age Ageing*. 1995;24:131–6.
47. Rothan-Tondeur M, Meaume S, Girard L, Weill-Engerer S, Lancien E, Abdelmalak S, Rufat P, Le Blanche AF. Risk factors for nosocomial pneumonia in a geriatric hospital: a control-case one-center study. *J Am Geriatr Soc*. 2003;51(7):997–1001.
48. Potter JM, Langhorne P, Roberts M. Routine protein energy supplementation in adults: systematic review. *BMJ*. 1998;317:495–501.
49. Geeganage C, Beavan J, Ellender S, Bath PM. Interventions for dysphagia and nutritional support in acute and subacute stroke. *Cochrane Database Syst Rev*. 2012;10:CD000323.
50. Gillick M. Rethinking the role of tube feeding in patients with advanced dementia. *N Engl J Med*. 2000;342:206–10.
51. Sitzmann JV. Nutritional support of the dysphagic patient: methods, risks, and complications of therapy. *J Parenter Enteral Nutr*. 1990;14(1):60–3.
52. Johnson ER, McKenzie SW, Sievers A. Aspiration pneumonia in stroke. *Arch Phys Med Rehabil*. 1993;74:973–6.
53. Kidd D, Lawson J, Nesbitt R, MacMahon J. The natural history and clinical consequences of aspiration in acute stroke. *Q J Med*. 1995;88:409–13.
54. Harkness GA, Bentley DW, Roghmann KJ. Risk factors for nosocomial pneumonia in the elderly. *Am J Med*. 1990;89:457–63.
55. Croghan JE, Burke EM, Caplan S, Denman S. Pilot study of 12-month outcomes of nursing home patients with aspiration on videofluoroscopy. *Dysphagia*. 1994;9:141–6.
56. Feinberg MJ, Knebl J, Tully J. Prandial aspiration and pneumonia in an elderly population followed over 3 years. *Dysphagia*. 1996;11:104–9.
57. Peck A, Cohen C, Mulvihill MN. Long-term enteral feeding of aged demented nursing home patients. *J Am Geriatr Soc*. 1990;38:1195–8.
58. Dziewas R, Ritter M, Schilling M, et al. Pneumonia in acute stroke patients fed by nasogastric tube. *J Neurol Neurosurg Psychiatry*. 2004;75:852–6.
59. Finucane TE, Bynum JP. Use of tube feeding to prevent aspiration pneumonia. *Lancet*. 1996;348:1421–4.
60. Nakajoh K, Nakagawa T, Sekizawa K, et al. Relation between incidence of pneumonia and protective reflexes in post-stroke patients with oral or tube feeding. *J Intern Med*. 2000;247:39–42.
61. Wolfsen HC, Kozarek RA, Ball TJ, et al. Long term survival in patients undergoing percutaneous endoscopic gastrostomy and jejunostomy. *Am J Gastroenterol*. 1990;85:1120–2.
62. Abuksis G, Mor M, Segal N, Shemesh I, Plout S, Sulkes J, Fraser GM, Niv Y. Percutaneous endoscopic gastrostomy: high mortality rates in hospitalized patients. *Am J Gastroenterol*. 2000;95(1):128–32.
63. Nakayama K, Sekizawa K, Sasaki H. ACE inhibitor and swallowing reflex. *Chest*. 1998;113 (5):1425.
64. Yamaya M, Yanai M, Ohrui T, et al. Antithrombotic therapy for prevention of pneumonia. *J Am Geriatr Soc*. 2001;49:687–8.
65. Feinberg MJ, Knebl J, Tully J. Prandial aspiration and pneumonia in an elderly population followed over 3 years. *Dysphagia*. 1996;11(2):104–9.

66. Hirschmann JV, Lipsky BA. The pneumococcal vaccine after 15 years of use. *Arch Intern Med.* 1994;154:373–7.
67. Fedson DS, Shapiro ED, LaForce FM, et al. Pneumococcal vaccine after 15 years of use: another view. *Arch Intern Med.* 1994;154:2531–5.
68. Prevention of pneumococcal disease: recommendations of the Advisory Committee on Immunization Practice (ACIP). *MMWR Recomm Rep.* 1997;46(RR-8):1–24.
69. Sisk JE, Moskowitz AJ, Whang W, et al. Cost-effectiveness of vaccination against pneumococcal bacteremia among elderly people. *JAMA.* 1997;278:1333–9.
70. Peck A, Cohen CE, Mulvihill MN. Long-term enteral feeding of aged demented nursing home patients. *J Am Geriatr Soc.* 1990;38(11):1195–8.
71. Nair S, Hertan H, Pitchumoni CS. Hypoalbuminemia is a poor predictor of survival after percutaneous endoscopic gastrostomy in elderly patients with dementia. *Am J Gastroenterol.* 2000;95(2):133–6.
72. Canel DF, Vane DW, Goto S, et al. Reduction of lower esophageal sphincter pressure with Stamm gastrostomy. *J Pediatr Surg.* 1987;22:54–7.
73. Grunow JE, Al-Hafidh AS, Tunell WP. Gastroesophageal reflux following percutaneous endoscopic gastrostomy in children. *J Pediatr Surg.* 1989;24:42–5.
74. Finucane TE, Christmas C, Travis K. Tube feeding in patients with advanced dementia: a review of the evidence. *JAMA.* 1999;282(14):1365–70.
75. Candy B, Sampson EL, Jones L. Enteral tube feeding in older people with advanced dementia: findings from a Cochrane systematic review. *Int J Palliat Nurs.* 2009;15(8):396–404.
76. Leibovitz A, Plotnikov G, Habot B, et al. Pathogenic colonization of oral flora in frail elderly patients fed by nasogastric tube or percutaneous enterogastric tube. *J Gerontol A Biol Sci Med Sci.* 2003;58:52–5.
77. Low JA, Chan DK, Hung WT, Chye R. Treatment of recurrent aspiration pneumonia in end-stage dementia: preferences and choices of a group of elderly nursing home residents. *Intern Med J.* 2003;33(8):345–9.
78. National Institute for Health and Excellence. Dementia: supporting people with dementia and their carers in health and social care. London: NICE; 2006.
79. Royal College of Physicians. Oral feeding difficulties and dilemmas: a guide to practical care towards the end of life, Royal College of Physicians. 2010. <http://www.rcplondon.ac.uk/sites/default/files/documents/oral-feeding-difficulties-and-dilemmas.pdf>. Accessed 2 May 2014.
80. Flynn EP, Smith CH, Walsh CD, Walshe M. Modifying the consistency of food and fluids for swallowing difficulties in dementia. *Cochrane Database Syst Rev.* 2014;4:CD011077.
81. Teasell R, Foley N, Fisher J, Finestone H. The incidence, management, and complications of dysphagia in patients with medullary strokes admitted to a rehabilitation unit. *Dysphagia.* 2002;17(2):115–20.
82. Karagiannis M, Karagiannis TC. Oropharyngeal dysphagia, free water protocol and quality of life: an update from a prospective clinical trial. *Hell J Nucl Med.* 2014;1:26–9.
83. Steele CM, Bayley MA, Pélaudeau-Pigeon M, Stokely SL. Tongue pressure profile training for dysphagia post stroke (TPPT): study protocol for an exploratory randomized controlled trial. *Trials.* 2013;14:126.
84. Karagiannis MJ, Chivers L, Karagiannis TC. Effects of oral intake of water in patients with oropharyngeal dysphagia. *BMC Geriatr.* 2011;1:11–9.
85. Whelan K. Inadequate fluid intakes in dysphagic acute stroke. *Clin Nutr.* 2001;20:423–8.
86. Goulding R, Bakheit AM. Evaluation of the benefits of monitoring fluid thickness in the dietary management of dysphagic stroke patients. *Clin Rehabil.* 2000;14:119–24.
87. Garon BR, Engle M, Ormiston C. A randomized control trial to determine the effects of unlimited oral intake of water in patients with identified aspiration. *J Neurol Rehabil.* 1997;11:139–48.
88. Brodner G, Van Aken H, Hertle L, Fobker M, Von Eckardstein A, Goeters C, et al. Multimodal perioperative management—combining thoracic epidural analgesia, forced

- mobilization, and oral nutrition—reduces hormonal and metabolic stress and improves convalescence after major urologic surgery. *Anesth Analg.* 2001;92(6):1594–600.
89. Sakashita R, Nishitani M, Ono H, Sato T and Hamada M. Impact of the consistency of food substances on the aspiration pneumonia of residents in welfare facilities for seniors. In: The 5th international symposium for inter oral health science, Sendai. 2014.
90. Tenovuo J. Antimicrobial function of human saliva—how important is it for oral health? *Acta Odontol Scand.* 1998;56(5):250–6.
91. Kaplan MD, Baum BJ. The functions of saliva. *Dysphagia.* 1993;8(3):225–9.
92. Palmer LB, Albulak K, Fields S, et al. Oral clearance and pathogenic oropharyngeal colonization in the elderly. *Am J Respir Crit Care Med.* 2001;164:464–8.
93. Leier H. Does gum chewing help prevent impaired gastric motility in the postoperative period? *J Am Acad Nurse Pract.* 2007;19(3):133–6.
94. Sakashita R, Inoue N, Kamegai T. From milk to solids: a reference standard for the transitional eating process in infants and preschool children in Japan. *Eur J Clin Nutr.* 2004;58(4):643–53.
95. Ono Y, Yamamoto T, Kubo KY, et al. Occlusion and brain function: mastication as a prevention of cognitive dysfunction. *J Oral Rehabil.* 2010;37:624–40.
96. Weijenberg RAF, Scherder EJA, Lobbezoo F. Mastication for the mind: the relationship between mastication and cognition in ageing and dementia. *Neurosci Biobehav Rev.* 2011;35:483–97.
97. Lexomboon D, Trulsson M, Wårdh I, Parker MG. Chewing ability and tooth loss: association with cognitive impairment in an elderly population study. *J Am Geriatr Soc.* 2012;60 (10):1951–6.
98. Stewart L. Development of the nutrition and swallowing checklist, a screening tool for nutrition risk and swallowing risk in people with intellectual disability. *J Intellect Dev Disabil.* 2003;28(2):171–87.
99. Wright L, Cotter D, Hickson M, Frost G. Comparison of energy and protein intakes of older people consuming a texture modified diet with a normal hospital diet. *J Hum Nutr Diet.* 2005;18(3):213–9.
100. Dahl WJ, Whiting SJ, Tyler RT. Protein content for pureed diets: implications for planning. *Can J Diet Pract Res.* 2007;68(2):99–102.
101. Beck AM, Hansen KS. Meals served in Danish nursing homes and to Meals-On-Wheels clients may not offer nutritionally adequate choices. *J Nutr Elder.* 2010;29(1):100–9.
102. Easterling CS, Robbins E. Dementia and dysphagia. *Geriatr Nurs.* 2008;29(4):275–85.
103. Ekberg O, Handy S, Woisard V, Wuttge-Hannig A, Ortega P. Social and psychological burden of dysphagia: its impact on diagnosis and treatment. *Dysphagia.* 2002;17:139–46.
104. Yamaki N, Shirasaka T, Sato M, Ichimura K. Effects of the introduction of soft food on the nutrition, food intake and swallowing ability of elderly residents of a nursing care home. *J Jpn Acad Gerontological Nurs.* 2012;17(1):83–90 (in Japanese).
105. Stodel EJ, Chambers LW. Assessing satisfaction with care in LTC homes: current and best practices. *Healthc Manage Forum.* 2006;19(3):45–52.
106. Wright L, Cotter D, Hickson M, Frost G. Comparison of energy and protein intakes of older people consuming a texture modified diet with a normal hospital diet. *J Hum Nutr Diet.* 2005;18(3):213–9.
107. Kumlien S, Axelsson K. Stroke patients in nursing homes: eating, feeding, nutrition and related care. *J Clin Nurs.* 2002;11(4):498–509.
108. Niezgoda H, Miville A, Chambers LW, Keller HH. Issues and challenges of modified-texture foods in long-term care: a workshop report. *Ann Long Term Care.* 2012;20(7):22–7.
109. Groher ME, McKaig TN. Dysphagia and dietary levels in skilled nursing facilities. *J Am Geriatr Soc.* 1995;43:528–32.
110. Krall E, Hayes C, et al. How dentition status and masticatory - Function affect nutrient intake. *J Am Dent Assoc.* 1998;129(9):1261–9.

111. Sheiham A, Steele JG, et al. The relationship among dental status, nutrient intake, and nutritional status in older people. *J Dent Res.* 2001;80(2):408–13.
112. Evidence-Based Medicine Working Group. Evidence-based medicine: a new approach to teaching the practice of medicine. *JAMA.* 1992;268(17):2420–5.
113. Black N. Why we need observational studies to evaluate the effectiveness of health care. *BMJ.* 1996;312(7040):1215–8.
114. Benson K, Hartz AJ. A comparison of observational studies and randomized, controlled trials. *N Engl J Med.* 2000;342(25):1878–86.
115. Concato J, Shah N, Horwitz RI. Randomized, controlled trials, observational studies, and the hierarchy of research designs. *N Engl J Med.* 2000;342(25):1887–92.
116. Horn SD, Gassaway J. Practice-based evidence study design for comparative effectiveness research. *Med Care.* 2007;45(10 Supl 2):S50–7.